Design and Synthesis of Covalent Inhibitors for the Protein Kinase MK2 and Exploration of Different Cysteine-Targeting Electrophiles

Dissertation

der Mathematisch-Naturwissenschaftlichen Fakultät

der Eberhard Karls Universität Tübingen

zur Erlangung des Grades eines

Doktors der Naturwissenschaften

(Dr. rer. nat.)

vorgelegt von

Lisa Haarer

aus Stuttgart

Tübingen

2024

Gedruckt mit Genehmigung der Mathematisch-Naturwissenschaftlichen Fakultät der Eberhard Karls Universität Tübingen.

Tag der mündlichen Qualifikation:	24.06.2024
Dekan:	Prof. Dr. Thilo Stehle
1. Berichterstatter/-in:	Prof. Dr. Matthias Gehringer
2. Berichterstatter/-in:	Prof. Dr. Stefan Laufer
3. Berichterstatter/-in:	Prof. Dr. Michael Lämmerhofer

Zusammenfassung der Dissertation

Die Proteinkinase MK2 (mitogen-activated protein kinase-activated protein kinase 2) gehört zu den Effektorproteinen des p38 MAP-Kinase Signalwegs und spielt eine wichtige Rolle in der Entstehung von Entzündungsreaktionen. Darüber hinaus zeigen neuere Erkenntnisse, dass MK2 an der Krebsentstehung und Tumorprogression beteiligt ist. Diese Eigenschaften machen die Kinase zu einem interessanten Arzneistofftarget.

Im Rahmen dieser Arbeit wurde ein kovalenter Designansatz zur Entwicklung neuer Inhibitoren der Proteinkinase MK2 verfolgt. Der Einsatz kovalenter Proteinkinaseinhibitoren ermöglicht eine Verbesserung der Aktivität, Selektivität und Verlängerung der Wirkdauer. Des Weiteren verhindert die erfolgreiche kovalente Bindung des Inhibitors dessen Verdrängung durch ATP, dem physiologischen Cosubstrat der Kinase. Die Ausbildung der kovalenten Bindung erfolgt dabei durch die Reaktion eines elektrophilen Strukturelements, dem sogenannten *warhead* des Inhibitors mit einem nucleophilen Zentrum im Protein, meist einer Aminosäuren-Seitenkette. Die hohe Nucleophilie der Thiolgruppe der Seitenkette der Aminosäure Cystein und der geringe Grad der Konservierung von Cysteinen im *Kinom*, machen diese zu attraktiven Zielstrukturen für kovalente Inhibitoren. Typischerweise setzt die Entwicklung kovalenter Kinaseinhibitoren die Anwesenheit eines Cysteins in bzw. in der Nähe der ATP-Bindungstasche voraus. Mit Cystein-140 besitzt die Proteinkinase MK2 ein solches adressierbares Cystein in der *hinge*-Region. Ein äquivalent positionierter Cysteinrest findet sich leidglich in vier weiteren Kinasen, FGFR4, MPS1, S6K2 und MK3, wodurch sich über die kovalente Adressierung auch eine Möglichkeit zur Verbesserung der Selektivität bietet.

Die Kombination eines bekannten, nicht-kovalent bindenden, tetracyclischen MK2 Inhibitors mit einem elektrophilen *warhead* stellt den initialen Designansatz dieser Arbeit dar. Die Optimierung der Synthese der Gerüststruktur, deren Modifikation zur Verbesserung der synthetischen Zugänglichkeit und Vereinfachung der Derivatisierung ermöglichte die Synthese diverser Analoga. Neben etablierten Acrylamid-basierten reaktiven Gruppen, konnten auch heteroaromatische Elektrophile erfolgreich als *warhead*-Strukturen eingebaut werden.

Dabei zeigten sowohl Acrylamid-basierte Derivate als auch solche, die auf einem Chlornitropyridin beruhen, sehr gute inhibitorische Aktivität im biochemischen Assay, sowie geringe intrinsische Reaktivität gegenüber Surrogatnucleophilen. Die erfolgreiche kovalente Adressierung konnte weiterhin durch, im Rahmen einer Kooperation erfolgte, massenspektrometrische Analyse des Inhibitor-gebundenen Proteins und Röntgenkristallstrukturuntersuchungen bestätigt werden.

Summary

The protein kinase MK2 (mitogen-activated protein kinase-activated protein kinase 2) belongs to the effector proteins of the p38 MAP kinase signaling pathway and plays an important role in the regulation of inflammatory processes. Furthermore, recent findings show the involvement of MK2 in carcinogenesis and tumor progression. These properties render the kinase an interesting target in drug discovery.

In this work, a covalent design approach was pursued for the development of new inhibitors against the protein kinase MK2. The application of covalent protein kinase inhibitors enables an improvement in activity, selectivity and extends the duration of action. Furthermore, the successful covalent binding of the inhibitor prevents its displacement by ATP, the physiological cosubstrate of the kinase. The covalent bond is formed by the reaction of an electrophilic group, the so-called *warhead* of the inhibitor, with a nucleophilic center in the protein, usually an amino acid side chain. Cysteine residues display attractive target structures for covalent targeting due to the high nucleophilicity of the thiol group of the side chain and the low degree of conservation in the kinome. Typically, the development of covalent kinase inhibitors requires the presence of a cysteine in or in proximity to the ATP binding pocket. With Cys140, the protein kinase MK2 possesses such an addressable cysteine in the hinge region. An equivalently positioned cysteine residue is also found in four other kinases, FGFR4, MPS1, S6K2 and MK3, which also offers the possibility of improving selectivity via the covalent approach.

The combination of a known, reversible binding, tetracyclic MK2 inhibitor with an electrophilic warhead represents the initial design approach of this work. The optimization of the synthesis of the core scaffold, modification thereof to improve synthetic accessibility and derivatization possibilities enabled the synthesis of various analogues. In addition to established acrylamide-based warheads, heteroaromatic electrophiles could also be successfully incorporated as reactive groups.

Both acrylamide-based derivatives and those based on a chloronitropyridine showed very good inhibitory activity in the biochemical assay, as well as low intrinsic reactivity towards surrogate nucleophiles. The successful covalent targeting was further confirmed through intact protein mass spectrometric and X-ray crystallography.

Abbreviations

5-LO	5-lipoxygenase
5'UTR	5’ untranslated region
AATF	apoptosis-antagonizing transcription factor
ACN	acetonitrile
ADMET	absorption, distribution, metabolism, excretion, toxicity
AMP-PNP	adenylyl-imidodiphosphate
AQ	AssayQuant®
Ar	argon
ARE	adenylate/uridylate-rich elements
ASK	apoptosis signal-regulating kinase
ATF	activating transcription factor
ATP	adenosine triphosphate
AUF1	AU-rich element RNA-binding protein 1
BE	biochemical efficacy
Bn	benzyl
Boc	*tert*-butyloxycarbonyl
Boc2O	di-*tert*-butyl dicarbonate, Boc anhydride
BRF1	butyrate response factor 1
Brij35	polyoxyethylene(23)laurylether
BSA	bovine serum albumin
CAF1	chromatin assembly factor 1
CAMK	Ca^{2+}/calmodulin-dependent protein kinases
Cbz	benzyloxycarbonyl
CCL	CC-chemokine ligand
CCR4	C-C-chemokine receptor 4
CD	common docking site
Cdc	cell division cycle
CDI	1,1'-Carbonyldiimidazole
CDK2	cyclin-dependent kinase 2
CDKN1B	$p27^{Kip1}$, cyclin-dependent kinase inhibitor 1B
CEP131	centrosomal protein of 131 kDa
Chk	checkpoint kinase
CK	casein kinase
COPD	chronic obstructive pulmonary disease
CRC	colorectal cancer
CREB	cAMP response element-binding protein

CRP	C-reactive protein
CS	centrosomal satellites
CXCL	C-X-C motif chemokine
CYP	cytochrome P450
DAD	diode array detector
DAMP	damage-associated molecular pattern
DAPK	death-associated protein kinase
DCM	dichloromethane
DDR	DNA damage response
DIPEA	diisopropylethylamine
DLK	dual leucine-zipper kinase
DMAP	4-(Dimethylamino)pyridine
DMARD	disease-modifying anti-rheumatic drug
DMF	*N,N*-dimethylformamide
DMSO	dimethyl sulfoxide
dppf	1,1'-bis(diphenylphosphino)ferrocene
DSF	differential scanning fluorimetry
DTT	dithioerythritol
E2F1	E2F transcription factor 1
EGTA	ethylene glycol-bis(β-aminoethyl ether)-N,N,N',N'-tetra acetic acid
eIF4E	eukaryotic translation initiation factor 4E
EMA	European Medicines Agency
ePKs	eukaryotic protein kinases
eq.	equivalent(s)
ER	endoplasmatic reticulum
ERK	extracellular-response kinase
ESI	electron spray ionisation
EtOAc	ethyl acetate
EtOH	ethanol
EWG	electron withdrawing group
FDA	US Food and Drug Administration
FGF	fibroblast growth factor
FGFR4	fibroblast growth factor receptor 4
GADD45α	growth arrest and DNA damage inducible α
GK	gatekeeper
GM-CSF	granulocyte-macrophage colony-stimulating factor
GSH	glutathione, γ-glutamylcysteinylglycine

HCC	hepatocellular carcinoma
HCV NS5B	hepatitis C virus nonstructural protein 5B
HDC	histidine decarboxylase
HDM2	human double minute 2
HEPES	4-(2-hydroxyethyl)-1-piperazineethanesulfonic acid
hnRNP A0	heterogenous nuclear ribonucleoprotein A0
HNSCC	head and neck cancer
HOAc	acetic acid
HPLC	high performance liquid chromatography
HRMS	high resolution mass spectrometry
HSF1	heat shock transcription factor 1
Hsp	heat-shock protein
HTS	high throughput screening
HuR	human antigen R
IC50	half maximal inhibitory concentration
IFN	interferon
IFNAR1	interferon alpha and beta receptor subunit 1
IGF	insulin-like growth factor
IL	interleukin
IMID	immune-mediated inflammatory disease
Imp	importins
IR	infrared (spectroscopy)
IκBα	nuclear factor of κ light polypeptide gene enhancer in B-cells inhibitor α
J	coupling constant (NMR)
JAK	Janus kinase
JNK	c-jun N-terminal kinase
KIM	kinase-interacting motif
KO*t*Bu	potassium *tert*-butanolat
KSHV	Kaposi's sarcoma-associated herpesvirus
LG	leaving group
LIMK1	LIM domain kinase 1
LPS	lipopolysaccharide
LSP1	lymphocyte-specific protein 1
MAP2K	MAPK kinase; MEK, MKK
MAP3K	mitogen-activated protein kinase kinase kinase
MAPK	mitogen-activated protein kinase
mCPBA	*meta*-chloroperbenzoic acid

MEKK	MEPK/ERK kinase kinase
MeOH	methanol
mGluR1/5	group I metabotropic glutamate receptors
MHC	major histocompatibility complex
MK2	mitogen-activated protein kinase activated protein kinase-2
MLCK	myosin light-chain kinase
MLK	mixed lineage kinase
MLM	mouse liver microsomes
MMP	matrix metalloproteinases
MNK1	MAP kinase signaling integrating kinase
MOM	methoxy methyl ether
MPS1	monopolar spindle 1
MRP2	multidrug resistance protein 2
MRTF-A	myocardin related transcription factor A
MS	mass spectrometry
MSK	mitogen- and stress-activated protein kinase
NADP	nicotinamide adenine dinucleotide phosphate
NBS	*N*-bromosuccinimide
ncRNA	non-coding RNA
NELFE	negative elongation factor complex (subunit E)
NES	nuclear export signal
NEXT	nuclear exosome targeting complex
NF-κB	nuclear factor 'κ-light-chain-enhancer' of activated *B*-cells
NGF	nerve growth factor
NLR	Nod-like receptor
NLS	nuclear localization signal
NMP	*N*-methyl-2-pyrrolidone
NMR	nuclear magnetic resonance spectroscopy
Nogo-B	neurite outgrowth inhibitor, Reticulon-4
NOS2	nitric oxide synthase 2
NSAID	nonsteroidal anti-inflammatory drug
NSCLC	non-small cell lung cancer
$p56^{lck}$	lymphocyte-specific protein tyrosine kinase
PABP1	poly(A)-binding protein 1
PAMP	pathogen-associated molecular pattern
PARN	poly(A)-specific ribonuclease
PBMCs	peripheral blood mononuclear cells

PDAC	pancreatic ductal adenocarcinoma
PDB	Protein Data Bank
PDE4	phosphodiesterase 4
PDGF	platelet-derived growth factor
PD-L1	programmed cell death ligand-1
PhK	Phosphorylase kinase
PIM1	proviral integration site for Moloney murine leukemia virus
PKA	protein kinase A
PKC	protein kinase C
PKI	protein kinase inhibitor
PKIDB	Protein Kinase Inhibitor Database
PKN2	serine/threonine-protein kinase N2
PLK	polo-like kinase
POI	protein of interest
PP2A/C	protein phosphatase 2A/C
PPARγ	peroxisome proliferator activated receptor-γ
PPh3	triphenylphosphine
ppm	parts per million
PRAK	p38-regulated/activated protein kinase, MK5
PTMs	post-translational modifications
QM/MM	quantum mechanics/ molecular mechanics
RA	rheumatoid arthritis
Raf	rapidly accelerated fibrosarcoma
RANKL	receptor activator of nuclear factor κ-B ligand
RBC	Reaction Biology Corporation®
RBM7	RNA binding motif protein 7
RIPK1	receptor-interacting protein kinase 1
ROCK	Rho-associated protein kinase
ROS	reactive oxygen species
RSK2	p90 ribosomal S6 kinase
rt	room temperature
S6K2	ribosomal protein S6 kinase β 2
SAR	structure-activity relationship
SASP	senescence-associated secretory phenotype
sat.	saturated
SCLC	small cell lung cancer
SEM	trimethylsilylethoxymethyl

shRNA	small hairpin RNA
S_NAr	nucleophilic aromatic substitution
Sox	sulfonamido-oxine
SRC3	steroid receptor coactivator 3
SRE	serum response elements
SRF	serum response factor
STAT3	signal transducer and activator of transcription 3
TAB1	transforming growth factor β-activated protein kinase binding protein 1
TAK	TGF-β activated kinase
TAO	thousand and one kinases
TBN	*tert*-butyl nitrite
*t*BuOH	*tert*-butanol
TCI	targeted covalent inhibitor
TEA	triethylamine
TFA	trifluoroacetic acid
TGFβ	transforming growth factor β
THF	tetrahydrofuran
TIPS	triisopropylsilyl
TIPSSH	triisopropylsilanethiol
TIR	Toll/IL-1 receptor
TLC	thin layer chromatography
TLR	Toll-like receptor
TME	tumor microenvironment
TNFα	tumor necrosis factor α
TPL2	tumor progression locus 2
t_{ret}	retention time
TRIM29	ATDC, tripartite motif containing 29
TSC2	tuberin, tuberous sclerosis complex 2
TTP	tristetraprolin
UBE2j1	ubiquitin-conjugating enzyme
UBE3A	ubiquitin-protein ligase E3A
VEGF	vascular endothelial growth factor
XantPhos	(9,9-Dimethyl-9*H*-xanthene-4,5-diyl)bis(diphenylphosphane)
XPhos	dicyclohexyl[2′,4′,6′-tris(propan-2-yl)[1,1′-biphenyl]-2-yl]phosphane
ZAK	leucine-zipper and sterile-α motif containing kinase
ZAP70	zeta-chain associated protein kinase 70 kDa
δ	chemical shift (NMR)

Table of Contents

1 Introduction

1.1 Inflammatory Processes and Related Diseases

1.1.1 Stress Response and Inflammation

The classical definition of inflammation was postulated by CELSUS and GALEN almost 2000 years ago and thereafter, inflammation is characterized by *dolor*, *calor*, *rubor*, *tumor* and *functio laesa*. [17]

Inflammatory processes can be described as the escalation of the stress response, occurring as physiological response to pathological conditions like hypoxia, heat shock and osmotic stress as a result of macroscopic or microscopic injury or change. [18] Possible stimulating events include trauma, infection, radiation, autoimmune disorders, toxins and non-communicable diseases like metabolic diseases and cancer. [17b, 18a] These incidences can induce antigen-dependent or non-antigenic signaling, each activating specific sensors resulting in the triggering of different neuroendocrine and stress response pathways. One of these involved pathways is the p38 mitogen-activated protein kinase (MAPK) pathway, which is discussed in detail in section 1.2. The complex inflammatory signaling network controls diverse physiological effects which are tightly regulated under physiological conditions to maintain or reinstate homeostasis after activation through stress-inducing factors. [18b]

The activating antigens can be sorted into two categories: pathogen-associated molecular patterns (PAMPs) and damage-associated molecular patterns (DAMPs). Both are recognized by pattern recognition receptors (PPR), for example Toll-like receptors (TLR) or NOD-like receptors (NLR). The subsequent activation of different cell types, primarily myeloid cells like monocytes and macrophages, leads to the expression of pro-inflammatory genes. [17a] These regulated genes include mediators, like chemokines (CC-chemokine ligand 2 (CCL2), C-X-C motif chemokine (CXCL8)) and further cytokines (interleukine-1 (IL-1), tumor necrosis factor α (TNFα)). [17b] Whilst chemokines are responsible for the recruitment of immune cells to the inflammation side, [17a] cytokines, in general, are small, secreted proteins (< 40 kDa), which have pleiotropic effects. Depending on the target cell, they play a major role in the regulation of the immune response and thereby are key mediators in inflammation.[19] Through the activation of epithelial cells, they promote an increase in vascular permeability facilitating the entrance of immune cells. In the blood stream, cytokines increase prostaglandin release and the activation of the complement system. [17a]

There is a distinction between acute and chronic inflammation. The aim of acute inflammation is the deletion of its cause, clearance of necrotic cells and inducing the following healing processes. [17a] After the acute phase, inflammatory signaling is down-regulated by anti-inflammatory mediators such as IL-10, IL-37 and interferon-β (IFNβ), soluble cytokine receptors and acute phase proteins. [17a]

While acute inflammation is an important physiological mechanism regulated through a complex signaling network, chronic inflammation is a pathophysiological state. These inflammatory processes

change during aging and their dysregulation is involved in many diseases.[17a] Elevated levels of C-reactive protein (CRP), IL-1β, IL-6 and TNFα are used as biomarkers for the detection of inflammatory processes.

Besides chronic inflammation being a symptom in several diseases, it also increases the risk of developing pathological sequelae like metabolic syndrome, diabetes mellitus, cancer and cardiovascular diseases.[20]

1.1.2 Inflammatory Diseases

About half of the deaths worldwide can be correlated to inflammation-related diseases.[20] The primary type of disease that comes to mind in this context are immune-mediated inflammatory diseases (IMIDs). IMIDs are a cluster of diseases characterized by chronic inflammation, caused by a dysregulated immune response. The Global Burden of Disease study 2019 listed a prevalence of 68 million cases, a number that significantly increased over the last 30 years, due to population growth, aging and environmental changes (e.g. air pollution, hygiene standards and nutrition).[21] The clinical picture of different IMIDs is divers, including for example bronchial asthma, atopic dermatitis, multiple sclerosis, type 1 diabetes mellitus, inflammatory bowel disease and rheumatoid arthritis (RA). According to the WHO, 18 million patients (2019) worldwide are living with RA[22], a number that doubled since 1990.[23] At the same time, the death rate decreased by 24% worldwide, and by even more than 40% in high-income countries.[23] These data indicate an improvement in diagnostics, including serological analysis and imaging techniques, as well as treatment options.[24] Early and effective treatment can reduce disease activity and thereby not only suffering and physical constrains in acute phases, but also systemic manifestation and disability.[24b]

While the clinical picture and primary localisation of the inflammatory processes diverge between the IMIDs, they share common mechanistic features in disease progression. Therefore, the treatment options overlap.

1.1.3 Treatment of Chronic Inflammation

Since inflammation-dependent diseases display a great burden, especially in their acute phases, and are increasing the risk for developing additional diseases, effective treatment strategies are important. Due to the chronic characteristics, treatment needs to be safe and effective on the long term and well tolerated at the same time.

A variety of treatment options are approved by the European Medicines Agency (EMA) to date. In the case of RA, remission can be achieved for many patients but no curative treatment or preventive intervention[25] is available. Additionally, not all patients respond to the applicable treatment options and many suffer from their side effects. The treatment options comprise four categories. The first component involves non-pharmacological options, including surgery, physiotherapy or lifestyle

changes. Secondly, there are symptomatic treatments. This includes e.g. non-steroidal anti-inflammatory drugs (NSAID) for RA [24b] and inhalative bronchodilators for bronchial asthma and chronic obstructive pulmonary disease (COPD). [26] The third component, local and/or systemic treatment with glucocorticoids, has a beneficial effect on inflammation, but is associated with severe side-effects for systemic use. Finally, disease-modifying anti-rheumatic drugs (DMARDs) including conventional DMARDs (e.g. methotrexate, hydroxychloroquine), Janus kinase (JAK) inhibitors and biological DMARDs, aim for slowing down disease progression and minimizing symptoms.

For the development of further improved treatments with higher response rates and reduced side effects, new targets and mechanisms of action are continuously investigated.

Intracellular pathways regulating the stress response and inflammation are potential targets in drug discovery. A pathway that came into focus around three decades ago is the p38 MAP kinase pathway. [27] In addition to its key kinase p38, which has been intensively studied during that time span, the downstream MAP kinase-activated protein kinase 2 (MK2) represents an interesting yet less explored target, not only for the treatment of inflammatory diseases, but also in cancer research.

1.2 Protein Kinases and the p38 MAP Kinase Pathway

1.2.1 Protein Kinases

As multicellular systems, complex organisms had to develop a strategy to communicate within and between cells, and furthermore between larger assemblies like organs. [28] The DNA encodes a great variety of proteins, involved in every kind of physiological process. Post-translational modifications (PTMs) of proteins increase the variety of functions proteins can adapt. Glycosylation, acetylation, ubiquitination and phosphorylation are only four among several other possible PTMs. [29] As one of the most important PTMs for regulating protein function, protein phosphorylation is catalyzed by protein kinases, which transfer the γ-phosphate group of adenosine triphosphate (ATP) – the protein kinases' co-substrate – onto a target protein. The phosphorylation status not only controls enzymatic activity, but also the interactions and localization of a protein. [30] In addition to the phosphorylation of proteins, phosphate groups may also be attached to lipids, sugars and other suitable, biologically functional molecules by distinct kinase classes. [31] In the following, the focus will be laid on protein kinases, since MK2, the target enzyme of this dissertation, belongs to this class of kinase enzymes.

In eukaryotic cells, proteins can be phosphorylated at hydroxy groups of amino acid side chains, namely at the three following: tyrosine, serine, threonine. Depending on the addressed amino acid, protein kinases can be classified into three groups: serine/threonine, tyrosine and bispecific kinases. In the human genome, 518 genes encoding protein kinases were initially identified by MANNING *et al*. [32] and this number has further increased to at least 538 protein kinase genes in the meantime. [33] Eukaryotic protein kinases (ePKs) can be classified into seven groups of classical protein kinases, based on their structural and functional similarities, and the "atypical" kinases. Atypical kinases lack the typical

structure elements of the kinase domain but are still catalytically active. The seven groups of typical ePKs are: 1. AGC kinases (PKA, PKG, PKC); 2. Calcium/calmodulin-dependent kinases (CAMK); 3. Casein kinases 1 (CK1); 4. Cyclin-dependent kinases, MAP kinases, glycogen synthase kinases, casein kinases 2 (CMGC); 5. The homologues of yeast Sterile 7, Sterile 11, Sterile 20 kinases (STE20); 6. Tyrosine kinases (TK); 7. Tyrosine kinase-like (TKL).

Protein kinases display a two-lobe structure (see Figure 1), with a smaller N-lobe, in which the prevalent secondary structure is comprised of β-sheets. The second lobe, the C-lobe, is mostly constructed of helices. The C-lobe contains the activation segment starting from the DFG motif and terminated by the APE motif and including the activation loop. The catalytic loop is also part of the C-lobe and located between β6 and β7. [34] The C-lobe and the N-lobe are connected by a short flexible part, the so-called hinge region, which is part of the ATP binding pocket and a central anchoring point for the co-substrate.

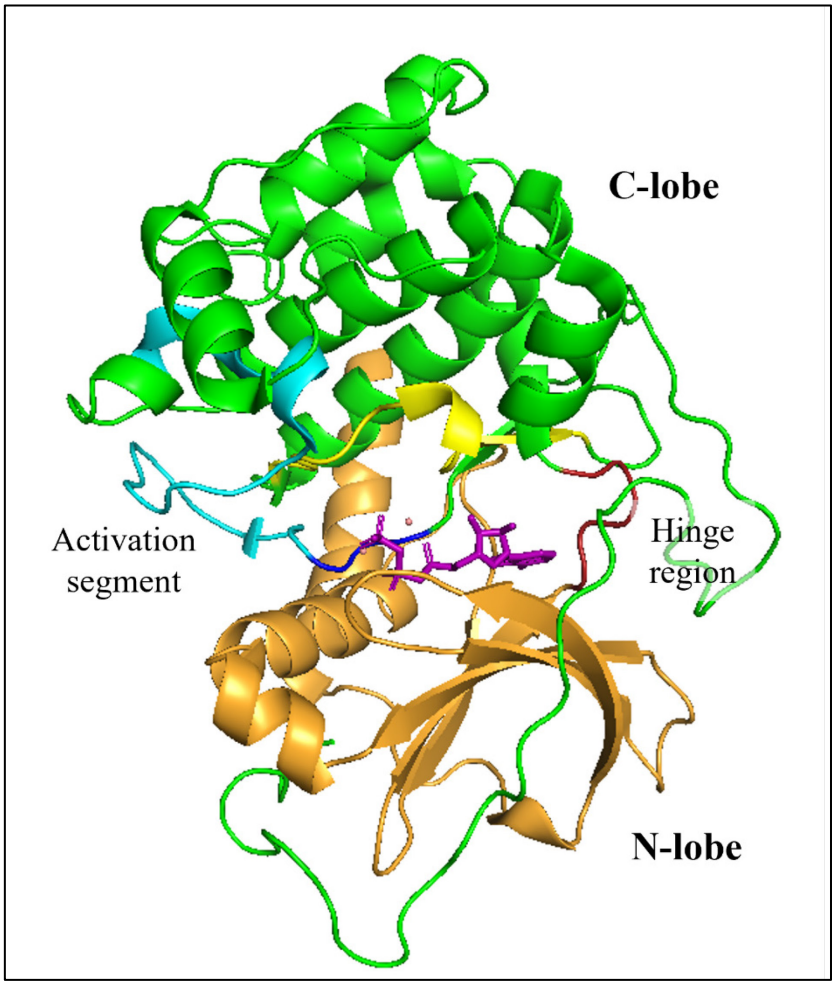

Figure 1: Crystal structure of protein kinase A (PKA) bound to AMP-PNP (PDB (protein data bank): 4DH7 [7]), the C-lobe is depicted in green, the N-lobe in orange, AMP-PNP in purple, the hinge region is colored in red, the catalytic loop in yellow, the activation segment in cyan and the DFG motif in blue.

The ATP binding pocket is highly conserved amongst the protein kinases. It contains a hydrophobic adenine-binding region, which is occupied by the adenine moiety of ATP (Figure 2B). The ribose part of ATP and the three phosphate groups interact with the hydrophilic environment in the ribose- and phosphate-binding region of the ATP binding pocket.[33a] The binding mode of the ATP-derivative adenylyl-imidodiphosphate (AMP-PNP) in the Proteinkinase A (PKA), as shown in Figure 2, showcases the crucial interactions.[7]

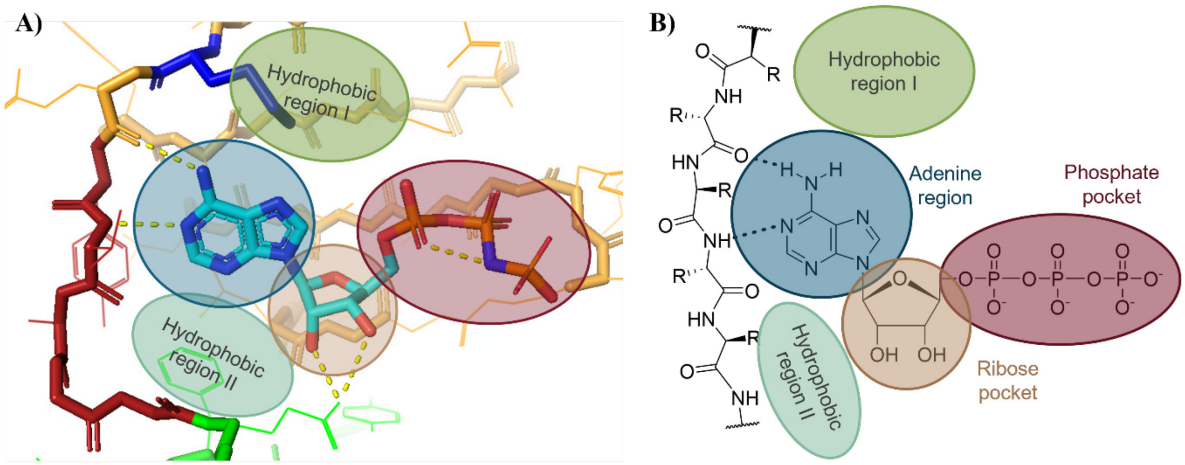

Figure 2: ATP binding pocket of PKA bound to AMP-PNP (colored by element), adenine binding region marked in blue, ribose pocket in orange, phosphate pocket in red, hydrophobic regions in green; A) 3D-depiction based on the crystal structure (PDB:4HD7[7], hinge region in red, gatekeeper in blue); B) 2D-depiction of the ATP binding mode.

Four conserved residues, the K/E/D/D motif, play an important role in the catalysis of the transfer of phosphate groups and are displayed in Figure 3A.[35] A conserved lysine (Lys72 in PKA), located in the N-lobe, positions the α- and β-phosphate. This residue forms a salt bridge to a glutamic acid (Glu91 in

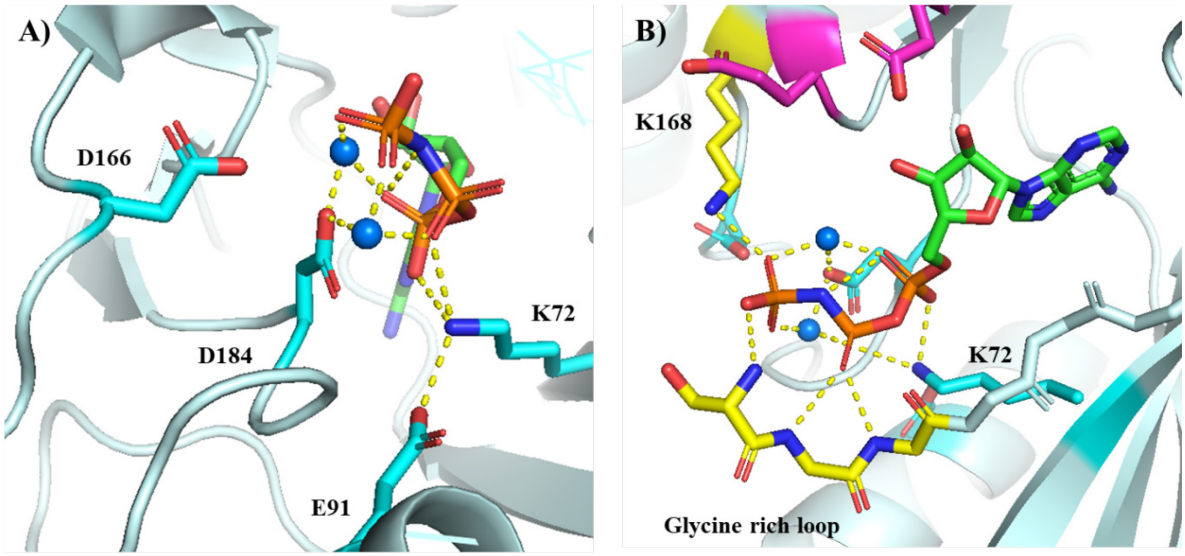

Figure 3: Anchoring of the phosphate groups of AMP-PNP in PKA (PDB: 4DH7[7]) (AMP-PNP is colored by element, Mg^{2+}-ions indicated by blue spheres, polar interactions indicated by yellow dotted lines); A) Interactions with the K/E/D/D-motif (light blue); B) Additional interactions with the glycine rich loop and K168 (involved amino acids colored in yellow)

PKA), which contributes to the stabilization of the position of the phosphate groups. The first aspartate residue (Asp166 in PKA), part of the catalytic loop, acts as catalytic base by abstracting a proton from the substrate protein. The final residue of the K/E/D/D motif is the aspartate of the DFG motif (Asp184 in PKA). This residue is coordinated to two Mg^{2+}-ions (blue spheres in Figure 3), which coordinate the β- and γ-phosphate. Additionally, residues of the glycine rich loop contribute to the binding of the latter phosphate groups (Ser53/Phe54/Gly55 in PKA, shown in Figure 3B, colored in yellow). As shown in Figure 3B (yellow residue at the bottom), the γ-phosphate interacts with another conserved lysine (Lys168). Together, these interactions position and activate the γ-phosphate for being transferred on a substrate protein.

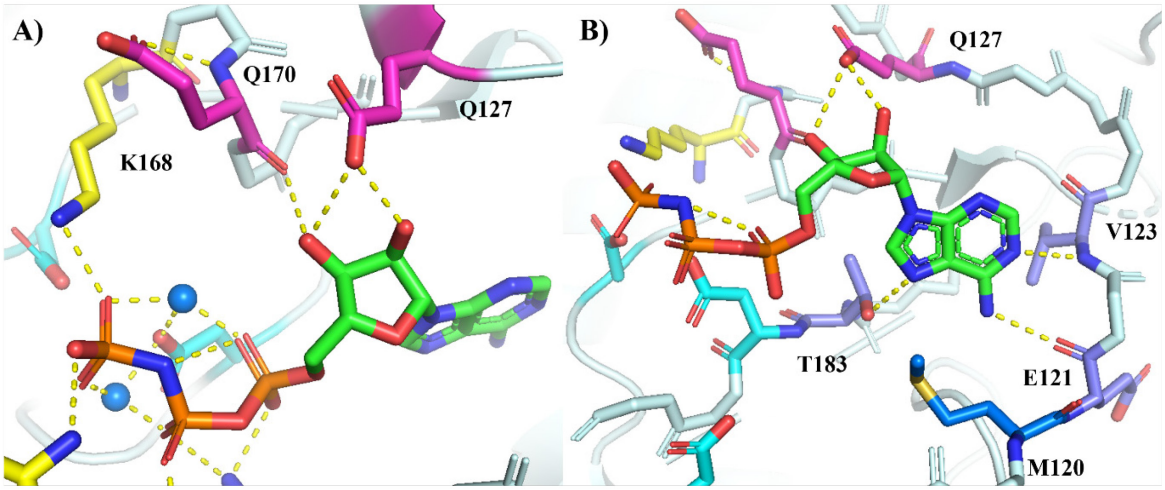

Figure 4: Depiction of the binding mode of AMP-PNP (colored by element) towards PKA (PDB: 4DH7 [7]); A) Interaction of the ribose residue of AMP-PNP (relevant residues in pink); B) Interactions of the adenine ring in the binding pocket (residues contributing to adenine binding colored in purple, gatekeeper residue M120 in blue).

Besides contributing to ATP binding, the conformation of DFG motif influences the activation state. Active kinases display the "DFG-in" conformation enabling the aforementioned contribution to phosphate binding, while in the "DFG-out" conformation the phenylalanine is oriented towards the binding pocket, blocking ATP binding.

The ribose is anchored by two glutamine (Gln, Q) residues, as shown in Figure 4A. Gln127 is the first amino acid following the hinge region and Gln170 is located in the catalytic loop. As mentioned, the adenine is bound to the flat and hydrophobic adenine-binding region in proximity to the hinge region. Here, its 6-amino group interacts with the backbone carbonyl group of the first amino acid of the hinge region (Glu121, shown in Figure 4B, purple residues). Two cyclic nitrogen atoms, *N*1 and *N*7, bind to the hinge region (Val123) and the activation segment (Thr183), respectively. In addition, the nucleotide is fixed by hydrophobic interactions to the N- and C-lobe. [35] The neighboring hydrophobic regions (highlighted in green in Figure 2), not involved in ATP binding, display a lower degree of conservation between different kinases. The size and access of the hydrophobic region I is regulated by the gatekeeper residue (Met120 in PKA, colored in blue in Figure 2A). Additionally, the gatekeeper and mutations of this residue can influence the activity of the kinase. [36]

1.2.2 MAP Kinase Pathways

Phosphorylation processes control enzymatic activity and possess the ability to either amplify (more common) or attenuate signals in signaling cascades, which is often used to translate extracellular signals into cellular responses. These complex signaling networks include multiple steps, enable crosstalk and feedback mechanisms, and are crucial for development and survival. On the other hand, dysregulation of such intricate signaling pathways can lead to pathophysiological conditions. The MAP kinase signaling pathways are one example for such regulatory pathways.

Three main families of MAP kinases have been identified in mammals: extracellular-response kinases (ERK1/-2, ERK5), c-jun N-terminal kinases (JNK), and p38 MAP kinases. [37] The members of the ERK family, ERK1, -2 and -5, are predominantly activated by growth factors and mitogens, regulating cell proliferation and growth. [38] The JNK pathway, activated by environmental stress, inflammatory cytokines and growth factors, governs inflammation, metabolism and apoptosis. [37a, 39] The function of the third family, the p38 MAP kinases, as well as its activation and downstream signaling, will be discussed in more detail in the following chapters.

The activation of the MAP kinases follows a three-step cascade, initiated by the activation of mitogen-activated protein kinase kinase kinases (MAP3Ks). Subsequently, MAP3Ks phosphorylate MAP kinase kinases (MAP2Ks, MKKs or MEKs), culminating in MAPK activation. The different MAP kinases share a common dual phosphorylation motif (Thr-X-Tyr) in the activation loop. Each pathway includes a distinct, yet partially overlapping, set of kinases in the cascade. [40]

There are several classes of MAP3Ks: MAPK/ERK kinase kinases (MEKK), mixed lineage kinases (MLKs), thousand and one kinases (TAOs) and Raf (rapidly accelerated fibrosarcoma). [41] MEKKs include MEKK1-4, TGF-β activated kinase 1 (TAK1), apoptosis signal-regulating kinase 1 (ASK1) and tumor progression locus 2 (TPL2). [42] MLKs are comprised of MLK2 and -3, dual leucine-zipper kinase (DLK) and leucine-zipper and sterile-α motif containing kinase (ZAK). [42d, 43] Both MLK classes include distinct kinases involved in activation of the different MAPK pathways. Additionally, TAO1-3 and their splice variants are capable of activating the p38 and JNK pathways. [44] The members of the Raf-family, such as A-Raf, B-Raf and C-Raf, activate the ERK pathway. [42d]

Compared to MAP3Ks, the number of MAP2Ks is considerably smaller and they display a notable target specificity. For instance, the MAPKs ERK1 and ERK2 are activated by MKK1 and MKK2, while ERK5 is activated by MKK5. Signal transduction in the JNK pathway is mediated by MKK4 and MKK7. In the p38 signaling pathway, MKK3 and MKK6 serve as the two key activating kinases. [37a, 45]

1.2.3 The p38 MAP Kinase

The p38 MAP kinase is the central kinase in its respective pathway. It was first identified in 1994 by three independent research groups and described as being activated by endotoxic lipopolysaccharides (LPS), hyperosmolarity, and heat shock. [46] Additionally, these studies demonstrated the downstream phosphorylation of other kinases and small heat shock proteins (Hsp) as a consequence of p38 activation, along with the regulation of cytokine levels. [27, 47]

Since its discovery, four isoforms of p38 have been identified. While p38α and β are expressed ubiquitously, the γ and δ isoforms are only present in specific tissues. [48] The p38γ isoform is predominantly expressed in skeletal muscle, whereas the p38δ isoform is found in the kidney, intestine, testis and pancreas. [49] Among the isoforms, the α-isoform stands out as the most extensively studied family member. It is the main form involved in inflammatory signaling and crucial for MK2 phosphorylation. [50]

1.2.4 Activation of the p38 MAP Kinase

The p38 MAP kinase pathway can be activated by various extracellular stimuli. In addition to cytokines (IL-1, IL-6, IL-17, IL-18, TNFα, transforming growth factor-β (TGFβ)), growth factors (granulocyte-macrophage colony-stimulating factor (GM-CSF), fibroblast growth factor (FGF), erythropoietin, nerve growth factor (NGF), insulin-like growth factor (IGF), vascular endothelial growth factor (VEGF), platelet-derived growth factor (PDGF), IL-3, IL-2, IL-7), intestinal signaling peptides (cholecystokinin, vasoactive peptides), and thrombin act as activators. Endotoxins and classical activators of the immune response, such as LPS, phorbol myristate acetate, PAMPs and DAMPs, can also activate the p38 pathway. Furthermore, physiological responses to environmental stress, like UV light, heat shock, stretching, osmolarity or hypoxia can trigger p38 activation. [46, 51] Additionally, certain chemical drugs, for example

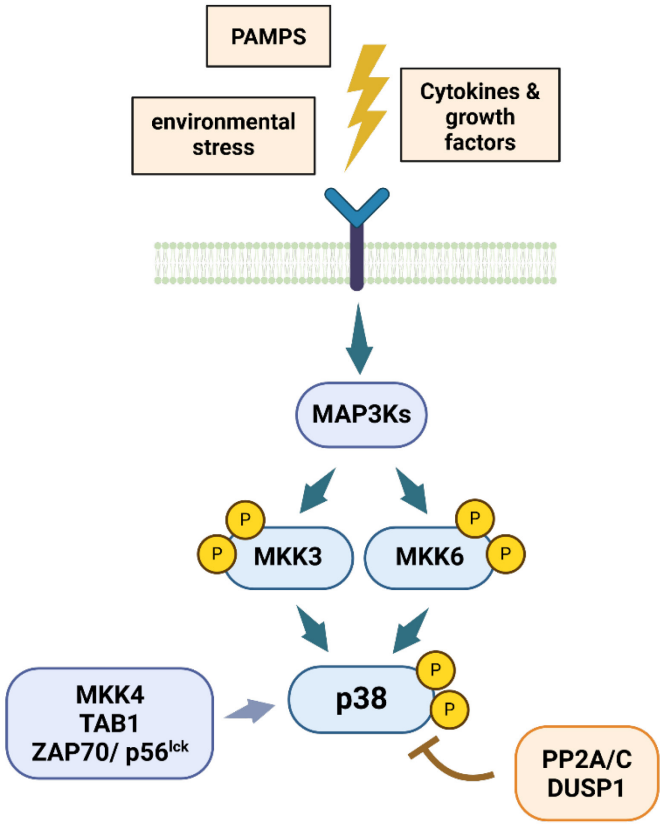

Figure 5: Activation of p38 MAP kinase (Created with BioRender.com).

anisomycin, hydroxyurea, or DNA-damage-inducing drugs like cisplatin or doxorubicin can induce cell stress and thereby activate p38. [51b, 51c]

A variety of receptors are involved in the activation of the p38 pathway. Among these, G-protein coupled receptors [51a] and members of the Toll/IL-1 receptor (TIR) superfamily, including the IL-1 receptor and TLR, play significant roles in p38 signaling and activate MAP3Ks. [52] The MAP3Ks acting upstream of p38 include MEKK1-4, ASK1, DLK1, TAK1, TAO1/2, ZAK1, TPL2, MLK3. [40-41, 42d, 51d] The distinct upstream signal transduction leading to p38 MAP kinase activation is highly dependent on the type of stimulus and the specific cell type. [43c, 51b, 53] For example, TNFα signal transduction is mediated through ASK1 and TAK1, while activation by reactive oxygen species (ROS) is transmitted by MEKK4 and ASK1. [51b]

The activation of p38 MAP kinase involves the phosphorylation of two MAP2Ks, MKK3 and MKK6, by upstream MAP3Ks (shown in Figure 5), such as TAK1, at serine and threonine residues within the activation loop. [45, 54] Activators and substrates of MAP kinases typically contain a docking (D) or kinase-interacting motif (KIM), with basic residues like arginine and/or lysine that bind to a negatively charged groove. Specificity of the interaction between distinct MAPKs and their activators or substrates is mediated by hydrophobic interactions. [55] In the case of p38α MAPK, MKK6 binds via its basic KIM motif to the common docking (CD) site. [56] The interaction of this N-terminal linker of MKK6 is important for substrate specificity and proper activation. Upon binding and additional interactions, conformational changes are induced, enabling access to the p38 phosphorylation side in the A-loop. [56a] Subsequently, p38 is activated by dual phosphorylation at Thr180 and Tyr182. [46, 57] The resulting conformational changes also stabilize the binding of Mg^{2+} and ATP. [56a] Binding to its activator not only activates the kinase, it also stabilizes the interacting proteins, thereby increasing their cellular concentration. [55]

While MKK3 and 6 are the main activators of p38 MAP kinase, BRANCHO *et al.* [58] found MKK4 to be involved in its activation after UV radiation. Furthermore, MAP2K-independent activation mechanisms have been discovered. For instance, in response to ischemia or hypoxia, interaction with TAB1 (transforming growth factor β-activated protein kinase binding protein-1) can induce autophosphorylation of p38α by an allosteric mechanism. [59] Additionally, SALVADOR *et al.* [60] described an autophosphorylation mechanism in T-cells mediated by ZAP70 (zeta-chain associated protein kinase 70 kDa) and $p56^{lck}$ (lymphocyte-specific protein tyrosine kinase) (Figure 5).

Several mechanisms contribute to fine-tuning the activity of p38 MAP kinase. One such mechanism involves the modulation of the binding affinity towards upstream kinases or the phosphorylation by the latter. For example, death-associated protein kinase 1 (DAPK1) enhances phosphorylation by MKK3. Posttranscriptional modification of the kinase itself or upstream components of the activation pathway also influence protein levels and activity. [51b] Another parameter is the localization of the kinase, which affects the phosphorylated substrate set. While p38α and β are manly located in the cytoplasm in the

resting state in most cells [61], their shuttling to the nucleus, independent of the phosphorylation state, is promoted by importins (Imp3, 7 and 9). [61-62]

The level of activity of the p38 pathway is also influenced by the type of activation pathway and feedback or cross-linked pathways. [51b] Inactivation of p38 signaling can be induced through phosphatases like protein phosphatase 2A (PP2A) and PP2C, which dephosphorylate threonine or both tyrosine and threonine residues, as observed with dual specificity phosphatase 1 (DUSP1). [51d, 63]

1.2.5 Physiological Functions of the p38 MAPK

The main functions of p38 MAPK were described in the mid-90s, including its involvement in cell proliferation, cell growth, differentiation and cell cycle control. [64] Subsequent research has further unraveled the effectors of p38 signaling in detail. One example is the importance of p38α for placental angiogenesis, as evidenced by embryonic lethality in p38α null mice. [40, 65]

The amino acid sequence recognized and phosphorylated by p38 typically contains a serine or threonine followed by a proline. [51d] Several downstream kinases phosphorylated and thereby activated by p38 kinases and thus contributing to their physiological effects were identified. These include mitogen-activated protein kinase activated protein kinase 2 (MAPKAPK2/MK2), MK3, p38-regulated/activated protein kinase (PRAK, MK5), ribosomal S6 kinase-B (RSK-B), MAP kinase signaling integrating kinase (MNK1), and mitogen- and stress-activated protein kinase 1 (MSK1). [66] Moreover, transcription factors such as activating transcription factor 2 (ATF2) and cAMP response element-binding protein (CREB) are well-established targets of p38 and are only two examples of the various transcription factors regulated by this pathway. [51d] Besides kinases and transcription factors, p38 isoforms also modulate DNA/RNA binding proteins, and various regulatory and structural proteins. More than 100 proteins were identified as direct phosphorylation targets of p38 kinases, while signal transduction via downstream targets further expand the number of effectors and the diversity of the network. [51b]

One of the main roles of the p38 MAP kinase pathway is the regulation of the stress response and inflammatory signaling, which involves the modulation of cytokine levels, for example TNFα, IL-1, IL-6 and IL-18. [49] The effects are mediated by the phosphorylation of transcription factors (e.g. NF-κB (nuclear factor 'κ-light-chain-enhancer' of activated B-cells), ATF1) and stabilization of mRNA. [51a] Notably, the stability of mRNA in this context is controlled by tristetraprolin (TTP) and human antigen R (HuR), two mRNA binding proteins. TTP is phosphorylated by MK2 (for further explanation see section 1.3.3). HuR is phosphorylated by p38, supporting cytoplasmatic localisation, [67] while both, p38 and MK2, appear to cooperate in enhanced shuttling of HuR to the cytosol. [50, 68]

Furthermore, the downstream kinase MSK1 exerts a regulatory role in controlling the expression of anti-inflammatory genes, like IL-10, TTP and DUSP1, through phosphorylation of transcription factors (e.g. CREB) and components of the nucleosome. [69]

Activation of p38 induces the senescence-associated secretory phenotype (SASP), which is associated with cell cycle arrest and involved in aging-related processes, tissue regeneration and cancer

development.[70] In addition, p38α is implicated in the DNA damage response (DDR), regulating cell cycle checkpoints (G1/S and G2/M phase), repair mechanisms and enhancing cell viability.[51b, 51d, 53b] Enhanced cell viability after metabolic stress is also mediated by p38 signaling.[51b, 71]
In contrast, the activation level of p38α also regulates proliferation in various cell types,[51d, 72] with strong sustained activation in cancer cells being linked to terminal cell differentiation, apoptosis and senescence[73], while low activity supports cell survival.[51d] This highlights the pleiotropic functions and intricate regulation of this signaling pathway.

1.2.6 Pathophysiological Role of the p38 Signaling Pathway

The regulation of inflammatory signaling represents the most prominent role of the p38 MAPK pathway, and therefore research focus laid on the pathophysiological role in chronic inflammation like rheumatoid arthritis. However, the influence of inflammatory processes on disease development is quite diverse and p38 signaling is involved in a variety of disease states beyond "classical" inflammatory phenotypes as outlined below.

Neurodegenerative diseases

The p38 pathway is involved in neuronal excitability, synaptic plasticity and myelination, but it is also associated with neuronal pathologies.[51b] Neuroinflammatory processes and high levels of IL-1, IL-10 TNFα and IL-6 were found to correlate with increased risk for neurodegenerative diseases like Alzheimer's and Parkinson´s disease.[50, 74] Moreover, p38 kinases have been found to promote Tau phosphorylation and subsequent aggregation, a mechanism strongly linked to Alzheimer's disease progression.[75]

Metabolic diseases

Through the regulation of glucose and lipid metabolism, the p38 kinases contribute to the development of obesity and metabolic diseases like diabetes.[50, 76] Hyperglycemia-induced ROS release can activate p38 signaling, thereby engendering cardiovascular complications, neuropathy and nephropathy.[50, 75d]

Cancer

The role of p38 signaling in cancer development is complex and multifaceted. While it was found to induce tumor growth in some models, a role as tumor suppressor is apparent in other experiments. Its role appears to depend on various factors including cell type, kinase expression levels, crosstalk, and feedback mechanisms due to the pleiotropic effects and complex pathological mechanisms in cancer development.[51d] One example for the tumor suppressing role of p38α is the activation of a negative feedback loop by inhibiting Ras-dependent gene expression and cell growth, important for lung tissue homeostasis.[77] A similar negative feedback mechanism was identified in liver cells, in which deletion of p38α promotes cancer development.[78] In a colorectal cancer model, enhanced metastasis in lung tissue was observed after p38 knockdown, which thereby promoted cancer progression.[79]

Conversely, increased p38 activation has been observed in lung cancer and head and neck squamous-cell carcinoma (HNSCC) samples, suggesting a promoting role in these malignancies. [80] In colon and liver cancer, p38γ has been shown to be implicated in tumor promotion. [81]

p38 activity also contributes to the development of chemoresistance. Besides enhancing expression of P-glycoprotein in gastric cancer cells [82], its role in the DDR and cell cycle control affects treatment response as for taxanes, 5-fluoruracil and cisplatin treatment. [63, 83] Furthermore, resistance to sorafenib treatment in hepatocellular carcinoma (HCC) correlates with p38α activity and resulting activation of MEK-ERK and ATF2. Inhibition of p38α using small hairpin RNA (shRNA) or the selective small molecule inhibitors skepinone-L and PH-797804 restored sorafenib sensitivity in a HCC cell line and animal models. [84]

Additionally, chronic inflammatory processes associated with cancer can create a tumor microenvironment (TME) that promotes tumor progression and metastasis. [50, 85] Cytokine and growth factor secretion, regulated by the p38 pathway, can promote tumor invasiveness and metastasis in different cancer types (e.g. breast cancer, fibrosarcoma and glioblastoma) by boosting angiogenesis, glycogen mobilization and motility. [85b, 86] In colorectal cancer (CRC), liver metastasis and dormancy can be connected to excretion of signaling molecules, e.g. TGF-β, matrix metalloproteinases (MMPs), IL-6, TNFα, to the TME and increased p38 activity, respectively. [87]

In conclusion, the role of the p38 pathway in cancer development and progression is versatile and dependent on several factors including involved cell types, isoform and the stage of tumor development. [88]

1.3 The Protein Kinase MK2

The growing understanding of the role of p38 MAPKs in pathological settings has intensified the interest in its downstream targets. A central one is MK2, which was first discovered over 30 years ago by STOKOE *et al.* [89], with the heat shock proteins Hsp25 and Hsp27 identified as its initial phosphorylation targets. [90]

The kinase belongs to the superfamily of Ca^{2+}/calmodulin-dependent protein kinases (CAMK), a family of serine/threonine kinases sharing a similar regulatory mechanism. [11, 91]

Knock-out experiments showed that $MK2^{-/-}$ mice are viable and fertile without other obvious peculiarities, but they exhibited decreased levels of phosphorylated Hsp25 after LPS stimulation (in heart tissue). Additionally, a reduction of TNFα, IFNγ, IL-1β and IL-6 levels was observed, suggesting a role in inflammatory processes. [92]

MK2 is expressed ubiquitously [93], with recent proteome analyses indicating especially high levels in immune organs and gastrointestinal tissues and low expression in muscles. [40]

Two main splice variants of MK2, with a molecular mass of 60 kDa and 53 kDa, can be detected in western blot analysis. [89, 92, 94] The longer 60 kDa variant is translated from an alternative CUG translation initiation start site in the 5' untranslated region (5'UTR) of the mRNA and contains an

additional phosphorylation site in the extended N-terminus. Nonetheless, only the shorter splice variant fits the known open reading frame and expected molecular mass and is capable of mediating some core functions like phosphorylation of Hsp27. Therefore, it is considered the main form regarding structure and numbering.[95] An additional, rare variant was discovered by Zu *et al.,* lacking the nuclear localization signal (NLS) and p38 docking domain.[96]

MK2 shares a high level of homology with MK3 (MAPKAPK3) which is significantly less explored. Consequences of this similarity will be discussed section 1.3.5.

1.3.1 Structure of the Protein Kinase MK2

The protein kinase MK2 consists of 400 amino acids organized in the kinase-typical two-lobe structure, along with an additional regulatory domain (depicted in Figure 6).[97] The N-terminus comprises two proline-rich segments (1-40) [[98], followed by the kinase domain (64-325) [[99] and the subsequent C-terminal regulatory domain.[97] The P-loop (64-82, orange in Figure 6) contains the ATP binding and glycine-rich motif (GXGXXG, 71-76, green in Figure 6), and is followed by the hinge region (Figure 6, colored in red).[11] The C-lobe contains the activation segment (Figure 6, colored in purple). MK2 can be classified into the group of RD kinases, wherein the catalytic aspartate (Asp186 in MK2) is preceded by an arginine (Arg185). Another widespread property within this group is the requirement of phosphorylation of the activation segment for activation. In MK2, the relevant residue is a threonine (T222).[11] The activation segment is a dynamic structure in the inactive kinase[11], commonly defined as the sequence starting with the DFG motif (residues 207-209, yellow in Figure 6) and terminated by the APE motif (231-233, light blue in Figure 6).[34, 100] The C-terminal regulatory domain of MK2 (328-400, crystalized part in colored in rose in Figure 6) contains the autoinhibitory region, nuclear export signal (NES, 345-368), and the bipartite NLS (373-389).[97] Two phosphorylation sites, Thr334 and Thr338, are located in this

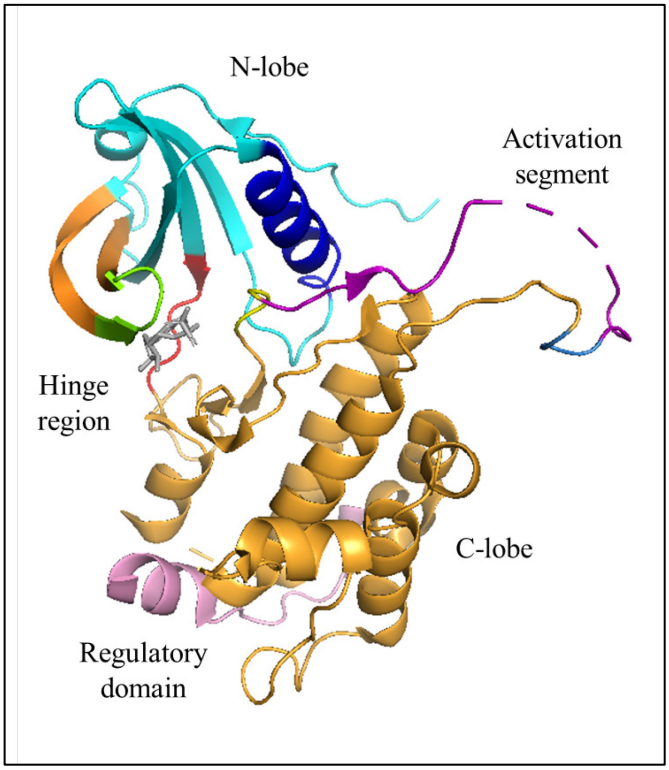

Figure 6: Structure of MK2 (PDB: 1NY3, residues 46-345[11]); N-lobe at the top (basis in cyan), C-lobe at the bottom (gold), C-terminal regulatory domain (rose), αC-helix in blue, glycine-rich motif (green) in the P-loop (orange on the left), hinge region (red, background), ADP (grey), activation segment in purple between the DFG (yellow) and APE motif (light blue).

domain. The latter, Thr 338, is most likely auto-phosphorylated, while Thr334 is phosphorylated by p38α/β and located at the C-terminus of the autoinhibitory region. [97, 101]

The binding mode of ADP and Staurosporin is similar to other kinase structures bound to ADP or ATP mimetics. [11] The adenine ring forms two hydrogen bonds towards the backbone *NH* of Leu141 and the carbonyl oxygen of Glu139, located in the hinge region (shown in Figure 7A). The ribose moiety of ATP interacts with the "sugar pocket" (orange in Figure 7) formed by Glu145, Glu190, Leu70, Gly71 and Leu72. [99] With methionine (Met138, colored blue in Figure 7A) as a considerably large gatekeeper residue, the ATP binding pocket is comparably small. [99]

The phosphate groups form polar interactions with Asn191, Asp207, Lys93 and Ile74 (Figure 7A, residues of the K/E/D/D motif colored in cyan in). The orientation of Lys93 is stabilized by a salt bridge towards Glu104 in the αC-helix, indicating the active state and enabling binding to the α- and β-phosphate of ATP (illustrated by yellow dotted lines in Figure 7). [11] Additionally, the catalytic aspartate (Asp186) completes the K/E/D/D motif, abstracting a hydrogen from the substrate.

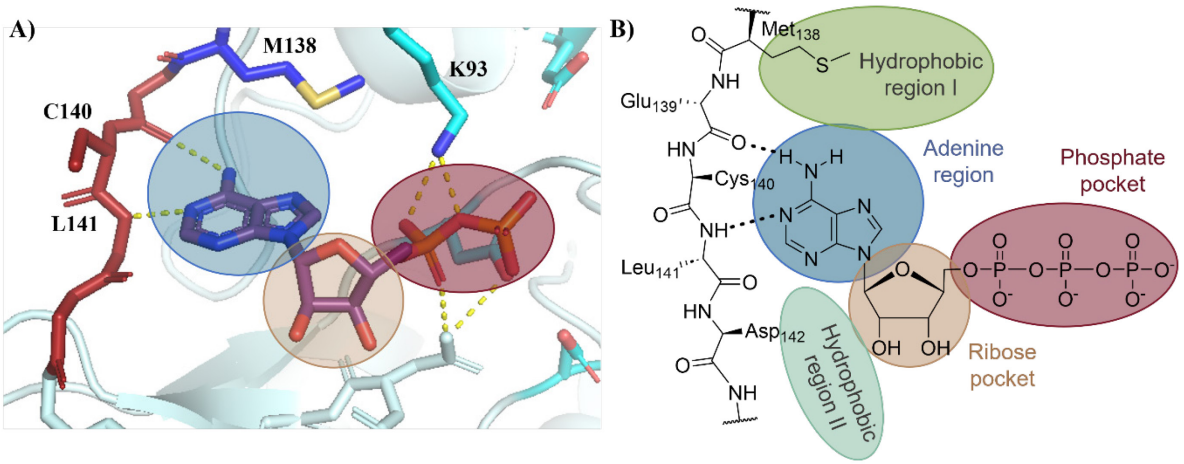

Figure 7: ATP binding site of MK2. Adenine binding region in blue, ribose pocket in orange, phosphate pocket in red; A) Crystal structure of DAP-bound MK2 (PDB: 1NY3 [11]; ADP purple, colored by element; hinge region in red, M138 in blue; residues of the K/E/D/D-motif in cyan, polar interactions shown as yellow dotted lines); B) 2D depiction of the binding mode of ATP to the hinge region of MK2 (hydrophobic regions highlighted in green).

Despite several conserved regions and shared structural characteristics among different protein kinases, each exhibits unique interaction patterns and structural features. This also applies to the structural features of MK2. The proline-rich domains and C-terminus share no significant sequence homology to kinases outside the group of MAPKAPK proteins (75% with MK3 and 45% with PRAK). The kinase domain bears low sequence homology to other serine/threonine kinases, except MK3. [11, 97] MK2 possesses structural similarities with PKA, CAMK (especially II and IV), and titin (TTN), a large molecule from muscle cells possessing a kinase domain [102], and shares similar regulatory mechanisms with these kinases. Furthermore, similarities of the catalytic domain with phosphorylase b kinase (PhK), myosin light-chain kinase (MLCK, from rabbit), and p90 ribosomal S6 kinase-II (RSK2, from mouse) were identified. [11] This results in a few shared substrates but significantly differing biological functions. [93a, 103]

1.3.2 Activation of MK2

In an inactive state, MK2 is primarily located in the nucleus. [93a, 98] There, it can form a complex with p38α. The formation of this complex not only enables activation but also has an additional stabilizing effect on the kinase. [104] Three phosphorylation sites were identified as relevant for the activation of MK2: Thr222, Ser272 and Thr334 (highlighted in yellow in Figure 8). All of these sites can be phosphorylated by p38α/β, and double phosphorylation is sufficient for activation. [101] An additional autophosphorylation sites was also discovered on MK2, Thr338. Phosphorylation at a threonine residue in the N-terminal region, Thr25, has also been observed, though it is not involved in activation, and the relevance of this event has not yet been fully elucidated. [101] Additional phosphorylation occurrences are possible at two serine residues, Ser9 and Ser328, but no functional relevance has been described for these events. [99]

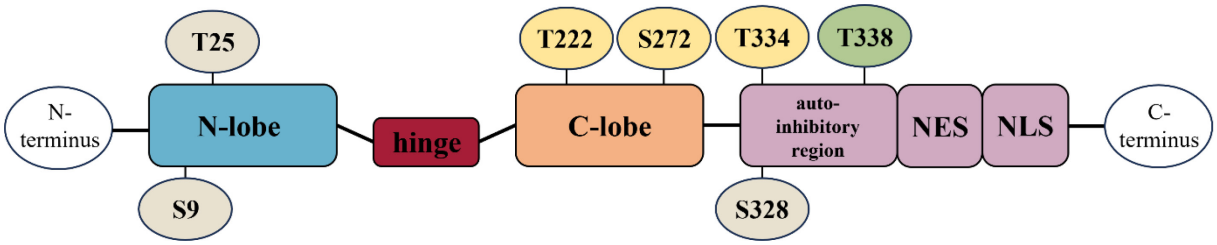

Figure 8: Localization of the phosphorylation sites in MK2 (regulatory domain in light purple; p38-mediated phosphorylation sites in yellow, autophosphorylation site in green).

The p38α-docking domain in MK2 is located in the C-lobe, with residues 366-390 being especially relevant for the formation of the high-affinity complex. [105] In the resulting complex, the kinases bind head-to-head, with their respective N-lobes interacting with each other, and the same applies to the C-lobes. The interaction interface also covers the regulatory domain of MK2 (345-390) including the aforementioned crucial residues. [105b] Additionally, the conformation of the activation segment is stabilized by these interactions. [105b] Upon phosphorylation of p38 and the resulting conformational change, the three phosphorylation sites in MK2 become accessible to the p38 active site. Phosphorylation of Thr334 unmasks the NES, resulting in translocation of the complex (Figure 9). [105-106] Furthermore, phosphorylation of MK2 induces a conformational change of the APE motif, resulting in a fully activated kinase complex. [55]

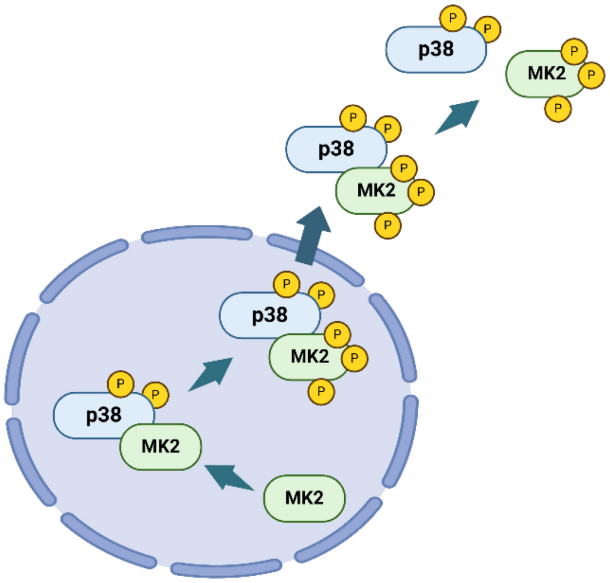

Figure 9: Activation and translocation of MK2 (graphic created with BioRender.com).

After activation, MK2 first activates nuclear targets before being shuttled to the cytoplasm. [107]
After activation by p38, the complex dissociates, and MK2 is degraded after ubiquitination by MDM2. Subsequently, MK2 is re-expressed and stabilized by binding to unphosphorylated p38 after pathway activation is terminated. Under conditions of sustained stress and stimulation of the pathway, MK2 levels are reduced, and cell death induced. [108]

1.3.3 Substrates and Functions of MK2

The minimal sequence requirements for phosphorylation of a substrate by MK2, identified in 1993 by STOKOE *et al.* can be summarized as HydXRXXSXX (with 'Hyd' representing a hydrophobic amino acid). [93a] A more recent and detailed version of the interaction pattern by MANKE *et al.* provided an updated sequence: (Leu/Phe/Ile)-(Xxx)-(Arg)-(Gln/Ser/Thr)-(Leu)-(**Ser**/Thr)-(Hydrophobic). [91]
Although including threonine in addition to serine as a possible phosphorylation site, efficient phosphorylation was only observed at serine residues, [91] consistent with the findings of STOKOE *et al.*, in which replacement of the serine abolished phosphorylation. [93a]
The underlying preference for this specific pattern can be attributed to the intermolecular interactions between the substrate and the kinase. The hydrophobic residue located five residues N-terminal to the phosphorylation site (at Ser –5) is oriented towards Ile255, while the arginine residue three residues before the serine (Ser –3) forms interactions with glutamic acid in position 145 of MK2. Moreover, the hydrophobic residue at Ser +1, namely valine, leucine, alanine, or glutamic acid [93a] is hosted in a hydrophobic pocket defined by four residues -Pro223, Pro227, Val234, and Leu235-, in proximity to the APE motif. [91]
A broad array of substrates for MK2 have been identified, although the physiological relevance of certain molecules is not completely understood yet, e.g. the phosphorylation of tyrosine hydroxylase. [109] In other cases, extensive investigation has shed light on the multifaceted role of MK2 in the regulation of several physiological processes like transcription, mRNA stabilization, cell cycle progression and cell mobility. The molecular mechanisms underlying these functions are outlined in Figure 10 and will be described in this section.
As already described for the p38 pathway, MK2 serves as a key regulator of the stress response and inflammation. Its physiological role has been investigated across various cell types, and its contribution to the adaptive immune response in epithelial and myeloid cells [110], as well as the regulation of epithelial cell migration during wound healing, has been described. [111]

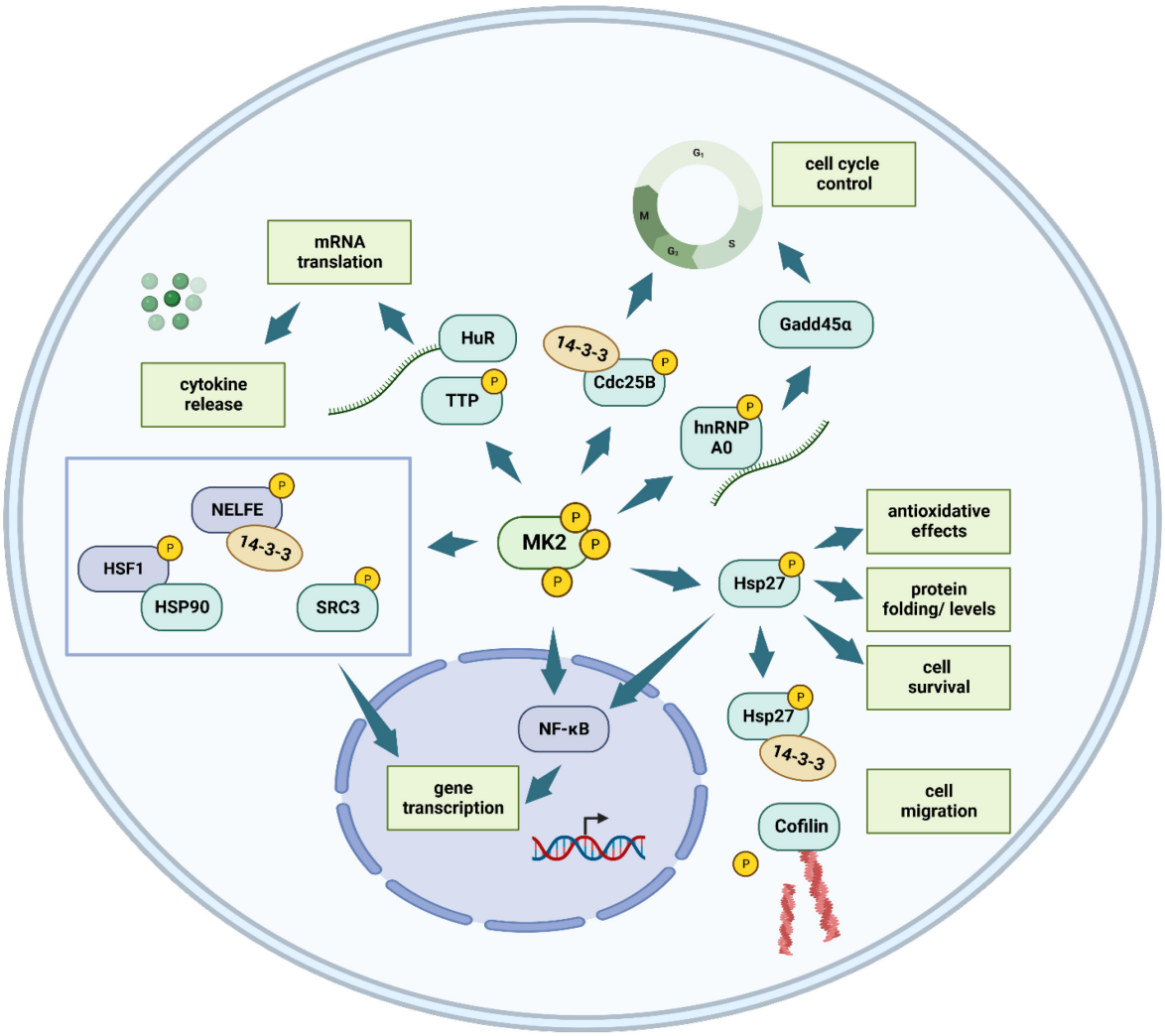

Figure 10: Downstream effectors of MK2 (graphic created with BioRender.com).

Stabilization of mRNA and translation

MK2 knockout or inhibition impedes the progression of asthma, skin inflammation and colitis in animal models correlating with decreased levels of inflammatory cytokines.[112] This effect is primarily mediated by the regulation of the respective mRNA stability, as briefly discussed in chapter 1.2.5. The stability of mRNA is an important regulator of protein expression, facilitating rapid responses to stimuli. Adenylate/uridylate-rich elements (AREs), often located in the 3'UTR of mRNAs, serve as destabilizing components of mRNA. In this context, the cytokines levels of IL-1β and IL-6 are two relevant examples controlled by ARE-dependent mRNA destabilization.[113] These AREs can be recognized and bound by various proteins, like TTP and HuR, which alter mRNA stability and thereby protein synthesis. The ability of TTP and HuR to bind to AREs is regulated by MK2 and the related processes will be outlined below.

Tristetraprolin (TTP, encoded by Zfp36) belongs to a family of proteins characterized by tandem CCCH zinc fingers. [114] Initially identified as targeting TNFα [115] and GM-CSF [116] mRNAs, TTP has since been implicated in the regulation of over 1000 mRNA targets. [117] BROOKS and BLACKSHEAR [114] collected more than forty proposed TTP-regulated mRNAs and a selection of relevant targets is displayed below in Table 1. [114, 118]

Table 1: TTP-regulated mRNA and the associated proteins. CXCL = C-X-C motif chemokine ligand; CCL = C-C motif chemokine ligand; COX2 = cyclooxygenase 1; PLK3 = Polo-like kinase 3; UBE3A = Ubiquitin-protein ligase E3A; PIM1 = proviral integration site for Moloney murine leukemia virus 1; NOS2 = nitric oxide synthase; MMP = matrix metalloproteinases; PD-L1 = Programmed cell death ligand-1.

Classification	Proteins
Inflammatory cytokines	IL-1α/β, IL-6, IL-12, IL-17, IL-23, IFNγ
Anti-inflammatory cytokines	IL-10
Growth factors	GM-CSF, VEGF, IL-2, IL-3
Chemokines	CXCL1/2, CCL3, CCL20, IL-8
Enzymes	COX2, PLK3, UBE3A, DUSP6, PIM1, NOS2, MMP2/9
mRNA binding proteins	TTP
Additional proteins	TLR4, Myc, PD-L1

When unphosphorylated, TTP binds to the target mRNA, initiating deadenylation through the CCR4/CAF1/NOT deadenylase complex (CCR4 = C-C-chemokine receptor 4; CAF1 = chromatin assembly factor 1; NOT = general negative regulator of transcription subunit 3), leading to the degradation of the transcript. Phosphorylation of TTP by MK2 disrupts this interaction, induces complex formation with 14-3-3 proteins and preventing TTP from destabilization of the mRNA [114] Consequently, HuR, another RNA binding protein, can bind to the mRNA and promote translation, [68] with MK2 activation enhancing the cytoplasmatic localization of HuR. [86f]

In addition, PABP1 (poly(A)-binding protein 1), PARN (poly(A)-specific ribonuclease) and hnRNP A0 (heterogenous nuclear ribonucleoprotein A0) are phosphorylated by MK2 and are also involved in the regulation of mRNA stability. [119]

MK2 signaling is implicated in stress-induced changes in the noncoding transcriptome mediated via the nuclear exosome targeting complex (NEXT). Phosphorylation of RBM7 (RNA binding motif protein 7), a member of the NEXT, reduces affinity for target ncRNAs (non-coding RNAs) and impede their degradation. [120]

Phosphorylation of eIF4E-binding protein 1 (eukaryotic translation initiation factor 4E binding protein 1), essential for protein synthesis, is usually inhibited by TSC2 (tuberin or tuberous sclerosis

complex 2). In turn, phosphorylation of TSC2 by MK2 increases its binding to 14-3-3 proteins enabling activation of eIF4E-binding protein-1. [96c, 121]

Furthermore, MK2 signaling is involved in aging-related processes, particularly through the regulation of the senescence-associated secretory phenotype (SASP). In addition to the TTP-mediated mRNA stabilization, MK2 contributes to this phenotype by stabilizing mRNA of SASP components through phosphorylation of butyrate response factor 1 (BRF1), thereby activating an immune escape mechanisms and reinforcing senescence, supporting the development of an age-related pathologic phenotype and potentially promoting tumorigenesis. [122]

Transcription

Heat shock transcription factor 1 (HSF1) induces the transcription of several heat shock proteins while repressing transcription of several cytokines such as IL-6 and TNFα. [40] Phosphorylation of HSF1 by MK2 increases its affinity and binding to Hsp90, thereby inactivating the transcription factor and abolishing its function as repressor of proinflammatory gene expression. [123]

MK2 phosphorylates and activates steroid receptor coactivator 3 (SRC3), a coactivator for several transcription factors including E2F transcription factor 1 (E2F1) and NF-κB, and regulator for the expression of IL-6. [124]

Furthermore, MK2-mediated phosphorylation of negative elongation factor complex (NELF) subunit E (NELFE) enhances its binding to 14-3-3 proteins, resulting in dissociation from chromatin and subsequent transcription of genes mainly involved in cell cycle control, RNA metabolism and DNA repair. [125]

MK2 signaling, mediated by Hsp27, is also involved in the regulation of NF-κB signaling, which control expression of pro-inflammatory genes. Specifically, in endothelial cells, MK2 is essential for sustaining the nuclear localization of NF-κB by decreasing the transcription of its exporter IκBα (nuclear factor of κ light polypeptide gene enhancer in B-cells inhibitor α). [112a]

In response to cellular stress, MK2 contributes to the phosphorylation of CREB, impacting cell cycle control and proliferation. [40] Depending on the stimulus, CREB phosphorylation can occur through different pathways, such as the ERK pathway and MSK1. [126] The extend of MK2 involvement requires further investigation. [53a, 127]

MK2 was identified to phosphorylate serum response factor (SRF), a regulator of immediate early genes like c-fos, c-jun and c-myc through its binding to serum response elements (SRE) and thereby influencing cell cycle, cell differentiation and immune response but the role of this event is unknown. [40, 127b] The same was found for MRTF-A (myocardin related transcription factor A), a transcription factor activated by actin polymerization. [40, 128]

Regulation cell cycle and survival

MK2 is involved in the cell cycle regulation after DNA damage. This role is especially pronounced in p53-deficient cells, a mutation frequently occurring in cancer cell lines. In this setting MK2 is responsible for cell cycle arrest at the G_2/M and the G_1/S checkpoint. [91]

The development of chemoresistance against DNA damaging agents like cisplatin and doxorubicin is promoted by MK2 activity. Upon DNA damage induced by UV-light or inhibition of the topoisomerase by doxorubicin, MK2 mediates Cdc25B binding to 14-3-3 proteins through phosphorylation and thereby inhibiting its activity. [91] Since Cdc25B inhibition is critical for cell-cycle escape after DNA damage, MK2 mediated regulation leads to arrest at the G_2/M checkpoint. Similarly, in p53-deficient cells, cisplatin treatment leads to S phase arrest, mediated by MK2. [129]

In p53-deficient cells, the phosphorylation of hnRNP A0 by MK2 is essential for cell cycle arrest. hnRNP A0 modulates mRNA stability of CDKN1B ($p27^{Kip1}$, cyclin-dependent kinase inhibitor 1B) and growth arrest and DNA damage inducible-α (GADD45α). While CDKN1B induces the G_1/S checkpoint, GADD45α controls the establishment of the G_2/M checkpoint. [130] Depletion of MK2 drives cells into mitotic catastrophe. As mentioned above, phosphorylation of PARN by MK2 increases mRNA stability. One of the targeted mRNAs encodes GADD45α, where PARN phosphorylation is involved alongside hnRNP A0 for stabilization. [40, 119b]

MK2 also influences p53 signaling. Phosphorylation of human double minute 2 (HDM2) by MK2 induces p53 degradation and promotes cell survival. [131] Moreover, MK2 suppresses the expression of p53-driven pro-apoptotic proteins through phosphorylation of the transcription factor apoptosis-antagonizing transcription factor (AATF). [132]

Furthermore, phosphorylation of PLK1 by MK2 is required for centrosome maturation and mitotic progression, [133] while enhanced phosphorylation of TRIM29 (ATDC, tripartite motif containing 29) by MK2 correlates with resistance to radiation in pancreatic cancer cells, acting as regulator of the DNA-damage response. [134]

Additional mechanisms were reported, through which MK2 contributes to the control of cell survival. Phosphorylation of NELFE or RBM7 by MK2 promotes cell survival by enhancing RNA polymerase II transcriptional activity. [51b] MK2 suppresses receptor-interacting protein kinase 1 (RIPK1) activity by phosphorylation, enhancing cell survival. RIPK1 induces cell death in response to inflammatory signaling by TNFα and LPS. [135] Under starvation conditions, MK2 and MK3 phosphorylate Beclin-1, inducing autophagy. [136]

In an oncogenic setting, Ras activates a negative feedback loop, mediated by the p38 pathway, including MK2, which promotes antiproliferative effects. [77a]

The regulation of the cell cycle by kinase signaling networks is, however, complex and depends on several factors, including the stimulus and cell type. In a study by XIAO *et al.*, it is shown that only knockdown of Chk1 (checkpoint kinase 1), and not Chk2 and MK2, prevents S-phase and G_2/M checkpoint arrest in a human cell lines (HeLa and H1299). Interestingly, a MK2/Chk1 double knockdown even partially rescues the effect of Chk1 single knockdown. [137] A recent study by LUO *et al.* in contrast supports the involvement of MK2 in cell cycle regulation. [138] Further research is required to clarify the contribution of distinct kinases under specific conditions.

Cell migration and mobility

Cell migration is essential for healthy tissue regeneration and wound healing, but also for immune response and metastasis. [139] Epithelial cell migration in wound healing is mediated by MK2/3. [111] The same relation was observed in smooth muscle cells in which cell migration influences remodeling and hypertrophy. [140] An important downstream target in this process is Hsp27, which executes diverse functions in response to stressors, e.g. mechanical stress. Hsp27 acts as a chaperone, supporting proper folding of damaged proteins post heat shock and controlling protein degradation. [40, 141] Following phosphorylation, it is involved in the control of apoptosis and cell migration by regulating actin remodeling. [51b, 132, 142] Unphosphorylated Hsp27 acts as an F-actin capping protein inhibiting actin polymerization, while phosphorylation weakens this binding enabling actin polymerization and cell migration. Phosphorylated Hsp27 competes with pCofilin for binding to 14-3-3 proteins. Replacement and dephosphorylation of Cofilin enable its binding to actin and subsequent remodeling. [96c]

Moreover, Hsp27 exhibits antioxidative effects, inhibiting oxidant stress-induced cellular damage by stimulating glucose-6-phosphat dehydrogenase, maintaining glutathione (GSH) levels, and possessing iron-chelating activity. [40, 98, 141a] Activation of Hsp27 also has anti-apoptotic effects by interacting with mitochondrial-dependent and independent apoptotic pathways (Fas-FasL mediated, caspase-dependent), thereby protecting against neuronal and ischemic injuries. [132, 141a] However, high Hsp27 expression correlates with aggressive tumor growth and poor prognosis [132], with phosphorylation of Hsp27 inducing up-regulation of MMP-2 and cell invasion in prostate cancer after TGF-β stimulation [143]

Additionally, MK2 activation influences actin remodeling through various targets like LIM domain kinase-1 (LIMK1) [144], lymphocyte-specific protein-1 (LSP1) [145] and CapZ-interacting protein. [96c] Cell migration and motility can also be modulated by MK2 through intermediate filament functions, MMPs, NOGO-B (neurite outgrowth inhibitor), RSK and structural features of the kinase itself. [40, 96c, 146]

Furthermore, MK2 is involved in the regulation of protein degradation by phosphorylating the E2 ubiquitin-conjugating enzyme UBE2j1, affecting protein degradation of e.g. major histocompatibility complex-1 (MHC1) and influencing TNFα expression. [147] Reorganization of CS (centrosomal satellites) during mitosis is also modulated by phosphorylation of centrosomal protein 131 (CEP131) by MK2 [148] as well as its contribution to fine-tuning cAMP levels by phosphorylation of phosphodiesterase 4 (PDE4), which reduces its activation by PKA. [149] Phosphorylation of 5-lipoxygenase (5-LO) by MK2 adds another contribution to inflammation to the portfolio, modulating its activity and cellular localization. [150]

In neurons, MK2 is activated by mGluR1/5 (group I metabotropic glutamate receptors) and is involved in mediating synaptic plasticity. [52b] At the same time, the neuronal response to inflammatory signals and stress, like ROS accumulation and increased apoptosis, is mediated by MK2. [151]

An overview of the manifold physiological and disease-related functions of MK2 is depicted in Figure 11. The diversity of stimuli and complexity of processes controlled by MK2 underline its important role. Therefore, dysregulation potentially leads to imbalances in the many processes regulated by this kinase and disease development.

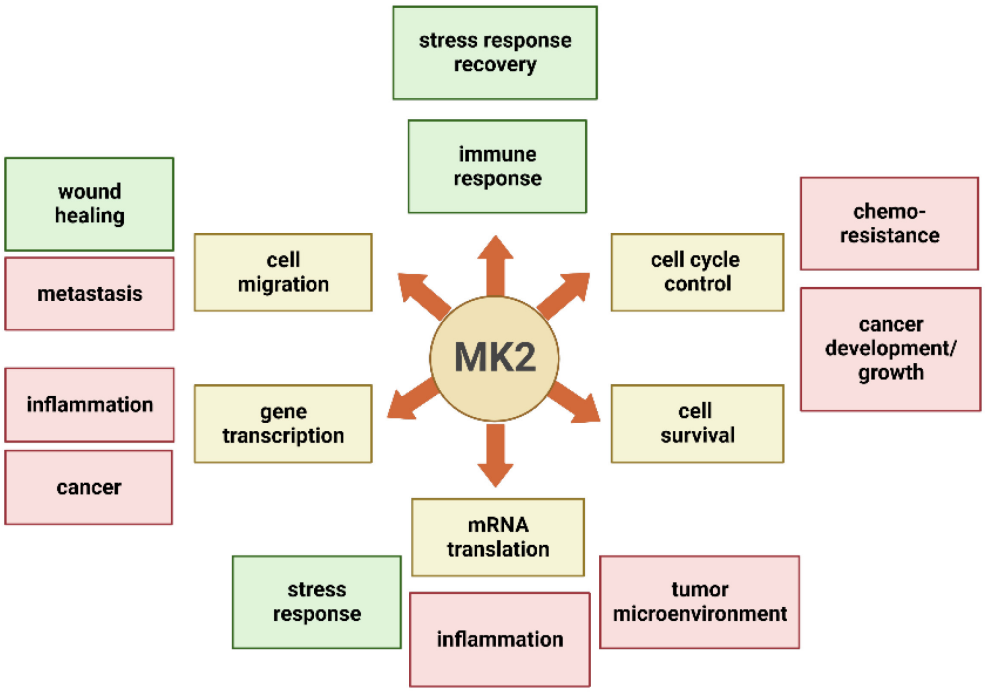

Figure 11: The role of MK2 in health and disease. Processes controlled by MK2 colored in yellow, resulting physiological processes in green and the pathophysiological events in red.

1.3.4 Pathophysiological Role of MK2 in Cancer

Due to its central role in inflammatory processes, research initially focused on the involvement of MK2 in this setting. As mentioned above, deletion of MK2 function in animal models has been found to prevent the development of asthma, skin inflammation and colitis. [112] Moreover, the cancerogenic role of inflammation has been associated with MK2 activity. Blockade (knockdown or inhibition) of MK2 hinders inflammation-driven development of colon and skin cancer, [152] suggesting its potential as a therapeutic target in cancer treatment. MK2 levels have been found altered in different tumor settings. Increased MK2 levels correlate with worse prognosis in certain cancers such as nasopharyngeal carcinoma [153], head and neck squamous cell carcinoma [154] and lung cancer. [155] In gastric cancer, high levels of MK2 or cytokines correlate with increased metastasis. [156] McCormick and Ganem were also able to reveal a link between the development of Kaposi's sarcoma and cytokine levels. [157] RANKL-mediated differentiation of bone marrow cells is mediated by the p38 MAP kinase pathway. [158] MK2 has been found to be a key regulator in the development of osteoclasts, and inhibition can reduce bone

loss caused by tumor metastases or chemotherapy. [159] Indeed, inhibition of p38α and MK2 was effective in reducing metastasis and related bone loss in mice even while no reduction of tumor growth could be achieved. [159]

Conversely, reduced copy numbers of MK2 and MKK3 have been observed in non-small cell lung cancer (NSCLC) samples, proposing a tumor suppressive role in this setting. [160] Additionally, MK2/p53 deficient NSCLC cells displayed increased tumor growth. [161]

Furthermore, MK2 is involved in the regulation of therapy resistance against cancer treatment, promoting different outcomes. For instance, high MK2 expression levels in multiple myeloma are associated with worse prognosis, whilst knockdown decreases the proliferation of myeloma cells. The combination of an MK2 inhibitor with bortezomib, doxorubicin or dexamethasone increases efficacy. [162] Similarly, inhibition of MK2 not only sensitizes tumors to radiotherapy by decreasing radiotherapy induced inflammation and influencing DDR [134, 154] but also restores etoposide sensitivity in small cell lung cancer (SCLC) cell lines with p53 mutation. [163] In contrast, therapy sensitivity towards gemcitabine in pancreatic cancer is mediated by MK2 activity. [164]

1.3.4.1 MK2 Signaling and the Tumor Microenvironment

Metastasis of cancer is connected to poor prognosis. The tumor microenvironment (TME) plays a crucial role in cancer development, progression, and metastasis, and is characterized by immune cell invasion and inflammatory processes. [165] Increased activity of MMPs, regulated by p38α, contributes to the inflammatory microenvironment and correlates with metastasis. [85b] Inhibition of the p38 MAPK pathway has been shown to reduce MMP activity in various cancer cell lines (bladder, breast, prostate), suggesting its potential as a therapeutic strategy. [86h, 166] The p38-driven influences in pro-metastatic changes in the microenvironment of the tumor are described in section 1.2.6. In Bladder cancer, KUAR and coworkers identified MK2 as the responsible downstream effector of p38α, influencing MMP-2 and MMP-9 levels through mRNA stabilization. [167] These two proteins belong to the best studied members of this TME and are involved in tumor progression. [143, 167-168] In various tumor settings, an increase in MMP activity is induced by MK2/Hsp27 signaling. [98, 143, 167]

The inflammatory processes in the tumor surrounding are driven by secretion of cytokines, a process also influenced by MK2. Increased expression levels of cytokines are promoted through mRNA stabilization (further described in section 1.3.3), especially IL-6, TNFα, TGFβ and IL-10 appear to be relevant. [169] In HNSCC, elevated levels of inflammatory cytokines, e.g. IL-6, IL-1α and TNFα have been linked to migration and invasion. [170] High levels of IL-6 in patients also correlate with poor prognosis such as tumor progression in glioblastoma. [171] In addition, upregulation of PD-L1 in cancer cells is mediated by TTP phosphorylation and has been shown to exert an immunosuppressive effect in the tumor microenvironment, enhancing tumor invasion. [172]

1.3.5 The Protein Kinase MK3 and its Interplay with MK2

MK2 shares a high level of homology and 75% sequence identity with MK3, exhibiting homologous phosphorylation sites, and a virtually identical ATP binding site, and therefore overlapping interaction patterns. [11, 173] Double MK2/MK3 knock-out mice are viable, fertile and behave normally. In contrast to MK2 knock-out, MK3 knock-out mice have displayed no significant changes in LPS-induced cytokine levels, like IL-6, IL-10 or TNFα, and levels of TTP and p38. The cellular levels of MK3 are tissue dependent, elevated levels were found in spleen, lung and skeletal muscle, and are independent of MK2. While MK3 can partially compensate MK2 depletion, complete compensation is not achieved due to its lower expression levels. [92, 96b] Overexpression of MK3 can compensate for some functions of MK2, like phosphorylation of Hsp25 (the rodent equivalent of Hsp27) and stabilization of mRNA (CXCL1, GM-CSF). [94]

In macrophage response to LPS, MK2 and MK3 display a complex interplay. Knock-out studies revealed a cooperative relationship for the regulation of TNFα, CXCL2 and IL-10, most likely to some extent mediated by TTP. [174] For other examples, like histidine decarboxylase (HDC) or CXCL9 one can compensate for loss of the other kinase. Additionally, mutual feedback loops have been observed, exemplified by the regulation of IFNβ expression levels which are upregulated by MK2, but downregulated by MK3 in absence of MK2 via reduced expression of IκBα and subsequent inhibition of NF-κB translocation. A contrasting example is the activation of signal transducer and activator of transcription 3 (STAT3) by LPS, mainly mediated by IFNβ and thereby enhanced by MK2. In absence of MK2, additional MK3 deficiency is able to restore activity. [175]

1.4 Protein Kinase Inhibitors

The US Food and Drug Administration (FDA) approved 81 small molecule protein kinase inhibitors as of April 2024. [176] The Protein Kinase Inhibitor Database (PKIDB) lists 372 molecules currently under investigation in clinical trials (last updated March 2024). [177] The success story of this class of therapeutics began with the approval of imatinib in 2001, the first protein kinase inhibitor (PKI) developed for a specific target enzyme. Similar to imatinib, another 68 PKIs are indicated for different types of neoplasms, underscoring the importance of kinase inhibitors in cancer treatment. [176a] However, the approval of tofacitinib by the FDA in 2012 marked a significant milestone as the first PKI for an indication outside the field of cancer. [178] Its approval for a chronic disease requires fulfilment of higher standards, regarding long-term tolerability, safety and selectivity. While multi-targeting drugs may offer benefits in some cases, off-target effects are often associated with adverse effect and dose limitations. [179] Therefore, the development of highly selective molecules is essential, not only from a clinical perspective, but also for research on a biochemical or cellular level. For the latter purpose, highly selective compounds, so-called “chemical probes” are helpful for the investigation of biochemical pathways and enzyme-specific functions.

Classical kinase inhibitors bind to the ATP binding site and therefore face competition by the high intracellular ATP concentrations (1-5 mM). In addition, selectivity is one of the major challenges in kinase inhibitor development, due to the kinases' high similarity in the ATP binding pocket. [180] To overcome these challenges, different types of binding modes have been explored. Type 1 inhibitors, like gefitinib (**1**), target the ATP binding pocket of the active form of the kinase, whereas Type 2 inhibitors, like imatinib and sorafenib, bind to the inactive form of the kinase. [181] The inactive state of the kinase differs more between kinases and typically displays lower affinity towards ATP, enhancing the potential

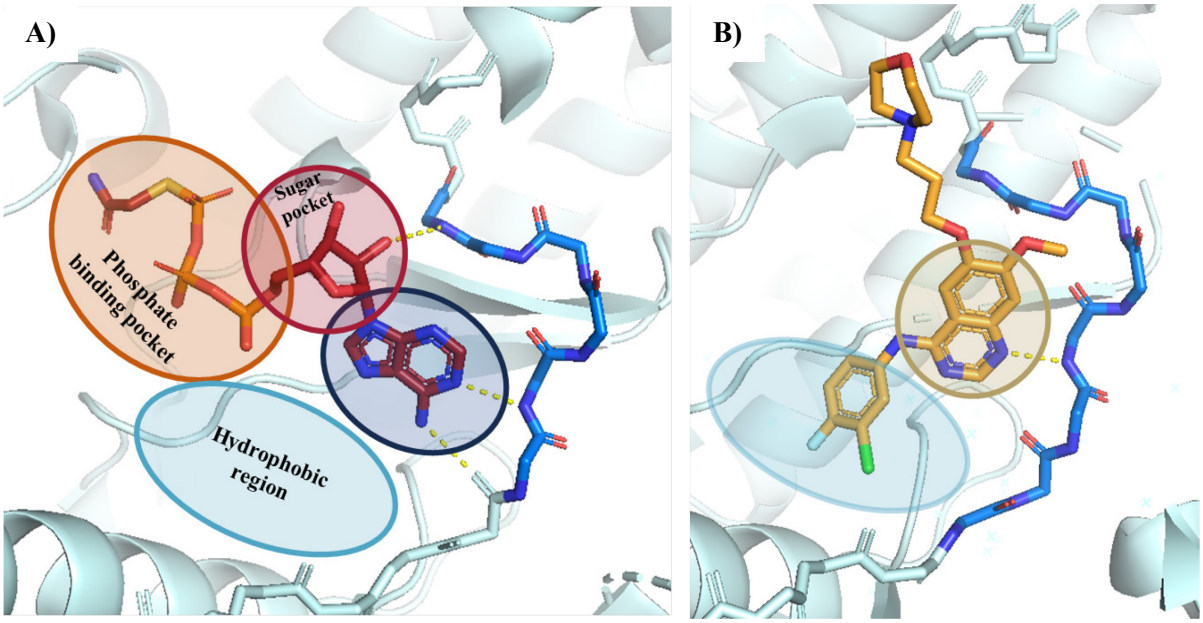

Figure 13: Crystal structure of EGFR kinase domain; A) Binding mode of an ATP-analog to EGFR (PDB: 2GS6 [6]), relevant regions of the binding pocket labeled and colored; B) Co-crystal structure of gefitinib **1** bound to EGFR (PDB: 4WKQ [4]), hinge binding motif marked in gold, hydrophobic region and the respective moiety of the inhibitor in light blue.

of increased activity and selectivity. Allosteric binding constitutes the third type of binding, relying on interactions outside the ATP binding site to alter kinase activity. Another possibility is the use of covalent inhibition, where a covalent bond is formed between the compound and the target and which can be applied to all the aforementioned types of binders. As a central topic to this thesis, covalent inhibitors will be discussed in detail in chapter 1.4.3.

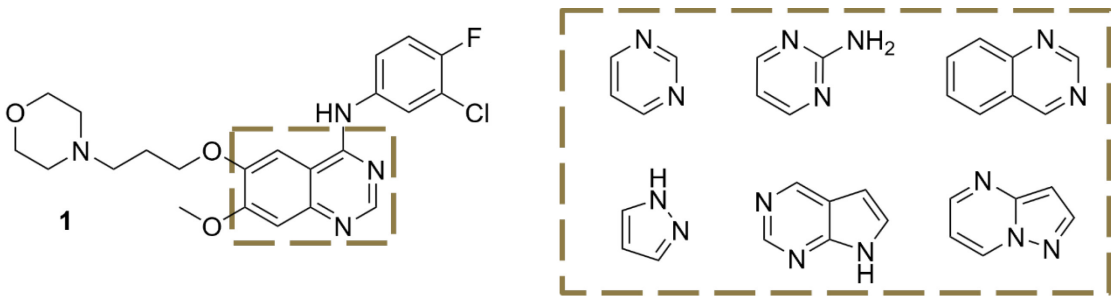

Figure 12: Structure of gefitinib **1** (hinge-binding motif marked in gold) and additional hinge binders, present in kinase inhibitors. [8]

The majority of protein kinase inhibitors bind to the ATP binding site, as shown for gefitinib **1** in Figure 13. The high degree of conservation of the active site combined with the increasing number of available crystal structures provides a starting point for the rational design of these inhibitors. They generally consist of a heterocyclic structure, such as the quinazoline in gefitinib **1** (Figure 12), which builds up one, two or three hydrogen bond interactions to the hinge region. Other common hinge-binding motifs are shown in Figure 12. The addition of variable substituents to the core allows interaction with additional parts of the binding pocket, such as the hydrophobic pocket behind the gatekeeper residue (sometimes referred to as the hydrophobic region I), as shown for gefitinib in Figure 13. This pocket is not occupied by ATP and thus considerably less conserved, which can be utilized to promote selectivity between different kinases.

1.4.1 Inhibitors of the p38 MAPK Pathway

Taken together, the knowledge outlined in the last sections underscores the potential of targeting the p38 MAPK pathway, not only in the context of inflammatory diseases but also in cancer therapy, with discussions extending to its possible application in the treatment of COVID-19 infection.[182] While some efforts have been made to inhibit upstream activators of p38, like MKK3/MKK6 and TAK1, the majority of drug discovery programs focused on p38α/β.[183] Several p38 inhibitors have demonstrated efficacy in disease models of inflammatory diseases and entered clinical trials, yet none successfully reached approval. Hepatotoxicity[184] and cardiotoxicity[185] were observed as limiting factors of treatment with p38 inhibitors. Besides toxicity issues, the lack of long-term efficacy was one of the major issues occurring during these trials.[49] Despite initial reductions in inflammatory signaling and biomarkers, like C-reactive protein (CRP), following p38 inhibition, relapse was observed over time (4-12 weeks).[186] These observations are likely attributed to inhibition of feedback loops, other anti-inflammatory mechanisms (IL-10), and downstream targets.[184b]

Beyond the classical ATP-competitive kinase inhibitors (structures displayed in Figure 14), like pamapimod (**2**)[187], SB203580 (**3**)[188] or skepinone-L (**4**)[189], several structures displaying alternative binding modes were discovered. One example is doramapimod (BIRB-796, **5**) which binds to the DFG out conformation (Type 2 binding) and thereby additionally occupies an allosteric binding pocket.[190] Moreover, selective inhibitors (CMPD1 (**6**) and zunsemetinib (**7**), displayed in Figure 14) against the activation of downstream targets, namely MK2, were developed and will be elaborated in the subsequent section.

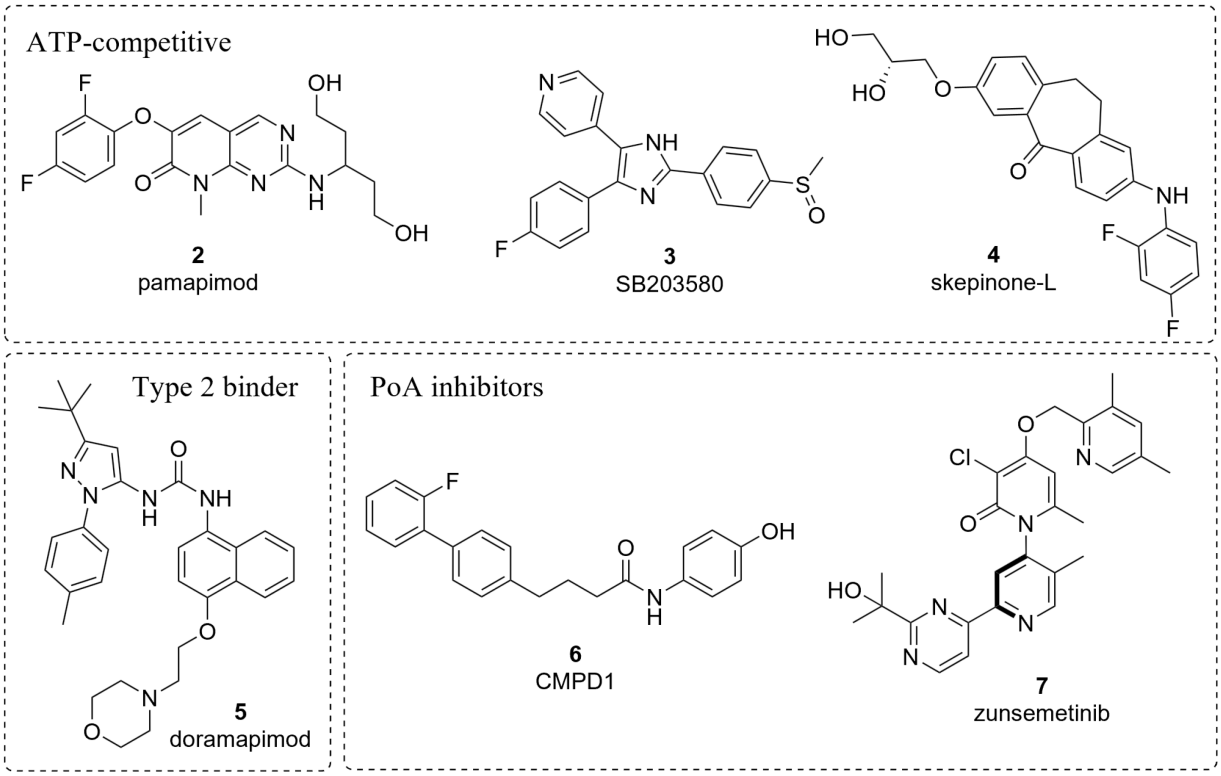

Figure 14: Structures of exemplary p38 kinase inhibitors; PoA = point of activation.

Following the lack of success in the treatment of inflammatory diseases, p38 pathway inhibitors like talmapimod (SCIO-469) and LY3007113 were also investigated in clinical trials for malignant diseases. [51d] However, dose-limiting tolerability issues of LY3007113 led to the termination of further investigations. [191] Notably, inhibition of p38 activates different feedback loops mediated by MSK, resulting in increased activation of the JNK pathway and inhibiting expression of DUSP1 and anti-inflammatory cytokines, IL-10 and IL-1RA. [192] These mechanism may contribute to the low levels of efficacy of p38 inhibitors in clinical trials.

1.4.2 Kinase Inhibitors Targeting MK2

To overcome the challenges associated with direct inhibition of p38, research turned its focus to other parts of the pathway, leading to the emergence of MK2 as a promising alternative target. [49, 192b]

Several activation inhibitors aimed at interrupting the interaction between p38α and MK2 have been developed and reached clinical trials. CMPD1 (**6**, Figure 14), described in 2004 by a group at Boehringer Ingelheim, binds to p38α and selectively inhibits MK2 phosphorylation in a non-ATP-competitive manner. [193] Zunsemetinib (CDD-450, ATI-450, **7**, Figure 14), an inhibitor of MK2 activity acting through the prevention of MK2 phosphorylation by p38α, demonstrated promising anti-inflammatory effects in a Phase IIa clinical trial, overcoming the typical challenges associated with p38 inhibition. [194] However, the phase IIb study for the treatment of rheumatoid arthritis failed to reach the efficacy goals, leading to the discontinuation of further development. A similar derivative, ATI-2231 (not shown), is

still in clinical trials for metastatic breast cancer and pancreatic cancer.[195] Additionally, chemists at AstraZeneca developed different series of prevention of activation inhibitors with an ATP-competitive binding mode, unfortunately, the project was terminated due to decreased IL-10 expression, which was hypothesized to limit efficacy.[196]

Over the past two decades, a variety of classical ATP-competitive inhibitors for MK2 has been developed. However, this approach has proven to be challenging, with most structures displaying unsatisfactory biochemical efficiency (BE) values, the discrepancy between activity in biochemical assays and cellular efficacy. Given that the majority of marketed drugs have a biochemical efficacy (BE) greater than 0.4, achieving this threshold is desirable goal in inhibitor development.[197] Here, one obstacle is the relatively high affinity of MK2 towards ATP, with a K_m value of 30 µM for the active form and 43 µM for the inactive form,[66, 180] coupled with the high intracellular ATP concentration (1-5 mM) [[180] the inhibitor has to compete with. As mentioned before, another challenge is achieving selectivity in kinase inhibitors, which is particularly challenging for MK2 due to the closed conformation of the nucleotide binding loop, resulting in a small and narrow binding pocket. Combined with a methionine residue as a gatekeeper this feature limits possibilities for compound derivatization.[10, 99] Consequently, planar compounds are preferred to accommodate the pocket in MK2, albeit at the expense of suitable physicochemical properties like solubility, also hampering cellular activity.[99] The similarity to the binding sites in other kinases like MK3, PRAK, PKA, cyclin-dependent kinase 2 (CDK2), and CaMKII, poses an additional challenge.[99]

In 2015, FIORE, FORLI and MANETTI[99] reviewed a variety of published MK2 inhibitors including aminopyrazinylthiourea (**8**), carbolines (**9**), aminopyrimidines (**10**), squarates (**11**), meroterpenoids (**12**) from marine sponges and 5,6-ring fused bicyclic scaffolds like pyrazolopyrimidines (**13**). However, these inhibitors exhibit insufficient activity, efficacy in cells, or suitable pharmacokinetic parameters.[99, 198] Peptide-derived inhibitors were investigated for their potential to reduce scar formation and hyperplasia in mouse vein graft models, with nanoparticle delivery methods used to enhance bioavailability and stability.[199] Furthermore, non-ATP-competitive furan-2-carboxamide (**14**) and uncompetitive anilinoquinolines (**15**) were developed to address challenges accompanying ATP competitive inhibitors, albeit with limitations including metabolic stability, cytotoxicity and low permeability.[99]

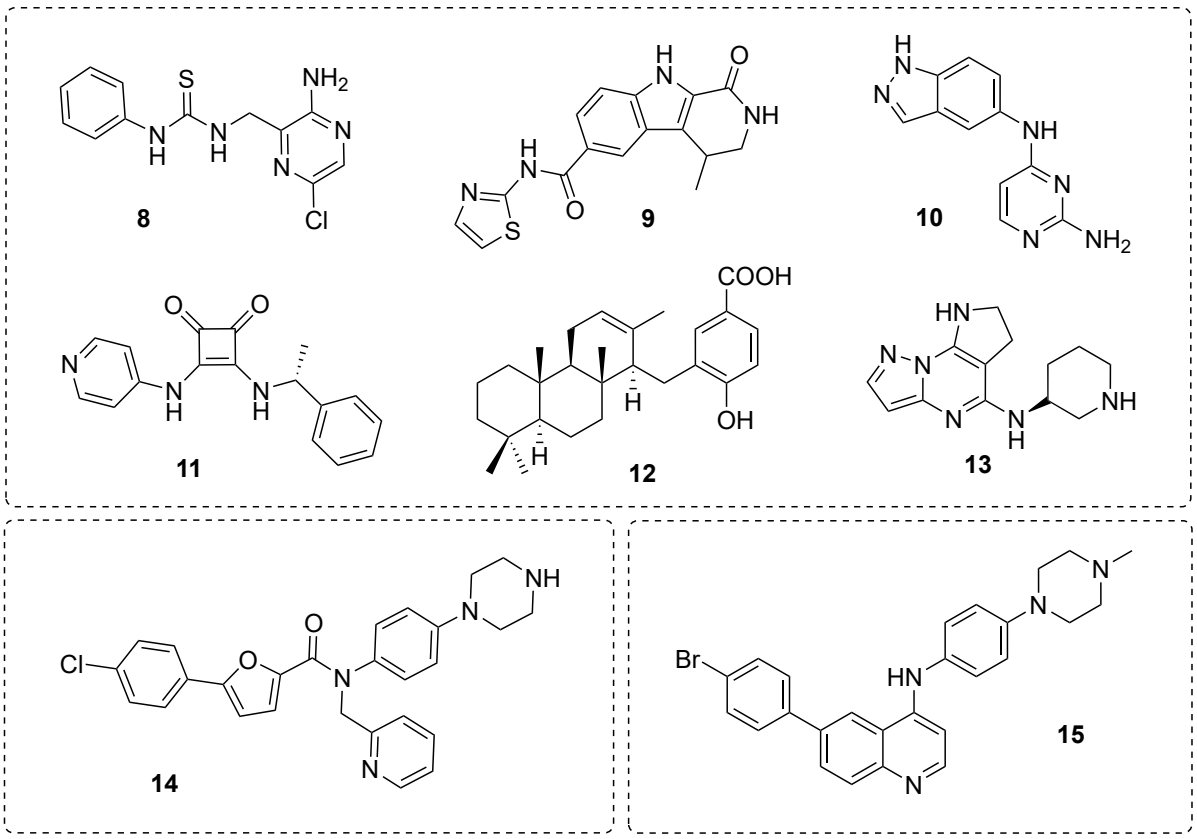

Figure 16: Examples of published MK2 inhibitors from different structural classes.

An alternative inhibitory mechanism was shown to be effective in vitro and in vivo by TRAN *et al*. They investigated the anti-inflammatory mechanism of the natural product andrographolide **16** and identified it as a degrader for the MK2 protein. After binding to the activation loop, andrographolide promotes proteasomal degradation. [200] This concept was further investigated by Kymera Therapeutics, who developed PROTACs by combining known MK2 inhibitor scaffold with E3-binding motifs (**17**, shown in Figure 15) and published their results in a patent recently. [201]

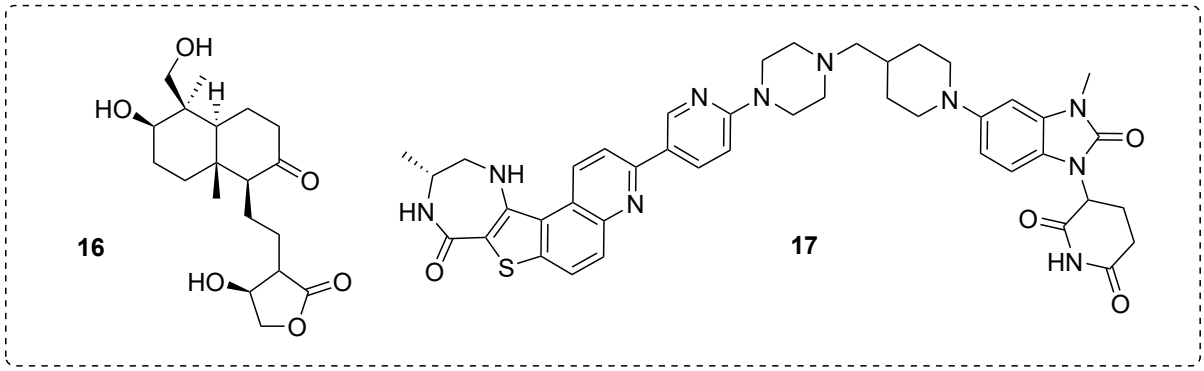

Figure 15: Compounds promoting degradation of MK2.

Two relevant structural classes of ATP-competitive MK2 inhibitors were not discussed here so far and deserve a closer consideration, the benzothiophene derivatives (exemplified by **19**, Figure 17) and the pyrrolopyridinone-related structures (Figure 18 and Figure 20) discussed in the following section

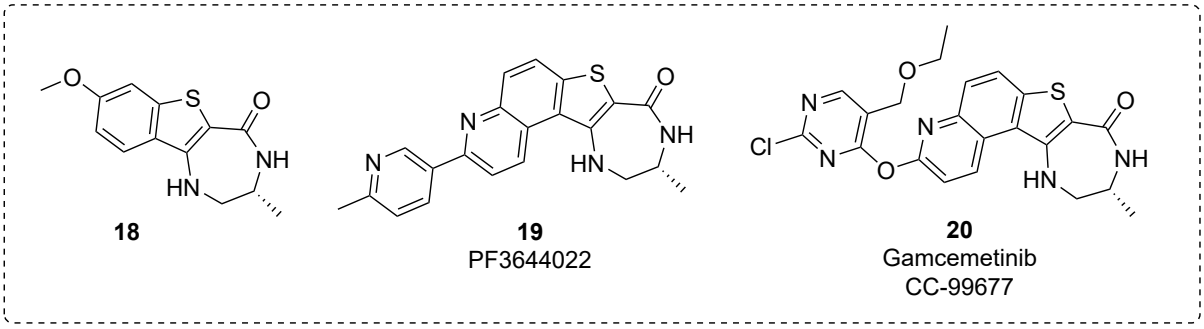

Figure 17: Benzothiophene-based MK2 inhibitors **18**, PF3644022 **19** and gamcemetinib **20**.

In 2009, ANDERSON and coworkers at Pfizer published a novel class of MK2 inhibitors with a benzothiophene core.[9] Optimization of the initial tricyclic structure **18** led to the discovery of the tetracyclic compound PF3644022 (**19**) with an IC_{50} value of 5 nM, which inhibits TNFα-release in U937 cells (IC_{50} = 150 nM). Even though, they could achieve good selectivity against CDK2 (IC_{50} = 7.9 µM), overall selectivity was insufficient (16 out of 200 kinases inhibited > 50% @ 1 µM). Among the affected kinase, eleven belonged to the CAMK-family.[202] Compound **19** is listed as a high-quality chemical probe against MK2 in the Chemical Probes Portal[203] and was further evaluated in a rat model for chronic inflammation showing good pharmacokinetic parameters and efficacy in the animal model. However, experiments in beagle dogs and monkeys unfortunately showed acute liver toxicity, due to off-target activity against hepatobiliary transporters activity (e.g. multidrug resistance protein-2 (MRP2)).[204] Although, the liver toxicity could be successfully reduced by structural changes, the development was discontinued due to reduced cellular potency of the optimized compounds and low safety margins. The core structure, however, was not completely forgotten, and Celgene/Bristol Myers Squibb included it in their development program for covalent inhibitors.[15, 205] The combination of the benzothiophene core with an electron-deficient heterocycle equipped with a leaving group led to the development of gamcemetinib (CC-99677, **20**), which entered clinical trials. The development will be further elucidated in section 1.4.4.

A second series of MK2 inhibitors with a 1,5,6,7-tetrahydro-4*H*-pyrrolo[3,2-c]pyridine-4-one core, hereafter referred to as pyrrolopyridinone (compounds **21** and **22**), developed by ANDERSON *et al.*[206], shares a similar binding mode and common structural features with the related structures discussed below.

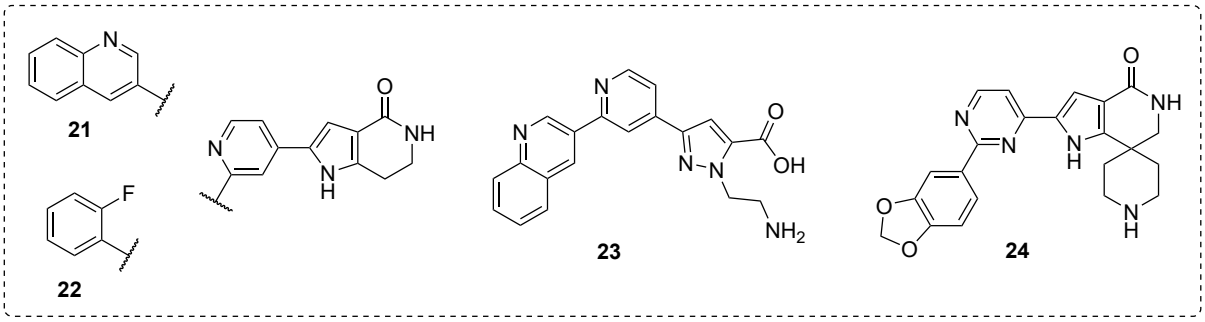

Figure 18: MK2 inhibitors with pyrrolopyridinone (**21**, **22**, **24**) and pyrazol-3-carboxylic acid (**23**) core structure.

X-ray crystal structure analysis revealed the binding mode of **21 (**Figure 19**)**. The pyridine nitrogen exhibits an H-bond to the backbone *NH* of Leu141 in the hinge region while the carbonyl of the lactam moiety interacts with the side chain amine of Lys93 and the lactam-*NH* forms an H-bond to the side chain of Asp207. Additional van-der-Waals-interactions with the gatekeeper residue Met138 and hydrophobic interactions in the active site were detected. More detailed analysis indicated water-mediated hydrogen bond formation of the pyrrole nitrogen to the backbone of Leu70, which is located at the beginning of the nucleotide binding loop. [10]

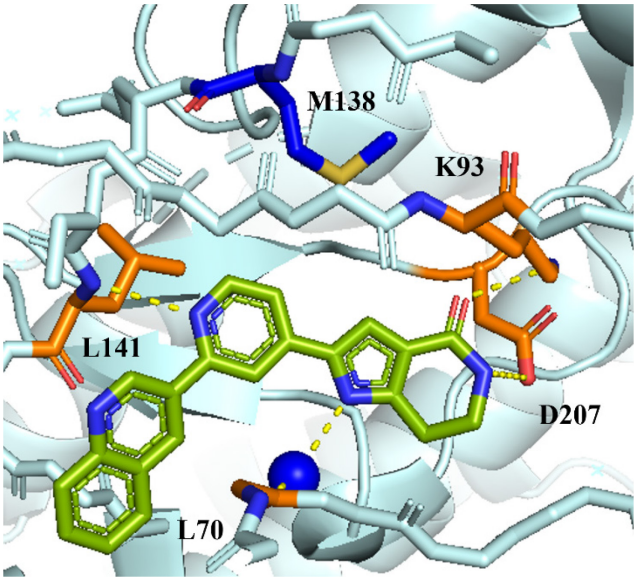

Figure 19: X-ray crystal structure of MK2-bound pyrrolopyridinone-based inhibitor **21** (in green) (PDB: 2JBO [10]; mediating water molecule shown as blue sphere, amino acids involved in binding colored in orange, gatekeeper Met138 in blue).

The 2-fluor-phenyl derivative **22** was further evaluated as **21** demonstrated poor physicochemical properties. Even though good selectivity against CDK2 was achieved, only a low degree of selectivity towards MK3 (10-fold) and PRAK (1.5-fold) was found. Compound **22** inhibits MK2 with an IC_{50} value of 126 nM and has a sufficient aqueous solubility (160 µM), but efficacy in cells dropped significantly with an EC_{50} of 4800 nM. Nevertheless, an effect on TNFα expression was detected in cells and in an animal model of acute inflammation. Despite of this, challenges remained in achieving suitable pharmacokinetic properties. [206-207]

The combination of the pyrrolopyridinone scaffold and a pyrazole-3-carboxylic acid derivative (**23**) from patent literature [208] served as the starting point for a drug discovery project at Merck. [209] They developed a series of spiropiperidines (**24**) with biochemical activity in a nanomolar range and cellular activity below 1 µM. Unfortunately, the membrane permeability for this series was insufficient. [210]

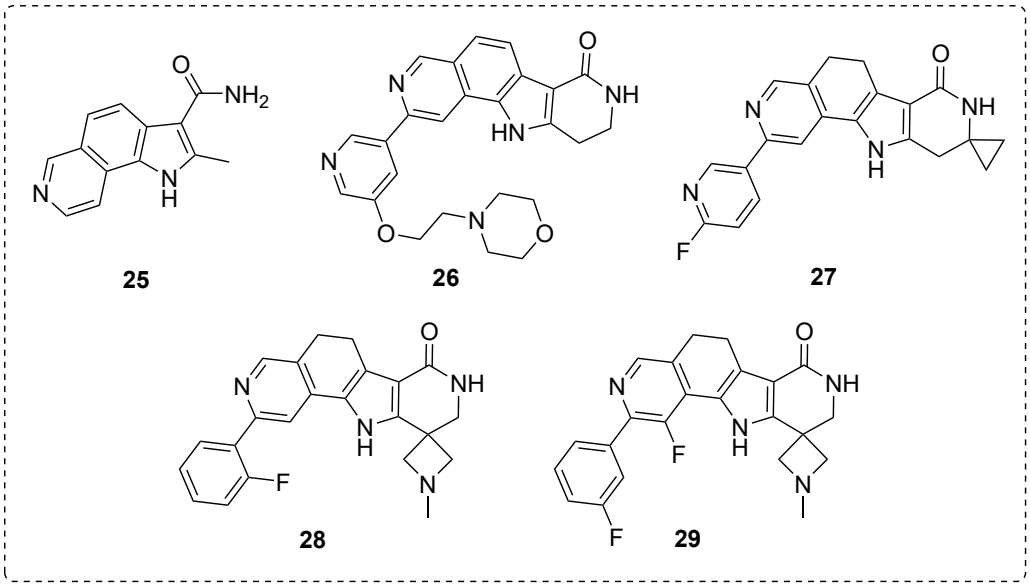

Figure 20: Tri- and tetracyclic MK2 inhibitors.

A high-throughput screening (HTS) campaign at Novartis identified the tricyclic compound **25** as a modest MK2 inhibitor (IC_{50} = 3.8 µM). Rigidization of the free amide into a 6-membered lactam ring, in analogy to the inhibitors discussed above, was beneficial on the activity. Alkylation or replacement of the amide by a ketone reduced affinity, underlining the contribution of the lactam-NH to binding affinity. Compound **26** demonstrated good biochemical potency (IC_{50} = 12 nM) and activity in cells (EC_{50}(TNFα) = 260 nM), but low solubility (< 4 µM) and it lacked oral bioavailability, which might be

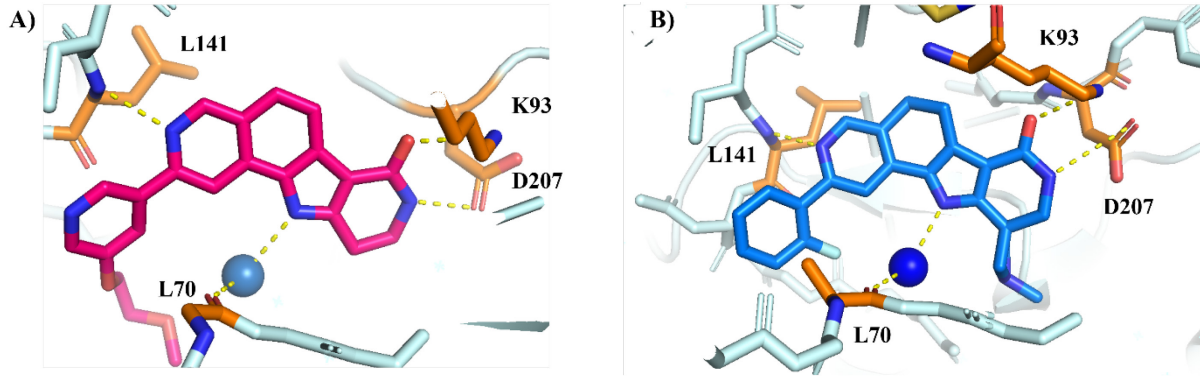

Figure 21: Crystal structure of MK2 bound to a tetracyclic inhibitor (relevant residues colored in orange; interaction indicated by yellow dotted lines); A) Compound **26** (colored in magenta) bound to MK2 (PDB: 3M42 [3]); B) Compound **28** (colored in marine) bound to MK2 (PDB: 3M2W [1]).

attributed to the highly planar nature of the tetracyclic system. [3] The co-crystal structures of **26** and the partially saturated derivative **28** bound to MK2 showed a comparable binding mode to the pyrrolopyridinone **21**. The tetracycle's pyridine acts as the hinge binder, interacting with Leu141. Additionally, the aforementioned hydrogen bond interactions of the lactam were detected and the pyrrole again forms a water mediated interaction to the backbone carbonyl of Leu70.

Dearomatization of the central ring of the tetracyclic core and introduction of small spiro cycles at the lactam ring, exemplified by compounds **28** and **27**, increased solubility and activity (**27**: IC_{50} = 50 nM,

EC_{50}(TNFα) = 300 nM, solubility 9 µM). Compound **27** showed good pharmacokinetic properties and reduced TNFα levels in mice after oral exposure. Replacement of the tetracycle's pyridine by a pyrimidine and methylation of the pyrrole reduced inhibitory activity but increased oral exposure. Fluorination at the 3-position (**29**) of the pyridine restored activity, in combination with better solubility, good oral bioavailability and low clearance. [211]

1.4.3 Covalent Kinase Inhibitors

The history of covalent drugs began in 1899 with the discovery of aspirin, although its mode of action was only revealed in the 1970s. Like other early drugs with a covalent mode of action, for example omeprazole and β-lactam antibiotics, the mechanisms were discovered later and often serendipitously involved a covalent binding event. Despite the success stories of these drugs, the deliberate development of covalently binding drugs was avoided for a long time due to concerns about potential toxic effects, which may be caused by unspecific binding of the reactive part to other biomolecules in the body beside the intended target or by the formation of haptens triggering an undesired immune response. [212] However, covalent target engagement also offers several advantages. This mode of binding can prolong the duration of action, enhance potency and specificity and limit competition with natural ligands or substrates. The approval and subsequent success of the first two purposely designed covalent kinase inhibitors, afatinib **30** and ibrutinib, in 2013 encouraged further research efforts. The compounds represent so-called targeted covalent inhibitors (TCIs), which combine a reversible binding core (highlighted in gold in Figure 22) with a weak electrophile, the so-called "warhead" (red in Figure 22).

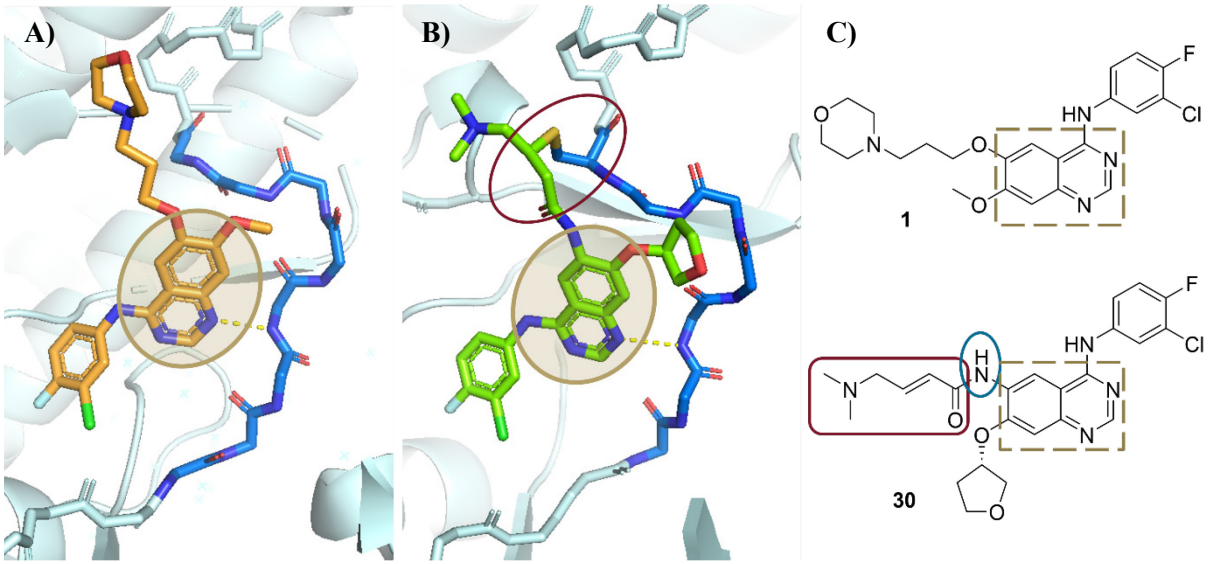

Figure 22: Co-crystal structure of inhibitor-bound EGFR (hinge region colored in blue, hydrogen bond interaction indicated by dotted yellow lines); A) Gefitinib **1** bound to the kinase domain of EGFR (PDB: 4WKQ [4], hinge binding motif marked in gold); B) Afatinib **30** bound to EGFR (PDB: 4G5J [13], hinge binding motif marked in gold, covalent bond in red; C) Structures of gefitinib **1** and afatinib **30** (core highlighted in gold, warhead in red and linker atom in blue).

To enable successful formation of the covalent bond (Figure 22B), the warhead is attached to the core at an appropriate position via a suitable linker (blue in Figure 22C). The electrophile then interacts with a nucleophilic amino acid residue of the target protein in a proximity-driven manner, strongly enhancing the reaction rate on target. The thiol side chains in cysteine, due to their strong nucleophilicity which is unique among proteinogenic amino acids, are often engaged in covalent binding interactions. Other nucleophilic residues, such as the amino and hydroxy groups of lysine, tyrosine or serine, are also possible targets for covalent engagement. [213] For example, two inhibitors against the hepatitis C virus NS3/4a protease, boceprevir and telaprevir, bind covalently to the catalytic serine using an α-ketoamide as warhead. Voxelotor, approved for the treatment of sickle cell anemia, covalently engages the terminal amino group of a valine in sickle cell hemoglobin using a salicylic aldehyde. [214] Although alternative target amino acids for covalent engagement and an increasing number of publications targeting different proteins and sites have emerged, all approved covalent kinase inhibitor are targeting a non-catalytic cysteine. [215] Until the end of 2023, the FDA approved ten covalent PKIs (acalabrutinib, afatinib, dacomitinib, futibatinib, ibrutinib, mobocertinib, neratinib, osimertinib, ritlecitinib. zanubrutinib). [176b, 216] Five additional covalent kinase inhibitors are approved outside the United States. [216] The selectivity of cysteine engagement is enhanced by the poor conservation of cysteine residues among protein kinases.

Out of the more than 500 protein kinases, at least 211 possess a cysteine in proximity to or within the ATP binding site. The targetable residues distribute over 27 different positions identified in a study by the groups of LAUFER and KNAPP. [217] Of these, more than 60 kinases have been successfully targeted until 2022, with this number continuously increasing. [218] The most commonly used warheads are α,β-unsaturated amides, which were successfully used to target the majority of the kinases mentioned above, displaying the variability of this warhead type. [218]

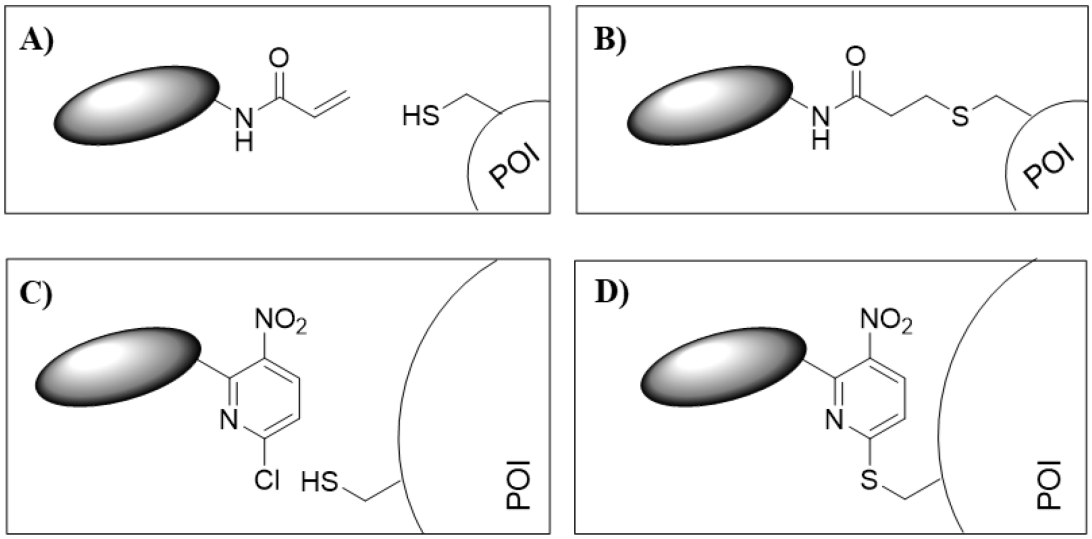

Figure 23: Schematic depiction of covalent warheads binding to the protein of interest (POI); A/B) Thia-Michael addition of an acrylamide; C/D) Covalent binding via S_NAr reaction by a heterocyclic warhead.

α,β-Unsaturated amides react with thiol groups via a thia-MICHAEL addition (Figure 23A/B) where the sulfur atom attacks the electrophilic β-position to form a β-thioether adduct. Alternative warhead types can further broaden the scope of covalent kinase inhibitors. [219] The possibility of cysteines reacting in a nucleophilic aromatic substitution (S_NAr), depicted in Figure 23C/D, can also be exploited for covalent targeting. The mechanism of this reaction type is usually described via the formation of an MEISENHEIMER complex (or σ-complex) as intermediate (shown in Figure 24A). [220] More recent data suggest a concerted mechanism, including a negatively charged instable transition state (Figure 24B). The mechanism thereby depends on the substitution of the aromatic system by electron withdrawing groups (EWG) and their ability to stabilize the MEISENHEIMER-like transition state. [221] Furthermore, the substitution pattern strongly influences reactivity and offers the opportunity to tune the warhead reactivity. Additionally, the aromatic ring and the incorporated heteroatoms influence the electronic properties and thereby reactivity. For example, including an additional nitrogen into a phenyl ring increases reactivity in a S_NAr reaction. Another factor influencing reactivity is the nature of the leaving group (LG). Most commonly, halogens serve as such, with aryl fluorides displaying the highest reactivity in this kind of reactions, followed by the chloride and bromide derivatives and the iodide substituted arenes being the least reactive aryl halides (F > Cl ~ Br > I). [213]

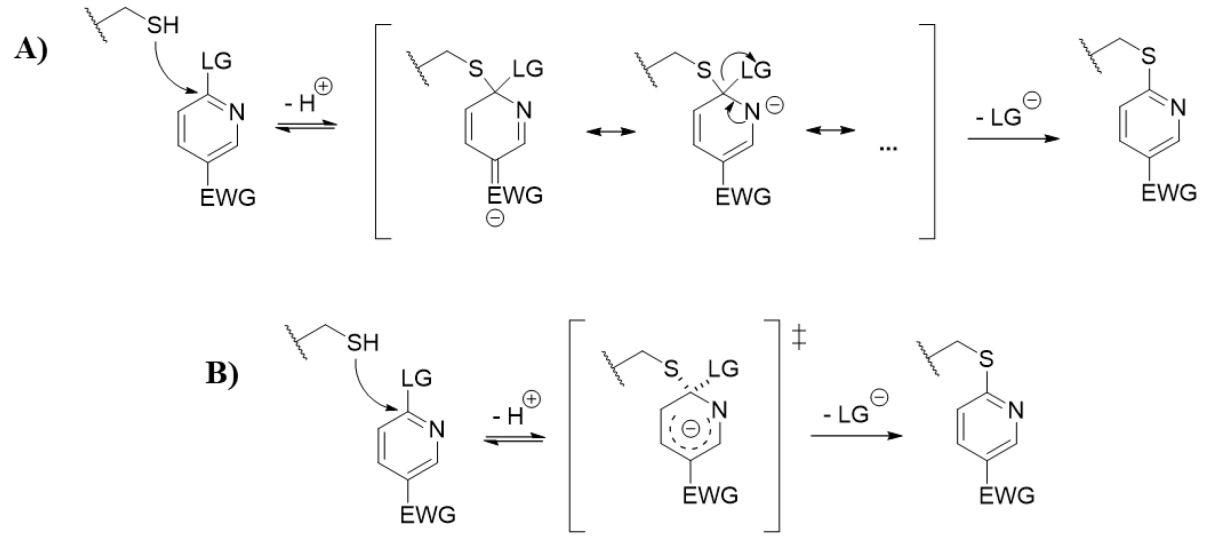

Figure 24: Mechanism of the S_NAr reaction between a thiol nucleophile and an electron deficient heteroarenes (LG = leaving group; EWG = electron withdrawing group); A) Reaction via MEISENHEIMER complex; B) Concerted mechanism via an instable transition state.

Early compounds containing an electron deficient (hetero)arene as warhead targeted the peroxisome proliferator activated receptor-γ (PPARγ) using 2-chloroquinoxaline (**31**) or a *p*-chloro-nitrobenzene (**32**), respectively, as electrophilic group. [222] Additionally, S_NAr based warheads targeting the hepatitis C virus nonstructural protein 5B (HCV NS5B) were published by CHEN *et al*. from Merck utilizing electron-deficient *p*-fluoronitro (**33**) or *p*-fluorosulfone substituted benzyl groups, covalently binding to Cys366, which was confirmed via X-ray crystallography. [223] The application of the S_NAr warhead for EGFR inhibition, as tested by HOU *et al.*, was not successful. Even though these inhibitors (exemplified

by compound **34**) showed good overall activity, no covalent modification could be proven. [224] This underlines the importance of the spatial alignment of the warhead to enable the covalent bond formation with the targeted residue.

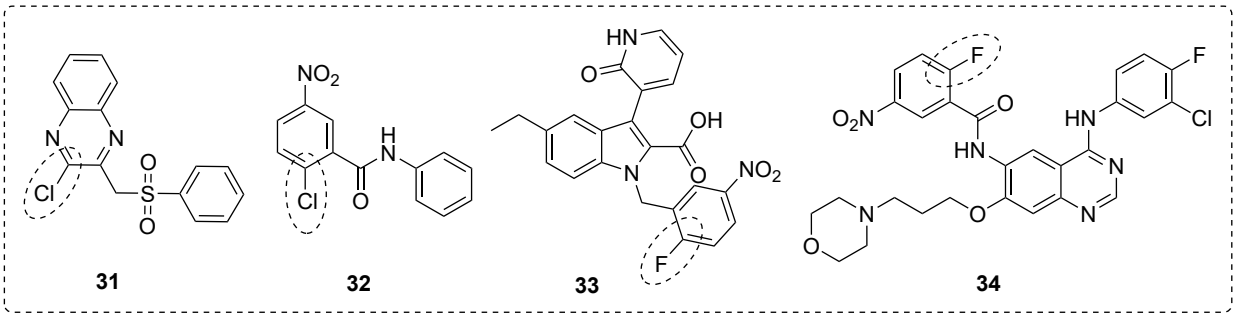

Figure 25: Cysteine-targeting compounds containing electron deficient (hetero)aromatic cycles as S_NAr warheads.

Interestingly, a HTS identified fragment-like compound **36** to covalently bind to a cysteine in the hinge region of fibroblast growth factor receptor-4 (FGFR4), a kinase amongst five kinases, possessing a cysteine at the gatekeeper+2 (GK+2) position. [12]

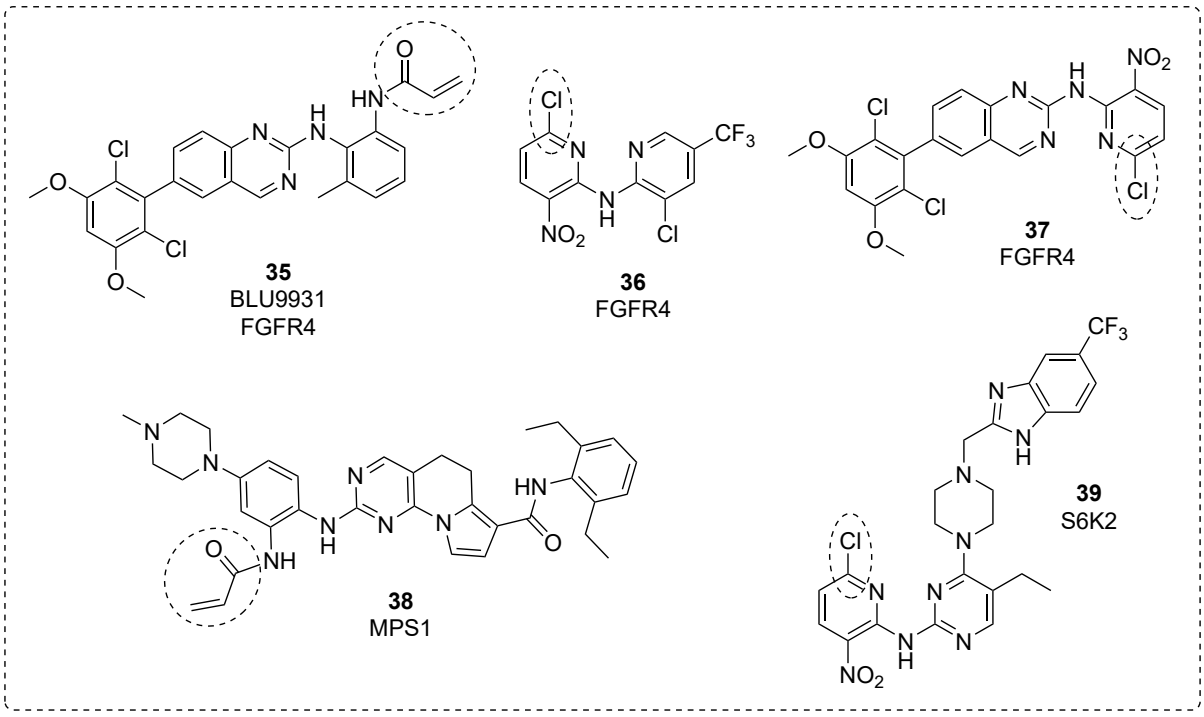

Figure 26: Covalent inhibitors engaging the GK+2 cysteines in FGFR4, MPS1 and S6K2. Acrylamide warhead and LG of the S_NAr warheads highlighted in dotted lines.

Besides FGFR4, monopolar spindle-1 (MPS1) and ribosomal protein S6 kinase β-2 (S6K2), MK2 and MK3 possess an equivalent cysteine. [217] The heterocyclic chloronitropyridine warhead in compound **36** also served as a starting point for the discovery of the first S6K2 inhibitor **39** in our research group. [225] Following the successful covalent targeting of FGFR4 by an acrylamide-based inhibitor (**35**) in 2015 [2], covalent ligands for the other kinases with a GK+2 cysteine, with the exception of MK3, have been published. Notably, beyond S6K2, our publications include the successful targeting MPS1 (**38**) [226] and

very recently FGFR4 (**37**).[227] In the latter study, we successfully combined the heterocyclic chloronitropyridine warhead of compound **36** with the hinge binding quinazoline core of BLU9931 (**35**), resulting in compound **37**.[227] In 2023, researchers from Bristol Myers Squibb published the discovery and properties of the benzothiophene-based MK2 inhibitor gamcemetinib (CC99677; **20**), the aforementioned S_NAr based clinical candidate, which will be further discussed in section 1.4.4.[228]

As briefly mentioned above, binding of a covalent inhibitor to its target can be described by a two-step mechanism (Figure 27). In the first step, there is a reversible binding event between the inhibitor and the protein. This initial interaction positions the warhead in proximity to the reactive amino acid residue, facilitating the formation of the covalent bond. While the covalent binding event is usually irreversible, reversible-covalent mechanisms are also possible, e.g. by using dually activated MICHAEL acceptors such as α-cyano-acrylamides as warhead.[217]

The activity of an inhibitor against its target is commonly described by the half maximal inhibitory concentration (IC_{50}) value. In the case of a covalently acting compound, the inhibition, however, is a time-dependent process, so the IC_{50} value changes when varying the incubation/reaction time leading to an increase in (apparent) potency with increasing incubation times.

Due to the more resource-demanding nature of the experiment, IC_{50} values are still common for activity assessment in the kinase field, especially at early project stages. To include the kinetic aspect of the activity for a covalent inhibitor, however the time-independent k_{inact}/K_I value is recommended for potency evaluation. The k_{inact}/K_I value is the second order rate constant of target inactivation.[229] The K_I value therein represents the required inhibitor concentration to achieve the half-maximal reaction rate of the covalent binding event. This term depends on efficient non-covalent binding in step 1 (see Figure 27). The covalent bond formation is described by k_{inact}, which is the reaction rate thereof essentially reflecting the velocity of covalent bond formation at full target occupancy.[230]

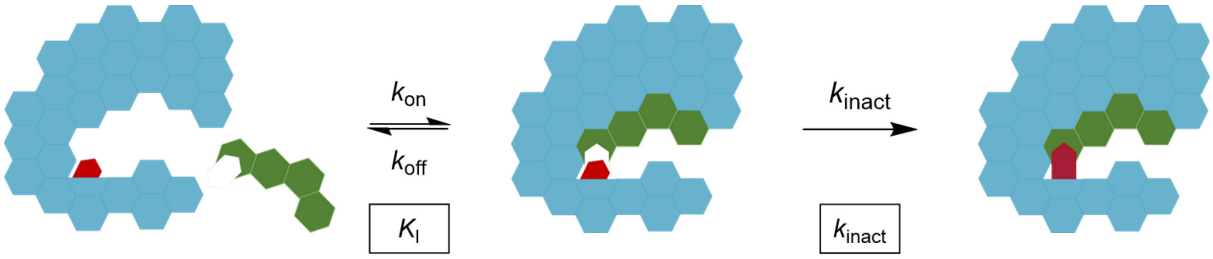

Figure 27: Two-step binding mechanism of a covalent inhibitor and its kinetic parameters; the protein is depicted in blue, the inhibitor in green, and the targeted residue in red.

The activity of covalent inhibitors is influenced by the reversible binding event, the intrinsic reactivity and the right orientation of the reactive group. The geometry is affected by the attachment positions of the linker to the core and the chosen linker/warhead combination. Balancing the reactivity of the electrophile is crucial to ensure effective target binding while avoiding unspecific binding to other proteins, DNA or small physiological molecules (e.g. GSH), which may cause off-target effects and toxicity or simply quench the inhibitor.[217, 231]

A common method to access reactivity towards thiol nucleophiles are stability assays using GSH or other surrogate nucleophiles bearing a thiol group. GSH is particularly suitable since it is present in cellular environment in high (typically low millimolar) concentrations. In addition, the use of GSH, compared to alternative surrogate molecules such as *N*-acetylcysteine and cysteamine, can distinguish the reactivity of a variety of warhead types in a more nuanced manner and covers a wide array of reactivities. [232] High-performance liquid chromatography (HPLC)-based methods are mostly used to measure degradation of the electrophilic compounds. To represent physiological conditions, an aqueous buffer at pH ~7.4 is typically used and the experiment is carried out at ~37 °C. However, differences in the experimental conditions like buffer system, type and amount of organic co-solvent and concentration of the reactive components, but also minor variations in pH and temperature, influence the obtained reaction rates and half-life ($t_{1/2}$) values, making quantitative comparisons challenging between different studies. [233] For drug-like molecules, a known inhibitor, like afatinib, is often included to be used as a reference value. [234]

1.4.4 Development of a Clinical Candidate Covalently Targeting MK2

The development of gamcemetinib (CC-99677, **20**, see Figure 17), the first covalent inhibitor targeting MK2, was published in 2022. [228, 235] Since the project for this thesis was already advanced at this point the findings of this study were not incorporated during our work. Nevertheless, it serves as a representative example of a covalent drug discovery project building on a related approach, and offers valuable insights into target-related aspects.

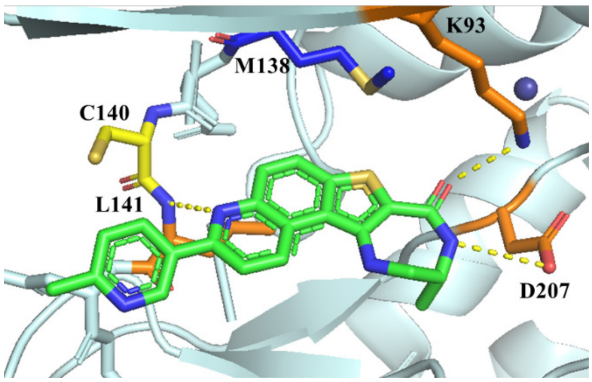

Figure 28: Binding mode of PF3644022 (**19**, in green) to MK2 (PDB: 7NRY [9]); gatekeeper Met138 in blue, Cys140 in yellow, amino acids involved in inhibitor binding in orange.

The design of gamcemetinib (**20**) started with the fusion of the established benzothiophene core (chapter 1.4.2, **19** (Figure 17)) and an S_NAr warhead. Even though the *p*-fluoronitro group (present in **33**, Figure 25) was included in the first patent [205a], the decision was made to utilize halopyrimidines as tunable warhead moieties. The crystal structure of the reversible benzothiophene based inhibitor PF3644022 (**19**), shown in Figure 28, reveals three relevant H-bond interactions. Specifically, the tetracycle's pyridine-nitrogen interacts with the backbone NH of Leu141 in the hinge-region, while two additional hydrogen bonds are formed between the lactam carbonyl oxygen and the ε-NH_2 of Lys93, and between the lactam *NH* and γ-carboxylate of Asp207 in the DFG-motif. [9] Analysis of crystal structure of an early covalent compound by MALONA *et al.* revealed an analogous binding mode. [228] Subsequently, the halopyrimidine in CC-99677 (**20**) forms a covalent bond with Cys140 (highlighted in yellow in Figure 28) via an S_NAr reaction.

Table 2: Compound series leading to the development of gamcemetinib (**20**).

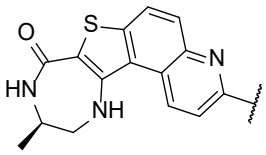 Benzothiophene core	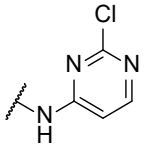 **40**	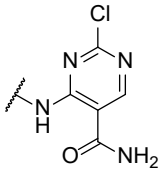 **41**	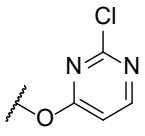 **42**	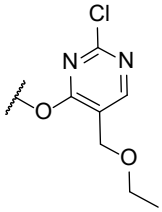 **20**
IC_{50} [nM]	35	4.7	53.9	156
Mass modification	0%	85%	63%	74%
Solubility [µM] pH2.0/ 7.4	13/ < 1	< 1/ < 1	54/ 59	15/ 19
Mouse S9 30 min (%remain)	70	57	40	72

However, their initial approach attaching a chloropyrimidine via a nitrogen linker, giving compound **40**, showed low intrinsic reactivity and no mass modification (see Table 2). Increasing the reactivity by adding an amide substituent led to a highly active compound **41** with an IC_{50} value in the low nanomolar range, but the nitrogen linked series showed low solubility and overall poor physicochemical properties. Incorporating an oxygen atom as linker improved solubility but negatively influenced metabolic degradation (shown in Table 2). Further optimization improved metabolic stability and led to the discovery of CC-99677 (**20**), exhibiting reasonable potency (IC_{50} = 156 nM, k_{inact}/K_I = (4.94 ± 0.63) x 10^3 $M^{-1}s^{-1}$), a good BE value (1.76) and suitable pharmacokinetic properties. [228]

CC-99677 (**20**) inhibits the release of CCL2, TNFα, GM-CSF and moderately of IL-6, while showing minimal impact on IL-1β levels in human peripheral blood mononuclear cells (PBMCs). [228] Additionally, the resynthesis rate of the kinase, which limits the duration of action, was assessed. The determined values indicated a slow resynthesis rate ($t_{1/2}$ ca. 27 h up to 44 ± 7 h; depending on the experimental setup), indicating suitability of MK2 for covalent targeting. Despite the inhibitor's short half-life (~ 2 to 7 hours in human) and limited selectivity, further data looked promising. The lack of selectivity, especially against kinases with an equivalent cysteine (GK+2), did not translate into cellular activity. Observed effects were attributed exclusively to MK2 inhibition and aligned with expected outcomes. CC-99677 reduced production of TNF, IL-6 and IL-17 in vitro by inhibiting the phosphorylation of TTP. Good efficacy in a rat model of spondyloarthropathy prompted further investigation humans and clinical trials. [235] Moreover, a Phase I first-in-human study revealed a linear PK profile and a favorable safety profile. Sustained reduction of TNFα levels in a cell-based model further supported progression to clinical studies. [235] However, a Phase II trial for active ankylosing spondylitis was terminated due to lack of efficacy in the short-term acute phase, while no toxicity issues were observed. [236]

2 Aims

The p38 MAP kinase signaling pathway is involved in important physiological and pathophysiological processes. [51b, 51d] One of the downstream targets of p38 MAP kinase is the protein kinase MK2, which plays an important role in inflammatory signaling. [237] In addition, more recent findings demonstrate its involvement in carcinogenesis and tumor progression. [40] Despite great efforts to target MK2 in several drug discovery projects, no small molecule inhibitor has yet succeeded in clinical trials. [33b, 99] A great portion of these drug design projects already failed in the early stages, due to the major challenges arising in terms of the high competing cellular ATP concentrations, kinase selectivity and the physicochemical properties. [99, 198] In 2023, two MK2 inhibitors, zunsemetinib (**7**) [195] and gamcemetinib (**20**) [236], for treatment of inflammatory diseases failed in clinical trials due to lack of efficacy, underlining the need for the development of drugs with further improved properties. [195, 236]

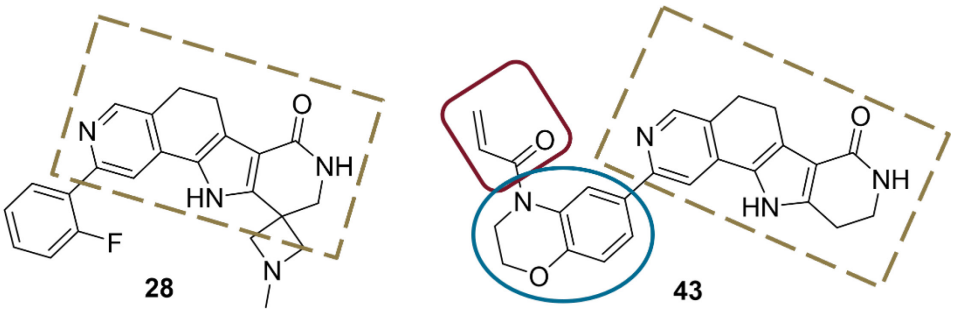

Figure 29: The MK2 inhibitors lead structures for this PhD project. Reversible binding core marked in gold, linker in blue and warhead in red.

The starting point for this PhD project were the known reversible MK2 inhibitor **28** [3] and the acrylamide-containing derivative **43** from the patent literature [15]. According to the limited data provided within the patent, attachment of the electrophilic warhead to the tetracyclic core (marked in gold in Figure 29) indeed enabled covalent targeting of a nucleophilic cysteine (Cys140) in the hinge region of MK2, located two residues C-terminal to the gatekeeper (Met138). We decided to pursue such a covalent approach to exploit the advantages of a long target-residence time and to improve on-target activity and selectivity. While MK2 is a suitable target for covalent approaches due to its low protein turnover, addressing Cys140 is also desirable to promote selectivity within the *kinome*, as only four other kinases (MK3, FGFR4, MPS1, S6K2) contain an equivalent cysteine. To enable the formation of a covalent bond with the kinase's cysteine, different electrophilic warheads (highlighted red in Figure 30) were incorporated into the molecule.

First, well-established acrylamide warheads were implemented to confirm covalent targetability of the respective cysteine. The same warhead type has been successfully used to target the equivalent cysteine in FGFR4 (**35**, BLU9931, Figure 30) [2], encouraging this approach. The second part of the project focused on installing an aromatic warhead, which forms the covalent bond via a S_NAr mechanism. [213] Notably, the fragment **36**, which comprises a 2-chloro-5-nitropyridine warhead, has been identified to covalently engage FGFR4 via the chloronitropyridine (Figure 30). [12] Consequently, we decided to attach its electron-deficient chloronitro aryl residue to the MK2 inhibitor core via a linker nitrogen atom.

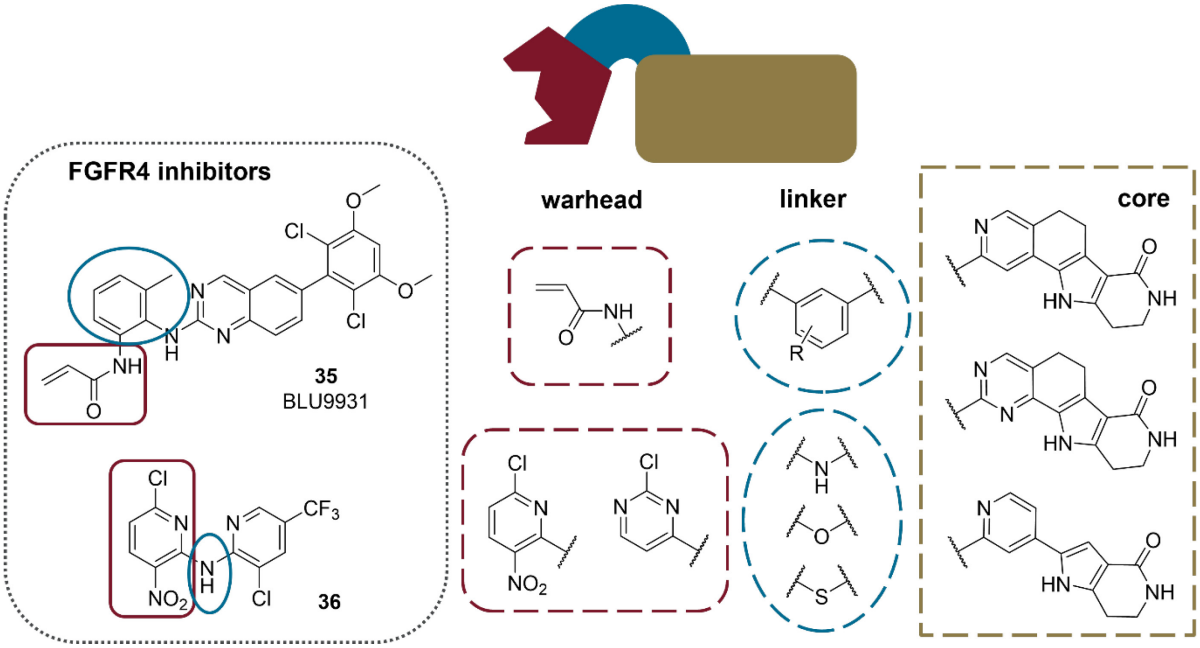

Figure 30: Schematic depiction of the design strategy. Known FGFR4 inhibitors on the top; linker highlighted in blue, warhead in red, reversible binding core in gold.

The inhibitor core was to be structurally modified to optimize the reversible binding properties and the orientation of the warhead, but also to facilitate chemical synthesis and thereby enabling generation of structure–activity relationships (SAR). The substitution at the pyrrole nitrogen was identified as interesting derivatization point and its influence in inhibitor binding and physicochemical behavior was to be examined. Furthermore, the variation of the linking atom and the warhead, particularly its substitution pattern, was envisaged to provide valuable insights into the potential influences of heterocyclic warheads on the reactivity and the physicochemical properties of the inhibitor.

3 Synthesis Part

3.1 Synthesis of Pyridine-based Tetracyclic Compounds

The first aim of the project was to prove the covalent targetability of the GK+2 cysteine in MK2, before varying the type of warhead used. The wealth of experience with acrylamide-based warheads supported the choice as a starting point. Not only is this structural group part of several approved drugs, [216] it is also suitable for targeting cysteine residues in different kinases and locations. [218] The wide application is accompanied by a variety of published synthetic methods, which can be useful for establishing a suitable synthetic route. In addition, the equivalent cysteine in FGFR4 has already been successfully targeted with an α,β-unsaturated amide. [2, 226] A patent disclosed by Celgene in 2014, covering several of the core structures, mentioned in section 1.4.2, combined with an acrylamide warhead, served as an inspiration for this project. [15] Considering the experimental results and the synthetic steps, including the accessibility of starting materials and the methods used, the tetracyclic structure, exemplified by compound **43** (Figure 31), was chosen as the starting point.

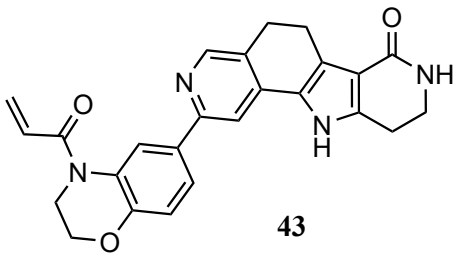

43

Figure 31: Structure of a covalent MK2 inhibitor **43** from the patent literature.

The pyridine-based tetracyclic core has been published in reversible MK2 inhibitors with IC_{50} values in the low nanomolar range in a biochemical assay, but lacking cellular activity. [3] The covalent binding mode is proposed to improve the cellular activity by escaping from competition with the high cellular ATP concentration after successful irreversible binding. [213] Compound **43** was reported to inhibit the kinase with an IC_{50} value ≤ 100 nM, furthermore the authors reported > 70% protein mass modification and labelling of Cys140 after trypsin digestion. [15] The synthesis of the tetracyclic core, which involves eight steps, is illustrated in Scheme 1.

The bicyclic isoquinolin-3-ol **47** was synthesized in a two-step procedure from benzylamine **45** and ethyl 2,2-diethoxyacetate **44**, in a manner analogous to that described in the literature. [5] To this end, after an initial ester aminolysis, the obtained amide intermediate **46** was cyclized to isoqunolin-3-ol **47** by stirring in sulfuric acid. The partial hydrogenation of **47** was carried out under strong acidic conditions (trifluoracetic acid (TFA), triflic acid) and catalyzed by PtO_2 under hydrogen pressure, as described by PAN *et al.* for the synthesis of sempervirine. [14] The following steps have been described in related patent literature and further optimized. [15-16] The obtained 5,6,7,8-tetrahydroisoqinolin-3-ol **48** was chlorinated with phosphoryl chloride ($POCl_3$) under heating to 170 °C in a pressure vessel. For the subsequent introduction of an oxime in the benzylic position, the bicyclic intermediate **49** was first partially deprotonated with potassium *tert*-butanolate (KO*t*Bu) in tetrahydrofuran (THF), before *tert*-butyl nitrite (TBN) was added. The oxime **50** was hydrolyzed to the ketone **51** in acetone. The concentration of the added hydrochloric acid (HCl) was critical for the outcome of the reaction, with a

mixture of concentrated HCl and 6N HCl giving the best results. The bromination at the α-position of ketone **51** led to the key intermediate **52**. The acidic environment allowed selective monohalogenation. The tetracyclic core **54** was completed by closure of the pyrrole ring via a HANTZSCH pyrrole synthesis which requires a primary amine and a 1,3-dicarbonyl besides the α-halo ketone. [238] Here *tert*-butyl 2,4-dioxopiperidine-1-carboxylate **53** was used as the dicarbonyl and condensed with ammonia and **52** to the pyrrole ring in **54**.

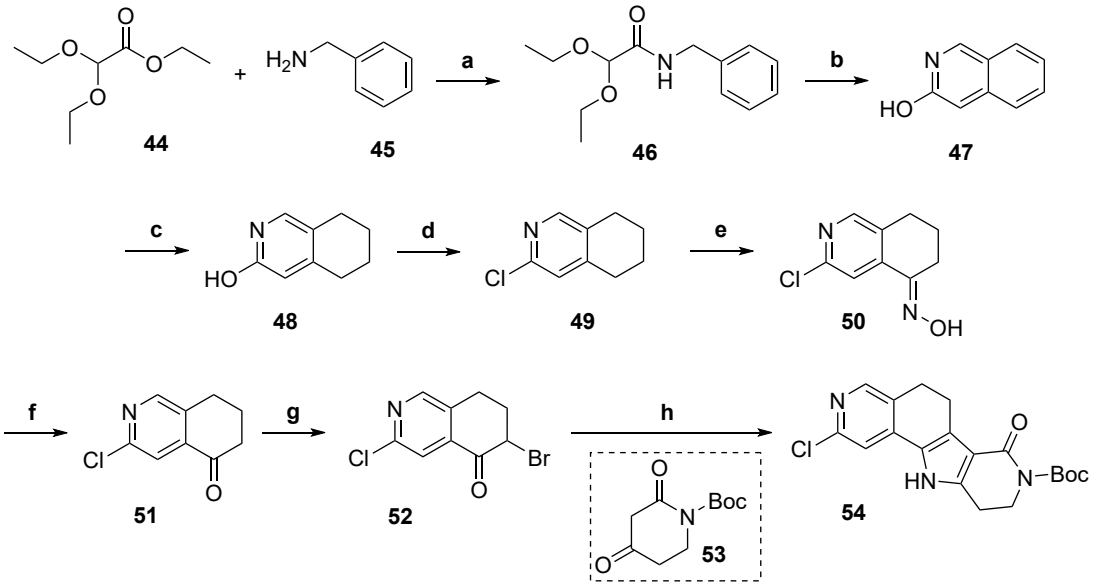

Scheme 1: Synthesis of the pyridine-based tetracyclic core: (a) 130 °C, 18 h, quant. [5]; (b) H_2SO_4, 0 °C (0.5 h) to rt (1 h), 98% [5]; (c) PtO_2, TFA/triflic acid, H_2 (3 bar), 18 h, 42% [14]; (d) $POCl_3$, 170 °C, 16 h, 47% [15]; (e) 1. KO*t*Bu, THF, 0 °C, 18 h; 2. TBN, 0 °C to rt, 3 h, 83% [16]; (f) HCl, acetone, reflux, 6 h, 77%; (g) Br_2, $HBr_{(aq)}$, acetic acid (HOAc), rt, 3 h, 73% [15]; (h) NH_4OAc, methanol (MeOH), reflux, 3 h, 47%. [15]

Methylation of the pyrrole nitrogen with methyl iodide worked as expected and **55** was obtained **(**see Scheme 2). The pre-substituted linker was attached to the isoquinoline-3-position of both, the methylated and unmethylated core via a SUZUKI coupling. The final steps are illustrated by the synthesis

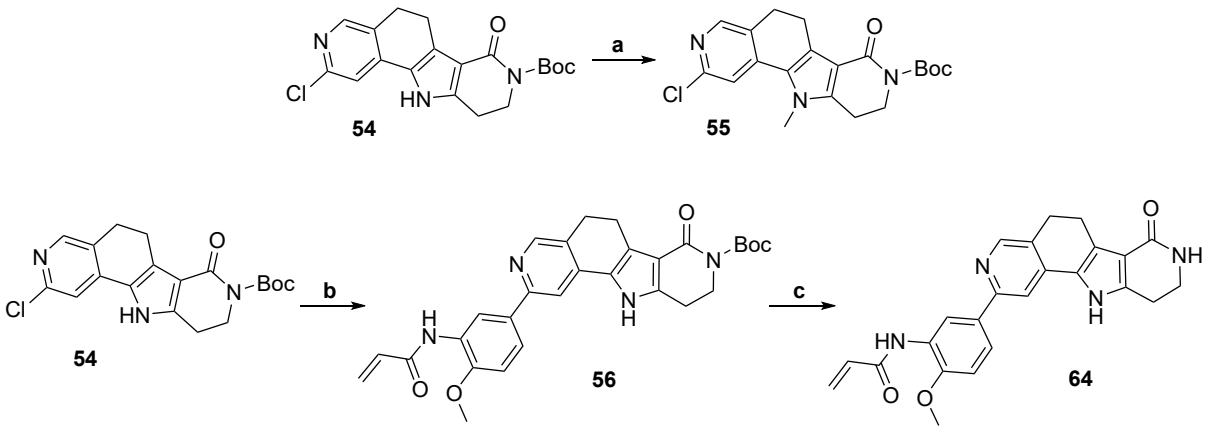

Scheme 2: Methylation of **55** and exemplary synthesis of the final inhibitor **64**; (a) CH_3I, Cs_2CO_3, *N,N*-dimethylformamide (DMF), rt, 2 h, 66%; (b) **76**, K_2CO_3, (tBu)$_3$P Pd G3, 1,4-dioxane/H_2O, 80 °C, 18 h, 77%; (c) TFA, dichloromethane (DCM), rt, 30 min, 68%.

of **64** (Scheme 2). The product of the Suzuki coupling **56** was deprotected by means of acid to give the final compound **64**.

This synthetic route allowed the synthesis of a series of compounds with a variety of aromatic linkers substituted in different ways. The corresponding unreactive control compounds, in which the acrylamide was replaced by a saturated propionamide, were synthesized in an analogous manner (see Scheme 3). The derivatives lacking the electrophilic group are useful for a first assessment of the relevance of the covalent binding step from the biochemical assay data. Due to their high structural similarity, an increase in inhibitory activity for the acrylamide-containing derivatives is likely to be related to covalent bond formation.

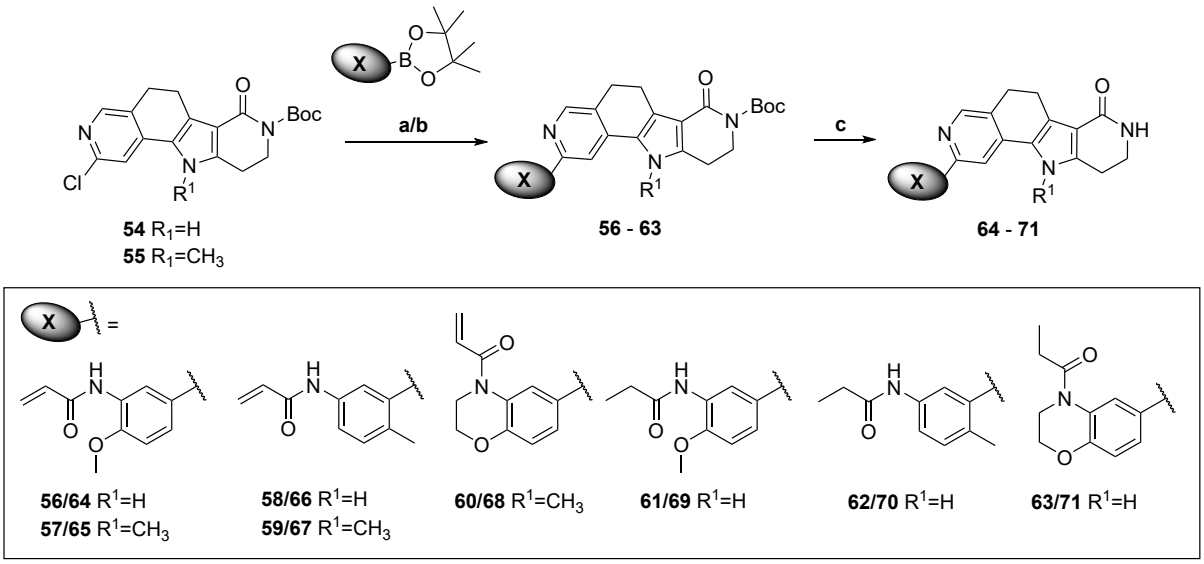

Scheme 3: Synthesis of the pyridine-based tetracyclic inhibitors; (a) K_2CO_3, (tBu)$_3$P Pd G3, 1,4-dioxane/H_2O, 80 °C, 18 h; (b) Na_2CO_3, $Pd(PPh_3)_4$, 1,2-dimethoxyethan/ethanol (EtOH)/H_2O, 90 °C, 6 h; (c) TFA, DCM, rt, 30 min.

The synthesis of the pre-substituted boronic acid esters **76** and **79** bearing an acrylamide or propionamide, which were used in the pre-final SUZUKI coupling step, is shown in Scheme 4. These *p*-methoxy substituted derivative (**76**/**79**) represent the ring-opened analog of the bicyclic linker of compound **43** from the patent literature (Figure 31). The precursor of the former are directly accessible from the aniline (**72**, Scheme 4), while the bicyclic oxazine **83** had to be built up first (Scheme 5). In addition to these two aromatic linker derivatives containing an ether substituent (**74** and **84**) the *ortho*-methyl linker, present in BLU9931 (**35**) was included as an alternative. The latter was successfully used to target the equivalent cysteine in FGFR4. [2] The *o*-substituent influences the orientation of

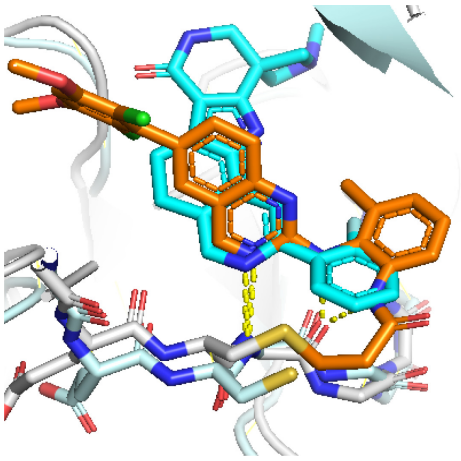

Figure 32: Overlay of the crystal structure of BLU9931 **35** (colored in orange) bound to FGFR4 (colored in grey; PDB: 4XCU [2]) and a tetracyclic inhibitor **28** (turquoise) bound to MK2 (colored in pale cyan; PDB: 3M2W [1]).

the linker moiety by promoting an out-of-plane torsion. An overlay of the X-ray crystal structures displayed a similar orientation of the hinge binding motif in the irreversible inhibitor BLU9931 (**35**) and the tetracyclic core of an MK2 inhibitor (**28**) related to the ones described here in the binding pocket of MK2 (Figure 32).

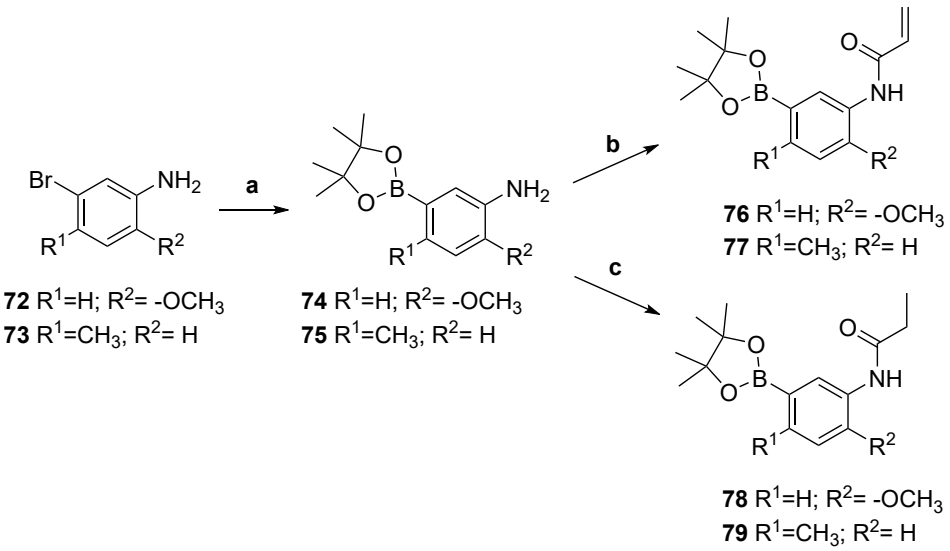

Scheme 4: Synthesis of the boronic acid pinacol esters of the aromatic linker; (a) B_2pin_2, KOAc, $Pd(dppf)Cl_2$, 1,4-dioxane, 80 °C, 5- 7 h, 57% (**74**)/ 87% (**75**); (b) acryloyl chloride, DIPEA, DCM, -80 °C to rt, 1 h, 75% (**76**)/ 66% (**77**); (c) propionyl chloride, TEA, DCM, 0 °C to rt, 16 h, 97% (**78**)/ 58% (**79**).

For the synthesis of the monocyclic linkers (shown in Scheme 4), the respective 3-bromoanilin derivatives **72**/**73** were first converted to the boronic acid pinacol esters **74**/**75**. The MIYAURA borylation was followed by an amide coupling with acryloyl chloride and *N,N*-diisopropylethylamine (DIPEA) to introduce the warhead (**76**/**77**) or propionyl chloride in combination with triethylamine (TEA) for the synthesis of the linkers **78**/**79** for the unreactive control compounds.

The bicyclic linker required for compounds **68** and **71** was synthesized from the aminophenol **80** (see Scheme 5). As described by ARMITAGE *et al.* [239], 2-amino-4-bromophenol **80** was reacted with 2-chloroacetyl chloride **81**. The resulting amide **82** was then reduced to the amine **83** using lithium aluminum hydride ($LiAlH_4$). The MIYAURA borylation (**84**) and the subsequent amide couplings were performed using the same procedure as described above (Scheme 4). The building blocks **85** and **86** were also attached to the core by SUZUKI coupling (Scheme 3).

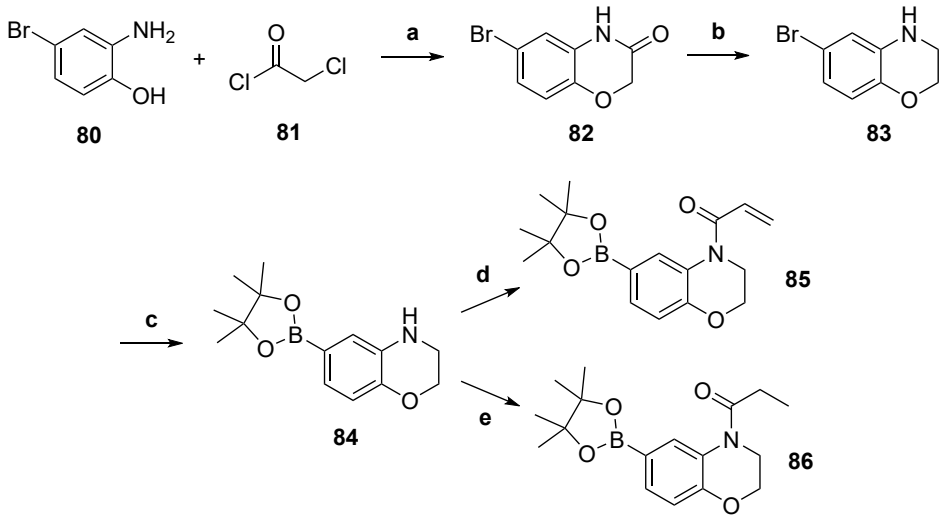

Scheme 5: Synthesis of the bicyclic linker moiety and attachment of the warhead; (a) 1) $NaHCO_3$, THF, < 5 °C, 30 min; 2) K_2CO_3, reflux, 2.5 h, 81%; (b) $LiAlH_4$, THF, 0 °C to rt, 18 h, 47%; (c) B_2pin_2, KOAc, $Pd(dppf)Cl_2$, 1,4-dioxane, 80 °C, 2 h, 76%; (d) acryloyl chloride, DIPEA, DCM, -80 °C to rt, 1 h, 72%; (e) propionyl chloride, TEA, DCM, 0 °C to rt, 16 h, 56%.

A series of compounds with the pyridine-derived tetracyclic core were successfully synthesized. However, several drawbacks became apparent during the synthesis. The harsh reaction conditions for the partial hydrogenation of the isoquinoline (Scheme 1, step **c**) with strong acidic conditions and hydrogen overpressure limited upscaling. Similarly, the subsequent chlorination step (Scheme 1, step **d**), performed at a temperature above the boiling point of $POCl_3$ and the resulting pressure conditions with this very aggressive reagent are a limiting factor. The insufficient reactivity of the 2-position of the terminal pyridine ring in cross-coupling and S_NAr reactions limits the derivatization possibilities and SAR studies. Attempts to replace the acrylamide warhead with a chloronitropyridine failed on this scaffold (see section 3.2.1 for planned synthetic route). To this end, replacing the chloride leaving group of the core with a nitrogen as a linker atom was not successful at all, using either S_NAr or transition metal catalyzed conditions, due to insufficient reactivity of the halide precursor and potential steric, electronic, and coordination effects of the entire tetracyclic core.

3.2 Synthesis of Pyrimidine-based Tetracyclic Compounds

The replacement of the terminal pyridine by a pyrimidine on tetracyclic MK2 inhibitors was described by SCHLAPBACH *et al.*[1] To this end, 2-chloropyridine in intermediate **54** was replaced by a 2-chloropyrimidine (**94**). The latter heterocycle is more electron deficient and should therefore be more reactive towards nucleophiles and in cross-coupling reactions.[240] In addition to the change in reactivity, the synthesis of the core has some significant advantages. The tetracyclic core could be built up from the cyclohexanone derivative **87** (see Scheme 6). Starting from this saturated ring avoided the hydrogenation, required for the pyridine-based tetracyclic derivative (section 3.1, Scheme 1).

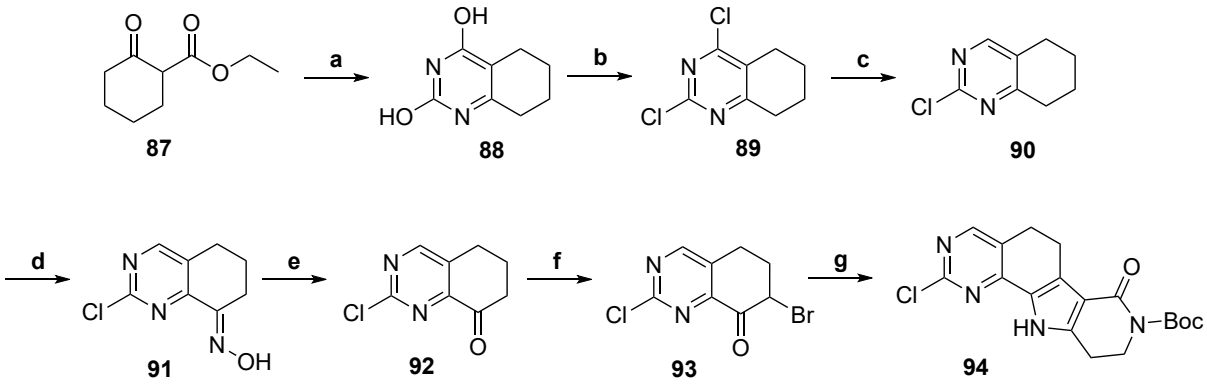

Scheme 6: Synthesis of the pyrimidine-based tetracyclic core **94**; (a) urea, NaOMe, EtOH, reflux, 16 h, 49%; (b) $POCl_3$, reflux, 2 h, 80%; (c) Zn, NH_4Cl, H_2O/acetone, reflux, 6 h, 60%; (d) KO*t*Bu, TBN, THF, -78 °C to rt; quant.; (e) HCl_{conc}, H_2O/acetone, 80 °C, 30 min, 23%; (f) Br_2, HCl_{conc}, 35 °C, 10 min, quant.; (g) **53**, NaOAc, NH_4OAc, MeOH, rt, 18 h, 52%.

Condensation of the dicarbonyl compound **87** with urea, as described by ORTEGA *et al.*[241], gave the "pyrimidine diol" **88** (Scheme 6). The chlorination was carried out under reflux conditions to give **89**. Selective monodehalogenation at the more electrophilic pyrimidine 4-position leading to **90** was performed under mild reductive conditions, using zinc dust and ammonium chloride. The reaction conditions had to be carefully balanced to avoid complete dehalogenation. The oxime of intermediate **91** was introduced at -78 °C to reduce by-product formation and the crude product was directly hydrolyzed to the ketone **92**. In analogy to a procedure described in the patent literature[16], the intermediate **92** was brominated at the carbonyl α-position under acidic conditions. The α-bromo ketone **93** was used to close the pyrrole ring with *tert*-butyl 2,4-dioxopiperidine-1-carboxylate **53** as discussed above to give the Boc-protected tetracyclic building block **94**[15] in satisfactory yields (52% over two steps).

The final steps to introduce the phenyl-linked warhead and finalize the inhibitor were performed as described in section 3.1 (Scheme 3). **95** was obtained after the successful SUZUKI coupling to the

warhead/linker moiety (shown in Scheme 7). In the final step, the *tert*-butoxycarbonyl (Boc) protecting group attached to the lactam was cleaved under acidic conditions to give **96**.

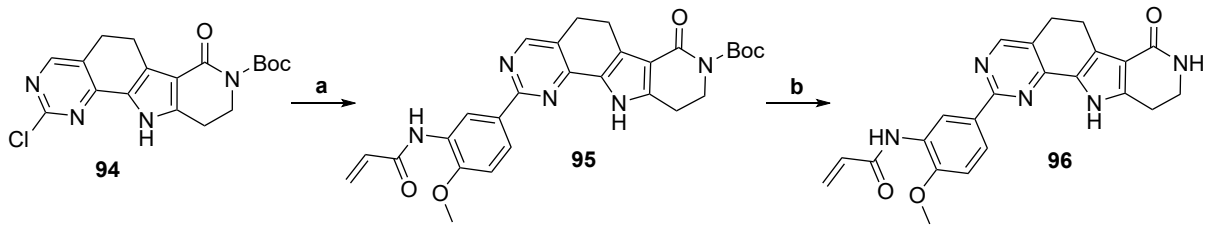

Scheme 7: Synthesis of the pyrimidine-based tetracyclic compound **96**; (a) **76**, K_2CO_3, (tBu)$_3$P Pd G3, 1,4-dioxane/H_2O, 80 °C, 18 h, 55 %; (b) TFA, DCM, rt, 30 min, 57%.

3.2.1 Synthesis of Pyrimidine-based Tetracyclic Compounds containing a S_NAr-based Warhead

After the successful implementation of the acrylamide, an alternative warhead strategy was to be applied to this project. As mentioned before, a chloronitropyridine residue was found to covalently bind the structurally equivalent cysteine in FGFR4 [12] and utilized by our group to successfully target S6K2 (compound **39**) by binding the corresponding residue. [225] An overlay of the crystal structure of inhibitor-bound MK2 with that of FGFR4 bound to the covalent fragment **36** showed a similar direction of the hinge binding motif and suggested a suitable orientation of the warhead to reach Cys140 in MK2 (Figure 33). Prior to the attachment of the warhead, this approach requires the introduction of the linking nitrogen atom. The introduction of the nitrogen to an electron-deficient heterocycle, such as pyrimidine, can be accomplished by a nucleophilic aromatic substitution (S_NAr) or catalyzed by transition metals, as in the ULLMANN or BUCHWALD-HARTWIG cross-coupling reactions.

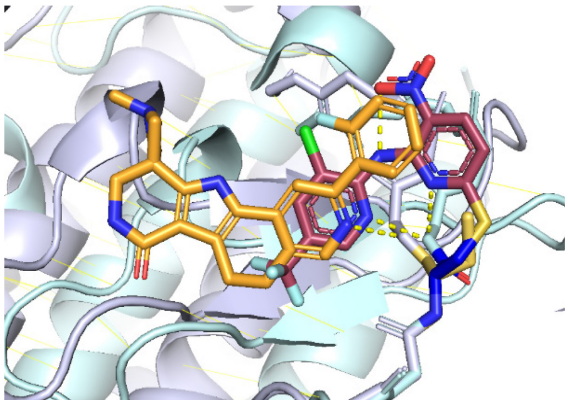

Figure 33: Overlay of inhibitor-bound MK2 (PDB: 3M2W [1]; kinase colored in grey, inhibitor **28** in orange, Cys140 in yellow) and FGFR4 bound to an covalent fragment **36** (PDB: 5NUD [12], kinase colored in pale cyan, fragment in raspberry); (polar interactions indicated by yellow dotted lines).

In order to exclude any interference of the free pyrrole with the synthetic route, the latter was *N*-methylated, to synthesize intermediate **97** as depicted in Scheme 8.

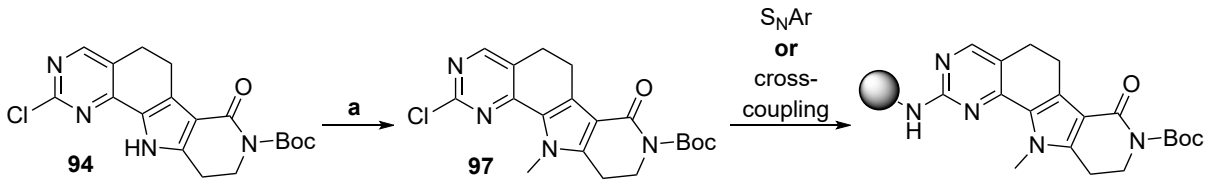

Scheme 8: Methylation of the pyrimidine-based tetracyclic core and schematic depiction of the amination; (a) CH_3I, Cs_3CO_3, DMF, rt, 2 h, 75%.

Initial attempts to use a nucleophilic aromatic substitution with ammonia or a suitable surrogate, such as benzylamine, were unsuccessful. Using a palladium-catalyzed BUCHWALD-HARTWIG coupling only worked when the pyrrole nitrogen was methylated. Thus, this approach was pursued, even though the inhibitory activity was expected to be lower than for analogs with the free pyrrole *NH*.[1] The monoprotection of the linking nitrogen was found to be necessary to avoid double arylation in the subsequent step as observed in the S6K2 project.[225] To choose a suitable protecting group, the deprotection method and the stability during the further synthetic route have to be considered. The deprotection conditions need to be compatible with the chemical reactivity of the warhead, since the groups are cleaved after the introduction of the warhead group. The latter is prone to react with nucleophiles, especially under basic conditions, which excludes most alkaline deprotection methods. Other common nitrogen protecting groups, such as the benzyl protection group, are removed under reductive conditions, potentially dehalogenating the warhead or reducing the nitro group. A global deprotection in the final step under acidic conditions was desirable, since the lactam was also protected by an acid-sensitive group. Thus, the use of the Boc protecting group met the requirements for adapting the synthetic route and structural characteristics. It was also previously shown to be stable under the reaction conditions of the subsequent steps.[225]

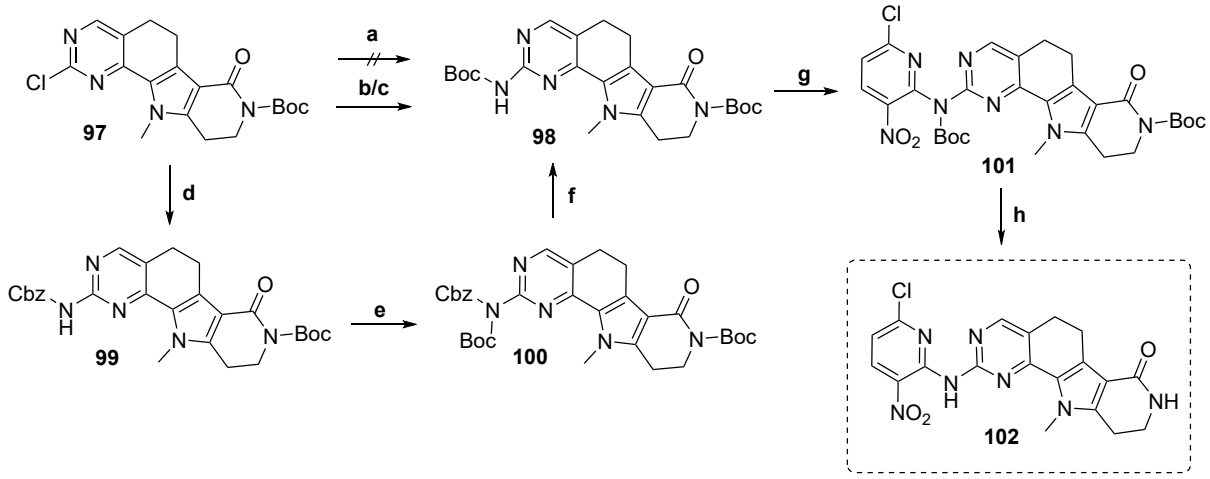

Scheme 9: Attachment of the nitrogen-bridged chloronitropyridine warhead to the tetracyclic core; (a) Boc-carbamate, XPhos Pd G4, K_2CO_3, 1,4-dioxane/*t*BuOH; (b) NaOCN, TEA, *t*BuXPhos, Pd_2dba_3, *t*BuOH, 130 °C, 18 h, 17%; (c) Boc-carbamate, Cs_2CO_3, XantPhos Pd G4, XantPhos, 1,4-dioxane, 100 °C, 4 h, 21%; (d) benzyl carbamate, Cs_2CO_3, XantPhos, $Pd(OAc)_2$, 1,4-dioxane, 120 °C, 16 h, 46%; (e) Boc_2O, TEA, 4-(dimethylamino)pyridine (DMAP), acetonitrile (ACN), rt, 18 h, 60%; (e) Pd/C, MeOH, H_2, rt, 5 h, 19%; (g) 2-bromo-6-chloro-3-nitropyridine **103**, Cs_2CO_3, XantPhos Pd G4, toluene, 55 °C, 4 days, 41%; (h) TFA, DCM, rt, 30 min, 31%.

The initial plan was to introduce the protected amine via a cross-coupling reaction with *tert*-butyl carbamate to synthesize intermidiate **98**. Compared to amines, carbamates exhibit lower nucleophilicity and the higher ability to form complexes with Pd catalysts.[242] These properties make them difficult substrates for cross-coupling reactions, and only a limited number of specific procedures have been described.[242a, 243] In initial attempts using a BUCHWALD-HARTWIG coupling protocol (XPhos Pd G4, K_2CO_3, 1,4-dioxane/tBuOH), no product could be isolated (Scheme 9, step **a**).

As observed in the derivatisation of coumarines by HICKEY *et al*., changing to benzylcarbamate as the coupling partner improved the reaction outcome. [244] The use of the benzyl carbamate indeed made the BUCHWALD cross-coupling more efficient. However, this strategy prolonged the synthetic route by two steps (Scheme 9). After the Pd-catalyzed introduction of the benzylcarbamate to obtain **99** (step **d**), the Boc protecting group was introduced (**100**). Selective removal of the benzyloxycarbonyl (Cbz) group under reductive conditions afforded the Boc-protected intermediate **98**. Notably this exchange of protecting groups was nescessary to avoid later incopatibilities between the reductive deprotection of the benzyl carbamate and the functional groups of the warhead. Due to the low yields and additional synthetic steps, an alternative approach was finally used.

The BUCHWALD group described the use of sodium cyanate in *tert*-butanol (*t*BuOH) to introduce Boc-protected amines [245], forming a isocyanate intermediate that reacts with the corresponding alcohol (here *t*BuOH) to form the carbamate. Unfortunately, the yield for the synthesis of **98** by an analogous procedure (Scheme 9, step **c**) was low (17%).

Optimization of the initial procedure using *tert*-butyl carbamate was achieved at a later stage of the project (for more detail see section 3.3.2.1.1). This resulted in shorter reaction time and improved reproducibility, although the yields remained low (21%).

The procedure used for introducing the heterocyclic warhead was based on the optimizations performed within the S6K2 project. [225] The proto warhead, 2-bromo-6-chloro-3-nitropyridine **103**, was connected to the core **98** through a BUCHWALD-type reaction. The final deprotection of **101** was performed as described for the acrylamide derivatives in section 3.1 to isolate compound **102**. Even though a synthetic route to obtain compound **102** was succesfully developed, the numerious synthetic steps required and the low yields impede the isolation of sufficient amounts of the key intermediates to further assess structure activity relationships on this tetarcyclic core.

To prevent hindering cross-coupling reactions by the free pyrrole *NH,* a protection group strategy should be implemented. As previously mentioned, an acid-labil group is the most suitable for this synthetic route. The 2-(trimethylsilyl)ethoxymethyl group (SEM) is a commonly used protection group for

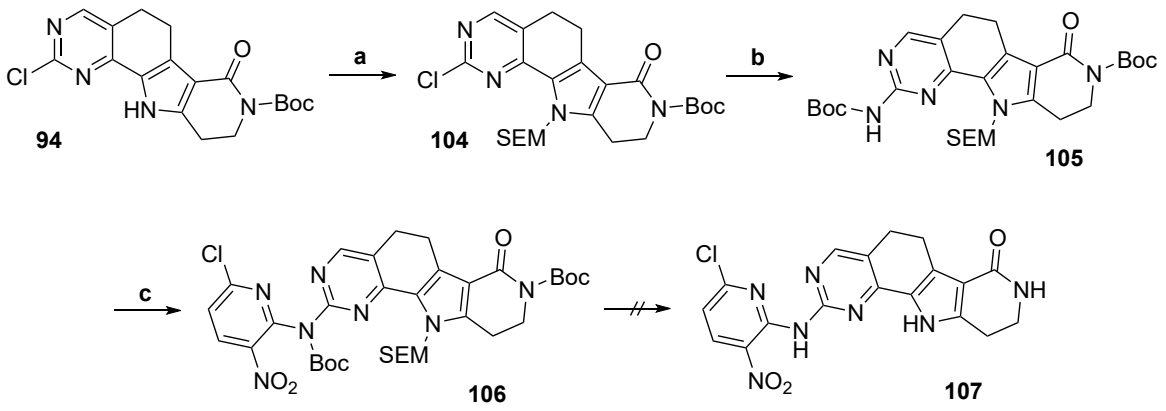

Scheme 10: Synthesis of the SEM-protected derivative; (a) SEM-Cl, NaH, DMF, rt, 18 h, 51%; (b) Boc carbamate, K_2CO_3, XPhos Pd G4, 1,4-dioxane/*t*BuOH (4:1), 90 – 100 °C, 42 h,36%; (c) 2-bromo-6-chloro-3-nitropyridine **103**, XantPhos Pd G4, Cs_2CO_3, toluene, 70 – 80 °C, 21 h, 16%.

heterocyclic nitrogens and can be cleaved by acids or flouride.[246] The attachment of this silyl-containing group (**104**) was achieved using SEM-chloride after deprotonation with sodium hydride. The two subsequent cross-coupling reactions to introduce the linker (step **b**, **105**) and the warhead (step **c**, **106**) afforded the desired products. However, the deprotection to isolate **107** was not successful, neither with TFA nor tetrabutylammonium fluoride.

3.3 Synthesis of Pyrrolopyridinone-Based Compounds

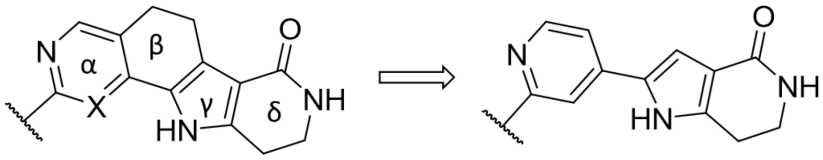

Scheme 11: General core structure of the tetracyclic core and the pyrrolopyridinone; X = C or N, labeling of the four rings α-δ adapted from REVESZ et al.[3]

To facilitate synthetic access and generation of SAR, we simplified the core structure by opening the partially saturated β-ring (Scheme 11). This derigidified pyrrolopyridinone based scaffold is found in inhibitors targeting MK2[206], and also used for targeting Cdc7[247], CK1γ[248], serine/threonine-protein kinase N2 (PKN2)[249]. In addition, several targets are mentioned in the patent literature.[250] The various possible substitution patterns allow for the introduction of selectivity promoting groups and expand the variety of applicable synthetic methods.

An overlay of the tetracyclic inhibitor **28** and the pyrrolopyridinone **21**, respectively, in the binding pocket of MK2, showed good alignment (Figure 34). Therefore, the warhead also should retain its orientation, when attached to the pyrrolopyridinone core. To verify the effective and covalent binding to the kinase the respective acrylamide **108** (Scheme 12), and its unreactive counterpart **109**, were synthesized first. In the following step the core structure was linked to the heterocyclic chloronitropyridine via the nitrogen atom, resulting in **110** (Scheme 12).

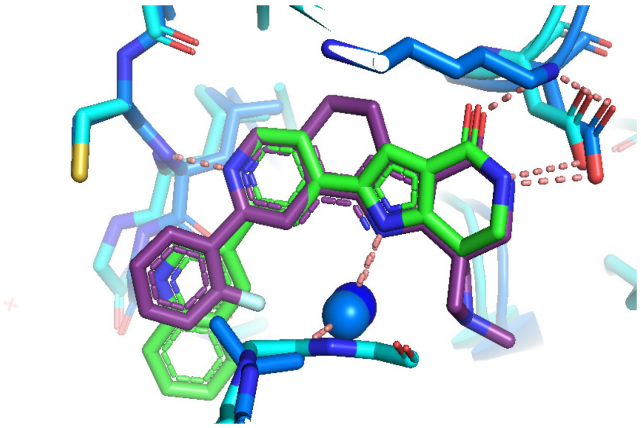

Figure 34: X-ray crystal structure overlay of two inhibitors bound to MK2. Tetracyclic inhibitor (**28**, colored in purple) bound to MK2 (colored in blue; PDB: 3M2W[1]) and pyrrolopyridinone-based inhibitor (**21**, colored in green) bound to MK2 (colored in turquoise; PDB: 2JBO[10]).

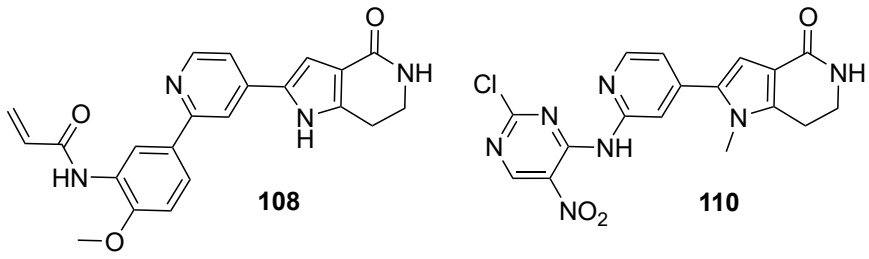

Scheme 13: Initially planned inhibitor structures **108** and **110** to proof the design hypothesis.

Two different synthetic routes (Scheme 13) were used to enable different derivatization strategies. The first route utilized the HANTZSCH pyrrole synthesis, which has already been employed to build up the tetracyclic cores (Scheme 1 and Scheme 7). The second variation involved a SUZUKI coupling to connect the pyridine (**III**) to the pyrrole part (**IV** in Scheme 13).

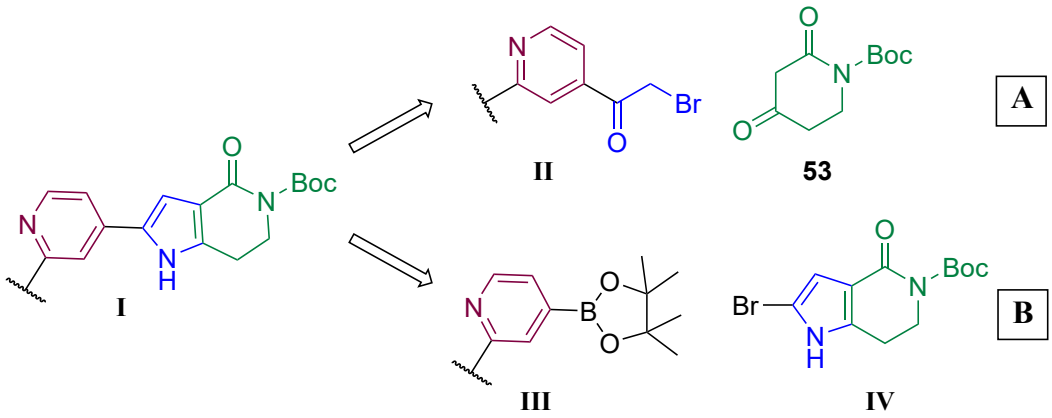

Scheme 12: General synthetic approaches to generate compounds with the pyrrolopyridinone core structure.

3.3.1 Synthesis of a Pyrrolopyridinone-based Inhibitor with an Acrylamide Warhead and the Corresponding Unreactive Analog

The pyrrolopyridinone core was synthesized from nicotinic acid *N*-oxide **111** using the general approach depicted in Scheme 13A. To enable ring closure by HANTZSCH pyrrole synthesis, the corresponding α-bromo ketone **115** was synthesized.

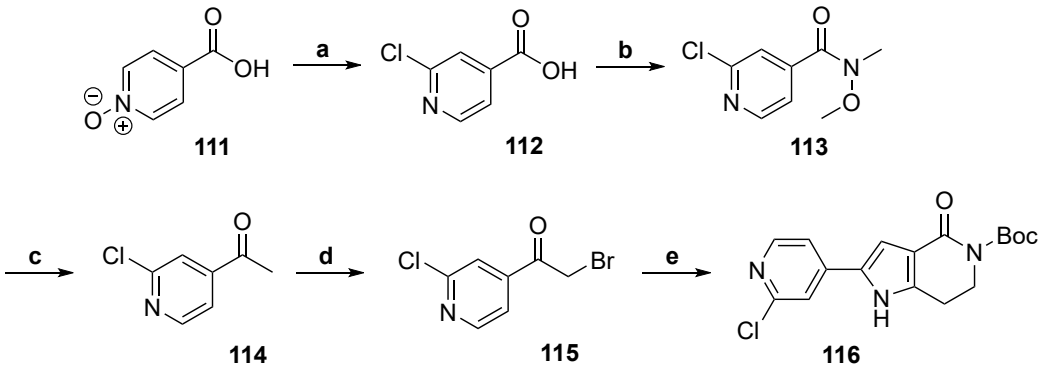

Scheme 14: Synthesis of the pyrrolopyridinone core **116**; (a) $POCl_3$, reflux, 7 h, 57%; (b) 1. $SOCl_2$, reflux, 5 h; 2. *N,O*-dimethyl hydroxylamine·HCl, NEt_3, DCM, 0°C to rt, 18 h, 91%; (c) MeMgBr, THF, 0°C to rt, 18 h, 93%; (d) 30% $HBr_{(HOAc)}$, Br_2, HOAc, rt, 2 h, 80%; (e) *tert*-butyl 2,4-dioxopiperidine-1-carboxylate **53**, NH_4OAc, EtOH, rt, 18 h, 48%.

The introduction of the chlorine at position 2 of the pyridine was carried out following the procedure described by ANDERSON *et al.* [251] Refluxing nicotinic acid *N*-oxide **111** in $POCl_3$ produced 2-chloronicotinic acid **112**. To convert the acid **112** into the ketone **114** using the WEINREB-NAHM ketone synthesis [252], the acid **112** was activated using $SOCl_2$ and transformed into the corresponding WEINREB amide **113**. [253] The WEINREB amid **113** was then reacted with methyl magnesium bromide in a GRIGNARD reaction to prepare the ketone **114** in good yields (93%). Subsequent α-bromination was performed following the procedure outlined by ANDERSON *et al.* [206] The resulting bromoketone **115·HBr** was isolated by filtration. The compound **115·HBr** was then cyclized with *tert*-butyl 2,4-dioxopiperidine-1-carboxylate **53** and ammonium acetate to yield the pyrrolopyridinone core in compound **116**.

The boronic acid pinacol esters of the substituted linker **76**/**78** were attached to the core **116** via a SUZUKI coupling using $(t\text{Bu})_3$P Pd G3 as the catalyst. The resulting compounds **117** and **118** were deprotected with TFA to yield compounds **108** and **109**.

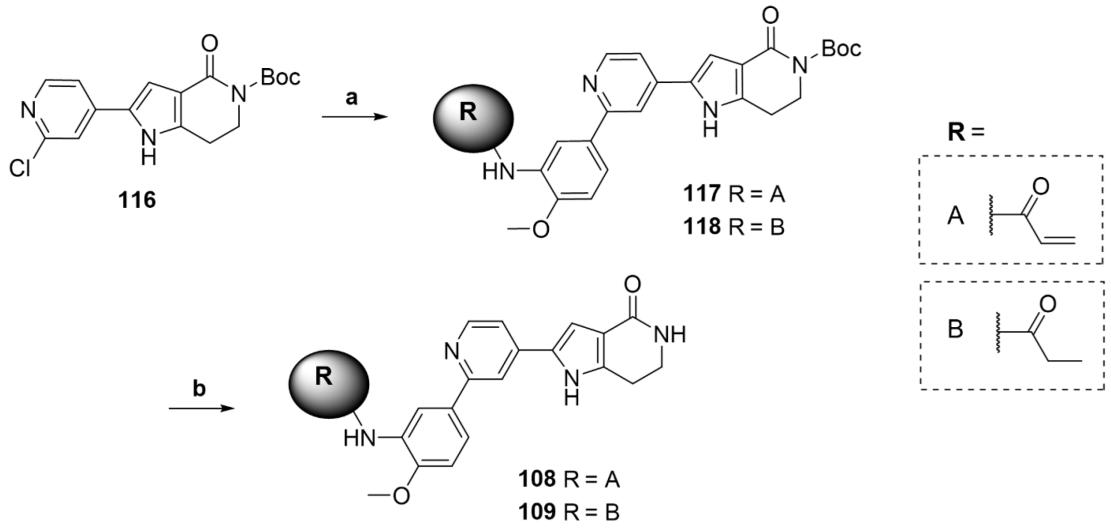

Scheme 15: Synthesis of a pyrrolopyridinone with an acrylamide warhead (**108**) and the unreactive control compound **109**; (a) **76**/ **78**, K_2CO_3, (tBu)$_3$P Pd G3, 1,4-dioxane/H_2O, 90 °C, 18 h; (b) TFA, DCM, rt, 15% (**108**)/ 35% (**109**) (over 2 steps)

3.3.2 Synthesis of Pyrrolopyridinone-based Inhibitors with Heterocyclic Warheads

After successfully synthesizing the acrylamide-based compound **108**, alternative heteroaromatic warheads were attached to the core to assess the structure–activity relationship (SAR). Starting from compound **110**, three sites were identified to be promising for further derivatization (Scheme 16). Replacing the warhead (red hexagon, Scheme 16) delivers insights into the correlation between the warhead's reactivity and inhibitory activity. Exchanging the linker atom (blue oval, Scheme 16) from nitrogen to an oxygen or sulfur can influence orientation of the warhead but also its reactivity, as well as physicochemical properties such as solubility. This was observed to be beneficial during the development of gamcemetinib (CC-9677, **20**), as discussed in section 1.4.4. [228] The substitution of the pyrrole nitrogen (golden triangle, Scheme 16) may offer a handle to fine-tune physicochemical properties but also affects inhibitory activity. A slightly unfavorable effect of the methyl group was observed for the tetracyclic acrylamides, consistent with the data published by REVESZ *et al.* on the

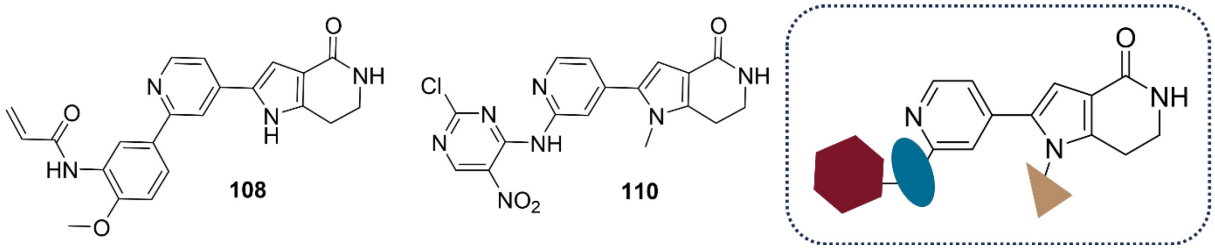

Scheme 16: Pyrrolopyridinone-based Inhibitors **108** and **110** and general structure with highlighted derivatization points (on the right).

tetracyclic scaffold. [3] Since the substitution of this hydrogen atom is necessary in several synthetic steps, the methyl group can be considered a compromise between synthetic convenience and inhibitory activity. Different attempts to replace the methyl group will be discussed in section 3.3.2.4.

3.3.2.1 Synthesis of Nitrogen-linked Pyrrolopyridinone Derivatives

Three different synthetic strategies were used to synthesize the key intermediate **119**, which contains the Boc-protected linking nitrogen, (Scheme 17). The mono-Boc protection of the nitrogen is necessary to prevent double attachment of the warhead, as mentioned previously (section 3.2.1). The attempt to introduce the carbamate via BUCHWALD coupling using *tert*-butyl carbamate to the chloride-containing precursor **120** was unsuccessful. Therefore, a three-step synthetic route, as shown in Scheme 19, was developed. The increased reactivity of the bromine derivative **121** in cross-coupling reactions was exploited, which was also beneficial for the introduction of the sulfur linker (explained in section 3.3.2.3). This was encouraging to re-investigate the initial synthetic strategy and finally enabled the direct attachment of the Boc-protected amine (Scheme 17A). Through optimization of the catalyst combination, the product **119** was isolated in satisfactory yield. An alternative approach was also developed (Scheme 17B) due to the initial problems with introducing the linker nitrogen at a late stage. Here, the protected nitrogen was attached in the first step before building up the core through the cyclisation method described for the halogenated derivatives (Scheme 14). The third strategy involves a SUZUKI cross-coupling reaction (Scheme 17C) where the protected amine was attached to the pyridine beforehand and then linked to the pyrrole-containing part.

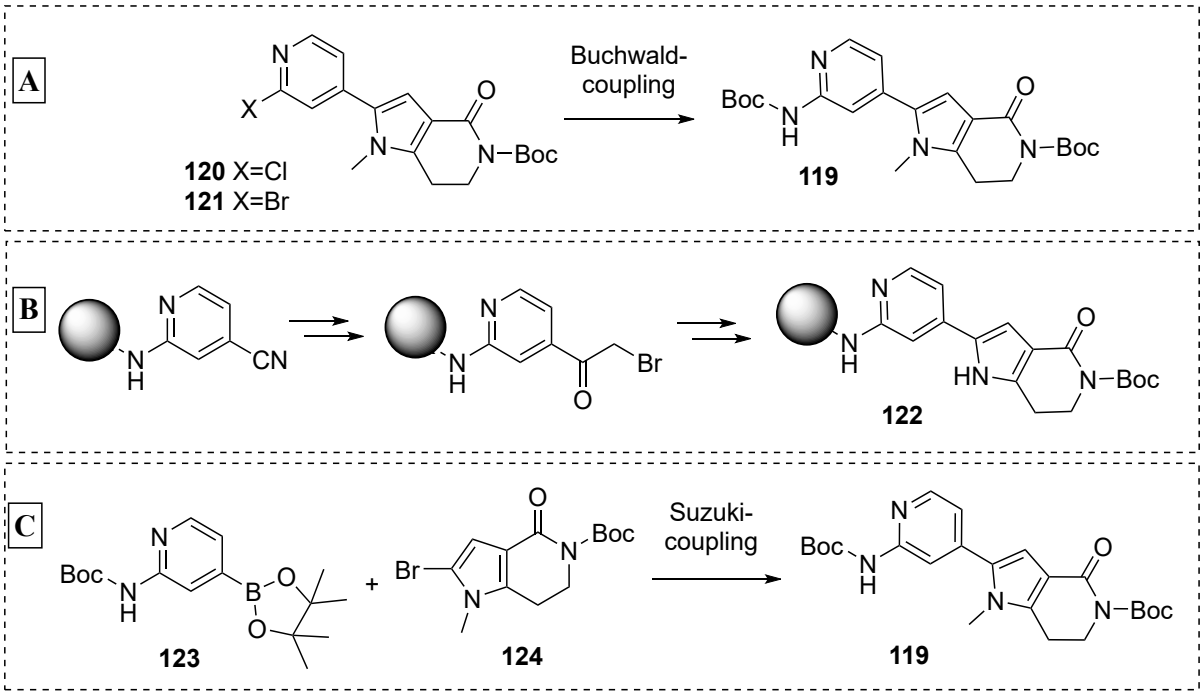

Scheme 17: Different approaches for the synthesis of amine-containing core **119**/**122**.

3.3.2.1.1 Introduction of the Nitrogen Linker via BUCHWALD Coupling

The synthesis of key intermediate **116** works well and was therefore initially identified as a suitable precursor for the warhead attachment. To prevent side reactions and interference with the catalyst in cross-coupling reactions [242a, 254], the pyrrole nitrogen was again methylated (Scheme 18). However, the attempted subsequent BUCHWALD coupling of **120** using Boc-carbamate as an ammonia surrogate did not work out, in line with the results previously obtained with the tetracyclic scaffold. Only partial conversion was achieved and due to problems in purification by column chromatography no pure product could be isolated.

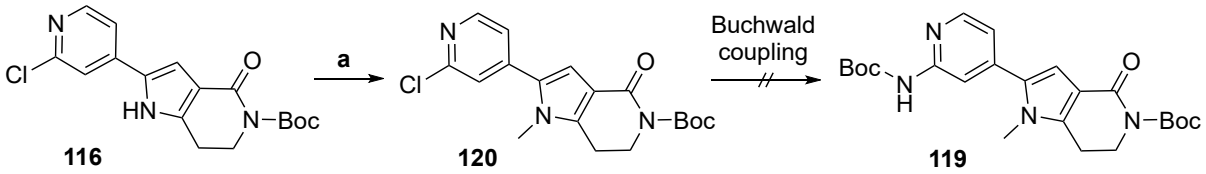

Scheme 18: Methylation of **116** and the planned subsequent coupling attempt; (a) CH_3I, Cs_2CO_3, DMF, rt, 18 h, 62%.

The low reactivity of the chlorine in oxidative additions, as previously observed for the tetracyclic derivatives (refer to section 3.1), would require harsher reaction conditions, including a higher temperature (> 100 °C) and potentially a stronger base. However, elevated temperatures and stronger bases are likely to result in increased side reactions and instability of the starting material, amongst others through loss of the Boc group. The successful conversion of **120** in a BUCHWALD-type reaction (step **a**, Scheme 19) was again achieved by exchanging the carbamate to the benzyl carbamate, resulting in Cbz-protected product **125**. The Cbz-protecting group was removed through hydrogenation before introducing the warhead moiety, as the latter is not stable under the required conditions. This process

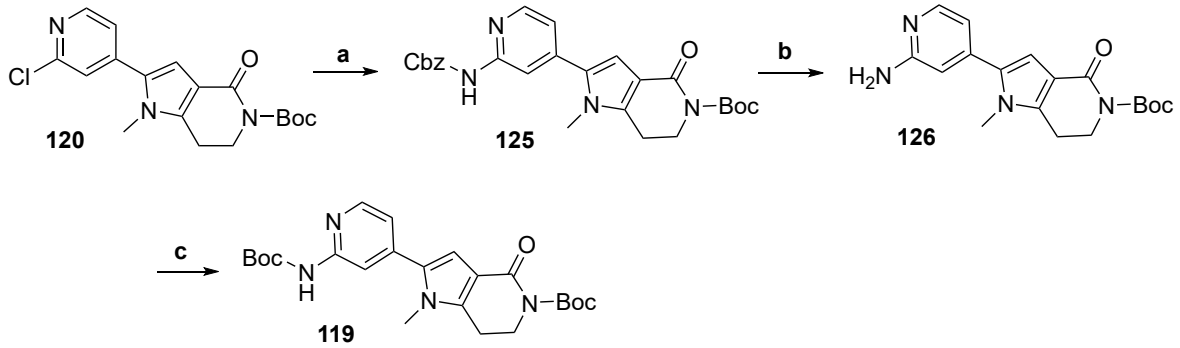

Scheme 19: Three step synthesis of **119** from **120**; a) benzyl carbamate, Cs_2CO_3, XantPhos, $Pd(OAc)_2$, 1,4-dioxane, 120 °C, 18 h, 56%; (b) Pd/C, H_2, MeOH, rt, 18 h, 90%; (b) Boc_2O, *t*BuOH, rt, 18 h, 87%.

involved two additional steps: deprotecting to the free amine **126** and the subsequent protection with di-*tert*-butyl dicarbonate (Boc_2O) to obtain the desired intermediate **119**. The selective attachment of a single Boc-group at the nitrogen required careful addition of the anhydride. Unfortunately, this synthetic approach resulted in a purity of only approximately 85% (HPLC) for **119** due to partial double attachment of the Boc group.

Therefore, the synthetic route was modified to improve the results. The Boc protection group was introduced to *NH*-acidic intermediate **125** under basic conditions using DMAP as the catalyst before removing the Cbz group. The selective deprotection of **127** through hydrogenation was successful, resulting in the key intermediate **119**.

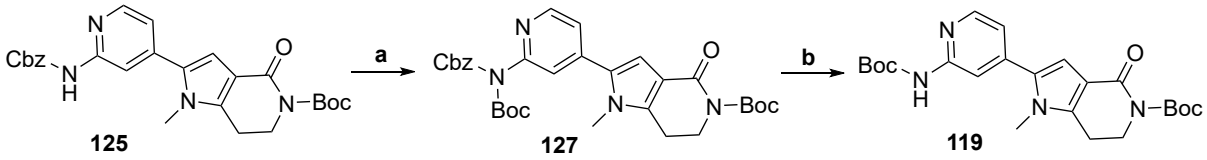

Scheme 20: Adjusted synthetic route for **119**; (a) Boc_2O, DMAP, TEA, ACN, rt, 18 h, 93%; (b) Pd/C, H_2, MeOH, rt, 2 h, 61%.

However, the additional steps required resulted in a decrease in overall yield. Furthermore, the upscaling of the initial BUCHWALD coupling with benzyl carbamate proved to be challenging, and the search for more robust conditions was unsuccessful. To enhance the reactivity of the of the hinge-binding heterocycle for this conversion the chlorine atom was replaced with a bromine, which is more reactive in cross-coupling reactions.[255] The respective bromo derivative **132** was synthesized in a similar manner to the chloro-substituted analog **116** (Scheme 14 and Scheme 21). The synthetic route started from the carboxylic acid **128**. The synthesis of the methyl pyridine ketone **130** was previously described in the literature.[256] To activate the carboxylic acid **128**, 1,1'-carbonyldiimidazole (CDI) was used, and the acid was converted to the WEINREB amide **129** with *N,O*-dimethyl hydroxylamine. The WEINREB-NAHM reaction with methyl magnesium bromide yielded the methyl ketone **130** in good yields (88%). The α-bromination method, adapted from HAY *et al.*[257], was successful even at a reduced temperature of 40 °C. The reaction of *tert*-butyl 2,4-dioxopiperidine-1-carboxylate **53** and NH_4OAc with the hydrobromic salt of **131** yielded pyrrolopyridinone **132**, which was isolated through filtration. The synthetic route for **132**, similar to that of the chloro-derivative **116** (Scheme 14), only required a single column chromatographic purification, i.e. of the ketone intermediate **130**.

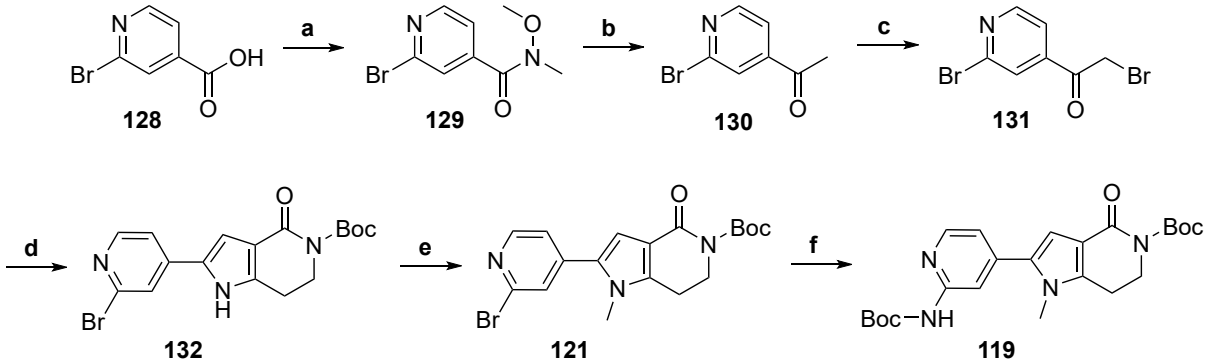

Scheme 21: Synthesis of the bromopyridinyl-pyrrolopyridinone core **132** and introduction of the amine (**119**): (a) 1. CDI, DCM, rt, 2 h; 2. *N,O*-dimethyl hydroxylamine·HCl, rt, 18 h, 96%; (b) MeMgBr, THF, 0°C, 2 h, 88%; (c) 30% $HBr_{(HOAc)}$, Br_2, HOAc, 15 °C to 40 °C, 1 h + 1 h, 98%; (d) *tert*-butyl 2,4-dioxopiperidine-1-carboxylate **53**, NH_4OAc, EtOH, rt, 18 h, 57%; (e) CH_3I, Cs_2CO_3, DMF, rt, 2 h, 91%; (f) Boc-carbamate, Cs_2CO_3, XantPhos Pd G4, XantPhos, 1,4-dioxane, 85 °C, 6 h, 51%.

After methylating the pyrrole in **132**, the Boc-protected amine was introduced using a BUCHWALD cross-coupling. Initial attempts with XPhos Pd G4 as the catalyst system did not result in the formation of the product **119**. However, when the XantPhos ligand was used instead, product formation was detected. The combination of XantPhos Pd G4 (5 mol%) and XantPhos ligand (5 mol%) increased product formation, but longer reaction times led to increased side product formation. Further attempts to improve the method, showed that decreasing the catalyst loading had the same effect. Additionally, increasing the amount of Boc-carbamate (from 2.00 to 3.00 equivalents) also resulted in higher formation of a by-product, whilst lowering the reaction temperature from 100 °C to 85 °C reduced the formation thereof. The optimized conditions enabled to isolate **119** with a yield of 51%.

3.3.2.1.2 Introduction of the Nitrogen Linker at an Early Stage

To overcome the initial challenges of introducing the nitrogen, a complementary approach was developed to introduce the amine at an early stage. In the first step the protected amine, 4-methoxybenzylamine **134**, was introduced through a nucleophilic aromatic substitution at 2-chloro-4-cyanopyridine **133**. The subsequent GRIGNARD reaction of the cyano group in **135** produced the methyl ketone **136**. The α-bromination of the carbonyl in acetic acid concomitantly removed the *p*-methoxybenzyl group. As a result, the product **137** contains the primary aromatic amine. To form **138**, the pyrrole ring was closed using *tert*-butyl 2,4-dioxopiperidine-1-carboxylate **53** and ammonium acetate, as previously described (Scheme 1, Scheme 6 and Scheme 14). To enable the single attachment of the warhead a mono-protection strategy was planned and developed, resulting in the isolation of key intermediate **139** with an unmethylated pyrrole. However, this strategy was not pursued further due to the low yields and the need for an additional step to protect the pyrrole.

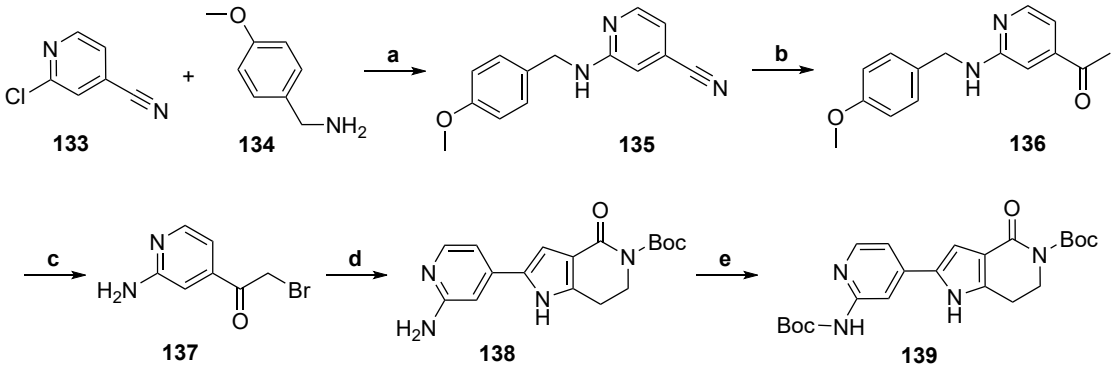

Scheme 22: Early-stage introduction of the amine; (a) DIPEA, *N*-methyl-2-pyrrolidinone (NMP), 120 °C, 18 h, 23%; (b) MeMgBr, Et_2O, reflux, 18 h, 82%; (b) 30% $HBr_{(HOAc)}$, Br_2, HOAc, 70 °C, 2 h, 80%; (d) *tert*-butyl 2,4-dioxopiperidine-1-carboxylate **53**, NH_4OAc, EtOH, rt, 18 h, 68%; (e) Boc_2O, *t*BuOH, rt, 6 h, 27%.

An acid-stable group at the amine was expected to remain intact during the entire buildup of the core, reducing disruptive influences and increasing the yield. In this approach benzylamine was used instead of its *p*-methoxybenzyl analog as the protected amine to synthesize **140** from 4-chloro-4-cyanopyridine **133** (Scheme 23). The subsequent step to generate the ketone **141** through a GRIGNARD-reaction worked as described above. The bromination using Br_2/HBr in HOAc produced the hydrobromide salt of **142**. Unlike the 4-methoxy benzyl group in **135**, which is not stable under these conditions (Scheme 22), the benzyl group is preserved. The pyrrolopyridinone derivative **143** was again obtained through subsequent condensation reaction with *tert*-butyl 2,4-dioxopiperidine-1-carboxylate **53**. Both free NH positions were then protected with a Boc group, resulting in the successful isolation of fully protected **144**. To attach the warhead, the benzyl group had to be selectively removed. However, the benzyl group was more stable under the selected conditions and could not be removed. Attempts to use palladium on charcoal and hydrogen under atmospheric pressure for reductive removal only resulted in trace amounts of conversion, which were detected by TLC-MS. This approach was thus abandoned due to the difficulties in the last deprotection step and the low yields (29% for introduction of the amine (step **a**, **140**) and 31% for the Boc-protection (step **e**, **144**)).

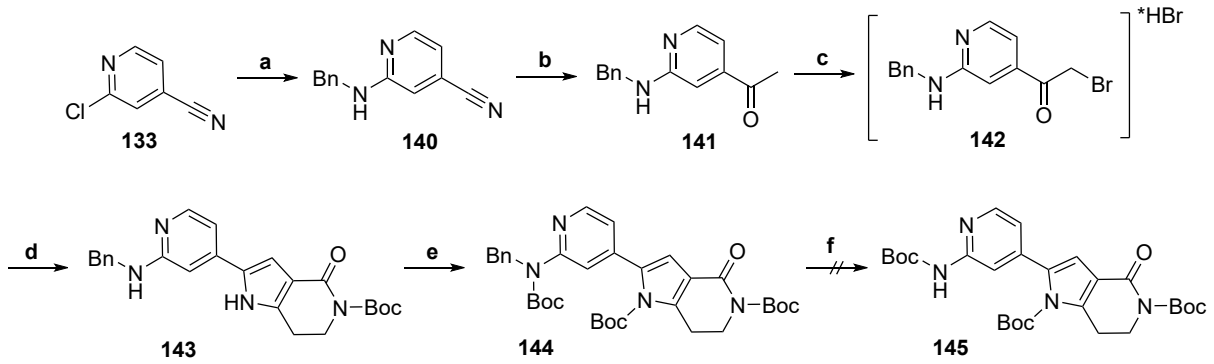

Scheme 23: Synthesis of the benzyl protected amine core; Bn = benzyl; (a) benzylamine **45**, NMP, DIPEA, 120 °C, 18 h, 29%; (b) MeMgBr, Et_2O, reflux, 18 h, 50 %; (b) 30% $HBr_{(HOAc)}$, Br_2, HOAc, 70 °C, 2 h, 90%; (d) *tert*-butyl 2,4-dioxopiperidine-1-carboxylate **53**, NH_4OAc, EtOH, rt, 18 h, 40%; (e) Boc_2O, TEA, DMAP, ACN, rt, 23 h, 31%; (f) Pd/C (10% wt), H_2, EtOH, rt, 18 h.

3.3.2.1.3 Synthesis of the Pyrrolopyridinone Core via SUZUKI Coupling

An alternative synthetic route was sought due to the difficulties encountered in incorporating the linking nitrogen. Linking the two aromatic heterocycles via SUZUKI coupling was identified as a complementary approach. The synthesis of the pyrrole component was adapted from the patent literature [258] and is depicted in Scheme 24. To this end, enamine **147** was obtained by condensing *tert*-butyl 2,4-dioxopiperidine-1-carboxylate **53** with aminoacetaldehyde dimethyl acetal **146**. The pyrrole ring in **148** was subsequently closed under acidic conditions via an intramolecular aldol condensation. In the next step, Boc protecting groups were attached to both nitrogen atoms resulting in **149**. Subsequently, the Boc protecting group at the pyrrole ring was selectively removed, resulting in the mono-protected bicyclic structure **150**. This selective cleavage was achieved by applying a mild deprotection procedure using ammonia. Typically, strong acids like HCl or TFA are used to remove the Boc-protecting group, but in this case, nucleophilic alkaline conditions were used to enable selective removal. [246b] Several alternative cleavage methods using nucleophilic or basic conditions are known for heterocycles, including pyrrole. [246a, 259] ROUTIER *et al.* suggested a nucleophilic attack at the carbonyl center of the carbamate by a nucleophile. [259] Considering this as the underlying mechanism, two properties primarily account for the preference of the deprotection pyrrole nitrogen in this case. The carbamate nitrogen's is part of the aromatic system of the pyrrole ring, which increases electrophilicity at the carbonyl and weakens the amide bond. Furthermore, the aromatic ring has favorable leaving group properties in the

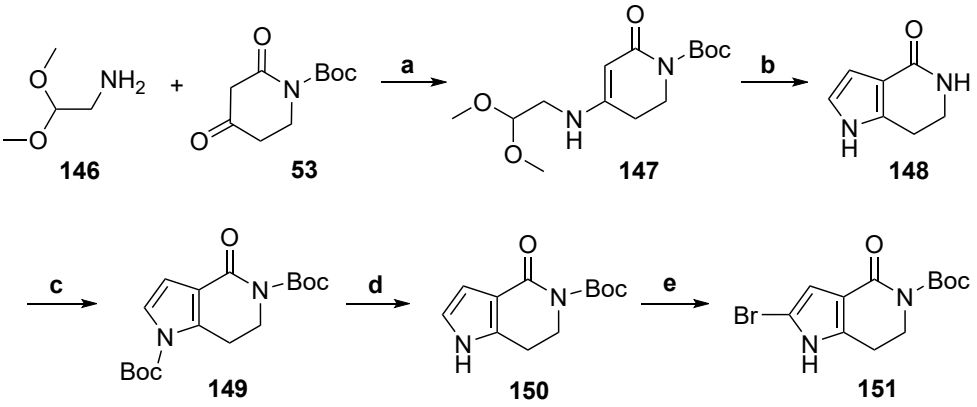

Scheme 24: Synthesis of the brominated precursor **151** for the SUZUKI-coupling to synthesis the pyrrolopyridinone core; (a) toluene, 70°C, 18 h, 99.5%; (b) TFA, DCM, 0 °C to rt, 2 h, 91%; (c) Boc_2O, DMAP, TEA, ACN, rt, 18 h, 49%; (d) $NH_{3(aq)}$, MeOH, reflux, 6 h, 85%; (e) NBS, THF, -70 °C, 30 min, 66%.

subsequent elimination step. It was crucial to balance temperature, reaction time, and the amount of the base to ensure selective, but complete cleavage of the pyrrole protection, while retaining the protecting group at the lactam. The procedure for bromination in the next step (Scheme 24, step **e**) was adapted from the literature. [260] *N*-Bromosuccinimide (NBS) was used in a solvent mixture of THF and methanol. To reduce double halogenation, it is necessary to cool the reaction due to the high reactivity of pyrrole towards electrophilic aromatic substitution. [261] The starting material can be easily separated from the mono-brominated product by column chromatography. However, the double-brominated derivate

displays similar behavior during chromatographic purification. Therefore, it is beneficial to ensure continuous stirring, even cooling, and to use less than 1.00 equivalent of NBS to isolate the pure mono-brominated product.

Using NBS as the brominating agent allows for selective substitution at the α-position of the pyrrole ring. [262] The latter is the kinetically favored substitution position, while the β-position is thermodynamically preferred. [263] Bromination at the β-position can be detected when using bromine (Br_2) as the brominating agent. A mixture of the α- and β-substituted pyrrole (and the results of multiple bromination) was isolated in this case, due to rearrangement under strongly acidic conditions after *in situ* generation of HBr. [264] The electrophilic attack at the α-position is preferred due to the mesomeric stabilization of the intermediate σ-complex (Scheme 25). [261, 265]

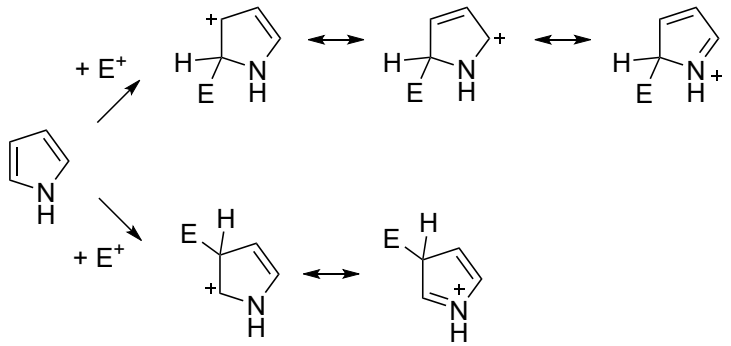

Scheme 25: Mesomeric stabilization of the σ-complex after electrophilic attack at the pyrrole at the α- and β- position, respectively.

The regiochemistry of the bromination was characterized by nuclear magnetic resonance spectroscopy (NMR). The remaining aromatic signal in the ^{1}H-spectrum indicates halogenation of the α-position as it gives a singlet, indicating no hydrogens at the neighboring atoms. As coupling with *NH* groups is often not visible in NMR experiments, **120** as synthesized as a reference compound. The same structure **120** was also synthesized using the procedure described in Scheme 14 and subsequently methylated (Scheme 18). The pyrrole nitrogen in **151** was therefore methylated and the resulting bromide **124** reacted with

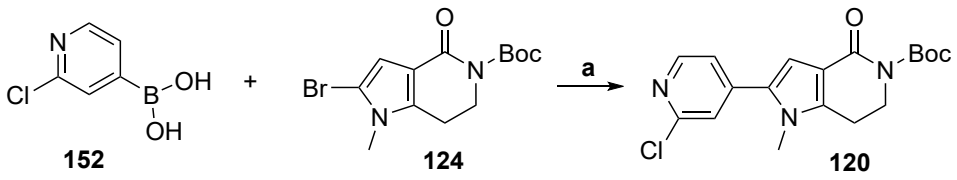

Scheme 26: Synthesis of the reference compound **120** using the SUZUKI coupling protocol; (a) Na_2CO_3, $Pd(dppf)Cl_2 \cdot CH_2Cl_2$, 1,4-dioxane/$H_2O$, 80 °C, 4 h, 40%.

(2-chloropyridin-4-yl)boronic acid **152** (Scheme 26) resulting in compound **120** to further confirm formation of the correct bromination derivative. The analytical data, particularly the NMR spectra, were compared to confirm the structural identity and the correct bromination position.

Prior to performing the SUZUKI coupling to link the pyrrole to the pyridine, it is necessary to protect the pyrrole-*NH* of the key intermediate **151** or to substitute the hydrogen. For the initial series, the methylated derivative **124** was utilized. The methylation was successfully carried out in DMF using methyl iodide as the methylating agent (Scheme 27).

The boronic acid required for the coupling was be obtained as the pinacol ester **123** through a two-step synthesis (Scheme 27). First, 2-amino-4-bromopyridine **153** was protected using Boc_2O. The resulting Boc-protected aminopyridine **154** was transformed into the boronic acid pinacol ester **123** using a MIYAURA borylation procedure (Scheme 27, step **c**). Finally, the pinacol ester **123** was reacted with aryl bromide **124** in a SUZUKI coupling, resulting in the amine-substituted core **119**. The reaction outcome is primarily limited by the debromination of the pyrrole. Therefore, the purity of the boronic acid derivative is crucial. Any remains of the borylation agent increase the rate of debromination. This observation and optimization of this reaction type is further discussed in section 3.3.2.2.

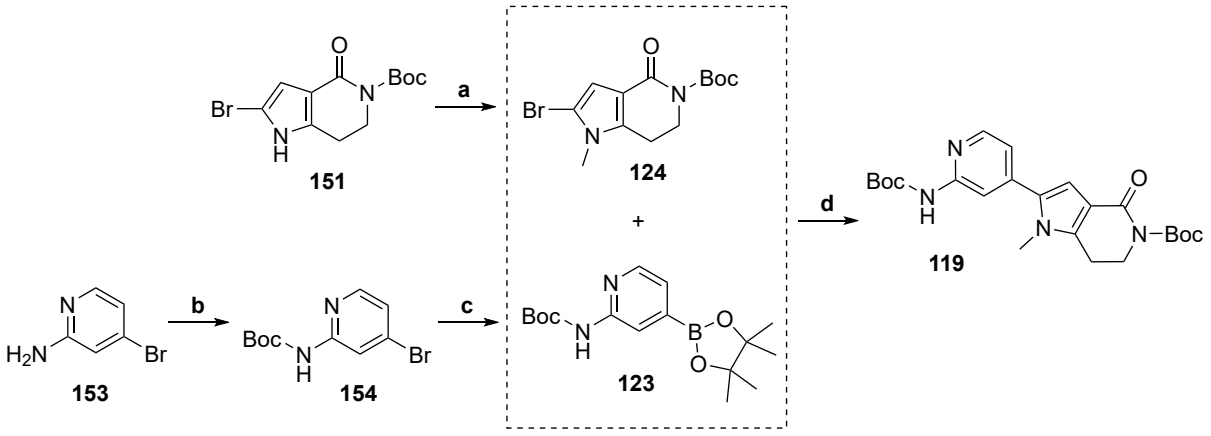

Scheme 27: SUZUKI coupling for the synthesis of **119**; (a) CH_3I, Cs_2CO_3, DMF, 0 °C to rt, 2 h, 88%; (b) Boc_2O, *t*BuOH, 50 °C, 4 h, 80%; (c) B_2pin_2, KOAc, XPhos Pd G4, 1,4-dioxane, 90 °C, 18 h, 54%; (d) Na_2CO_3, XPhos Pd G4, 1,4-dioxane/H_2O, 90 °C, 18 h, 40%.

When comparing the three synthetic strategies for the synthesis of **119** depicted in Scheme 17 and explained in the last three sections, it was found that the BUCHWALD coupling of the brominated pyridine **121** with *tert*-butyl carbamate was the most suitable approach to obtain the key intermediate. The synthesis of the core **132**/**121** only required chromatographic purification twice and avoided the use of large quantities of aggressive chemicals (such as TFA for the synthesis of **148** as precursor for **124**). The results of a first attempt to increase the scale (multigram scale) were encouraging.

3.3.2.1.4 Introduction of Heterocyclic Warheads to the Aminated and Methylated Core

The proto warhead 2-bromo-5-chloro-3-nitropyridine **103** was attached to **119** via a BUCHWALD-HARTWIG cross-coupling protocol, which was established and optimized for the synthesis of the S6K2

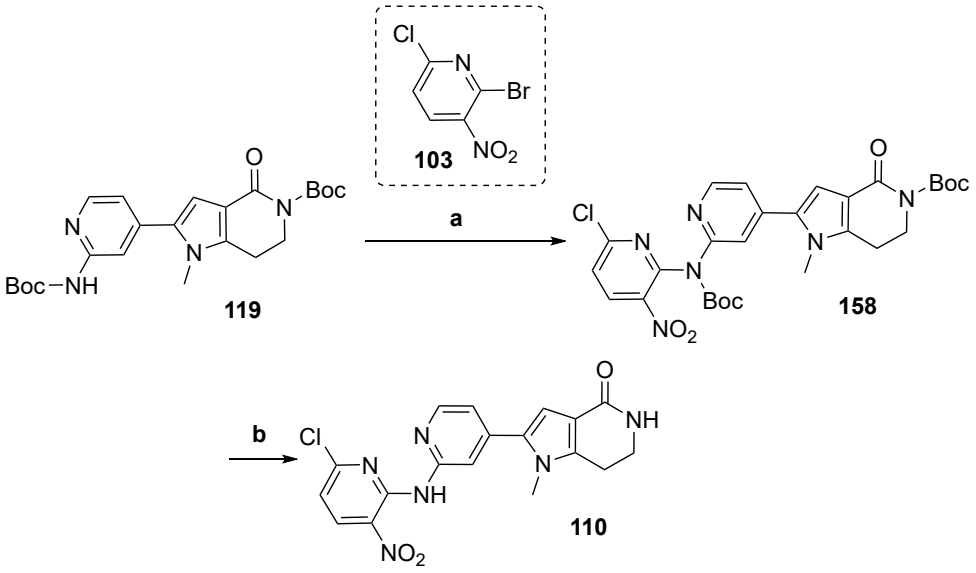

Scheme 28: Attachment of the warhead and global deprotection; (a) 2-bromo-6-chloro-3-nitropyridine **103**, Cs_2CO_3, XantPhos Pd G4, toluene, 60 °C, 18 h, 98%; (b) TFA, DCM, rt, 15 min, 68%.

inhibitor **39**, containing the same warhead moiety.[225] The procedure was successfully applied to this project, resulting in the Boc-protected coupling product **158** in excellent yields (98%). The desired compound **110** was obtained after removing both protection groups using TFA in DCM (Scheme 28). Fine-tuning of the reactivity can be achieved by changing the heterocycle or the leaving group of the warhead part. To explore the influence of the differences in reactivity between the different halogens, the respective bromo and fluoro derivatives **155** and **156** were synthesized. Additionally, the unreactive control compound **157**, which lacks the leaving group at the pyridine, was synthesized.

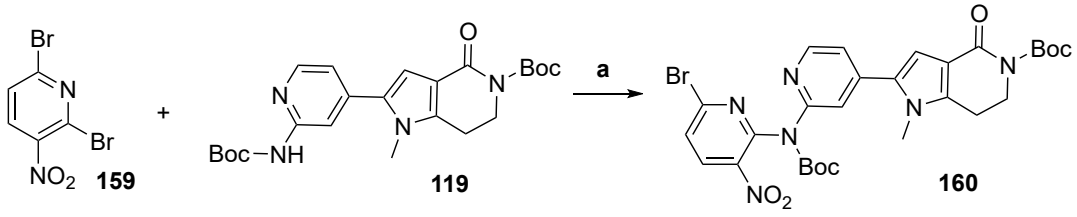

Scheme 29: Synthesis of compound **160** containing a bromine atom as leaving group; (a) Cs_2CO_3, XantPhos Pd G4, toluene, 70 °C, 18 h, 35%.

At first, the bromo derivative of **110** was prepared. Therefore, the dibromopyridine **159** was attached to the inhibitor core using a BUCHWALD-coupling method (Scheme 29). However, the purification of **160** proved to be more challenging due to the competing substitution at the C6 of the proto warhead, which occurred as a side reaction and could not be completely avoided. As a result, the yield and purity of the isolated compound **160** were rather low. Optimization of the reaction temperature could possibly improve the outcome of the reaction.

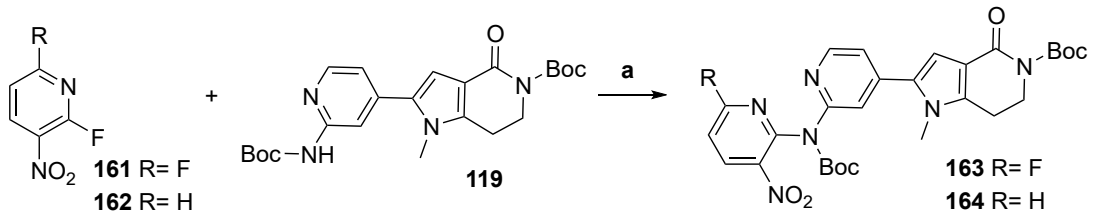

Scheme 30: Attachment of the warhead via S_NAr reaction; (a) NaH, DMF, 0 °C to rt, 3 d/ 18 h.

The respective fluorine derivative **163** and the unreactive control **164** were synthesized via a nucleophilic aromatic substitution (Scheme 30). The nitropyridines **161**/**162** contain a fluorine as the leaving group, which generally displays good properties for S_NAr reactions enabling the transformation at room temperature (rt) after deprotonation of the *NH*-acidic amino nucleophile.

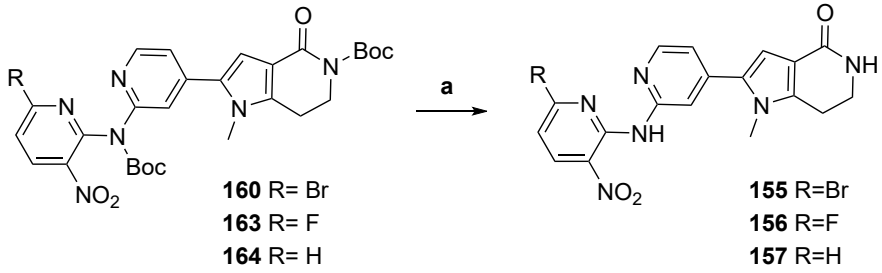

Scheme 32: Removal of the protecting groups to finalize compounds **155**, **156** and **157**; (a) TFA, DCM, rt, 30 min, 22-63%.

The three derivatives **155**, **156** and **157** were subsequently obtained by following the previously described procedure for removing the two protecting groups (Scheme 32). During the purification of the fluoro analog **156**, caution was necessary due to the increased reactivity of the fluorine. Unwanted substitution can occur in the presence of nucleophiles, such as H_2O or MeOH, especially under basic or acidic conditions and elevated temperatures, as depicted in Scheme 31.

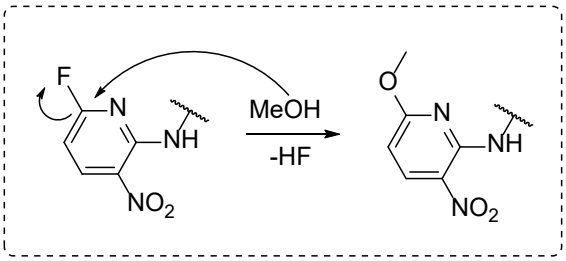

Scheme 31: Reaction of **156** with methanol via S_NAr.

In addition to halopyridines, sulfonylpyri(mi)dines are suitable electrophilic warheads for targeting cysteine residues.[266] MAUREL *et al.* described the synthesis of the sulfone from the corresponding chloro-derivative.[267] Following their procedure, sodium methanethiolate was used to introduce a

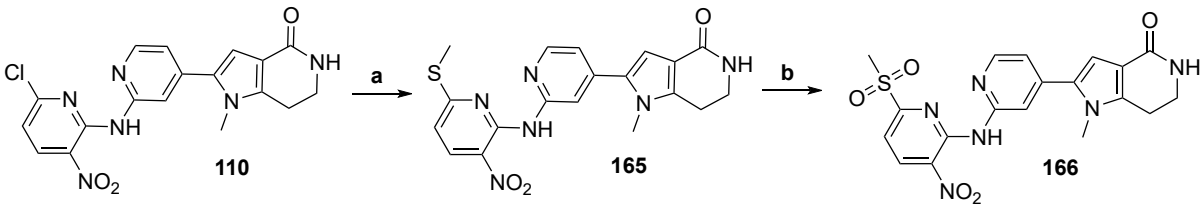

Scheme 33: Synthesis of the sulfone pyridine; (a) $NaSCH_3$, DMF, rt, 18 h, 57%; (b) *m*CPBA, DCM, 0 °C to rt, 3 h.

methylthiol to **110**. The resulting intermediate, **165**, was then oxidized with *meta*-chloroperoxybenzoic acid (*m*CPBA) to form the sulfone **166**. The final step has potential for further optimization, which was, however, not elaborated further due to time constraints. Adapting the added amount of *m*CPBA and reaction conditions to give complete oxidation to the sulfone without formation of an *N*-oxide should increase the yield. Furthermore, the high S_NAr reactivity of the sulfonyl group should be respected during workup and replacing the aqueous conditions could be beneficial.

3.3.2.2 Synthesis of Oxygen-linked Compounds

Replacing the nitrogen atom with an oxygen atom as the attachment point of the warhead could expand SAR analysis and potentially improve solubility due to higher flexibility and lack of the pseudobicyclic arrangement imposed by the aforementioned intramolecular hydrogen bond. The synthetic approach used for the nitrogen-linked compounds (Scheme 27), which is based on a SUZUKI coupling of the bromo pyrrole and the pyridin boronic acid, was retained. However, additional considerations were necessary for the oxygen-linked structures.

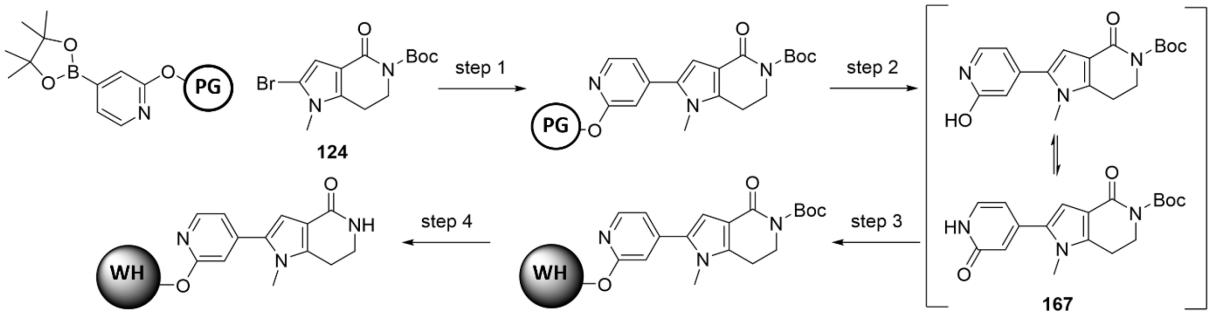

Scheme 34: Planned route for the synthesis of oxygen-linked compounds.

An initial attempt to directly borylate and couple the pyridin-2-one (2-hydroxy pyridine) moiety, as described in the literature [268], was unsuccessful. Therefore, a protected derivative was used (step 1, Scheme 34). The choice of the protecting group should enable selective deprotection (step 2), while maintaining protection of the lactam nitrogen. The benzyl group was used, enabling selective reductive removal. The introduction of the heterocyclic warhead (step 3) represents the key step of the synthesis. The attachment of the warhead is complicated by the lactam-/lactim tautomerism of the 2-pyridone/2-hydroxypyridine, which adds the challenge of *O*-selectivity.

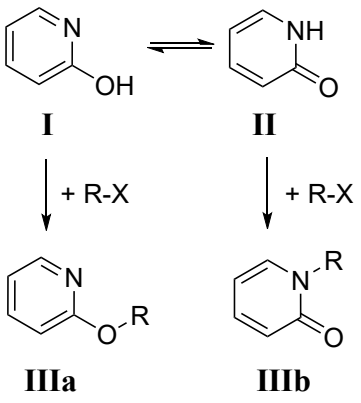

Scheme 35: Lactam-/ lactim tautomerism of pyridine-2-one (**II**) and the resulting substitution products (**III**).

Due to the presence of pyridin-2-one (**II**)/pyridin-2-ol (**I**) in diverse bioactive molecules, their reactions have been a subject of research for a long time. [269] In the gas phase, the 2-hydroxypyridin (**I**) was calculated to be the more stable tautomer. [270] But only the pyridinone (**II**) is present in crystals and is also the preferred tautomer in solution. The ratio of the two tautomers in solution depends on various factors

such as temperature, concentration, matrix and solvent, which influence pH and solvation. [270-271] The same applies to the substitution reaction, where the solvent and temperature can affect the amount of *N*- (**IIIb**) versus *O*-substitution (**IIIa**). [272] Quantum chemical calculation revealed that the *N*-substitution is thermodynamically favored, while a slightly higher intrinsic reactivity was calculated for the *O*-substitution. [273]

Nonetheless, some *O*-selective/preferring arylation and alkylation reactions are described in the literature. [269] While the position is not influenced by the leaving group at the electrophilic center [272a], the substitution pattern plays an important role, mainly for steric reasons. [272c, 274] The *N*-substitution is more sterically demanding, therefore *ortho*-substitution, *tert*-alkylhalids and demanding ligands in copper-catalyzed reactions favor *O*-substitution. [274-275] Selective *O*-arylation has been achieved using diaryliodonium salts [274a, 276], boronic acids [275] and aryl halides [274b], with the latter two utilizing copper catalysis for the reaction. Selective *O*-alkylation was described using gold catalysis [277], zinc(II) for benzyl-derivatives [278] and a microwave-assisted method utilizing silver carbonate. [279] The preference for *O*-alkylation when using silver carbonate compared to alkali salts was already observed by KORNBLUM *et al.* [280] in the 1950s. They attribute this to the ability of the silver salts to increase the carbenium character of the aryl halide. As a result, the reaction occurs at the position with higher electron density, in this case the oxygen, due to the increasing S_N1-character of the reaction. BREUGST and MAYR later revised this theory, suggesting the coordination of the silver ion, which hinders the *N*-substitution. In addition to the selectivity issues, identifying the resulting isomers, especially for more complex molecules, is not straightforward. The resulting shifts in the ^{13}C-NMR do not allow for clear differentiation, requiring more complex 2D-NMR experiments and interpretation of the IR (infrared) spectra for product identification. [271d, 273]

The first part of the synthesis was the preparation of the ether-substituted pyridine boronic acid **170**. To avoid the selectivity issue, mentioned in the previous section, the oxygen-atom was introduced via an S_NAr reaction by using benzyl alcohol (Scheme 36, step **a**) based on a literature procedure [281]. The borylation of **169** proceeded as anticipated, yielded the boronic acid pinacol ester **170** in good yields.

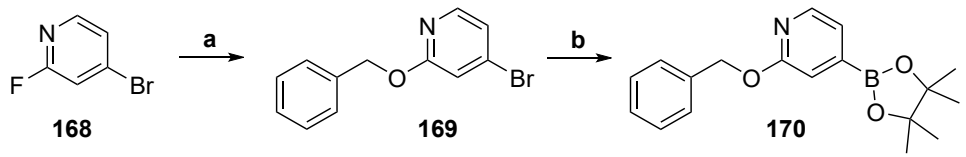

Scheme 36: Synthesis of the oxygen-containing hinge binder moiety; (a) benzyl alcohol, KO*t*Bu, THF, 0°C to rt, 18 h, 95%; (b) B_2pin_2, KOAc, XPhos Pd G4, 1,4-dioxane, 90 °C, 18 h, 71%.

The SUZUKI cross-coupling to obtain **171** was performed as shown in Scheme 37. Debromination of **124** was observed as a side reaction. It has been reported that electron-rich heterocycles tend to undergo dehalogenation in palladium-catalyzed reactions, either as a byproduct or as the desired outcome. [282] JEDINÁK *et al.* investigated the influence of several reaction parameters on the rate of dehalogenation of halopyrazoles. [282d] They found that the choice of base and temperature were important factors, as well

as the solvent and the catalyst system to reduce unwanted dehalogenation. Among the examined catalyst systems (XPhos Pd G4, $Pd(dppf)Cl_2$, XantPhos Pd G4, $P(tBu)_3$ Pd G3), the XPhos precatalyst gave the lowest rate of debromination, in the case on hand. The change of the base from sodium carbonate to potassium carbonate had only minor influence on the side reaction. The purity of the boronic acid ester (**170**) had the strongest influence. Remaining traces of B_2pin_2 from the prior borylation reaction increased dehalogenation, most likely due to their reductive properties. [283]

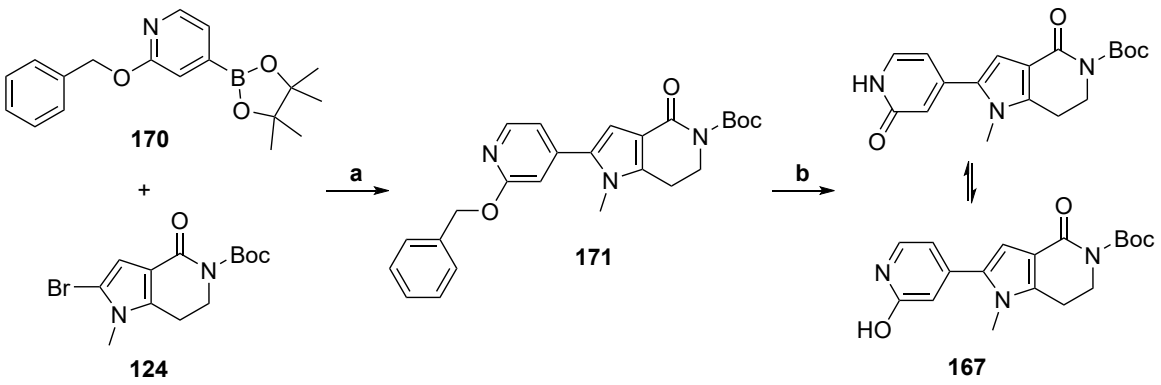

Scheme 37: Synthesis of the oxygen-containing core **167**; (a) Na_2CO_3, XPhos Pd G4, 1,4-dioxane/H_2O, 90 °C, 18 h + 5 h, 32%; (b) Pd/C (10% w/t), H_2, EtOH, 2 h, 96%.

The benzyl group was cleaved from **171** under reductive conditions with palladium on charcoal and hydrogen. The use of ethanol as solvent instead of methanol resulted in higher yields of **167** due to improved solubility of the reactant and hydrogen and cleaner conversion. Complete isolation of the product was ensured by rinsing the filter with ethyl acetate and DCM, as the product has limited solubility in alcohols, which finally afforded the product **167** in excellent yields (96%).

Since most of the described *O*-selective procedures require specific characteristics of the starting material, such as diaryliodonium salts [274a], boronic acids [275], or expensive gold catalysts [277], which were difficult to implement, the influence of different basic salts was assessed (Scheme 38).

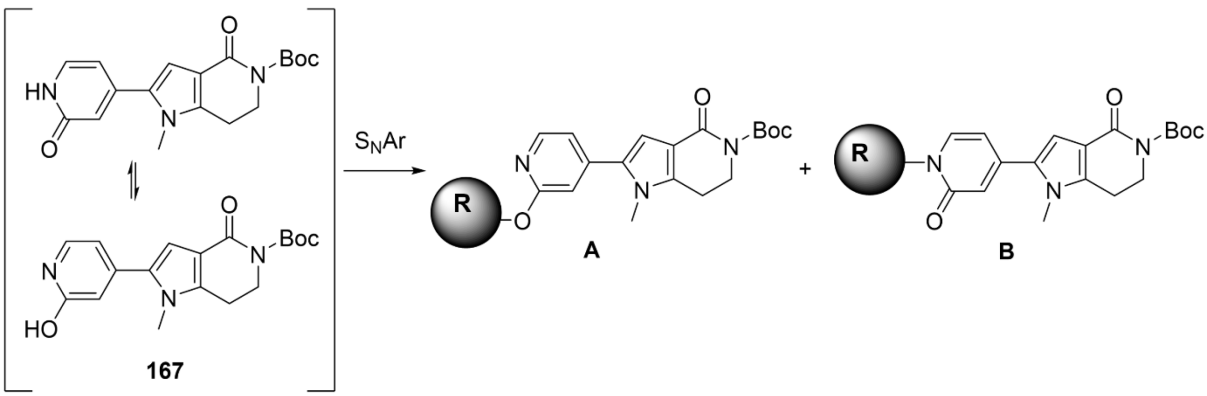

Scheme 38: Schematic depiction of the warhead attachment at the oxygen linker. Different heterocycles used as **R** are displayed in Scheme 39.

The reaction of **167** with **162** to give **179** was chosen for initial assessment of the substitution. The mono-halogenated pyridin **162** was preferred over dihalo-derivatives with a second leaving group to avoid potential regioselectivity issues on the warhead part. A clear difference was observed on the ratio

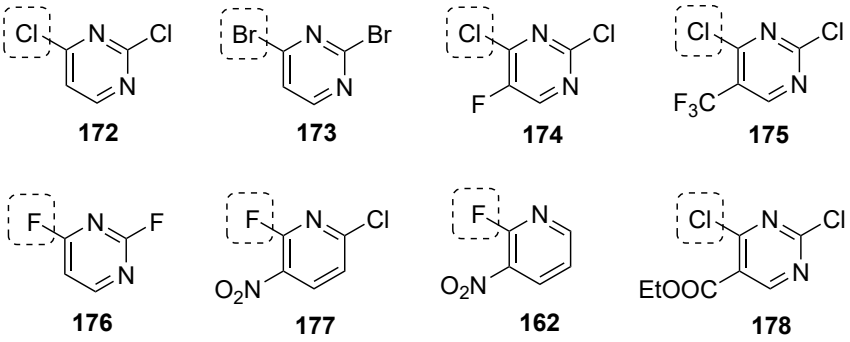

Scheme 39: Haloheterocycles utilized in the reaction with **167**. Leaving group marked in dotted squares.

of the formed products in the UV spectra from the HPLC chromatograms when using K_2CO_3 (9:3) or Ag_2CO_3 (4:13) as base. However, identifying the respective derivative **A** or **B** (Scheme 38) is not straightforward. The shifts in the NMR spectra differ between the two isolated fractions, but due to the complexity of the molecule, the assigment is complicated. As mentioned previously, BREUGST AND MAYR utilized IR spectroscopy for identification of their derivatives. They observed a band at ~1660 cm^{-1} for the *N*-substituted derivatives (**B**) and at ~1590 cm^{-1} for the *O*-substituted derivatives (**A**). Fraction **1** (HPLC: t_R=10.344 min (method C)) exhibited an absorbtion at 1591 cm^{-1}, indicating the substitution at the oxygen, consitent with the increased proportion in the reaction using the silver salt. The band at 1654 cm^{-1}, found in the second fraction **2** (HPLC: t_R=9.358 min (method C)) is close to the proposed value for the *N*-substituted derivative and supports the suggested assignment.

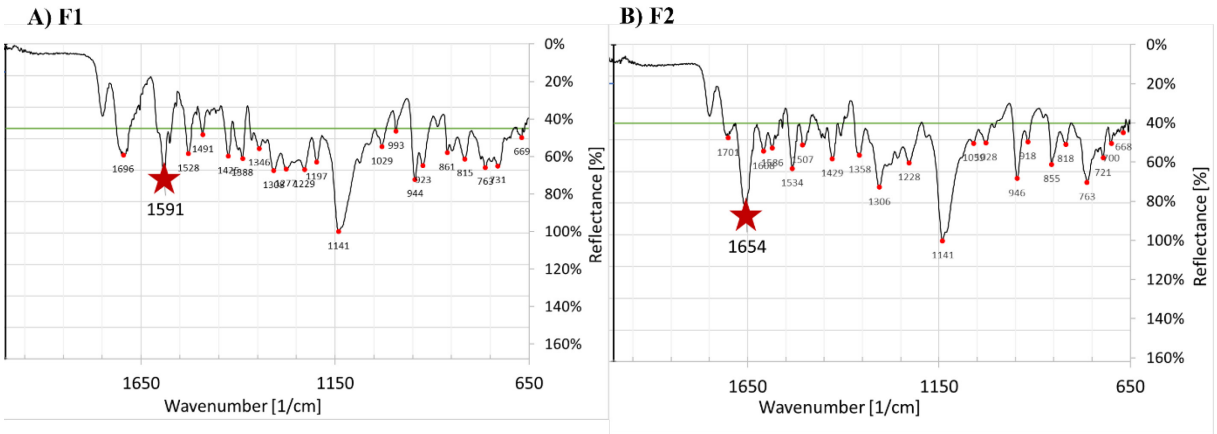

Figure 35: IR-spectra of **179**, characteristic peaks highlighted with red stars; A) spectra of **179**F1; B) spectra **179**F2.

To attach chloropyrimidine **172** to the core Ag_2CO_3, Li_2CO_3 and NaH were tested as bases. The HPLC analysis showed formation of 2-3 different products with $\Delta t_R < 0.5$ min (no baseline separation), which differed in the intensity depending on the base used. However, no pure fraction could be isolated by column chromatography. Similaryly, purification efforts for the transformation of **173**, **175**, **176**, **177** and **178** were unsuccessful, and no product could be isolated and identified. Eventhough, Ag_2CO_3 was

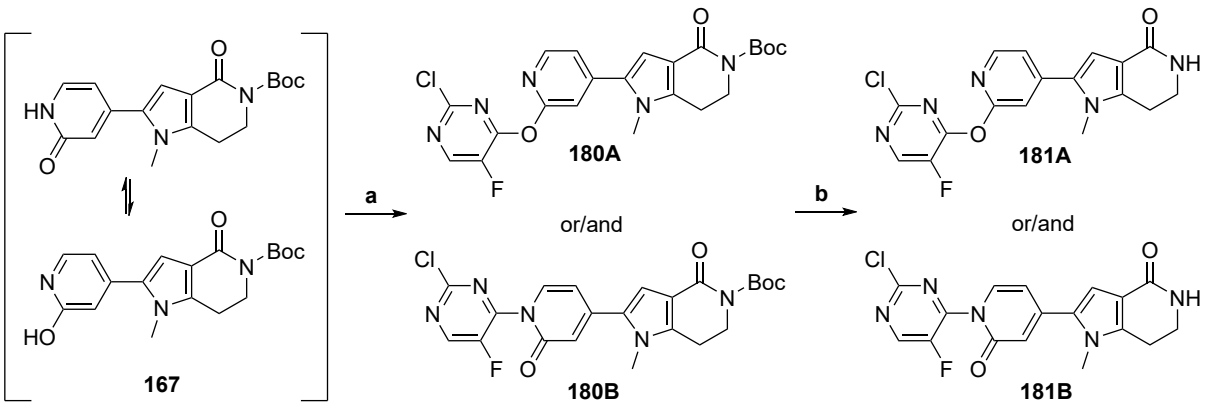

Scheme 40: Synthesis of **181A/B**; (a) Ag_2CO_3, 2,4-dichloro-5-fluoropyrimidine **174**, DMF, 90 °C, 18 h; 100 °C, 23 h, 40%; (b) DCM, TFA, rt, 30 min, 54%.

used as base in all cases, only the synthesis of **180** using 2,4-dichloro-5-fluoropyrimidine **174** yielded a pure main product after purification when Ag_2CO_3 was used in DMF. Identification of the isolated isomer via the IR spectra was not possible for **180**, due to the presence of a band at 1701 cm^{-1} and 1573 cm^{-1}. Similarily, in the decprotected final product **181** the IR spectra does not allow a clear assigment which regioisomer had been generated. Furthermore, crystalisation of compound **181** and its HCl salt through slow vapor diffusion was attempted but not succcessful until this point. However, compound **181** was tested in the biochemical HotSpot™ assay at Reaction Biology Corp. (Malvern, PA, USA, conditions described in detail in section 4.1) against MK2 but only showed weak inhbition (IC_{50}(MK2) = 4860 nM). Therefore, no further attempts were made for structural identification.

Further efforts on this series were abandoned because it was assumed that the regioselectivity issues could not be solved in a justifiable time frame. Most derivatives would have required clean conversion due to difficulties in removing side products. Establishing an *O*-selective substitution methode presents a considerable challenge, as seen in the examples displayed here and in the literature. In addition, the identification of the respective isomer requires extensive analytical efforts, such as crystallisation or 2D-NMR analysis, even during optimisation. As a result, this series was not pursued any further.

3.3.2.3 Synthesis of Sulfur-linked Compounds

To further explore SAR the linker nitrogen atom was exchanged to a sulfur. The high nucleophilicity of the sulfur atom should allow for its introduction to the scaffold via a S_NAr reaction. To this end, the reaction conditions previously established in the FGFR4 project [227] were tested. However, the desired displacement product could not be synthesized by refluxing the aryl halide with thiourea **184** in ethanol. Despite varying the solvent (ethanol, methanol, DMF, 1,4-dioxane) and using acidic or basic additives the desired product was not formed in significant amounts. To take advantage of the higher reactivity towards nucleophilic attack of fluoroarenes, the fluoropyridine precursor **183** was synthesized as shown in Scheme 41. In the initial borylation reaction 4-bromo-2-fluoropyridine **168** was transformed into the corresponding boronic acid pinacol ester **182**. The SUZUKI coupling with the bromo intermediate **124** then gave **183**. Although the fluoropyridine **183** was expected to show increased reactivity, no such advantage was observed in the reactions described in Scheme 41.

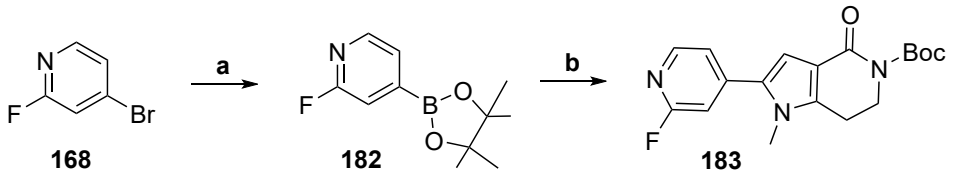

168 **182** **183**

Scheme 41: Synthesis of the fluorinated derivative **183**; (a) B_2pin_2, KOAc, $Pd(dppf)Cl_2 \cdot CH_2Cl_2$, 1,4-dioxane, 90 °C, 18 h, 69%; (b) **124**, Na_2CO_3, XPhos Pd G4, 1,4-dioxane/H_2O, 90 °C, 18 h, 35%.

When *n*- or *tert*-butanol were used as a solvent under acidic conditions (HCl), the corresponding aryl alkyl thioethers **187**/**188** were obtained instead of the desired pyridine thiol/thione (Scheme 42B). The *tert*-butyl group is described as a protecting group for thiols and various strategies for its cleavage have been published. However, removal of the *tert*-butyl substituent at the sulfur with HCl, as described in a publication by VAN VELDHOVEN *et al.* [284], was unsuccessful. Several alternative methods did not give the desired product in this case. [285]

Although ethanethiol was reported for the synthesis of 2-mercaptopyridine [286], only the 2-(ethylthio)pyridines **189** and **190** could be isolated. Therefore, another thiol surrogate, *p*-methoxybenzyl mercaptan (**191**), was selected. Here, according to the literature, the residue could be introduced by an S_NAr reaction, and the *p*-methoxybenzyl group subsequently be removed with TFA and *m*-cresol as a scavenger. [287] The proposed substitution reaction, however, did not work out and an alternative palladium-catalyzed reaction was carried out, which led to the desired (4-methoxybenzyl)sulfanyl derivative **192**.

Even though, the removal of the benzylic group could not be accomplished, the successful introduction of the sulfur encouraged further Pd-catalyzed options. This was even more promising, since the Boc protecting group at the lactam moiety was stable under these conditions.

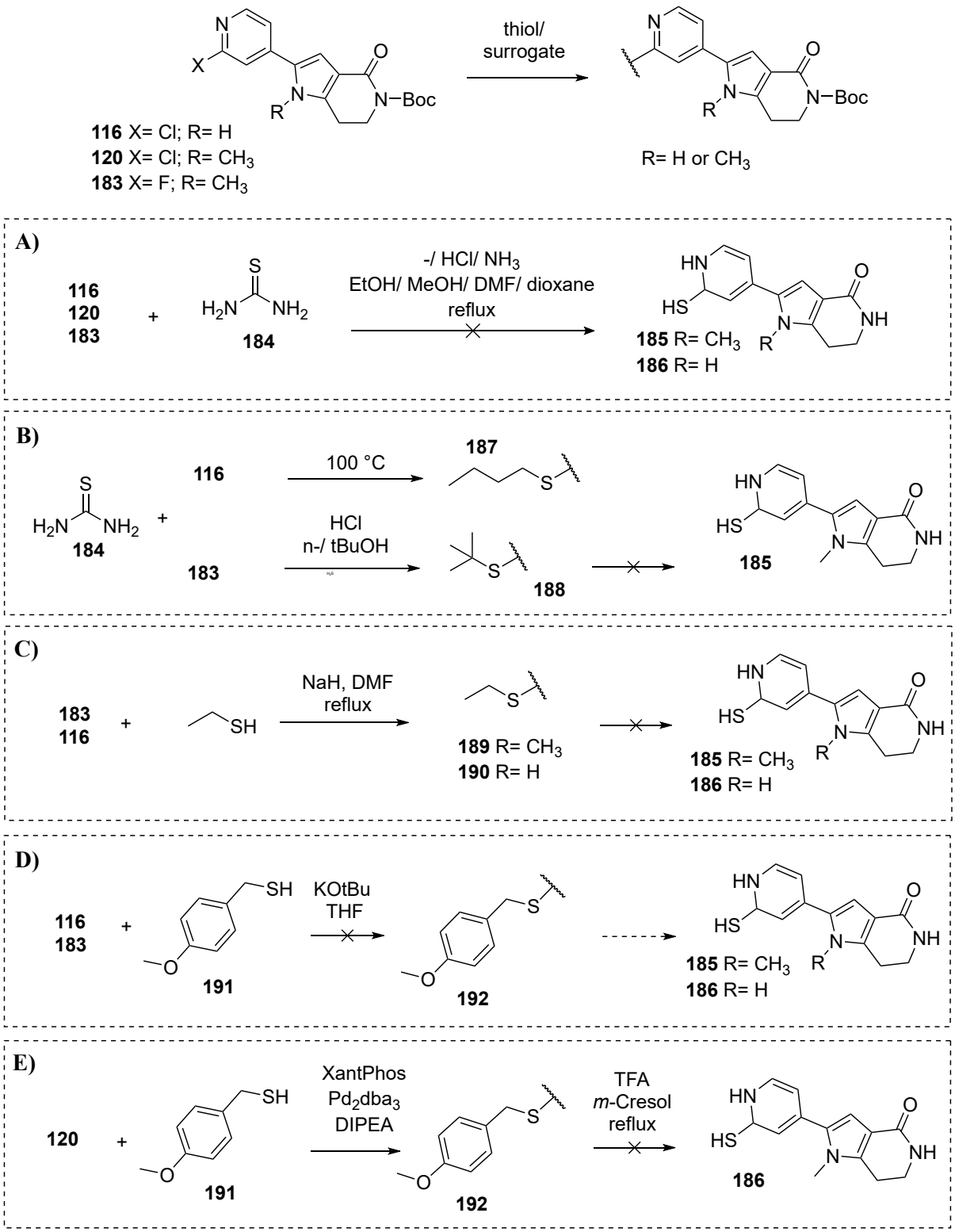

Scheme 42: Synthetic attempts to obtain 2-mercaptopyridine **185**/**186** via a S_NAr reaction or palladium-catalyzed procedure with a suitable thiol surrogate.

KREIS/BRÄSE published a method for synthesizing silyl-protected arylthiols using triisopropylsilanethiol (TIPSSH, **193**) and a palladium catalyst. [288] Unfortunately, the chloropyridine derivative **120** did not react under their cross-coupling conditions. However, the corresponding

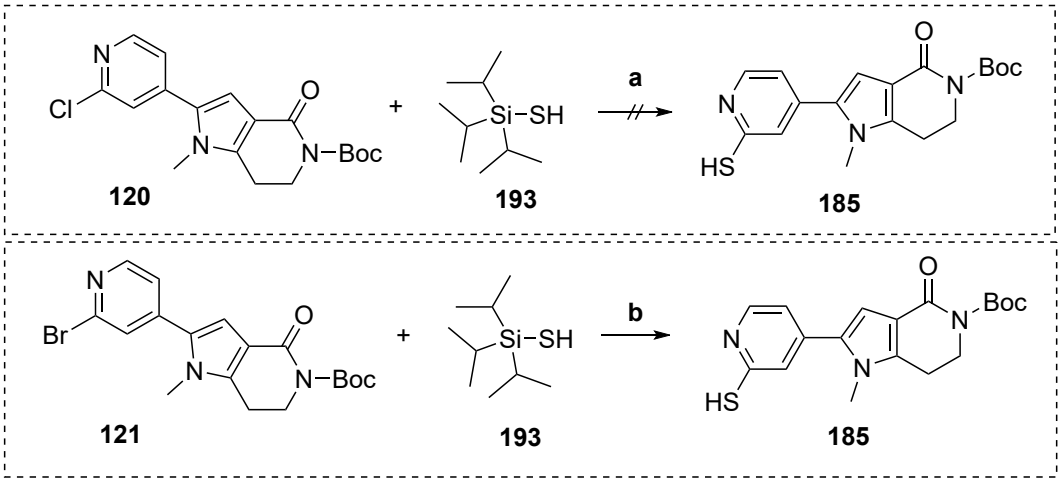

Scheme 43: Palladium-catalyzed reaction of TIPSSH **193** and the aryl halides **120** and **121**; (a) $Pd(OAc)_2$, PPh_3, Cs_2CO_3, toluene, 100 °C, 16 h.; (b) $Pd(PPh_3)_4$, XantPhos, DIPEA, toluene, 80 °C, 3 h, 92% (containing ~10% **196**).

bromoaryl **121** reacted with the thiol-surrogate in toluene using $Pd(OAc)_2$ and triphenylphosphine (PPh_3) for catalysis. As stated in the publication, the triisopropylsilyl (TIPS) group on the sulfur attached at electron-deficient (hetero)arenes is particularly susceptible to nucleophiles. In this case, the TIPS-substituted product could not even be observed since it is cleaved during the work-up or even the reaction. In the first attempts a significant amount of side products were isolated and identified as the

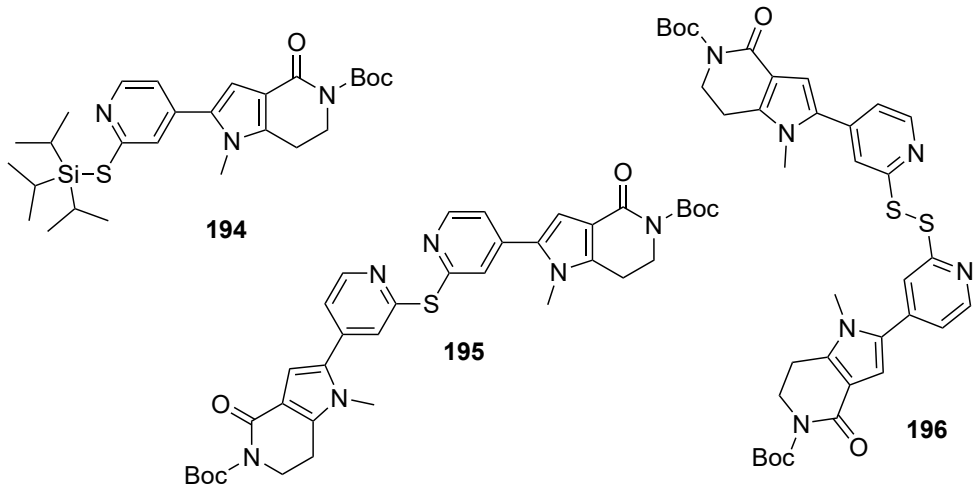

Scheme 44: Intermediate **194** and identified side products **195** and **196** of the Pd-catalyzed reaction with TIPSSH.

diarylsulfide **195** and the disulfide **196** (depicted in Scheme 44). Doubling the equivalents of the thiol (1.30 to 3.00 equivalents (eq.)) prevented the formation of the diarylsulfide **195** (Scheme 44). Attempts to reduce the disulfide with triphenyl-/tributylphosphin [289] or to use it directly in the next step to form the desired diheteroaryl thioether [290] were unsuccessful. Disulfide formation was reduced by optimizing

the coupling conditions. Good results were achieved using $Pd(PPh_3)_4$ as the catalyst and XantPhos as an additional ligand. Using DIPEA as the base and reduction of temperature (80 °C) and reaction time (3 h) were sufficient for obtaining good yields. Formations of the disulfide could still not be completely avoided using these conditions and the removal was difficult. Therefore, the product **185a** was used in the next step, even though it contains approximately 10% of the disulfide **196**.

The reactivity pattern in substitution reactions of the two nucleophilic centers in pyridin-2-(1*H*)thione (S and N) differs significantly from that of the corresponding pyridin-2-one discussed in section 3.3.2.2, with nucleophilic attack via the sulfur atom being largely preferred.[291] The differences in regio selectivity can be explained by transferring the knowledge about the reactivity of the ambident thiocyanate (SCN^-) and cyanate (OCN^-) ions to the cyclic structures. In both cases, nucleophilic attack via the oxygen or sulfur is kinetically preferred. The thermodynamic preference, however, favors *N*-substitution, and this effect is significantly mor pronounced for the pyridin-2-one leading to the observed dominance of its *N*-substitution product under most conditions. In contrast, the sulfur derivative primarily yields the *S*-substituted product.[291c]

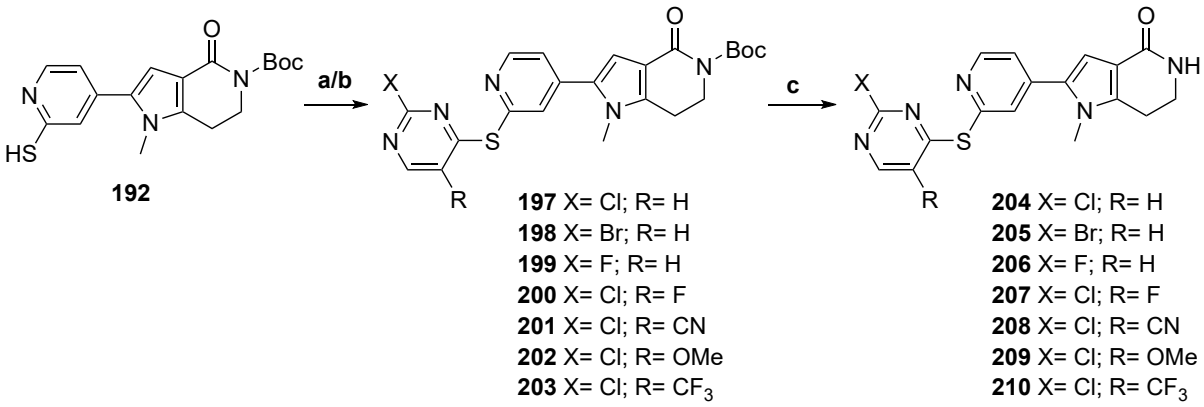

Scheme 45: Synthesis of the sulfur-linked compounds; (a) 2,4-dichloropyrimidine **172**, K_2CO_3, DMF, -78 °C to rt, 4 h, **197** 81%; (b) 2,4-dihalopyrimidine, K_2CO_3, DMF, 0°C to rt, 1-4 h, 21-98%; (c) TFA, DCM, rt, 15 min, 29-91%.

The heterocyclic warhead was introduced via a S_NAr reaction of pyridine-2-(1*H*)thione **185** with the respective 2,4-diaholpyrimidine (Scheme 45; **a**/**b**). Selectivity for substitution at the 4-posiiton of the pyrimidine was increased by initial cooling of the reaction. Removal of the Boc-protecting group yielded the desired compounds **204-210**. Mass spectrometric (MS) analytic of the Boc-deprotection process of **201** and **203** to yield compounds **208** and **210**, which include an additional electron-withdrawing group

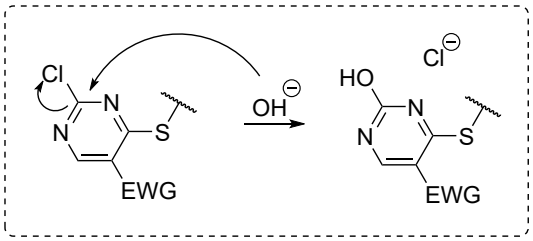

TLC-MS (**208**): ESI(-) calcd. for $[M\text{-}H]^+$: *m/z* = 395.1; found: 377.3.

TLC-MS (**210**): ESI(-) calcd. for $[M\text{-}H]^+$: *m/z* = 438.1; found: 420.0.

Scheme 46: Mechanism for the hydrolysis of electron-deficient heterocyclic moiety. The mass difference (ΔM) of 18u was found for the nitril- (**208**) and CF_3-derivates (**210**).

(EWG) at the halopyrimidine warhead, indicated hydrolytic instability during the basic work-up (Scheme 46). The finalization of these two derivatives was not pursued further, as the remaining compounds in this series (**204-207** and **209**) are sufficient for the initial proof of concept and SAR studies. The NMR spectra of the final compounds were measured in deuterated dimethyl sulfoxide (DMSO-d^6). Identifying the peaks assigned to the aliphatic CH_2 group neighboring the lactam nitrogen can be challenging in this solvent. The chemical shifts of these hydrogen signals in the ^1H NMR-spectrum are close to the peak caused by residual water, and there may be a partial overlap depending on the derivative and the water content of the solvent. The corresponding carbon signal in the ^{13}C spectrum is located in the area of the solvent residual peak (quintet). A 2D-NMR experiment (HSQC) of **209** enabled the identification of the structure and a clear assignment of the partially hidden peaks (shown in Figure 52, section 6.2.11).

The S_NAr strategy was found to be superior to an alternative approach of introducing the warhead via a palladium-catalyzed reaction due to side reactions, which negatively impacted purification and yield. Scheme 47 shows the only compound, dimethoxyquinazoline derivative **211**, which was synthesized using this alternative approach.

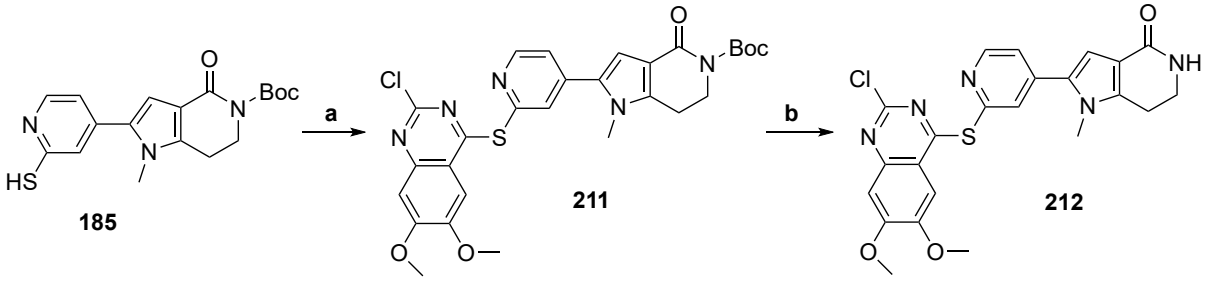

Scheme 47: Synthesis of the sulfur-linked dimethoxyquinazoline derivative **212**; (a) 2,4-dichloro-6,7-dimethoxyquinazoline, $Pd(OAC)_2$, XantPhos, K_3PO_4, DMF, 50 °C, 1 h, 46%; (b) TFA, DCM, rt, 15 min, 71%.

BANDARU *et al.* [292] proposed XantPhos as a suitable ligand for thioetherification, which worked well for synthesizing the pre-final derivative **211**. After deprotection under acidic conditions, the final compound **212**, was successfully isolated. However, its solubility in DMSO was too low (not dissolved @1.67 mM) for biochemical testing.

3.3.2.4 Variations of the Substitution at the Pyrrole Ring

The methylation of the pyrrole decreased inhibitory activity against MK2 compared to the free *NH* in this position, as described by REVESZ *et al.* [1] and observed for the tetracyclic acrylamide compounds synthesized in this work (section 4.1.1). On the other hand, *NH* substitution prevents the formation of side products and is often necessary during the synthetic route. Several synthetic steps required the masking of the pyrrole *NH*, including many cross-coupling reactions and the warhead attachment. Since the methyl group retains significant activity and introduction worked well, this group was maintained for SAR investigation on the linker and warhead part. Various protecting group strategies have been

attempted to introduce to the built-up core (**54**, **94**, **116**, **132**). In order to release the free pyrrole *NH* in a (pre)final step. However, most approaches were impeded by incomplete conversion to the protected derivative and difficulties in the purification process (i.e. tosyl, TIPS, methoxymethyl ether (MOM), *p*-methoxybenzyl group). Even if the attachment of the protection group was successful, stability in the following reaction steps (Boc) or the removal (SEM) appeared to be problematic. Switching to a SUZUKI coupling as the key synthetic step simplified the introduction of the linking heteroatom. Additionally, it allowed for variations in the pyrrole substitution. Attaching protective groups or alternative residues to the bicyclic intermediate **151** thus opens new possibilities. The introduction and purification also worked well for several different derivatives (Table 3). Furthermore, the subsequent reaction conditions are comparably mild, allowing the use of more susceptible groups. An overview of the compounds obtained by this route is given in Scheme 48. The derivatives containing a methyl group on the pyrrole nitrogen (R^1) have been discussed in previous chapters. The synthesis of **119** and **120** is explained in section 3.3.2.1.3. Compounds **171** and **183** are discussed in detail in sections 3.3.2.2 and 3.3.2.3, respectively. The remaining derivatives will be discussed in the following section.

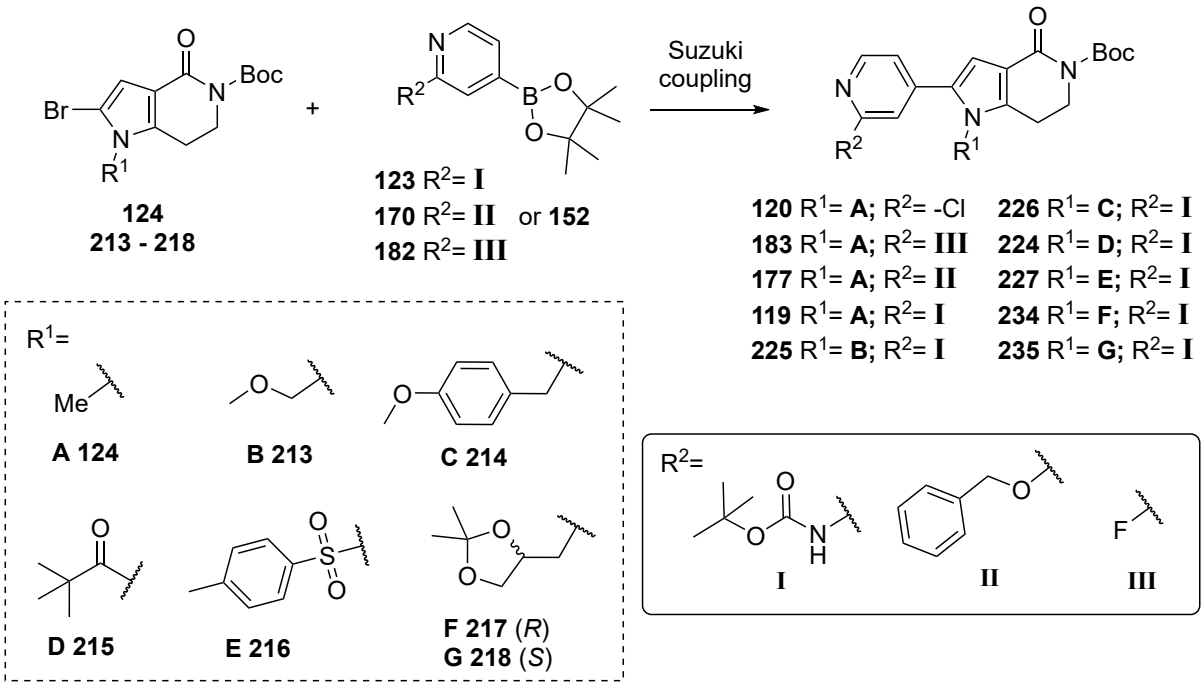

Scheme 48: Overview of advanced intermediates including various pyrrole *N*-substituents synthesized via SUZUKI coupling.

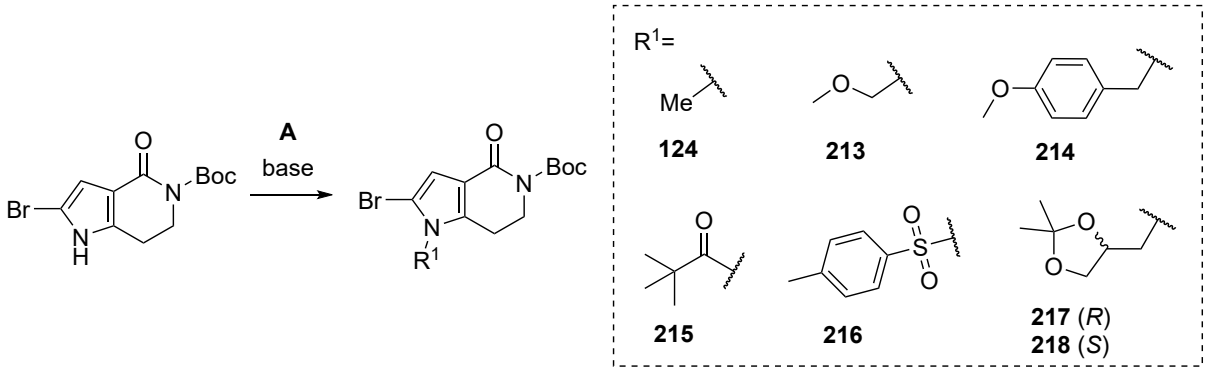

Scheme 49: Introduction of the masking groups at the pyrrole ring. Structure of R_1 in the box on the right, reaction conditions summarized in Table 3.

When the respective alkyl iodide (CH_3I), methoxybenzyl or MOM bromide (**220** or **219**) was used (Table 3, **124**, **213** and **214**), the attachment of the masking groups (Scheme 49) went smoothly under basic conditions. The addition of DMAP as catalyst was required when using a carboxylic acid chloride **221** (pivaloyl chloride) or tosyl chloride **222** (**215**, **216**). The synthesis of **217**/**218** is described in more detail below (Scheme 54). The introduction of the dioxolane **223** was carried out under FINKELSTEIN conditions.

Table 3: Reaction conditions for substitution at the pyrrole-*N* shown in Scheme 49.

#	A		Reaction conditions	Yield
124	CH_3I		Cs_2CO_3, DMF, 0°C to rt, 2 h	88%
213	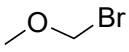 **219**		NaH, THF, 0 °C, 1 h	82%
214	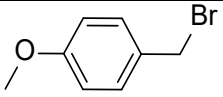 **220**		Cs_2CO_3, DMF, rt, 18 h	33%
215	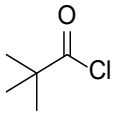 **221**		DMAP, TEA, DCM, 0 °C to rt, 18 h	61%
216	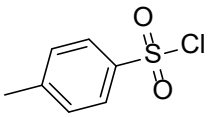 **222**		DMAP, TEA, ACN, rt, 18 h	78%
217 (*R*)	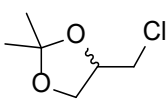 **223**	***S***	NaI, Cs_2CO_3, DMF, 110 °C, 48 h	60%
218 (*S*)		***R***		58%

The SUZUKI-coupling with the *N*-substituted pyrroles was performed in 1,4-dioxane, combined with an aqueous sodium carbonate solution. The initial reaction conditions employed $Pd_2(dba)_3$ as the palladium(0) source and XPhos as the ligand. During optimization the catalyst complex was substituted for the XPhos Pd G4 pre-catalyst.

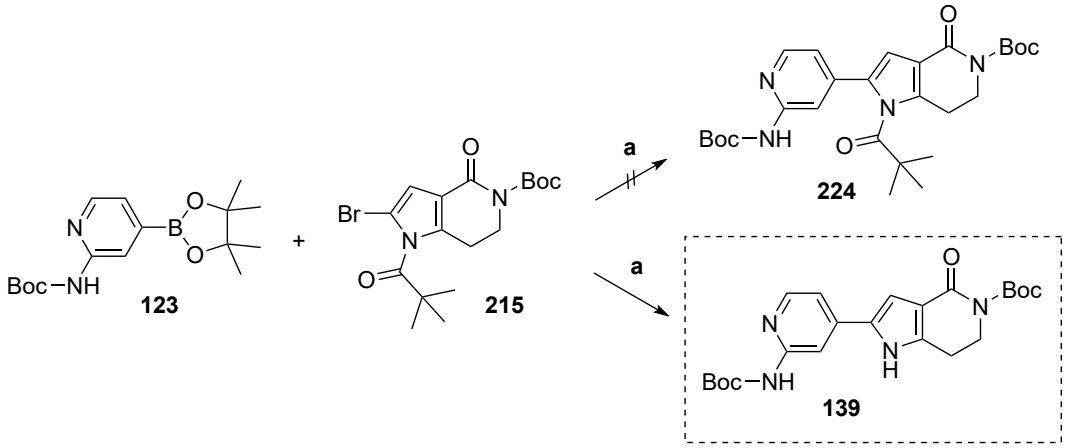

Scheme 50: SUZUKI coupling of the pivaloyl protected derivative **215**; (a) Na_2CO_3, XPhos Pd G4, 1,4-dioxane/H_2O, 80 °C to 90 °C, 18 h + 3 h, 19% **139**.

The pivaloyl-protected bromo intermediate **215** was intended to be coupled to the boronic acid ester **123** through a SUZUKI coupling. However, the pivaloyl protecting group proved to be unstable under these conditions, resulting in only a small amount of the coupling product without the pivaloyl substituent being detected and none of the pivaloyl protected derivative **224**. The main coupling product obtained was the free *NH* derivative **139**. The low yield (19%) underlined the relevance of masking the pyrrole for proper conversion.

The pyrrolopyridinone core structures **225**, **226**, and **227** were obtained by transforming the three pyrrole-*N*-protected intermediates **213**, **214**, and **216** in a SUZUKI coupling (Scheme 52). The introduction of the chloronitropyridine warhead proceeded as expected. However, none of the derivatives could be successfully deprotected.

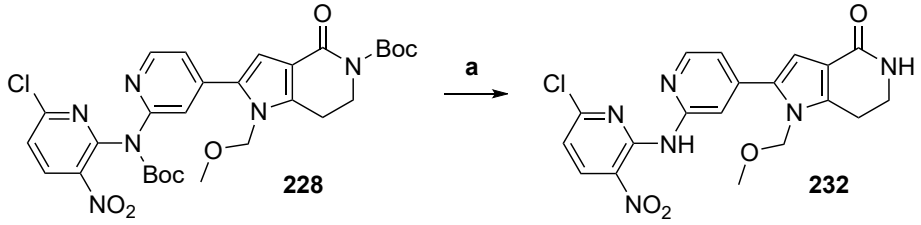

Scheme 51: Partial deprotection of **228** to yield **232**; (a) TFA, DCM, rt, 1 h, 51%.

Compounds **228** and **229** should undergo global deprotection using acidic conditions (TFA/HCl). However, the removal of the MOM-protection group and the *p*-methoxy benzyl did not proceed as expected. Only the Boc groups were completely removed under these conditions. The MOM-substituted derivative **232** was isolated (Scheme 51) and tested for its inhibitory activity.

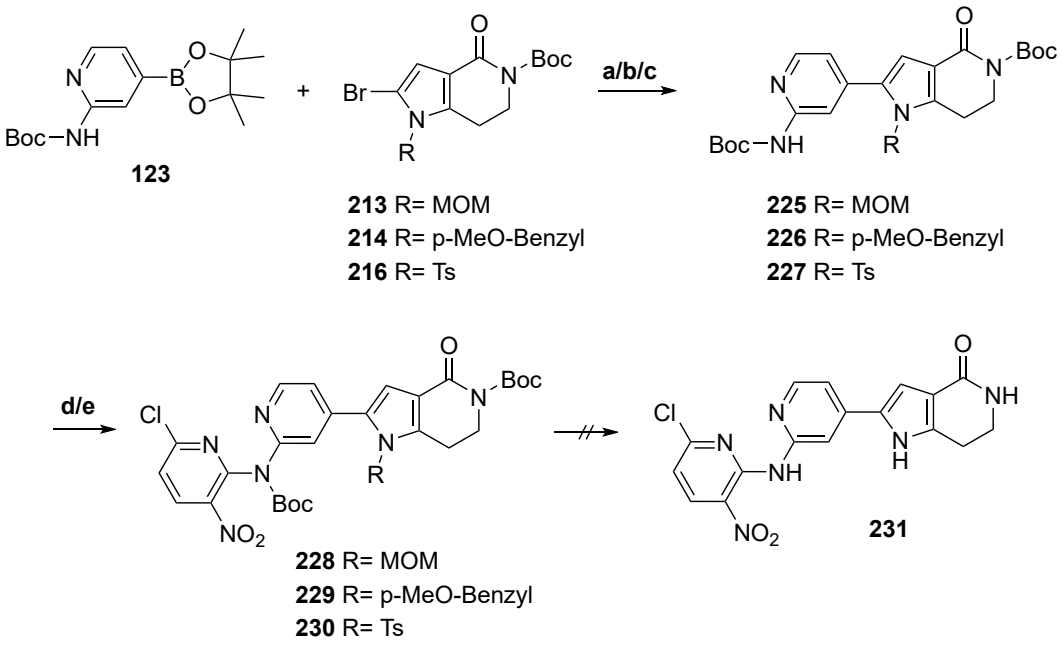

Scheme 52: Synthetic approach towards compounds with a free pyrrole-*NH*; (a) $Pd_2(dba)_3$, XPhos, Na_2CO_3, 1,4-dioxane/H_2O, 80 °C, 2 h, 36% (**225**); (b) $Pd_2(dba)_3$, XPhos, Na_2CO_3, 1,4-dioxane/H_2O, 90 °C, 16 h, 56% (**226**); (c) XPhos Pd G4, Na_2CO_3, 1,4-dioxane/H_2O, 80 °C, 18 h, 58% (**227**); (d) 2-bromo-6-chloro-3-nitropyridine **103**, Cs_2CO_3, XantPhos, $Pd(OAc)_2$, toluene, 70 °C, 48 h, 76% (**228**)/ 47% (**229**); (e) 2-bromo-6-chloro-3-nitropyridine **103**, Cs_2CO_3, XantPhos Pd G4, toluene, 70 °C, 16 h, 86% (**230**).

Deprotection of the tosyl-protected derivative **230** was expected to be challenging due to the basic/nucleophilic conditions required to remove this group. Under these conditions the warhead can undergo hydrolysis or other substitutions at the electrophilic position (Scheme 31). To avoid this issue, mild deprotection conditions were used, employing Cs_2CO_3 as a base in a MeOH/THF mixture were chosen. The tosyl-group was successfully removed under these conditions, but only the methoxy-substituted warhead derivative could be detected. Therefore, the order of the synthetic route was modified, and the tosyl-group removed prior to the incorporation of the warhead (Scheme 53).

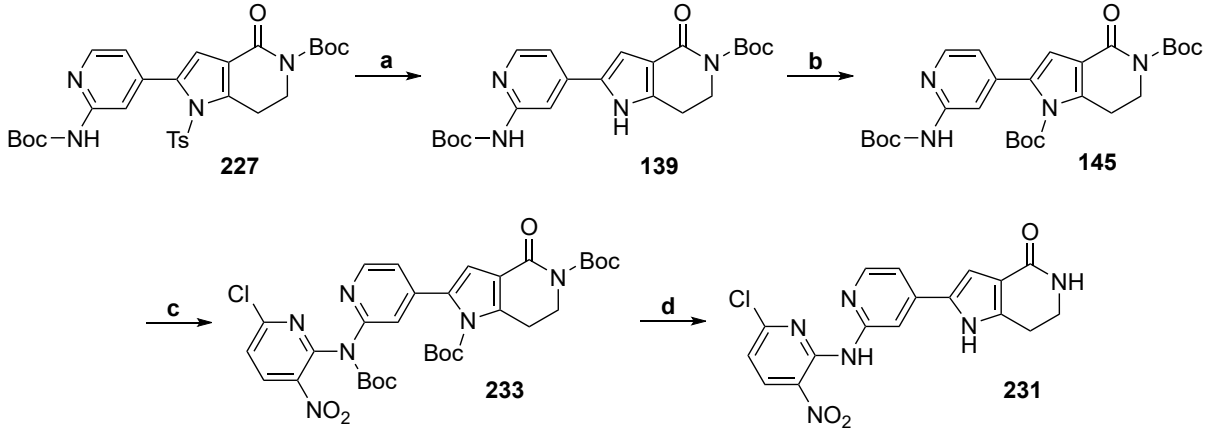

Scheme 53: Synthesis of compound **231**; (a) Cs_2CO_3, THF/MeOH, rt, 30 min, 46%; (b) Boc_2O, NaH, DMAP, DMF, rt, 42 h, 37%; (c) 5-chloro-2-flouro-3-nitropyridine **177**, NaH, DMF, 0 °C to rt, 18 h, 71%; (d) TFA, DCM, rt, 30 min, 28%.

Under the same conditions as described above, deprotection of **227** resulted in the free pyrrole derivative **139**. To ensure selective attachment of the warhead at the exocyclic nitrogen, a Boc-protecting group was attached to protect the pyrrole-*N* (**145**). The warhead was then introduced to **145** through nucleophilic aromatic substitution. The S_NAr procedure using a chlorofluoropyridine electrophile was chosen over the Pd-catalyzed procedure (Scheme 52) due to the lower temperature required increasing compatibility with the labile Boc-protecting group at the pyrrole (Scheme 53, step **c**). This approach allowed the isolation of **233** in good yield (71%). The final step involved globally cleaving the three protecting groups to obtain compound **231** with a free pyrrole *NH*.

During the development of the protection group strategy, repeated drawbacks were encountered, leading to the idea of introducing a beneficial substituent at the pyrrole *NH*. The crystal structure of a MK2 inhibitor revealed a water-mediated interaction between the pyrrole and the kinase (Figure 19). A polar group can mimic this interaction and, at the same time, improve the solubility of the inhibitors.

GOLDSTEIN *et al.* introduced a 2,3-dihydroxypropoxy group into their kinase inhibitors to improve solubility. Their compounds showed good pharmacokinetic properties and metabolic stability without cytotoxicity.[293] The same residue is present in skepinone-L (**4**), where it enhances hydrophilicity and cellular activity.[189] Encouraged by these examples, a ketal-protected 1,2-diol was chosen as a substituent in this case.

To introduce the desired group, (*R/S*-)4-(chloromethyl)-2,2-dimethyl-1,3-dioxolane **223** was attached to the pyrrole (Scheme 49). The initial approach used Cs_2CO_3 as a base and DMF as the solvent for a nucleophilic substitution, as applied for the methylation (**124**), however, attachment of the residue under these conditions was unsuccessful. To increase the reactivity of the alkyl chloride, the corresponding iodide was formed *in situ* under FINKELSTEIN conditions. A procedure from the patent literature[294] was followed, which involved changing the base to NaH to further enhance nucleophilicity of the pyrrol(at)e and heating the reaction to 120 °C. However, this resulted in the decomposition of the starting material. Attempting the reaction under more classical FINKELSTEIN conditions in acetone with Cs_2CO_3 as the base and heating it to reflux was also unsuccessful. When **223** was pre-stirred with NaI in acetone under reflux conditions for 18 hours before adding it to the pyrrole **151** and base (Cs_2CO_3) in DMF and heating to 100 °C, traces of the product could be detected. Isolating the corresponding alkyl iodide before adding it to the reaction did not improve the outcome. Changing the solvent to NMP or DMSO and replacing the base with Na_2CO_3 was also not beneficial. However, successful reaction conditions could be developed by removing possible disruptive factors and combining the knowledge gained from the initial attempts about the temperature-dependent stability and reactivity. To ensure the absence of residual water traces, the acetone was dried over sodium sulfate and the utilized salts were dried in the oven. The alkyl chloride **223** was activated by stirring it with sodium iodide in acetone for 1 hour. In a separate flask, Cs_2CO_3 was used to (partially) deprotonate the bromopyrrole **151** in DMF at 100 °C for 1 hour. The solution of the dioxolane was then filtered and added to the reaction mixture of the pyrrole. After allowing the acetone to evaporate through a canula perforating the septum, the reaction was stirred at

110 °C under an atmosphere of argon (Ar) to obtain the corresponding substitution products **217** and **218** in ~60% yield (Scheme 55Scheme 49: Introduction of the masking groups at the pyrrole ring. Structure of R_1 in the box on the right, reaction conditions summarized in Table 3.). The boronic acid ester **123** was reacted with these intermediates in a SUZUKI coupling (Scheme 54**a**) to obtain the intermediates **234**/**235**. The adapted BUCHWALD protocol described above (Scheme 28) was successfully used to attach the proto warhead **103**. The fully protected compounds **236**/ **237** were obtained in satisfactory yields (69% for **236**; 61% for **237**). The final compounds **238** and **239** were generated by the removal of the Boc protecting groups and the hydrolysis of the ketal in one step.

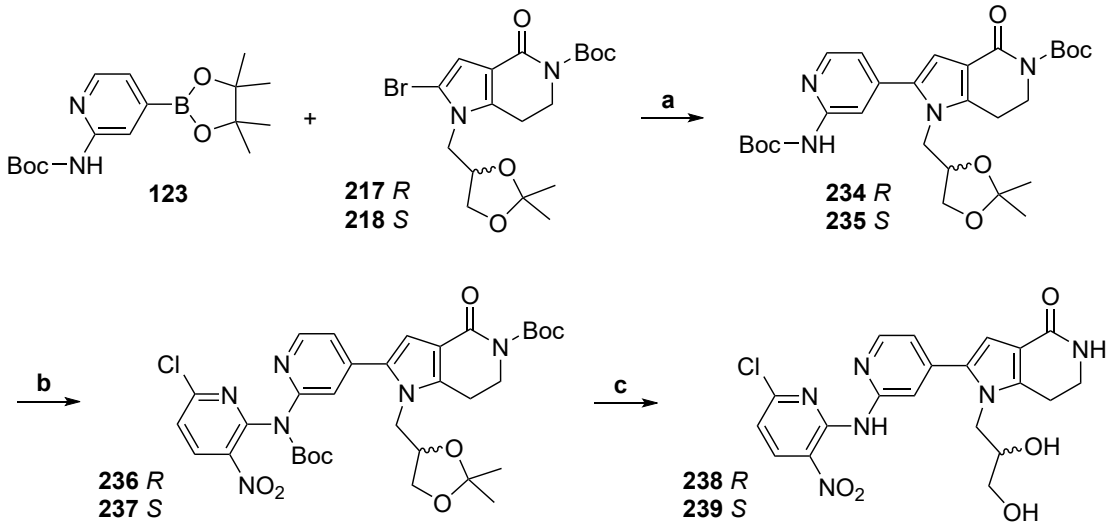

Scheme 54: Synthesis of the diole compounds **238** and **239**; (a) Na_2CO_3, XPhos Pd G4, 1,4-dioxane/H_2O, 90 °C, 6 h, 34% (**234**)/ 25% (**235**); (b) 2-bromo-6-chloro-3-nitropyridine **103**, Cs_2CO_3, XantPhos Pd G4, toluene, 55 °C/ 60 °C, 18 h, 69% (**236**)/ 61% (**237**); (c) TFA, DCM/H_2O, 6% (**238**)/ 8% (**239**).

To increase the rather poor isolated yield, it is important to consider the reactivity of the warhead and its increased aqueous solubility. When performing the aqueous workup to remove the acidic component, the compound may partially dissolve in the aqueous phase, making it difficult to extract it completely. The use of a mixture of DCM or ethyl acetate (EtOAc) with an alcohol for the extraction can be problematic, due to the nucleophilic properties of the hydroxy group. Elevated temperatures during evaporation of the solvent can cause substitution reactions at the warhead, as described in Scheme 46. Exchanging the workup and purification procedure may improve the outcome of this synthetic route.

4 Biochemical Evaluation and Discussion

4.1 Biochemical Evaluation

Kinase inhibitors are initially evaluated using specific biochemical assay formats, based on different technologies for detection. Assays that measure the activity of the kinase and reduction thereof by an inhibitor provide more descriptive results than binding assays. For kinases, the phosphorylation of a specific target can be used as an activity metric, enabling the determination of IC_{50} values.

Radiometric assays, which capture the phosphorylation reaction from radiolabeled ^{32}P-γ-ATP or ^{33}P-γ-ATP, are well established and provide reliable results.[295] The HotSpot™ kinase assay (performed at Reaction Biology Corp., Malvern, PA, USA), utilized for the determination of IC_{50} values of the compounds in this thesis (see sections 4.1.1 and 4.1.2), is based on this technology.[296] It should be noted that the handling of radiolabeled components requires specific precautions and cannot be handled in every setting. As an alternative, other detection technologies, such as fluorescence and luminescence, are used.[295] The PhosphoSens® technology, applied at AssayQuant® Technologies, Inc., and used for determination of activity and kinetic parameters discussed in section 4.2, is based on fluorescence measurement.[297] As previously discussed in section 1.4.3, the IC_{50} values do not take into account the kinetic aspects of the two-step binding mode of covalent inhibitors. However, they remain useful as a practicable approach for initial activity estimation. Additionally, kinetic parameters were measured for selected compounds and discussed in section 4.2.

4.1.1 Evaluation of Acrylamide-based Compounds

Inhibitory activity for the compounds synthesized during this thesis was measured in a commercial radiometric assay format at Reaction Biology Corp. (RBC), Malvern, PA, USA.

The pyridine-based tetracyclic inhibitors, containing an acrylamide warhead (shown in Table 4), achieved IC_{50} values down to 2.62 nM (**64**). As expected from the SAR studies on tetracyclic MK2 inhibitors by REVESZ *et al.*[1], the methylation of the pyrrole leads to a 20-fold decrease in activity (**65**, IC_{50}(MK2) = 57.8 nM). Replacement of the electrophilic warhead with a propionamide in **69** significantly reduces the activity (IC_{50}(MK2) = 995 nM). The weak activity of the non-reactive compound supports the proposed covalent binding mode, as the presence of the intact warhead increases the activity 400-fold. At the same time, the remaining inhibitory activity indicates an effective contribution of the reversible binding. The influence of the latter is most pronounced for the bicyclic linker in **71** since this saturated derivative still inhibits the kinase activity with an IC_{50} value of 55.4 nM. The reduced flexibility of the amide also increases the binding of the reactive derivative **68** when compared to the secondary amide **65** (IC_{50}(MK2) = 6.75 nM vs. 57.8 nM) supporting the notion that appropriate pre-orientation of the warhead supports effective covalent bond formation.

Table 4: Inhibitory activity of pyridine-based tetracyclic inhibitors with an acrylamide warhead (left) and the corresponding propionamide control compounds; IC_{50} values were determined in a HotSpot™ kinase assay at Reaction Biology Corp., using 5-point singlicate measurements with 5-fold dilution steps starting from 2 µM. The assay was performed at 10 µM ATP with 20 minutes of preincubation and 2-hour duration for the kinase reaction.

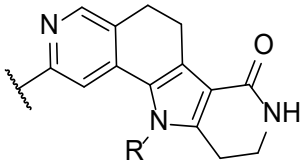

Acrylamid-based Inhibitors				Unreactive control compounds			
Structure	**#**	**R**	**IC_{50} (MK2)**	**Structure**	**#**	**R**	**IC_{50} (MK2)**
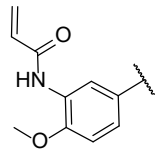	**65**	**CH_3**	57.8 nM	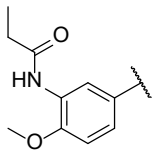	**69**	**H**	995 nM
	64	**H**	2.62 nM				
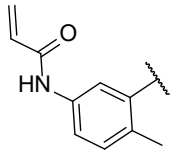	**67**	**CH_3**	610 nM	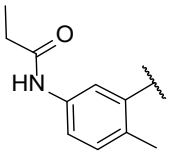	**70**	**H**	> 2.0 µM
	66	**H**	> 2.0 µM				
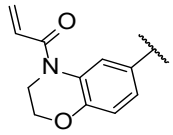	**68**	**CH_3**	6.75 nM	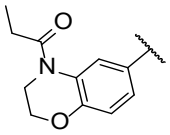	**71**	**H**	55.4 nM

The introduction of an *o*-methyl was found to be effective for covalent targeting of FGFR4 by a pyrimidine-based tetracyclic inhibitor [2], but had a negative effect on inhibitory activity in this case. Compounds **66** and **70** showed less than 50% inhibition of the kinase at the highest concentration tested (2.0 µM). The *o*-substituent forces an out-of-plane rotation of the linker, which is approximately 60° in BLU9931 (**35**). [2, 298] Even though, the overlay of the inhibitor-bound co-crystal structure displayed good alignment of the respective hinge binding motifs (Figure 32), the resulting orientation of the warhead appears to be unfavorable for covalent bond formation towards Cys140 in MK2. In contrast to the results discussed previously, the methylation at the pyrrole nitrogen in **67** restores a low level of inhibition (IC_{50}(MK2) = 610 nM).

Incorporation of the methoxy-substituted linker into the series of compounds including **65**, **64** and **69**, provided initial insights into the structure–activity relationships. The substitution pattern of the linker was therefore also used to evaluate alternative core structures.

Inclusion of an additional nitrogen to generate a pyrimidine-based tetracyclic core only had minor influence on the activity of the inhibitor. Pyrimidine-based tetracyclic compound **96** inhibited MK2 with an IC_{50} value of 1.96 nM (Table 5) and thus slightly better than the related pyridine-based tetracyclic derivative **64**.

Opening the β-ring of the tetracyclic pyridine-based core led to the pyrrolopyridinone derivatives with significantly improved synthetic accessibility. Attachment of the acrylamide warhead via the established methoxy-substituted phenyl linker yielded compound **108** which also featured an IC_{50} in the low nanomolar range (IC_{50}(MK2) = 9.59 nM). Thus, the ring opening reduced kinase inhibition by factor 4 (**108** vs. **64,** Table 5). The large decrease in activity for the saturated analog **109** (IC_{50}(MK2) = 1190 nM) indicates proper orientation of the warhead and formation of the proposed covalent bond in **108** (Table 5).

Table 5: Influence of the variation of the core structure on the inhibitory activity of the acrylamide-based inhibitors; IC_{50} values were determined in a HotSpot™ kinase assay at Reaction Biology Corp., using 5-point singlicate measurements with a) 5-fold dilution steps starting from 2 µM or b) 10-fold dilution steps starting from 5 µM. The assay was performed at 10 µM ATP with 20 minutes of preincubation and 2-hour duration for the kinase reaction.

	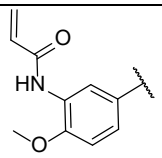		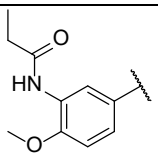	
	#	**IC_{50} (MK2)**	**#**	**IC_{50} (MK2)**
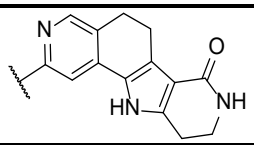	**64**	2.62 nM [a)]	**69**	995 nM [a)]
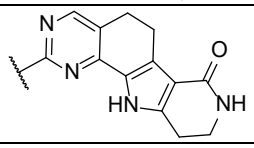	**96**	1.96 nM [b)]		
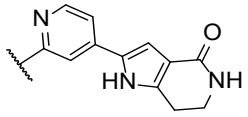	**108**	9.59 nM [a)]	**109**	1190 nM [b)]

4.1.2 Evaluation of Heterocyclic Warhead Structures

Attaching the known chloronitropyridine [12, 225] as a reactive group to the pyrimidine-based tetracyclic core in **102** increased the inhibitory activity (IC_{50} below the lowest concentration tested in this assay, i.e. < 3.20 nM, 7.7% residual activity @ 3.2 nM).

Consistent with the observation for the acrylamide-containing compounds, the activity of the derigidified pyrrolopyridinone compound decreases when compared to the tetracyclic core. Compound **110** inhibits the kinase with an IC_{50} value in the double-digit nanomolar range. Two separate measurements under the same conditions performed at RBC yielded IC_{50} values of 31.9 nM and 91.8 nM, respectively. For the comparison of activity data, the mean value of 61.6 nM will be used.

Table 6: Activity of the alternative heterocyclic warhead in comparison to the respective acrylamides; IC_{50} values were determined in a HotSpot™ kinase assay at Reaction Biology Corp., using 5-point singlicate ([c]) duplicate) measurements with [a] 5-fold dilution steps from 2 µM or [b] 10-fold dilution steps starting from 5 µM. [d] residual activity of the kinase with an inhibitor concentration of 3.20 nM, the lowest concentration tested in the assay.

	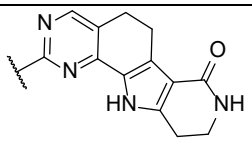		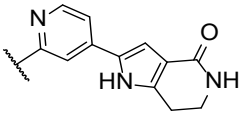	
	#	**IC_{50} (MK2)**	**#**	**IC_{50} (MK2)**
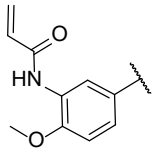	**96**	1.96 nM [b]	**108**	9.59 nM [a]
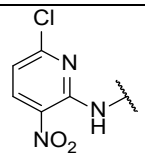	**102**	< 3.20 nM [a] 7.7% [d]	**110**	61.6 nM [b,c]

The non-reactive analog **157** lacks the chlorine as the leaving group, which results in a dramatic loss of activity (IC_{50}(MK2) = 4570 nM). Changing of the chlorine leaving group also displayed an effect on the IC_{50} values obtained. The bromine derivative **155** shows a similar level of activity (IC_{50}(MK2) = 73.7 nM). The value is in line with the expectations, since the reactivity of a bromine substituent is similar or slightly lower to that of chlorine in S_NAr reactions, according to the reactivity order discussed previously in section 1.4.3. [299] The fluorine substituted derivative **156** was expected to be more reactive towards nucleophiles, in line with common S_NAr reactivity trends and as observed in the GSH stability assay (section 4.6). However, despite the expected increase in potency promoted by the more reactive warhead, the IC_{50} value of compound **156** was approximately 1.5- to 2-fold higher than that of the other halogen derivatives **110** and **155** (IC_{50}(MK2, **156**) = 117 nM; IC_{50}(MK2, **110**) = 61.6 nM; IC_{50}(MK2, **155**) = 73.7 nM, Table 7). These values show that the inhibitory activity does not necessarily correlate with the reactivity of the warhead, since the half-life in the GSH assay of the chloro derivative **110** is three times longer than that of the fluoro compound **156** (124 h vs 35 h). The halogen substituent may contribute to the proper pre-orientation of the compound to allow nucleophilic attack of the cysteine side chain and covalent bond formation. Moreover, its impact on the electron density of the pyridine ring and the pKa of the linker *NH* may affect the binding properties of the ligan din the pre-reaction complex.

Table 7: Inhibitory activity of potential MK2 inhibitors with heterocyclic warheads; IC_{50} values were determined in a HotSpot™ kinase assay at Reaction Biology Corp., using 5-point singlicate ([a] duplicate) measurements with 10-fold dilution steps starting from 5 µM.

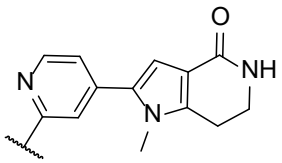

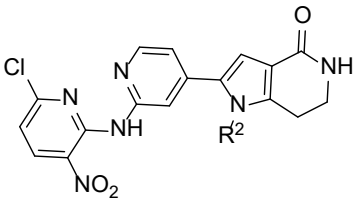

#	R	IC_{50} (MK2)	#	R	IC_{50} (MK2)	#	R^2	IC_{50} (MK2)
110	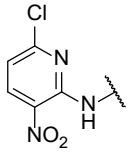	61.6 nM [a]	**204**	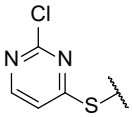	> 5 µM	**110**	**CH_3**	61.6 nM [a]
156		117 nM	**206**	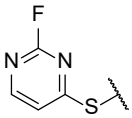	> 5 µM	**231**	**H**	0.36 nM
155	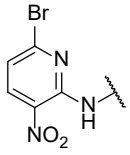	73.7 nM	**205**	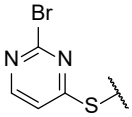	> 5 µM	**232**	**MOM**	1.36 nM
166	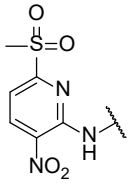	> 5 µM	**209**	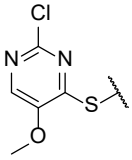	> 5 µM	**238**	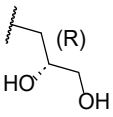	1070 nM
157	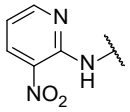	4.57 µM	**207**	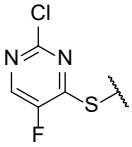	> 5 µM	**239**	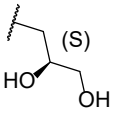	396 nM

Introduction of a sulfone residue instead of halides as the leaving group abolishes the activity of compound **166** (71% residual activity @ 5 µM). Considering the low stability towards GSH (see section 4.6), which is in line with their higher reactivity compared to aryl halides observed by others [266b], the compound is expected to react with dithioerythritol (DTT) (or other reaction buffer components) to a significant extent before being able to bind the kinase.

To evaluate the influence of the substitution at the pyrrole the prototype chloronitropyridine warhead was combined with variable residues attaches to the pyrrole nitrogen atom. Replacing the methyl group (**110**) with a methoxymethyl (**232**) reduced the IC_{50} value to the single digit nanomolar range (IC_{50}(MK2) = 1.36 nM). Although it cannot be fully excluded that this compound liberates the free pyrrole or its hemiaminal precursor during the assay runtime, the high chemical stability of this

compound, which also led to problems with removing the MOM-group during synthesis, indicates that this is rather unlikely (see section 3.3.2.1.3). Increasing the size of the substituent further to a 2,3-dihydroxypropan-1-yl (**238, 239**), a modification made with the aim of improving solubility, hinders inhibitor binding and decreases activity. While the *R*-enantiomer **238** has an IC_{50} value of 1.07 µM, the activity of the *S*-enantiomer **239** is 3 times higher (IC_{50}(MK2) = 396 nM) highlighting der different binding properties. Complete removal of the pyrrole *N*-substituent has the greatest positive effect on the potency. The unsubstituted compound **231** inhibits MK2 with an IC_{50} value of 0.36 nM.

Changing the linking atom from nitrogen to oxygen or sulfur did not lead to active compounds (Table 7). Notably, while the sulfur-linked congeners where synthetically quite accessible, the preparation of the oxygen-linked analogs proved to be notoriously challenging. Unfortunately, the sulfur-linked compounds **204**, **205**, **206** and **207** showed no inhibition at the highest concentration tested (5 µM). Compound **209** only showed low inhibitory activity at this concentration (85% residual activity @ 5 µM). However, the intrinsic reactivity towards GSH is similar when compared to the active inhibitors **64** and **110** ($t_{1/2}$(**204**) = 94 h, $t_{1/2}$(**64**) = 84.5 h, $t_{1/2}$(**110**) = 124 h, Figure 41). The sulfur atom is larger than the nitrogen ($r_{(S)}$=1.05 Å versus $r_{(N)}$= 0.71 Å) [300] and features increased bond lengths while also favoring different torsion angles, which alters the geometry of the linker. This may prevent suitable positioning of the warhead or even induce steric clashes. In addition, the linking *NH* is able to form an intramolecular hydrogen bond with the nitro group of the chloronitropyridine warhead, stabilizing the right orientation of the electrophilic center (shown in Figure 36). Replacing the nitro group and/or exchange of the linking heteroatom disrupts this interaction. The loss in activity for the sulfur derivatives was also observed, when targeting FGFR4 via a related strategy. [227]

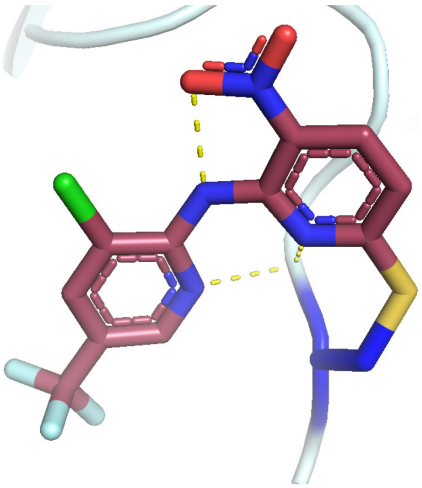

Figure 36: Covalent fragment **36** (colored in raspberry) bound to FGFR4 (PDB: 5NUD, covalent bound cysteine displayed as sticks in blue). Relevant hydrogen bond interactions to the hinge region and the intramolecular interactions shown as yellow dotted lines.

4.2 Evaluation of Kinetic Binding Parameters

Irreversible covalent inhibitors bind to the kinase via a two-step binding mechanism with covalent bond formation as the rate-limiting second step. Although the IC_{50} value is commonly used to initially estimate inhibitory activity, it neglects the time-dependency of this binding mechanism. A more accurate measure to compare covalent binders is the second order rate constant k_{inact}/K_I, which is a time-independent measure of potency governing both binding steps i.e. non-covalent complex formation (reflected by K_I) and the covalent reaction step (reflected by k_{inact}). Optimized irreversible kinase inhibitors typically display k_{inact}/K_I values between 10^5 $M^{-1}s^{-1}$ and 10^7 $M^{-1}s^{-1}$. [301] For Afatinib, the k_{inact}/K_I value is

$5.2 \cdot 10^6$ $M^{-1}s^{-1}$. [302] In this context, it is important to note that k_{inact} does not equal intrinsic chemical reactivity and although a correlation between these parameters is often observed, they may also show opposing trends. [215]

Table 8: Assessment of the affinity and kinetic parameters of compound **64** and **110**, performed at AssayQuant® Technologies, Inc.; values for gamcemetinib published by MALONA *et al.* [228]

		IC_{50} [nM]	K_i [nM]	k_{inact}/K_I [$M^{-1}s^{-1}$]	k_{inact} [s^{-1}]	K_I [µM]
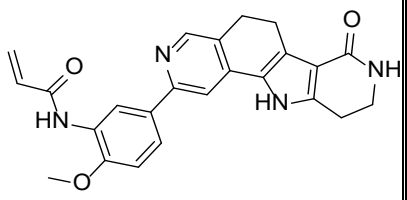	**64**	2.50	1.25	$2.58 \cdot 10^5$	$11.2 \cdot 10^{-3}$	0.0435
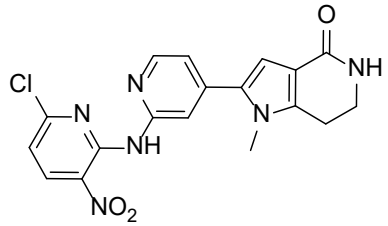	**110**	40.2	20.1	$5.01 \cdot 10^3$	$8.1 \cdot 10^{-3}$	1.65
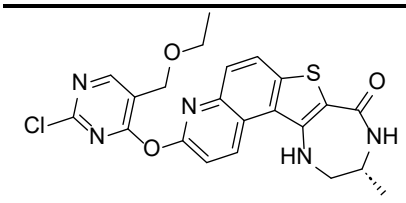	**Gamcemetinib**	156	-	$4.94 \cdot 10^3$	$0.82 \cdot 10^{-3}$	0.172

The time-dependent assay format was performed at AssayQuant® Technologies, Inc. (AQ), at their site in Marlboro, MA, US. They utilize a modified peptide substrate to continuously detect the reaction progress by a fluorescence reader. The attached sulfonamido-oxine (Sox) chromophore changes emission upon substrate phosphorylation through its chelating properties, enabling fluorescence-based read-out. [303] The kinetic parameters can then be gained from the resulting reaction progress curves. The IC_{50} values were calculated from the 20 min timepoint (Table 8). When compared to the values obtained in the HotSpot™ kinase assay at Reaction Biology (RBC), they were found to be in the same range (IC_{50}(AQ) = 2.50 nM vs. IC_{50}(RBC) = 2.62 nM for **64**; IC_{50}(AQ) = 40.1 nM vs. IC_{50}(RBC) = 61.6 nM for **110**). The inhibitory constant K_i is defined as the concentration of an inhibitor at equilibrium when 50% of the enzyme is occupied, while no competing substrate is present. The apparent K_i values can be calculated from the IC_{50} values using the CHENG-PRUSOFF equation under specific conditions. The apparent *K*i values for **64** and **110** are shown in Table 8. [304]

The k_{inact}/K_I value for the acrylamide compound **64** ($2.58 \cdot 10^5$ $M^{-1}s^{-1}$) falls within the same range of approved EGFR inhibitors compared by ZHAI *et al.* [302] (10^4-10^7 $M^{-1}s^{-1}$). The potency of **110** is 50 times lower ($5.01 \cdot 10^3$ $M^{-1}s^{-1}$) and is similar to the value published for the covalent MK2 inhibitor

gamcemetinib ($4.94 \cdot 10^3$ $M^{-1}s^{-1}$). Examining the values for k_{inact} and K_I separately allows for further interpretation. The K_I value describes the non-covalent binding affinity and is defined as the concentration at which the rate of covalent bond formation is half the maximum. Inhibitor **110** exhibits the lowest reversible binding affinity and therefore the highest K_I (K_I(**110**) = 1.65 µM). The affinity of **64** towards the binding pocket of MK2 is 40 times higher (K_I(**64**) = 0.0435 µM), which explains the difference in k_{inact}/K_I, since the values for k_{inact} are similar. The efficiency of the covalent bond formation from the properly arranged non-covalent pre-reaction complex is described by the second parameter, k_{inact}. The efficient bond formation of the heterocyclic warhead in **110**, with a similar k_{inact} to the acrylamide in **64**, underlines the potential of this warhead type. Although, **110** and gamcemetinib have a similar k_{inact}/K_I, the contribution of both terms differs. While the K_I value of gamcemetinib is 10 times lower, indicating improved reversible binding, the k_{inact} of **110** is 10 times higher despite the low intrinsic reactivity of this compound (*vide infra*). The potential for improving the reversible binding parameters of **110** is highlighted by these relations.

4.3 Investigations on the Covalent Binding Mode

To confirm the formation of the suggested covalent bond, various experimental options are available. A first indication can be gained from the biochemical assay. The inhibitory activity decreases when the reactive acrylamide is replaced by a saturated propionamide (IC_{50}(**64**) = 2.62 nM vs. IC_{50}(**69**) = 995 nM), suggesting that of the covalent bond formation contributes to the inhibitory activity. The same relationship was observed between the heterocyclic chloronitropyridine warhead in **110** and the analogous non-chlorinated nitropyridine in **157** (IC_{50}(**110**) = 61.6 nM vs. IC_{50}(**157**) = 4570 nM). Further experiments are, however, required to support the binding hypothesis. Therefore, modification of the target protein by the potential inhibitor was assessed by intact protein mass spectrometry at our cooperation partners from the group of Prof. Dr. STEFAN KNAPP (Institute for Pharmaceutical Chemistry, Structural Genomics Consortium, Goethe University, Frankfurt). If the protein is labeled successfully after incubation with the respective compound, the mass shift corresponding to the protein bound to the inhibitor can be detected in the mass spectrum. All four inhibitors tested (**64**, **96**, **108**, **102**) showed the expected shift in the analysis, i.e. addition of the inhibitor mass in the case of the acrylamides and the loss of the chloride for the chloronitropyridine compounds upon covalent bond formation via a S_NAr reaction. These results already strongly support the covalent mechanism via a thia-MICHAEL-addition and a S_NAr reaction, respectively. However, additional evaluations are necessary for further confirmation of the binding mode. To confirm the labeling of the desired cysteine, the protein labeling experiment should be combined with trypsin digestion of the labeled protein to identify the location of the labeled residue. [305] Additionally, the co-crystal structure of the inhibitor bound to the kinase can provides further insights (see section 4.4).

4.4 X-Ray Crystal Structure of 64 and 110 bound to the Proteinkinase MK2

X-ray crystallographic analysis of inhibitor-kinase complexes represents a valuable approach to elucidate the binding mode during compound evaluation. The crystal structure can furthermore support lead optimization and delivers a starting point for quantum mechanics/ molecular mechanics (QM/MM) calculations, shedding light on the details of the covalent binding mechanism. In the development process of covalent compounds, the formation of the covalent bond can be visualized in the crystal structure. GUIQUN WANG from the group of Prof. Dr. STEFAN KNAPP (Institute for Pharmaceutical Chemistry, Structural Genomics Consortium, Goethe University, Frankfurt) successfully crystallized MK2 bound to compound **64** and **110**, respectively. The co-crystal structure shows the expected covalent bond formation from Cys140 via MICHAEL-addition to the acrylamide warhead in compound **64** (Figure 37).

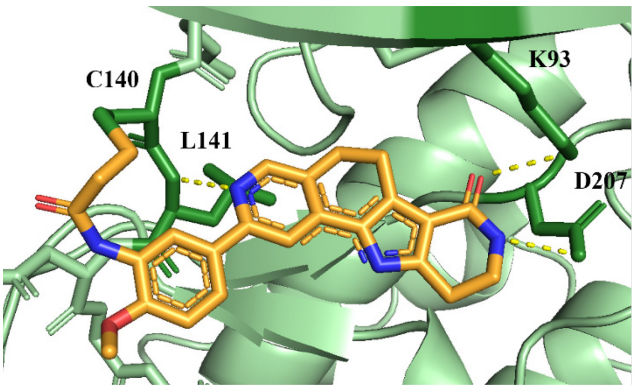

Figure 37: Co-crystal structure of MK2 bound to **64** generated by GUIQUN WANG; inhibitor colored in orange, kinase in light green, polar interactions indicated by yellow dotted lines; residues involved in inhibitor binding in forest green.

For compound **110**, the covalent binding by replacement of the chloride via a S_NAr reaction is also shown in the co-crystal structure (Figure 38). Furthermore, the orientation of both compounds (**64** and **110)** within the ATP binding pocket aligns with the expected binding mode (illustrated in Figure 37 and Figure 38). The pyridine nitrogen of the pyridine-based tetracyclic core of **64** and the pyridine core in **110** can interact with the backbone *NH* of Leu141. The crystal structure of **110** additionally shows a relatively coplanar orientation of the heterocyclic warhead, supported by a hydrogen bond interaction of the warhead residue to the backbone of Leu141. In addition, the orientation of the lactam moiety towards Lys93 and Asp207 is consistent with the binding mode observed for the reversible tetracyclic structures and the pyrrolopyridinone derivatives from the literature (displayed in Figure 19 and Figure 21, section 1.4.2).

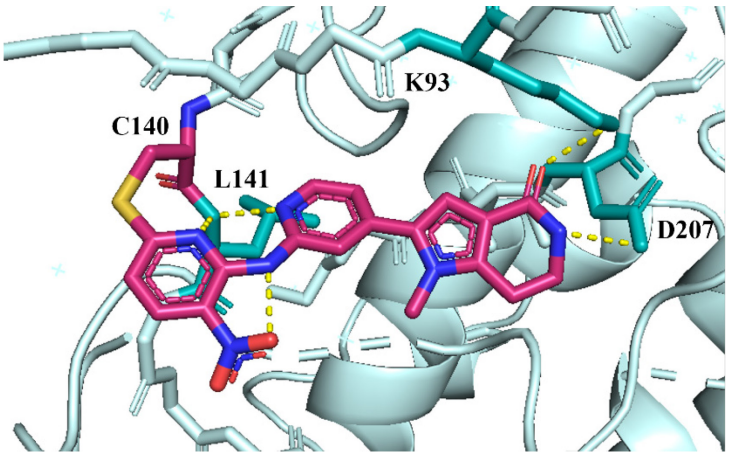

Figure 38: Co-crystal structure of MK2 bound to **110** generated by GUIQUN WANG; inhibitor colored in pink, kinase in pale cyan, polar interactions indicated by yellow dotted lines; residues involved in inhibitor binding in cyan.

4.5 Assessment of the Selectivity of Selected Compounds

Compounds **102** and **110** were tested against the subset of kinases with an equivalent positioned cysteine (FGFR4, MK3, S6K2 and MPS1). The data for the two compounds were determined at Reaction Biology Corp. in a radiometric HotSpot™ kinase assay and compared with the available data for gamcemetinib from the literature (Table 9). [228]

The experimental setting used did not allow differentiation of the binding affinity with the high activity of **102**. The four kinases, FGFR4, MK2, MK3 and S6K2 were inhibited with an IC_{50} value below the determination limit of the assay system used. However, only the inhibitory activity against MPS1 was significantly lower. This trend was even more pronounced for the compound **110**, where no inhibition of MPS1 could be measured at a compound concentration of 5 µM. Gamcemetinib also did not show any inhibition of MPS1. [228] The IC_{50} value for **110** against FGFR4 demonstrated good selectivity (IC_{50}(FGFR4) = 1.39 µM). Unfortunately, compound **110** did not exhibit selectivity against MK3 and S6K2, with IC_{50} values in the double-digit nanomolar range. Similarly, gamcemetinib showed only 20% inhibition of FGFR4@ 1 µM. In this case, the activity against MK3 and S6K2 is also similar to that observed for MK2.

Table 9: Inhibition of kinases with a cysteine in an equivalent positioned. IC_{50} values for **102** and **110** were determined via 5-point singlicate measurements (assay performed at Reaction Biology Corp.) with 10-fold dilution steps starting from 5 µM. Values for gamcemetinib were extracted from the literature. [228] a) Assay performed with 5-fold dilution steps, starting from 2 µM; b) percent inhibition of the kinase @ 1 µM concentration of the compound.

#	FGFR4	MK2	MK3	S6K2	MPS1
102	< 0.50 nM	< 3.20 nM a)	< 0.50 nM	< 0.50 nM	765 nM
110	1.39 µM	61.6 nM	21.5 nM	31.2 nM	> 5.00 µM
Gamcemetinib CC-99677	20% b)	156 nM 94% b)	73% b)	71 nM 89% b)	-

To estimate selectivity over a broader panel, compounds **64** and **109** were tested in a thermal shift assay against 102 kinases and compounds **96**, **102** and **108** against 100 kinases by our cooperation partners at the group of Prof. Dr. STEFAN KNAPP (Institute for Pharmaceutical Chemistry, Structural Genomics Consortium, Goethe University, Frankfurt) (selected values depicted in Table 10). Tetracyclic pyrimidine-based acrylamide compound **96** induces a shift in melting temperature above 10 °C for seven kinases, including the target protein MK2 (Table 4). This number decreases for the pyridine-based tetracyclic acrylamide structure **64** (4 enzymes with $\Delta T_m > 10$ °C). The pyrimidine-based tetracyclic compound with the alternative S_NAr warhead **102** exhibited a $\Delta T_m > 10$ °C for MK2 and one additional

kinase, DYRK2. For acrylamide-containing pyrrolopyridinone derivative **108** still 12 kinases displayed shifts $\Delta T_m \geq 5$ °C (see section 6.1). The corresponding unreactive propionamide-derivate **109** exhibited a significantly lower shift in melting temperature for MK2 ($\Delta T_m = 3.9$ °C) compared to acrylamide **108** ($\Delta T_m = 11.7$ °C for MK2), while the T_m-shifts of the other kinases stay in a similar range as observed for **108**. This indicates that binding to these kinases is not driven by covalent bond formation, but rather by non-covalent interactions. However, this assay format only determines the stabilizing effect of a compound on the protein which does not always correlate with the inhibitory activity of the compound. To confirm or rule out off-target activity the inhibitor must be tested against the kinases in question in a biochemical assay format or even in a cellular environment. MALONA *et al.* evaluated the effect of gamcemetinib on a subset of kinases that were inhibited in the biochemical assay on a cellular level. However, they found no effect on the suggested off-targets in cells. [228]

Table 10: Data from the thermal shift screening for **64**, **96**, **102**, **108** and **109**; $\Delta T_m > 10$ °C in bold; $\Delta T_m > 5$ °C in italic; relevant kinases selected, which show a greater shift for **96** than MK2.

	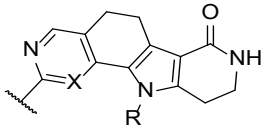			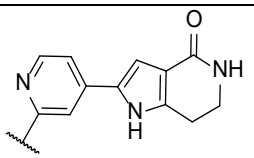	
	X = CH **R = H**	**X = N** **R = H**	**X = N** **R = CH_3**	-	-
	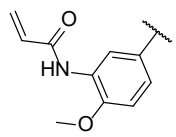	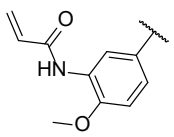	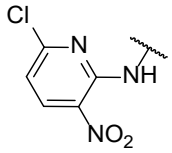	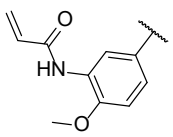	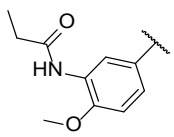
	64	**96**	**102**	**108**	**109**
Enzyme	**ΔT_m [°C]**			**ΔT_m [°C]**	
MAP3K5A	*9.49*	**14.59**	8.56	8.79	*6.00*
CAMKK2B	**12.60**	**14.07**	3.36	*8.68*	6.87
TOPKA	*6.82*	**12.89**	0.52	*8.67*	0.85
CLK1	*8.57*	**11.44**	*9.32*	5.98	3.53
STK17A	**10.36**	**11.17**	*8.29*	*8.22*	*7.74*
DYRK2A	**10.10**	**10.94**	**13.87**	*8.26*	*7.63*
GPRK5A	3.24	**10.55**	2.13	1.40	0.43
MAPKAPK2A	**10.66**	**10.51**	**10.32**	**11.67**	**3.87**
DYRK1A	*7.49*	*9.51*	*6.78*	5.19	3.89
TTK1A	*6.44*	*6.96*	2.39	2.08	1.88

4.6 Stability of Synthesized Inhibitors towards Nucleophiles

The mode of action of cysteine-targeting covalent inhibitors is determined by their electrophilic characteristics. It is important to balance these reactive properties to avoid off-target reactivity, which can cause unwanted side-effects and limit activity due to premature quenching of the compound. However, sufficient reactivity is necessary for efficient binding to the target structure. Optimized reversible binding properties of the inhibitor and positioning of the warhead allow for minimizing the warhead reactivity while maintaining adequate inactivation rates (k_{inact}). The reactivity of the warhead can be adjusted by changing its (chemo)type or modifying the substitution pattern.[213, 306] Highly reactive warheads are often used in early stages of drug discovery programs, such as target identification by means of "electrophile first" approaches. Drug-like inhibitors typically exhibit lower reactivity, often falling within the same range as established covalent inhibitors, such as afatinib or ibrutinib. Assessing warhead reactivity is a crucial step in inhibitor development and often involves evaluating its reactivity towards GSH.[215, 232, 306c]

As GSH assays tend to strongly depend on minor deviations in the assay conditions, afatinib was used as a control to obtain a comparative value for our adjusted assay conditions when compared to various literature protocols. The assay protocol used by KEELEY *et al.*[306a] was adapted to enable measurement of compounds with low solubility. The following modifications were already applied for reactivity assessment on the S6K2 and FGFR4 projects.[225, 227] The compound concentration was lowered to a final concentration of 100 µM and the amount of organic co-solvent increased to 50% of acetonitrile. The PBS buffer used in the literature procedure[306a] was exchanged to a HEPES (4-(2-hydroxyethyl)-1-piperazineethanesulfonic acid) buffer system, adapted from the buffer used for the biochemical assay at RBC[296]. To prevent interference with the compounds, the composition was adjusted by omitting DTT and BSA from the mixture. The half-life ($t_{1/2}$) of Afatinib was determined to be 8.8 hours under the modified conditions. The assay runtime was limited to a maximum between 16 and 20 hours and the half-life for compounds with low reactivity extrapolated from the linear regression.

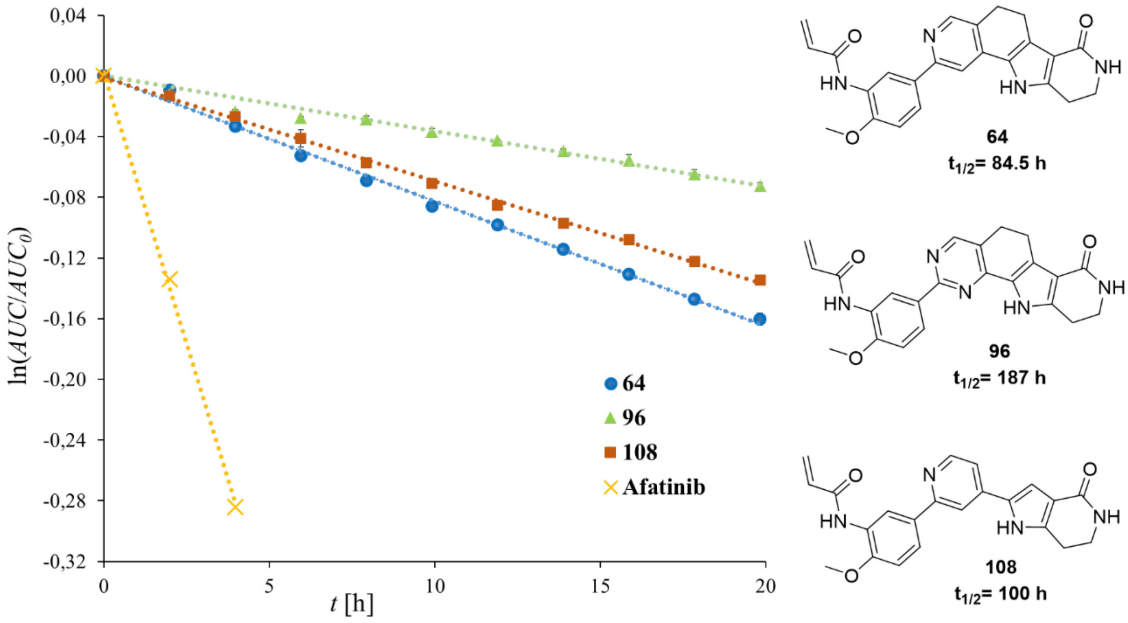

Figure 39: GSH-stability of selected acrylamide derivatives **64** (data depicted in blue), **96** (green) and **108** (orange), compared to afatinib (**30**, yellow).

The reactivity of the three acrylamide-containing compounds was determined to compare the impact of the different core structures. As expected, the core only had a minor influence on the reactivity of the warhead (see Figure 39). The determined half-life values were 10- to 20-fold higher than the value found for afatinib (84.5 h vs. 8.8 h), which may be rationalized by their more electron-rich aryl linker, which deactivates the acrylamide. Additionally, the *N,N*-dimethylaminomethyl substituent at the β-position of the acrylamide in afatinib **30**, can increase reactivity.[234b, 306c] The mass spectrometry analysis of the assay solution for **64** and **96** showed the formation of the expected product of a thia-MICHAEL-addition with GSH.

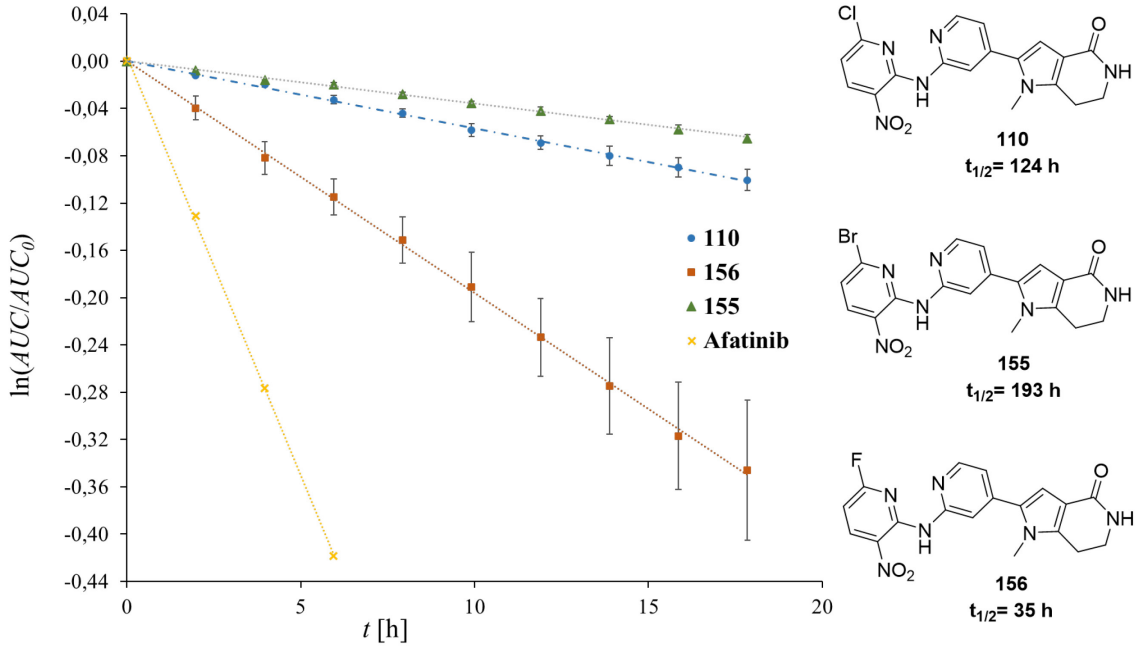

Figure 40: Stability of S_NAr-based inhibitors **110** (data depicted in blue), **155** (green) and **156** (orange) towards GSH compared to afatinib (**30**, yellow).

When the warhead was changed from the classical acrylamide in **108** (Figure 39) to the heterocyclic warhead in **110** (Figure 40), the reactivity did not change significantly ($t_{1/2}$(**108**) = 100 h to $t_{1/2}$(**110**) = 124 h), indicating a favorable and druglike reactivity range of the chloronitropyridine warhead. In the next step, the exchange of the halogen leaving group was investigated. In line with common reactivity trends for S_NAr reactions, the bromine derivative **155** exhibited a half-life similar to that of the chlorine compound **110** (see Figure 40). The significantly higher reactivity of the fluoropyridine inhibitor **156** was expected, as fluoroarenes are known to be more reactive in S_NAr reactions than the chloro and bromo derivatives. [299]

Mass spectrometric analysis supported the presumed reaction with GSH via an S_NAr mechanism (Scheme 55). The mass of the respective GSH adduct was found, and no hydrolysis could be detected. The higher reactivity of the warhead, however, does not translate into higher inhibitory activity of **156** (IC_{50}(MK2) = 117 nM) compared to the chlorine derivative **110** (IC_{50}(MK2) = 61.6 nM) highlighting the discrepancy between intrinsic reactivity and efficiency of covalent binding to the target.

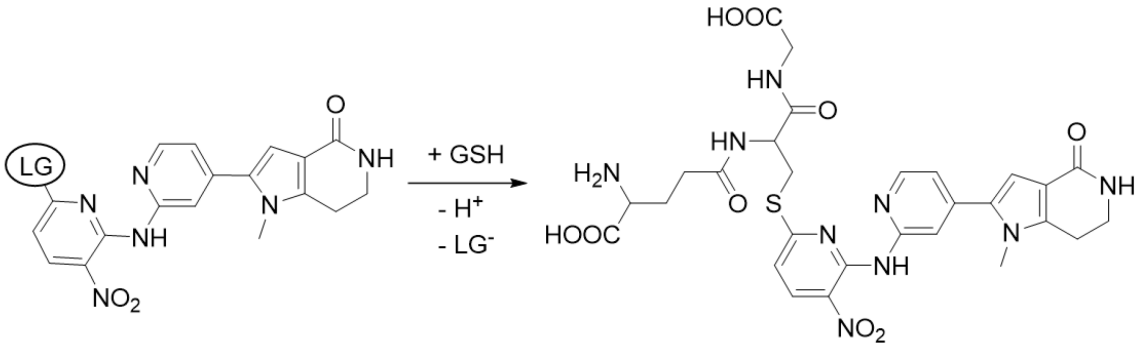

Scheme 55: Adduct formation of the halonitropyridine warhead with GSH; LG = leaving group.

ZAMBALDO *et al.* [266a] and PICHON *et al.* [266b] described sulfonyl-substituted heterocyclic derivatives as cysteine-reactive moieties. In their study, PICHON *et al.* performed an extensive evaluation of sulfonylpyrimidine reactivity showing, that sulfonyl leaving groups generally feature an increased reactivity compared to halides in this context. [266b] In line with these results, the sulfone-containing derivative **166**, which was synthesized with the aim of improving solubility, displayed extensive reactivity towards GSH, leading to complete degradation after two hours (exact half-life not determined). Adduct formation with GSH via the expected S_NAr mechanism could be confirmed by HPLC-MS analysis. The reactivity of **166** is significantly higher than that of the other compounds, including afatinib, which is a comparably reactive example of an approved TCI drug. Based on the substantial data available on the clinical use of afatinib, its reactivity seems to be suitable to define an upper limit for drug-like compounds to reduce the risk of toxicity related to promiscuous electrophilic reactivity. [307] Furthermore, fast degradation impedes biochemical evaluation. Since the reaction buffer typically contains DTT, a thiol-containing reducing agent used to stabilize the kinase, excessive reactivity towards thiols can result in reaction with the buffer component during incubation and thus premature degradation of the inhibitor.

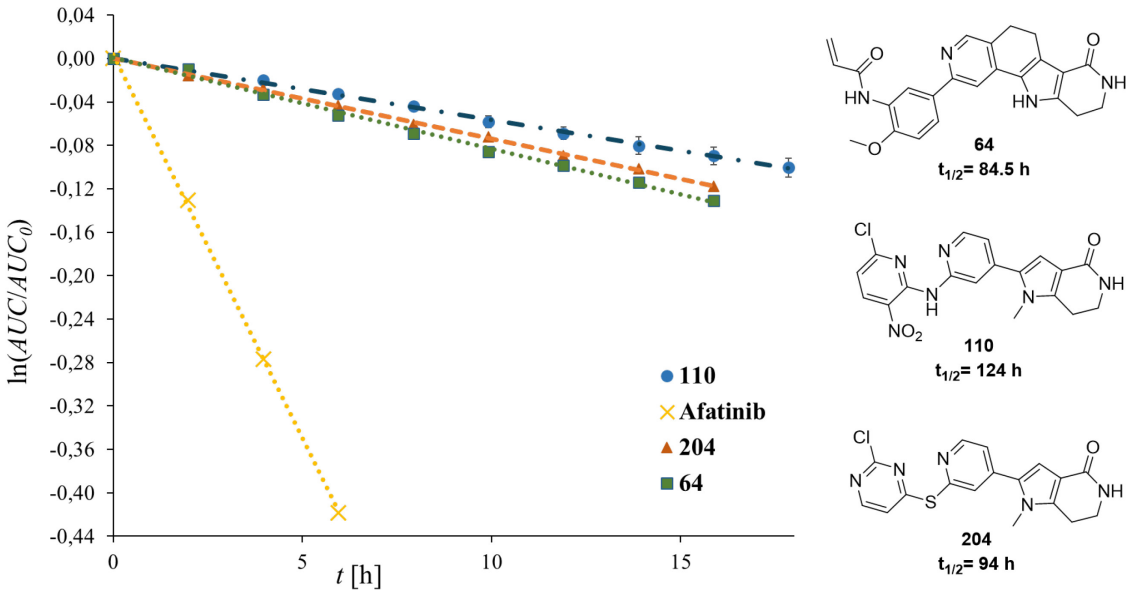

Figure 41: Comparison of the reactivity of different warhead structures present in **64** (data depicted in green), **110** (blue) and **204** (orange) compared to afatinib (**30**, yellow).

The sulfur-linked 2-chloropyrimidine compound **204** does not exhibit inhibitory activity against MK2 in the biochemical assay up to the highest concentration tested (5 µM). However, this lack of activity does not correlate with the intrinsic reactivity of the warhead. The determined half-life of 94 hours falls in the same range as the values obtained for compounds **64** and **110** (Figure 41).

The adjustments of the method for GSH assays, as described above and in section 6.1, due to the low solubility of the compounds, limit the comparability of the stability data with values from the literature. The better solubility of the diol-substituted inhibitor **239** in aqueous systems enables the determination of the reactivity in two additional settings. Initially, the stability was determined in a 50:50 buffer/ACN mixture, as used for the previous experiments to compare the value with the one obtained previously (Figure 42). The half-life of **110** is twice as long as for **239**, despite sharing the same warhead moiety.

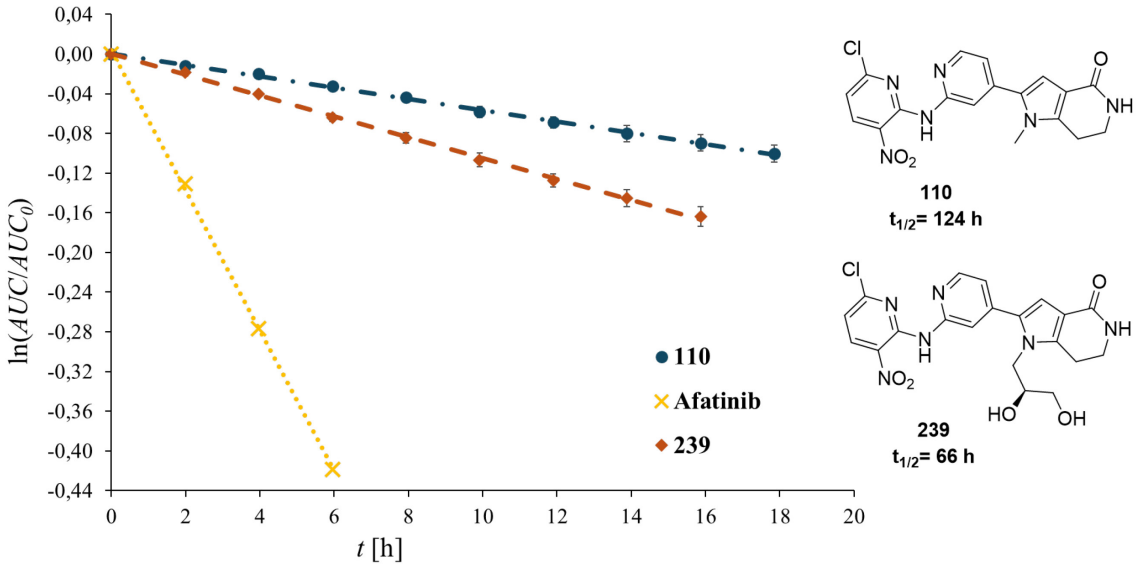

Figure 42: Comparison of the GSH-stability of **110** (data depicted in blue) and **239** (orange) in a 50:50 HEPES buffer/ACN mixture.

The higher reactivity of **239** is likely linked to better solvation of the molecule. Additionally, it is also conceivable that the diol moiety impacts reactivity by altering conformational preferences or assisting nucleophilic attack. Nevertheless, the compound remained in a favorable reactivity rage with a half-life ~8-times longer than afatinib.

When the amount of organic co-solvent was reduced to 10% ACN, the half-life decreased to 99 min (Figure 43A). The half-life of afatinib was also reduced to 26 min in buffer containing 10% ACN and 25 min in plain GSH-containing buffer. These values are consistent with those determined by WARD *et al.* in their assay system ($t_{1/2}$ = 25 min; LC-UV-MS-based, phosphate buffer pH = 7.4, 4.6 mM GSH, 37 °C).[307] When measuring the stability of **239** in HEPES buffer without additionally cosolvent the half-life increased to 124 min. However, this was accompanied by an increased deviation of the measured values, as indicated by the error bars in Figure 43B. These effects may be caused by limited solubility of compound **239** in this system. Significant precipitation of the compound was observed at room temperature (rt) (in solution A), which was not obvious in the reaction solution at 40 °C at which the GSH assays were performed. Nevertheless, this may have caused systematic errors during sample preparation and/or possibly during the runtime of the assay.

The aqueous stability of **239** was also assessed in HEPES buffer without the addition of GSH, and no degradation was observed after 3.40 h (displayed in orange in Figure 43B).

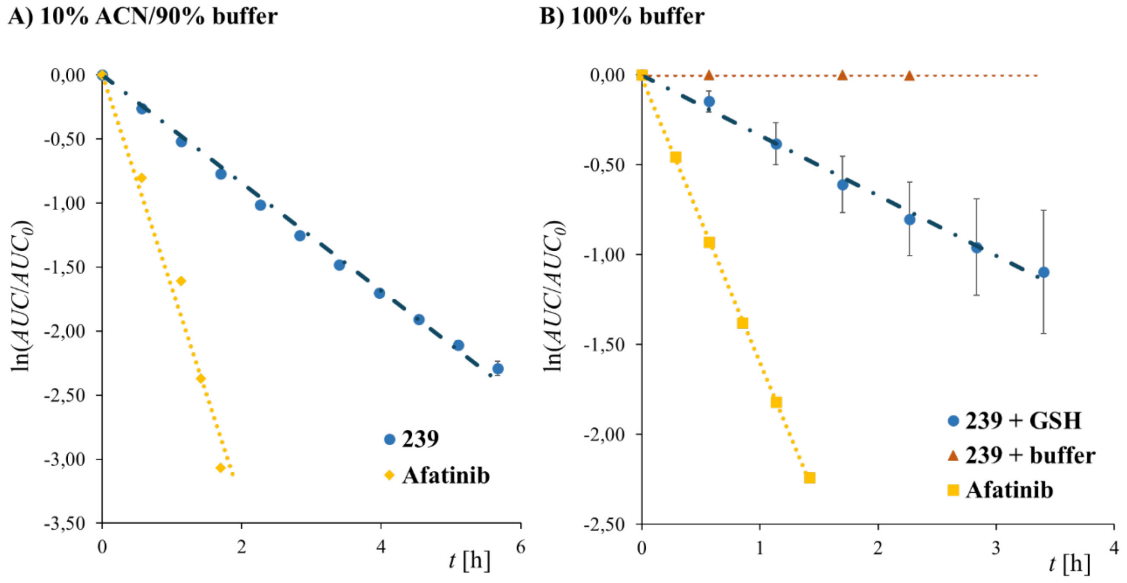

Figure 43: Stability of compound **239** (blue graph) and afatinib (in yellow) towards GSH; A) measurement in HEPES buffer with 10% ACN; B) in 100% HEPES buffer, values for aqueous stability of **239** in orange.

4.7 Metabolic Stability in Mouse Liver Microsomes

The metabolism of a molecule has significant impact on its pharmacokinetic behavior and its toxicity. Biotransformation processes are typically intended to facilitate the excretion and detoxification of xenobiotics. However, some metabolic processes can produce reactive and toxic intermediates.

Evaluating metabolic stability is a critical part of the drug discovery process. Liver enzymes play a crucial role in the metabolic process, and various model systems, such as the use of liver microsomes, hepatocytes or recombinant enzymes, have been established for *in vitro* assessment of liver metabolism. Using liver microsomes offers several experimental advantages, like low complexity for the test procedure, low costs and good stability during storage, making them a suitable model for early experiments. [308] Liver microsomes are a subcellular system, derived from the endoplasmic reticulum (ER) and isolated from liver tissue. They contain ER-associated enzymes, such as cytochrome P450 (CYP) and CYP reductase, which are involved in drug metabolism. These two enzyme classes are key enzymes in drug metabolism and are known to be involved in the biotransformation of aromatic nitro groups, such as those present in the heterocyclic warhead of **110**, as well as various oxidative processes. Nitroaromatic compounds have been linked to liver toxicity and mutagenicity due to highly reactive intermediates formed during reductive metabolism that are able to bind proteins and DNA. However, not all nitroarene compounds undergo reductive metabolism, as the reactivity of the nitro group towards

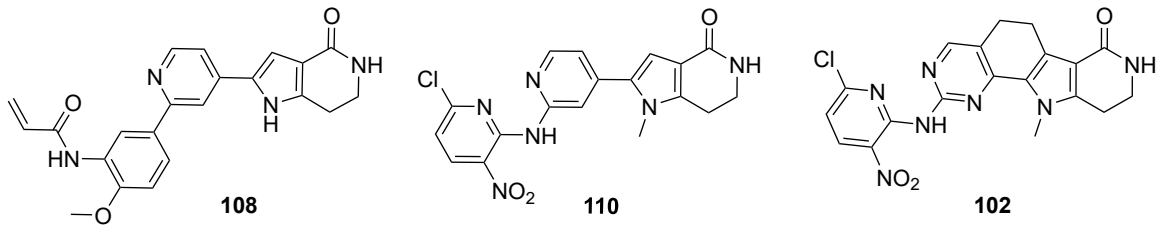

Figure 44: Selected compounds **108**, **110**, and **102** tested for metabolic stability in MLM.

metabolism is influenced by different structural features. [309] Notably, a variety of nitro-containing drugs is approved. [310] In order to detect metabolic soft spots, the microsomal metabolism of three selected compounds **108**, **110** and **102** was investigated in mouse liver microsomes (MLM). The experiments were conducted by MARK KUDOLO and ALEXANDER RASCH from the group of Prof. Dr. STEFAN LAUFER (Institute of Pharmaceutical Chemistry, Eberhard Karls University, Tübingen).

The acrylamide derivative **108** showed good metabolic stability, with 93% of the compound remaining after 90 min, indicating no specific metabolic hotspot related to the pyrrolopyridinone core. In contrast, the metabolic degradation of S_NAr-based inhibitors **102** and **110** was significantly increased. Compound **102** underwent 83% conversion of the parent compound within 90 min, leaving only 17% intact. Inhibitor **110** displayed better stability, with 54% of the compound remaining after 120 min. Based on the experimental results from other projects, the warhead appears to be metabolically stable in both the S6K2 inhibitor **39** [225] and the quinazoline-based FGFR4 inhibitor **37**. [227] The absence of any reduction of the nitro group suggests that metabolism occurs at the core structure. Mass analysis of the metabolite revealed a difference in *m/z* of +16 Da, indicating oxidation of the compound. Hydroxylation and *N*-oxide formation are known metabolic pathways for pyridines and are consistent with the observed mass shift, while hydroxylation of a benzylic CH-group may also be possible. [311] Additionally, a second metabolite with a mass shift of -2 Da was detected for compound **110**. The detected *m/z* of 397.8 (Δm = -2 Da) was suggested to be due to desaturation of the lactam ring. The metabolic stability of **110**

was found to be similar to the published data for gamcemetinib.[228] MALONA *et al.* measured the metabolic stability in mouse S9 fraction, a subcellular fraction which contains microsomal and cytosolic enzymes involved in metabolism, and found that 72% of the compound remained after 30 min (63% for **110** after 30 min).[228]

4.8 Determination of the Solubility of Selected Compounds

Physicochemical properties of a compound such as solubility and lipophilicity determine its pharmacokinetic behavior and ADMET (absorption, distribution, metabolism, excretion, toxicity) properties in a broader sense. Furthermore, these characteristics can influence *in vitro* assays, in the early stages of drug development. Low solubility of a compound and resulting precipitation can lead to systematic and time-dependent deviation during dilution processes, resulting in misinterpretation of measured values and underestimation of the activity.[312] Increased size, planarity, number of aromatic rings, and certain hydrogen bond donor/acceptor patterns negatively affect solubility.[313] In the development of protein kinase inhibitors these properties are particularly relevant because they are often directly linked to compound activity and selectivity. The narrow binding pocket of MK2 favors planar molecules, which hampers solubility.[99] Here, kinetic solubility was tested by adding a stock solution of the compound in DMSO to aqueous HEPES buffer. The resulting concentration after stirring for 17 h was determined by HPLC/UV measurements.

Table 11: Solubility of a subset of compounds in HEPES buffer (pH 7.5). Values for the calibration curves were measured as triplicates; [a)] calibration curve measured as singlicate.

#	**64**	**102**	**108**	**110**	**232**	**157**	**181**	**204**	**239**
Solubility [µM]	6.78 [a)]	1.1	102	< 0.50	2.35	< 0.50	99.9	13.5	14.0

Compounds **64** and **102**, which are based on tetracyclic core structures, only displayed a solubility below 10 µM in the buffer system (Table 1). Opening of the β-ring in the pyrrolopyridinone derivative increased the solubility for the acrylamide-containing compounds by 10-fold (6.78 µM (**64**) vs. 102 µM (**108**)). The attachment of the nitropyridine via a nitrogen linker resulted in a significant loss in solubility (< 0.50 µM for compound **110** and **157**). Replacing the linker atom with sulfur, as in compound **204**, was beneficial for solubility (13.5 µM). Notably, during the development of gamcemetinib, which was published later, it was shown that the replacement of the amino linker by an ether significantly increased solubility.[228] Additionally, the nitro group of the warhead is able to form an intramolecular hydrogen bond to the linking *NH* (shown in Figure 36), which stabilizes a pseudobicyclic planar conformation presumably resulting in a further loss in solubility. Replacing the pyrrole *N*-methyl group with the propyl diol in chloronitropyridine derivative **239** significantly increased the solubility (14.0 µM), while the MOM group (**232**) had only a minor solubilizing effect.

5 Conclusion and Outlook

Three related MK2 inhibitor core structures were employed within this thesis. All of them were successfully equipped with electrophilic warheads resulting in compounds which displayed high potency against MK2 with IC_{50} values down to the single digit nanomolar range (**64**, **102**, **231**). Here, different warhead types were installed. "Classical" acrylamide warheads were successfully attached to all three cores. The resulting inhibitor structures showed good potency in the nanomolar range and the expected mass shift for the covalent modification of the kinase was observed in intact protein mass spectrometry experiments (performed by GUIQUN WANG from the group of Prof. Dr. STEFAN KNAPP, Institute for Pharmaceutical Chemistry, Structural Genomic Consortium, Goethe University, Frankfurt). Additionally, the kinetic binding parameters of **64** proved to be very good, with a k_{inact}/K_I of $2.58 \cdot 10^5$ $M^{-1}s^{-1}$. Moreover, in comparison to afatinib, **64** displayed a significantly lower intrinsic reactivity towards thiols as shown in a GSH stability assay ($t_{1/2}$ = 84.5 h vs. $t_{1/2}$ = 8.8 h).

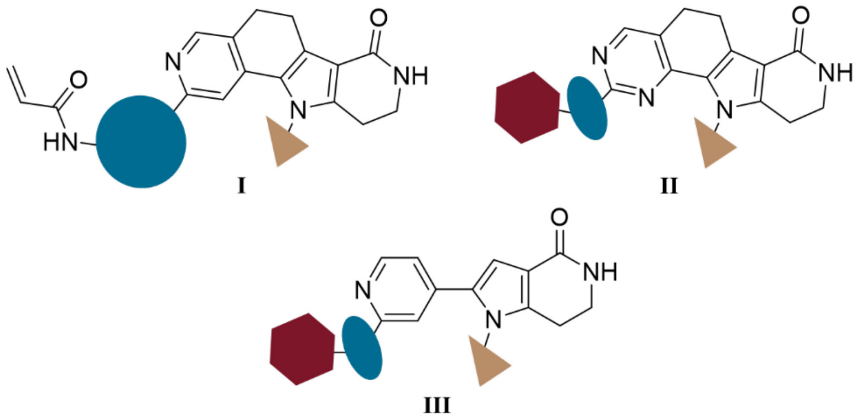

Figure 45: Overview of the different core structures and derivatization possibilities (linker colored in blue, warhead in red, pyrrole substituent in gold. **I**: tetracyclic pyridine-based compounds; **II**: tetracyclic pyrimidine-based compounds; **III**: pyrrolopyridinone derivatives

For compound **102** (tetracyclic core structure **II**, Figure 45), replacing the acrylamide warhead with an alternative heterocyclic warhead maintained the high potency (IC_{50} < 3 nM). The electron-deficient chloronitropyridine warhead, is supposed to react with the target via an S_NAr reaction. Due to synthetic reasons, further SAR studies concerning this warhead type were performed on the simplified pyrrolopyridinone core **III** (Figure 45). The resulting ring-opened derivative **110** (**III**) retained satisfying potency (IC_{50} = 61.6 nM). Changing the heteroatom linking the warhead to the core structure (highlighted in blue in Figure 45) to a sulfur atom, however, abolished inhibitory activity. As expected, removal of the chloride leaving group from a nitrogen-linked analog also strongly decreased inhibitory activity (**157**, IC_{50} = 4.6 µM), in line with a covalent mode of action which was again confirmed by intact protein MS.

Exchanging the chloride leaving group to fluorine, bromine or sulfone did not show any benefit either, which is interesting since the fluorine and the sulfone derivatives show enhanced intrinsic reactivity. This behavior deserves further investigations.

Finally, various substituents were introduced at the pyrrole nitrogen atom (golden triangle in Figure 45). Removing the methyl group, which had been introduced for synthetic convenience, increased potency (**231**, IC_{50} = 0.36 nM), enabling additional polar interactions with the target. Larger substituents, such as the dihydroxy propyl in **238** and **239**, decrease inhibitory activity but improve solubility (< 0.5 µM (**110**) vs. 14.0 µM (**239**)). Additional derivatization at this position could be beneficial for balancing activity and physiochemical properties. Another possibility for further inhibitor development is the variation of the warhead substitution pattern to enable tuning of warhead reactivity and potentially increase solubility, especially replacement of the nitro group is a desirable goal. It remains to be tested if activity can be retained by alternative, more drug-like functional groups which are capable of making a similar intramolecular hydrogen bond as the nitro group.

Importantly, it should be noted that significant obstacles had to be overcome in the chemical synthesis of the compounds presented herein and these efforts, the methods developed, and the lessons learned could significantly facilitate further SAR exploration.

After the protein MS experiments had already confirmed the successful covalent labeling of MK2, our cooperation partners from the group of Prof. Dr. STEFAN KNAPP (Institute for Pharmaceutical Chemistry, Goethe University, Frankfurt, experiments conducted by GUIQUN WANG) recently solved the X-ray crystal structures of the two key compounds **64** and **110**. These structures confirm the desired covalent binding of Cys140 in MK2 by the electrophilic warhead via a thia-MICHAEL addition in case of **64** and a S_NAr mechanism for **110**. In addition, they show the expected non-covalent binding interactions, which are in line with the data from the literature for the reversible analogs [1, 3, 206], confirming the initial design hypothesis. Furthermore, X-ray crystal structures can now be utilized to design further improved inhibitors and to elucidate the details of the binding mechanism, e.g. by applying QM/MM calculations.

Beyond this, the most promising compounds were shared with our colleagues at the University Hospital Tübingen (group of Dr. DANIEL DAUCH). Their obtained results showed a very interesting activity of the S_NAr based compounds in cells and organoid cultures of CRC and pancreatic ductal adenocarcinoma (PDAC), which was superior to the efficacy of acrylamide-based analogs. Despite being still preliminary, these results encourage the further exploration of SNAr-based MK2 inhibitors in an anticancer setting.

6 Experimental Part

6.1 Materials and Methods

Chemistry

Starting materials and reagents for the chemical synthesis were purchased from commercial suppliers and were used without purification. Anhydrous and oxygen-free solvents were also commercially acquired and stored over molecular sieve under an inert atmosphere. Thin layer chromatography (TLC) was performed using Merck 60 F254 silica plates (Merck KGaA, Darmstadt, Germany) and the spots were detected under UV light (254 nm or 366 nm). Purification of the compounds was performed by preparative column chromatography using either an Interchim PuriFlash XS420 (Interchim S.A., Montlucon, Allier, France) or a LaFlash V2.3 system (VWR International®). For normal phase separation Grace Davison Davisil LC60A 20-45 micron Silica (W.R. Grace and Company, Columbia, MD, USA) and Merck Geduran Si60 633200 micron silica (Merck KGaA, Darmstadt, Germany), or pre-packed columns from the puriFlash® SIHP series (60 Å, 500 m^2/g, 30 µM dp, 12/25/40 g; Interchim® S.A., Montlucon, Allier, France) were used. Reverse phase preparative column chromatography was conducted using a CHROMABOND® Flash RS 40 C 18 ec column (Machery-Nagel GmbH & Co. KG, Düren, Germany).

High-performance liquid chromatography (HPLC)

Method A:

The purity of the compounds was determined using Agilent 1100 systems (injection module, ColCom setup, degasser and binary pump, diode array detector (DAD) detector module; Agilent Technologies Inc., Santa Clara, CA, USA). A Phenomenex Luna® 5 µM C8 RP (150 mm x 4.6 mm, 5 µM, 100 Å) was used with an injection volume of 10 µL and a flow rate of 1.5 mL/min mL/min at 35 °C. Detection was performed at two different wavelengths, 254 nm and 230 nm.

0 min min: 40% MeOH, 60% phosphate buffer (0.01 M) pH 2.3

8 min: 85% MeOH, 15% phosphate buffer (0.01 M) pH 2.3

13 min: 85% MeOH, 15% phosphate buffer (0.01 M) pH 2.3

14 min: 40% MeOH, 60% phosphate buffer (0.01 M) pH 2.3

16 min: 40% MeOH, 60% phosphate buffer (0.01 M) pH 2.3

Method B/C:

The purity of the compounds was determined using an Agilent 1100 system (injection module with thermostat module, ColCom setup, degasser and binary pump; Agilent Technologies Inc., Santa Clara, CA, USA) coupled to an Agilent 1260 DAD detector module. Both methods used a Phenomenex Kinetex® 2.6 µM C8 100 Å (150 × 4.6 mm) column with an injection volume of 5 µL and a flow rate of 0.5 mL/min at 23 °C. Detection was performed at two different wavelengths, 254 nm and 230 nm.

Method B:

0 min: 40% MeOH, 60% phosphate buffer (0.01 M) M) pH 2.3

15 min: 85% MeOH, 15% phosphate buffer (0.01 M) M) pH 2.3

20 min: 85% MeOH, 15% phosphate buffer (0.01 M) M) pH 2.3

22 min: 40% MeOH, 60% phosphate buffer (0.01 M) M) pH 2.3

28 min: 40% MeOH, 60% phosphate buffer (0.01 M) M) pH 2.3

Method C:

0 min: 40% MeOH, 60% phosphate buffer (0.01 M) M) pH 2.3

9 min: 85% MeOH, 15% phosphate buffer (0.01 M) M) pH 2.3

10 min: 85% MeOH, 15% phosphate buffer (0.01 M) M) pH 2.3

11 min: 40% MeOH, 60% phosphate buffer (0.01 M) M) pH 2.3

16 min: 40% MeOH, 60% phosphate buffer (0.01 M) M) pH 2.3

Nuclear magnetic resonance (NMR) spectroscopy

NMR spectra were acquired using Bruker Avance III HD 200/400/600 spectrometers (Bruker Corporation, Billerica, MA, USA). Deuterated solvents were used to dissolve the samples. The residual solvent signal according to FULMER *et al.*[314] was used to calibrate the chemical shift relative to tetramethylsilane (TMS) as δ [ppm] = 0. The following indications were given for the multiplicity of signals: s = singlet, d = doublet, dd = doublet of doublet, t = triplet, q = quartet, b = broad singlet and m = multiplet.

Mass spectrometry

TLC-MS: MS data for intermediates was acquired using an Advion TLC-MS interface (Advion, Ithaca, NY, USA) based on electrospray ionization (ESI) in positive or negative mode. ESI voltage = 3.50 kV; capillary voltage = 187 V; source voltage = 44 V; capillary temperature = 250 °C; desolvation gas temperature = 250 °C; gas flow = 5 L/min nitrogen.

HPLC-MS: The HPLC-MS measurements were performed at the MS department of the Institute of Organic Chemistry at the Eberhard Karls University, Tübingen. An Agilent 1260 Infintiy II system was used to perform separation by HPLC. A gradient elution at a flow rate of 0.3 mL/min mL/min was employed. Detection was carried out using a DAD detector combined with an MS system (Bruker AmaZon SL, ESI in positive mode).

*Method A (**64**, **239**, **166**, **110**, **156**):*

The separation was performed on a Luna Omega polar 100 C18 column (length: 15 cm; diameter: 4.6 mm, T: 30 °C, C-18 modified silica, particle size: 3µm).

Gradient:

0 min: 90% H_20 with 0.01% formic acid, 10% ACN with 0.01% formic acid
30 min: 100% ACN with 0.01% formic acid
40 min: 100% ACN with 0.01% formic acid

41 min: 90% H_20 with 0.01% formic acid, 10% ACN with 0.01% formic acid
50 min: 90% H_20 with 0.01% formic acid, 10% ACN with 0.01% formic acid

*Method B (**96**):*

The separation was performed on a Reprosil 100 C18 column (length: 10 cm; diameter: 3 mm, T: 30 °C, C-18 modified silica, particle size: 3µm). Mass data was additionally acquired in the negative mode of the ESI.

Gradient B:

0 min: 80% H_20 with 0.01% formic acid, 20% MeOH with 0.01% formic acid

20 min: 100% MeOH with 0.01% formic acid

30 min: 100% MeOH with 0.01% formic acid

High-resolution MS (HRMS): The HRMS measurements were conducted at the MS department of the Institute of Organic Chemistry, using a Bruker maXIs 4G ESI-TOF (Bruker Corporation, Billerica, MA, USA) based on ESI in positive mode. Dry heater = 200 °C; nebulizer = 1.2 bar; dry gas flow = 6.0 L/min; capillary voltage = 4500 V; endplate voltage Offset = 2500 V.

Infrared spectroscopy (IR)

The IR spectra were obtained using an Agilent Cary 630 FTIR (Agilent Technologies Inc., Santa Clara, CA, USA) with the pure substances.

PYMOL™

X-ray crystal structures and overlays thereof were analyzed using The PyMOL Molecular Graphics System, Version 2.5.7. Schrödinger, LLC.

Biochemical assay performed at Reaction Biology Corp.

The IC_{50} values were determined using a HotSpot™ Kinase assay [296], a radiometric assay format, which employed ^{33}P-ATP for the phosphorylation reaction. The assay was performed by the commercial provider Reaction Biology® Corp. at their site in Malvern, PA, USA. The resulting radioactive labeling of a suitable substrate was measured to determine the amount of phosphorylation in relation to a control reaction and assessed as a function of the inhibitor concentration. Five-point measurements were performed starting from 5 µM following a 10-fold or from 2 µM in a 5-fold dilution scheme, respectively. The IC_{50} value was determined as the concentration of half-maximal inhibition of the enzymatic activity. The assay was performed in HEPES buffer system at pH 7.5, which consisted of 20 mM HEPES, 10 mM $MgCl_2$, 1 mM EGTA (ethylene glycol-bis(β-aminoethyl ether)-N,N,N',N'-tetraacetic acid), 0.01% Brij35 (polyoxyethylene(23)laurylether), 0.02 mg/ml BSA (bovine serum albumine), 0.1 mM Na_3VO_4, 2 mM DTT, and 1% DMSO.

1. The oligopeptide [KKLNRTLSVA] is added as a substrate (20 µM) to the buffer, followed by the necessary cofactors and the specific kinase.
2. The compound is added and incubated for 20 min at rt (non-competitive phase).
3. ^{33}P-ATP (10 µM) is added and incubated for 2 h at rt (competitive phase).

4. Unreacted ATP is removed by spotting the reaction onto P81 ion exchange filter paper and washing.
5. The amount of phosphorylated substrate is quantified by an undisclosed method, relying on measuring the radioactivity of ^{33}P.

Table 12: Inhibitory activity (IC_{50}) against MK2; [a] 5-fold dilution from 2 µM; [b] 10-fold dilution starting from 5 µM.

Acrylamide-based Inhibitors			Unreactive control compounds		
#	Structure	IC_{50} (MK2)	#	Structure	IC_{50} (MK2)
65	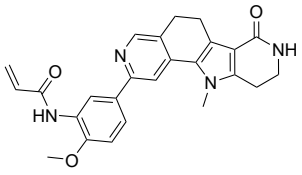	**57.8 nM** [a]	**69**	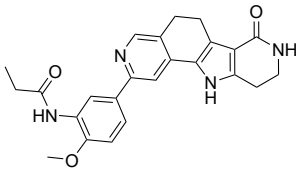	**995 nM** [a]
64	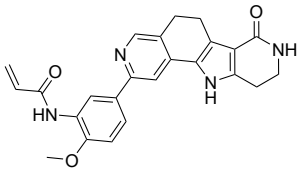	**2.62 nM** [a]			
67	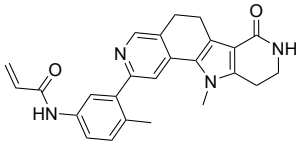	**610 nM** [a]	**70**	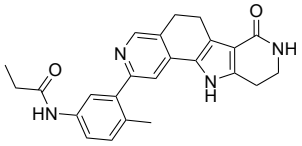	**> 2.0 µM** [a]
66	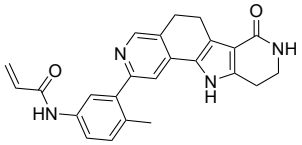	**> 2.0 µM** [a]			
68	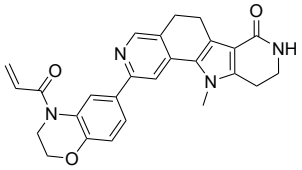	**6.75 nM** [a]	**71**	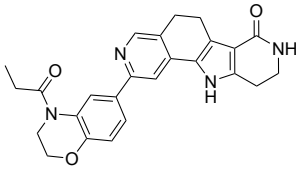	**55.4 nM** [a]
96	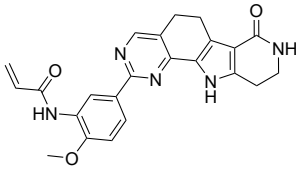	**1.96 nM** [b]			
108	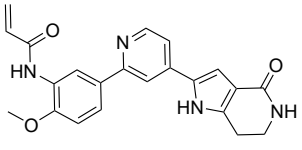	**9.59 nM** [a]	**109**	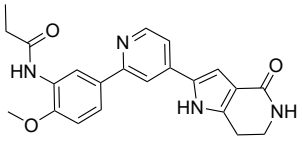	**1190 nM** [b]
Tetracyclic compound with heterocyclic warhead					
102	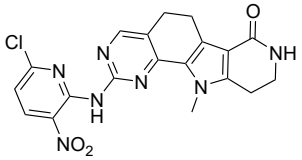	**< 3.20 nM** [a]			

Pyrrolopyridinone derivatives with heterocyclic warhead					
Nitrogen-linked compounds with methylated pyrrole					
110	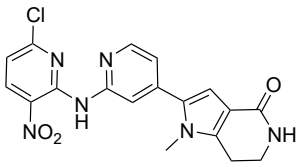	**61.58 ± 15 nM** [b] **(n=2)**	**157**	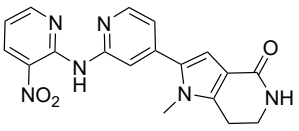	**4570 nM** [b]
155	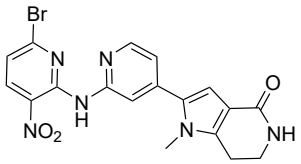	**73.7 nM** [b]	**166**	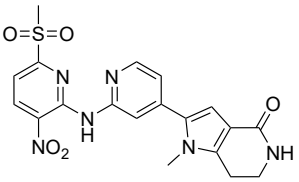	**> 5 µM** [b]
156	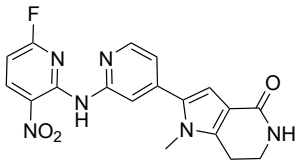	**117 nM** [b]			
Nitrogen-linked compounds with varying substitution at the pyrrole					
232	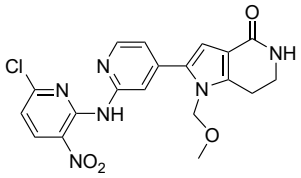	**1.36 nM** [b]	**238**	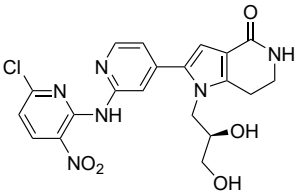	**1070 nM** [b]
231	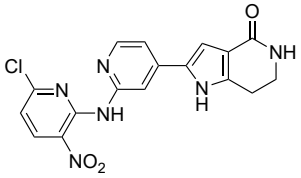	**0.36 nM** [b]	**239**	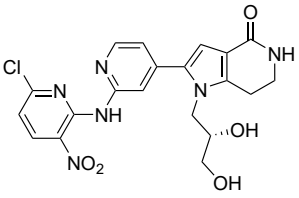	**396 nM**[b]
Sulfur-linked compounds					
204	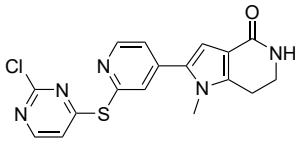	**> 5.0 µM** [b]	**209**	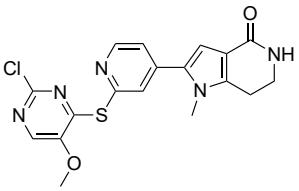	**> 5.0 µM** [b]
205	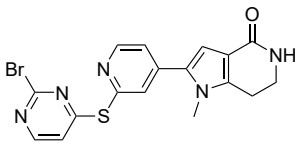	**> 5.0 µM** [b]	**207**	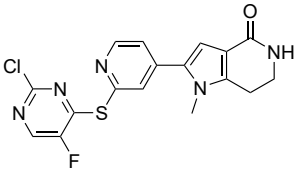	**> 5.0 µM** [b]
206	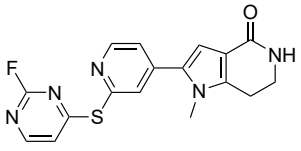	**> 5.0 µM** [b]			

The biochemical activities of **102** and **110** against kinases with an equivalent positioned cysteine (FGFR4, MK3, S6K2, MPS1) was determined using the HotSpot™ kinase assay by Reaction Biology® as previously described. The substrate was adjusted to the respective kinase ([KKLNRTLSVA] for MK3, [l]KKRNRTLTK] for S6K2, poly[Glu:Tyr] (4:1) for FGFR4 and MPS1).

Table 13: Inhibition of kinases with an equivalent positioned cysteine. IC_{50} values for **102** and **110** were determined via 5-point singlicate measurements with 10-fold dilution steps starting from 5 µM. [a)] Assay performed with 5-fold dilution steps, starting from 2 µM.

#	FGFR4	MK2	MK3	S6K2	MPS1
102	< 0.50 nM	**< 3.20 nM** [a)]	< 0.50 nM	< 0.50 nM	765 nM
110	1.39 µM	**61.6 nM**	21.5 nM	31.2 nM	> 5.00 µM

Biochemical activity determined at AssayQuant®

IC_{50} and K_i values for compounds **64** and **110** were additionally determined using a fluorescence-based kinase assay with the PhosphoSense® technology at AssayQuant® Technologies, Inc., Marlboro, MA, US. The assay was performed in 50 mM HEPES buffer at pH 7.5. The final reaction solution contained 1.0 mM DTT, 0.01% Brij-35, 0.5 mM EGTA, 1% glycerol, 10 mM $MgCl_2$, 0.20 mg/mL BSA, 15 µM AQT sensor substrate AQT0425, 2% DMSO, 10.1 µM ATP and the kinase (1 nM MK2, full length (1-400), N-terminal GST fusion, Carna (cat. # 02-142/ Lot: 22CBS-0444 B)). The compound was diluted in a 3-fold serial dilution from 10 µM concentration and 16 (**64**) and 18 (**110**) data points were included in the evaluation. The kinase reaction was conducted at a final volume of 15 µL in a 384-well microplate (purchased from Perkin Elmer, white, low-volume, sealed with optically-clear adhesive film (TopSealA-plus plate seal, Perkin Elmer)) and incubated at 30 °C for 240 min. The reaction was detected using a Biotek Synergy Neo 2 microplate reader with excitation (360 nm) and emission (485 nm) wavelengths.

Table 14: Determination of IC_{50} and K_i values for **64** and **110** at AssayQuant®.

#	Structure	IC_{50} [nM]	K_i [nM]
64	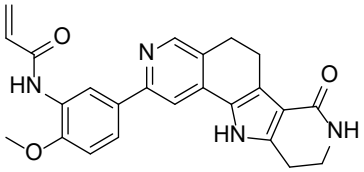	2.50	1.25
110	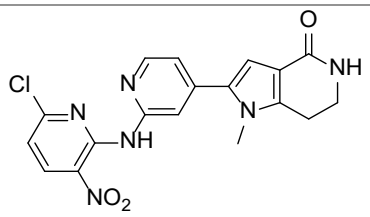	40.2	20.1

Assessment of the Kinetic Binding Parameters

The binding of a covalent inhibitor can be described as a two-step mechanism and the binding is time-dependent. Therefore, the k_{inact}/K_I values describe the activity of irreversible inhibitors better than the IC_{50} values. To determine the k_{inact}/K_I values of **64** and **110**, a PhosphoSens® CSox-based continuous assay format was used at AssayQuant® Technologies, Inc. The assay was performed in 50 mM HEPES buffer at pH 7.5. The final reaction solution contained 1.0 mM DTT, 0.01% Brij-35, 0.5 mM EGTA, 1% glycerol (from EDB), 10 mM $MgCl_2$, 0.20 mg/mL BSA (from EDB), 15 µM AQT sensor substrate AQT0425, 1% DMSO, 10.1 µM ATP and the kinase (1 nM MK2, full length (1-400), N-term GST fusion, Carna (cat. # 02-142/ Lot: 22CBS-0444 B)). The compound was diluted in a 1.5-fold serial dilution from 0.5 µM concentration and 24 data points were measured. For the reaction setup 0.3 µL of a 100x compound solution in 100% DMSO, 3.0 µL of 10x Sox-based substrate, and 3.0 µL of 10x ATP were combined. The mixture was incubated for 30 min at rt, while reaction mix is prepared. 23.7 µL of reaction mix with 1.4x enzyme was added. The kinase reaction was performed at a final volume of 30 µL in a 384-well microplate (purchased from Perkin Elmer, white, low-volume, sealed with optically-clear adhesive film (TopSealA-plus plate seal, Perkin Elmer)) at 30 °C for 240 min. The reaction was measured with a Biotek Synergy Neo 2 microplate reader, using excitation and emission wavelengths of 360 nm and 485 nm, respectively.

Table 15: Kinetic binding parameters determined for **64** and **110** at Assay Quant®.

#	**Structure**	k_{inact}/K_I [$M^{-1}s^{-1}$]	k_{inact} [s^{-1}]	K_I [µM]
64	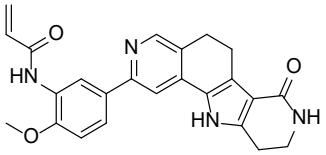	$2.58 \cdot 10^5$	0.0112	0.0435
110	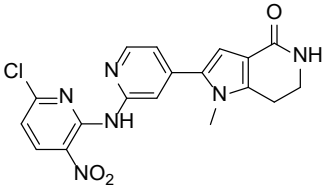	$5.01 \cdot 10^3$	0.0081	1.65

Differential Scanning Fluorimetry (DSF) Assay

The Differential scanning fluorimetry (DSF) or thermal shift assay is used in the context of drug discovery as a high-throughput method for evaluating ligand binding and selectivity in the early stages. The method is based on the ligand's ability to stabilize the protein fold as a result of a binding event to the respective protein. The folding state stabilization can then be measured as change in the melting temperature (T_m) of the protein. The melting temperature (T_m) is defined as the temperature at which 50% of the protein is in the unfolded stage. The folding stage of the protein can be tracked by measuring

the fluorescence of a suitable dye, such as SYPRO Orange, which is used for the experiment described herein. [315] SYPRO Orange interacts with the hydrophobic regions of the protein that become accessible during unfolding. The fluorescence is increased by these interactions, allowing for the tracking of changes in the folding stage through changes in dye fluorescence emission. [316]

The DSF assay was conducted in the group of Prof. Dr. STEFAN KNAPP (Institute for Pharmaceutical Chemistry, Structural Genomics Consortium, Goethe University, Frankfurt), following the procedure described in FEDOROV *et al.* [315b] Purified proteins were buffered in 25 mM HEPES (pH 7.5) containing 500 mM NaCl and were assayed in a 384-well plate with a final protein concentration of 2 µM in a 10 µL assay volume. Inhibitors were added to a final concentration of 10 µM using an ECHO 550 acoustic dispenser (Labcyte, San José, CA, USA). A 1:5000 dilution of SYPRO-Orange (Molecular Probes, Eugene, OR, USA) was used as a fluorescence probe. The filters for excitation and emission were set to 465 nm and 590 nm, respectively. The temperature was increased from 25 °C at a rate of 3 °C/min to a final temperature of 95 °C while scanning with the QuantStudio5 (Applied Biosystems, Waltham, MA, USA). The data were analyzed using the Boltzmann equation in the Protein Thermal Shift software (Applied Biosystems, Waltham, MA, USA). The samples were measured in technical duplicates.

Table 16: Data from the thermal shift screening; $\Delta T_m > 10$ °C in bold; $\Delta T_m > 5$ °C in italic; empty cells not determined.

Enzyme	64	96	102	108	109	Stauro-sporine pos. control
MAP3K5A	*9,49*	**14,59**	*8,56*	*8,79*	*6,00*	**17,60**
CAMKK2B	**12,60**	**14,07**	3,36	*8,68*	*6,87*	**25,14**
TOPKA	*6,82*	**12,89**	0,52	*8,67*	0,85	*8,14*
CLK1A	*8,57*	**11,44**	*9,32*	*5,98*	3,53	**13,70**
STK17AA	**10,36**	**11,17**	*8,29*	*8,22*	*7,74*	**12,36**
DYRK2A	**10,10**	**10,94**	**13,87**	*8,26*	*7,63*	*7,04*
GPRK5A	3,24	**10,55**	2,13	1,40	0,43	*8,56*
MK2	**10,66**	**10,51**	**10,32**	**11,67**	3,87	3,43
DYRK1AA	*7,49*	*9,51*	*6,78*	*5,19*	3,89	**10,68**
CLK3A	3,74	*9,20*	*6,12*	2,21	0,83	*7,46*
RPS6K5A		*8,35*	*6,63*	*5,53*		**15,00**
DAPK3A	*7,07*	*8,24*	3,98	*7,46*	*5,15*	**18,73**
MELKA	*6,72*	*8,22*	3,59	*5,00*	3,04	**14,09**
GAKA	*6,60*	*7,92*	2,84	4,05	4,03	*9,53*
GSK3BB	4,73	*7,59*	4,44	4,07	4,15	**12,21**

BMP2KA	4,65	*7,56*	*5,59*	*5,87*	*5,25*	**19,25**
STK10A	2,98	*7,42*	1,02	3,00	1,65	**24,40**
MAPK15HSD	*5,51*	*7,01*	*6,86*	2,52	1,58	**14,17**
CSNK2A2A	*5,43*	*6,97*	1,48	*5,03*	4,50	*5,68*
TTKA	*6,44*	*6,96*	2,39	2,08	1,88	**12,44**
ABL1A	1,78	*6,62*	0,91	1,66	1,36	**10,27**
CHEK2A	*6,17*	*6,27*	2,71	2,42	2,74	**18,30**
BMPR2A	2,91	*6,07*	0,67	2,80	1,41	2,91
FGFR3A	2,97	*5,58*	1,21	1,92	0,79	**13,67**
SLKA		*5,31*	0,73	1,60		**20,78**
PLK4A	4,68	*5,28*	3,12	3,67	2,65	**19,00**
FLT1A	*6,12*	*5,17*	0,71	1,38	3,14	**12,53**
PIM3A	*5,72*	*5,16*	2,02	2,89	3,23	**18,43**
PHKG2A	4,18	*5,14*	*8,16*	1,25	0,71	**22,50**
CK2A1A		4,83	1,95	4,38		4,40
STK6A	2,00	4,40	0,69	2,55	2,01	**17,29**
GSG2A	4,34	4,38	1,44	1,31	0,72	*7,93*
AAK1A	3,17	4,37	2,66	3,05	3,70	**12,23**
NEK2A	0,13	3,87	2,16	1,90	-0,33	2,24
PIM1A	*6,18*	3,85	3,93	2,52	3,41	**11,48**
CSNK1DA	3,45	3,84	2,50	2,32	1,70	2,49
STK17BA	4,71	3,65	*5,95*	-0,04	0,80	*8,57*
DAPK1A	3,95	3,61	3,50	1,94	1,95	*9,61*
ULK3A	1,94	3,41	0,55	1,04	0,74	**17,38**
SRPK1A	4,31	3,13	3,55	0,74	0,58	*7,42*
STK38LA	1,72	2,87	0,54	0,74	0,30	**11,26**
FGFR2A	1,24	2,47	0,24	1,14	0,16	*8,65*
MAPK8B	4,25	2,05	2,28	2,80	0,92	*7,71*
RIOK1A		1,89	0,92	*5,73*		-0,22
MAPK10A	2,57	1,82	1,89	1,56	0,28	*8,21*
CAMK2DA	1,30	1,46	2,21	-0,11	-0,08	**17,47**
RPS6KA1A	1,41	1,39	1,07	0,44	-0,07	4,58
VRK1A	3,25	1,32	2,09	0,58	0,31	3,37
CDK2A	0,63	1,29	2,53	-0,05	0,03	**15,29**
STK3A	0,48	1,04	0,26	0,24	0,08	**14,81**

STK39A	0,03	0,98	0,96	0,33	-0,23	*9,27*
FESA	0,36	0,90	0,60	0,24	0,09	*7,49*
MAP2K4A	0,49	0,86	2,80	0,78	0,18	**12,48**
MAPK1A	0,82	0,79	1,02	0,20	0,09	-0,37
MERTKA	0,41	0,78	0,63	0,58	0,19	*5,95*
EPHB3A	0,68	0,69	-0,17	-0,26	-0,45	*6,65*
MARK3A	0,73	0,68	0,60	0,97	0,60	**19,24**
FGFR1B	0,13	0,64	0,09	0,21	-0,10	*5,96*
CDKL1A	0,13	0,62	-0,05	-0,10	0,20	3,96
EPHA2A	-0,01	0,61	0,26	0,18	0,01	*7,81*
BRPF1B	1,30	0,60	0,50	0,77	0,84	1,30
PAK1A	-0,76	0,57	-0,45	-0,31	-0,52	*7,43*
EPHA5A	0,47	0,51	-0,11	-0,41	-0,23	*8,67*
CAMK4A	0,40	0,49	0,46	-0,01	0,10	*8,95*
AKT3A	0,51	0,49	0,69	0,27	0,38	*7,77*
AURKBA	1,83	0,42	2,33	-2,41	-0,68	**14,06**
MAPK6		0,33	0,70	0,39		0,99
OSR1A	0,11	0,33	0,30	0,05	0,31	*7,57*
PAK4A	-0,05	0,31	0,75	-0,09	-0,25	**14,87**
BRAFA	0,44	0,29	1,59	0,38	0,11	0,36
MARK4A	1,21	0,26	-0,66	-0,26	0,06	**18,34**
MAP2K6A	0,09	0,25	0,73	0,41	-0,09	**12,51**
PCTK1A	0,36	0,19	0,24	0,10	-0,06	*8,87*
WNK1A	-0,24	0,19	0,00	0,18	-0,08	1,42
BMXA	0,85	0,14	-0,38	0,08	-0,34	*7,16*
DMPK1A	0,43	0,08	0,28	-0,29	-0,34	*9,75*
CAMK2BA	1,48	0,07	1,36	-0,68	0,22	**11,42**
STK4A	0,17	-0,02	-0,27	-0,37	0,06	**15,52**
MAPK14A	-0,15	-0,02	0,42	-0,76	-0,13	-0,05
RPS6KA6A		-0,03	0,10	0,38		1,00
MST3A	1,48	-0,04	-0,09	-0,99	0,38	*6,46*
MAPK13A	0,34	-0,06	0,99	-0,23	0,30	*6,21*
MAPK9A	2,81	-0,14	0,53	1,25	-1,29	4,83
NEK1A	0,80	-0,15	0,02	0,64	0,04	-0,69
PKMYT1A	0,18	-0,21	0,66	-0,73	-0,79	-1,07

CAMK1DA	-1,08	-0,21	0,55	0,01	-1,47	**10,49**
TAF1A	-0,52	-0,29	-0,09	-0,15	-0,40	0,43
SRCA	-0,18	-0,31	-0,02	-0,04	0,10	*5,09*
MAP2K1A		-0,32	-0,38	-0,21		1,62
EPHA7A	0,09	-0,48	-0,01	0,10	-0,18	**12,72**
DCAMKL1A	2,60	-0,57	0,27	-1,36	1,24	*6,32*
CASKA	-0,06	-0,69	-0,49	-0,64	0,02	*5,11*
TLK1A	0,03	-0,73	-0,09	0,00	0,08	*8,88*
MST4A	0,15	-1,03	-0,16	-2,37	-0,23	4,56
PDK4A		-1,22	-0,05	0,02		0,07
CDC42BPAA	0,28	-1,30	0,01	-0,06	0,42	2,18
CAMK1GA	0,93	-1,68	-0,95	-0,72	-0,06	**10,46**
NEK7A	-0,39	-1,81	-0,59	-0,56	-0,99	-0,20
BRD4A	0,23	-1,92	-0,43	-1,03	-0,96	-0,81
RIOK2A		-2,98	1,59	0,86		2,29
CSNK1EA	2,45				0,51	
CSNK2A1A	*5,60*				4,17	
EPHA4A	0,16				0,07	
EPHB1A	0,11				-0,02	
FECH	2,50				-0,16	
HIPK2	1,86				0,35	
MAP2K7A	*9,57*				0,86	
NQO2A	0,27				0,55	
RPS6kA5A	*7,32*				4,26	
TIF1A	0,28				-0,26	
ULK1A	2,27				0,23	

GSH stability assay

The stability of a representative subset of compounds towards nucleophiles was evaluated. Reduced glutathione, which is present under physiological conditions and the thiol exhibits high nucleophilicity, is commonly used. Several different methods for this purpose can be found in the literature, differing in the concentration of the reaction partners, buffer composition and organic cosolvent. [306a, 306c, 306d, 307, 317] For this evaluation, the procedure from KEELEY *et al.* [306a] was adapted. To adjust for the low solubility of most of the compounds, the method required modifications as already used for the published data on the S6K2 and FGFR4 projects. [225] The buffer was changed from a PBS buffer to a HEPES buffer (20 mM HEPES, 1 mM EGTA, 10 mM $MgCl_2$, 0.01% Brij35, 0.1 mM Na_3VO_4; pH adjusted to 7.5 by

dropwise addition of 1 M HCl or 1 M NaOH), which was adapted from the buffer used in the biochemical assay at Reaction Biology Corp. to prevent interference with the compounds, the composition was adjusted by omitting DTT and BSA from the mixture. Additionally, a 50:50 mixture of the buffer with acetonitrile was used and the final compound concentration was reduced to 100 µM. Indoprofen was used as an internal standard at a final concentration of 100 µM. To ensure pseudo-first order kinetics, the GSH concentration in the final solution was 5 mM. The assay was performed at 40 °C. Compound stability was measured in duplicates. Afatinib stability was assessed simultaneously as a positive control. To prepare the assay solution, 20 µL of a 10 mM compound solution in DMSO was diluted with 980 µL of 1:1 HEPES buffer (pH 7.5)/ACN (Solution A). For compound **110** the concentration of the DMSO solution was 5 mM. Therefore, 40 µL of the 5 mM solution in DMSO were diluted with 470 µL ACN and 490 µL HEPES buffer (pH 7.5). A 200 µM solution of indoprofen with 10 mM GSH in 1:1 HEPES buffer (pH7.5)/ACN was freshly prepared (solution B).

A mixture of 250 µL of solution A and B was monitored for reaction using a HPLC-based method. The decreasing area under the curve for the compound was measured relative to the internal standard indoprofen.

The kinetic parameters of the reaction were calculated by linearizing the data. The half-life $t_{1/2}$ for the pseudo-first order reaction can be calculated using the following formula:

$$t_{1/2} = \frac{ln2}{k}$$

The reaction rate constant, *k,* can be obtained from the linear regression by plotting the natural logarithm of AUC divided by AUC_0 against the time. The slope of the trend line represents the value for k.

General formula for the linear regression:

$$y = k * x$$

Formula for the reaction rate:

$$\ln\left(\frac{AUC}{AUC_0}\right) = k * t$$

Less soluble compounds showed an increase of the compound AUC at t_1, due to increased solubility at 40 °C compared to rt. The corrected value for AUC_0 ($AUC_{0(corr)}$) was calculated from the linearization, which did not affect the values for *k* or $t_{1/2}$ but allowed for better comparison and depiction.

After the assay was completed, selected reaction mixtures were analyzed by HPLC-MS at the MS department of the Institute of Organic Chemistry (Eberhard Karls University, Tübingen) to identify the reaction products formed. Besides the mass of the internal standard, the parent compound and the GSH-adduct could be identified in the mass spectrum. No hydrolysis product was identified.

Table 17: Measurements of GSH-stability for selected compounds. Structures of the compound and the corresponding GSH adduct are shown when reaction products were analyzed by mass spectrometry. Plots and values for the half-life $t_{1/2}$ are presented in the plots. HPLC-MS methods are described in the experimental section; [a] Method A; [b] Method B.

#	Structure	Experimental data
64	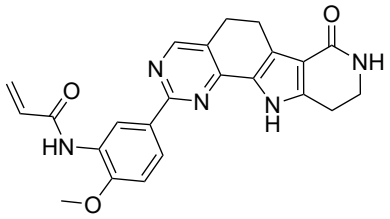 Exact Mass: 414.16919 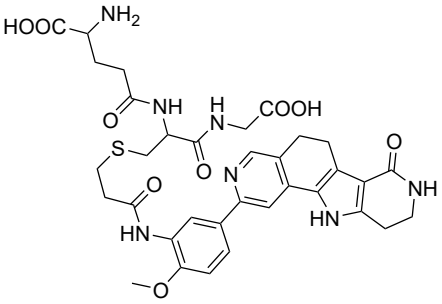 **64GSH** Exact Mass: 721.25300	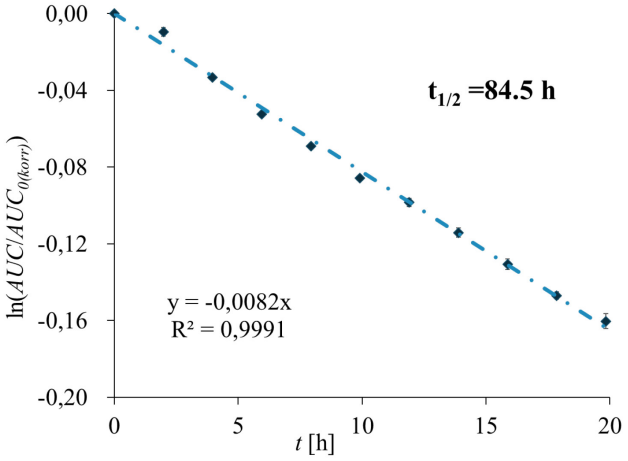 **HPLC-MS:**[a] $m/z_{14.90min(1)}$ = 361.74 (**64GSH**+2H$^+$) $m/z_{14.90min(2)}$ = 722.37 (**64GSH**+H$^+$)
96	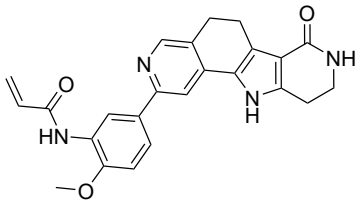 Exact Mass: 415.16444 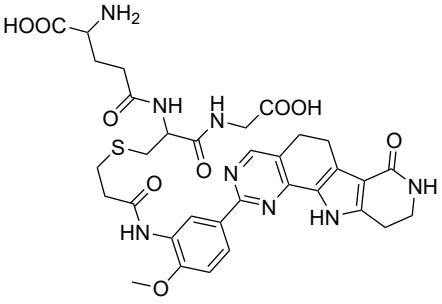 **96GSH** Exact Mass: 722.24825	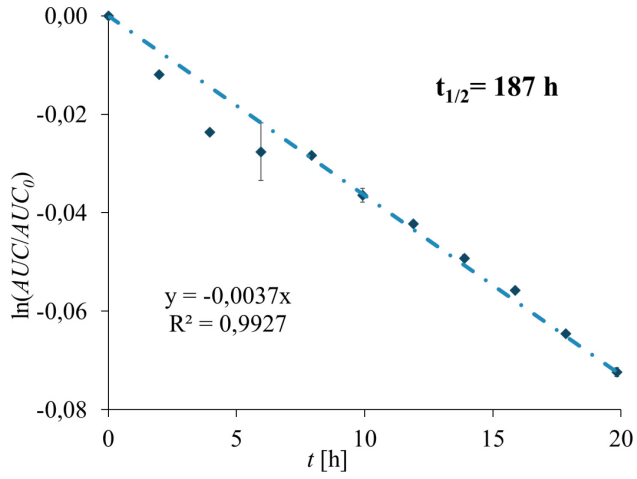 **HPLC-MS:**[b] $m/z_{14.55min(1)}$ = 362.18 (**96GSH**+2H$^+$) $m/z_{14.55min(2)}$ = 723.32 (**96GSH**+H$^+$)

108	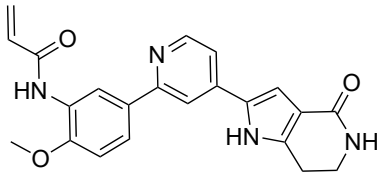 Exact Mass: 388,15354	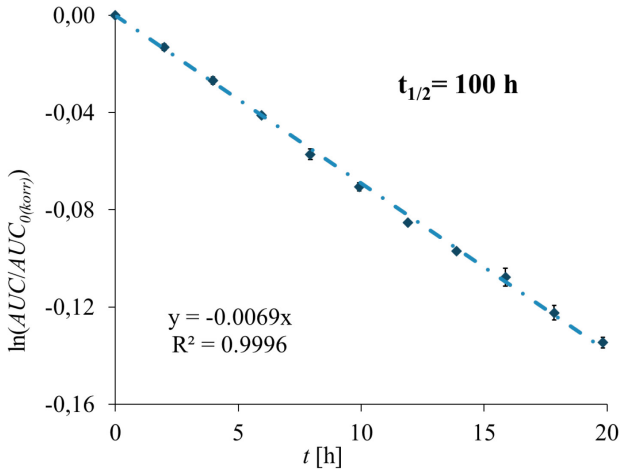
110	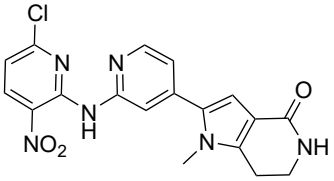 Exact Mass: 398.08942 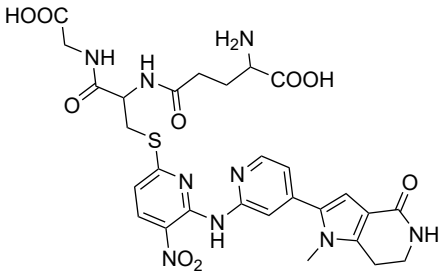 **110GSH** Exact Mass: 669.19654	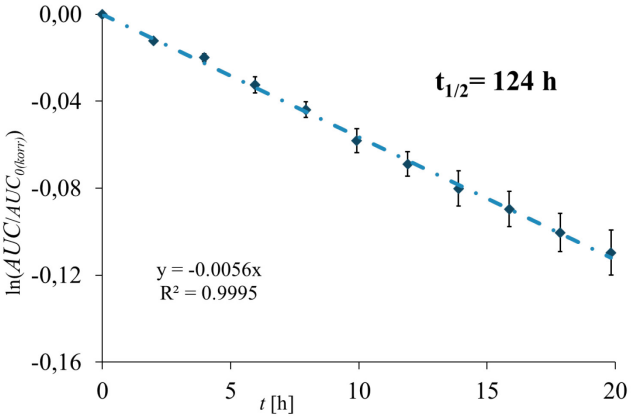 **HPLC-MS:**[a)] $m/z_{16.30min(1)}$ = 335.71 (**110GSH**+2H⁺) $m/z_{16.30min(2)}$ = 670.30 (**110GSH**+H⁺)
156	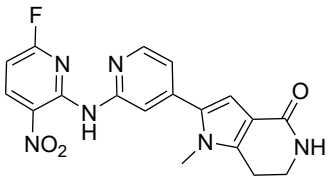 Exact Mass: 382.11897 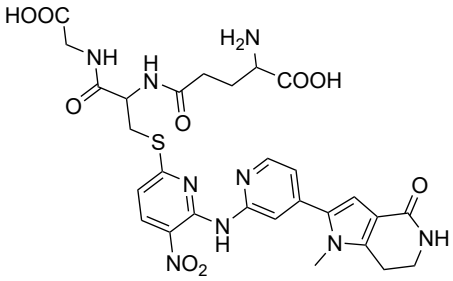 **156GSH** Exact Mass: 669.19654	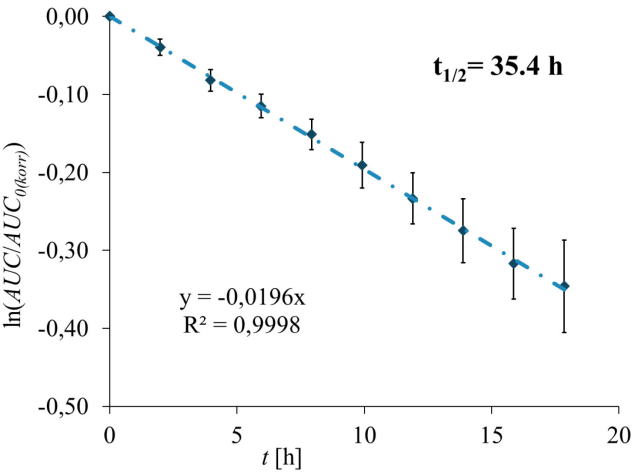 **HPLC-MS:**[a)] $m/z_{16.70min(1)}$ = 335.71 (**156GSH**+2H⁺) $m/z_{16.70min(2)}$ = 670.31 (**156GSH**+H⁺)

155

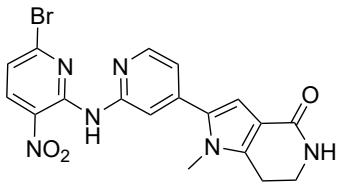

Exact Mass: 442.03890

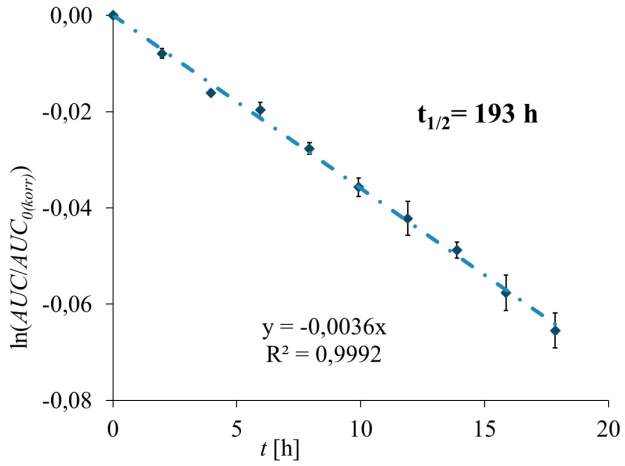

204

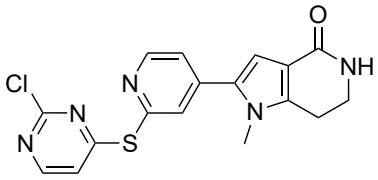

Exact Mass: 371.06076

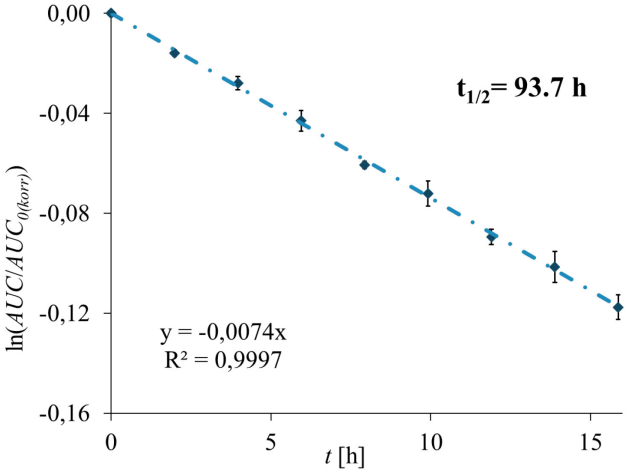

239

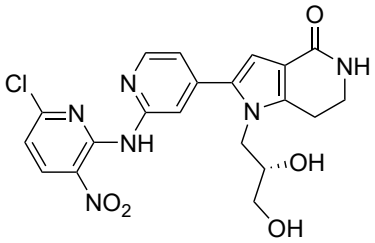

Exact Mass: 458.11055

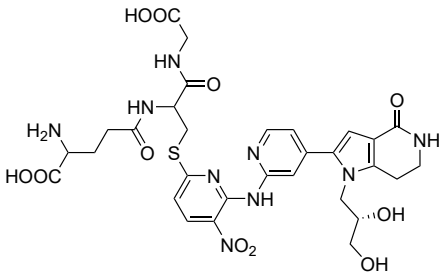

239GSH
Exact Mass: 729.21767

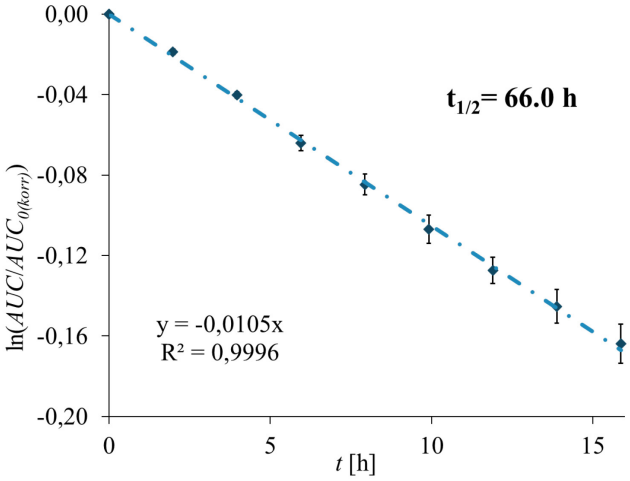

HPLC-MS: [a)]

$m/z_{14.92min(1)}$ = 365.71 (**239GSH**+2H$^+$)

$m/z_{14.92min(2)}$ = 730.31 (**239GSH**+H$^+$)

30	**Afatinib** 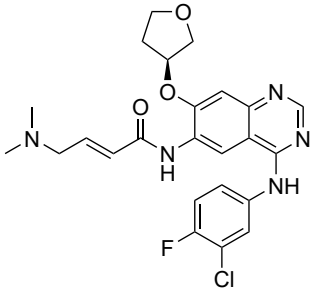	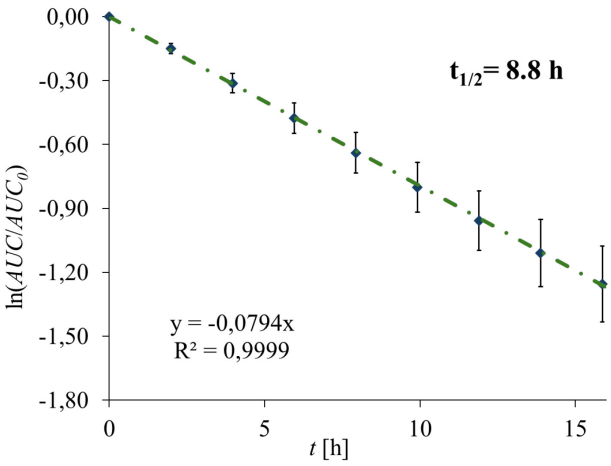

No half-life could be determined for the sulfone-containing derivative **166**, due to its fast degradation. The first measurement (t_0) already showed significant degradation (Figure 46). The solution was analyzed using HPLC-MS (Method A), which identified the degradation product as the GSH adduct of compound **166** ($m/z_{16.33min(1)}$= 335.71 (**166GSH**+2H$^+$); $m/z_{16.33min(2)}$= 670.20 (**166GSH**+H$^+$)). After two hours (t_1) the parent compound **166** could not be detected anymore. In order to determine the half-life for compounds with higher reactivity, adjustments to the method are necessary. Firstly, the time between the addition of solution B and the injection must be minimized to reduce degradation at the t_0 time point. Furthermore, reducing the assay temperature can slow down adduct formation. However, it is desired to have lower reactivity in comparison to afatinib (**30**, $t_{1/2}$ = 8.8 h).[233, 307] Therefore, an exact determination of highly reactive compounds is not required.

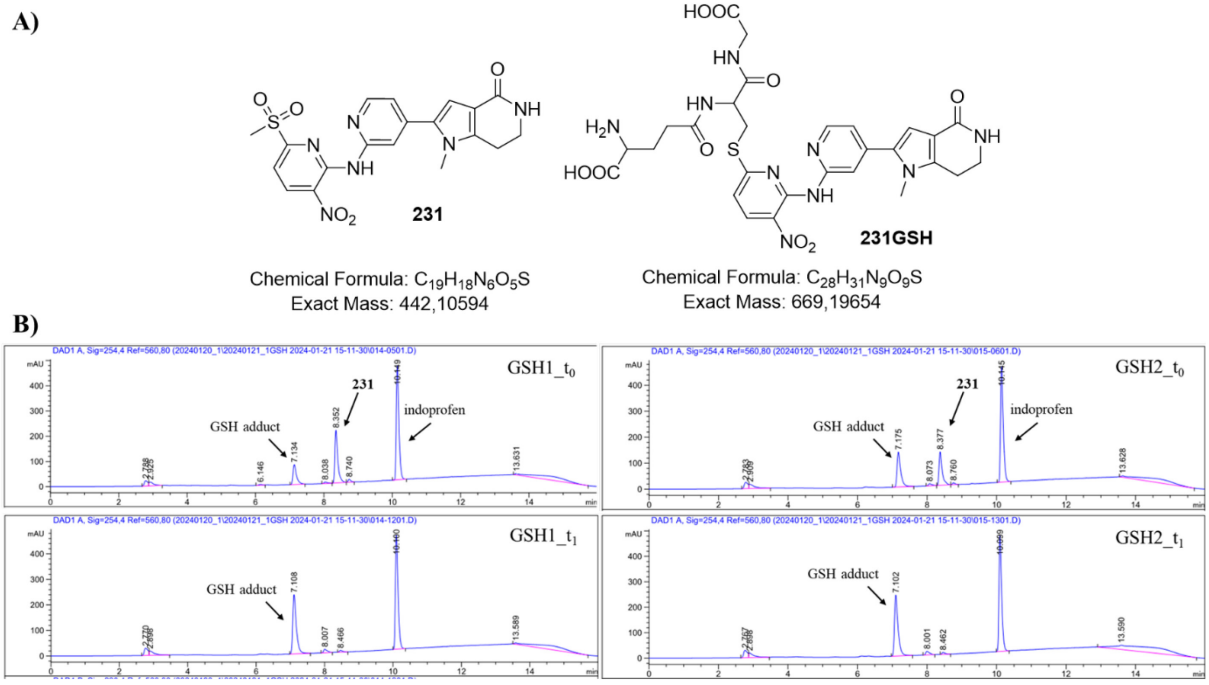

Figure 46: A) Structure of compound **166** and the respective GSH adduct. B) HPLC chromatograms of the GSH stability assay of **166** for time point t_0 and t_1.

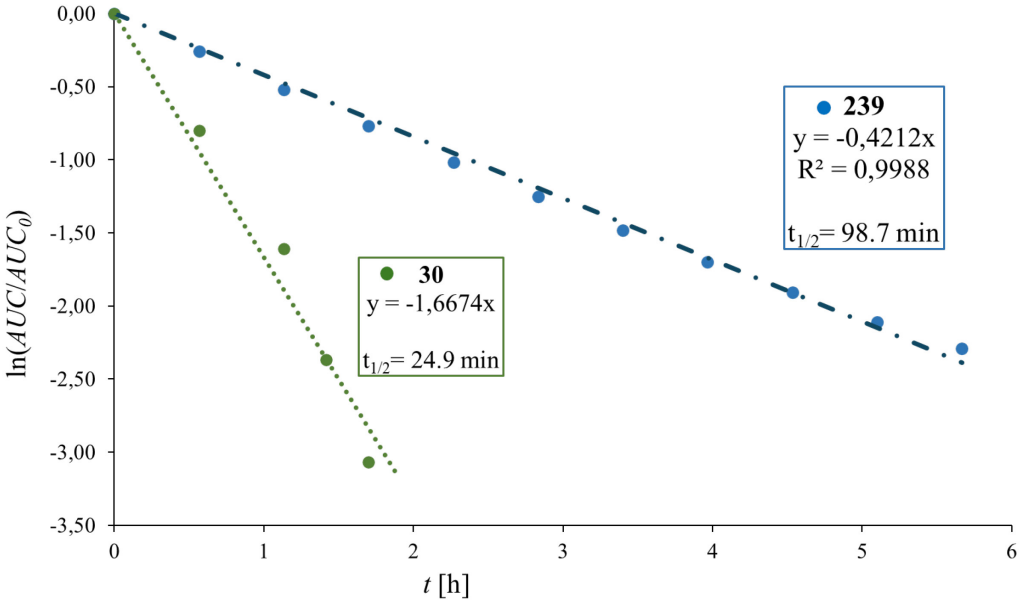

Figure 47: GSH-stability of **239** (date depicted in blue) and afatinib **30** (in green) in HEPES buffer (pH 7.5) with 10% ACN.

Compound **239** has higher solubility in water. Therefore, the GSH stability for this compound was assessed using two additional methods. The first method uses 10% ACN as cosolvent in the reaction buffer (Figure 48), analog to the literature procedure described in the literature by KEELEY *et al.* [306a] Additionally, the stability measurement was performed in plan buffer without any additional organic cosolvent (1% of DMSO from the compound stock solution)(Figure 47). Solutions A and B were prepared with the respective solvent mixture and treated as described previously.

The half-life for afatinib in 100% HEPES buffer and 90% buffer/ 10% ACN was also determined and a value of 26 min and 25 min, respectively, was obtained. The aqueous stability of **239** was also assessed in HEPES buffer. No degradation was observed after 3.40 h (displayed in orange in Figure 47).

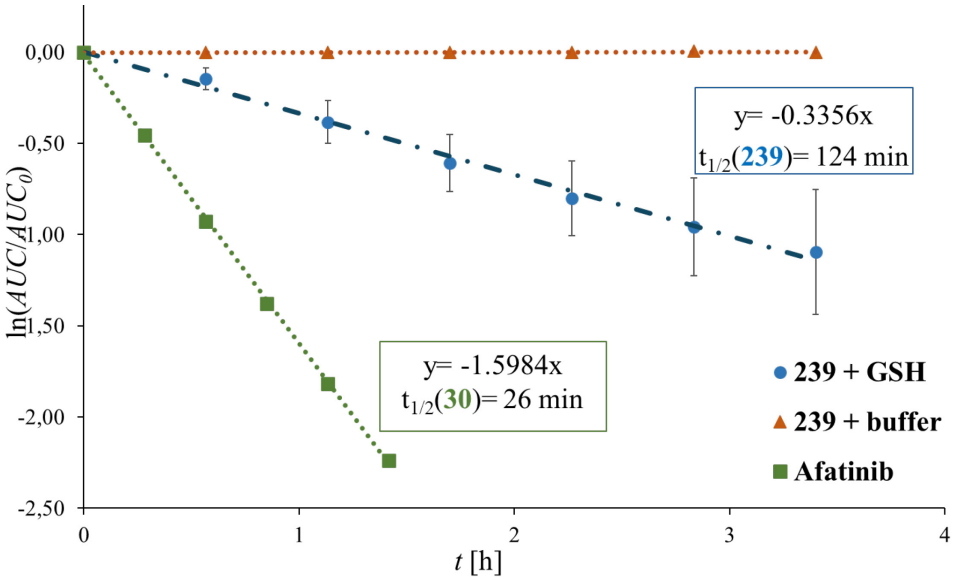

Figure 48: GSH-stability of **239** (data depicted in blue) and afatinib **30** (in green) in 100% HEPES buffer (pH 7.5) and stability of **239** in plain buffer (orange).

Metabolic stability in Mouse Liver Microsomes

The metabolic stability assays were conducted by MARK KUDOLO (for **102** and **108**) and ALEXANDER RASCH (for **110**) (group of Prof. Dr. STEFAN LAUFER, Institute for Pharmaceutical Chemistry, Eberhard Karls University, Tübingen), respectively, using mouse liver microsomes (MLM) in the presence of an NADPH (nicotinamide adenine dinucleotide phosphate)-regenerating system. The system consisted of 5 mM glucose-6-phosphate, 5 U/mL glucose-6-phosphate dehydrogenase, and 1 mM $NADP^+$. Liver microsomes (20 mg/mL), NADPH-regenerating system, and 4 mM $MgCl_2 \cdot 6\ H_2O$ in 0.1 M TRIS-HCl buffer (pH 7.4) were preincubated for 5 min at 37 °C and 750 rpm on a shaker. The reaction was initiated by adding the preheated compounds in DMSO at concentrations of 5 mM (**110**) and 10 mM (**102**, **108**), respectively, resulting in respective final concentrations of 0.050 mM (**110**) and 0.1 mM (**102**, **108**). The reaction was terminated at selected time points (0, 10, 20, 30, 60, and 120 min) by adding 100 µL of internal standard (ketoprofen) in ACN at a concentration of 0.050 mM (**110**, **102**, **108**). The samples were vortexed for 30 s and then centrifuged (21910 relative centrifugal force, 4 °C, 20 min). The resulting supernatant was used directly for LC-MS analysis. All compound incubations were conducted at least in triplicate. Additionally (for **110**), a negative control containing BSA (20 mg/mL) instead of liver microsomes and a positive control using Verapamil instead of the compound were performed. A limit of 1% organic solvent during incubation was not exceeded. Pooled liver microsomes from mice (male) were purchased from Sekisui XenoTech, LLC, Kansas City, KS, USA.

Sample separation and detection were performed using an Alliance 2695 Separations Module HPLC system (Waters Corporation, Milford, MA, USA) equipped with a Phenomenex Kinetex 2.6 µm XB-C18 100 Å 50 x 3 mm column (Phenomenex Inc., Torrance, CA, USA) coupled to an Alliance 2996 Photodiode Array Detector and a MICROMASS QUATTRO micro API mass spectrometer (both Waters Corporation, Milford, MA, USA) with electrospray ionization in positive mode.

Mobile phase A: 90% water, 10% acetonitrile and additionally 0.1% formic acid (v/v), mobile phase B: 100% acetonitrile with additionally 0.1% formic acid (v/v). The gradient was set to: 0-2.5 min 0% B, 2.5-10 min from 0 to 40% B, 10-12 min 40% B, 12-12.01 min from 40 to 0% B, 12.01-17 min 0% B at a flow rate of 0.7 mL/min (**110**) and 0-2.5 min 10% B, 2.5-12.5 min from 10 to 50% B, 12.5-15 min 50% B, 15-15.01 min from 50 to 10% B, 15.01-18 min 10% B at a flow rate of 0.6 mL/min mL/min (**102**) and 0-2.5 min 0% B, 2.5-11 min from 0 to 20% B, 11-12 min 20% B, 12.5-12.51 min from 20 to 10% B, 12.51-17 min 10% B at a flow rate of 1.2 mL/min (**108**). Samples were maintained at 10 °C, the column temperature was set to 20 °C with an injection volume of 5 µL. Spray, cone, extractor, and RF lens voltages were at 4 kV, 30 V, 8 V and 2 V, respectively. The source and desolvation temperatures were set to 120 °C and 350 °C, respectively, and the desolvation gas flow was set to 750 L/h (**110**) or 650 L/h (**102**, **108**), respectively. MassLynx 4.1 software (Waters Corporation, Milford, MA, USA) was used for data analysis.

The plotted data for metabolic stability is depicted in Figure 49 (**102**), Figure 50, (**108**) and Figure 51 (**110**).

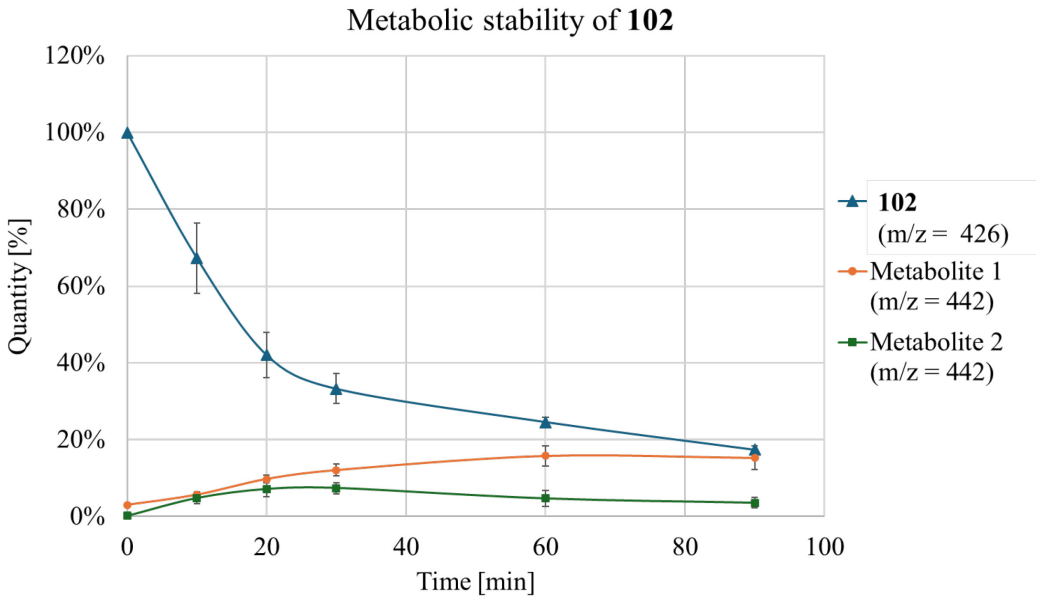

Figure 49: Metabolic stability in MLM of compound **102**.

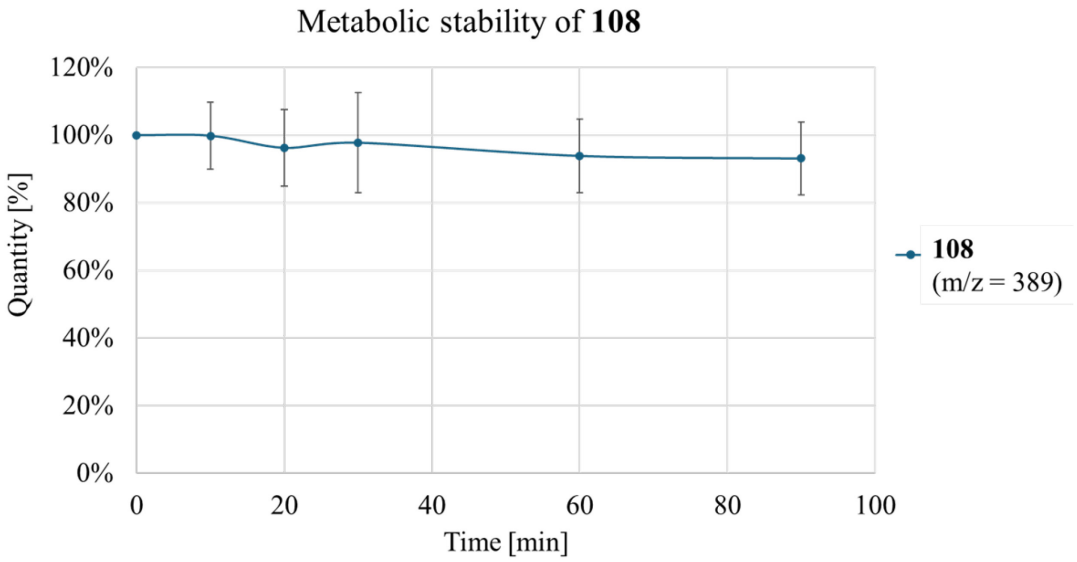

Figure 50: Metabolic stability in MLM of compound **108.**

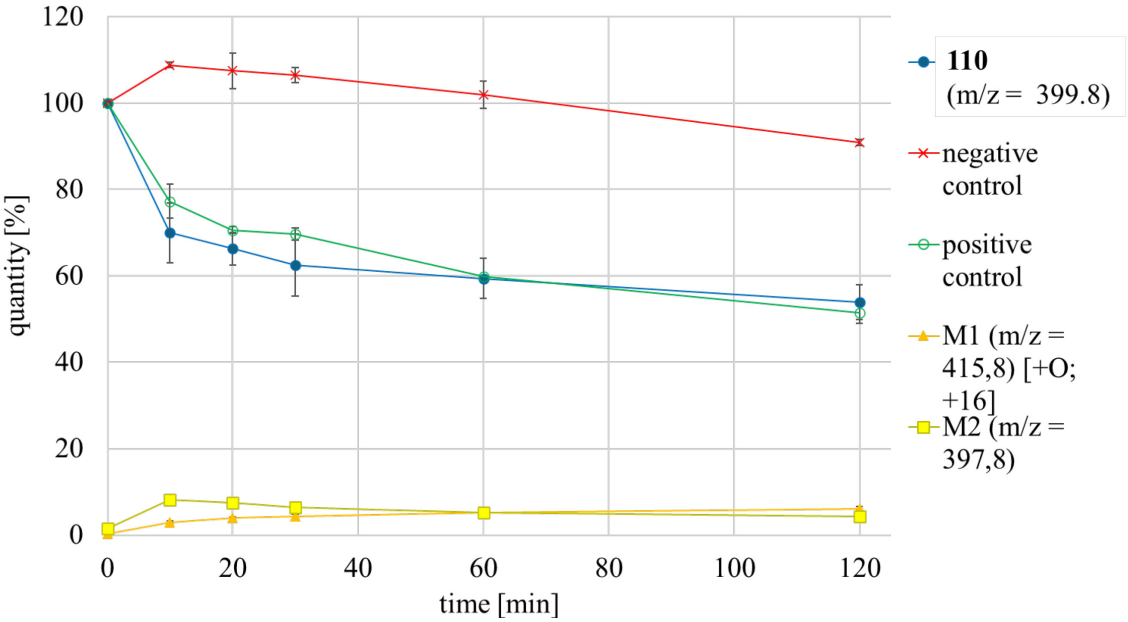

Figure 51: Metabolic stability in MLM of compound **110**.

Solubility assay

The aqueous solubility was determined using a HPLC-based method in a buffer system with HEPES buffer (pH 7.5), which is similar to the one used in the HotSpot™ Kinase Assay at Reaction Biology. To prevent unwanted reactions between the buffer components and the compounds, DTT and BSA were excluded from the buffer. The same buffer composition was used for the GSH stability assay and was described previously. A calibration curve was generated using calibration points were set at 5, 10, 25, and 50 µM in either singlicate or triplicate measurements. Linear regression was used to fit to fit the calibration curve, with the axis origin being a fixed artificial fifth calibration point. To determine the solubility of the compound, 990 µL of HEPES buffer and 10 µL of a 10 mM solution of the compound in DMSO were combined in an HPLC vial, equipped with a stir bar. The mixture was stirred for 17 hours at rt and then centrifuged at g = 35060 (14000 rpm with 16.53 cm radius) for 30 minutes at 20 °C. Next, 700 µL of the mixture were decanted and centrifuged again at g = 35060 for 30 minutes at 20 °C. Finally, 500 µL were decanted and analyzed by HPLC (method C). The solubility was calculated by dividing the slope of the calibration curve by the AUC of the residual compound peak (singlicate measurements).

Table 18: Solubility of a subset of compounds in HEPES buffer (pH 7.5). Values for the calibration curves were measured as triplicates; [a)] calibration curve measured as singlicate.

#	**64**	**102**	**108**	**110**	**232**	**157**	**181**	**204**	**239**
Solubility [µM]	6.78 [a)]	1.1	102	< 0.50	2.35	< 0.50	99.9	13.5	14.0

Intact protein mass spectrometry

The mass spectrum can detect the covalent modification of the target protein by an irreversible inhibitor. The analysis was performed by GUIQUN WANG from the group of Prof. Dr. STEFAN KNAPP (Institute for Pharmaceutical Chemistry, Structural Genomic Consortium, Goethe University, Frankfurt). The protein (concentration: 50 µM) was incubated with the acrylamide compounds **64**, **96** and **108** were incubated for two hours at rt with at a compound concentration of 250 µM. The experiment showed complete labelling of the protein by the inhibitors (Table 19). Compound **102** was incubated at rt at concentration of 50 µM for the protein and 25 µM for the inhibitor for 3 min min. Significant labeling of the protein was detected after this short incubation time.

Table 19: Results from intact protein MS experiments performed by GUIQUN WANG.

M_w(MK2): 37560	Δm	*m/z* (ESI^-)	
64	414.2	37973.58	80% 1-site bound 20% 2-site bound
96	415.2	37974.45	90% 1-site bound 10% 2-site bound
108	388.2	37947.24	90% 1-site bound 10% 2-site bound
102	389.1	37559.1	

6.2 Synthesis

6.2.1 General Synthetic Procedures (GSP)

GSP 1: MIYAURA borylation A

The corresponding 3-bromo-aniline (1.00 eq.), bis(pinacolato)diboron (1.20 eq.), potassium acetate (5.00 eq.) and Pd(dppf)Cl_2 (20 mol%) were dissolved in 1,4-dioxane (dry, degassed, 1 mL/mmol) and the reaction stirred at 80 °C for 7 h. After cooling to rt the reaction was diluted with EtOAc and filtered through a patch of celite. The solution was washed with brine three times, the organic layer dried over Na_2SO_4 and the solvent evaporated. The residue was purified by flash column chromatography.

GSP 2: MIYAURA borylation B

The corresponding 3-bromoaniline (1.00 eq.), bis(pinacolato)diboron (1.20 eq.) and potassium acetate (5.00 eq.) were dissolved in 1,4-dioxane (dry, 7 mL/mmol) and argon bubbled through the solution for 10 min. XPhos Pd G3 (2 mol%) was added and the reaction stirred at 90 °C for 18 h. After cooling to rt, the reaction was diluted with EtOAc and filtered through a patch of celite. The solution was washed

with brine three times, the organic layer dried over Na_2SO_4 and the solvent evaporated. The residue was purified by flash column chromatography.

GSP 3: Acrylamide introduction

The corresponding aniline (1.00 eq) was dissolved in dry DCM (5 mL/mmol) under an atmosphere of argon and DIPEA (3.00 eq.) was added. The solution was cooled in a N_2/acetone bath (-92 °C) and acryloyl chloride added slowly (1.00 eq). The reaction was allowed to warm up to rt and stirred for 1 h. The reaction was monitored by TLC and acryloyl chloride added, if the conversion was not completed, and the reaction stirred another 30 min. After complete conversion the reaction was quenched by the addition of water (20 mL) and the layers were separated. The organic layer was dried over Na_2SO_4 and the solvent evaporated. The residue was purified by flash column chromatography.

GSP 4: Amide coupling using Propionyl Chloride

The corresponding aniline (1.10 eq.) was dissolved in DCM (dry, 10 mL/mmol) under Ar atmosphere and cooled to 0 °C, followed by the addition of TEA (1.10 eq.). Propionyl chloride (as 1M solution in DCM, 1.00 eq.) was added dropwise at 0 °C and the reaction stirred for 16 h at rt. The reaction was quenched by the addition of saturated (sat.) Na_2CO_3 solution and the layers separated. The aqueous layer was extracted with DCM (50 mL) and the combined organic phases washed with 1 M $HCl_{(aq)}$ (20 mL) and dried over Na_2SO_4. The solvent was removed under reduced pressure to afford the product.

GSP 5: Introduction of the pre-substituted linker via SUZUKI coupling A

The aryl halide of the core (1.00 eq.), boronic acid pinacol ester and (tBu)$_3$P Pd G3 (3 mol%) were weighed into a flask, purged with argon and dissolved in degassed 1,4-dioxane (1 mL/0.04 mmol). An aqueous solution of K_2CO_3 (0.5 mol/L, 3.00 eq) was added dropwise to the stirred solution. The reaction was heated to 80 °C for 18 h. After the reaction was finished, the mixture was diluted with EtOAc and washed with NH_4Cl solution, water and brine. The organic layer was dried over Na_2SO_4 and the solvent removed. The raw product was purified by flash column chromatography.

GSP 6: Introduction of the pre-substituted linker via SUZUKI coupling B

The aryl halide of the core (1.00 eq.) and boronic acid pinacol ester (3.00 eq.) were dissolved in a mixture of 1,2-dimethoxyethan and ethanol (10:1) and a saturated solution of Na_2CO_3 in water (1.10 mL/ 0.05 mmol) was added. The solution was degassed with argon for 10 min and $Pd(PPh_3)_4$ (20 mol%) was added. After degassing for additional 10 min the reaction was stirred at 90 °C for 6 h. After cooling to rt, water and EtOAc (1:1) were added to the reaction and the layers separated. The aqueous layer was extracted with EtOAc and combined organic layers were dried over Na_2SO_4 and the solvent removed under reduced pressure. The residue was purified by flash column chromatography.

GSP 7: Cleavage of Boc protection groups

The corresponding protected amine or amide was dissolved in DCM (dry) and TFA (10% V/V) was added. The reaction was stirred at rt until conversion is completed and then diluted with toluene (twice the volume of DCM). The volatiles were removed under reduced pressure and the residue purified.

GSP 8: Introduction of the heterocyclic warhead via BUCHWALD coupling

The corresponding Boc-protected amine (1.00 eq.), 2-bromo-6-chloro-3-nitropyridine (**103**, 1.50 eq) and Cs_2CO_3 (4.00 eq.) were weighed into a flask. The flask was evacuated and backfilled with argon three times. XantPhos Pd G4 (5 mol%) was added, and toluene (degassed, dry) was added to the solids. The reaction was heated until complete consumption of the amine. The reaction mixture was then subjected to an aqueous workup and the crude product purified by flash column chromatography.

GSP 9: Introduction of the pyrimidine warhead to thiol-derivative

tert-Butyl 2-(2-mercaptopyridin-4-yl)-1-methyl-4-oxo-1,4,6,7-tetrahydro-5*H*-pyrrolo[3,2-*c*]pyridine-5-carboxylate (**185**) (1.00 eq) and K_2CO_3 (2.00 eq) were dissolved in DMF (dry, ~1 mL/0.10 mmol) and cooled to 0 °C. After stirring for 15 min the corresponding halopyrimidine (1.10 eq) was added and stirred at rt until complete conversion. The solvent was evaporated and the residue dissolved in DCM (10 mL/0.1 mmol) and washed with sat. NH_4Cl solution (10 mL/0.1 mmol). The aqueous phase was extracted with DCM twice. The combined organic layers were dried over Na_2SO_4 and the solvent evaporated. The raw product was purified by flash column chromatography.

6.2.2 Synthesis of Compounds described in Section 3.1

N-Benzyl-2,2-diethoxyacetamide (46)

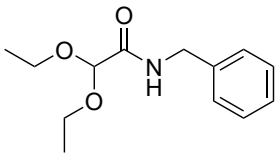

46
Chemical Formula: $C_{13}H_{19}NO_3$
Exact Mass: 237.13649
Molecular Weight: 237.29900

Synthesis of **46**, and subsequent **47**, was carried out in an analogous manner as described in the literature.[5] A mixture of benzylamine **45** (30.0 g, 0.280 mol, 1.00 eq.) and ethyl 2,2-diethoxyacetate **44** (54.3 g, 0.308 mol, 1.10 eq.) was heated to 130 °C and stirred for 18 h. After cooling to room temperature, the volatiles were removed under reduced pressure. The residue was diluted with toluene and remaining volatiles and solvent removed under reduced pressure. The crude product **46** was isolated as yellow oil (67.0 g, quant.) and used in the next step without further purification.

^{1}H NMR (200 MHz, $CDCl_3$) δ 7.32 (dd, *J* = 10.4, 4.9 Hz, 5H), 6.95 (s, 1H), 4.85 (s, 1H), 4.47 (d, *J* = 6.0 Hz, 2H), 3.66 (dd, *J* = 9.1, 5.7 Hz, 4H), 1.24 (dd, *J* = 8.5, 5.5 Hz, 6H). **^{13}C NMR** (50 MHz, $CDCl_3$) δ 167.85, 138.03, 128.78, 127.81, 127.54, 98.40, 62.44, 42.68, 15.11. **TLC-MS:** ESI(+) calcd. for $[M+Na]^+$: *m/z* = 260.1; found: 259.9. **HPLC:** t_{ret} = 6.53 min (method A).

Isoquinolin-3-ol (47)

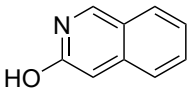

47

Chemical Formula: C_9H_7NO
Exact Mass: 145.05276
Molecular Weight: 145.16100

A flask containing *N*-benzyl-2,2-diethoxyacetamide (**46**, 61.2 g, 0.258 mol) was equipped with a stir bar and cooled to 0 °C using an ice bath. 150 mL of sulfuric acid (conc.) were added dropwise at 0 °C. After complete addition of the acid the solution was stirred for 30 min at 0 °C, warmed up to rt and stirred for one hour. The reaction was poured onto ice and the pH adjusted to 10 by slow addition of ammonia to precipitate the product. The product was isolated by filtration and dried under vacuum to afford the product **47** (36.6 g, 0.252 mol, 98%) as a yellow powder.

^{1}H NMR (200 MHz, DMSO) δ 8.90 (s, 1H), 7.93 (d, *J* = 8.1 Hz, 1H), 7.69 (d, *J* = 8.4 Hz, 1H), 7.56 (t, *J* = 7.5 Hz, 1H), 7.41 – 7.17 (m, 2H), 6.88 (s, 1H). **^{13}C NMR** (50 MHz, DMSO) δ 160.70, 150.14, 139.41, 130.44, 127.73, 125.07, 123.58, 123.37, 100.36. **HPLC:** t_{ret} = 2.87 min (91.1% at 254 nm, 94.8% at 230 nm, method A).

5,6,7,8-Tetrahydroisoquinolin-3-ol (48)

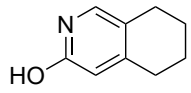

48

Chemical Formula: $C_9H_{11}NO$
Exact Mass: 149.08406
Molecular Weight: 149.19300

In an analogue manner to the procedure described by PAN *et al.* [14] to isoquinolin-3-ol (**47**, 10.0 g, 68.9 mmol, 1.00 eq) in a pressure reactor was added PtO_2 (0.234 g, 1.03 mmol, 1.5 mol%). The solids were dissolved in 25 mL TFA and 2.5 mL triflic acid under argon atmosphere. Then the reactor was purged with hydrogen and the reaction stirred under 3 bar H_2 for 18 h. After complete conversion the reaction mixture was filtered through celite and ice water was added. The solution was basified to pH 8 by adding sat. Na_2CO_3 solution and extracted with EtOAc (4x 250 mL). The organic phases were dried over Na_2SO_4 and the solvent removed. The product **48** (28.9 mmol, 4.33 g, 42%) was afforded as yellow solid, which was used in the next step without further purification. A small fraction was purified by column chromatography (Silica gel, 0% - 10% DCM/MeOH) and identified by NMR.

^{1}H NMR (200 MHz, MeOH) δ 7.17 (s, 1H), 6.30 (s, 1H), 2.69 (s, 2H), 2.57 (s, 2H), 1.91 – 1.57 (m, 4H). **^{13}C NMR** (50 MHz, MeOH) δ 164.72, 156.80, 133.29, 119.65, 117.81, 30.35, 26.06, 23.73, 23.19.

3-Chloro-5,6,7,8-tetrahydroisoquinoline (49)

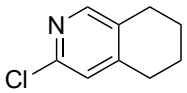

49

Chemical Formula: $C_9H_{10}ClN$
Exact Mass: 167.05018
Molecular Weight: 167.63600

According to the procedure described in patent literature [15], 5,6,7,8-Tetrahydroisoquinolin-3-ol (**48**, 2.00 g, 13.4 mmol, 1.00 eq.) was dissolved in 7.5 mL phosphorus oxychloride in a pressure tube and heated to 170°C for 16 h. After cooling to rt, the reaction was quenched by pouring it into ice water and neutralized by careful addition of Na_2CO_3 solution. The aqueous mixture was extracted three times with EtOAc (500 mL), the organic phases dried over Na_2SO_4 and the solvent

evaporated. The crude product was purified by flash column chromatography (Silica gel, 0 – 70% hexane/EtOAc) which afforded the product **49** (1.06 g, 6.30 mmol, 47%) as yellow oil.

^{1}H NMR (200 MHz, $CDCl_3$) δ 8.04 (s, 1H), 6.99 (s, 1H), 2.69 (s, 4H), 1.78 (s, 4H). **^{13}C NMR** (50 MHz, $CDCl_3$) δ 150.20, 149.91, 148.40, 132.34, 124.07, 29.00, 26.00, 22.69, 22.33. **HPLC:** t_{ret} = 7.40 min (87.9% at 254 nm, 68.4% at 230 nm, method A)

3-Chloro-7,8-dihydroisoquinolin-5(6H)-one oxime (50)

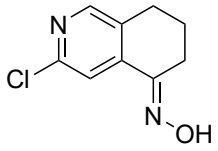

50
Chemical Formula: $C_9H_9ClN_2O$
Exact Mass: 196.04034
Molecular Weight: 196.63400

Potassium *tert*-butoxide (4.61 g, 41.1 mmol, 2.00 eq.) was suspended in 30 mL THF (dry) under an argon atmosphere and a solution of **49** (3.43 g, 20.5 mmol, 1.00 eq.) in 5 mL THF (dry) was added dropwise. After stirring for 18 h the reaction was cooled to 0 °C (ice) and *tert*-butyl nitrite (6.35 g, 7.33 mL, 61.6 mmol, 3.00 eq.) was added and stirred for 3 h at rt. The reaction was quenched by addition of 200 mL brine and then extracted with EtOAc (4x 100 mL), the organic phases dried over Na_2SO_4 and the solvent removed under reduced pressure. The residue was washed with *n*-pentane to afford the product **50** (3.35 g, 17.0 mmol, 83%) as brown solid.

^{1}H NMR (200 MHz, DMSO) δ 11.86 (s, 1H), 8.29 (s, 1H), 7.66 (s, 1H), 2.77 – 2.58 (m, 4H), 1.85 – 1.65 (m, 2H). **^{13}C NMR** (50 MHz, DMSO) δ 150.50, 150.30, 148.02, 141.83, 133.05, 116.54, 25.25, 22.79, 20.18. **TLC-MS:** ESI(+) calcd. For $[M+H]^+$: *m/z* = 197.0; found: 196,9. **HPLC:** t_{ret} = 5.66 min (98.1 % at 254 nm, 88.5 % at 230 nm, method A).

3-Chloro-7,8-dihydroisoquinolin-5(6H)-one (51)

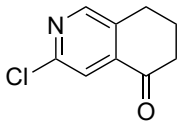

51
Chemical Formula: C_9H_8ClNO
Exact Mass: 181.02944
Molecular Weight: 181.61900

3-Chloro-7,8-dihydroisoquinolin-5(6*H*)-one oxime (**50**, 2.8 g, 14.2 mmol, 1.00 eq.) was dissolved in 50 mL acetone and a mixture of 15 mL 6 N HCl and 15 mL conc. HCl was added. The mixture was heated to reflux for 6 h. After cooling to rt the reaction was poured into 150 mL of saturated Na_2CO_3 solution and extracted with EtOAc (3x 150 mL). The organic phases were dried over Na_2SO_4 and the solvent evaporated. The residue was purified by flash column chromatography (silica gel, 10 – 70% hexane/ EtOAc). The product containing fractions were purified a second time (silica gel, 10 – 40% hexane/EtOAc) which afforded the product **51** (2.12 g, 11.0 mmol, 77%) as yellow oil.

^{1}H NMR (200 MHz, $CDCl_3$) δ 8.38 (s, 1H), 7.71 (s, 1H), 2.92 (t, *J* = 6.1 Hz, 2H), 2.74 – 2.57 (m, 2H), 2.27 – 2.03 (m, 2H). **^{13}C NMR** (50 MHz, $CDCl_3$) δ 196.19, 151.20, 150.22, 140.23, 136.38, 120.13, 38.83, 25.73, 22.63. **TLC-MS:** ESI(+) calcd. for $[M+H]^+$: *m/z* = 182.0; found: 181.9. **HPLC:** t_{ret} = 5.38 min (83.0 % at 254 nm, 97.8 % at 230 nm, method A).

6-Bromo-3-chloro-7,8-dihydroisoquinolin-5(6H)-one (52)

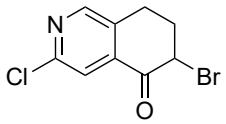

52

Chemical Formula: $C_9H_7BrClNO$
Exact Mass: 258.93995
Molecular Weight: 260.51500

3-Chloro-7,8-dihydroisoquinolin-5(6*H*)-one (**51**, 2.70 g, 14.9 mmol, 1.00 eq.) was dissolved in 30 mL acetic acid and bromine (2.38 g, 0,76 mL, 14.87 mmol, 1.00 eq.) and HBr_{aq} (47% m/m, 1.20 g, 1.67 mL, 14.9 mmol, 1 eq.) added. The reaction was stirred at rt for 3 h and then poured into sat. Na_2CO_3 solution and extracted with EtOAc (3x 100 mL). The organic phases were dried over Na_2SO_4, the solvent removed under reduced pressure. The crude product was washed with n-pentane and purified by flash column chromatography (silica gel, 0 – 50% hexane/EtOAc) to isolate the product **52** (2.82 g, 10.9 mmol, 73%) as yellow solid.

^{1}H NMR (200 MHz, $CDCl_3$) δ 8.41 (s, 1H), 7.75 (s, 1H), 4.69 (t, *J* = 3.8 Hz, 1H), 3.35 – 3.02 (m, 1H), 2.91 (dt, *J* = 17.3, 4.1 Hz, 1H), 2.64 – 2.21 (m, 2H). **^{13}C NMR** (50 MHz, $CDCl_3$) δ 188.77, 151.60, 150.77, 138.24, 135.05, 121.58, 49.12, 31.14, 22.59. **HPLC:** t_{ret} = 7.06 min (94.7 % at 254 nm, 96.0 % at 230 nm, method A).

tert-Butyl 2-chloro-7-oxo-5,6,7,9,10,11-hexahydro-8H-pyrido[3',4':4,5]pyrrolo[2,3-f]isoquinoline-8-carboxylate (54)

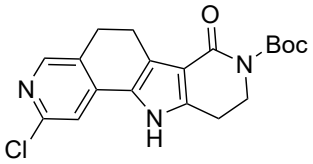

54

Chemical Formula: $C_{19}H_{20}ClN_3O_3$
Exact Mass: 373.11932
Molecular Weight: 373.83700

In analogous manner to the described procedure in patent literature [15] 6-Bromo-3-chloro-7,8-dihydroisoquinolin-5(6*H*)-one (**52**, 0.763 g, 2.93 mmol, 1.00 eq.) was dissolved in 25 mL MeOH and *tert*-butyl 2,4-dioxopiperidine-1-carboxylate (**53**, 0.874 g, 4.10 mmol, 1,4 eq.) and ammonium acetate (1.13 g, 14.64 mmol, 5 eq.) were added. The reaction was refluxed for 3h and then the solvent removed under reduced pressure. The residue was dissolved in 50 mL EtOAc and washed with water (50 mL) and brine (50 mL). The organic phase was dried over Na_2SO_4 and the solvent evaporated. The residue was purified by flash column chromatography (silica gel, 1 – 4% DCM/MeOH) which afforded the product **54** (0.527 g, 1.41 mmol, 47%) as brown powder.

^{1}H NMR (200 MHz, CDCl3) δ 11.31 (s, 1H), 8.04 (s, 1H), 7.25 (s, 1H), 4.10 (d, J = 6.0 Hz, 2H), 3.03 (d, J = 6.7 Hz, 4H), 2.83 (t, J = 7.5 Hz, 2H), 1.51 (s, 9H). **^{13}C NMR** (50 MHz, CDCl3) δ 164.37, 153.26, 149.96, 147.52, 142.36, 139.36, 128.48, 126.55, 126.14, 114.32, 113.09, 83.37, 45.96, 28.52, 25.52, 23.53, 20.64. **TLC-MS:** ESI(+) calcd. for $[M+Na]^+$: *m/z* = 396.1; found: 396.0. ESI(-) calcd. for $[M-H]^-$: *m/z* = 372.1; found: 372.0. **HPLC:** t_{ret} = 8.21 min (95.8% at 254 nm, 95.4% at 230 nm, method A).

tert-Butyl 2-chloro-11-methyl-7-oxo-5,6,7,9,10,11-hexahydro-8H-pyrido[3',4':4,5]pyrrolo[2,3-f]-isoquinoline-8-carboxylate (55)

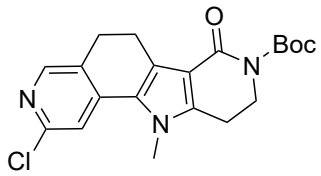

55

Chemical Formula: $C_{20}H_{22}ClN_3O_3$
Exact Mass: 387.13497
Molecular Weight: 387.86400

tert-Butyl 2-chloro-7-oxo-5,6,7,9,10,11-hexahydro-8*H*-pyrido[3',4':4,5]pyrrolo[2,3-*f*]isoquinoline-8-carboxylate (**54**, 0.465 g, 1.24 mmol, 1.00 eq.) was dissolved in 11 mL DMF (dry) under an argon atmosphere and Cs_2CO_3 (0.892 g, 2.74 mmol, 2.20 eq.) was added. After 1 h of pre-stirring at rt iodomethane (0.389 g, 0.170 mL, 2.74 mmol, 2.20 eq.) was added. The reaction was stirred for 2 h at rt. When the conversion was completed DCM (20 mL) and water (20 mL) were added and the layers separated. The organic phase was dried over Na_2SO_4, the solvent evaporated and the residue was purified by flash column chromatography (silica gel, 20 – 80% hexane/EtOAc). The product **55** (0.317 g, 0.722 mmol, 66%) was isolated as an off-white powder.

^{1}H NMR (200 MHz, $CDCl_3$) δ 8.08 (s, 1H), 7.18 (s, 1H), 4.06 (t, *J* = 6.3 Hz, 2H), 3.77 (s, 3H), 2.99 (t, *J* = 7.5 Hz, 2H), 2.87 (t, *J* = 6.3 Hz, 2H), 2.72 (t, *J* = 7.5 Hz, 2H), 1.52 (s, 9H). **^{13}C NMR** (50 MHz, $CDCl_3$) δ 162.49, 153.47, 149.89, 147.92, 142.34, 138.48, 128.76, 127.75, 127.16, 113.81, 112.06, 82.74, 44.43, 33.46, 28.18, 25.92, 22.00, 20.30. **TLC-MS:** ESI(+) calcd. for $[M+Na]^+$: *m/z* = 410.1; found: 410.0. **HPLC:** t_{ret} = 7.95 min (98.9% at 254 nm, 99.0% at 230 nm, method A).

tert-Butyl 2-(3-acrylamido-4-methoxyphenyl)-7-oxo-5,6,7,9,10,11-hexahydro-8H-pyrido[3',4':4,5]-pyrrolo[2,3-f]isoquinoline-8-carboxylate (56)

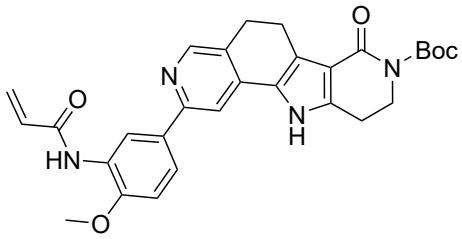

56

Chemical Formula: $C_{29}H_{30}N_4O_5$
Exact Mass: 514.22162
Molecular Weight: 514.58200

tert-Butyl 2-chloro-7-oxo-5,6,7,9,10,11-hexahydro-8*H*-pyrido[3',4':4,5]pyrrolo[2,3-*f*]isoquinoline-8-carboxylate (**54**, 0.100 g, 0.268 mmol, 1.00 eq.) and *N*-(2-methoxy-5-(4,4,5,5-tetramethyl-1,3,2-dioxaborolan-2-yl)phenyl)acrylamide (**76**, 0.122 g, 0.401 mmol, 1.50 eq.) were coupled under the conditions described in GSP 5. The raw product was purified by flash column chromatography (Silica gel, 0 – 5% DCM/MeOH) which afforded the product **56** (0.100 g, 0.195 mmol, 73%) as beige powder.

^{1}H NMR (200 MHz, $CDCl_3$) δ 11.38 (s, 1H), 8.71 (s, 1H), 8.18 (s, 1H), 7.95 (s, 1H), 7.25 (d, *J* = 4.6 Hz, 1H), 7.04 (s, 1H), 6.49 – 6.17 (m, 3H), 5.71 (d, *J* = 8.5 Hz, 1H), 4.03 – 3.91 (m, 2H), 3.59 (s, 3H), 3.09 – 2.79 (m, 4H), 2.72 (t, *J* = 7.7 Hz, 2H), 1.52 (s, 9H). **^{13}C NMR** (50 MHz, $CDCl_3$/10% CD_3OD) δ 163.88, 163.59, 155.24, 153.49, 148.98, 147.12, 140.69, 136.62, 131.72, 131.11, 127.69, 127.00, 126.81, 126.68, 124.26, 122.96, 118.65, 112.63, 110.37, 110.24, 82.61, 55.69, 45.18, 27.99, 25.16, 24.44, 22.77. **TLC-MS:** ESI(+) calcd. for $[M+H]^+$: *m/z* = 515.2; found: 515.2. **HPLC:** t_{ret} = 5.91 min (92.5% at 254 nm, 90.3% at 230 nm, method A).

tert-Butyl 2-(3-acrylamido-4-methoxyphenyl)-11-methyl-7-oxo-5,6,7,9,10,11-hexahydro-8H-pyrido[3',4':4,5]pyrrolo[2,3-f]isoquinoline-8-carboxylate (57)

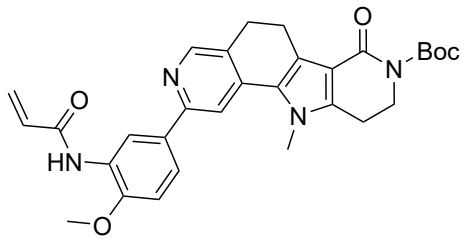

57
Chemical Formula: $C_{30}H_{32}N_4O_5$
Exact Mass: 528.23727
Molecular Weight: 528.60900

tert-Butyl 2-chloro-11-methyl-7-oxo-5,6,7,9,10,11-hexahydro-8*H*-pyrido[3',4':4,5]pyrrolo[2,3-*f*]isoquinoline-8-carboxylate (**55**, 70.0 mg, 0.180 mol, 1.00 eq) and *N*-(2-methoxy-5-(4,4,5,5-tetramethyl-1,3,2-dioxaborolan-2-yl)phenyl)acrylamide (**76**, 0.109 g, 0.361 mmol, 2.00 eq.) were weighed into a flask an subjected to GSP 5. The raw product was purified by flash column chromatography (Silica gel, 0 - 6% DCM/MeOH) which afforded the product **57** (82.0 mg, 0.155 mmol, 86%) as yellow solid.

^{1}H NMR (200 MHz, $CDCl_3$) δ 8.97 (s, 1H), 8.38 (s, 1H), 7.97 (s, 1H), 7.75 (dd, *J* = 8.6, 2.2 Hz, 1H), 7.62 (s, 1H), 6.92 (d, *J* = 8.7 Hz, 1H), 6.34 (t, *J* = 5.5 Hz, 2H), 5.73 (dd, *J* = 8.6, 2.8 Hz, 1H), 4.05 (t, *J* = 6.0 Hz, 2H), 3.88 (s, 3H), 3.83 (s, 3H), 3.04 (t, *J* = 7.3 Hz, 2H), 2.89 – 2.73 (m, 4H), 1.54 (s, 9H). **^{13}C NMR** (50 MHz, $CDCl_3$) δ 163.42, 162.66, 155.71, 153.54, 148.46, 148.17, 141.54, 136.30, 132.57, 131.52, 128.15, 127.44, 127.25, 126.34, 122.63, 118.03, 111.73, 110.67, 110.09, 82.46, 55.81, 44.42, 33.49, 28.11, 26.10, 24.72, 21.93. **TLC-MS:** ESI(+) calcd. for $[M+H]^+$: *m/z* = 529.2; found: 529.0 . **HPLC:** t_{ret} = 5.51 min (96.9% at 254 nm, 96.8% at 230 nm, method A).

tert-Butyl 2-(5-acrylamido-2-methylphenyl)-7-oxo-5,6,7,9,10,11-hexahydro-8H-pyrido[3',4':4,5]-pyrrolo[2,3-f]isoquinoline-8-carboxylate (58)

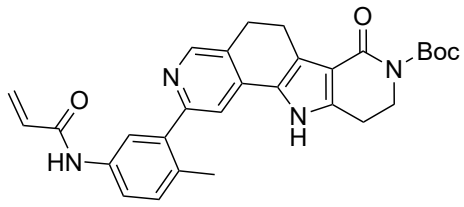

58
Chemical Formula: $C_{29}H_{30}N_4O_4$
Exact Mass: 498.22671
Molecular Weight: 498.58300

tert-Butyl 2-chloro-7-oxo-5,6,7,9,10,11-hexahydro-8*H*-pyrido[3',4':4,5]pyrrolo[2,3-f]isoquinoline-8-carboxylate (**54**, 0.100 g, 0.268 mmol, 1.00 eq.) and *N*-(4-methyl-3-(4,4,5,5-tetramethyl-1,3,2-dioxaborolan-2-yl)phenyl)acrylamide (**77**, 0.230 g, 0.800 mmol, 3.00 eq.) were dissolved in a mixture of 1,2-dimethoxyethane and EtOH (8 mL, 10:1) and subjected to GSP 6. The crude product was purified by flash column chromatography (Silica gel, 0 – 8% DCM/MeOH) which afforded the product **58** (60.0 mg, 59.0 µmol, 22%) as light-yellow solid and was directly used in the next step.

TLC-MS: ESI(+) calcd. for $[M+H]^+$: *m/z* = 499.2; found: 499.1. **HPLC:** t_{ret} = 5.60 min (100% at 254 nm, 100% at 230 nm, method A).

tert-Butyl 2-(5-acrylamido-2-methylphenyl)-11-methyl-7-oxo-5,6,7,9,10,11-hexahydro-8H-pyrido[3',4':4,5]pyrrolo[2,3-f]isoquinoline-8-carboxylate (59)

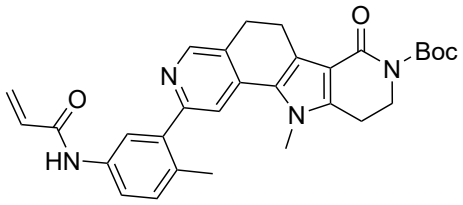

59

Chemical Formula: $C_{30}H_{32}N_4O_4$
Exact Mass: 512.24236
Molecular Weight: 512.61000

tert-Butyl 2-chloro-11-methyl-7-oxo-5,6,7,9,10,11-hexahydro-8*H*-pyrido[3',4':4,5]pyrrolo[2,3-*f*]isoquinoline-8-carboxylate (**55**, 70.0 mg, 0.180 mmol, 1.00 eq.) and *N*-(4-Methyl-3-(4,4,5,5-tetramethyl-1,3,2-dioxaborolan-2-yl)phenyl)acrylamide (**77**, 0.104 g, 0.361 mmol, 2.00 eq.) were treated according to GSP 5 and purified by flash column chromatography (Silica gel, 0 – 6% DCM/MeOH). The fraction, which contained product, were purified by a second column (Silica gel, 1 – 5% DCM/MeOH) which afforded the product **59** (47.0 mg, 90.3 µmol, 50%) as yellowish solid.

^{1}H NMR (200 MHz, CDCl3) δ 8.78 (s, 1H), 8.41 (s, 1H), 7.50 (d, J = 9.6 Hz, 2H), 7.31 (s, 1H), 7.13 (d, J = 7.9 Hz, 1H), 6.33 (dd, J = 15.1, 12.4 Hz, 2H), 5.64 (dd, J = 9.0, 2.6 Hz, 1H), 4.08 (t, J = 6.0 Hz, 2H), 3.75 (s, 3H), 3.07 (t, J = 7.5 Hz, 2H), 2.84 (d, J = 5.9 Hz, 4H), 2.27 (s, 3H), 1.55 (s, 9H). **^{13}C NMR** (50 MHz, $CDCl_3$) δ 164.1, 162.9, 158.4, 153.7, 147.9, 141.9, 140.8, 136.3, 131.6, 131.6, 131.2, 128.6, 128.0, 127.4, 127.0, 121.6, 120.6, 114.6, 112.1, 82.8, 44.6, 33.6, 28.3, 26.5, 22.22, 20.7, 19.8. **TLC-MS:** ESI(+) calcd. for $[M+H]^+$: *m/z* = 513.2; found: 523.2. **HPLC:** t_{ret} = 5.483 min (100% at 254 nm, 100% at 230 nm, method A).

tert-Butyl 2-(4-acryloyl-3,4-dihydro-2H-benzo[b][1,4]oxazin-6-yl)-11-methyl-7-oxo-5,6,7,9,10,11-hexahydro-8H-pyrido[3',4':4,5]pyrrolo[2,3-f]isoquinoline-8-carboxylate (60)

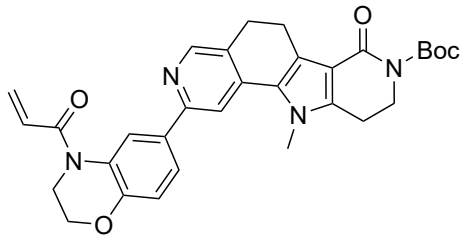

60

Chemical Formula: $C_{31}H_{32}N_4O_5$
Exact Mass: 540.23727
Molecular Weight: 540.62000

tert-Butyl 2-chloro-11-methyl-7-oxo-5,6,7,9,10,11-hexahydro-8*H*-pyrido[3',4':4,5]pyrrolo[2,3-*f*]isoquinoline-8-carboxylate (**55**, 70.0 mg, 0.180 mmol, 1.00 eq.) and 1-(6-(4,4,5,5-tetramethyl-1,3,2-dioxaborolan-2-yl)-2,3-dihydro-4*H*-benzo[*b*][1,4]oxazin-4-yl)prop-2-en-1-one (**85**, 0.114 g, 0.361 mmol, 2.00 eq.) were subjected to GSP 5 and purified by flash column chromatography (Silica gel, 0 – 6% DCM/MeOH) which afforded the product **60** (71.0 mg, 0.131 mmol, 73%) as brown oil which was used in the next step without further purification.

^{1}H NMR (200 MHz, $CDCl_3$) δ 8.41 (s, 1H), 7.77 (s, 1H), 7.66 (dd, *J* = 8.6, 2.1 Hz, 1H), 7.54 (s, 1H), 6.98 (d, *J* = 8.6 Hz, 1H), 6.92 – 6.61 (m, 2H), 6.48 (dd, *J* = 16.8, 1.9 Hz, 1H), 5.77 (dd, *J* = 10.2, 1.9 Hz, 1H), 4.43 – 4.29 (m, 2H), 4.14 – 4.00 (m, 4H), 3.84 (s, 3H), 3.07 (t, *J* = 7.6 Hz, 2H), 2.98 – 2.74 (m, 5H), 1.55 (s, 9H). **^{13}C NMR** (50 MHz, $CDCl_3$) δ 164.31, 162.73, 155.42, 153.72, 148.66, 147.54, 141.70, 136.60, 132.32, 129.12, 128.61, 128.20, 126.84, 125.80, 124.79, 122.77, 117.65, 112.11, 110.45, 82.79,

75.03, 67.15, 44.56, 33.52, 28.27, 26.30, 24.90, 22.17, 20.58. **TLC-MS:** ESI(+) calcd. for $[M+H]^+$: *m/z* = 541.2; found:541.1. **HPLC:** t_{ret} = 5.66 min (80.7% at 254 nm, 80.6% at 230 nm, method A).

tert-Butyl 2-(4-methoxy-3-propionamidophenyl)-7-oxo-5,6,7,9,10,11-hexahydro-8H-pyrido[3',4':4,5]pyrrolo[2,3-f]isoquinoline-8-carboxylate (61)

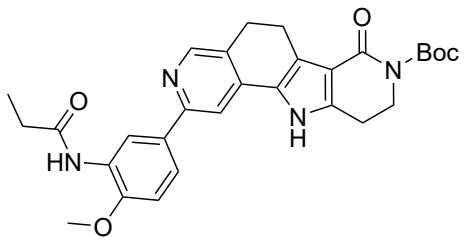

61
Chemical Formula: $C_{29}H_{32}N_4O_5$
Exact Mass: 516.23727
Molecular Weight: 516.59800

A mixture of *tert*-Butyl 2-chloro-7-oxo-5,6,7,9,10,11-hexahydro-8H-pyrido[3',4':4,5]pyrrolo[2,3-f]isoquinoline-8-carboxylate (**54**, 70.0 mg, 0.187 mmol, 1.00 eq.) and *N*-(2-methoxy-5-(4,4,5,5-tetramethyl-1,3,2-dioxaborolan-2-yl)phenyl)propionamide (**78**, 0.114 g, 0.562 mmol, 2.00 eq.) was subjected to GSP 5. After 18 h an additional portion of $(t\text{Bu})_3$P Pd G3 (3.21 mg, 5.62 µmol, 3.00 mol%) was added and the reaction continued for 18 h at 90 °C. After the aqueous work-up the raw product was purified by flash column chromatography (Silica gel, 40 – 100% hexane/EtOAc). The product containing fractions were purified in a second step (Silica gel, 2 – 6 % DCM/MeOH) which afforded the product **61** (27.0 mg, 52.4 µmol, 28%) as light-yellow powder. Due to low solubility in NMR solvents the product was directly transferred to the next step.

TLC-MS: ESI(+) calcd. for $[M+H]^+$: *m/z* = 517.2; found: 517.1. **HPLC:** t_{ret} = 13.16 min (99.1% at 254 nm, 98.8% at 230 nm, method B).

tert-Butyl 2-(2-methyl-5-propionamidophenyl)-7-oxo-5,6,7,9,10,11-hexahydro-8H-pyrido[3',4':4,5]pyrrolo[2,3-f]isoquinoline-8-carboxylate (62)

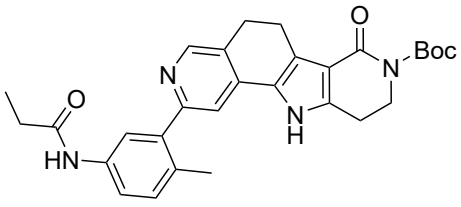

62
Chemical Formula: $C_{29}H_{32}N_4O_4$
Exact Mass: 500.24236
Molecular Weight: 500.59900

tert-Butyl 2-chloro-7-oxo-5,6,7,9,10,11-hexahydro-8H-pyrido[3',4':4,5]pyrrolo[2,3-f]isoquinoline-8-carboxylate (**54**, 70.0 mg, 0.187 mmol, 1.00 eq.) and boronic acid derivative **79** (0.108 g, 0.375 mmol, 2.00 eq.) were subjected to GSP 5. After the reaction was stirred for 18 h an additional portion of boronic acid derivative **79** (54.1 mg, 0.188 mmol, 1.00 eq.)and $(t\text{Bu})_3$P Pd G3 (3.20 mg, 5,62 µmol, 3 mol%) were added and the reaction stirred for another 18 h. The reaction was then treated as described in GSP 5 and purified by flash column chromatography (Silica, 0 – 6% DCM/MeOH) which afforded the product **62** (40.0 mg, 80.4 µmol, 43%) as light-green powder. Due to low solubility in NMR solvents the product was directly transferred to the next step.

TLC-MS: ESI(+) calcd. for $[M+H]^+$: *m/z* = 501.2 ; found: 501.1. **HPLC:** t_{ret} = 5.69 min (97.2% at 254 nm, 95.1% at 230 nm, method A).

tert-Butyl 7-oxo-2-(4-propionyl-3,4-dihydro-2H-benzo[b][1,4]oxazin-6-yl)-5,6,7,9,10,11-hexahydro-8H-pyrido[3',4':4,5]pyrrolo[2,3-f]isoquinoline-8-carboxylate (63)

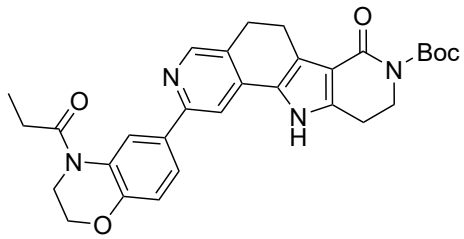

63

Chemical Formula: $C_{30}H_{32}N_4O_5$
Exact Mass: 528.23727
Molecular Weight: 528.60900

tert-Butyl 2-chloro-7-oxo-5,6,7,9,10,11-hexahydro-8H-pyrido[3',4':4,5]pyrrolo[2,3-f]isoquinoline-8-carboxylate (**54**) (70.0 mg, 0.187 mmol, 1.00 eq.) and 1-(6-(4,4,5,5-tetramethyl-1,3,2-dioxaborolan-2-yl)-2,3-dihydro-4*H*-benzo[*b*][1,4]oxazin-4-yl)propan-1-one (**86**, 0.119 g, 0.374 mmol, 2.00 eq.) were subjected to GSP 5. After the reaction was stirred for 18 h an additional portion of 1-(6-(4,4,5,5-tetramethyl-1,3,2-dioxaborolan-2-yl)-2,3-dihydro-4*H*-benzo[*b*][1,4]oxazin-4-yl)propan-1-one (**86**, 59.5 mg, 0.187 mmol, 1.00 eq.)and (tBu)$_3$P Pd G3 (3.20 mg, 5,62 µmol, 3 mol%) were added and the reaction stirred for another 18 h. The reaction was then treated as described in GSP 5 and purified by flash column chromatography (Silica, 0 – 6% DCM/MeOH) which afforded the product **63** (47.0 mg, 80.7 µmol, 47%) as a light-brown oil.

^{1}H NMR (200 MHz, $CDCl_3$) δ 11.08 (s, 1H), 8.26 (s, 1H), 7.54 (s, 2H), 6.79 (d, J = 8.6 Hz, 1H), 4.23 (s, 2H), 4.04 (d, J = 5.3 Hz, 2H), 3.80 (s, 2H), 3.11 – 2.91 (m, 2H), 2.93 – 2.73 (m, 4H), 2.53 (dd, J = 14.4, 7.0 Hz, 3H), 1.53 (s, 9H), 1.17 – 1.02 (m, 3H). **^{13}C NMR** (50 MHz, $CDCl_3$) δ 164.60, 163.59, 153.67, 147.78, 140.82, 136.57, 131.95, 127.39, 127.06, 124.75, 124.46, 122.61, 117.48, 112.92, 110.0, 82.79, 75.20, 45.41, 28.31, 27.97, 25.55, 24.97, 23.06, 20.64, 9.72. **TLC-MS:** ESI(+) calcd. for $[M+H]^+$: m/z = 529.2; found: 529.1. **HPLC:** t_{ret} = 6.02 min (100 % at 254 nm, 95.7% at 230 nm, method A).

N-(2-methoxy-5-(7-oxo-6,7,8,9,10,11-hexahydro-5H-pyrido[3',4':4,5]pyrrolo[2,3-f]isoquinolin-2-yl)phenyl)acrylamide (64)

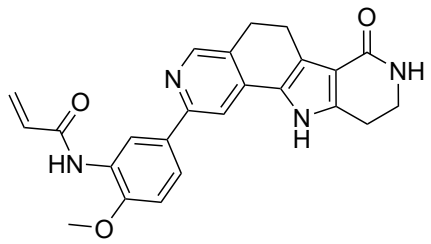

64

Chemical Formula: $C_{24}H_{22}N_4O_3$
Exact Mass: 414.16919
Molecular Weight: 414.46500

tert-Butyl 2-(3-acrylamido-4-methoxyphenyl)-7-oxo-5,6,7,9,10,11-hexahydro-8*H*-pyrido[3',4':4,5]pyrrolo[2,3-*f*]isoquinoline-8-carboxylate (**56**, 0.100 g, 0.194 mmol) was dissolved in DCM (5 mL) and subjected to GSP 7 and stirred for 30 min. The residue was dissolved in a 9:1 mixture of DCM and MeOH (5 mL) and washed with sat. Na_2CO_3 solution (3 mL). The aqueous phase was extracted with DCM/MeOH (9:1, 2x 5 mL) and the combined organic layers dried over Na_2SO_4 and the solvent evaporated. The residue was purified by flash column chromatography (Silica gel, 1 – 7% DCM/MeOH). The product containing fractions were combined, the solvent removed and purified by reverse phase column chromatography (43 g, CHROMABOND® Flash RS 40 C_{18} ec, 5 – 40% water/MeCN + 0.2%TFA, 60 min). The pure product containing fractions were lyophilized to afford the product **64** (54.8 mg, 0.132 mmol, 68%) as yellow solid.

^{1}H NMR (200 MHz, DMSO) δ 11.99 (s, 1H), 9.49 (s, 1H), 8.70 (s, 1H), 8.34 (s, 1H), 7.90 – 7.75 (m, 2H), 7.19 (d, *J* = 8.7 Hz, 1H), 7.03 (s, 1H), 6.73 (dd, *J* = 16.8, 10.1 Hz, 1H), 6.27 (dd, *J* = 17.1, 1.9 Hz, 1H), 5.81 – 5.68 (m, 1H), 3.91 (s, 3H), 3.42 (d, *J* = 5.9 Hz, 2H), 2.88 (p, *J* = 6.5 Hz, 6H). **^{13}C NMR** (50 MHz, DMSO) δ 165.52, 163.39, 154.53, 150.78, 147.61, 138.89, 136.41, 132.02, 131.45, 127.02, 126.71, 126.29, 125.07, 122.89, 121.97, 120.84, 111.93, 111.22, 108.81, 55.90, 48.59, 25.02, 22.16, 20.18. **HRMS:** ESI(+) calcd. for $[M+H]^+$: *m/z* = 415.17647; found: 415.17667; rel. deviation: 0.49 ppm. **HPLC:** t_{ret} = 7.29 min (95.1% at 254 nm, 95.2% at 230 nm, method B). **IR** (ATR) [cm^{-1}]: 3235, 3068, 3022, 2946, 2902, 2844, 1653, 1623, 1511, 1437, 1420, 1395, 1327, 1268, 1196, 1176, 1126, 1056, 1018, 979, 877, 797, 746, 718, 663.

N-(2-methoxy-5-(11-methyl-7-oxo-6,7,8,9,10,11-hexahydro-5H-pyrido[3',4':4,5]pyrrolo[2,3-f]isoquinolin-2-yl)phenyl)acrylamide (65)

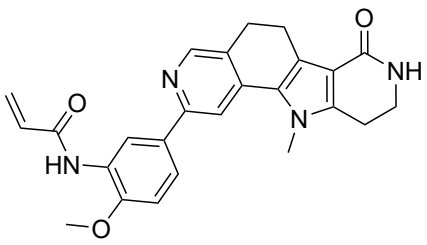

65
Chemical Formula: $C_{25}H_{24}N_4O_3$
Exact Mass: 428.18484
Molecular Weight: 428.49200

tert-Butyl 2-(3-acrylamido-4-methoxyphenyl)-11-methyl-7-oxo-5,6,7,9,10,11-hexahydro-8*H*-pyrido[3',4':4,5]pyrrolo[2,3-*f*]isoquinoline-8-carboxylate (**57**, 16.3 mg, 30.8 µmol, 1.00 eq.) was dissolved in DCM (4 mL) and subjected to GSP 7 (stirred for 30 min). A saturated solution of Na_2CO_3 was added to the residue and extracted with EtOAc (2x 10 mL). The organic phases were dried over Na_2SO_4 and the solvent removed under reduced pressure and the raw product was purified by flash column chromatography (Silica gel, 0 – 10% DCM/MeOH). The product was washed with n-pentane and dried in vacuum which afford the product **65** (8.00 mg, 18.5 µmol, 60%) as yellow powder. **^{1}H NMR** (200 MHz, CDCl3/10% CD3OD) δ 8.75 (s, 1H), 8.25 (s, 1H), 7.62 (s, 2H), 6.96 (d, J = 8.3 Hz, 1H), 6.31 (d, J = 5.1 Hz, 2H), 5.78 – 5.65 (m, 1H), 3.87 (s, 3H), 3.84 (s, 3H), 3.51 (t, J = 6.9 Hz, 2H), 2.93 (d, J = 7.4 Hz, 2H), 2.83 (t, J = 7.2 Hz, 4H). **^{13}C NMR** (50 MHz, CDCl310% CD3OD) δ 166.94, 164.25, 155.22, 149.53, 145.80, 141.73, 138.29, 131.19, 130.88, 128.73, 127.73, 127.34, 127.26, 126.75, 123.50, 118.89, 111.70, 110.73, 110.61, 55.85, 40.14, 33.58, 26.15, 21.48, 20.26. **HRMS:** ESI(+) calcd. for $[M+H]^+$: *m/z* = 429.19212; found: 429.19250; rel. deviation 1.7 ppm. **HPLC:** t_{ret} = 2.82 min (96.6% at 254 nm, 95.0% at 230 nm, method A). **IR** (ATR) [cm^{-1}]: 3322, 3257, 3232, 3211, 3139, 3105, 3083, 3069, 3019, 2921, 2849, 2651, 1653, 1618, 1592, 1528, 1491, 1448, 1420, 1323, 1261, 1198, 1173, 1128, 1072, 1018, 986, 893, 861, 799, 720, 668.

N-(4-Methyl-3-(7-oxo-6,7,8,9,10,11-hexahydro-5H-pyrido[3',4':4,5]pyrrolo[2,3-f]isoquinolin-2-yl)phenyl)acrylamide (66)

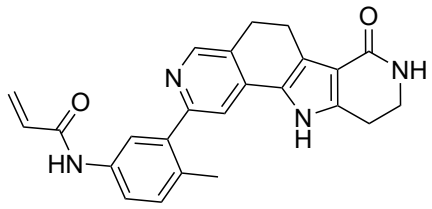

66
Chemical Formula: $C_{24}H_{22}N_4O_2$
Exact Mass: 398.17428
Molecular Weight: 398.46600

tert-Butyl 2-(5-acrylamido-2-methylphenyl)-7-oxo-5,6,7,9,10,11-hexahydro-8*H*-pyrido[3',4':4,5]pyrrolo[2,3-*f*]isoquinoline-8-carboxylate (**58**, 60.0 mg, 0.120 mmol) was dissolved in DCM (4 mL) and subjected to GSP 7. Sat. Na_2CO_3 solution was added to the residue and extracted with EtOAc (2x 10 mL). The combined organics were dried over Na_2SO_4 and the solvent evaporated. The raw product was purified by flash column chromatography (Silica gel, 3 – 10% DCM/MeOH) which afforded the product **66** (25.0 mg, 62.7 µmol, 52%) as beige powder.

^{1}H NMR (200 MHz, DMSO) δ 11.88 (s, 1H), 10.17 (s, 1H), 8.38 (s, 1H), 7.77 (d, *J* = 2.0 Hz, 1H), 7.60 (dd, *J* = 8.3, 2.3 Hz, 1H), 7.46 (s, 1H), 7.23 (s, 1H), 7.04 (s, 1H), 6.52 – 6.18 (m, 2H), 5.74 (d, *J* = 12.3 Hz, 1H), 3.44 – 3.37 (m, 2H), 2.86 (dt, *J* = 13.5, 5.2 Hz, 5H), 2.31 (s, 3H). **^{13}C NMR** (50 MHz, DMSO) δ 165.48, 163.06, 157.48, 147.35, 140.70, 139.06, 136.82, 135.89, 131.89, 130.90, 130.31, 126.72, 126.27, 124.82, 122.19, 120.44, 118.91, 113.17, 111.96, 25.01, 22.15, 22.12, 20.13, 19.68. **HRMS:** ESI(+) calcd. for $[M+H]^+$: *m/z* = 399.18155; found: 399.18202; rel. deviation: 1.16 ppm. **HPLC:** t_{ret} = 2.47 min (97.7% at 254 nm, 97.8% at 230 nm, method A). **IR** (ATR) [cm^{-1}]: 3218, 3111, 3056, 2948, 2926, 2857, 1635, 1605, 1540, 1499, 1437, 1401, 1360, 1330, 1284, 1233, 1204, 1182, 1156, 1137, 1115, 1052, 985, 947, 893, 819, 797, 778, 731, 710, 690, 664.

N-(4-Methyl-3-(11-methyl-7-oxo-6,7,8,9,10,11-hexahydro-5H-pyrido[3',4':4,5]pyrrolo[2,3-f]isoquinolin-2-yl)phenyl)acrylamide (67)

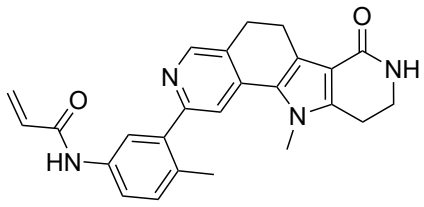

67
Chemical Formula: $C_{25}H_{24}N_4O_2$
Exact Mass: 412.18993
Molecular Weight: 412.49300

tert-butyl 2-(5-acrylamido-2-methylphenyl)-11-methyl-7-oxo-5,6,7,9,10,11-hexahydro-8*H*-pyrido[3',4':4,5]pyrrolo[2,3-*f*]isoquinoline-8-carboxylate (**59**, 47.0 mg, 91.7 µmol) was dissolved in DCM (5 mL, dry) and subjected to GSP 7. The residue was dissolved in a 9:1 mixture of DCM and MeOH (15 mL) and washed with sat. Na_2CO_3 solution (15 mL). The aqueous phase was extracted with DCM/MeOH (9:1, 2x 15 mL) and the combined organic layers dried over Na_2SO_4. The solvent was removed under reduced pressure and the residue purified by flash column chromatography (Silica gel, 1 – 9% DCM/MeOH) which afforded the product **67** (23.0 mg, 55.8 µmol, 61%) as yellow powder.

^{1}H NMR (400 MHz, DMSO) δ 10.18 (s, 1H), 8.46 (s, 1H), 7.76 (d, *J* = 1.6 Hz, 1H), 7.69 – 7.62 (m, 1H), 7.50 (s, 1H), 7.26 (d, *J* = 8.3 Hz, 1H), 7.12 (s, 1H), 6.43 (dd, *J* = 16.9, 10.1 Hz, 1H), 6.24 (dd, *J* = 16.9, 1.6 Hz, 1H), 5.79 – 5.69 (m, 1H), 3.81 (s, 3H), 3.45 – 3.37 (m, 2H), 2.95 – 2.77 (m, 6H), 2.33 (s,

3H). **^{13}C NMR** (101 MHz, DMSO) δ 165.11, 163.00, 157.36, 147.32, 141.06, 140.53, 136.77, 135.92, 131.89, 130.82, 130.36, 127.69, 126.55, 126.05, 124.33, 120.66, 119.02, 114.05, 110.76, 54.78, 33.17, 25.76, 21.05, 20.08, 19.66. **HRMS:** ESI(+) calcd. for $[M+H]^+$: *m/z* = 413.19720; found: 413.19751; rel. deviation: 0.74 ppm. **HPLC:** t_{ret} = 6.63 min (95.6% at 254 nm, 96.3% at 230 nm, method B). **IR** (ATR) [cm^{-1}]: 3308, 3058, 2949, 2924, 2850, 1676, 1640, 1590, 1554, 1529, 1512, 1487, 1437, 1401, 1356, 1328, 1251, 1237, 1195, 1170, 1067, 976, 943, 914, 893, 873, 826, 782, 756, 731, 699, 668.

2-(4-Acryloyl-3,4-dihydro-2H-benzo[b][1,4]oxazin-6-yl)-11-methyl-5,6,8,9,10,11-hexahydro-7H-pyrido[3',4':4,5]pyrrolo[2,3-f]isoquinolin-7-one (68)

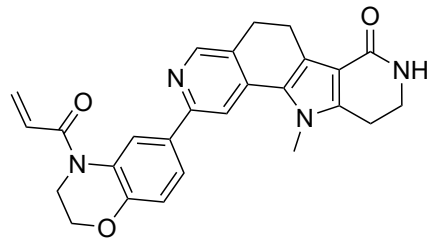

68
Chemical Formula: $C_{26}H_{24}N_4O_3$
Exact Mass: 440.18484
Molecular Weight: 440.50300

tert-Butyl 2-(4-acryloyl-3,4-dihydro-2*H*-benzo[*b*][1,4]oxazin-6-yl)-11-methyl-7-oxo-5,6,7,9,10,11-hexahydro-8*H*-pyrido[3',4':4,5]pyrrolo[2,3-f]isoquinoline-8-carboxylate (**60**, 71.0 mg, 0.131 mmol) was dissolved in DCM (dry, 4 mL) and subjected to GSP 7. The residue was dissolved in a 9:1 mixture of DCM and MeOH (15 mL) and washed with sat. Na_2CO_3 solution (15 mL). The aqueous phase was extracted with DCM/MeOH (9:1, 2x 15 mL). The combined organic layers were dried over Na_2SO_4 and the solvent was removed under reduced pressure. The raw product was purified by flash column chromatography (Silica gel, 1 – 10% DCM/MeOH) which afforded the product **68** (9.00 mg, 20.4 µmol, 16%) as brown solid.

^{1}H NMR (200 MHz, $CDCl_3$/10% CD_3OD) δ 8.31 (s, 1H), 7.82 – 7.44 (m, 3H), 6.96 (d, *J* = 8.8 Hz, 1H), 6.78 (dd, *J* = 16.4, 10.3 Hz, 1H), 6.42 (d, *J* = 16.6 Hz, 1H), 5.76 (d, *J* = 9.8 Hz, 1H), 4.31 (d, *J* = 5.0 Hz, 2H), 4.00 (d, *J* = 5.0 Hz, 2H), 3.81 (s, 3H), 3.54 (t, *J* = 6.8 Hz, 2H), 2.95 (d, *J* = 7.4 Hz, 2H), 2.84 (t, *J* = 7.0 Hz, 4H). **^{13}C NMR** (50 MHz, $CDCl_3$/10% CD_3OD) δ 166.72, 164.45, 154.85, 147.33, 147.00, 140.57, 137.09, 131.22, 129.01, 128.69, 128.36, 127.04, 125.89, 125.11, 124.90, 122.42, 117.40, 110.82, 110.47, 76.99, 66.48, 39.96, 33.23, 25.86, 21.30, 20.04. **HRMS:** ESI(+) calcd. for $[M+H]^+$: *m/z* = 441.19212; found: 441.19268; rel. deviation: 1.27 ppm. **HPLC:** t_{ret} = 1.497 min (87.6% at 254 nm, 92.0% at 230 nm, method A, overlaying injection peak). **IR** (ATR) [cm^{-1}]: 2920, 2852, 1636, 1594, 1507, 1457, 1405, 1363, 1320, 1254, 1219, 1198, 1170, 1112, 1067, 1041, 977, 944, 894, 860, 820, 784, 724, 700, 668.

N-(2-methoxy-5-(7-oxo-6,7,8,9,10,11-hexahydro-5H-pyrido[3',4':4,5]pyrrolo[2,3-f]isoquinolin-2-yl)phenyl)propionamide (69)

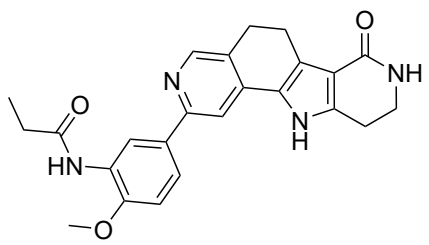

69

Chemical Formula: $C_{24}H_{24}N_4O_3$
Exact Mass: 416.18484
Molecular Weight: 416.48100

tert-Butyl 2-(4-methoxy-3-propionamidophenyl)-7-oxo-5,6,7,9,10,11-hexahydro-8*H*-pyrido[3',4':4,5]pyrrolo[2,3-*f*]isoquinoline-8-carboxylate (**61**, 27.0 mg, 52.2 µmol) was dissolved in 4 mL DCM (dry) and subjected to GSP 7. The reaction was stirred for 30 min. The raw product was dissolved in a DCM/MeOH mixture (5% MeOH, 10 mL) and washed with sat, Na_2CO_3 solution (5 mL). the organic layer was dried over Na_2SO_4 and the solvent evaporated. The residue was purified by flash column chromatography (Silica gel, 1 – 10% DCM/MeOH). The isolated product was washed with n-pentane and dried in vacuum which afforded the product **69** (18.0 mg, 43.2 µmol, 83%) as a beige powder.

^{1}H NMR (400 MHz, DMSO) δ 11.99 (s, 1H), 9.13 (s, 1H), 8.61 (s, 1H), 8.33 (s, 1H), 7.83 (s, 1H), 7.77 (dd, *J* = 8.6, 2.0 Hz, 1H), 7.16 (d, *J* = 8.7 Hz, 1H), 7.05 (s, 1H), 3.89 (s, 3H), 3.40 (td, *J* = 6.8, 2.4 Hz, 2H), 2.89 (ddd, *J* = 18.6, 9.7, 4.6 Hz, 6H), 2.42 (q, *J* = 7.5 Hz, 2H), 1.10 (dd, *J* = 10.1, 5.0 Hz, 3H).**^{13}C NMR** (101 MHz, DMSO) δ 172.06, 165.42, 154.63, 150.50, 147.51, 138.78, 136.32, 131.45, 127.40, 126.15, 125.00, 122.32, 121.88, 120.52, 111.89, 111.00, 108.73, 55.78, 40.03, 29.12, 24.95, 22.10, 20.11, 9.65. **HRMS:** ESI(+) calcd. for $[M+H]^+$: *m/z* = 417.19212; found: 417,19253; rel. deviation 0.98 ppm. **HPLC:** t_{ret} = 3.25 min (100% at 254 nm, 100% at 230 nm, method A). **IR** (ATR) [cm^{-1}]: 3339, 2962, 2930, 2895, 2836, 1603, 1536, 1506, 1483, 1440, 1401, 1363, 1331, 1274, 1257, 1140, 1113, 1057, 1032, 910, 869, 809, 782, 753, 723, 700, 678.

N-(4-methyl-3-(7-oxo-6,7,8,9,10,11-hexahydro-5H-pyrido[3',4':4,5]pyrrolo[2,3-f]isoquinolin-2-yl)phenyl)propionamide (70)

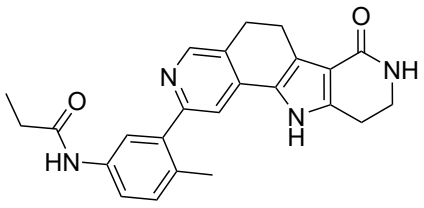

70

Chemical Formula: $C_{24}H_{24}N_4O_2$
Exact Mass: 400.18993
Molecular Weight: 400.48200

tert-Butyl 2-(2-methyl-5-propionamidophenyl)-7-oxo-5,6,7,9,10,11-hexahydro-8*H*-pyrido[3',4':4,5]pyrrolo[2,3-*f*]isoquinoline-8-carboxylate (**62**, 40.0 mg, 79.9 µmol) was dissolved in DCM (dry, 5 mL) subjected to GSP 7. The residue was dissolved in a 9:1 mixture of DCM and MeOH (5 mL) and washed with sat. Na_2CO_3 solution (3 mL). The aqueous phase was extracted with the 9:1 mixture of DCM and MeOH (2x 5 mL) and the combined organic extracts were dried over Na_2SO_4 and the solvent removed. The raw product was purified by flash column chromatography (Silica gel, 1 – 8% DCM/MeOH)which afforded the product **70** (6.5 mg, 16.2 µmol, 20%) as yellow solid.

^{1}H NMR (200 MHz, DMSO) δ 11.89 (s, 1H), 9.87 (s, 1H), 8.37 (s, 1H), 7.69 (s, 1H), 7.51 (d, *J* = 9.7 Hz, 1H), 7.45 (s, 1H), 7.20 (d, *J* = 8.2 Hz, 1H), 7.04 (s, 1H), 3.40 (d, *J* = 6.2 Hz, 2H), 2.95 – 2.75 (m,

5H), 2.39 – 2.19 (m, 5H), 1.08 (t, *J* = 7.5 Hz, 3H). **^{13}C NMR** (50 MHz, DMSO) δ 171.82, 165.45, 157.65, 140.62, 139.02, 137.15, 135.80, 130.69, 129.57, 126.16, 124.82, 122.10, 120.16, 113.12, 111.93, 29.48, 25.02, 22.13, 20.13, 19.61, 9.70. **HRMS:** ESI(+) calcd. for $[M+H]^+$: *m/z* = 401.19720; found: 401.19726; rel. deviation 0.15 ppm. **HPLC:** t_{ret} = 2.63 min (96.7% at 254 nm, 94.6% at 230 nm, method A).

2-(4-Propionyl-3,4-dihydro-2H-benzo[b][1,4]oxazin-6-yl)-5,6,8,9,10,11-hexahydro-7H-pyrido[3',4':4,5]pyrrolo[2,3-f]isoquinolin-7-one (71)

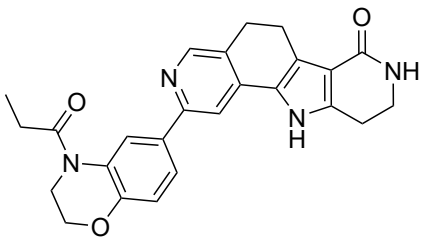

71
Chemical Formula: $C_{25}H_{24}N_4O_3$
Exact Mass: 428.18484
Molecular Weight: 428.49200

tert-Butyl 7-oxo-2-(4-propionyl-3,4-dihydro-2*H*-benzo[*b*][1,4]oxazin-6-yl)-5,6,7,9,10,11-hexahydro-8*H*-pyrido[3',4':4,5]pyrrolo[2,3-*f*]isoquinoline-8-carboxylate (**63**, 47.0 mg, 88.9 µmol) was dissolved in DCM (dry, 5 mL) and subjected to GSP 7. The residue was dissolved in a 9:1 mixture of DCM and MeOH (10 mL) and washed with sat. Na_2CO_3 solution (5 mL). The aqueous phase was extracted with DCM/MeOH (9:1, 10 mL). The combined organic extracts were dried over Na_2SO_4 and the solvent was removed under reduced pressure. The raw product was purified by flash column chromatography (Silica gel, 2 – 8% DCM/MeOH) which afforded the product **71** (23.0 mg, 20.4 µmol, 23%) as yellow powder.

^{1}H NMR (400 MHz, DMSO) δ 11.92 (s, 1H), 8.50 (s, 1H), 8.33 (s, 1H), 7.84 (s, 1H), 7.71 (d, J = 7.6 Hz, 1H), 7.01 (d, J = 8.4 Hz, 2H), 4.35 – 4.28 (m, 2H), 3.94 – 3.86 (m, 2H), 3.45 – 3.36 (m, 2H), 2.88 (dt, J = 12.9, 6.7 Hz, 6H), 2.63 (dd, J = 14.6, 7.2 Hz, 2H), 1.09 (t, J = 7.3 Hz, 3H). **^{13}C NMR** (101 MHz, DMSO) δ 171.85, 165.44, 154.31, 147.41, 146.99, 138.93, 136.48, 130.86, 126.42, 126.29, 125.01, 123.06, 122.15, 122.06, 116.88, 111.95, 108.82, 66.27, 66.25, 40.06, 27.00, 24.96, 22.15, 20.13, 9.32. **HRMS:** ESI(+) calcd. for $[M+H]^+$: *m/z* = 429.19212; found:429.19244 ; rel. deviation: 0.76 ppm. **HPLC:** t_{ret} = 3.23 min (98.4% at 254 nm, 97.0% at 230 nm, method A). **IR** (ATR) [cm^{-1}]: 3213, 2921, 2850, 1663, 1610, 1497, 1443, 1384, 1325, 1285, 1251, 1217, 1197, 1115, 1043, 952, 934, 887, 847, 819, 781, 723, 691, 668, 651.

2-Methoxy-5-(4,4,5,5-tetramethyl-1,3,2-dioxaborolan-2-yl)aniline (74)

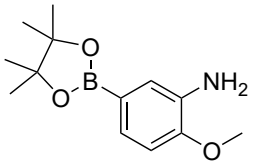

74
Chemical Formula: $C_{13}H_{20}BNO_3$
Exact Mass: 249.15362
Molecular Weight: 249.11700

5-Bromo-2-methoxyanilin (**72**, 0.500 g, 2.50 mmol, 1.00 eq.) was dissolved in 1,4 dioxane (3 mL) subjected to GSP1, heated for 7 h and purified by flash chromatography (Silica gel, 0 – 20% hexane/EtOAc) which afforded the product **74** (0.352 g, 1.41 mmol, 57%) as a yellow oil.

^{1}H NMR (200 MHz, $CDCl_3$) δ 7.33 (d, *J* = 8.0 Hz, 1H), 7.26 (s, 1H), 6.88 (d, *J* = 8.0 Hz, 1H), 3.94 (s, 3H), 3.81 (s, 2H), 1.42 (s, 12H). **^{13}C NMR** (50 MHz, $CDCl_3$) δ 150.00, 135.57, 126.07,

120.99, 120.96, 109.70, 83.48, 55.34, 24.87. **TLC-MS:** ESI(+) calcd. for $[M+H]^+$: *m/z* = 249.2; found: 250.0. **HPLC:** t_{ret} = 4.319 min (96.9% at 254 nm, 91.5% at 230 nm, method A).

4-Methyl-3-(4,4,5,5-tetramethyl-1,3,2-dioxaborolan-2-yl)aniline (75)

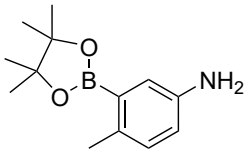

75

Chemical Formula: $C_{13}H_{20}BNO_2$
Exact Mass: 233.15871
Molecular Weight: 233.11800

3-Bromo-4-methylaniline (**73**, 1.50 g, 8.06 mmol, 1.00 eq.) was subjected to GSP 1, using 15 mL of 1,4-dioxane as solvent and stirring for 5 h. The raw product was purified by flash column chromatography (Silica gel, 0 – 20% hexane/EtOAc) which afforded the product **75** (1.63 g, 7.01 mmol, 87%) as an orange-brown solid.

^{1}H NMR (200 MHz, $CDCl_3$) δ 7.14 (d, *J* = 2.5 Hz, 1H), 6.98 (d, *J* = 8.0 Hz, 1H), 6.69 (dd, *J* = 8.1, 2.6 Hz, 1H), 3.53 (s, 2H), 2.45 (s, 3H), 1.35 (s, 12H). **^{13}C NMR** (50 MHz, $CDCl_3$) δ 143.35, 134.85, 130.83, 122.61, 118.12, 83.55, 25.05, 21.24. **TLC-MS:** ESI(+) calcd. for $[M+H]^+$: *m/z* = 234.2; found: 234.0. **HPLC:** t_{ret} = 6.36 min (98.4% at 254 nm, 99.6% at 230 nm, method A).

N-(2-Methoxy-5-(4,4,5,5-tetramethyl-1,3,2-dioxaborolan-2-yl)phenyl)acrylamide (76)

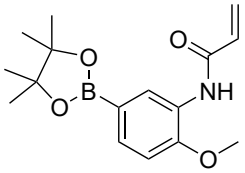

76

Chemical Formula: $C_{16}H_{22}BNO_4$
Exact Mass: 303.16419
Molecular Weight: 303.16500

2-Methoxy-5-(4,4,5,5-tetramethyl-1,3,2-dioxaborolan-2-yl)aniline (**74**, 0.280 g, 1.12 mmol, 1.00 eq.) was subjected to GSP 3. After 1 h another portion of acryloyl chloride (50.0 mg, 42.0 µL, 0.560 mmol, 0.50 eq.) was added and the reaction stirred for 30 min. The described purification procedure by column chromatography (Silica gel, 0 – 70% hexane/EtOAc) afforded the product **76** (0.256 g, 0.841 mmol, 75%) as white powder.

^{1}H NMR (200 MHz, CDCl3) δ 8.83 (s, 1H), 7.81 (s, 1H), 7.52 (dd, J = 8.1, 1.4 Hz, 1H), 6.86 (d, J = 8.2 Hz, 1H), 6.35 (qd, J = 16.8, 5.8 Hz, 2H), 5.72 (dd, J = 9.6, 2.0 Hz, 1H), 3.88 (s, 3H), 1.30 (s, 12H). 13**C NMR** (50 MHz, $CDCl_3$) δ 162.70, 150.36, 131.25, 131.00, 127.05, 126.66, 125.94, 109.03, 83.24, 55.34, 24.60. **TLC-MS:** ESI(+) calcd. for [M+Na]+: *m/z* = 236.2; found: 326.0. **HPLC:** tret = 14.60 min (100% at 254 nm, 94.6 % at 230 nm, method B).

N-(4-Methyl-3-(4,4,5,5-tetramethyl-1,3,2-dioxaborolan-2-yl)phenyl)acrylamide (77)

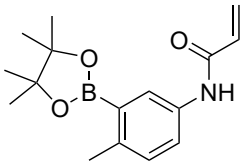

77

Chemical Formula: $C_{16}H_{22}BNO_3$
Exact Mass: 287.16927
Molecular Weight: 287.16600

4-Methyl-3-(4,4,5,5-tetramethyl-1,3,2-dioxaborolan-2-yl)aniline (**75**, 0.500 g, 2.14 mmol, 1.00 eq.) was subjected to GSP 3 and purified by flash column chromatography (0 – 70% hexane/EtOAc) which afforded the product **77** (0.428 g, 1.41 mmol, 66%) as white powder.

^{1}H NMR (200 MHz, $CDCl_3$) δ 7.85 (d, *J* = 7.1 Hz, 1H), 7.64 (s, 1H), 7.45 (s, 1H), 7.14 (d, *J* = 8.3 Hz, 1H), 6.27 (dt, *J* = 16.8, 12.9 Hz, 2H), 5.71 (d, *J* = 9.8 Hz, 1H), 2.49 (s, 3H), 1.33 (s, 12H). **^{13}C NMR** (50 MHz, $CDCl_3$) δ 163.91, 141.06, 134.84, 131.50, 130.44, 127.54, 127.21, 123.17, 83.58, 24.91, 21.53. **TLC-MS:** ESI(+) calcd. for [M+Na]+: *m/z* = 310.2; found: 310.0. **HPLC:** t_{ret} = 9.17 min (96.0 % at 254 nm, 97.5% at 230 nm, method A).

N-(2-methoxy-5-(4,4,5,5-tetramethyl-1,3,2-dioxaborolan-2-yl)phenyl)propionamide (78)

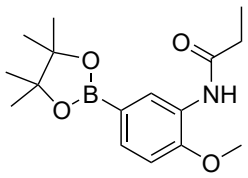

78

Chemical Formula: $C_{16}H_{24}BNO_4$
Exact Mass: 305.17984
Molecular Weight: 305.18100

2-Methoxy-5-(4,4,5,5-tetramethyl-1,3,2-dioxaborolan-2-yl)aniline (**74**, 0.920 g, 3.69 mmol, 1.10 eq) was subjected to GSP 4 which afforded the product **78** (1.10 g, 3.58 mmol, 97%) as an off-white solid.

^{1}H NMR (200 MHz, $CDCl_3$) δ 8.76 (s, 1H), 7.67 (s, 1H), 7.50 (d, *J* = 8.0 Hz, 1H), 6.86 (d, *J* = 8.1 Hz, 1H), 3.89 (s, 3H), 2.42 (q, *J* = 7.5 Hz, 2H), 1.31 (s, 12H), 1.24 (t, *J* = 7.6 Hz, 3H). **^{13}C NMR** (50 MHz, $CDCl_3$) δ 171.67, 150.45, 150.34, 130.86, 127.32, 126.18, 109.19, 83.83, 55.65, 31.07, 25.02, 9.68. **TLC-MS:** ESI(+) calcd. for $[M+Na]^+$: *m/z* = 328.2; found: 327.9. **HPLC:** t_{ret} = 7.68 min (100% at 254 nm, 99.3% at 230 nm, method A).

N-(4-methyl-3-(4,4,5,5-tetramethyl-1,3,2-dioxaborolan-2-yl)phenyl)propionamide (79)

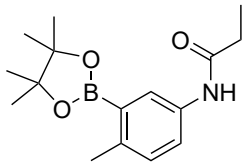

79

Chemical Formula: $C_{16}H_{24}BNO_3$
Exact Mass: 289.18492
Molecular Weight: 289.18200

4-Methyl-3-(4,4,5,5-tetramethyl-1,3,2-dioxaborolan-2-yl)aniline (**75**, 0.499 g, 2,14 mmol, 1.10 eq.) was subjected to GSP 4 which afforded the product **79** (0.370 g, 1.21 mmol, 58%) as beige solid.

^{1}H NMR (200 MHz, $CDCl_3$) δ 7.75 (dd, *J* = 8.3, 2.0 Hz, 1H), 7.60 (s, 1H), 7.51 (s, 1H), 7.10 (d, *J* = 8.2 Hz, 1H), 2.47 (s, 3H), 2.34 (q, *J* = 7.6 Hz, 2H), 1.31 (s, 12H), 1.20 (t, *J* = 7.5 Hz, 3H). **^{13}C NMR** (50 MHz, $CDCl_3$) δ 172.19, 140.72, 135.06, 130.48, 127.09, 122.96, 83.61, 30.64, 24.96, 21.61, 9.82. **TLC-MS:** ESI(+) calcd. for $[M+Na]^+$: *m/z* = 312.2 ; found: 312.0. **HPLC:** t_{ret} = 9.21 min (97,3% at 254 nm, 97.7% at 230 nm, method A).

6-Bromo-2H-benzo[b][1,4]oxazin-3(4H)-one (82)

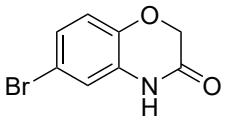

82
Chemical Formula: $C_8H_6BrNO_2$
Exact Mass: 226.95819
Molecular Weight: 228.04500

Following the procedure described by ARMITAGE *et al.*[239], 2-amino-4-bromophenol (**80**, 5.00 g, 26.6 mmol, 1.00 eq.) and $NaHCO_3$ (4.47 g, 53.2 mmol, 2.00 eq.) were suspended in 80 mL THF (dry)(solution A) and cooled to 6 °C. 2-Chloroacetyl chloride (**81**, 3.15 g, 2.22 mL, 27.9 mmol, 1.05 eq.) was dissolved in 10 mL THF and added to solution A over a time period of 20 min, while the inner temperature was kept below 5 °C. The reaction was stirred 20 min before 1.00 mL 2-chloroacetyl chloride (**81**) was added and stirred for 10 min. K_2CO_3 (7.35 g, 53.2 mmol, 2.00 eq.) was added and the mixture refluxed for 2.5 h. After cooling to rt, EtOAc (60 mL) was added and the suspension was stirred for 20 minutes. The precipitate was filtered of and washed with 30 mL EtOAc. The filtrate was concentrated and the resulting pink solid suspended in water (60 mL) and stirred for 1 h. The product was isolated by filtration, washed with water (30 mL) twice and dried to afford a rose-colored powder **82** (4.93 g, 4.93 mmol, 81%).

^{1}H NMR (200 MHz, DMSO) δ 10.81 (s, 1H), 7.11 – 6.99 (m, 2H), 6.91 (d, *J* = 8.5 Hz, 1H), 4.59 (s, 2H). **^{13}C NMR** (50 MHz, DMSO) δ 164.52, 142.66, 128.82, 124.97, 118.09, 117.99, 66.65. **TLC-MS:** ESI(-) calcd. for $[M-H]^-$: *m/z* = 226.0; found: 225.8. **HPLC:** t_{ret} = 6.54 min (99.1 % at 254 nm, 98.8 % at 230 nm, method A).

6-Bromo-3,4-dihydro-2H-benzo[b][1,4]oxazine (83)

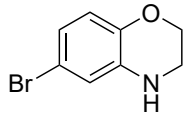

83
Chemical Formula: C_8H_8BrNO
Exact Mass: 212.97893
Molecular Weight: 214.06200

$LiAlH_4$ (2.50 g, 65.8 mmol, 15.0 eq.) was suspended in 20 mL THF (dry) and cooled to 0 °C in an ice bath. A solution of 6-bromo-2*H*-benzo[*b*][1,4]oxazin-3(4*H*)-one (**82**, 1.00 g, 4.39 mmol, 1.00 eq) in 20 mL THF (dry) was added dropwise. The reaction was allowed to warm up to rt and stirred for 18 h. After the reaction was complete it was cooled to 0 °C and quenched by addition of 40 mL of 1N KOH solution. The organic solvent was removed under reduced pressure and water and EtOAc were added. The precipitate was filtered off and the phases separated. The organic layer was dried over Na_2SO_4 and the solvent evaporated. The raw product was purified by flash column chromatography (Silica gel, 0 – 30% hexane/EtOAc) which afforded the product **83** (0.500 g, 2.06 mmol, 47%) as a colorless oil.

^{1}H NMR (200 MHz, $CDCl_3$) δ 6.77 – 6.61 (m, 3H), 4.24 – 4.10 (m, 2H), 3.80 (s, 1H), 3.41 – 3.26 (m, 2H). **^{13}C NMR** (50 MHz, $CDCl_3$) δ 142.93, 135.16, 120.81, 117.96, 117.54, 113.07, 64.90, 40.49. **HPLC:** t_{ret} = 7.05 min (99.3% at 254 nm, 99.3% at 230 nm, method A).

6-(4,4,5,5-Tetramethyl-1,3,2-dioxaborolan-2-yl)-3,4-dihydro-2H-benzo[b][1,4]oxazine (84)

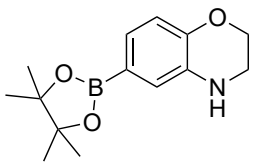

84
Chemical Formula: $C_{14}H_{20}BNO_3$
Exact Mass: 261.15362
Molecular Weight: 261.12800

6-Bromo-3,4-dihydro-2*H*-benzo[*b*][1,4]oxazine (**83**, 0.579 g, 2.69 mmol, 1.00 eq) was dissolved in 1,4-dioxane (8 mL) and subjected to GSP 1. After stirring for 2 h, the work-up was carried out as described and the raw product purified by flash column chromatography (0 – 70% hexane/EtOAc) to afford the product **84** (0.529 g, 2.03 mmol, 76%) as a colorless oil.

^{1}H NMR (200 MHz, $CDCl_3$) δ 7.14 (d, *J* = 7.9 Hz, 1H), 7.06 (s, 1H), 6.78 (d, *J* = 7.9 Hz, 1H), 4.30 – 4.17 (m, 2H), 3.59 (s, 1H), 3.43 – 3.31 (m, 2H), 1.32 (s, 12H). **^{13}C NMR** (50 MHz, $CDCl_3$) δ 147.31, 133.54, 126.31, 122.33, 116.56, 83.79, 65.85, 41.17, 25.15. **TLC-MS:** ESI(+) calcd. for $[M+H]^+$: *m/z* = 262.2; found: 261.9. **HPLC:** t_{ret} = 7.51 min (99.2% at 254 nm, 99.4% at 230 nm, method A).

1-(6-(4,4,5,5-Tetramethyl-1,3,2-dioxaborolan-2-yl)-2,3-dihydro-4H-benzo[b][1,4]oxazin-4-yl)prop-2-en-1-one (85)

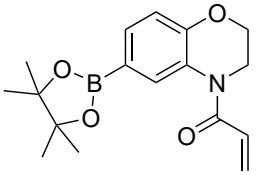

85
Chemical Formula: $C_{17}H_{22}BNO_4$
Exact Mass: 315.16419
Molecular Weight: 315.17600

6-(4,4,5,5-tetramethyl-1,3,2-dioxaborolan-2-yl)-3,4-dihydro-2*H*-benzo[*b*][1,4]oxazine (**84**, 0.165 g, 0.630 mmol, 1.00 eq.) was subjected to GSP 3 and purified by column chromatography (Silica gel, 0 – 70% hexane/EtOAc) to afford the product **85** (0.143 mg, 0.454 mmol, 72%) as a yellow oil.

^{1}H NMR (200 MHz, $CDCl_3$) δ 7.49 (s, 1H), 7.45 (s, 1H), 6.84 (d, *J* = 8.2 Hz, 1H), 6.70 (dd, *J* = 16.8, 10.1 Hz, 1H), 6.44 (dd, *J* = 16.8, 1.9 Hz, 1H), 5.73 (dt, *J* = 16.3, 8.1 Hz, 1H), 4.34 – 4.19 (m, 2H), 3.99 – 3.77 (m, 2H), 1.26 (s, 12H). **^{13}C NMR** (50 MHz, $CDCl_3$) δ 164.04, 149.46, 133.08, 130.91, 129.11, 128.52, 125.20, 120.68, 116.79, 83.68, 67.02, 39.89, 24.77. **TLC-MS:** ESI(+) calcd. for $[M+Na]^+$: *m/z* = 338.2; found: 338.0. **HPLC:** t_{ret} = 8.70 min (92.6% at 254 nm, 82.7% at 230 nm, method A).

1-(6-(4,4,5,5-Tetramethyl-1,3,2-dioxaborolan-2-yl)-2,3-dihydro-4H-benzo[b][1,4]oxazin-4-yl)propan-1-one (86)

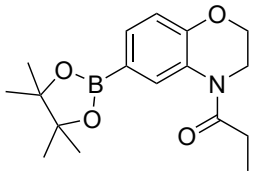

86
Chemical Formula: $C_{17}H_{24}BNO_4$
Exact Mass: 317.17984
Molecular Weight: 317.19200

6-(4,4,5,5-Tetramethyl-1,3,2-dioxaborolan-2-yl)-3,4-dihydro-2*H*-benzo[*b*][1,4]oxazine (**84**, 0.287 g, 1.10 mmol, 1.10 eq.) was subjected to GSP 4 to afford the product **86** (0.196 g, 0.616 mmol, 56%) as yellow oil.

^{1}H NMR (200 MHz, $CDCl_3$) δ 7.65 (s, 1H), 7.51 (d, *J* = 8.1 Hz, 1H), 6.89 (d, *J* = 8.2 Hz, 1H), 4.44 – 4.16 (m, 2H), 4.01 – 3.54 (m, 2H), 2.64 (q, *J* = 7.3 Hz, 2H), 1.32 (s, 12H), 1.18 (t, *J* = 7.3 Hz, 3H). **^{13}C NMR** (50 MHz, $CDCl_3$) δ 172.69, 149.56, 132.85,

130.91, 126.05, 116.75, 83.66, 67.09, 28.61, 27.42, 24.81, 9.63, 8.34. **TLC-MS:** ESI(+) calcd. for $[M+Na]^+$: *m/z* = 340.2; found: 340.0. **HPLC:** t_{ret} = 8.93 min (99.9% at 254 nm, 99.9% at 230 nm, method A).

6.2.3 Synthesis of Compounds described in Section 3.2

5,6,7,8-Tetrahydroquinazoline-2,4-diol (88)

According to the procedure described by ORTEGA et al. [241], urea (37.5 g, 0.625 mol, 5.00 eq.), sodium methanolate (30.4 g, 0.563 mol, 4.50 eq.) and ethyl 2-oxocyclohexanecarboxylate (**87**, 20.0 mL, 21.3 g, 0.125 mol, 1.00 eq.) were dissolved in EtOH (400 mL) and stirred for 16 h at reflux. The solvent was removed under reduced pressure and the residue diluted with water. The pH of the mixture was adjusted to pH 8-9 by addition careful of HCl solution. The suspension was cooled in an ice bath and filtered. The residue was washed with cold methanol (300 mL) and diethyl ether (300 mL) and dried under high vacuum which afforded the product **88** (10.3 g, 61.3 mmol, 49 %) as white powder.

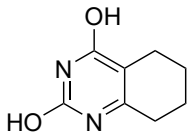

88

Chemical Formula: $C_8H_{10}N_2O_2$
Exact Mass: 166.07423
Molecular Weight: 166.18000

^{1}H NMR (200 MHz, DMSO) δ 10.80 (s, 2H), 2.42 – 2.19 (m, 2H), 2.19 – 1.97 (m, 2H), 1.76 – 1.39 (m, *J* = 4.8 Hz, 4H). **^{13}C NMR** (50 MHz, DMSO) δ 164.40, 150.89, 148.88, 105.72, 25.70, 21.36, 21.04, 20.48. **TLC-MS:** ESI(+) calcd. for $[M+Na]^+$: *m/z* = 189.1; found: 189.1; ESI(-) calcd. for $[M-H]^-$: *m/z* = 165.1; found: 165.0. **HPLC:** t_{ret} = 2.40 min (100% at 254 nm, 100% at 230 nm, method A).

2,4-Dichloro-5,6,7,8-tetrahydroquinazoline (89)

5,6,7,8-Tetrahydroquinazoline-2,4-diol (**88**, 7.10 g, 43.0 mmol, 1.00 eq.) was suspended in phosphorus oxychloride (50 mL) and stirred for 2 h at reflux. After cooling to rt the reaction was quenched by pouring it into ice (200 g) and allowed to warm to rt. The pH of the mixture was neutralized by slow addition of NaOH and a solution of Na_2CO_3. The solution was extracted with EtOAc which afforded the product **89** (7.00g, 34.4 mmol, 80%) as yellow powder.

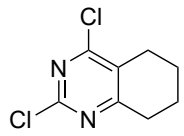

89

Chemical Formula: $C_8H_8Cl_2N_2$
Exact Mass: 202.00645
Molecular Weight: 203.06600

^{1}H NMR (200 MHz, $CDCl_3$) δ 2.77 (s, 2H), 2.62 (s, 2H), 1.79 (dd, *J* = 6.2, 3.1 Hz, 4H). **^{13}C NMR** (50 MHz, $CDCl_3$) δ 171.02, 161.99, 156.45, 127.75, 32.26, 25.16, 21.61, 21.43. **TLC-MS:** ESI(+) calcd. for $[M+H]^+$: *m/z* = 203.0; found: 202.8. **HPLC:** t_{ret} = 7.086 min (97.4% at 254 nm, 99.1% at 230 nm, method A).

2-Chloro-5,6,7,8-tetrahydroquinazoline (90)

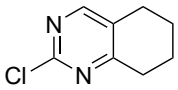

90

Chemical Formula: $C_8H_9ClN_2$
Exact Mass: 168.04543
Molecular Weight: 168.62400

To a mixture of 2,4-dichloro-5,6,7,8-tetrahydroquinazoline (**89**, 3.70 g, 18.2 mmol, 1.00 eq.), zinc dust (8.23 g, 128 mmol, 7.00 eq.) and ammonium chloride (1.27 g, 23.7 mmol, 1.30 eq.) water (40 mL) and acetone (40 mL) were added and the reaction stirred at reflux for 6 h. After cooling to rt, the mixture was filtered through celite and the solvent partially removed under reduced pressure and DCM (50 mL) was added. The pH of the aqueous phase was adjusted to pH 8 by addition of a 2 M NaOH solution. The layers were separated and the aqueous phase extracted with DCM (2x 50 mL). The combined organic layers were dried over Na_2SO_4 and the solvent removed under reduced pressure. The raw product was purified by flash column chromatography (Silica gel, 0 – 60% hexane/EtOAc) which afforded the product **90** (1.90 g, 11.3 mmol, 60%) as an off-white powder.

^{1}H NMR (200 MHz, $CDCl_3$) δ 8.25 (s, 1H), 2.85 (t, *J* = 5.3 Hz, 2H), 2.71 (t, *J* = 5.4 Hz, 2H), 1.85 (dt, *J* = 9.4, 6.0 Hz, 4H). **^{13}C NMR** (50 MHz, $CDCl_3$) δ 169.82, 159.31, 158.37, 128.89, 31.92, 25.09, 21.91, 21.88. **TLC-MS:** ESI(+) calcd. for $[M+H]^+$: *m/z* = 169.0; found: 168.9. **HPLC:** t_{ret} = 9.56 min (93.8% at 254 nm, 98.0% at 230 nm, method B).

2-Chloro-6,7-dihydroquinazolin-8(5H)-one oxime (91)

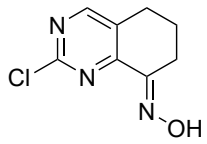

91

Chemical Formula: $C_8H_8ClN_3O$
Exact Mass: 197.03559
Molecular Weight: 197.62200

2-Chloro-5,6,7,8-tetrahydroquinazoline (**90**, 2.00 g, 11.9 mmol, 1.00 eq) was dissolved in THF (dry, 150 mL) under argon and cooled in an N_2/acetone mixture (-78 °C). Potassium *tert*-butoxide (2.66 g, 23.7 mmol, 2.00 eq.) was suspended in THF (dry, 25 mL) and added dropwise under stirring. The mixture was stirred for 15 min and *tert*-butyl nitrite (8.47 mL, 7.34 g, 71.1 mmol, 6.00 eq.) added dropwise while cooling was maintained. The reaction was stirred for 15 min while slowly warming up to rt. After the reaction was completed, the solution was poured into a mixture of water and acetic acid (1.5 mL acetic acid in 1200 mL water) and extracted with EtOAc (5x 300 mL). The combined organic phases were dried over Na_2SO_4 and evaporated to dryness which afforded the product **91** (2.36 g, quant.) as brown solid which was used in the next step without further purification.

^{1}H NMR (200 MHz, $CDCl_3$) δ 14.59 (s, 1H), 8.69 (s, 1H), 2.86 – 2.65 (m, 4H), 2.16 – 1.91 (m, 2H). **^{13}C NMR** (50 MHz, $CDCl_3$) δ 161.92, 156.30, 155.28, 144.94, 129.71, 30.48, 25.57, 21.59. **TLC-MS:** ESI(+) calcd. for $[M+Na]^+$: *m/z* = 220.0; found: 219.9.; ESI(-) calcd. for $[M-H]^-$: *m/z* = 196.0; found: 195.9:. **HPLC:** t_{ret} = 3.25 min (83.0% at 254 nm, 92.1% at 230 nm, method A).

2-Chloro-6,7-dihydroquinazolin-8(5H)-one (92)

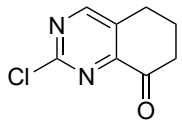

92
Chemical Formula: $C_8H_7ClN_2O$
Exact Mass: 182.02469
Molecular Weight: 182.60700

2-Chloro-6,7-dihydroquinazolin-8(5*H*)-one oxime (**91**, 1.20 g, 6.07 mmol, 1.00 eq.) was dissolved in conc. HCl (14 mL) and water (100 mL) and acetone (24 mL) were added. The mixture was stirred at 80 °C for 30 min. After cooling to rt, the reaction was poured into a solution of Na_2CO_3 (24 g/ 300 mL water) and extracted with EtOAc (3x 200 mL). The combined organic layers were dried over Na_2SO_4 and the solvent removed under reduced pressure. The residue was purified by flash column chromatography (Silica gel, 10 – 100% hexane/EtOAc) which afforded the product **92** (0.278 mg, 1.40 mmol, 23%) as light-yellow solid.
^{1}H NMR (200 MHz, $CDCl_3$) δ 14.59 (s, 1H), 8.69 (s, 1H), 2.86 – 2.65 (m, 4H), 2.16 – 1.91 (m, 2H). **^{13}C NMR** (50 MHz, $CDCl_3$) δ 161.92, 156.30, 155.28, 144.94, 129.71, 30.48, 25.57, 21.59. **TLC-MS:** ESI(+) calcd. for $[M+Na]^+$: *m/z* =195.0; found: 195.0. **HPLC:** t_{ret} = 2.121 min (66.9% at 254 nm (minimum of the UV spectra at 254 nm), 96.6% at 230 nm, method A).

7-Bromo-2-chloro-6,7-dihydroquinazolin-8(5H)-one (93)

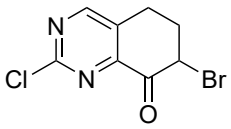

93
Chemical Formula: $C_8H_6BrClN_2O$
Exact Mass: 259.93520
Molecular Weight: 261.50300

In analogous manner to the procedure described in patent literature [16] 2-Chloro-6,7-dihydroquinazolin-8(5*H*)-one (**92**, 1.60 g, 8.76 mmol, 1.00 eq.) was dissolved in conc. HCl (60 mL) and a solution of bromine (0.495 mL, 1.54 g, 9.64 mmol, 1.1 eq.) in conc. HCl (9.5 mL) was added dropwise and the solution stirred at 35 °C for 10 min. The reaction was poured into water (50 mL) and extracted with EtOAc (3x 100 mL). The combined organic layers were dried over Na_2SO_4 and evaporated to dryness which afforded the crude product **93** (2.64 g, quant.) as a brown oil. The crude product was directly used in the next step instability.

tert-Butyl 2-chloro-7-oxo-5,6,7,9,10,11-hexahydro-8H-pyrido[3',4':4,5]pyrrolo[3,2-h]quinazoline-8-carboxylate (94)

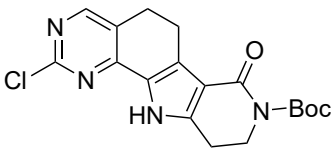

94
Chemical Formula: $C_{18}H_{19}ClN_4O_3$
Exact Mass: 374.11457
Molecular Weight: 374.82500

According to the procedure described in the patent literature [15] 7-Bromo-2-chloro-6,7-dihydroquinazolin-8(5*H*)-one (**93**, 0.510 g, 1.95 mmol, 1.00 eq.), *tert*-butyl 2,4-dioxopiperidine-1-carboxylate (**53**, 0.624 g, 2.93 mmol, 1.5 eq.) and sodium acetate (0.160 g, 1.95 mmol, 1.00 eq.) were dissolved in MeOH (20 mL) and stirred for 10 min. After addition of ammonium acetate (0.301 g, 3.90 mmol, 2.00 eq), the reaction was stirred for 18 h at rt. After the reaction was completed, the solvent was removed under reduced pressure and

the residue purified by flash column chromatography (Silica gel, 0 – 100 % hexane/EtOAc) which afforded the product **94** (0.379 g, 1.01 mmol, 52%) as light-yellow powder.

^{1}H NMR (400 MHz, $CDCl_3$) δ 10.37 (s, 1H), 8.26 (s, 1H), 4.09 (t, *J* = 6.3 Hz, 2H), 3.17 (t, *J* = 7.9 Hz, 2H), 3.00 – 2.87 (m, 4H), 1.55 (s, 9H). **^{13}C NMR** (101 MHz, $CDCl_3$) δ 162.68, 159.06, 156.18, 155.71, 153.47, 142.95, 131.17, 125.90, 124.59, 114.23, 83.06, 44.98, 28.29, 24.44, 23.22, 20.17. **TLC-MS:** ESI(+) calcd. for $[M+Na]^+$: *m/z* = 397.1; found: 397.1.; ESI(-) calcd. for $[M-H]^-$: *m/z* = 373.1; found: 373.2. **HPLC:** t_{ret} = 15.413 min (96.0% at 254 nm, 95.6% at 230 nm, method B).

tert-Butyl 2-(3-acrylamido-4-methoxyphenyl)-7-oxo-5,6,7,9,10,11-hexahydro-8H-pyrido[3',4':4,5]pyrrolo[3,2-h]quinazoline-8-carboxylate (95)

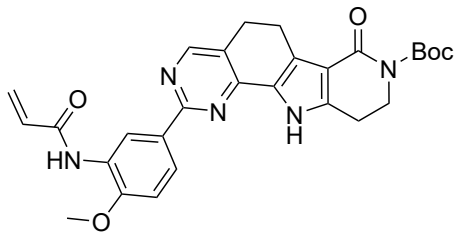

95

Chemical Formula: $C_{28}H_{29}N_5O_5$
Exact Mass: 515.21687
Molecular Weight: 515.57000

tert-Butyl 2-chloro-7-oxo-5,6,7,9,10,11-hexahydro-8*H*-pyrido[3',4':4,5]pyrrolo[3,2-*h*]quinazoline-8-carboxylate (**94**, 0.250 g, 0.667 mmol, 1.00 eq.) and *N*-(2-methoxy-5-(4,4,5,5-tetramethyl-1,3,2-dioxaborolan-2-yl)phenyl)acrylamide (**76**, 0.404 g, 1.33 mmol, 2.00 eq) were subjected to GSP 5. The raw product was purified by flash column chromatography (Silica gel, 0 - 5% DCM/MeOH) which afforded the product **95** (0.189 mg, 0.367 mmol, 55%) as light-yellow solid.

^{1}H NMR (400 MHz, $CDCl_3$) δ 11.65 (s, 1H), 9.36 (s, 1H), 8.23 (s, 1H), 8.09 (s, 1H), 8.03 (dd, *J* = 8.6, 1.9 Hz, 1H), 6.80 (d, *J* = 8.7 Hz, 1H), 6.39 – 6.25 (m, 2H), 5.71 (dd, *J* = 9.6, 1.6 Hz, 1H), 4.00 (t, *J* = 6.1 Hz, 2H), 3.79 (s, 3H), 3.07 (t, *J* = 7.9 Hz, 2H), 2.89 (t, *J* = 6.1 Hz, 2H), 2.83 (t, *J* = 7.9 Hz, 2H), 1.50 (s, 9H). **TLC-MS:** ESI(+) calcd. for $[M+Na]^+$: *m/z* = 538.2; found: 538.2. ESI(-) calcd. for $[M-H]^-$: *m/z* = 514.2; found: 513.7. **HPLC:** t_{ret} = 8.43 min (98.0% at 254 nm, 97.5% at 230 nm, method A).

N-(2-Methoxy-5-(7-oxo-6,7,8,9,10,11-hexahydro-5H-pyrido[3',4':4,5]pyrrolo[3,2-h]quinazolin-2-yl)phenyl)acrylamide (96)

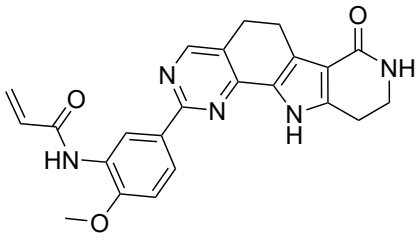

96

Chemical Formula: $C_{23}H_{21}N_5O_3$
Exact Mass: 415.16444
Molecular Weight: 415.45300

tert-Butyl 2-(3-acrylamido-4-methoxyphenyl)-7-oxo-5,6,7,9,10,11-hexahydro-8*H*-pyrido[3',4':4,5]pyrrolo[3,2-*h*]quinazoline-8-carboxylate (**95**, 0.189 g, 0.367 mmol) was dissolved in DCM (5 mL), subjected to GSP 7 and stirred for 30 min. The raw product was dissolved in a DCM/MeOH (5%) mixture (10 mL) and washed with sat, Na_2CO_3 solution (5 mL). the organic layer was dried over Na_2SO_4 and the solvent evaporated. The residue was purified by flash column chromatography (Silica gel, 1 – 10% DCM/MeOH). The isolated product was washed with n-pentane and dried in vacuum which afforded the product **96** (86.5 mg, 0.209 mmol, 57%) as yellow solid.

^{1}H NMR (400 MHz, DMSO) δ 12.06 (s, 1H), 9.50 (s, 1H), 8.94 (s, 1H), 8.45 (s, 1H), 8.30 (dd, *J* = 8.6, 2.1 Hz, 1H), 7.18 (d, *J* = 8.8 Hz, 1H), 7.13 (s, 1H), 6.70 (dd, *J* = 17.0, 10.2 Hz, 1H), 6.26 (dd, *J* = 17.0, 1.9 Hz, 1H), 5.74 (dd, *J* = 10.4, 2.0 Hz, 1H), 3.93 (s, 3H), 3.40 (td, *J* = 6.7, 2.3 Hz, 2H), 2.96 (d, *J* = 6.9 Hz, 2H), 2.88 (dd, *J* = 14.9, 7.4 Hz, 4H). **^{13}C NMR** (101 MHz, DMSO) δ 165.24, 163.33, 161.33, 153.51, 152.30, 140.87, 132.00, 130.06, 126.81, 126.67, 126.51, 125.28, 124.98, 122.78, 112.33, 110.81, 55.89, 24.30, 22.20, 19.86. **HRMS:** ESI(+) calcd. for $[M+H]^+$: *m/z* = 416.17172; found: 416.17211; rel. deviation: 0.95 ppm. **HPLC:** t_{ret} = 5.02 min (100% at 254 nm, 97.8% at 230 nm, method A). **IR** (ATR) [cm^{-1}]: 3338, 3014, 2958, 2890, 2835, 1686, 1617, 1581, 1545, 1507, 1477, 1438, 1395, 1361, 1327, 1289, 1257, 1215, 1179, 1128, 1055, 1026, 966, 950, 917, 890, 838, 798, 782, 712, 671.

6.2.4 Synthesis of Compounds described in Section 3.2.1

tert-Butyl 2-chloro-11-methyl-7-oxo-5,6,7,9,10,11-hexahydro-8H-pyrido[3',4':4,5]pyrrolo[3,2-h]quinazoline-8-carboxylate (97)

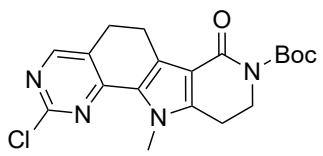

97

Chemical Formula: $C_{19}H_{21}ClN_4O_3$
Exact Mass: 388.13022
Molecular Weight: 388.85200

tert-Butyl 2-chloro-7-oxo-5,6,7,9,10,11-hexahydro-8*H*-pyrido[3',4':4,5]pyrrolo[3,2-*h*]quinazoline-8-carboxylate (**94**, 0.410 g, 1.09 mmol, 1.00 eq.) and Cs_2CO_3 (0.784 g, 2.41 mmol, 2.2 eq.) were dissolved in DMF (dry, 12 mL) under an atmosphere of argon and stirred for 1 h at rt. Then methyl iodide (0.150 mL, 0.342 g, 2.41 mmol, 2.2 eq.) was added and the reaction stirred for 2 h at rt. After the reaction was completed, DCM (50 mL) and water (50 mL) were added and the layers separated. The organic layer was dried over Na_2SO_4 and the solvent removed under reduced pressure. The raw product was purified by flash column chromatography (Silica gel, 30 – 100% hexane/EtOAc) which afforded the product **97** (0.320 g, 0.818 mmol, 75%) as light-yellow powder.

^{1}H NMR (400 MHz, $CDCl_3$) δ 8.19 (s, 1H), 4.10 (t, *J* = 6.3 Hz, 2H), 4.01 (s, 3H), 3.14 (t, *J* = 7.9 Hz, 2H), 2.89 (t, *J* = 6.3 Hz, 2H), 2.84 (t, *J* = 7.9 Hz, 2H), 1.56 (s, 9H). **^{13}C NMR** (101 MHz, $CDCl_3$) δ 162.39, 158.91, 157.39, 155.56, 153.56, 144.31, 131.97, 126.20, 125.03, 112.60, 82.99, 44.47, 33.66, 28.31, 24.82, 22.03, 20.26. **TLC-MS:** ESI(+) calcd. for $[M+Na]^+$: *m/z* = 411.1; found: 411.3; ESI(-) calcd. for $[M-H]^-$: *m/z* = 387.1; found: 387.2. **HPLC:** t_{ret} = 16.55 min (95.9% at 254 nm, 96.3% at 230 nm, method B).

tert-Butyl 2-((tert-butoxycarbonyl)amino)-11-methyl-7-oxo-5,6,7,9,10,11-hexahydro-8H-pyrido[3',4':4,5]pyrrolo[3,2-h]quinazoline-8-carboxylate (98)

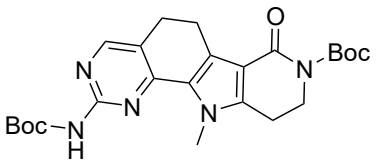

98

Chemical Formula: $C_{24}H_{31}N_5O_5$
Exact Mass: 469.23252
Molecular Weight: 469.54200

A) *tert*-Butyl 2-chloro-11-methyl-7-oxo-5,6,7,9,10,11-hexahydro-8*H*-pyrido[3',4':4,5]pyrrolo[3,2-*h*]quinazoline-8-carboxylate (**97**, 0.100 g, 0.257 mmol, 1.00 eq.) and sodium cyanate (41.8 mg, 0.643 mmol, 2.50 eq.) were dissolved in *t*BuOH (7.0 mL). TEA (42.9 µL, 31.3 mg, 1.20 eq.) was added and the solution degassed with argon. *t*BuXPhos (7.86 mg, 18.5 µmol, 7.2 mol%) and $Pd_2(dba)_3$ (7.06 mg, 7.71 µmol, 3 mol%) were added and the reaction heated to 130 °C under for 18 h. After cooling to rt, the solvent was evaporated and the residue purified by flash column chromatography (Silica gel, 10 – 100% hexane/EtOAc). The purification afforded the product **98** (42.0 mg, 44.7 µmol, 17%) as off-white solid.

TLC-MS: ESI(+) calcd. for $[M+H]^+$: *m/z* = 492.2; found: 492.5. **HPLC:** t_{ret} = 8.658 min (96.9% at 254 nm, 97.9% at 230 nm, method A).

B) *tert*-Butyl 2-chloro-11-methyl-7-oxo-5,6,7,9,10,11-hexahydro-8*H*-pyrido[3',4':4,5]pyrrolo[3,2-*h*]quinazoline-8-carboxylate (**97**, 0.150 g, 0.386 mmol, 1.00 eq.), *tert*-butyl carbamate (90.5 mg, 0.772 mmol, 2.00 eq.) and Cs_2CO_3 (0.377 g, 1.16 mmol, 3.00 eq.) was evacuated and back filled with argon 3 times. XantPhos Pd G4 (18.6 mg, 19.3 µmol, 5 mol%) and XantPhos (11.2 mg, 19.3 µmol, 5 mol%) were added and the flask evacuated and backfilled again. 1,4-dioxane (dry, degassed, 4 mL) was added and the reaction heated to 100 °C for 4 h. After cooling to rt, the mixture was concentrated and the residue diluted with EtOAc (20 mL). The suspension was filtered through a pad of celite and the solvent removed under reduced pressure. The residue was purified by flash column chromatography (Silica gel, 50 – 100% hexane/EtOAc). The product containing fractions were subjected to a second flash chromatography method (Silica gel, 1 – 5% DCM/MeOH) which afforded the product **98** (38 mg, 81.0 µmol, 21%) as off-white solid.

^{1}H NMR (400 MHz, $CDCl_3$) δ 8.21 (s, 1H), 7.45 (s, 1H), 4.13 – 4.05 (m, 5H), 3.11 (t, *J* = 7.8 Hz, 2H), 2.88 (t, *J* = 6.3 Hz, 2H), 2.80 (t, *J* = 7.8 Hz, 2H), 1.57 (s, 9H), 1.53 (s, 9H). **^{13}C NMR** (101 MHz, $CDCl_3$) δ 162.67, 155.96, 155.88, 154.64, 153.80, 150.69, 143.55, 131.04, 126.99, 121.11, 112.35, 82.89, 81.09, 44.60, 33.59, 28.41, 28.36, 24.92, 22.03, 20.67. **TLC-MS:** ESI(+) calcd. for $[M+H]^+$: *m/z* = 492.2; found: 491.9. **HPLC:** t_{ret} = 15.65 min (99.1% at 254 nm, 97.0% at 230 nm, method B).

C) *tert*-Butyl 2-(((benzyloxy)carbonyl)(tert-butoxycarbonyl)amino)-11-methyl-7-oxo-5,6,7,9,10,11-hexahydro-8*H*-pyrido[3',4':4,5]pyrrolo[3,2-*h*]quinazoline-8-carboxylate (**100**, 70.0 mg, 0.135 mmol, 1.00 eq.) was dissolved in MeOH (5.0 mL). Pd on charcoal (10% wt, 7.00 mg, 10% m/m) was added and hydrogen bubbled through the mixture. After stirring for 5 h at rt, the mixture was filtered through a pad of silica. The solvent was removed under reduced pressure which afforded the product **98** (12.0 mg, 25.6 µmol, 19%) as white powder.

^{1}H NMR (400 MHz, $CDCl_3$) δ 8.20 (s, 1H), 7.53 (s, 1H), 4.10 (d, *J* = 4.7 Hz, 5H), 3.11 (t, *J* = 7.8 Hz, 2H), 2.87 (dd, *J* = 13.2, 6.9 Hz, 2H), 2.80 (t, *J* = 7.8 Hz, 2H), 1.57 (s, 9H), 1.53 (s, 9H). **^{13}C NMR** (101 MHz, $CDCl_3$) δ 162.70, 155.96, 155.86, 154.58, 153.79, 150.71, 143.56, 131.05, 126.96, 121.08, 112.31, 82.91, 81.09, 44.59, 33.59, 28.40, 28.34, 24.91, 22.00, 20.59. **TLC-MS:** ESI(+) calcd. for $[M+H]^+$: *m/z* = 492.2; found: 492.4. **HPLC:** t_{ret} = 15.016 min (95.9% at 254 nm, 88.4% at 230 nm, method B).

tert-Butyl 2-(((benzyloxy)carbonyl)amino)-11-methyl-7-oxo-5,6,7,9,10,11-hexahydro-8H-pyrido[3',4':4,5]pyrrolo[3,2-h]quinazoline-8-carboxylate (99)

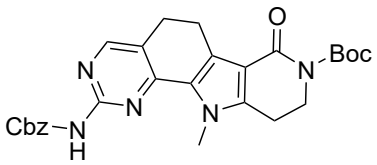

99
Chemical Formula: $C_{27}H_{29}N_5O_5$
Exact Mass: 503.21687
Molecular Weight: 503.55900

tert-Butyl 2-chloro-11-methyl-7-oxo-5,6,7,9,10,11-hexahydro-8*H*-pyrido[3',4':4,5]pyrrolo[3,2-*h*]quinazoline-8-carboxylate (**97**, 0.100 g, 0.257 mmol, 1.00 eq.), benzyl carbamate (0.194 g, 1.29 mmol, 5.00 eq.) and Cs_2CO_3 (0.168 g, 0.514 mmol, 2.00 eq.) were weighed into a Schlenk tube and evaporated and backfilled with argon. XantPhos (22.3 mg, 38.6 µmol, 15 mol%) and $Pd(OAc)_2$ (5.77 mg, 25.7 µmol 10 mol%) were added and 1,4-dioxane (3.0 mL) added. The reaction was heated to 120 °C for 16 h. After cooling to rt, the solvent was removed under reduced pressure. The residue was dissolved in EtOAc and washed with sat. solution of NH_4Cl, water and brine. The organic layer was dried over Na_2SO_4 and the solvent evaporated. The residue was purified by flash column chromatography (Silica gel, 0 – 100% hexane/EtOAc) which afforded the product **99** (60.0 mg, 0.118 mmol, 46%) as white solid.

^{1}H NMR (400 MHz, $CDCl_3$) δ 10.03 (s, 1H), 7.88 (s, 1H), 7.36 – 7.29 (m, 5H), 5.13 (d, *J* = 16.8 Hz, 2H), 4.06 (s, 3H), 4.02 (s, 2H), 2.98 (t, *J* = 7.8 Hz, 2H), 2.79 (t, *J* = 6.2 Hz, 2H), 2.47 (t, *J* = 7.8 Hz, 2H), 1.50 (s, 9H). **^{13}C NMR** (101 MHz, $CDCl_3$) δ 162.69, 155.96, 155.78, 154.13, 153.69, 152.06, 143.75, 135.87, 131.05, 128.84, 128.79, 128.63, 128.20, 126.97, 120.86, 112.22, 82.83, 67.31, 44.55, 33.40, 28.29, 24.66, 21.92, 20.54. **TLC-MS:** ESI(+) calcd. for $[M+H]^+$: *m/z* = 526.2; found: 526.4. **HPLC:** t_{ret} = 16.711 min (100% at 254 nm, 99.4% at 230 nm, method B).

tert-Butyl 2-(((benzyloxy)carbonyl)(tert-butoxycarbonyl)amino)-11-methyl-7-oxo-5,6,7,9,10,11-hexahydro-8H-pyrido[3',4':4,5]pyrrolo[3,2-h]quinazoline-8-carboxylate (100)

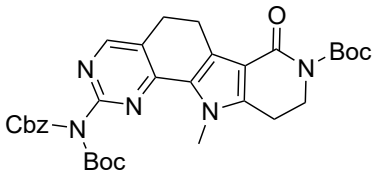

100
Chemical Formula: $C_{32}H_{37}N_5O_7$
Exact Mass: 603.26930
Molecular Weight: 603.67600

tert-Butyl 2-(((benzyloxy)carbonyl)amino)-11-methyl-7-oxo-5,6,7,9,10,11-hexahydro-8*H*-pyrido[3',4':4,5]pyrrolo[3,2-*h*]quinazoline-8-carboxylate (**99**, 0.100 g, 0.199 mmol, 1.00 eq.) and DMAP (4.86 mg, 39.8 µmol, 0.20 eq.) were dissolved in ACN (3.0 mL, dry)(Ar). After the addition of Boc_2O (68.6 µL, 65,1 mg, 0.298 mmol, 1.50 eq.) and TEA (49.9 µL, 36.2 mg, 0.358 mmol, 1.20 eq.), the reaction was stirred at rt for 18 h. After complete

conversion, the mixture was diluted with DCM (20 mL) and water (20 mL). The layers were separated and the organic layer dried over Na_2SO_4. The solvent was evaporated and the residue purified by flash column chromatography (Silica gel, 20 – 100% hexane/EtOAc) which afforded the product **100** (72.0 mg, 0.119 mmol, 60%) as white powder.

^{1}H NMR (400 MHz, $CDCl_3$) δ 8.28 (s, 1H), 7.22 – 7.16 (m, *J* = 7.4 Hz, 5H), 5.16 (s, 2H), 4.01 (t, *J* = 6.2 Hz, 2H), 3.76 (s, 3H), 3.08 (t, *J* = 7.8 Hz, 2H), 2.80 (dt, *J* = 9.5, 7.1 Hz, 4H), 1.49 (s, 9H), 1.36 (s, 9H). **^{13}C NMR** (101 MHz, $CDCl_3$) δ 162.46, 156.64, 155.93, 154.97, 153.53, 152.32, 150.75, 143.73, 135.39, 131.02, 128.41, 128.20, 127.97, 126.45, 125.00, 112.29, 83.73, 82.83, 68.29, 44.44, 33.45, 28.22, 27.88, 24.97, 21.88, 20.18. **TLC-MS:** ESI(+) calcd. for $[M+H]^+$: *m/z* = 626.3; found: 626.5. **HPLC:** t_{ret} = 18.147 min (95.3% at 254 nm, 95.5% at 230 nm, method B).

tert-Butyl 2-((tert-butoxycarbonyl)(6-chloro-3-nitropyridin-2-yl)amino)-11-methyl-7-oxo-5,6,7,9,10,11-hexahydro-8H-pyrido[3',4':4,5]pyrrolo[3,2-h]quinazoline-8-carboxylate (101)

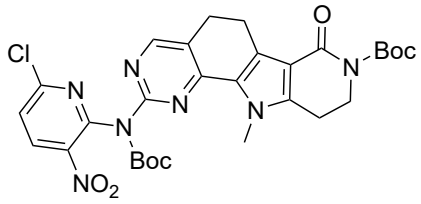

101
Chemical Formula: $C_{29}H_{32}ClN_7O_7$
Exact Mass: 625.20517
Molecular Weight: 626.06700

tert-Butyl 2-((*tert*-butoxycarbonyl)amino)-11-methyl-7-oxo-5,6,7,9,10,11-hexahydro-8*H*-pyrido[3',4':4,5]pyrrolo[3,2-*h*]quinazoline-8-carboxylate (**98**, 37.0 mg, 78.8 µmol, 1.00 eq.) was subjected to GSP 8 and suspended in 1.0 mL of toluene. After stirring at 55 °C for 4 days, the reaction mixture was filtered through a pad of celite and the solvent evaporated, without aqueous work-up. The residue was purified by flash column chromatography (silica gel, 0.5 – 5% DCM/MeOH) which afforded the product **101** (20 mg, 31.9 µmol, 41%) as yellow oil.

^{1}H NMR (400 MHz, $CDCl_3$) δ 8.40 (d, *J* = 8.5 Hz, 1H), 8.22 (s, 1H), 7.40 (d, *J* = 8.4 Hz, 1H), 4.08 (t, *J* = 6.2 Hz, 2H), 3.80 (s, 3H), 3.14 (t, *J* = 7.8 Hz, 2H), 2.84 (dd, *J* = 13.9, 7.1 Hz, 4H), 1.57 (s, 9H), 1.44 (s, 9H). **^{13}C NMR** (101 MHz, $CDCl_3$) δ 162.57, 157.39, 155.98, 154.69, 153.75, 153.69, 150.64, 147.98, 143.63, 136.49, 131.13, 126.86, 123.47, 123.25, 112.47, 84.08, 82.94, 44.54, 33.33, 28.36, 27.96, 24.98, 22.00, 20.42. **TLC-MS:** ESI(+) calcd. for $[M+Na]^+$: *m/z* = 648.2; found: 648.5. **HPLC:** t_{ret} = 18.184 min (97.9% at 254 nm, 97.5% at 230 nm, method B).

2-((6-Chloro-3-nitropyridin-2-yl)amino)-11-methyl-5,6,8,9,10,11-hexahydro-7H-pyrido[3',4':4,5]pyrrolo[3,2-h]quinazolin-7-one (102)

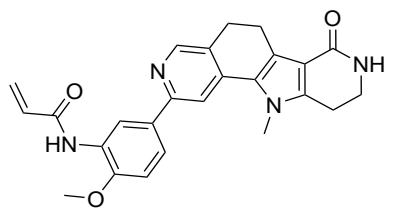

102
Chemical Formula: $C_{19}H_{16}ClN_7O_3$
Exact Mass: 425.10032
Molecular Weight: 425.83300

tert-Butyl 2-((*tert*-butoxycarbonyl)(6-chloro-3-nitropyridin-2-yl)amino)-11-methyl-7-oxo-5,6,7,9,10,11-hexahydro-8*H*-pyrido[3',4':4,5]pyrrolo[3,2-*h*]quinazoline-8-carboxylate (**101**, 19 mg, 30.4 µmol, 1.00 eq.) was subjected to GSP 7 and stirred for 30 min. the residue was dissolved in DCM (5 mL) and washed with a sat. solution of Na_2CO_3. The organic phase was dried over Na_2SO_4 and the solvent evaporated. The crude product was purified by flash column chromatography (Silica gel, 1,5 – 7% MeOH/DCM) and the isolated product washed with n-pentane which afforded the product **102** (4.0 mg, 9.39 µmol, 31%) as orange powder.

^{1}H NMR (400 MHz, DMSO) δ 10.68 (s, 1H), 8.48 (d, *J* = 8.5 Hz, 1H), 8.18 (s, 1H), 7.31 (d, *J* = 8.5 Hz, 1H), 7.14 (s, 1H), 3.95 (s, 3H), 3.40 (td, *J* = 6.8, 2.4 Hz, 2H), 2.92 (t, *J* = 7.7 Hz, 2H), 2.84 (t, *J* = 6.8 Hz, 2H), 2.76 (t, *J* = 7.8 Hz, 2H). **^{13}C NMR** (101 MHz, DMSO) δ 164.83, 155.82, 155.01, 153.95, 152.18, 146.27, 143.08, 137.96, 133.96, 128.60, 124.73, 120.36, 117.40, 111.26, 32.92, 24.24, 20.80, 20.77, 20.01. **HRMS:** ESI(+) calcd. for $[M+H]^+$: *m/z* = 426.10759; found: 426.10722; rel. deviation: 0.88 ppm. **HPLC:** t_{ret} = 13.879 min (97.4% at 254 nm, 97.6% at 230 nm, method B). **IR** (ATR) [cm^{-1}]: 3311, 2975,2918, 2840, 1641, 1577, 1535, 1511, 1491, 1457, 1429, 1380, 1344, 1288, 1241, 1211, 1152, 1060, 1002, 979, 934, 899, 835, 761, 718, 680.

tert-Butyl 2-chloro-7-oxo-11-((2-(trimethylsilyl)ethoxy)methyl)-5,6,7,9,10,11-hexahydro-8H-pyrido[3',4':4,5]pyrrolo[3,2-h]quinazoline-8-carboxylate (104)

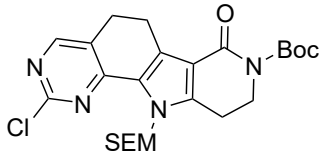

104
Chemical Formula: $C_{24}H_{33}ClN_4O_4Si$
Exact Mass: 504.19596
Molecular Weight: 505.08700

Sodium hydride (60% in mineral oil, 32.0 mg, 0.800 mmol, 1.50 eq.) was added to *tert*-Butyl 2-chloro-7-oxo-5,6,7,9,10,11-hexahydro-8*H*-pyrido[3',4':4,5]pyrrolo[3,2-*h*]quinazoline-8-carboxylate (**94**, 0.200 mg, 0.534 mmol, 1.00 eq.) and suspended in DMF (20 mL). After stirring at rt for 30 min, SEM-Cl was added (0.238 mL, 0.214 mg, 1.07 mmol, 2.00 eq.) and the reaction stirred for 18 h. Water (50 mL) was added to stop the reaction and the mixture extracted with DCM (3x 50 mL). The organic phases were dried over Na_2SO_4 and the solvent removed under reduced pressure. The residue was purified by flash column chromatography (Silica gel, 0 – 70% hexane/EtOAc) which afforded the product **104** (0.138 g, 0.273 mmol, 51%) as yellowish oil.

^{1}H NMR (400 MHz, $CDCl_3$) δ 8.20 (s, 1H), 5.91 (s, 2H), 4.08 (t, *J* = 6.6 Hz, 2H), 3.65 – 3.58 (m, 2H), 3.14 (t, *J* = 7.9 Hz, 2H), 2.98 (t, *J* = 6.3 Hz, 2H), 2.84 (t, *J* = 7.9 Hz, 2H), 1.54 (s, 9H), 0.93 – 0.87 (m, 2H), -0.09 (s, 9H). **^{13}C NMR** (101 MHz, $CDCl_3$) δ 162.37, 158.73, 157.05, 155.77, 153.41, 145.43, 132.17, 125.91, 125.15, 113.69, 83.00, 73.93, 66.22, 44.54, 28.25, 24.62, 22.20, 20.14, 17.94, -1.43.

TLC-MS: ESI(+) calcd. for $[M+Na]^+$: *m/z* = 527.2; found: 527.2. **HPLC:** t_{ret} = 11.212 min (95.4% at 254 nm, 95.6% at 230 nm, method A).

tert-Butyl 2-((tert-butoxycarbonyl)amino)-7-oxo-11-((2-(trimethylsilyl)ethoxy)methyl)-5,6,7,9,10,11-hexahydro-8H-pyrido[3',4':4,5]pyrrolo[3,2-h]quinazoline-8-carboxylate (105)

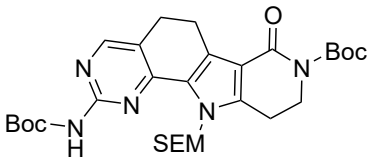

105
Chemical Formula: $C_{29}H_{43}N_5O_6Si$
Exact Mass: 585.29826
Molecular Weight: 585.77700

tert-Butyl 2-chloro-7-oxo-11-((2-(trimethylsilyl)ethoxy)methyl)-5,6,7,9,10,11-hexahydro-8*H*-pyrido[3',4':4,5]pyrrolo[3,2-*h*]quinazoline-8-carboxylate (**104**, 0.120 g, 0.238 mmol, 1.00 eq.), Boc carbamate (55.7 mg, 0.475 mmol, 2.00 eq.) and K_2CO_3 (98.5 mg, 0.713 mmol, 3.00 eq.) were weigh into a Schlenk tube, the tube evaporated and backfilled with argon. A solvent mixture of 1,4-dioxane and *t*BuOH (4:1) (10 mL) was added. After addition of XPhos Pd G4 (2.04 mg, 2.38 µmol, 1 mol%), the reaction was stirred at 90 °C for 18 h. Boc-carbamate (27.8 mg, 0.238 mmol, 1.00 eq.) and XPhos Pd G4 (1.02 mg, 1.19 µmol, 0.5 mol%) were added and the reaction heated to 100 °C for 24 h. After cooling to rt, the mixture was diluted with EtOAc (20 mL) and washed with water (30 mL). The organic layer was dried over Na_2SO_4 and the solvent removed under reduced pressure. The residue was purified by flash column chromatography (Silica gel, 10 – 80% hexane/EtOAc) which afforded the product **105** (50.0 mg, 85.5 µmol, 36%) as off-white solid.
^{1}H NMR (400 MHz, $CDCl_3$) δ 8.77 (s, 1H), 8.24 (s, 1H), 6.19 (s, 2H), 4.08 (dd, *J* = 12.0, 5.8 Hz, 2H), 3.63 – 3.57 (m, 2H), 3.12 (t, *J* = 7.9 Hz, 2H), 2.98 (t, *J* = 6.3 Hz, 2H), 2.80 (t, *J* = 7.9 Hz, 2H), 1.55 (s, 9H), 1.53 (s, 9H), 0.89 – 0.83 (m, 2H), -0.12 (s, 9H). **TLC-MS:** ESI(+) calcd. for $[M+Na]^+$: *m/z* = 608.3; found: 608.6. **HPLC:** t_{ret} = 11.150 min (99.1% at 254 nm, 98.7% at 230 nm, method A).

tert-Butyl 2-((tert-butoxycarbonyl)(6-chloro-3-nitropyridin-2-yl)amino)-7-oxo-11-((2-(trimethylsilyl)ethoxy)methyl)-5,6,7,9,10,11-hexahydro-8H-pyrido[3',4':4,5]pyrrolo[3,2-h]quinazoline-8-carboxylate (106)

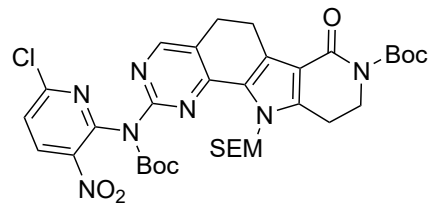

106
Chemical Formula: $C_{34}H_{44}ClN_7O_8Si$
Exact Mass: 741.27092
Molecular Weight: 742.30200

tert-Butyl 2-((tert-butoxycarbonyl)amino)-7-oxo-11-((2-(trimethylsilyl)ethoxy)methyl)-5,6,7,9,10,11-hexahydro-8*H*-pyrido[3',4':4,5]pyrrolo[3,2-*h*]quinazoline-8-carboxylate (**105**, 25.0 mg, 42.7 µmol, 1.00 eq.) was subjected to GSP 8. After stirring at 70 °C for 18 h, 2-bromo-6-chloro-3-nitropyridine (5.07 mg, 21.3 µmol, 0.50 eq.) and XantPhos Pd G4 (2.05 mg, 21.3 µmol, 5 mol%) were added and the stirring continued at 80 °C for 3 h. The reaction was cooled to rt and diluted with EtOAc (10 mL). The mixture was washed with water and a solution of NH_4Cl (10 mL) and the organic layer tried over Na_2SO_4. The solvent was removed under reduced

pressure and the residue purified by flash column chromatography (Silica gel, 10 – 50% hexane/EtOAc) which afforded the product **106** (5.00 mg, 6.74 µmol, 16%) as yellow powder.

^{1}H NMR (400 MHz, $CDCl_3$) δ 8.41 (d, *J* = 8.5 Hz, 1H), 8.22 (s, 1H), 7.41 (d, *J* = 8.5 Hz, 1H), 5.86 (s, 2H), 4.08 (t, *J* = 6.3 Hz, 2H), 3.52 – 3.43 (m, 2H), 3.16 (t, *J* = 7.9 Hz, 2H), 2.97 (t, *J* = 6.3 Hz, 2H), 2.87 (t, *J* = 7.9 Hz, 2H), 1.57 (s, 9H), 1.43 (s, 9H), 0.84 – 0.78 (m, 2H), -0.09 (s, 9H). **TLC-MS:** ESI(+) calcd. for $[M+Na]^+$: *m/z* = 764.3; found: 764.5. **HPLC:** t_{ret} = 11.947 min (83.0% at 254 nm, 84.5% at 230 nm, method A).

6.2.5 Synthesis of Compounds described in Section 3.3.1

2-Chloroisonicotinic acid (112)

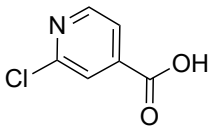

112
Chemical Formula: $C_6H_4ClNO_2$
Exact Mass: 156.99306
Molecular Weight: 157.55300

Pyridine-4-carboxylic acid *N*-oxid (**111**, 14.0 g, 0.100 mol) was suspended on $POCl_3$ (60 mL) and treated according to the procedure described by ANDERSON *et al.* [251]After the mixture was heated to reflux for 7 h and cooled to rt, it was poured into ice water (300 mL) and the precipitate filtered. The solid was recrystallized from EtOAc and dried which afforded the product **112** (8.90 g, 56.0 mmol, 57%) as light-brown solid.

^{1}H NMR (400 MHz, DMSO) δ 13.99 (s, 1H), 8.61 (dd, *J* = 5.0, 0.7 Hz, 1H), 7.90 – 7.74 (m, 2H). **^{13}C NMR** (101 MHz, DMSO) δ 164.84, 151.12, 151.10, 141.76, 123.48, 122.24. **TLC-MS:** ESI(-) calcd. for $[M-H]^-$: *m/z* = 156.0; found: 156.0. **HPLC:** t_{ret} = 5.48 min (96.7% at 254 nm, 96.5% at 230 nm, method B).

2-Chloro-N-methoxy-N-methylisonicotinamide (113)

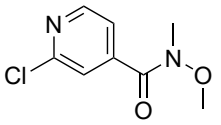

113
Chemical Formula: $C_8H_9ClN_2O_2$
Exact Mass: 200.03526
Molecular Weight: 200.62200

In an analogous manner to the procedure described by ANSIDERI *et al.*, [253] 2-Chloroisonicotinic acid (**112**, 5.50 g, 34.9 mmol, 1.00 eq.) was suspended in $SOCl_2$ (35mL) and heated to reflux for 5 h. After cooling to rt, the excess of reagent was removed under reduced pressure to isolate the crude acidic chloride which was then dissolved in DCM (dry, 10 mL). *N,O*-dimethylhydroxylamine hydrochloride (4.08 g, 41.9 mmol, 1.2 eq.) and NEt_3 (11.6 mL, 8.48 mmol, 2.4 eq.) were dissolved in DCM (dry, 15 mL), cooled in an ice bath and the solution of the acid chloride added dropwise. The reaction was warmed up to rt and stirred for 18 h. The solvent was evaporated and water (150 mL) added to the residue. The solution was extracted with DCM (150 mL) and the organic layer dried over Na_2SO_4. The solution was evaporated to dryness which afforded the product **113** (6.35 g, 31.8 mmol, 91%) as brown solid.

^{1}H NMR (400 MHz, $CDCl_3$) δ 8.46 (d, *J* = 5.1 Hz, 1H), 7.55 (s, 1H), 7.44 (d, *J* = 5.0 Hz, 1H), 3.54 (s, 3H), 3.35 (s, 3H). **^{13}C NMR** (101 MHz, $CDCl_3$) δ 166.22, 151.82, 149.96, 144.71, 123.06, 120.93, 61.70,

33.11. **TLC-MS:** ESI(+) calcd. for $[M+H]^+$: *m/z* =201.0; found: 201.2. **HPLC:** t_{ret} = 7.12 min (99.3% at 254 nm, 96.9% at 230 nm, method B).

1-(2-Chloropyridin-4-yl)ethan-1-one (114)

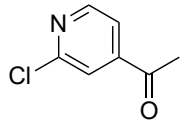

114
Chemical Formula: C_7H_6ClNO
Exact Mass: 155.01379
Molecular Weight: 155.58100

2-Chloro-*N*-methoxy-*N*-methylisonicotinamide (**113**, 5.80 g, 29.0mmol, 1.00 eq.) was dissolved in THF (dry, 90 mL) under an atmosphere of argon and cooled in a cooling bath (ice/NaCl). A solution of MeMgBr (3 M, 14.5 mL, 43.5 mmol, 1.50 eq.) in diethyl ether was added dropwise. After the addition was completed, the reaction was allowed to warm up to rt and stirred for 18 h. The reaction was then quenched by addition of NH_4Cl solution (100 mL) and extracted with EtOAc (3x 150 mL). The combined organic layers were dried over Na_2SO_4 and the solvent evaporated which afforded the product **114** (4.20 g, 27.0 mmol, 93%) as brown oil.

^{1}H NMR (400 MHz, DMSO) δ 8.63 (d, *J* = 5.0 Hz, 1H), 7.91 (s, 1H), 7.81 (d, *J* = 5.1 Hz, 1H), 2.64 (s, 3H). **^{13}C NMR** (101 MHz, DMSO) δ 196.80, 151.41, 151.18, 146.06, 122.41, 120.74, 27.11. **TLC-MS:** ESI(+) calcd. for $[M+H]^+$: *m/z* = 156.0; found: 156.0; ESI(-) calcd. for $[M-H]^-$: *m/z* = 154.0; found: 154.0. **HPLC:** t_{ret} = 7.88 min (93.8% at 254 nm, 97.7% at 230 nm, method B).

2-Bromo-1-(2-chloropyridin-4-yl)ethan-1-one hydrobromide (115·HBr)

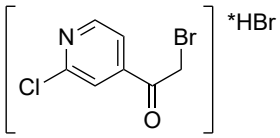

115·HBr
Chemical Formula: $C_7H_5BrClNO$
Exact Mass: 232.92430
Molecular Weight: 315.38900

2-Bromo-1-(2-chloropyridin-4-yl)ethan-1-one·HBr (**115·HBr**) was synthesized according to the procedure described by ANDERSON *et al.* [206]1-(2-Chloropyridin-4-yl)ethan-1-one (**114**, 2.37 g, 15.2 mmol, 1.00 eq.) was dissolved in acetic acid (65 mL) and bromine (0.86 mL, 2.68 g, 16.8 mmol, 1.1 eq.) and hydrobromic acid (30% in acetic acid, 4.10 mL, 15.2 mmol, 1.0 eq) were added. The reaction mixture was stirred at rt for 2 h. Diethyl ether was added to precipitate the product which was then isolated by filtration. The raw product **115·HBr** (3.83 g, 12.2 mmol, 80%, light-yellow powder) was dried in vacuum and used in the next step without further purification. **TLC-MS:** ESI(-) calcd. for $[M-H]^-$: *m/z* = 231.9; found: 232.0.

tert-Butyl 2-(2-chloropyridin-4-yl)-4-oxo-1,4,6,7-tetrahydro-5H-pyrrolo[3,2-c]pyridine-5-carboxylate (116)

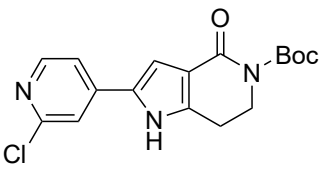

116

Chemical Formula: $C_{17}H_{18}ClN_3O_3$
Exact Mass: 347.10367
Molecular Weight: 347.79900

2-Bromo-1-(2-chloropyridin-4-yl)ethan-1-one hydrobromide (**115·HBr**, 0.925 g, 7.19 mmol, 1.00 eq.), *tert*-butyl 2,4-dioxopiperidine-1-carboxylate (**53**, 1.71 g, 8.02 mmol, 1.10 eq.) and ammonium acetate (2.25 g, 29.2 mmol, 4.00 eq.) were dissolved in EtOH (30 mL, HPLC grade) and stirred at rt for 18 h. Water (40 mL) was added to the reaction and the mixture was stirred for one hour. The precipitate was collected by filtration, washed with water and diethyl ether and dried in vacuum which afforded the product **116** (1.31 g, 3.50 mmol, 48%) as white powder.

^{1}H NMR (400 MHz, DMSO) δ 12.23 (s, 1H), 8.32 (d, *J* = 5.3 Hz, 1H), 7.78 (d, *J* = 1.1 Hz, 1H), 7.67 (dd, *J* = 5.4, 1.6 Hz, 1H), 7.25 (d, *J* = 2.4 Hz, 1H), 3.96 (t, *J* = 6.3 Hz, 2H), 2.95 (t, *J* = 6.3 Hz, 2H), 1.46 (s, 9H). **^{13}C NMR** (101 MHz, DMSO) δ 161.62, 152.94, 151.26, 150.19, 141.92, 141.92, 128.50, 117.31, 117.15, 115.67, 108.83, 81.28, 45.01, 27.77, 22.08. **TLC-MS:** ESI(+) calcd. for $[M+Na]^+$: *m/z* = 370.1; found: 370.4; ESI(-) calcd. for $[M-H]^-$: *m/z* = 346.1; found: 346.3. **HPLC:** t_{ret} = 14.57 min (97.1% at 254 nm, 96.5% at 230 nm, method B).

tert-Butyl 2-(2-(3-acrylamido-4-methoxyphenyl)pyridin-4-yl)-4-oxo-1,4,6,7-tetrahydro-5H-pyrrolo[3,2-c]pyridine-5-carboxylate (117)

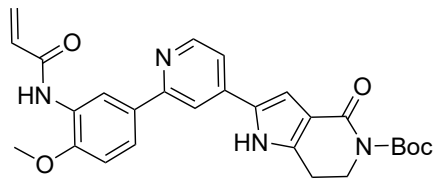

117

Chemical Formula: $C_{27}H_{28}N_4O_5$
Exact Mass: 488.20597
Molecular Weight: 488.54400

tert-Butyl 2-(2-chloropyridin-4-yl)-4-oxo-1,4,6,7-tetrahydro-5*H*-pyrrolo[3,2-*c*]pyridine-5-carboxylate (**116**, 0.200 g, 0.575 mmol, 1.00 eq.) and *N*-(2-methoxy-5-(4,4,5,5-tetramethyl-1,3,2-dioxaborolan-2-yl)phenyl)acrylamide (**76**, 0.262 g, 0.863 mmol, 1.50 eq.) were subjected to GSP 5, but heated at 90 °C for 18 h. The crude product was purified by flash column chromatography (Silica gel, 1 – 8% MeOH) which afforded the product **117** (91.5 mg, 0.190 mmol, 33%) as light-yellow solid.

^{1}H NMR (400 MHz, $CDCl_3$) δ 11.40 (s, 1H), 8.70 (s, 1H), 8.25 (d, *J* = 5.3 Hz, 1H), 7.92 (s, 1H), 7.58 (s, 1H), 7.48 (dd, *J* = 8.5, 1.8 Hz, 1H), 7.19 – 7.04 (m, 1H), 6.90 (d, *J* = 2.1 Hz, 1H), 6.64 (d, *J* = 8.7 Hz, 1H), 6.30 (qd, *J* = 16.8, 5.6 Hz, 2H), 5.75 – 5.63 (m, 1H), 3.97 (t, *J* = 6.2 Hz, 2H), 3.70 (s, 3H), 2.82 (t, *J* = 6.2 Hz, 2H), 1.51 (s, 9H). **^{13}C NMR** (101 MHz, $CDCl_3$) δ 163.68, 163.22, 156.88, 153.42, 149.22, 149.16, 140.93, 139.78, 131.60, 131.27, 130.77, 127.90, 126.90, 123.26, 119.03, 116.45, 116.13, 114.45, 110.03, 107.41, 82.56, 55.79, 45.35, 28.21, 22.59. **TLC-MS:** ESI(+) calcd. for $[M+Na]^+$: *m/z* = 511.2; found: 511.7; ESI(-) calcd. for $[M-H]^-$: *m/z* = 487.2; found: 487.7. **HPLC:** t_{ret} = 14.69 min (99.6% at 254 nm, 99.5% at 230 nm, method B).

N-(2-Methoxy-5-(4-(4-oxo-4,5,6,7-tetrahydro-1H-pyrrolo[3,2-c]pyridin-2-yl)pyridin-2-yl)phenyl)acrylamide (108)

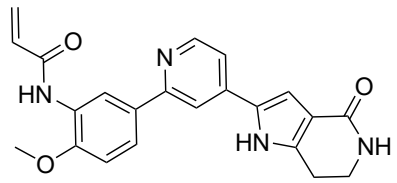

108

Chemical Formula: $C_{22}H_{20}N_4O_3$
Exact Mass: 388.15354
Molecular Weight: 388.42700

tert-Butyl 2-(2-(3-acrylamido-4-methoxyphenyl)pyridin-4-yl)-4-oxo-1,4,6,7-tetrahydro-5*H*-pyrrolo[3,2-*c*]pyridine-5-carboxylate (**117**, 91.5 mg, 0.190 mmol) was dissolved in DCM (20 mL) and subjected to GSP 7. To the residue saturated Na_2CO_3 solution (10 mL) and DCM (10 mL) was added. The precipitate was isolated by filtration which afforded a first fraction of product. In addition, the phases were separated and the aqueous phase extracted with DCM (2x 10 mL). the organic phases were dried over Na_2SO_4 and evaporated to dryness which afforded the product **108** (combined fraction; 34.0 mg, 88.7 µmol, 47%) as beige powder.

^{1}H NMR (400 MHz, DMSO) δ 12.02 (s, 1H), 9.48 (s, 1H), 8.79 (s, 1H), 8.52 (d, *J* = 5.1 Hz, 1H), 8.09 (s, 1H), 7.93 (d, *J* = 8.3 Hz, 1H), 7.52 (d, *J* = 4.7 Hz, 1H), 7.19 (d, *J* = 8.7 Hz, 1H), 7.08 (d, *J* = 26.6 Hz, 2H), 6.72 (dd, *J* = 16.8, 10.3 Hz, 1H), 6.27 (d, *J* = 17.2 Hz, 1H), 5.74 (d, *J* = 10.3 Hz, 1H), 3.92 (s, 3H), 3.42 (d, *J* = 4.9 Hz, 2H), 2.88 (t, *J* = 6.6 Hz, 2H). **^{13}C NMR** (101 MHz, DMSO) δ 164.81, 163.37, 156.31, 151.05, 149.67, 139.75, 138.85, 132.01, 131.09, 128.74, 127.03, 126.62, 123.31, 121.29, 115.81, 115.63, 112.93, 111.11, 106.45, 69.75, 55.88, 21.86. **HRMS:** ESI(+) calcd. for $[M+H]^+$: *m/z* = 389.16082; found: 389.16089; rel. deviation: 0.20 ppm. **HPLC:** t_{ret} = 7.90 min (99.1% at 254 nm, 98.9% at 230 nm, method B). **IR** (ATR) [cm^{-1}]: 3189, 2919, 2850, 1647, 1607, 1534, 1491, 1457, 1411, 1374, 1330, 1255, 1217, 1169, 1128, 1073, 1041, 1021, 990, 962, 877, 810, 772, 737, 701, 670.

tert-Butyl 2-(2-(4-methoxy-3-propionamidophenyl)pyridin-4-yl)-4-oxo-1,4,6,7-tetrahydro-5H-pyrrolo[3,2-c]pyridine-5-carboxylate (118)

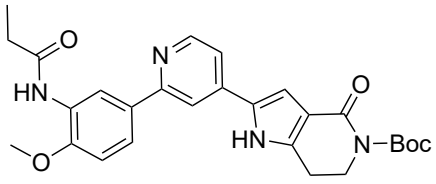

118

Chemical Formula: $C_{27}H_{30}N_4O_5$
Exact Mass: 490.22162
Molecular Weight: 490.56000

tert-Butyl 2-(2-chloropyridin-4-yl)-4-oxo-1,4,6,7-tetrahydro-5*H*-pyrrolo[3,2-*c*]pyridine-5-carboxylate (**116**, 0.150 g, 0.431 mmol, 1.00 eq.) and *N*-(3-(4,4,5,5-tetramethyl-1,3,2-dioxaborolan-2-yl)phenyl)propionamide (**78**, 0.197 g, 0.647 mmol, 1.50 eq.) were subjected to GSP 5 and heated to 90 °C. After 18 h of stirring, an additional portion of *N*-(3-(4,4,5,5-tetramethyl-1,3,2-dioxaborolan-2-yl)phenyl)propionamide (**78**, 65.8 mg, 0.216 mmol, 0.50 eq.) and $(tBu)_3P$ Pd g3 (2.46 mg, 4.30 µmol, 1.00 mol%) were added and the reaction stirred at 100 °C for 24 h. After cooling to rt, the solvent was evaporated and the residue diluted with EtOAc. The mixture washed with NH_4Cl solution, water and brine. The organic layer was dried over Na_2SO_4 and the solvent removed. The residue was purified by flash column chromatography (Silica gel,0 – 10% DCM/MeOH) which afforded the raw product **118**, which was used in the next step without further

purification. **TLC-MS:** ESI(+) calcd. for $[M+Na]^+$: *m/z* = 513.2; found: 513.3; ESI(-) calcd. for $[M-H]^-$: *m/z* = 489.2; found: 489.3. **HPLC:** t_{ret} = 12.59 min (68.9% at 254 nm, 69.3% at 230 nm, method B).

N-(2-methoxy-5-(4-(4-oxo-4,5,6,7-tetrahydro-1H-pyrrolo[3,2-c]pyridin-2-yl)pyridin-2-yl)phenyl)propionamide (109)

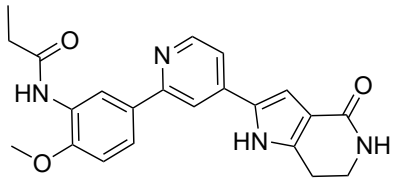

109

Chemical Formula: $C_{22}H_{22}N_4O_3$
Exact Mass: 390.16919
Molecular Weight: 390.44300

The crude product obtained for *tert*-butyl 2-(2-(4-methoxy-3-propionamidophenyl)pyridin-4-yl)-4-oxo-1,4,6,7-tetrahydro-5*H*-pyrrolo[3,2-*c*]pyridine-5-carboxylate (**118**) was dissolved in DCM (5 mL) and subjected to GSP 7 and stirred for 30 min. The residue was dissolved in DCM (10 mL) and washed with sat. Na_2CO_3 solution. The organic layer was dried over Na_2SO_4 and the solvent evaporated. The raw product was purified by flash column chromatography (Silica gel, 0 – 10% DCM/MeOH) which afforded the product **109** (59.0 mg, 0.151 mmol, 35% over 2 steps) as off-white solid.

^{1}H NMR (400 MHz, DMSO) δ 12.00 (s, 1H), 9.12 (s, 1H), 8.70 (s, 1H), 8.51 (d, *J* = 5.3 Hz, 1H), 8.08 (s, 1H), 7.89 (dd, *J* = 8.6, 1.8 Hz, 1H), 7.51 (dd, *J* = 5.3, 1.5 Hz, 1H), 7.15 (d, *J* = 8.7 Hz, 1H), 7.11 (d, *J* = 2.3 Hz, 1H), 7.06 (s, 1H), 3.90 (s, 3H), 3.43 (td, *J* = 6.8, 2.4 Hz, 2H), 2.87 (t, *J* = 6.8 Hz, 2H), 2.42 (q, *J* = 7.4 Hz, 2H), 1.09 (t, *J* = 7.5 Hz, 3H). **^{13}C NMR** (101 MHz, DMSO) δ 172.15, 164.86, 156.42, 150.90, 149.68, 139.76, 138.88, 131.05, 128.77, 127.41, 122.84, 121.19, 115.80, 115.65, 112.94, 111.00, 106.50, 55.84, 29.19, 21.89, 9.76. **HRMS:** ESI(+) calcd. for $[M+H]^+$: *m/z* = 391.17647; found: 391.17671; rel. deviation: 0.61 ppm. **HPLC:** t_{ret} = 6.85 min (98.6% at 254 nm, 94.2% at 230 nm, method B). **IR** (ATR) [cm^{-1}]: 3397, 3232, 3192, 3065, 2932, 2834, 1639, 1607, 1539, 1491, 1464, 1412, 1375, 1327, 1263, 1217, 1168, 1129, 1062, 1020, 990, 808, 767, 733, 703, 656.

6.2.6 Synthesis of Compounds described in Section 3.3.2.1.1

tert-Butyl 2-(2-chloropyridin-4-yl)-1-methyl-4-oxo-1,4,6,7-tetrahydro-5H-pyrrolo[3,2-c]pyridine-5-carboxylate (120)

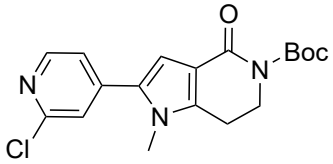

120

Chemical Formula: $C_{18}H_{20}ClN_3O_3$
Exact Mass: 361.11932
Molecular Weight: 361.82600

A) *tert*-Butyl 2-(2-chloropyridin-4-yl)-4-oxo-1,4,6,7-tetrahydro-5*H*-pyrrolo[3,2-*c*]pyridine-5-carboxylate (**116**, 0.450 g, 1.29 mmol, 1.00 eq.) and Cs_2CO_3 (0.927 g, 2.85 mmol, 2.20 eq.) were dissolved in DMF (dry, 20 mL) and stirred at rt for 30 min. After addition of methyl iodide (0.177 mL, 0.404 g, 2.85 mmol, 2.2 eq.) the reaction was stirred at rt for 18 h. The solvent was removed under reduced pressure and the residue dissolved in EtOAc (50 mL). The mixture was washed with sat. NH_4Cl solution, water and brine (50 mL) and the organic layer dried over Na_2SO_4. The solvent was evaporated and the crude product purified by flash column chromatography

(Silica gel, 0 – 100% hexane/EtOAc) which afforded the product **120** (0.290 g, 0,801 mmol, 62%) as white powder.

^{1}H NMR (400 MHz, DMSO) δ 8.42 (d, *J* = 5.2 Hz, 1H), 7.64 (d, *J* = 1.0 Hz, 1H), 7.55 (dd, *J* = 5.2, 1.6 Hz, 1H), 6.88 (s, 1H), 3.98 (t, *J* = 6.3 Hz, 2H), 3.65 (s, 3H), 2.97 (t, *J* = 6.3 Hz, 2H), 1.47 (s, 9H). **^{13}C NMR** (101 MHz, DMSO) δ 161.36, 152.92, 150.92, 150.04, 142.89, 142.24, 131.41, 121.68, 121.26, 114.24, 109.91, 81.31, 44.63, 32.65, 27.78, 21.53. **TLC-MS:** ESI(+) calcd. for $[M+Na]^+$: *m/z* = 384.1; found: 384.2. **HPLC:** t_{ret} = 14.09 min (97.0% at 254 nm, 96.9% at 230 nm, method B).

B) An alternative approach for the synthesis of **120** is described in section 6.2.8

tert-Butyl 2-(2-(((benzyloxy)carbonyl)amino)pyridin-4-yl)-1-methyl-4-oxo-1,4,6,7-tetrahydro-5H-pyrrolo[3,2-c]pyridine-5-carboxylate (125)

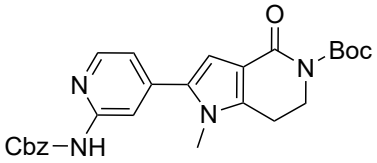

125

Chemical Formula: $C_{26}H_{28}N_4O_5$
Exact Mass: 476.20597
Molecular Weight: 476.53300

tert-Butyl 2-(2-chloropyridin-4-yl)-1-methyl-4-oxo-1,4,6,7-tetrahydro-5*H*-pyrrolo[3,2-*c*]pyridine-5-carboxylate (**120**, 0.100 g, 0.276 mmol, 1.00 eq.), benzyl carbamate (0.209 g, 1.38 mmol, 5.00 eq.) and Cs_2CO_3 (76.4 mg, 0.553 mmol, 2.00 eq.) were dissolved in 1,4-dioxane (3.0 mL, dry, degassed). After adding XantPhos (24.0 mg, 41.5 µmol, 15 mol%) and $Pd(OAc)_2$ (6.21 mg, 27.6 µmol, 10 mol%), the reaction was heated to 120 °C for 18 h. The mixture was allowed to cool to rt and the solvent removed under reduced pressure. The residue was dissolved in DCM and washed with a solution of NH_4Cl and water. The organic layer was dried over Na_2SO_4 and the solvent evaporated. The residue was purified by flash column chromatography (Silica gel, 0 – 100% hexane/EtOAc) which afforded the product **125** (73.0 mg, 0,155 mmol, 56%) as white solid.

^{1}H NMR (400 MHz, $CDCl_3$) δ 10.57 (s, 1H), 8.02 (d, *J* = 5.4 Hz, 2H), 7.31 (ddd, *J* = 7.4, 3.9, 1.5 Hz, 5H), 6.75 (s, 1H), 6.73 (dd, *J* = 5.3, 1.4 Hz, 1H), 5.15 (s, 2H), 4.05 (t, *J* = 6.2 Hz, 2H), 3.56 (s, 3H), 2.81 (t, *J* = 6.3 Hz, 2H), 1.49 (s, 9H).**^{13}C NMR** (101 MHz, $CDCl_3$) δ 162.35, 153.68, 153.64, 152.68, 147.98, 141.83, 141.27, 135.78, 133.67, 128.72, 128.60, 117.45, 115.44, 110.53, 109.84, 82.58, 67.34, 44.74, 32.72, 28.24, 22.28. **TLC-MS:** ESI(+) calcd. for $[M+H]^+$: *m/z* = 499.2; found: 499.2. **HPLC:** t_{ret} = 16.486 min (97.8% at 254 nm, 97.8% at 230 nm, method B).

tert-Butyl 2-(2-aminopyridin-4-yl)-1-methyl-4-oxo-1,4,6,7-tetrahydro-5H-pyrrolo[3,2-c]pyridine-5-carboxylate (126)

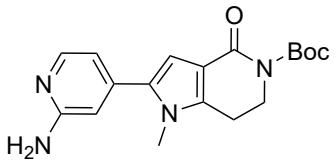

126
Chemical Formula: $C_{18}H_{22}N_4O_3$
Exact Mass: 342.16919
Molecular Weight: 342.39900

tert-Butyl 2-(2-(((benzyloxy)carbonyl)amino)pyridin-4-yl)-1-methyl-4-oxo-1,4,6,7-tetrahydro-5*H*-pyrrolo[3,2-*c*]pyridine-5-carboxylate (**125**, 0.173 g, 0.363 mmol, 1.00 eq.) was suspended in MeOH (15 mL, HPLC grade). Pd/C (10%wt ,17.3 mg, 10% m/m) was added and the H_2 bubbled through the mixture. The reaction was stirred for 18 h under H_2 atmosphere. After complete conversion, the suspension was filtered and the solvent removed under reduced pressure which afforded the product **126** (0.111 g, 0.322 mmol, 90%) as white powder.

^{1}H NMR (400 MHz, DMSO) δ 7.93 (d, *J* = 5.3 Hz, 1H), 6.58 (dd, *J* = 5.3, 1.3 Hz, 1H), 6.53 (s, 1H), 6.50 (s, 1H), 5.99 (s, 2H), 3.97 (t, *J* = 6.3 Hz, 2H), 3.57 (s, 3H), 2.94 (t, *J* = 6.3 Hz, 2H), 1.46 (s, 9H). **^{1}H NMR** (400 MHz, $CDCl_3$) δ 8.03 (d, *J* = 5.3 Hz, 1H), 6.69 (s, 1H), 6.60 (d, *J* = 5.3 Hz, 1H), 6.51 (s, 1H), 4.78 (s, 2H), 4.10 (t, *J* = 6.3 Hz, 2H), 3.56 (s, 3H), 2.86 (t, *J* = 6.3 Hz, 2H), 1.54 (s, 9H).**^{13}C NMR** (101 MHz, $CDCl_3$) δ 162.58, 158.86, 153.66, 147.87, 141.36, 140.76, 134.17, 115.26, 113.31, 109.00, 107.49, 82.68, 44.85, 32.52, 28.27, 22.27. **TLC-MS:** ESI(+) calcd. for $[M+H]^+$: *m/z* = 343.2; found:343.5. **HPLC:** t_{ret} = 7.423 min (95.7% at 254 nm, 93.4% at 230 nm, method B).

tert-Butyl 2-(2-((tert-butoxycarbonyl)amino)pyridin-4-yl)-1-methyl-4-oxo-1,4,6,7-tetrahydro-5H-pyrrolo[3,2-c]pyridine-5-carboxylate (119)

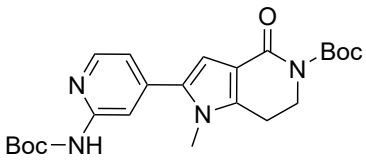

119
Chemical Formula: $C_{23}H_{30}N_4O_5$
Exact Mass: 442.22162
Molecular Weight: 442.51600

A) *tert*-Butyl 2-(2-aminopyridin-4-yl)-1-methyl-4-oxo-1,4,6,7-tetrahydro-5*H*-pyrrolo[3,2-*c*]pyridine-5-carboxylate (**126**, 15.0 mg, 43.8 µmol, 1.00 eq.) and Boc_2O (14.3 mg, 65.7 µmol, 1.50 eq.) was dissolved in *tert*-butanol (2 mL) at stirred at rt. After stirring for 18 h, the solvent was evaporated and the residue purified by flash column chromatography (Silica gel, 0 – 5% DCM/MeOH) which afforded the product **119** (16.5 mg, 34.1 µmol, 87%) as white solid.

^{1}H NMR (400 MHz, $CDCl_3$) δ 8.85 (s, 1H), 8.23 (d, *J* = 5.2 Hz, 1H), 8.00 (s, 1H), 6.91 (dd, *J* = 5.2, 1.0 Hz, 1H), 6.78 (s, 1H), 4.07 (t, *J* = 6.3 Hz, 2H), 3.60 (s, 3H), 2.83 (t, *J* = 6.3 Hz, 2H), 1.50 (s, 9H), 1.47 (s, 9H).**^{13}C NMR** (101 MHz, $CDCl_3$) δ 162.44, 153.78, 152.73, 152.72, 147.79, 141.89, 141.17, 133.88, 117.43, 115.49, 110.87, 109.87, 82.68, 81.25, 44.83, 32.81, 28.44, 28.31, 22.35. **TLC-MS:** ESI(+) calcd. for $[M+Na]^+$: *m/z* = 465.2; found: 465.7. **HPLC:** t_{ret} = 15.897 min (85.6% at 254 nm, 69.7% at 230 nm, method B).

B) *tert*-Butyl 2-(2-(((benzyloxy)carbonyl)(*tert*-butoxycarbonyl)amino)pyridin-4-yl)-1-methyl-4-oxo-1,4,6,7-tetrahydro-5*H*-pyrrolo[3,2-*c*]pyridine-5-carboxylate (**127**, 0.113 g, 0.195 mmol, 1.00 eq.) was dissolved in MeOH (3.0 mL, HPLC-grade). Palladium on charcoal (10% wt, 11.3 mg, 10% m/m) was

added and H_2 bubbled through the mixture. After stirring for 2 h at rt under H_2 atmosphere, the mixture was filtered through a pad of silica gel. The filtrate was collected and the solvent evaporated which afforded the product **119** (53.0 mg, 0.125 mmol, 61%) as yellowish solid.

^{1}H NMR (400 MHz, $CDCl_3$) δ 9.23 (s, 1H), 8.31 (d, *J* = 5.2 Hz, 1H), 8.07 (s, 1H), 6.97 (d, *J* = 4.5 Hz, 1H), 6.83 (s, 1H), 4.12 (t, *J* = 6.2 Hz, 2H), 3.65 (s, 3H), 2.88 (t, *J* = 6.2 Hz, 2H), 1.55 (s, 9H), 1.53 (s, 9H). **^{13}C NMR** (101 MHz, $CDCl_3$) δ 162.42, 153.78, 152.90, 152.80, 147.97, 141.78, 141.09, 133.92, 117.35, 115.45, 110.89, 109.75, 82.63, 81.14, 44.82, 32.78, 28.45, 28.29, 22.33. **TLC-MS:** ESI(+) calcd. for $[M+Na]^+$: *m/z* = 465.2; found: 465.4. **HPLC:** t_{ret} = 15.808 min (97.7% at 254 nm, 97.5% at 230 nm, method B).

C) A flask containing *tert*-Butyl 2-(2-bromopyridin-4-yl)-1-methyl-4-oxo-1,4,6,7-tetrahydro-5*H*-pyrrolo[3,2-*c*]pyridine-5-carboxylate (**121**, 0.500 g, 1.23 mmol, 1.00 eq.), *tert*-butyl carbamate (0.288 g, 2.46 mmol, 2.00 eq.) and Cs_2CO_3 (1.20 g, 3.69 mmol, 3.00 eq.) was evacuated and back filled with argon 3 times. XantPhos Pd g4 (59.2 mg, 61.5 µmol, 5 mol%) and XantPhos (35.6 mg, 61.5 µmol, 5 mol%) were added and the flask evacuated and backfilled again. 1,4-dioxane (dry, degassed, 10 mL) was added and the reaction heated to 85 °C for 6 h. After cooling to rt the mixture was concentrated and the residue diluted with EtOAc (25 mL). The suspension was filtered through celite and the solvent removed under reduced pressure. The residue was purified by flash column chromatography (Silica gel, 30 – 100% hexane/EtOAc). The product containing fractions were subjected to a second flash chromatography method (Silica gel, 1 – 5% DCM/MeOH) which afforded the product **119** (0.279 g, 0.628 mmol, 51%) as white solid.

^{1}H NMR (400 MHz, $CDCl_3$) δ 8.52 (s, 1H), 8.29 (s, 1H), 8.04 (s, 1H), 6.97 (d, *J* = 4.2 Hz, 1H), 6.83 (s, 1H), 4.13 (t, *J* = 6.0 Hz, 2H), 3.65 (s, 3H), 2.88 (t, *J* = 6.1 Hz, 2H), 1.56 (s, 9H), 1.53 (s, 9H). **^{13}C NMR** (101 MHz, $CDCl_3$) δ 162.69, 154.04, 153.40, 153.19, 148.43, 141.98, 141.31, 134.27, 117.58, 115.71, 111.27, 109.93, 82.86, 81.31, 45.12, 33.02, 28.76, 28.57, 22.61. **TLC-MS:** ESI(+) calcd. for $[M+Na]^+$: *m/z* = 465.2; found: 465.2. **HPLC:** t_{ret} = 16.19 min (98.6% at 254 nm, 97.8% at 230 nm, method B).

D) Alternative synthetic method based on a SUZUKI coupling procedure is described in section 6.2.8.

tert-Butyl 2-(2-(((benzyloxy)carbonyl)(tert-butoxycarbonyl)amino)pyridin-4-yl)-1-methyl-4-oxo-1,4,6,7-tetrahydro-5H-pyrrolo[3,2-c]pyridine-5-carboxylate (127)

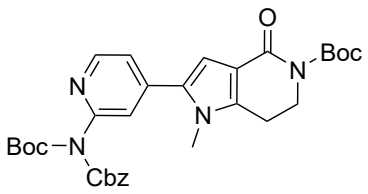

127

Chemical Formula: $C_{31}H_{36}N_4O_7$
Exact Mass: 576.25840
Molecular Weight: 576.65000

tert-Butyl 2-(2-(((benzyloxy)carbonyl)amino)pyridin-4-yl)-1-methyl-4-oxo-1,4,6,7-tetrahydro-5*H*-pyrrolo[3,2-*c*]pyridine-5-carboxylate (**125**, 0.100 g, 0.210 mmol, 1.00 eq.) and DMAP (5.1 mg, 42.0 µmol, 0.20 eq.) were dissolved in ACN (3.0 mL, dry) under an atmosphere of argon. Boc_2O (72.3 µL, 68.7 mg, 0.315 mmol, 1.50 eq.) and TEA (52.7 µL, 38.3 mg, 0.378 mmol, 1.20 eq.) were added and the rection stirred for 18 h. The reaction was diluted with DCM (20 mL) and water (20 mL) and the layers separated. The organic phase was dried over Na_2SO_4 and the solvent evaporated. The residue was

purified by flash column chromatography (Silica gel, 20 – 100% hexane/EtOAc) which afforded the product **127** (0.113 g, 0.195 mmol, 93%) as light-yellow solid. **^{1}H NMR** (400 MHz, $CDCl_3$) δ 8.45 (d, *J* = 5.1 Hz, 1H), 7.28 – 7.16 (m, 7H), 6.76 (s, 1H), 5.18 (s, 2H), 4.17 – 3.98 (m, 2H), 3.46 (s, 3H), 2.84 (t, *J* = 6.3 Hz, 2H), 1.51 (s, 9H), 1.37 (s, 9H).**^{13}C NMR** (101 MHz, $CDCl_3$) δ 162.22, 153.57, 152.41, 152.18, 150.81, 149.23, 141.73, 141.27, 135.19, 132.72, 128.54, 128.39, 128.02, 121.52, 120.50, 115.62, 109.98, 83.95, 82.67, 68.51, 44.70, 32.40, 28.21, 27.85, 22.21. **TLC-MS:** ESI(+) calcd. for $[M+Na]^+$: *m/z* = 599.3; found: 599.4. **HPLC:** t_{ret} = 17.059 min (94.8% at 254 nm, 94.3% at 230 nm, method B).

2-Bromo-N-methoxy-N-methylisonicotinamide (129)

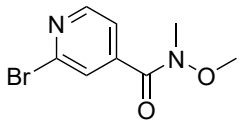

129
Chemical Formula: $C_8H_9BrN_2O_2$
Exact Mass: 243.98474
Molecular Weight: 245.07600

2-Bromoisonicotinic acid (**128**, 13.0 g, 64.4 mmol, 1.00 eq.) was treated according to the procedure described in patent literature.[256] The acid was dissolved in DCM (dry, 120 mL) and 1,1′-carbonyldiimidazole (11.5 g, 70.8 mmol, 1.10 eq.) was added. The reaction was stirred at rt for 2 h. N,O-dimethylhydroxylamine hydrochloride (9.41 g, 96.5 mmol, 1.50 eq.) was added and the reaction stirred for 18 h. The reaction was quenched with 0.1 N NaOH solution (60 mL) and diluted with water (60 mL). The layers were separated and the aqueous layer extracted with DCM (2x 125 mL). The combined organic layers were dried over Na_2SO_4 and evaporated to dryness which afforded the product **129** (15.1 g, 61.8 mmol, 96%) as colorless oil. **^{1}H NMR** (400 MHz, $CDCl_3$) δ 8.44 (d, J = 5.0 Hz, 1H), 7.71 (s, 1H), 7.47 (dd, J = 5.0, 1.3 Hz, 1H), 3.55 (s, 3H), 3.36 (s, 3H). **^{13}C NMR** (101 MHz, $CDCl_3$) δ 166.09, 150.34, 144.40, 142.34, 126.72, 121.22, 61.67, 33.20. **HPLC:** t_{ret} = 7.83 min (98.5% at 254 nm, 96.2% at 230 nm, method B).

1-(2-Bromopyridin-4-yl)ethan-1-one (130)

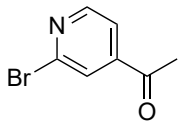

130
Chemical Formula: C_7H_6BrNO
Exact Mass: 198.96328
Molecular Weight: 200.03500

1-(2-Bromopyridin-4-yl)ethan-1-one **130** was synthesized in a similar manner as described in literature[256], therefore 2-Bromo-*N*-methoxy-*N*-methylisonicotinamide (**129**, 5.00 g, 20.4 mmol, 1.00 eq.) was dissolved in THF (dry, 30 mL) under an argon atmosphere and stirred for 15 min at 0 °C. Methyl magnesium bromide (3 M solution in diethyl ether, 8.16 mL, 24.5 mmol, 1.20 eq.) was added slowly and stirred for 2 h at 0 °C. After complete conversion the reaction was quenched by the addition of sat. NH_4Cl solution (30 mL) and extracted with EtOAc (2x 50 mL). The combined organic layers were washed with brine (50 mL) and dried over Na_2SO_4. The solvent was evaporated and the residue purified by flash column chromatography (Silica gel, 10 – 70 % hexane/EtOAc) which afforded the product **130** (3.59 g, 18.0 mmol, 88%) as white crystals.

^{1}H NMR (400 MHz, $CDCl_3$) δ 8.48 (dd, J = 5.1, 0.6 Hz, 1H), 7.84 (dd, J = 1.4, 0.7 Hz, 1H), 7.63 (dd, J = 5.1, 1.5 Hz, 1H), 2.56 (s, 3H). **^{1}H NMR** (400 MHz, DMSO) δ 8.60 (dd, J = 5.0, 0.6 Hz, 1H), 8.03 –

8.01 (m, 1H), 7.83 (dd, J = 5.0, 1.4 Hz, 1H), 2.62 (s, 3H). **^{13}C NMR** (101 MHz, DMSO) δ 196.92, 151.80, 145.76, 142.45, 126.12, 121.11, 27.20. **HPLC:** t_{ret} = 8.63 min (95.2% at 254 nm, 95.3% at 230 nm, method B).

2-Bromo-1-(2-bromopyridin-4-yl)ethan-1-one hydrobromide (131·HBr)

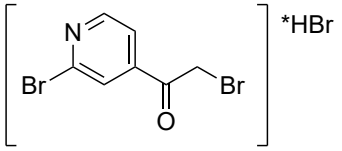

131
Chemical Formula: $C_7H_5Br_2NO$
Exact Mass: 276.87379
Molecular Weight: 359.84300

The synthesis was performed in a similar manner as described by HAY *et al.* [257]. 1-(2-Bromopyridin-4-yl)ethan-1-one (**130**, 6.02 g, 30.1 mmol, 1.00 eq.) was dissolved in acetic acid (10 mL) and 30% HBr/HOAc (50 mL) was added and the solution cooled to 15 °C. Bromine (1.55 mL, 3.38 g, 30.1 mmol, 1.00 eq.) was added in two portions and the reaction was stirred at 20 °C for 1 h. After heating the reaction to 40 °C for 1 h it was cooled to rt and diluted with Et_2O (30 mL). The suspension was cooled to 0°C and stirred for 30 min. The precipitate was isolated by filtration and dried in vacuum which afforded the product **131·HBr** (10.6 g, 29.5 mmol, 98%) as light-yellow powder.
HPLC: t_{ret} = 11.52 min (98.9% at 254 nm, 97.0% at 230 nm, method B).

tert-Butyl 2-(2-bromopyridin-4-yl)-4-oxo-1,4,6,7-tetrahydro-5H-pyrrolo[3,2-c]pyridine-5-carboxylate (132)

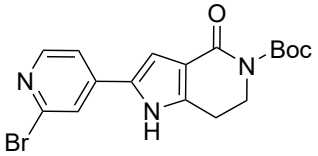

132
Chemical Formula: $C_{18}H_{19}BrN_2O_3$
Exact Mass: 390.05791
Molecular Weight: 391.26500

2-Bromo-1-(2-bromopyridin-4-yl)ethan-1-one hydrobromide (**131·HBr**, 10.6 g, 29.5 mmol, 1.00 eq.), *tert*-butyl 2,4-dioxopiperidine-1-carboxylate (**53**, 6.60 g, 30.9 mmol, 1.05 eq.) and ammonium acetate (9.10 g, 117.8 mmol, 4.00 eq.) were dissolved in EtOH (90 mL) and stirred at rt for 18 h. Water (50 mL) was added to the reaction and the product collected by filtration. Drying the solid in vacuum afforded the product **132** (6.26 g, 16.8 mmol, 57%) as white powder.

^{1}H NMR (400 MHz, DMSO) δ 12.23 (s, 1H), 8.29 (d, *J* = 5.3 Hz, 1H), 7.91 (d, *J* = 0.8 Hz, 1H), 7.69 (dd, *J* = 5.3, 1.4 Hz, 1H), 7.25 (d, *J* = 2.3 Hz, 1H), 3.97 (t, *J* = 6.3 Hz, 2H), 2.94 (t, *J* = 6.3 Hz, 2H), 1.46 (s, 9H). **^{13}C NMR** (101 MHz, DMSO) δ 161.68, 152.99, 150.66, 142.47, 142.02, 141.65, 128.38, 120.97, 117.51, 115.71, 108.90, 81.35, 45.05, 27.81, 22.11. **TLC-MS:** ESI(+) calcd. for $[M+Na]^+$: *m/z* = 414.1; found: 414.5; ESI(-) calcd. for $[M-H]^-$: *m/z* = 390.1; found: 390.5. **HPLC:** t_{ret} = 15.18 min (98.9% at 254 nm, 99.5% at 230 nm, method B).

tert-Butyl 2-(2-bromopyridin-4-yl)-1-methyl-4-oxo-1,4,6,7-tetrahydro-5H-pyrrolo[3,2-c]pyridine-5-carboxylate (121)

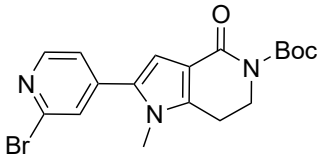

121
Chemical Formula: $C_{19}H_{21}BrN_2O_3$
Exact Mass: 404.07356
Molecular Weight: 405.29200

tert-Butyl 2-(2-bromopyridin-4-yl)-4-oxo-1,4,6,7-tetrahydro-5*H*-pyrrolo[3,2-*c*]pyridine-5-carboxylate (**132**, 2.50 g, 6.37 mmol, 1.00 eq.) and Cs_2CO_3 (4.57 g, 14.0 mmol, 2.20 eq.) were dissolved in DMF (dry, 80 mL) under an argon atmosphere. And stirred at rt for 30 min. After addition of methyl iodide (0.992 mL, 2.26 g, 15.9 mmol, 2.5 eq.), the reaction was stirred at rt for 2 h. Sat. NH_4Cl solution (80 mL) was added to terminate the reaction and the precipitate was isolated by filtration to collect a first portion of crude product. The filtrate was extracted with EtOAc (2x 100 mL) and the organic layers dried over Na_2SO_4. The solvent was evaporated to isolate a second portion of crude product. The two portions of product were combined and purified by flash column chromatography (Silica gel, 0 – 6% DCM/MeOH) which afforded the product **121** (2.36 g, 14.5 mmol, 91%) as light-yellow solid.

^{1}H NMR (400 MHz, $CDCl_3$) δ 8.36 (d, *J* = 5.1 Hz, 1H), 7.46 (s, 1H), 7.24 (d, *J* = 4.8 Hz, 1H), 6.82 (s, 1H), 4.12 (t, *J* = 6.2 Hz, 2H), 3.61 (s, 3H), 2.89 (t, *J* = 6.2 Hz, 2H), 1.54 (s, 9H). **^{13}C NMR** (101 MHz, $CDCl_3$) δ 162.14, 153.60, 150.38, 142.81, 142.20, 141.66, 131.96, 126.17, 121.45, 115.90, 110.70, 82.83, 44.71, 32.67, 28.27, 22.30. **TLC-MS:** ESI(+) calcd. for $[M+H]^+$: *m/z* = 428.1; found: 428.6. **HPLC:** t_{ret} = 14.72 min (100% at 254 nm, 97.9% at 230 nm, method B).

6.2.7 Synthesis of Compounds described in Section 3.3.2.1.2

2-((4-Methoxybenzyl)amino)isonicotinonitrile (135)

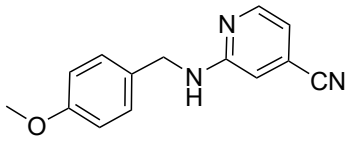

135
Chemical Formula: $C_{14}H_{13}N_3O$
Exact Mass: 239.10586
Molecular Weight: 239.27800

2-Chloro-4-cyanopyridin (**133**, 5.00 g, 36.1 mmol, 1.00 eq.) was dissolved in NMP (8.0 mL, dry). After addition of 4-methoxybenzylamine (**134**, 5.19 mL, 5.55 g, 39.7 mmol, 1.10 eq.) and DIPEA (9.15 mL, 7.01 g, 54.1 mmol, 1.50 eq.), the reaction was heated to 120 °C for 18 h. The mixture was allowed to cool to rt and the solvent removed under reduced pressure. The residue was dissolve din EtOAc (50 mL) and washed with a solution of NH_4Cl (50 mL) and water (50 mL). the organic layer was dried over Na_sSO_4 and the solvent removed in vacuum. The residue was purified by flash column chromatography (Silica gel, 0 – 80% hexane/EtOAc) which afforded the product **135** (2.03 g, 8.30 mmol, 23%) as yellowish solid.

^{1}H NMR (400 MHz, DMSO) δ 8.16 (dd, *J* = 5.2, 0.6 Hz, 1H), 7.55 (t, *J* = 5.8 Hz, 1H), 7.25 (d, *J* = 8.7 Hz, 2H), 6.91 – 6.86 (m, 2H), 6.83 (s, 1H), 6.79 (dd, *J* = 5.2, 1.3 Hz, 1H), 4.40 (d, *J* = 5.9 Hz, 2H), 3.72

(s, 3H). **^{13}C NMR** (101 MHz, $CDCl_3$) δ 159.28, 158.51, 149.63, 129.99, 128.89, 121.48, 117.40, 114.37, 113.79, 109.09, 55.46, 45.76. **TLC-MS:** ESI(-) calcd. for $[M-H]^-$: *m/z* = 238.1; found: 238.2. **HPLC:** t_{ret} = 12.449 min (99.6% at 254 nm, 99.2% at 230 nm, method B).

1-(2-((4-Methoxybenzyl)amino)pyridin-4-yl)ethan-1-one (136)

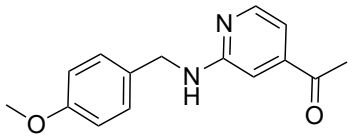

136
Chemical Formula: $C_{15}H_{16}N_2O_2$
Exact Mass: 256.12118
Molecular Weight: 256.30500

2-((4-Methoxybenzyl)amino)isonicotinonitrile (**135**, 0.600 g, 2.51 mmol, 1.00 eq.) was dissolved in Et_2O (20 mL, dry) and cooled to 0°C. A solution of MeMgBr (5.02 mL, 3M in THF, 15.1 mmol, 6.00 eq.) was added dropwise and the reaction heated under reflux for 18 h. After cooling to rt, the mixture was poured into ice (50 mL) and $HCl_{conc.}$ (2 mL) added and stirred for 1 h. the mixture was neutralized using NH_3 solution and extracted with EtOAc (3x 50 mL). The organic layer was dried over Na_2SO_4 and the solvent evaporated. The residue was purified by flash column chromatography (Silica gel, 0 – 60% hexane/EtOAc) which afforded the product **136** (0.218 g, 3.06 mmol, 82%) as yellow solid.
^{1}H NMR (400 MHz, $CDCl_3$) δ 8.08 (dd, *J* = 5.2, 0.7 Hz, 1H), 7.21 – 7.13 (m, 2H), 6.86 (dd, *J* = 5.3, 1.4 Hz, 1H), 6.80 – 6.74 (m, 2H), 6.74 – 6.69 (m, 1H), 5.26 (t, *J* = 5.0 Hz, 1H), 4.37 (d, *J* = 5.6 Hz, 2H), 3.68 (s, 3H), 2.41 (s, 3H). **^{13}C NMR** (101 MHz, $CDCl_3$) δ 198.16, 159.48, 158.96, 149.33, 144.60, 130.78, 128.85, 114.10, 110.62, 105.00, 55.30, 45.79, 26.79. **TLC-MS:** ESI(+) calcd. for $[M+H]^+$: *m/z* = 257.1; found: 257.1; ESI(-) calcd. for $[M-H]^-$: *m/z* = 255.1; found: 255.2. **HPLC:** t_{ret} = 6.112 min (99.2% at 254 nm, 98.0% at 230 nm, method B).

1-(2-Aminopyridin-4-yl)-2-bromoethan-1-one hydrobromide (137·HBr)

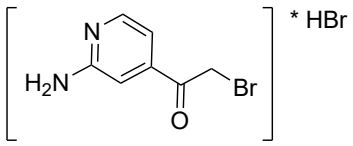

137·HBr
Chemical Formula: $C_7H_7BrN_2O$
Exact Mass: 213.97418
Molecular Weight: 295.96200

1-(2-((4-Methoxybenzyl)amino)pyridin-4-yl)ethan-1-one (**136**, 0.490 g, 1.91 mmol, 1.00 eq.) was dissolved in HAc (8 mL) and Br_2 (98.2 µmL, 310 mg, 1.91 mmol, 1.00 eq.) was added. After adding HBr (3M in HAc, 1.65 mL, 6.12 mmol, 3.20 eq.), the mixture was stirred at 70°C for 2 h. The reaction was cooled to rt and the solvent evaporated. Then DCM was added to crystallize the product and isolated through filtration. This afforded the crude product **137·HBr** (0.580 g, 1.53 mmol, 80%) which was used in the next step without further purification.

tert-Butyl 2-(2-aminopyridin-4-yl)-4-oxo-1,4,6,7-tetrahydro-5H-pyrrolo[3,2-c]pyridine-5-carboxylate (138)

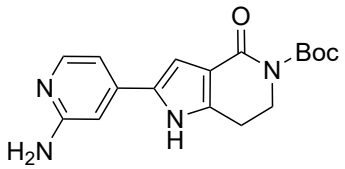

138
Chemical Formula: $C_{17}H_{20}N_4O_3$
Exact Mass: 328.15354
Molecular Weight: 328.37200

1-(2-aminopyridin-4-yl)-2-bromoethan-1-one hydrobromide (**137·HBr**, 0.430 g, 1.45 mmol, 1.00 eq.), *tert*-butyl 2,4-dioxopiperidine-1-carboxylate (**53**, 0.341 g, 1.60 mmol, 1.10 eq.) and NH_4OAc (0.448 g, 5.81 mmol, 4.00 eq.) were dissolved in EtOH (10 mL, HPLC grad). After stirring for 18 h at rt, the solvent was removed under reduced pressure and residue purified by flash column chromatography (Silica gel, 3 – 15% DCM/MeOH) which afforded the product **138** (0.256 g, 0.986 mmol, 68%) as light-yellow powder.

^{1}H NMR (400 MHz, DMSO) δ 12.13 (s, 1H), 7.88 (d, *J* = 5.7 Hz, 1H), 6.93 (d, *J* = 2.2 Hz, 1H), 6.88 (dd, *J* = 5.8, 1.6 Hz, 1H), 6.73 (d, *J* = 1.6 Hz, 1H), 6.41 (s, 2H), 3.96 (t, *J* = 6.2 Hz, 2H), 2.93 (t, *J* = 6.3 Hz, 2H), 1.46 (s, 9H). **^{13}C NMR** (101 MHz, DMSO) δ 172.04, 161.76, 158.46, 153.06, 145.06, 141.40, 130.12, 115.33, 107.59, 107.10, 101.92, 81.25, 45.10, 27.80, 21.07. **TLC-MS:** ESI(+) calcd. for $[M+Na]^+$: *m/z* = 351.2; found: 351.3; ESI(-) calcd. for $[M-H]^-$: *m/z* = 327.2; found: 327.2. **HPLC:** t_{ret} = 8.459 min (95.1% at 254 nm, 97.4% at 230 nm, method B).

tert-Butyl 2-(2-((tert-butoxycarbonyl)amino)pyridin-4-yl)-4-oxo-1,4,6,7-tetrahydro-5H-pyrrolo[3,2-c]pyridine-5-carboxylate (139)

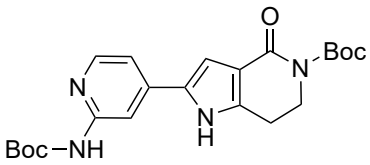

139
Chemical Formula: $C_{22}H_{28}N_4O_5$
Exact Mass: 428.20597
Molecular Weight: 428.48900

A) *tert*-Butyl 2-(2-aminopyridin-4-yl)-4-oxo-1,4,6,7-tetrahydro-5*H*-pyrrolo[3,2-*c*]pyridine-5-carboxylate (**138**, 42.0 mg, 0.128 mmol, 1.00 eq.) was dissolved in tBuOH (1.0 mL) and Boc_2O (27.6 µmol, 28.2 mg, 0.129 mmol, 1.01 eq.) added. The reaction was stirred at rt for 6 h. After complete conversion the solvent was removed under reduced pressure and the residue dissolved in EtOAc (20 mL). The mixture was washed with water (20 mL) and the organic layer dried over Na_2SO_4 . The solvent was evaporated and the residue purified by flash column chromatography (Silica gel, 0 – 10% DCM/MeOH) which afforded the product **139** (15.0 mg, 34.6 µmol, 27%) as yellow oil.

^{1}H NMR (400 MHz, Acetone) δ 11.42 (s, 1H), 8.13 (d, *J* = 5.4 Hz, 1H), 7.98 (d, *J* = 4.5 Hz, 1H), 7.55 – 7.37 (m, 1H), 7.18 (s, 1H), 7.06 (dt, *J* = 5.3, 2.5 Hz, 1H), 4.06 – 3.98 (m, 3H), 2.94 (q, *J* = 6.2 Hz, 3H), 1.47 (ddd, *J* = 7.3, 4.0, 2.3 Hz, 18H). **TLC-MS:** ESI(+) calcd. for $[M+Na]^+$: *m/z* = 451.2; found: 451.4; ESI(-) calcd. for $[M-H]^-$: *m/z* = 427.2; found: 427.4. **HPLC:** t_{ret} = 14.664min (94.9% at 254 nm, 94.3% at 230 nm, method B).

B/C) Synthetic methods **B** and **C,** based on a SUZUKI coupling procedure are described in section 6.2.12.

2-(Benzylamino)isonicotinonitrile (140)

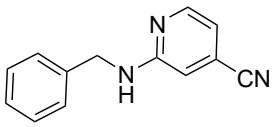

140
Chemical Formula: $C_{13}H_{11}N_3$
Exact Mass: 209.09530
Molecular Weight: 209.25200

2-Chloro-4-cyanopyridine (**133**, 0.500 g, 3.61 mmol, 1.00 eq,) was dissolved in NMP (1.0 mL) and benzylamine (0.434 mL, 0.425 g, 3.97 mmol, 1.10 eq.) added. After addition of DIPEA (0.944 mL, 0.698 g, 5.41 mmol, 1.50 eq.) the reaction was stirred for 18 h at 120 °C. After cooling to rt, the solvent was evaporated and the residue dissolved in EtOAc (20 mL). The organic solution was washed with water (20 mL) and the organic layer dried over Na_2SO_4. The solvent was removed under reduced pressure and the residue purified by flash column chromatography (Silica gel, 0 – 80% hexane/EtOAc) which afforded the product **140** (0.219 g, 1.05 mmol, 29%) as light-yellow solid. **^{1}H NMR** (400 MHz, $CDCl_3$) δ 8.06 (dd, *J* = 5.1, 0.6 Hz, 1H), 7.31 – 7.16 (m, 5H), 6.65 (dd, *J* = 5.1, 1.3 Hz, 1H), 6.53 – 6.39 (m, 1H), 5.41 (s, 1H), 4.43 (d, *J* = 5.8 Hz, 2H). **^{13}C NMR** (101 MHz, $CDCl_3$) δ 158.55, 149.64, 138.05, 128.92, 127.72, 127.48, 121.39, 117.36, 113.76, 108.98, 46.13. **TLC-MS:** ESI(-) calcd. for $[M-H]^-$: *m/z* = 208.1; found: 208.0. **HPLC:** t_{ret} = 12.452 min (96.6% at 254 nm, 95.7% at 230 nm, method B).

1-(2-(Benzylamino)pyridin-4-yl)ethan-1-one (141)

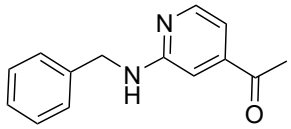

141
Chemical Formula: $C_{14}H_{14}N_2O$
Exact Mass: 226.11061
Molecular Weight: 226.27900

2-(Benzylamino)isonicotinonitrile (**140**, 0.220 g, 1.05 mmol, 1.00 eq.) was dissolved in Et_2O (8.0 mL, dry) and cooled to 0 °C. A solution of MeMgBr (3 M in THF, 2.10 mL, 6.31 mmol, 6.00 eq.) was added dropwise. After complete addition the reaction was refluxed for 18 h. The reaction was cooled to rt and poured into ice (50 mL) and conc. HCl (2.0 mL) added to the mixture. After stirring for 1 h ammonia was added to neutralize the pH of the solution. The mixture was extracted with EtOAc (100 mL) and the organic layer dried over Na_2SO_4. The solvent was removed under reduced pressure and the residue purified by flash column chromatography (Silica gel, 0 – 50% hexane/EtOAc) which afforded the product **141** (0.100 mg, 0.389 mmol, 37%) as yellow solid.

^{1}H NMR (400 MHz, $CDCl_3$) δ 8.12 (d, *J* = 5.2 Hz, 1H), 7.31 – 7.14 (m, 5H), 6.89 (dd, *J* = 5.2, 1.4 Hz, 1H), 6.74 (s, 1H), 5.20 (d, *J* = 4.7 Hz, 1H), 4.46 (d, *J* = 5.7 Hz, 2H), 2.42 (s, 3H). **^{13}C NMR** (101 MHz, $CDCl_3$) δ 198.14, 159.49, 149.36, 144.76, 138.80, 128.81, 127.58, 127.51, 110.86, 105.07, 46.38, 26.88. **TLC-MS:** ESI(+) calcd. for $[M+H]^+$: *m/z* =227.1; found: 227.1; ESI(-) calcd. for $[M-H]^-$: *m/z* =225.1; found: 224.9.

1-(2-(Benzylamino)pyridin-4-yl)-2-bromoethan-1-one hydrobromide (142·HBr)

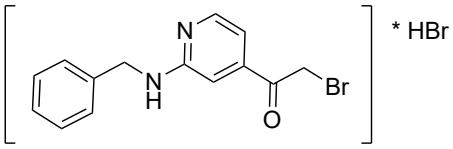

142·HBr
Chemical Formula: $C_{14}H_{13}BrN_2O$
Exact Mass: 304.02113
Molecular Weight: 386.08700

1-(2-(Benzylamino)pyridin-4-yl)ethan-1-one (**141**, 0.100 g, 0.442 mmol) was dissolved in HOAc (4.0 mL). Br_2 (22.7 µL, 70.6 mg, 0.442 mmol, 1.00 eq.) and HBr (3 M in HAc, 0.381 mL, 1.41 mmol, 3.20 eq.) were added and the reaction heated to 70 °C for 2 h. The solvent was evaporated and the crude product **142·HBr** (0.154 g, 90%) used in the next step without purification.

tert-Butyl 2-(2-(benzylamino)pyridin-4-yl)-4-oxo-1,4,6,7-tetrahydro-5H-pyrrolo[3,2-c]pyridine-5-carboxylate (143)

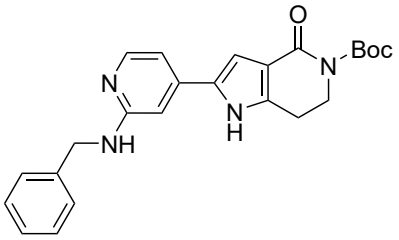

143
Chemical Formula: $C_{24}H_{26}N_4O_3$
Exact Mass: 418.20049
Molecular Weight: 418.49700

1-(2-(Benzylamino)pyridin-4-yl)-2-bromoethan-1-one hydrobromide (**142·HBr**, 0.154 mg, 0.399 mmol, 1.00 eq.), *tert*-butyl 2,4-dioxopiperidine-1-carboxylate (**53**, 0.128 g, 0.598 mmol, 1.5 eq.) and NH_4OAc (0.123 g, 1.60 mmol, 4.00 eq.) were dissolved in EtOH (10 mL, HPLC grade). After stirring the reaction for 18 h at rt, the solvent was evaporated. The residue was purified by flash column chromatography (Silica gel, 2 – 10% DCM/MeOH) which afforded the product **143** (67.0 mg, 0.160 mmol, 40%) as yellow solid. The isolated product was directly used in the next step.

TLC-MS: ESI(+) calcd. for $[M+Na]^+$: *m/z* = 441.2; found: 441.4; ESI(-) calcd. for $[M-H]^-$: *m/z* = 417.2; found: 417.3.

Di-tert-butyl 2-(2-(benzyl(tert-butoxycarbonyl)amino)pyridin-4-yl)-4-oxo-6,7-dihydro-1H-pyrrolo[3,2-c]pyridine-1,5(4H)-dicarboxylate (144)

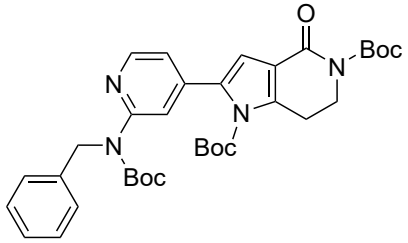

144
Chemical Formula: $C_{34}H_{42}N_4O_7$
Exact Mass: 618.30535
Molecular Weight: 618.73100

tert-Butyl 2-(2-(benzylamino)pyridin-4-yl)-4-oxo-1,4,6,7-tetrahydro-5*H*-pyrrolo[3,2-*c*]pyridine-5-carboxylate (**143**, 67.0 mg, 0.160 mmol, 1.00 eq.) and DMAP (9.8 mg, 80.1 µmol, 0.5 eq.) were dissolved in ACN (15 mL, dry) under an argon atmosphere). Boc_2O (0.147 mL, 0.140 g, 0.641 mmol, 4.00 eq.) and TEA (0.112 mL, 81.1 mg, 0.801 mmol, 5.00 eq.) were added and the reaction stirred for 18 h. To enable complete conversion another portion of Boc_2O (29.4 µL, 28.0 mg, 0.128 mmol, 0.80 eq.) and DMAP (2.0 mg, 16.0 µmol, 0.1 eq.) were added and the reaction prolonged for 5 h. The reaction mixture was diluted with DCM (20 mL) and H_2O (20 mL). The layers were separated and the organic layer dried over

Na_2SO_4. The residue was purified by flash column chromatography (Silica gel, 0 – 50% hexane/EtOAc) which afforded the product **144** (31.0 mg, 49.7 µmol, 31%) as rose-colored oil.

^{1}H NMR (400 MHz, $CDCl_3$) δ 8.36 (d, *J* = 5.1 Hz, 1H), 7.77 (s, 1H), 7.28 (ddd, *J* = 25.5, 14.3, 6.8 Hz, 5H), 6.94 (dd, *J* = 5.1, 1.2 Hz, 1H), 6.72 (s, 1H), 5.28 (s, 2H), 4.13 (t, *J* = 6.4 Hz, 2H), 3.25 (t, *J* = 6.4 Hz, 2H), 1.59 (s, 9H), 1.43 (s, 9H), 1.30 (s, 9H). **^{13}C NMR** (101 MHz, $CDCl_3$) δ 161.98, 154.32, 154.11, 153.31, 148.52, 146.77, 142.68, 142.10, 139.47, 133.86, 128.30, 127.36, 126.86, 119.32, 118.76, 118.40, 112.81, 86.20, 83.02, 81.69, 49.78, 44.74, 28.27, 27.42, 24.71. **TLC-MS:** ESI(+) calcd. for $[M+Na]^+$: *m/z* = 641.3; found: 641.6; ESI(-) calcd. for $[M-H]^-$: *m/z* = 617.3; found: 617.6. **HPLC:** t_{ret} = 22.260 min (98.3% at 254 nm, 98.6% at 230 nm, method B).

Di-tert-butyl 2-(2-((tert-butoxycarbonyl)amino)pyridin-4-yl)-4-oxo-6,7-dihydro-1H-pyrrolo[3,2-c]pyridine-1,5(4H)-dicarboxylate (145)

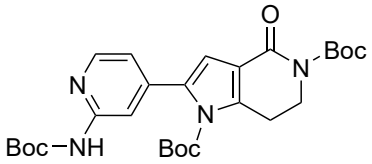

145

Chemical Formula: $C_{27}H_{36}N_4O_7$
Exact Mass: 528.25840
Molecular Weight: 528.60600

Di-*tert*-butyl 2-(2-(benzyl(*tert*-butoxycarbonyl)amino)pyridin-4-yl)-4-oxo-6,7-dihydro-1*H*-pyrrolo[3,2-*c*]pyridine-1,5(4*H*)-dicarboxylate (**144**, 31.0 mg, 49.7 µmol, 1.00 eq.) was dissolved in EtOH (2.0 mL, HPLC grade) and Palladium on charcoal added (10% wt, 3.0 mg, 10% m/m). H_2 was bubbled through the reaction. After 18h only traces of the product **145** could be detected by TLC-MS (ESI(+) calcd. for $[M+Na]^+$: *m/z* = 551.3; found: 551.6). A successful method for the synthesis of intermediate **145** is described in section 6.2.12

6.2.8 Synthesis of Compounds described in Section 3.3.2.1.3

tert-Butyl 4-((2,2-dimethoxyethyl)amino)-6-oxo-3,6-dihydropyridine-1(2H)-carboxylate (147)

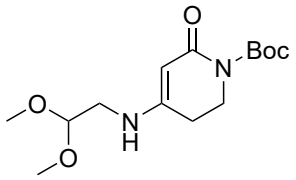

147

Chemical Formula: $C_{14}H_{24}N_2O_5$
Exact Mass: 300.16852
Molecular Weight: 300.35500

tert-Butyl 4-((2,2-dimethoxyethyl)amino)-6-oxo-3,6-dihydropyridine-1(2*H*)-carboxylate (**147**) was synthesized in a similar manner as described in the patent literature.[258a] *tert*-Butyl 2,4-dioxopiperidine-1-carboxylate (**53**, 10.0 g, 46.9 mmol, 1.00 eq.), molecular sieve (4Å, 4.00 g) and aminoacetaldehyde dimethyl acetal (5.38 mL, 4.93 g, 46.9 mmol, 1.00 eq.) were weighed into a flask and toluene (dry, 100 mL) was added. The reaction was stirred for 18 h at 70 °C under an atmosphere of argon. After cooling to rt, the mixture was filtered and the filtrate evaporated to dryness which afforded the product **147** (14.0 g, 46.7 mmol, 99.5%) as yellow solid.

^{1}H NMR (400 MHz, DMSO) δ 11.13 (s, 1H), 6.94 (s, 1H), 6.65 (t, *J* = 2.4 Hz, 1H), 6.21 (d, *J* = 2.1 Hz, 1H), 3.35 (t, *J* = 6.9 Hz, 2H), 2.73 (t, *J* = 6.9 Hz, 2H). **^{13}C NMR** (101 MHz, DMSO) δ 165.71, 135.59, 117.67, 113.31, 105.52, 40.38, 21.84. **TLC-MS:** ESI(+) calcd. for $[M+Na]^+$: *m/z* = 323.2; found: 323.3;

ESI(-) calcd. for $[M-H]^-$: *m/z* = 299.2; found: 299.1. **HPLC:** t_{ret} = 9.69 min (96.3% at 254 nm, 98.0% at 230 nm, method B).

1,5,6,7-Tetrahydro-4H-pyrrolo[3,2-c]pyridin-4-one (148)

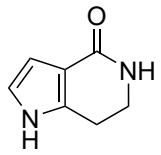

148
Chemical Formula: $C_7H_8N_2O$
Exact Mass: 136.06366
Molecular Weight: 136.15400

tert-Butyl 4-((2,2-dimethoxyethyl)amino)-6-oxo-3,6-dihydropyridine-1(2*H*)-carboxylate (**147**, 14.1 g, 46.9 mmol, 1.00 eq.) was dissolved in DCM (dry, 25 mL) and added dropwise to cold TFA (120 mL) in an ice bath. [258a] The reaction was stirred at rt for 2 h and the solvent removed under reduced pressure. After adding MTBE (200 mL) to the residue, the mixture was stirred at rt for 2 h. The precipitate was filtered off and again suspended in MTBE (100 mL) and stirred at 50 °C for 24 h. After cooling to rt the mixture was filtered. The filtrates were combined and the solvent reduced to a volume of 100 mL. Cyclohexane (200 mL) was added and the first fraction of product collected by filtration. The filtrate was evaporated and treated with cyclohexane again to precipitate a second fraction of product which was collected by filtration. The fractions of product were combined and dried in vacuum which afforded the product **148** (5.82 g, 42.7 mmol, 91 %) as white solid.

^{1}H NMR (400 MHz, DMSO) δ 11.13 (s, 1H), 6.98 (s, 1H), 6.65 (d, *J* = 2.2 Hz, 1H), 6.21 (d, *J* = 2.2 Hz, 1H), 3.36 (t, *J* = 6.9 Hz, 2H), 2.73 (t, *J* = 6.9 Hz, 2H). **^{13}C NMR** (101 MHz, DMSO) δ 165.75, 135.65, 117.77, 117.72, 105.54, 40.39, 21.82. **TLC-MS:** ESI(+) calcd. for $[M+Na]^+$: *m/z* = 159.1; found: 158.9. **HPLC:** t_{ret} = 3.48 min (97.8% at 254 nm, 95.6% at 230 nm, method B).

Di-tert-butyl 4-oxo-6,7-dihydro-1H-pyrrolo[3,2-c]pyridine-1,5(4H)-dicarboxylate (149)

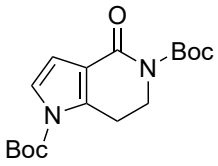

149
Chemical Formula: $C_{17}H_{24}N_2O_5$
Exact Mass: 336.16852
Molecular Weight: 336.38800

1,5,6,7-Tetrahydro-4*H*-pyrrolo[3,2-*c*]pyridin-4-one (**148**, 4.00 g, 29.4 mmol, 1,00 eq.), Boc_2O (20.5 g, 94.0 mmol, 3.20 eq.) and DMAP (0.359 g, 2.94 mmol, 0.10 eq.) were dissolved in acetonitrile (dry). [258a] After addition of triethylamine (15.6 mL, 11.9 g, 117 mmol, 4.00 eq.) the reaction was stirred at rt for 18 h. The solvent was removed under reduced pressure and the residue purified by flash column chromatography (Silica gel, 10 – 60% hexane/EtOAc) which afforded the product **149** (4.80 g, 14.1 mmol, 49%) as light-yellow solid.

^{1}H NMR (400 MHz, $CDCl_3$) δ 7.14 (d, *J* = 3.5 Hz, 1H), 6.60 (d, *J* = 3.5 Hz, 1H), 4.05 (t, *J* = 6.4 Hz, 2H), 3.19 (t, *J* = 6.4 Hz, 2H), 1.60 (s, 9H), 1.55 (s, 9H). **^{13}C NMR** (101 MHz, $CDCl_3$) δ 162.43, 153.46, 148.64, 139.33, 121.71, 119.55, 109.59, 85.39, 82.85, 44.86, 28.27, 28.08, 24.35.**TLC-MS:** ESI(+) calcd. for $[M+Na]^+$: *m/z* = 359.2; found: 359.2. **HPLC:** t_{ret} = 17.5 min (99.2% at 254 nm, 97.3% at 230 nm, method B).

tert-Butyl 4-oxo-1,4,6,7-tetrahydro-5H-pyrrolo[3,2-c]pyridine-5-carboxylate (150)

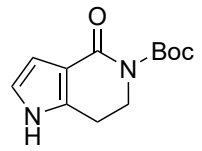

150
Chemical Formula: $C_{12}H_{16}N_2O_3$
Exact Mass: 236.11609
Molecular Weight: 236.27100

Di-*tert*-butyl 4-oxo-6,7-dihydro-1*H*-pyrrolo[3,2-*c*]pyridine-1,5(4*H*)-dicarboxylate (**149**, 4.86 g, 14.4 mmol) was dissolved in MeOH (120 mL). After the addition of ammonia solution (4 mL, 25% in water) the reaction was stirred at reflux for 6 h.[258a] After cooling to rt, the solvent was removed and the residue dissolved in DCM (50 mL). By adding MTBE (150 mL) the product was precipitated and collected by filtration which afforded a first fraction of product. The filtrate was evaporated and the residue purified by flash column chromatography (Silica gel, 2 – 8% DCM/MeOH) which afforded a second product fraction. The two fractions of product **150** (light-yellow powder, 2.88 g, 12.2 mmol, 85%) were combined.

^{1}H NMR (400 MHz, $CDCl_3$) δ 9.53 (s, 1H), 6.73 – 6.64 (m, 1H), 6.56 (t, *J* = 2.5 Hz, 1H), 4.06 (t, *J* = 6.4 Hz, 2H), 2.90 (t, *J* = 6.3 Hz, 2H), 1.54 (s, 8H). **^{13}C NMR** (101 MHz, $CDCl_3$) δ 163.84, 153.57, 137.95, 119.38, 114.84, 107.90, 82.55, 45.70, 28.32, 22.84. **TLC-MS:** ESI(+) calcd. for $[M+Na]^+$: *m/z* = 259.1; found: 259.1. **HPLC:** t_{ret} = 9.90 min (99.3% at 254 nm, 98.5% at 230 nm, method B).

tert-Butyl 2-bromo-4-oxo-1,4,6,7-tetrahydro-5H-pyrrolo[3,2-c]pyridine-5-carboxylate (151)

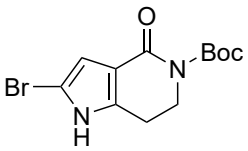

151
Chemical Formula: $C_{12}H_{15}BrN_2O_3$
Exact Mass: 314.02661
Molecular Weight: 315.16700

tert-Butyl 4-oxo-1,4,6,7-tetrahydro-5*H*-pyrrolo[3,2-*c*]pyridine-5-carboxylate (**150**, 1.50 g, 6.35 mmol, 1.00 eq.) was dissolved in a mixture of THF (dry, 39 mL) and MeOH (12 mL) and cooled to -70 °C (acetone/N_2 bath). *N*-Bromosuccinimide (1.02 g, 5.72 mmol, 0.90 eq.) was added in 2 portions and the reaction stirred for 30 min while cooling was maintained. Then the reaction was allowed to warm to rt and the reaction was quenched by addition of $Na_2S_2O_3$ solution (10%, 20 mL). The organic solvent was removed under reduced pressure and the mixture extracted with DCM (3x 50 mL). The combined organic layers were dried over Na_2SO_4 and the solvent evaporated. Purification by flash column chromatography (Silica gel, 30 – 80% hexane/EtOAc) afforded the product **151** (1.32g, 4.20 g, 66%) as white solid.

^{1}H NMR (400 MHz, DMSO) δ 12.10 (s, 1H), 6.35 (s, 1H), 3.90 (t, *J* = 6.3 Hz, 2H), 2.81 (t, *J* = 6.3 Hz, 2H), 1.45 (s, 9H). **^{13}C NMR** (101 MHz, DMSO) δ 160.97, 153.04, 139.46, 115.06, 108.14, 99.52, 81.22, 45.07, 27.77, 21.92. **TLC-MS:** ESI(+) calcd. for $[M+Na]^+$: *m/z* = 337.0; found: 337.1; ESI(-) calcd. for $[M-H]^-$: *m/z* = 313.0; found: 312.9. **HPLC:** t_{ret} = 13.47 min (98.9% at 254 nm, 96.9% at 230 nm, method B).

tert-Butyl 2-bromo-1-methyl-4-oxo-1,4,6,7-tetrahydro-5H-pyrrolo[3,2-c]pyridine-5-carboxylate (124)

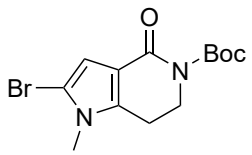

124
Chemical Formula: $C_{13}H_{17}BrN_2O_3$
Exact Mass: 328.04226
Molecular Weight: 329.19400

tert-Butyl 2-bromo-4-oxo-1,4,6,7-tetrahydro-5*H*-pyrrolo[3,2-*c*]pyridine-5-carboxylate (**151**, 1.20 g, 3.82 mmol, 1.00 eq.) and Cs_2CO_3 (2.74 g, 8.41 mmol, 2.20 eq.) were dissolved in DMF (dry, 30 mL) under an argon atmosphere and stirred at rt for 15 min. The solution was cooled to 0 °C (ice bath) and methyl iodide (0.523 mL, 1.19 g, 8.41 mmol, 2.20 eq.). After the reaction was stirred at rt for 2 h, the solvent was evaporated and the residue diluted with EtOAc (50 mL). The solution was washed with sat. NH_4Cl solution, water and brine (50 mL) and the aqueous phase extracted with EtOAc (50 mL) the combined organic layers were dried over Na_2SO_4 and the solvent removed under reduced pressure. The crude product was purified by flash column chromatography (Silica gel, 30 – 80% hexane/EtOAc) which afforded the product **124** (1.11 g, 7.40 mmol, 88%) as white powder.

^{1}H NMR (400 MHz, $CDCl_3$) δ 6.60 (s, 1H), 4.08 – 4.03 (m, 2H), 3.48 (s, 3H), 2.82 – 2.76 (m, 2H), 1.53 (s, 9H). **^{13}C NMR** (101 MHz, $CDCl_3$) δ 161.65, 153.70, 138.62, 115.75, 109.93, 104.87, 82.68, 44.74, 32.41, 28.26, 22.52. **TLC-MS:** ESI(+) calcd. for $[M+Na]^+$: *m/z* = 351.0; found: 351.2. **HPLC:** t_{ret} = 14.32 min (98.6% at 254 nm, 98.3 % at 230 nm, method B).

tert-Butyl 2-(2-chloropyridin-4-yl)-1-methyl-4-oxo-1,4,6,7-tetrahydro-5H-pyrrolo[3,2-c]pyridine-5-carboxylate (120)

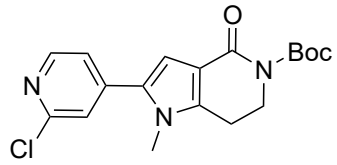

120
Chemical Formula: $C_{18}H_{20}ClN_3O_3$
Exact Mass: 361.11932
Molecular Weight: 361.82600

A) Alternative method **A** is described in section 6.2.6.

B) *tert*-Butyl 2-bromo-1-methyl-4-oxo-1,4,6,7-tetrahydro-5*H*-pyrrolo[3,2-*c*]pyridine-5-carboxylate (**124**, 50.0 mg, 0.152 mmol, 1.00 eq.) and (2-chloropyridin-4-yl)boronic acid (**152**, 28.7 mg, 0.182 mmol, 1.20 mmol) were dissolved in 1,4-dioxane (degassed, 1 mL) under argon atmosphere and $Pd(dppf)Cl_2 \cdot CH_2Cl_2$ (12.4 mg, 15.2µmol, 10 mol%) was added. A 2 M Na_2CO_3 solution (0.235 mL, 0.471 mmol, 3.10 eq.) was added and the reaction heated to 80 °C. After stirring for 4 h, the reaction was cooled to rt and diluted with EtOAc (20 mL). The mixture was filtered through a pad of celite and washed with sat. NH_4Cl solution, water and brine (20 mL). The organic layer was dried over Na_2SO_4 and evaporated. The residue was purified by flash column chromatography (Silica gel, 30 – 100% hexane/EtOAc) which afforded the product **120** (22.0 mg, 60.8 µmol, 40%) as light-yellow powder.

^{1}H NMR (400 MHz, $CDCl_3$) δ 8.38 (d, *J* = 5.2 Hz, 1H), 7.30 (d, *J* = 0.9 Hz, 1H), 7.20 (dd, *J* = 5.2, 1.5 Hz, 1H), 6.83 (s, 1H), 4.13 (t, *J* = 6.3 Hz, 2H), 3.62 (s, 3H), 2.90 (t, *J* = 6.3 Hz, 2H), 1.55 (s, 9H). **^{13}C NMR** (101 MHz, $CDCl_3$) δ 162.19, 153.63, 152.21, 150.06, 142.47, 141.63, 132.18, 122.44, 121.13,

115.88, 110.63, 82.85, 44.72, 32.68, 28.27, 22.31. **TLC-MS:** ESI(+) calcd. for $[M+Na]^+$: *m/z* = 384.1; found: 384.0. **HPLC:** t_{ret} = 14.37 min (90.6% at 254 nm, 97.1% at 230 nm, method B).

tert-Butyl (4-bromopyridin-2-yl)carbamate (154)

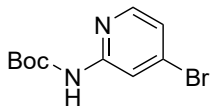

154

Chemical Formula: $C_{10}H_{13}BrN_2O_2$
Exact Mass: 272.01604
Molecular Weight: 273.13000

2-Amino-4-bromopyridine (**153**, 4.00 g, 23.1 mmol, 1.00 eq.) and di-*tert*-butyl dicarbonate (5.30 g, 24.3 mmol, 1.05 eq.) were suspended in *t*BuOH (25 mL). After stirring the reaction at 50 °C for 4 h, the solvent was removed under reduced pressure and the residue purified by flash column chromatography (Silica gel, hexane/7% EtOAc) which afforded the product **154** (5.07 g, 18.5 mmol, 80%) as white solid.

^{1}H NMR (400 MHz, $CDCl_3$) δ 9.36 (s, 1H), 8.27 (s, 1H), 8.14 (d, *J* = 5.4 Hz, 1H), 7.11 (dd, *J* = 5.4, 1.5 Hz, 1H), 1.54 (s, 9H). **^{13}C NMR** (101 MHz, $CDCl_3$) δ 153.42, 152.47, 148.18, 134.66, 121.52, 115.66, 81.41, 28.33. **TLC-MS:** ESI(+) calcd. for $[M+Na]^+$: *m/z* = 295.0; found: 295.0. **HPLC:** t_{ret} = 17.14 min (97.8% at 254 nm, 96.1% at 230 nm, method B).

tert-Butyl (4-(4,4,5,5-tetramethyl-1,3,2-dioxaborolan-2-yl)pyridin-2-yl)carbamate (123)

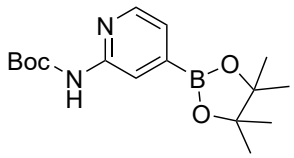

123

Chemical Formula: $C_{16}H_{25}BN_2O_4$
Exact Mass: 320.19074
Molecular Weight: 320.19600

tert-Butyl (4-bromopyridin-2-yl)carbamate (**154**, 4.50 g, 16.5 mmol, 1.00 eq.), bis(pinacolato)diboron (4.60 g, 18.3 mmol, 1.10 eq.) and potassium acetate (4.85 g, 49.4 mmol, 3,00 eq.) were suspended in 1,4-dioxane (dry, 90 mL) and degassed (Ar). After addition of XPhos Pd g4 (0.142 g, 0.16 mmol, 0.01 eq.) the reaction was heated to 90 °C for 18 h. After cooling to room temperature, the reaction was filtered over a pad of celite and the solvent evaporated. The residue was treated with EA and a first fraction of product isolated by filtration. The filtrate was evaporated and purified by column chromatography (Silica gel, 10 – 100% hexane/EtOAc) to isolate a second product fraction. The product portions were combined to yield the product **123** (2.87 g, 8.90 mmol, 54%) as white powder.

^{1}H NMR (400 MHz, $CDCl_3$) δ 9.50 (s, 1H), 8.36 (d, *J* = 4.8 Hz, 1H), 8.32 (s, 1H), 7.27 (d, *J* = 4.8 Hz, 1H), 1.53 (s, 9H), 1.32 (s, 12H). **^{13}C NMR** (101 MHz, $CDCl_3$) δ 152.97, 152.48, 147.05, 139.95, 123.07, 117.83, 84.51, 80.68, 28.50, 24.96. **TLC-MS:** ESI(+) calcd. for $[M+Na]^+$: *m/z* = 343.2; found: 343.3; ESI(-) calcd. for $[M-H]^-$: *m/z* = 319.2; found: 319.1.

tert-Butyl 2-(2-((tert-butoxycarbonyl)amino)pyridin-4-yl)-1-methyl-4-oxo-1,4,6,7-tetrahydro-5H-pyrrolo[3,2-c]pyridine-5-carboxylate (119)

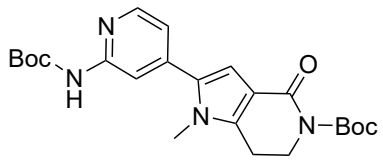

119

Chemical Formula: $C_{23}H_{30}N_4O_5$
Exact Mass: 442.22162
Molecular Weight: 442.51600

To a mixture of *tert*-Butyl 2-bromo-1-methyl-4-oxo-1,4,6,7-tetrahydro-5*H*-pyrrolo[3,2-*c*]pyridine-5-carboxylate (**124**, 0.500 g, 1.52 mmol, 1.00 eq.) and *tert*-Butyl (4-(4,4,5,5-tetramethyl-1,3,2-dioxaborolan-2-yl)pyridin-2-yl)carbamate (**123**, 0.535 g, 1.67 mmol, 1.10 eq.) in a argon-purged flask 1,4-dioxane (degassed, 15 mL)) was added and a degassed 2 M Na_2CO_3 solution (2.28 mL, 4.56 mmol, 3.00 eq.) was added dropwise. After adding XPhos Pd g4 (65.3 mg, 95.9 µmol, 5 mol%) the reaction was heated at 90 °C and stirred for 18 h. After cooling to rt, the reaction was diluted with EtOAc (30 mL) and filtered through a pad of celite. The solution was washed with sat. NH_4Cl solution, water and brine (50 mL) and the organic layer dried over Na_2SO_4. After the solvent was removed under reduced pressure, the residue was purified by flash column chromatography (Silica gel, 40 – 100% hexane/EtOAc) which afforded the product **119** (0.269 g, 0.608 mmol, 40%) as off-white solid.

^{1}H NMR (400 MHz, DMSO) δ 9.86 (s, 1H), 8.27 (d, *J* = 5.2 Hz, 1H), 7.87 (s, 1H), 7.14 (d, *J* = 4.5 Hz, 1H), 6.66 (s, 1H), 3.98 (t, *J* = 6.1 Hz, 2H), 3.61 (s, 3H), 2.96 (t, *J* = 6.1 Hz, 2H), 1.47 (d, *J* = 3.7 Hz, 19H). **^{13}C NMR** (101 MHz, DMSO) δ 161.55, 153.03, 152.87, 148.27, 142.28, 140.50, 133.28, 116.97, 113.95, 110.51, 108.22, 81.30, 79.76, 44.74, 32.56, 28.05, 27.82, 21.55. **TLC-MS:** ESI(+) calcd. for $[M+Na]^+$: *m/z* = 465.2; found: 465.3. **HPLC:** t_{ret} = 16.04 min (97.0% at 254 nm, 96.3% at 230 nm, method B).

Alternative methods for the synthesis of **119** are described in section 6.2.6.

6.2.9 Synthesis of Compounds described in Section 3.3.2.1.4

tert-Butyl 2-(2-((tert-butoxycarbonyl)(6-chloro-3-nitropyridin-2-yl)amino)pyridin-4-yl)-1-methyl-4-oxo-1,4,6,7-tetrahydro-5H-pyrrolo[3,2-c]pyridine-5-carboxylate (158)

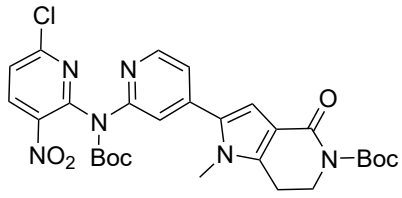

158

Chemical Formula: $C_{28}H_{31}ClN_6O_7$
Exact Mass: 598.19428
Molecular Weight: 599.04100

tert-Butyl 2-(2-((*tert*-butoxycarbonyl)amino)pyridin-4-yl)-1-methyl-4-oxo-1,4,6,7-tetrahydro-5*H*-pyrrolo[3,2-*c*]pyridine-5-carboxylate (**119**, 0.500 g, 1.13 mmol, 1.00 eq.) was subjected to GSP 8. The reaction mixture in toluene (12 mL) was heated to 60 °C for 18 h. After cooling to rt the reaction mixture was diluted with DCM (50 mL) and washed with sat. $NaHCO_3$ solution (50 mL). The aqueous phase was extracted with DCM (2x 50 mL) and the combined organic layers were dried over Na_2SO_4. The solvent was evaporated and the residue purified by flash column chromatography

(Silica gel, 0.5 – 5% DCM/MeOH) which afforded the product (**158**, 0.661 g, 1.10 mmol, 98%) as yellow solid.

^{1}H NMR (400 MHz, $CDCl_3$) δ 8.44 (d, *J* = 8.5 Hz, 1H), 8.18 (d, *J* = 5.2 Hz, 1H), 7.87 (s, 1H), 7.47 (d, *J* = 8.5 Hz, 1H), 7.06 (dd, *J* = 5.2, 1.5 Hz, 1H), 6.85 (s, 1H), 4.15 (t, *J* = 6.3 Hz, 2H), 3.67 (s, 3H), 2.91 (t, *J* = 6.3 Hz, 2H), 1.57 (s, 9H), 1.41 (s, 9H). **^{13}C NMR** (101 MHz, $CDCl_3$) δ 162.42, 153.88, 153.83, 153.62, 151.18, 148.21, 147.89, 142.06, 141.31, 141.17, 136.53, 133.54, 124.05, 119.56, 117.19, 115.64, 109.88, 84.27, 82.72, 44.82, 32.72, 28.33, 27.95, 22.37. **TLC-MS:** ESI(+) calcd. for $[M+Na]^+$: *m/z* = 621.2; found: 621.0. **HPLC:** t_{ret} = 17.60 min (97.3% at 254 nm, 97.4% at 230 nm, method B).

2-(2-((6-Chloro-3-nitropyridin-2-yl)amino)pyridin-4-yl)-1-methyl-1,5,6,7-tetrahydro-4H-pyrrolo[3,2-c]pyridin-4-one (110)

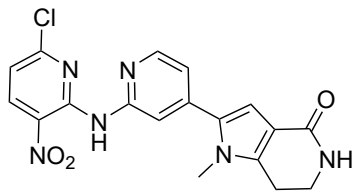

110

Chemical Formula: $C_{18}H_{15}ClN_6O_3$
Exact Mass: 398.08942
Molecular Weight: 398.80700

tert-Butyl 2-(2-((*tert*-butoxycarbonyl)(6-chloro-3-nitropyridin-2-yl)amino)pyridin-4-yl)-1-methyl-4-oxo-1,4,6,7-tetrahydro-5*H*-pyrrolo[3,2-*c*]pyridine-5-carboxylate (**158**, 0.528 g, 0.881 mmol) was dissolved in DCM (dry, 10 mL), subjected to GSP 7and stirred for 15 min. The residue was dissolved in DCM (20 mL) and washed with sat. Na_2CO_3 solution. The aqueous phase was extracted with EtOAc (5x 15 mL). The combined organic layers were dried over Na_2SO_4 and the solvent removed under reduced pressure. The residue was purified by flash column chromatography (Silica gel, 4 – 8% DCM/MeOH) and the raw product washed with n-hexane, which afforded the product **110** (0.238 g, 0.599 mmol, 68%) as yellow powder.

^{1}H NMR (400 MHz, DMSO) δ 10.48 (s, 1H), 8.63 (d, *J* = 8.6 Hz, 1H), 8.34 (d, *J* = 5.2 Hz, 1H), 8.26 (s, 1H), 7.31 (dd, *J* = 5.2, 1.5 Hz, 1H), 7.22 (d, *J* = 8.6 Hz, 1H), 7.10 (s, 1H), 6.70 (s, 1H), 3.76 (s, 3H), 3.47 – 3.41 (m, 2H), 2.89 (t, *J* = 6.9 Hz, 2H). **^{1}H NMR** (400 MHz, $CDCl_3$/TFA) δ 11.37 (s, 1H), 8.70 (d, *J* = 8.6 Hz, 1H), 8.58 (d, *J* = 9.4 Hz, 1H), 8.38 (d, *J* = 6.7 Hz, 1H), 8.04 (d, *J* = 1.8 Hz, 1H), 7.53 (dd, *J* = 6.7, 1.8 Hz, 1H), 7.36 (d, *J* = 8.7 Hz, 1H), 7.23 (s, 1H), 3.86 (d, *J* = 4.6 Hz, 5H), 3.09 (t, *J* = 7.3 Hz, 2H). **^{13}C NMR** (101 MHz, $CDCl_3$/TFA) δ 167.94, 155.11, 148.56, 147.44, 146.44, 145.71, 138.99, 137.52, 131.18, 130.19, 120.18, 117.79, 114.58, 112.90, 112.46, 40.63, 33.84, 21.13. **HRMS:** ESI(+) calcd. for $[M+H]^+$: *m/z* = 399.09669; found: 399.09685; rel. deviation: 0.40 ppm. **HPLC:** t_{ret} = 13.63 min (98.6% at 254 nm, 99.1% at 230 nm, method B). **IR** (ATR) [cm^{-1}]: 3321, 3188, 3056, 2966, 2946, 2919, 2878, 1647, 1582, 1485, 1459, 1437, 1410, 1388, 1363, 1324, 1298, 1264, 1217, 1183, 1142, 1042, 992, 970, 894, 850, 805, 759, 652.

tert-Butyl 2-(2-((6-bromo-3-nitropyridin-2-yl)(tert-butoxycarbonyl)amino)pyridin-4-yl)-1-methyl-4-oxo-1,4,6,7-tetrahydro-5H-pyrrolo[3,2-c]pyridine-5-carboxylate (160)

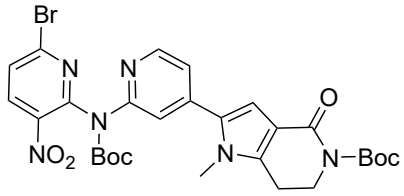

160

Chemical Formula: $C_{28}H_{31}BrN_6O_7$
Exact Mass: 642.14376
Molecular Weight: 643.49500

tert-Butyl 2-(2-((*tert*-butoxycarbonyl)amino)pyridin-4-yl)-1-methyl-4-oxo-1,4,6,7-tetrahydro-5*H*-pyrrolo[3,2-*c*]pyridine-5-carboxylate (**119**, 55.0 mg, 0.124 mmol, 1.00 eq.) and 2,6-dibromo-3-nitropyridine (**159**, 52.6 mg, 0.186 mmol, 1.50 eq.) were treated in an analogous manner as described in GSP 8 and dissolved in toluene (5 mL). After stirring for 18 h at 70 °C the mixture was cooled to rt and concentrated under reduced pressure. The residue was diluted with DCM (20 mL) and washed with sat. NH_4Cl solution (20 mL). The aqueous layer was extracted with DCM (2x 20 mL) and the combined organic layers dried over Na_2SO_4. The solvent was removed under reduced pressure and the raw product purified by flash column chromatography (Silica gel, 1 – 6% DCM/MeOH) which afforded the product **160** (28.0 mg 43.5 µmol, 35%) as yellow oil.

^{1}H NMR (400 MHz, $CDCl_3$) δ 8.47 (d, *J* = 5.2 Hz, 1H), 8.25 (d, *J* = 8.8 Hz, 1H), 7.96 (d, *J* = 8.8 Hz, 1H), 7.36 (d, *J* = 0.8 Hz, 1H), 7.26 (s, 1H), 6.87 (s, 1H), 4.14 (t, *J* = 6.3 Hz, 2H), 3.65 (s, 3H), 2.91 (t, *J* = 6.3 Hz, 2H), 1.56 (s, 9H), 1.44 (s, 9H). **^{13}C NMR** (101 MHz, $CDCl_3$) δ 162.33, 155.86, 153.75, 153.50, 152.15, 149.38, 142.47, 141.76, 141.34, 135.97, 132.97, 132.17, 121.76, 121.67, 117.02, 115.79, 109.98, 84.24, 82.81, 44.80, 32.69, 28.31, 28.13, 22.36. **TLC-MS:** ESI(+) calcd. for $[M+Na]^+$: *m/z* =665.1; found: 665.5; ESI(-) calcd. for $[M\text{-Boc-H}]^-$: *m/z* =541.1; found: 541.5. **HPLC:** t_{ret} = 17.99 min (92.3% at 254 nm, 91.3% at 230 nm, method B).

^{1}H NMR (400 MHz, $CDCl_3$) δ 8.71 (dd, *J* = 4.7, 1.7 Hz, 1H), 8.47 (dd, *J* = 8.1, 1.7 Hz, 1H), 8.20 (d, *J* = 5.2 Hz, 1H), 7.88 (s, 1H), 7.48 (dd, *J* = 8.1, 4.7 Hz, 1H), 7.05 (dd, *J* = 5.2, 1.5 Hz, 1H), 6.84 (s, 1H), 4.13 (t, *J* = 6.8 Hz, 2H), 3.66 (s, 3H), 2.90 (t, *J* = 6.3 Hz, 2H), 1.56 (s, 9H), 1.39 (s, 9H). **^{13}C NMR** (101 MHz, $CDCl_3$) δ 162.73, 154.22, 154.13, 153.16, 151.80, 148.43, 148.08, 143.54, 141.70, 141.52, 134.56, 133.83, 123.65, 119.71, 117.78, 115.92, 110.22, 84.22, 83.01, 45.12, 33.02, 28.62, 28.23, 22.65. **TLC-MS:** ESI(+) calcd. for $[M+Na]^+$: *m/z* = 587.2; found: 587.2. **HPLC:** t_{ret} = 11.16 min (97.4% at 254 nm, 96.5% at 230 nm, method B).

tert-Butyl 2-(2-((tert-butoxycarbonyl)(3-nitropyridin-2-yl)amino)pyridin-4-yl)-1-methyl-4-oxo-1,4,6,7-tetrahydro-5H-pyrrolo[3,2-c]pyridine-5-carboxylate (164)

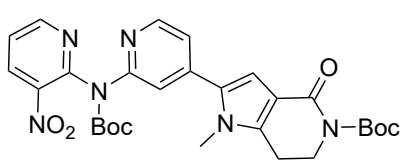

164

Chemical Formula: $C_{28}H_{32}N_6O_7$
Exact Mass: 564.23325
Molecular Weight: 564.59900

tert-Butyl 2-(2-((*tert*-butoxycarbonyl)amino)pyridin-4-yl)-1-methyl-4-oxo-1,4,6,7-tetrahydro-5*H*-pyrrolo[3,2-*c*]pyridine-5-carboxylate (**119**, 50.0 mg, 0.113 mmol, 1.00 eq.) was dissolved in DMF (dry, 2 mL) under an argon atmosphere and cooled to 0 °C. NaH (9.04 mg, 60% dispersion mineral oil, 0.226 mmol, 2.00 eq.) was added and the mixture stirred at rt for 1 h. 2-fluoro-3-nitropyridin (**162**, 44.6 µL, 64.2 mg,

0.452 mmol, 4.00 eq.) was added and the reaction stirred at rt for 3 days. After addition of sat. NH_4Cl solution (10 mL) the mixture was extracted with EtOAc (3x 15 mL). The combined organic layers were dried over Na_2SO_4 and the solvent removed under reduced pressure. The residue was purified by flash column chromatography (Silica gel, 20 – 100% hexane/EtOAc) and the product-containing fractions evaporated. A second purification step by flash column chromatography (Silica gel, 0 – 8% DCM/MeOH) afforded the product **164** as yellow solid, which was directly used in the next step (**157**).

tert-Butyl 2-(2-((tert-butoxycarbonyl)(6-fluoro-3-nitropyridin-2-yl)amino)pyridin-4-yl)-1-methyl-4-oxo-1,4,6,7-tetrahydro-5H-pyrrolo[3,2-c]pyridine-5-carboxylate (163)

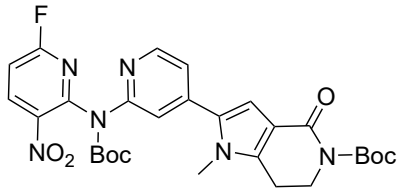

163

Chemical Formula: $C_{28}H_{32}N_6O_7$
Exact Mass: 564.23325
Molecular Weight: 564.59900

tert-Butyl 2-(2-((*tert*-butoxycarbonyl)amino)pyridin-4-yl)-1-methyl-4-oxo-1,4,6,7-tetrahydro-5*H*-pyrrolo[3,2-*c*]pyridine-5-carboxylate (**119**, 0.120 g, 0.271 mmol, 1.00 eq.) was dissolved in DMF (dry, 2 mL) under argon atmosphere and cooled to 0 °C. After NaH (60% dispersion in mineral oil, 32.5 mg, 0.814 mmol, 3.00 eq.) was added, the reaction was stirred at rt for 1 h. 2,6-Difluoro-3-nitropyridine (**161**, 0.112 mL, 0.174 g, 4.00 eq.) was added at 0 °C and the reaction stirred at rt for 18 h. The solvent was evaporated and the residue dissolved in DCM (10 mL) and washed with sat. NH_4Cl solution (10 mL). The aqueous layer was extracted with DCM (2x 10 mL). The combined organic layers were dried over Na_2SO_4 and the solvent removed under reduced pressure. The residue was purified by flash column chromatography (Silica gel, 0.5 – 3% DCM/MeOH). The product containing fractions were combined and the solvent evaporated. The raw product was purified by a second flash chromatography column (Silica gel, 1 - 10% DCM/THF) which afforded the product **163** (33.0 mg, 56.6 µmol, 21%) as yellow solid.

^{1}H NMR (400 MHz, $CDCl_3$) δ 8.52 (dd, *J* = 16.4, 7.3 Hz, 2H), 8.02 (d, *J* = 8.8 Hz, 1H), 7.30 (s, 2H), 6.86 (s, 1H), 4.14 (t, *J* = 6.2 Hz, 2H), 3.65 (s, 3H), 2.91 (t, *J* = 6.2 Hz, 2H), 1.56 (s, 9H), 1.44 (s, 9H). **^{13}C NMR** (101 MHz, $CDCl_3$) δ 162.29, 156.33 (d, *J* = 14.0 Hz), 153.97 (d, *J* = 252.2 Hz), 153.71, 153.30, 151.98, 149.55, 142.00, 141.45, 138.54, 132.83, 127.49 (d, *J* = 20.5 Hz), 122.13, 121.86, 115.86, 114.72 (d, *J* = 5.2 Hz), 110.16, 84.47, 82.83, 44.79, 32.63, 28.31, 28.09, 22.36. **TLC-MS:** ESI(+) calcd. for $[M+Na]^+$: *m/z* = 605.2; found: 604.8. **HPLC:** t_{ret} = 17.05 min (93.3% at 254 nm, 91.5% at 230 nm, method B).

2-(2-((6-Bromo-3-nitropyridin-2-yl)amino)pyridin-4-yl)-1-methyl-1,5,6,7-tetrahydro-4H-pyrrolo[3,2-c]pyridin-4-one (155)

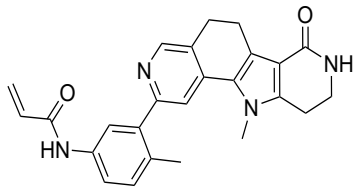

155

Chemical Formula: $C_{18}H_{15}BrN_6O_3$
Exact Mass: 442.03890
Molecular Weight: 443.26100

tert-Butyl 2-(2-((6-bromo-3-nitropyridin-2-yl)(tert-butoxycarbonyl)amino)pyridin-4-yl)-1-methyl-4-oxo-1,4,6,7-tetrahydro-5*H*-pyrrolo[3,2-*c*]pyridine-5-carboxylate (**160**, 28.0 mg, 43.5 µmol) was dissolved in DCM (dry, 3 mL) and subjected to GSP 7 and stirred for 30 min. The residue was dissolved in DCM (20 mL) and washed with sat. Na_2CO_3 solution (10 mL). The aqueous phase was extracted with DCM until the yellow color was removed. The combined organic extracts were dried over Na_2SO_4 and the solvent evaporated. The raw product was purified by flash column chromatography (Silica gel, 3 – 10% DCM/MeOH) which afforded the product **155** (12.0 mg, 27.4 µmol, 63%) as yellow powder.

^{1}H NMR (400 MHz, DMSO) δ 10.92 (s, 1H), 8.43 (d, *J* = 9.0 Hz, 1H), 8.33 (d, *J* = 5.3 Hz, 1H), 7.97 (d, *J* = 8.8 Hz, 1H), 7.77 (s, 1H), 7.21 (dd, *J* = 5.3, 1.5 Hz, 1H), 7.09 (s, 1H), 6.65 (s, 1H), 3.71 (s, 3H), 3.44 (td, *J* = 6.8, 2.4 Hz, 2H), 2.88 (t, *J* = 6.9 Hz, 2H). **^{13}C NMR** (101 MHz, DMSO) δ 164.57, 155.39, 152.84, 147.99, 141.13, 140.53, 137.71, 137.00, 132.96, 131.47, 116.79, 114.33, 110.50, 110.07, 107.85, 39.84, 32.78, 21.16. **HRMS:** ESI(+) calcd. for $[M+H]^+$: *m/z* = 443.04618; found: 443.04639; rel. deviation: 0.49 ppm. **HPLC:** t_{ret} = 13.13 min (96.5% at 254 nm, 96.5% at 230 nm, method B). **IR** (ATR) [cm^{-1}]: 3280, 2920, 2877, 1643, 1579, 1554, 1497, 1466, 1429, 1400, 1319, 1226, 1205, 1179, 1033, 890, 825, 808, 765, 656.

2-(2-((6-Fluoro-3-nitropyridin-2-yl)amino)pyridin-4-yl)-1-methyl-1,5,6,7-tetrahydro-4H-pyrrolo[3,2-c]pyridin-4-one (156)

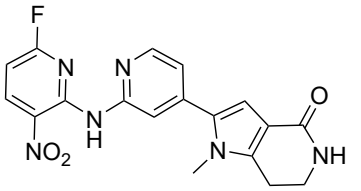

156

Chemical Formula: $C_{18}H_{15}FN_6O_3$
Exact Mass: 382.11897
Molecular Weight: 382.35540

tert-Butyl 2-(2-((*tert*-butoxycarbonyl)(6-fluoro-3-nitropyridin-2-yl)amino)pyridin-4-yl)-1-methyl-4-oxo-1,4,6,7-tetrahydro-5*H*-pyrrolo[3,2-*c*]pyridine-5-carboxylate (**163**, 33.0 mg, 56.6 µmol, 1.00 eq.) was dissolved in DCM (3 mL, dry) and subjected to GSP 7. After stirring for 30 min and the general workup, the residue was dissolved in DCM (5 mL) and washed with Na_2CO_3 solution (5 mL). The aqueous phase was extracted with DCM (5 mL) twice and the combined organic layers dried over Na_2SO_4. The solvent was removed under reduced pressure and the residue purified by flash column chromatography (Silica gel, 2 – 8% DCM/MeOH) which afforded the product **156** (9.0 mg, 23.5 µmol, 41%) as yellow solid.

^{1}H NMR (400 MHz, $CDCl_3$) δ 10.78 (s, 1H), 8.73 (dd, *J* = 8.8, 7.0 Hz, 1H), 8.44 (s, 1H), 8.39 (d, *J* = 5.2 Hz, 1H), 7.15 (dd, *J* = 5.2, 1.5 Hz, 1H), 6.89 (s, 1H), 6.52 (dd, *J* = 8.9, 3.7 Hz, 1H), 5.46 (s, 1H), 3.78 (s, 3H), 3.68 (td, *J* = 6.9, 2.4 Hz, 2H), 2.95 (t, *J* = 6.9 Hz, 2H). **^{13}C NMR** (101 MHz, DMSO) δ

164.56, 156.06 (d, *J* = 11.8 Hz), 154.75 (d, *J* = 241.5 Hz), 152.59, 148.08, 141.16, 140.58, 138.71, 131.43, 123.13 (d, *J* = 20.0 Hz), 117.09, 114.32, 111.00, 108.88 (d, *J* = 3.8 Hz), 107.86, 39.84, 32.62, 21.16. **HRMS:** ESI(+) calcd. for $[M+H]^+$: *m/z* = 383.12624; found: 383.12656; rel. deviation: 0.82 ppm. **HPLC:** t_{ret} = 10.291 min (96.7% at 254 nm, 98.0% at 230 nm, method B). **IR** (ATR) [cm^{-1}]: 3294, 3273, 3059, 2937, 2919, 2889, 1649, 1592, 1492, 1453, 1409, 1313, 1226, 1203, 1180, 1086, 886, 839, 811, 760, 690, 665.

1-Methyl-2-(2-((3-nitropyridin-2-yl)amino)pyridin-4-yl)-1,5,6,7-tetrahydro-4H-pyrrolo[3,2-c]pyridin-4-one (157)

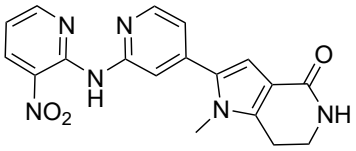

157
Chemical Formula: $C_{18}H_{16}N_6O_3$
Exact Mass: 364.12839
Molecular Weight: 364.36500

tert-Butyl 2-(2-((*tert*-butoxycarbonyl)(3-nitropyridin-2-yl)amino)pyridin-4-yl)-1-methyl-4-oxo-1,4,6,7-tetrahydro-5*H*-pyrrolo[3,2-*c*]pyridine-5-carboxylate (**164**) was dissolved in DCM (dry, 2 mL) and subjected to GSP 7 and stirred for 30 min. The residue was dissolved in DCM (10 mL) and washed with sat. Na_2CO_3 solution (10 mL). The organic layer was dried over Na_2SO_4 and the solvent removed under reduced pressure. The residue was purified by flash column chromatography (Silica gel, 5 – 10% DCM/MeOH) which afforded the product **157** (9.00 mg, 24.9 µmol, 22% over 2 steps) as yellow solid.

^{1}H NMR (400 MHz, DMSO) δ 10.39 (s, 1H), 8.68 (dd, *J* = 4.6, 1.6 Hz, 1H), 8.61 (dd, *J* = 8.3, 1.6 Hz, 1H), 8.37 (s, 1H), 8.31 (d, *J* = 5.2 Hz, 1H), 7.23 (d, *J* = 5.2 Hz, 1H), 7.17 (dd, *J* = 8.3, 4.5 Hz, 1H), 7.09 (s, 1H), 6.64 (s, 1H), 3.69 (s, 3H), 3.44 (dd, *J* = 6.9, 4.7 Hz, 2H), 2.88 (t, *J* = 6.9 Hz, 2H). **HRMS:** ESI(+) calcd. for $[M+H]^+$: *m/z* = 365.13566; found: 365.13576; rel. deviation: 0.27 ppm. **HPLC:** t_{ret} = 6.25 min (97.2% at 254 nm, 95.5% at 230 nm, method B). **IR** (ATR) [cm^{-1}]: 3334, 3314, 1642, 1577, 1497, 1402, 1374, 1355, 1296, 1231, 1196, 1148, 1087, 1046, 991, 876, 841, 821, 758, 706, 651.

1-Methyl-2-(2-((6-(methylthio)-3-nitropyridin-2-yl)amino)pyridin-4-yl)-1,5,6,7-tetrahydro-4H-pyrrolo[3,2-c]pyridin-4-one (165)

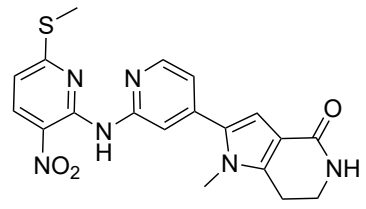

165
Chemical Formula: $C_{18}H_{15}BrN_6O_3$
Exact Mass: 442.03890
Molecular Weight: 443.26100

Following an analogous procedure as described by MAUREL *et al.*,[267] 2-(2-((6-Chloro-3-nitropyridin-2-yl)amino)pyridin-4-yl)-1-methyl-1,5,6,7-tetrahydro-4H-pyrrolo[3,2-c]pyridin-4-one (**110**, 50.0 mg, 0.125 mmol, 1.00 eq.) and $NaSCH_3$ (22.0 mg, 0.313 mmol, 2.50 eq.) were dissolved in DMF (2 mL, dry) and stirred at rt for 18 h. After the reaction was completed, the mixture was poured into water (10 mL) and extracted with EtOAc (10 mL). The organic layer was washed with water (10 mL) and brine (10 mL) and dried over Na_2SO_2. The solvent was removed under reduced pressure and the residue purified by flash column chromatography (Silica gel, 2 – 10% DCM/MeOH) which afforded the product **165** (29.0 mg, 71.3 µmol, 57%) as yellow solid.

^{1}H NMR (400 MHz, DMSO) δ 10.67 (s, 1H), 8.47 – 8.37 (m, 2H), 8.35 (d, J = 5.2 Hz, 1H), 7.27 (dd, J = 5.2, 1.3 Hz, 1H), 7.08 (s, 1H), 7.03 (d, J = 8.9 Hz, 1H), 6.65 (s, 1H), 3.69 (s, 3H), 3.48 – 3.38 (m, 2H), 2.88 (t, J = 6.9 Hz, 2H), 2.59 (s, 3H). **^{13}C NMR** (101 MHz, DMSO) δ 168.61, 164.56, 151.69, 148.44, 147.34, 141.31, 140.41, 135.14, 131.71, 126.08, 117.80, 114.38, 112.42, 112.12, 107.74, 39.84, 32.66, 21.15, 13.78. **TLC-MS:** ESI(+) calcd. for $[M+Na]^+$: *m/z* = 433.1; found: 432.9; ESI(-) calcd. for $[M-H]^-$: *m/z* = 409.1; found: 409.1. **HPLC:** t_{ret} = 14.14 min (99.2% at 254 nm, 96.1% at 230 nm, method B).

1-Methyl-2-(2-((6-(methylsulfonyl)-3-nitropyridin-2-yl)amino)pyridin-4-yl)-1,5,6,7-tetrahydro-4H-pyrrolo[3,2-c]pyridin-4-one (166)

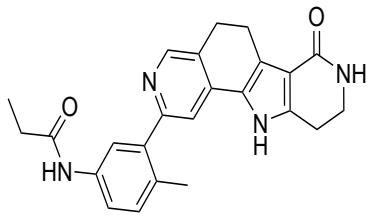

166
Chemical Formula: $C_{19}H_{18}N_6O_5S$
Exact Mass: 442,10594
Molecular Weight: 442.45000

1-Methyl-2-(2-((6-(methylthio)-3-nitropyridin-2-yl)amino)pyridin-4-yl)-1,5,6,7-tetrahydro-4H-pyrrolo[3,2-c]pyridin-4-one (**165**, 29.0 mg, 71.3 µmol, 1.00 eq.) was dissolved in DCM (1.5 mL, dry) under an argon atmosphere and cooled to 0 °C. After the addition of mPa (36.7 mg, 0.212 mmol, 3.00 eq.), the reaction as allowed to warm up to rt and stirred for 3 h. The mixture was then poured into $NaHCO_3$ solution (10 mL) and the layers separated. The aqueous layer was extracted with DCM (10 mL) twice and the combined organics dried over Na_2SO_4. After the removal of the solvent the residue was purified by flash column chromatography (Silica gel, 3 – 10% DCM/MeOH) which afforded the product **166** (1.0 mg, 3%) as orange solid.

^{1}H NMR (400 MHz, $CDCl_3$) δ 10.72 (s, 1H), 8.84 (d, J = 8.4 Hz, 1H), 8.47 (s, 1H), 8.40 (d, J = 5.3 Hz, 1H), 7.69 (d, J = 8.3 Hz, 1H), 7.19 (d, J = 4.0 Hz, 1H), 6.87 (s, 1H), 5.43 (s, 1H), 3.74 (s, 3H), 3.70 – 3.64 (m, 2H), 3.14 (d, J = 7.8 Hz, 3H), 2.95 (t, J = 6.8 Hz, 2H). **^{13}C NMR** (101 MHz, $CDCl_3$) δ 166.16, 160.39, 155.64, 155.35, 151.23, 148.82, 148.28, 142.54, 138.64, 119.55, 112.71, 112.17, 109.20, 40.96, 40.91, 32.89, 22.01. **HRMS:** ESI(+) calcd. for $[M+Na]^+$: *m/z* = 465.09516; found: 465.09519; rel. deviation: 0.07 ppm. **HPLC:** t_{ret} = 4.73 min (97.3% at 254 nm, 95.0% at 230 nm, method A).

6.2.10 Synthesis of compounds described in Section 3.3.2.2

2-(Benzyloxy)-4-bromopyridine (169)

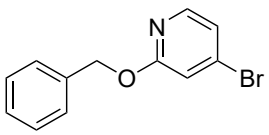

169
Chemical Formula: $C_{12}H_{10}BrNO$
Exact Mass: 262.99458
Molecular Weight: 264.12200

2-(Benzyloxy)-4-bromopyridine (**169**) was synthesized as described in the patent literature [281]. 4-Bromo-2-fluoropyridine (**168**, 1.73 mL, 3.00 g, 17.2 mmol, 1.00 eq.) and benzyl alcohol (1.79 mL, 1.86 g, 17.2 mmol, 1.00 eq.) were dissolved in THF (dry, 25 mL) under argon atmosphere. The reaction mixture was cooled to 0 °C in an ice bath and potassium *tert*-butoxide (1.93 g, 17.2 mmol, 1.00 eq.) was added in small portions to the stirred solution while cooling was maintained. The reaction was slowly warmed to rt and stirred for 18 h. After

adding water (2 mL) to the reaction, the organic solvent was removed under reduced pressure. The residue was diluted with water (20 mL) and extracted with hexane (4x 20 mL). The combined organic layers were dried over Na_2SO_4 and evaporated to dryness to isolate the product **169** (4.31 g, 16.4 mmol, 95%) as colorless oil.

^{1}H NMR (400 MHz, $CDCl_3$) δ 8.00 (d, *J* = 5.5 Hz, 1H), 7.44 (d, *J* = 7.3 Hz, 2H), 7.41 – 7.29 (m, 3H), 7.04 (dd, *J* = 5.5, 1.6 Hz, 1H), 7.02 (d, *J* = 1.0 Hz, 1H), 5.38 (s, 2H). **^{13}C NMR** (101 MHz, $CDCl_3$) δ 164.37, 147.56, 137.00, 134.04, 128.64, 128.12, 120.64, 114.68, 68.18. **HPLC:** t_{ret} = 18.69 min (92.8% at 254 nm, 93.4% at 230 nm, method B).

2-(Benzyloxy)-4-(4,4,5,5-tetramethyl-1,3,2-dioxaborolan-2-yl)pyridine (170)

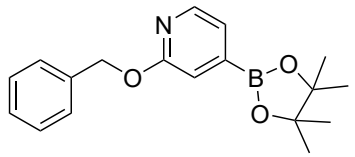

170
Chemical Formula: $C_{12}H_{10}BrNO$
Exact Mass: 262.99458
Molecular Weight: 264.12200

2-(Benzyloxy)-4-bromopyridine (**169**, 1.60 g, 6.06 mmol, 1.00 eq.), bis(pinacolato)diboron (1.62 g, 6.36 mmol, 1.05 eq.) and potassium acetate (1.78 g, 18.17 mmol, 3.00 eq.) were suspended in 1,4-dioxane (dry, 60 mL) and argon bubbled through the mixture. XPhos Pd g4 (5.21 mg, 60.6 µmol, 10 mol%) was then added and the reaction was stirred at 90 °C for 18 h. After cooling to rt, the reaction was diluted with EtOAc and filtered through a pad of celite. The solvent was removed under reduced pressure and the residue purified by flash column chromatography (Silica gel, 0 – 70% hexane/EtOAc) which afforded the product **170** (1.35 g, 4.30 mmol, 71%) as white solid.

^{1}H NMR (400 MHz, $CDCl_3$) δ 8.19 (d, *J* = 4.9 Hz, 1H), 7.45 (d, *J* = 7.1 Hz, 2H), 7.39 – 7.27 (m, 3H), 7.23 – 7.18 (m, 2H), 5.38 (s, 2H), 1.34 (s, 12H). **^{13}C NMR** (101 MHz, $CDCl_3$) δ 163.54, 146.43, 137.73, 128.52, 127.83, 127.77, 121.56, 117.21, 84.55, 67.48, 24.99. **TLC-MS:** ESI(+) calcd. for $[M+Na]^+$: *m/z* = 334.2; found: 334.3. **HPLC:** t_{ret} = 14.19 min (86.7% at 254 nm, 88.2% at 230 nm, method B, unstable under column conditions).

tert-Butyl 2-(2-(benzyloxy)pyridin-4-yl)-1-methyl-4-oxo-1,4,6,7-tetrahydro-5H-pyrrolo[3,2-c]pyridine-5-carboxylate (171)

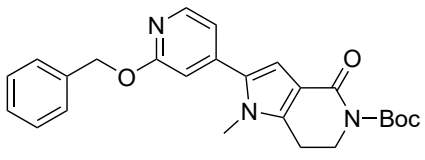

171
Chemical Formula: $C_{25}H_{27}N_3O_4$
Exact Mass: 433.20016
Molecular Weight: 433.50800

tert-Butyl 2-bromo-1-methyl-4-oxo-1,4,6,7-tetrahydro-5*H*-pyrrolo[3,2-*c*]pyridine-5-carboxylate (**124**, 0.400 g, 1.22 mmol, 1.00 eq.) and 2-(Benzyloxy)-4-(4,4,5,5-tetramethyl-1,3,2-dioxaborolan-2-yl)pyridine (**170**, 0.416 g, 1.34 mmol, 1.10 eq.) were weighed into a flask and purged with argon before 1,4-dioxane (degassed, 12 mL) was added. XPhos Pd g4 (31.4 mg, 36.5 µmol, 3 mol%) and 2M Na_2CO_3 solution (degassed, 1.82 mL, 3.65 mmol, 3.00 eq.) were added and the reaction stirred at 90 °C for 18 h. Another portion of 2-(Benzyloxy)-4-(4,4,5,5-tetramethyl-1,3,2-dioxaborolan-2-yl)pyridine (**170**, 37.8 mg, 0.122 mmol, 0.10 eq.) and XPhos Pd g4 (10.5 mg, 12.2 µmol, 1 mol%) were added and the

reaction stirred for 5 h at 90 °C. After cooling to rt, the mixture was diluted with EtOAc (30 mL) and filtered through a pad of celite. The solution was washed with sat. NH_4Cl solution, water and brine (30 mL) and the organic layer dried over Na_2SO_4 and the solvent removed. The residue was purified by flash column chromatography (Silica gel, 30 – 80% hexane/EtOAc) which afforded the product **171** (0.170 g, 0.389 mmol, 32%) as white solid.

^{1}H NMR (400 MHz, $CDCl_3$) δ 8.18 (dd, *J* = 5.3, 0.5 Hz, 1H), 7.47 (dd, *J* = 7.8, 0.8 Hz, 2H), 7.42 – 7.28 (m, 3H), 6.89 (dd, *J* = 5.3, 1.5 Hz, 1H), 6.80 – 6.75 (m, 2H), 5.40 (s, 2H), 4.12 (t, *J* = 6.3 Hz, 2H), 3.57 (s, 3H), 2.87 (t, *J* = 6.3 Hz, 2H), 1.55 (s, 9H), 1.23 (s, 2H). **^{13}C NMR** (101 MHz, $CDCl_3$) δ 164.14, 162.40, 153.77, 147.30, 142.20, 140.89, 137.21, 133.60, 128.59, 128.15, 128.03, 116.57, 115.44, 109.55, 109.44, 82.64, 75.06, 67.95, 44.75, 32.53, 28.27, 24.93, 22.27. **TLC-MS:** ESI(+) calcd. for $[M+Na]^+$: *m/z* = 456.2; found: 456.1. **HPLC:** t_{ret} = 17.82 min (98.8% at 254 nm, 98.7% at 230 nm, method B).

tert-Butyl 1-methyl-4-oxo-2-(2-oxo-1,2-dihydropyridin-4-yl)-1,4,6,7-tetrahydro-5H-pyrrolo[3,2-c]pyridine-5-carboxylate (167)

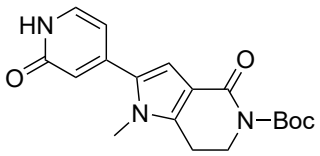

167
Chemical Formula: $C_{18}H_{21}N_3O_4$
Exact Mass: 343,15321
Molecular Weight: 343,3830

tert-Butyl 2-(2-(benzyloxy)pyridin-4-yl)-1-methyl-4-oxo-1,4,6,7-tetrahydro-5*H*-pyrrolo[3,2-*c*]pyridine-5-carboxylate (**171**, 0.264 g, 0.609 mmol, 1.00 eq.) was dissolved in ethanol (5 mL) and palladium on charcoal (10% w/t, 26.4 mg, 10% m/m). Hydrogen was bubbled through the mixture for 2 h. After conversion was completed, the mixture was filtered through a pad of celite and the filter rinsed with EtOAc and DCM (20 mL). The solution was evaporated to dryness which afforded the product **167** (0.200 mg, 0.585 mmol, 96%) as white powder.

^{1}H NMR (400 MHz, DMSO) δ 11.55 (s, 1H), 7.39 (d, *J* = 6.8 Hz, 1H), 6.69 (s, 1H), 6.36 (d, *J* = 1.4 Hz, 1H), 6.32 (dd, *J* = 6.8, 1.8 Hz, 1H), 3.96 (t, *J* = 6.3 Hz, 2H), 3.60 (s, 3H), 2.93 (t, *J* = 6.3 Hz, 2H), 1.46 (s, 9H). **^{13}C NMR** (101 MHz, DMSO) δ 162.40, 161.56, 153.03, 143.29, 142.67, 135.40, 132.70, 116.31, 113.96, 108.82, 105.13, 81.37, 44.71, 32.81, 27.84, 21.58. **TLC-MS:** ESI(+) calcd. for $[M+H]^+$: *m/z* = 366.2; found: 365.9; ESI(-) calcd. for $[M-H]^-$: *m/z* = 342.2; found: 341.9. **HPLC:** t_{ret} = 8.45 min (96.2% at 254 nm, 99.5% at 230 nm, method B).

tert-Butyl 1-methyl-2-(2-((3-nitropyridin-2-yl)oxy)pyridin-4-yl)-4-oxo-1,4,6,7-tetrahydro-5H-pyrrolo[3,2-c]pyridine-5-carboxylate (179A)/ tert-Butyl 1-methyl-2-(3'-nitro-2-oxo-2H-[1,2'-bipyridin]-4-yl)-4-oxo-1,4,6,7-tetrahydro-5H-pyrrolo[3,2-c]pyridine-5-carboxylate (179B)

I) *tert*-Butyl 1-methyl-4-oxo-2-(2-oxo-1,2-dihydropyridin-4-yl)-1,4,6,7-tetrahydro-5*H*-pyrrolo[3,2-*c*]pyridine-5-carboxylate (**167**, 20.0 mg, 34.9 µmol, 1.00 eq.), 2-fluoro-3-nitropyridine (**162**, 6.00 mg, 41.9 µmol, 1.20 eq.) and K_2CO_3 (5.8 mg, 41.9 µmol, 1.20 eq.) were dissolved in THF (0.5 mL) and DMSO (0.5 mL) and stirred at 40 °C for 18 h. After complete conversion the mixture was diluted with EtOAc (10 mL) and washed with water (10 mL). The organic layer was dried over Na_2SO_4 and the solvent was evaporated. The residue was combined with **II** and purified by flash column (Silica gel, 50 – 100% hexane/EtOAc, method continued with pure EtOAc additional 5 minutes) which afforded two main fractions.

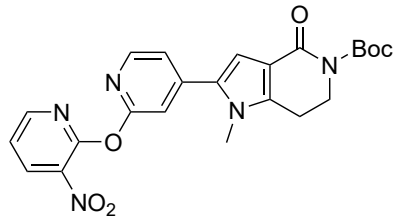

179A

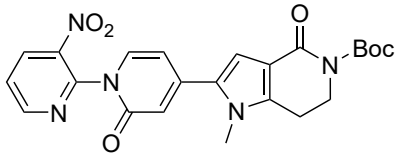

179B

Chemical Formula: $C_{23}H_{23}N_5O_6$
Exact Mass: 465.16483
Molecular Weight: 465.46600

II) *tert*-Butyl 1-methyl-4-oxo-2-(2-oxo-1,2-dihydropyridin-4-yl)-1,4,6,7-tetrahydro-5*H*-pyrrolo[3,2-*c*]pyridine-5-carboxylate (**167**, 20.0 mg, 34.9 µmol, 1.00 eq.), 2-fluoro-3-nitropyridine (**162**, 6.00 mg, 41.9 µmol, 1.20 eq.) and Ag_2CO_3 (11.6 mg, 41.9 µmol, 1.20 eq.) were dissolved in DMF (1.0 mL) and stirred at 60 °C for 18 h. The mixture was diluted with EtOAc (10 mL) and washed with water (10 mL). The organic layer was dried over Na_2SO_4 and the solvent was evaporated. The residue was combined with **I** and purified as explained above.

Fraction **1**: **^{1}H NMR** (400 MHz, $CDCl_3$) δ 8.54 (dd, *J* = 4.8, 1.8 Hz, 1H), 8.46 (dd, *J* = 8.0, 1.8 Hz, 1H), 8.22 (d, *J* = 5.2 Hz, 1H), 7.35 (dd, *J* = 8.0, 4.8 Hz, 1H), 7.16 (dd, *J* = 5.2, 1.4 Hz, 1H), 7.13 (s, 1H), 6.89 (s, 1H), 4.15 (t, *J* = 6.3 Hz, 2H), 3.66 (s, 3H), 2.91 (d, *J* = 6.3 Hz, 2H), 1.56 (s, 9H). **^{13}C NMR** (101 MHz, $CDCl_3$) δ 162.28, 161.63, 154.10, 153.77, 152.52, 148.21, 143.74, 141.48, 136.95, 135.71, 132.87, 120.91, 119.79, 115.83, 111.92, 110.43, 82.81, 44.76, 32.75, 28.32, 22.36. **TLC-MS:** ESI(+) calcd. for $[M+Na]^+$: *m/z* = 488.2; found: 488.0. **HPLC:** t_{ret} = 10.344 min (95.5% at 254 nm, method C). **IR** (ATR) [cm^{-1}]: 2976, 2923, 2855, 1696, 1591, 1528, 1491, 1425, 1388, 1346, 1308, 1277, 1229, 1197, 1141, 1029, 993, 944, 923, 861, 815, 763, 731, 669.

Fraction **2**: **^{1}H NMR** (400 MHz, $CDCl_3$) δ 8.79 (dd, *J* = 4.8, 1.6 Hz, 1H), 8.41 (dd, *J* = 8.1, 1.6 Hz, 1H), 7.83 – 7.74 (m, 1H), 7.59 (dd, *J* = 8.1, 4.8 Hz, 1H), 6.99 (s, 1H), 6.51 (d, *J* = 6.7 Hz, 2H), 4.16 – 4.11 (m, 2H), 3.70 (s, 3H), 2.91 (t, *J* = 6.3 Hz, 2H), 1.56 (s, 9H). **^{13}C NMR** (101 MHz, $CDCl_3$) δ 162.16, 161.14, 153.65, 152.34, 144.20, 144.00, 142.67, 142.64, 135.10, 133.72, 132.19, 124.33, 115.98, 115.73, 111.73, 107.71, 82.89, 44.68, 33.38, 28.31, 22.41. **TLC-MS:** ESI(+) calcd. for $[M+Na]^+$: *m/z* = 488.2; found: 488.0. **HPLC:** t_{ret} = 9.358 min (93.8% at 254 nm, method C); t_{ret} = 12.682 min (93.7% at 254

nm, method B). **IR** (ATR) [cm^{-1}]: 3082, 2973, 2923, 2850, 1701, 1654, 1608, 1586, 1534, 1507, 1429, 1358, 1306, 1228, 1141, 1059, 1028, 946, 918, 855, 818, 763, 721, 700, 668.

tert-Butyl 2-(2-((2-chloro-5-fluoropyrimidin-4-yl)oxy)pyridin-4-yl)-1-methyl-4-oxo-1,4,6,7-tetrahydro-5H-pyrrolo[3,2-c]pyridine-5-carboxylate/ tert-butyl 2-(1-(2-chloro-5-fluoropyrimidin-4-yl)-2-oxo-1,2-dihydropyridin-4-yl)-1-methyl-4-oxo-1,4,6,7-tetrahydro-5H-pyrrolo[3,2-c]pyridine-5-carboxylate (180)

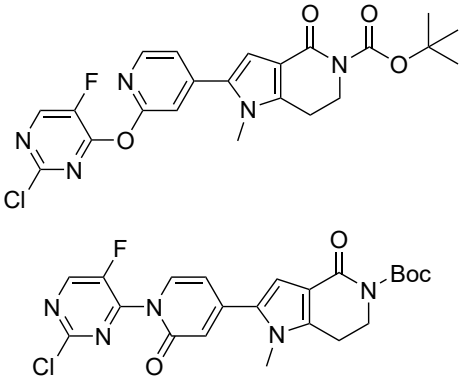

180

Chemical Formula: $C_{22}H_{21}ClFN_5O_4$
Exact Mass: 473.12661
Molecular Weight: 473.88940

tert-Butyl 1-methyl-4-oxo-2-(2-oxo-1,2-dihydropyridin-4-yl)-1,4,6,7-tetrahydro-5*H*-pyrrolo[3,2-*c*]pyridine-5-carboxylate (**167**, 50.0 mg, 0.146 mmol, 1.00 eq.) and Ag_2CO_3 (24.1 mg, 87.4 µmol, 0.60 eq.) were dissolved under an argon atmosphere in DMF (dry, 5 mL)and stirred for 30 min. 2,4-Dichloro-5-fluoropyrimidine (18.2 µL, 29.2 mg, 0.175 mmol, 1.20 eq.) and stirred at 90 °C for 18 h. The reaction was heated up to 100 °C and stirred for 5 h. Another portion of 2,4-Dichloro-5-fluoropyrimidine (**174**, 9.10 µL, 14.7 mg, 87.4 µmol, 0.60 eq.) and Ag_2CO_3 (12.1 mg, 43.7 µmol, 0.30 eq.) were added and the reaction stirred at 100 °C for 18 h. After cooling to rt, sat. NH_4Cl solution (20 mL) was added and extracted with DCM (3x 20 mL). The organic layer was dried over Na_2SO_4 and the solvent evaporated. The residue was purified by flash column chromatography (Silica gel, 1 – 8% DCM/MeOH) which afforded the product **180** (35.0 mg, 58.9µmol, 40%) as white solid. The obtained regio isomer could not be identified, for detailed discussion see section 3.3.2.2.

^{1}H NMR (400 MHz, $CDCl_3$) δ 8.46 (d, *J* = 1.7 Hz, 1H), 8.33 (d, *J* = 5.2 Hz, 1H), 7.26 (dd, *J* = 5.2, 1.4 Hz, 1H), 7.14 (s, 1H), 6.90 (s, 1H), 4.15 (t, *J* = 6.3 Hz, 2H), 3.67 (s, 3H), 2.92 (t, *J* = 6.3 Hz, 2H), 1.56 (s, 9H). **^{13}C NMR** (101 MHz, $CDCl_3$) δ 161.90, 159.28, 157.32 (d, *J* = 11.8 Hz), 153.41, 148.39, 146.90 (d, *J* = 20.6 Hz), 146.67 (d, *J* = 266.8 Hz), 143.53, 141.36, 132.24, 120.63, 115.63, 112.24, 110.32, 82.56, 44.42, 32.45, 27.99, 22.05. **TLC-MS:** ESI(+) calcd. for $[M+H]^+$: *m/z* = 496.1; found: 496.2. **HPLC:** t_{ret} = 10.65 min (98.6% at 254 nm, 96.0% at 230 nm, method C). **IR** (ATR) [cm^{-1}]: 2920, 2850, 1701, 1606, 1573, 1424, 1388, 1365, 1340, 1307, 1237, 1197, 1141, 1030, 946, 899, 849, 759, 673.

2-(2-((2-Chloro-5-fluoropyrimidin-4-yl)oxy)pyridin-4-yl)-1-methyl-1,5,6,7-tetrahydro-4H-pyrrolo[3,2-c]pyridin-4-one/ 2-(1-(2-chloro-5-fluoropyrimidin-4-yl)-2-oxo-1,2-dihydropyridin-4-yl)-1-methyl-1,5,6,7-tetrahydro-4H-pyrrolo[3,2-c]pyridin-4-one (181)

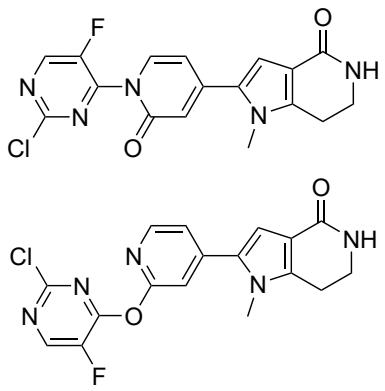

181
Chemical Formula: $C_{17}H_{13}ClFN_5O_2$
Exact Mass: 373.07418
Molecular Weight: 373.77240

tert-Butyl 2-(2-((2-chloro-5-fluoropyrimidin-4-yl)oxy)pyridin-4-yl)-1-methyl-4-oxo-1,4,6,7-tetrahydro-5*H*-pyrrolo[3,2-*c*]pyridine-5-carboxylate/ tert-butyl 2-(1-(2-chloro-5-fluoropyrimidin-4-yl)-2-oxo-1,2-dihydropyridin-4-yl)-1-methyl-4-oxo-1,4,6,7-tetrahydro-5*H*-pyrrolo[3,2-*c*]pyridine-5-carboxylate (**180**, 35.0 mg, 73.9 µmol, 1.00 eq.) was dissolved in DCM (dry, 3 mL) and subjected to GSP 7. After stirring for 30 min and the described work-up, the residue was dissolved in a mixture of DCM with 5% MeOH (10 mL). The solution was washed with sat. Na_2CO_3 solution (10 mL) and the aqueous layer extracted with DCM (2x 10 mL). The combined organic layers were dried over Na_2SO_4 and the solvent removed under reduced pressure. The crude product was purified by flash column chromatography (Silica gel, 3 – 10% DCM/MeOH) which afforded the product **181** (15.0 mg, 39.9 µmol, 54%) as off-white solid. The final regio isomer could not be identified, for detailed discussion see section 3.3.2.2.

^{1}H NMR (400 MHz, $CDCl_3$) δ 8.45 (d, *J* = 1.8 Hz, 1H), 8.31 (d, *J* = 5.2 Hz, 1H), 7.27 – 7.24 (m, 1H), 7.15 (s, 1H), 6.86 (s, 1H), 6.12 (s, 1H), 3.68 (s, 3H), 3.65 (d, *J* = 6.8 Hz, 2H), 2.91 (t, *J* = 6.9 Hz, 2H). **^{13}C NMR** (101 MHz, $CDCl_3$) δ 166.49, 159.90, 157.99 (d, *J* = 11.7 Hz), 154.00 (d, *J* = 4.9 Hz), 148.92, 147.48 (d, *J* = 20.6 Hz), 147.30 (d, *J* = 266.7 Hz), 144.45, 140.68, 132.14, 121.16, 115.11, 112.66, 109.80, 41.12, 33.14, 22.26. **HRMS:** ESI(+) calcd. for $[M+Na]^+$: *m/z* = 396.06340; found: 396.06408; rel. deviation: 1.72 ppm. **HPLC:** t_{ret} = 10.49 min (98.4% at 254 nm, 98.8% at 230 nm, method B). **IR** (ATR) [cm^{-1}]: 3200, 3049, 1650, 1605, 1580, 1543, 1503, 1466, 1430, 1400, 1339, 1232, 1210, 1177, 1159, 1117, 959, 890, 813, 767, 688, 671.

6.2.11 Synthesis of Compounds described in Section 3.3.2.3

2-Fluoro-4-(4,4,5,5-tetramethyl-1,3,2-dioxaborolan-2-yl)pyridine (182)

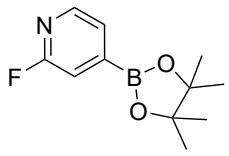

182
Chemical Formula: $C_{11}H_{15}BFNO_2$
Exact Mass: 223.11799
Molecular Weight: 223.05440

4-Bromo-2-fluoropyridine (**168**, 0.585 mL, 1.00 g, 5.68 mmol, 1.00 eq.), bis(pinacolato)diboron (1.59 g, 6.25 mmol, 1.10 eq.), potassium acetate (1.67 g, 17.05 mmol, 3.00 eq.) and Pd(dppf)Cl_2·CH_2Cl_2 were weighed into a round bottom flask and purged with argon. 1,4-dioxane (degassed, dry, 40 mL) was added and the reaction stirred at 90 °C for 18 h. After cooling down to rt, the mixture was filtered through a pad of celite and the solvent evaporated. The residue was purified by flash column chromatography (silica gel, 0 – 50% hexane/EtOAc) which afforded the product **182** (0.871 g, 3.92 mmol, 69%) as white solid.

^{1}H NMR (400 MHz, $CDCl_3$) δ 7.98 (d, *J* = 4.7 Hz, 1H), 7.28 – 7.23 (m, 1H), 7.02 (d, *J* = 2.0 Hz, 1H), 1.10 (s, 12H). **^{13}C NMR** (101 MHz, $CDCl_3$) δ 163.33 (d, *J* = 240.1 Hz), 146.89 (d, *J* = 13.5 Hz), 125.85 (d, *J* = 4.1 Hz), 114.39 (d, *J* = 35.1 Hz), 84.53, 24.50. **HPLC:** t_{ret} = 6.42 min (99.3% at 254 nm, 99.3% at 230 nm, method B).

tert-Butyl 2-(2-fluoropyridin-4-yl)-1-methyl-4-oxo-1,4,6,7-tetrahydro-5H-pyrrolo[3,2-c]pyridine-5-carboxylate (183)

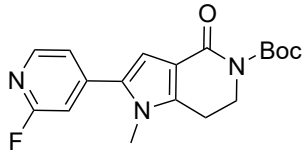

183
Chemical Formula: $C_{18}H_{20}FN_3O_3$
Exact Mass: 345.14887
Molecular Weight: 345.37440

tert-Butyl 2-bromo-1-methyl-4-oxo-1,4,6,7-tetrahydro-5*H*-pyrrolo[3,2-*c*]pyridine-5-carboxylate (**124**, 0.200 g, 0.608 mmol, 1.00 eq.), 2-fluoro-4-(4,4,5,5-tetramethyl-1,3,2-dioxaborolan-2-yl)pyridine (**182**, 0.149 g, 0.668 mmol, 1.10 eq.) and XPhos Pd g4 (26.1 mg, 30.4 µmol, 5 mol%) were weighed into a flask and purged with argon. The solids were dissolved in 1,4-dioxane (degassed, 6 mL) and a 2 M Na_2CO_3 solution (0.911 mL, 1.82 mmol, 3.00 eq.) was added and the reaction stirred at 90 °C for 18 h. After cooling to rt the reaction was diluted with EtOAc (30 mL) and filtered through a pad of celite. The solution was washed with sat. NH_4Cl solution, water and brine (30 mL). The organic layer was dried over Na_2SO_4 and the solvent evaporated. The residue was purified by flash column chromatography (Silica gel, 10 – 100% hexane/EtOAc) which afforded the product **183** (91.6 mg, 0.212 mmol, 35%) as white powder.

^{1}H NMR (400 MHz, $CDCl_3$) δ 8.22 (d, *J* = 5.3 Hz, 1H), 7.17 (dt, *J* = 5.2, 1.6 Hz, 1H), 6.89 (s, 1H), 6.84 (s, 1H), 4.13 (t, *J* = 6.3 Hz, 2H), 3.63 (s, 3H), 2.90 (t, *J* = 6.3 Hz, 2H), 1.54 (s, 9H). **^{13}C NMR** (101 MHz, $CDCl_3$) δ 164.29 (d, *J* = 238.6 Hz), 162.21, 153.69, 148.19 (d, *J* = 15.8 Hz), 144.79 (d, *J* = 8.6 Hz), 141.60, 132.47 (d, *J* = 3.7 Hz), 120.27 (d, *J* = 4.0 Hz), 115.88, 110.59, 107.67 (d, *J* = 38.5 Hz), 82.86,

44.73, 32.70, 28.30, 22.33. **TLC-MS:** ESI(+) calcd. for $[M+Na]^+$: *m/z* = 368.1; found: 368.0. **HPLC:** t_{ret} = 13.42 min (99.4% at 254 nm, 99.4% at 230 nm, method B).

2-(2-(Butylthio)pyridin-4-yl)-1,5,6,7-tetrahydro-4H-pyrrolo[3,2-c]pyridin-4-one (187)

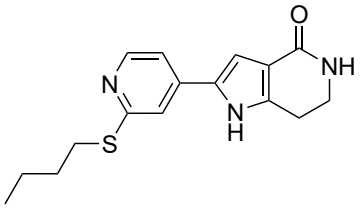

187
Chemical Formula: $C_{16}H_{19}N_3OS$
Exact Mass: 301.12488
Molecular Weight: 301.40800

tert-Butyl 2-(2-chloropyridin-4-yl)-4-oxo-1,4,6,7-tetrahydro-5*H*-pyrrolo[3,2-*c*]pyridine-5-carboxylate (**116**, 22.0 mg, 63.4 µmol, 1.00 eq.) and thiourea (14.5 mg, 0.190 mmol, 3.00 eq.) were dissolved in *n*-butanol (5 mL) and three drops of HCl (in dioxane) were added. The reaction was heated to 100 °C for 18 h. After cooling to rt, the solvent was evaporated and the residue purified by flash column chromatography (Silica gel, 3 – 10% DCM/MeOH). The product **187** was isolated for identification.

^{1}H NMR (400 MHz, $CDCl_3$) δ 9.89 (s, 1H), 8.34 – 8.23 (m, 1H), 7.27 (s, 1H), 7.08 (dd, *J* = 5.4, 1.7 Hz, 1H), 7.00 (d, *J* = 2.5 Hz, 1H), 5.58 (d, *J* = 2.8 Hz, 1H), 3.62 (td, *J* = 6.9, 2.5 Hz, 2H), 3.20 – 3.12 (m, 2H), 2.98 (t, *J* = 6.9 Hz, 2H), 1.75 – 1.59 (m, 2H), 1.45 (dw, *J* = 14.6, 7.3 Hz, 2H), 0.92 (t, *J* = 7.3 Hz, 3H). **TLC-MS:** ESI(+) calcd. for $[M+H]^+$: *m/z* = 302.1; found: 302.2; **HPLC:** t_{ret} = 9.435 min (95.3% at 254 nm, method C).

2-(2-(tert-Butylthio)pyridin-4-yl)-1,5,6,7-tetrahydro-4H-pyrrolo[3,2-c]pyridin-4-one (188)

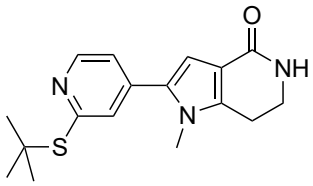

188
Chemical Formula: $C_{17}H_{21}N_3OS$
Exact Mass: 315.14053
Molecular Weight: 315.43500

tert-Butyl 2-(2-fluoropyridin-4-yl)-1-methyl-4-oxo-1,4,6,7-tetrahydro-5*H*-pyrrolo[3,2-*c*]pyridine-5-carboxylate (**183**, 25.0 mg, 72.4 µmol, 1.00 eq.) and thiourea (11.0 mg, 0.145 mmol, 2.00 eq.) were dissolved in *tert*-butanol (1.0 mL). After adding HCl (in dioxane, 0.1 mL), the reaction as heated to 120 °C in a pressure tube for 18 h. After cooling to rt, the mixture was diluted with EtOAc (10 mL) and filtered. The solution was washed with water (10 mL) and Na_2CO_3 solution (10 mL). The organic layer was dried over Na_2SO_4 and the solvent removed under reduced pressure. The residue was purified by flash column chromatography (Silica gel, 1 – 10% DCM/MeOH). The product **188** (12.0 mg, 38.4 µmol, 53%) was isolated as light brown powder.

^{1}H NMR (400 MHz, $CDCl_3$) δ 8.52 (d, *J* = 4.8 Hz, 1H), 7.33 (d, *J* = 0.9 Hz, 1H), 7.08 (dd, *J* = 5.2, 1.7 Hz, 1H), 6.77 (s, 1H), 5.71 (s, 1H), 3.65 (td, *J* = 6.9, 2.4 Hz, 2H), 3.61 (s, 3H), 2.90 (t, *J* = 6.9 Hz, 2H), 1.53 (s, 9H). **TLC-MS:** ESI(+) calcd. for $[M+Na]^+$: *m/z* = 338.1; found: 338.3; **HPLC:** t_{ret} = 9.561 min (88.5% at 254 nm, 88.7% at 230 nm, method C).

2-(2-(Ethylthio)pyridin-4-yl)-1,5,6,7-tetrahydro-4H-pyrrolo[3,2-c]pyridin-4-one (190)

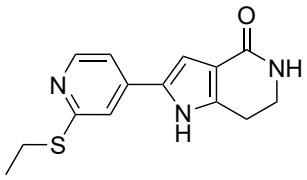

190

Chemical Formula: $C_{14}H_{15}N_3OS$
Exact Mass: 273.09358
Molecular Weight: 273.35400

Following the procedure published by WANG *et al.*[286a], NaH (60% dispersion in mineral oil, 88.6 mg, 2.21 mmol, 7.70 eq.) was suspended in DMF (1.0 mL, dry) and the mixture cooled to 0 °C. Ethanethiol (0.164 mL, 0.138 g, 2.21 mmol, 7.70 eq.) was added and the reaction stirred for 30 min at rt. After adding *tert*-Butyl 2-(2-chloropyridin-4-yl)-4-oxo-1,4,6,7-tetrahydro-5*H*-pyrrolo[3,2-*c*]pyridine-5-carboxylate (**116,** 0.100 g, 0.288 mmol, 1.00 eq.) the reaction was heated to reflux for 48 h. The reaction was cooled to rt and the solvent removed under reduced pressure. The residue was diluted with water (15 mL) and the pH adjusted to 7 by addition of diluted HCl. The mixture was extracted with DCM (3x 15 mL) and the combined organic layers dried over Na_2SO_4. The solvent was removed under reduced pressure and the residue purified by flash column chromatography (Silica gel, 1 – 10% DCM/MeOH). The product **190** was isolated for identification.

^{1}H NMR (400 MHz, $CDCl_3$) δ 8.44 (dd, *J* = 5.4, 0.8 Hz, 1H), 7.17 (dd, *J* = 1.7, 0.8 Hz, 1H), 7.00 (dd, *J* = 5.3, 1.6 Hz, 1H), 6.78 (s, 1H), 5.52 (s, 1H), 3.65 (dt, *J* = 6.9, 3.4 Hz, 2H), 3.21 (q, *J* = 7.4 Hz, 2H), 2.90 (t, *J* = 6.9 Hz, 2H), 1.40 (t, *J* = 7.4 Hz, 3H). **TLC-MS:** ESI(+) calcd. for $[M+Na]^+$: *m/z* = 296.1; found: 296.1.

2-(2-(Ethylthio)pyridin-4-yl)-1-methyl-1,5,6,7-tetrahydro-4H-pyrrolo[3,2-c]pyridin-4-one (189)

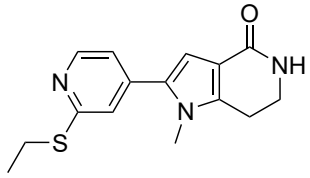

189

Chemical Formula: $C_{15}H_{17}N_3OS$
Exact Mass: 287.10923
Molecular Weight: 287.38100

To NaH (60% dispersion in mineral oil, 11.0 mg, 0.268 mmol, 7.70 eq.) DMF (1.0 mL, dry) was added and the mixture cooled to 0 °C. Ethanethiol (19.8 µL, 16.6 mg, 0.268 mmol, 7.70 eq.) was added. After stirring the reaction at rt for 30 min, *tert*-butyl 2-(2-fluoropyridin-4-yl)-1-methyl-4-oxo-1,4,6,7-tetrahydro-5*H*-pyrrolo[3,2-*c*]pyridine-5-carboxylate (**183,** 12.0 mg, 34.7 µmol, 1.00 eq.) and the reaction heated to reflux for 4 h. The reaction was cooled to rt and the solvent removed under reduced pressure. The mixture was diluted with water (15 mL) and the pH adjusted to 7 by addition of HCl (2M). The mixture was extracted with EtOAc (3x 15 mL) and the combined organic layers dried over Na_2SO_4. The solvent was removed under reduced pressure and the residue purified by flash column chromatography (Silica gel, 1 – 10% DCM/MeOH). The product **189** was isolated for identification.

^{1}H NMR (400 MHz, $CDCl_3$) δ 8.44 (d, *J* = 5.3 Hz, 1H), 7.17 (s, 1H), 7.00 (dd, *J* = 5.3, 1.5 Hz, 1H), 6.78 (s, 1H), 5.52 (s, 1H), 3.65 (td, *J* = 6.9, 2.4 Hz, 2H), 3.62 (s, 3H), 3.21 (q, *J* = 7.4 Hz, 2H), 2.90 (t, *J* = 6.9 Hz, 2H), 1.40 (t, *J* = 7.4 Hz, 3H). **TLC-MS:** ESI(+) calcd. for $[M+Na]^+$: *m/z* = 310.1; found: 310.1.

tert-Butyl 2-(2-((4-methoxybenzyl)thio)pyridin-4-yl)-1-methyl-4-oxo-1,4,6,7-tetrahydro-5H-pyrrolo[3,2-c]pyridine-5-carboxylate (192)

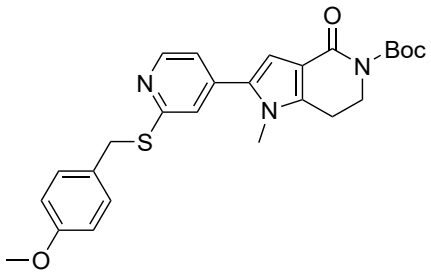

192
Chemical Formula: $C_{26}H_{29}N_3O_4S$
Exact Mass: 479.18788
Molecular Weight: 479.59500

tert-Butyl 2-(2-chloropyridin-4-yl)-1-methyl-4-oxo-1,4,6,7-tetrahydro-5*H*-pyrrolo[3,2-*c*]pyridine-5-carboxylate (**120,** 50.0 mg, 0.138 mmol, 1.00 eq.) and DIPEA (46.7 µL, 35.7 mg, 0.276 mmol, 2.0 eq.) were dissolved in dioxane (2.0 mL, dry) and the solution degassed (Ar). (4-methoxyphenyl)methanethiol (**191**, 19.9 µmol, 21.3 mg, 0.138 mmol, 1.00 eq.) was added and the degassing progress continued. After adding XantPhos (4.00 mg, 6.9 µmol, 5 mol%) and $Pd_2(dba)_3$ (3.16 mg, 3.5 µmol, 2.5 mol%) the reaction was heated to 100 °C for 21 h. The reaction was cooled to rt and diluted with EtOAc (10 mL). The mixture was washed with H_2O (10 mL) and the organic layer dried over Na_2SO_4. The solvent was removed under reduced pressure and the residue purified by flash column chromatography (Silica gel, 10 – 80% hexane/EtOAc) which afforded the product **192** (41.0 mg, 85.6 µmol, 62%) as white powder.

^{1}H NMR (400 MHz, $CDCl_3$) δ 8.47 (d, *J* = 5.2 Hz, 1H), 7.33 (d, *J* = 8.7 Hz, 2H), 7.11 (d, *J* = 0.6 Hz, 1H), 6.99 (dd, *J* = 5.2, 1.5 Hz, 1H), 6.86 – 6.80 (m, 2H), 6.77 (s, 1H), 4.40 (s, 2H), 4.12 (t, *J* = 6.3 Hz, 2H), 3.77 (s, 3H), 3.53 (s, 3H), 2.87 (t, *J* = 6.3 Hz, 2H), 1.55 (s, 9H). **TLC-MS:** ESI(+) calcd. for $[M+Na]^+$: *m/z* = 502.2; found: 502.6. **HPLC:** t_{ret} = 17.743 min (98.9% at 254 nm, 96.6% at 230 nm, method B).

tert-Butyl 2-(2-mercaptopyridin-4-yl)-1-methyl-4-oxo-1,4,6,7-tetrahydro-5H-pyrrolo[3,2-c]pyridine-5-carboxylate (185)

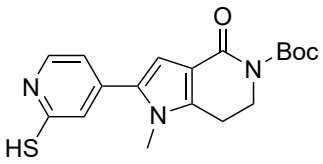

185
Chemical Formula: $C_{18}H_{21}N_3O_3S$
Exact Mass: 359.13036
Molecular Weight: 359.44400

tert-Butyl 2-(2-bromopyridin-4-yl)-1-methyl-4-oxo-1,4,6,7-tetrahydro-5*H*-pyrrolo[3,2-*c*]pyridine-5-carboxylate (**121**, 0.846 g, 2.08 mmol, 1.00 eq) was dissolved in toluene (degassed, dry, 15 mL) and triisopropylsilanethiol (1.28 mL, 0.989 g, 6.25 mmol, 3.00 eq.) and DIPEA (1.09 mL, 0.808 g, 6.25 mmol, 3.00 eq.) were added. After addition of tetrakis(triphenylphosphin)palladium(0) (0.120 g, 0.104 mmol, 5 mol%) and XantPhos (0.120 mg, 0.208 mmol, 10 mol%) the reaction was heated to 80 °C and stirred for 3 h. After cooling to rt, the solvent was removed under reduced pressure and the residue purified by flash column chromatography (Silica gel, 0 – 10% DCM/MeOH) which afforded the product **185** (0.689 g, 5.75 mmol, 92%) (containing ~ 10% of disulfide, which could be easily removed in the next step) as yellow solid.

^{1}H NMR (400 MHz, DMSO) δ 13.32 (s, 1H), 7.64 (d, *J* = 6.2 Hz, 1H), 7.32 (s, 1H), 6.89 (dd, *J* = 6.6, 1.4 Hz, 1H), 6.83 (s, 1H), 3.97 (s, 2H), 3.62 (s, 3H), 2.95 (t, *J* = 6.2 Hz, 2H), 1.46 (s, 9H). **^{13}C NMR**

(101 MHz, DMSO) δ 161.30, 152.93, 143.48, 139.51, 137.69, 131.61, 128.77, 114.36, 111.91, 110.25, 81.36, 44.57, 32.89, 27.78, 21.56. **TLC-MS:** ESI(+) calcd. for $[M+H]^+$: *m/z* = 382.1; found: 381.9; ESI(-) calcd. for $[M-H]^-$: *m/z* =358.1; found: 357.9. **HPLC:** t_{ret} = 10.59 min (85.6% at 254 nm, 84.2% at 230 nm, method B).

tert-Butyl 2-(2-((2-chloropyrimidin-4-yl)thio)pyridin-4-yl)-1-methyl-4-oxo-1,4,6,7-tetrahydro-5H-pyrrolo[3,2-c]pyridine-5-carboxylate (197)

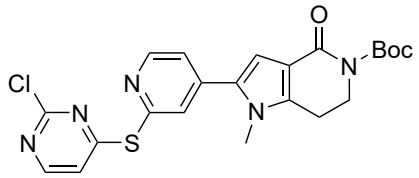

197
Chemical Formula: $C_{22}H_{22}ClN_5O_3S$
Exact Mass: 471.11319
Molecular Weight: 471.96000

tert-Butyl 2-(2-mercaptopyridin-4-yl)-1-methyl-4-oxo-1,4,6,7-tetrahydro-5*H*-pyrrolo[3,2-*c*]pyridine-5-carboxylate (**185**, 0.150 g, 0.417 mmol, 1.00 eq.) and K_2CO_3 (0.115 g, 0.835 mmol, 2.00 eq.) were dissolved in DMF (dry, 4 mL) under an argon atmosphere and cooled to -78 °C. 2,4-Dichloropyrimidine (**172**, 68.4 mg, 0.459 mmol, 1.10 eq.) was added and the reaction allowed to slowly warm up to rt. After stirring for 4 h the solvent was evaporated and sat. NH_4Cl solution (20 mL) and DCM (20 mL) were added. The layers were separated and the aqueous phase extracted with DCM (20 mL). The combined organic layers were dried over Na_2SO_4 and the solvent evaporated. The residue was purified by flash column chromatography (Silica gel, 1 – 10 % DCM/MeOH) which afforded the product **197** (0.160 g, 0.338 mmol, 81%) as light-yellow solid.
^{1}H NMR (400 MHz, $CDCl_3$) δ 8.57 (dd, *J* = 5.2, 0.5 Hz, 1H), 8.27 (d, *J* = 5.4 Hz, 1H), 7.65 (d, *J* = 0.9 Hz, 1H), 7.28 (dd, *J* = 5.2, 1.6 Hz, 1H), 7.22 (d, *J* = 5.4 Hz, 1H), 6.80 (s, 1H), 4.07 (t, *J* = 6.3 Hz, 2H), 3.65 (s, 3H), 2.87 (t, *J* = 6.4 Hz, 2H), 1.49 (s, 9H). **^{13}C NMR** (101 MHz, $CDCl_3$) δ 172.27, 162.45, 162.06, 160.57, 157.80, 153.33, 151.69, 150.94, 141.67, 141.12, 132.17, 127.09, 122.35, 117.49, 115.69, 110.44, 82.58, 44.64, 32.81, 28.11, 22.15. **TLC-MS:** ESI(+) calcd. for $[M+Na]^+$: *m/z* = 494.1; found: 494.0; ESI(-) calcd. for $[M-H]^-$: *m/z* = 470.1; found: 470.0. **HPLC:** t_{ret} = 15.13 min (96.2% at 254 nm, 94.3% at 230 nm, method B).

tert-Butyl 2-(2-((2-bromopyrimidin-4-yl)thio)pyridin-4-yl)-1-methyl-4-oxo-1,4,6,7-tetrahydro-5H-pyrrolo[3,2-c]pyridine-5-carboxylate (198)

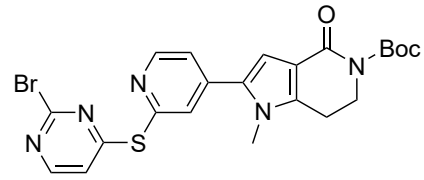

198
Chemical Formula: $C_{22}H_{22}BrN_5O_3S$
Exact Mass: 515.06267
Molecular Weight: 516.41400

tert-Butyl 2-(2-mercaptopyridin-4-yl)-1-methyl-4-oxo-1,4,6,7-tetrahydro-5*H*-pyrrolo[3,2-*c*]pyridine-5-carboxylate (**185**, 40.0 mg, 0.111 mmol, 1.00 eq.) and 2,4-dibromopyrimidine (**173**, 29.1 mg, 0.122 mmol, 1.10 eq.) were subjected to GSP 9 and stirred for 2 h. The residue was purified by flash column chromatography (Silica gel, 2 – 6% DCM/MeOH) which afforded the product **198** (56.0 mg, 0.219 mmol, 98%) as beige solid. **^{1}H NMR** (400 MHz, $CDCl_3$) δ 8.63 (dd, *J* = 5.2, 0.5 Hz, 1H), 8.26 (d, *J* = 5.4 Hz, 1H), 7.69 (d, *J* = 0.9 Hz, 1H), 7.34 (dd, *J* =

5.2, 1.7 Hz, 1H), 7.30 (d, *J* = 5.4 Hz, 1H), 6.88 (s, 1H), 4.13 (t, *J* = 6.3 Hz, 2H), 3.69 (s, 3H), 2.91 (t, *J* = 6.3 Hz, 2H), 1.55 (s, 9H). **^{13}C NMR** (101 MHz, $CDCl_3$) δ 172.07, 162.16, 157.63, 153.60, 152.37, 151.87, 151.06, 141.71, 141.31, 132.32, 127.22, 122.52, 117.95, 115.95, 110.70, 82.82, 44.73, 33.02, 28.27, 22.32. **TLC-MS:** ESI(+) calcd. for $[M+H]^+$: *m/z* = 538.1; found: 538.0. **HPLC:** t_{ret} = 15.57 min (96.0% at 254 nm, 96.8% at 230 nm, method B).

tert-Butyl 2-(2-((2-fluoropyrimidin-4-yl)thio)pyridin-4-yl)-1-methyl-4-oxo-1,4,6,7-tetrahydro-5H-pyrrolo[3,2-c]pyridine-5-carboxylate (199)

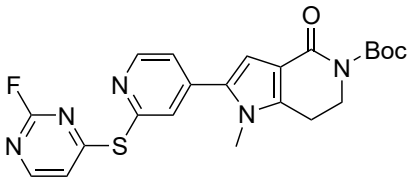

199
Chemical Formula: $C_{22}H_{22}FN_5O_3S$
Exact Mass: 455.14274
Molecular Weight: 455.50840

tert-Butyl 2-(2-mercaptopyridin-4-yl)-1-methyl-4-oxo-1,4,6,7-tetrahydro-5*H*-pyrrolo[3,2-*c*]pyridine-5-carboxylate (**185**, 80.0 mg, 0.223 mmol, 1.00 eq.) and 2,4-difluoropyrimidine (**176**, 20.9 µmol, 28.4 mg, 0.245 mmol, 1.10 eq.) were subjected to GSP 9 and stirred for 2 h. The residue was purified by flash column chromatography (Silica gel, 2 – 8% DCM/MeOH) which afforded the product **199** (36.8 mg, 61.9 µmol, 28%) as light-yellow solid.

^{1}H NMR (400 MHz, $CDCl_3$) δ 8.64 (d, *J* = 5.2 Hz, 1H), 8.36 (dd, *J* = 5.3, 1.9 Hz, 1H), 7.75 (d, *J* = 1.0 Hz, 1H), 7.35 (dd, *J* = 5.2, 1.6 Hz, 1H), 7.27 – 7.23 (m, 1H), 6.88 (s, 1H), 4.18 – 4.09 (m, 2H), 3.70 (s, 3H), 2.91 (t, *J* = 6.3 Hz, 2H), 1.55 (s, 9H). **^{13}C NMR** (101 MHz, $CDCl_3$) δ 173.72 (d, *J* = 12.3 Hz), 162.20 (d, *J* = 220.8 Hz), 162.18, 159.24 (d, *J* = 12.6 Hz), 153.64, 151.52, 150.94, 141.82, 141.33, 132.36, 127.67, 122.60, 117.07 (d, *J* = 4.7 Hz), 116.00, 110.74, 82.85, 44.74, 32.81, 28.29, 22.35. **TLC-MS:** ESI(+) calcd. for $[M+H]^+$: *m/z* = 478,1; found: 478.1; ESI(-) calcd. for $[M-H]^-$: *m/z* = 454.1; found: 454.1. **HPLC:** t_{ret} = 14.34 min (99.2% at 254 nm, 95.0% at 230 nm, method B).

tert-Butyl 2-(2-((2-chloro-5-fluoropyrimidin-4-yl)thio)pyridin-4-yl)-1-methyl-4-oxo-1,4,6,7-tetrahydro-5H-pyrrolo[3,2-c]pyridine-5-carboxylate (200)

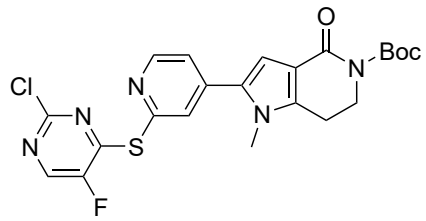

200
Chemical Formula: $C_{22}H_{21}ClFN_5O_3S$
Exact Mass: 489.10377
Molecular Weight: 489.95040

tert-Butyl 2-(2-mercaptopyridin-4-yl)-1-methyl-4-oxo-1,4,6,7-tetrahydro-5*H*-pyrrolo[3,2-*c*]pyridine-5-carboxylate (**185**, 50.0 mg, 0.139 mmol, 1.00 eq.) and 2,4-dichloro-5-fluoropyrimidine (**174**, 15.7 µmol, 25.6 mg, 0.153 mmol, 1.10 eq.) were subjected to GSP 9 and stirred for 4 h. The residue purified by flash column chromatography (Silica gel, 1 – 3% DCM/MeOH) which afforded the product **200** (64 mg, 0,131 mmol, 94%) as off-white solid.

^{1}H NMR (400 MHz, $CDCl_3$) δ 8.60 (d, *J* = 5.1 Hz, 1H), 8.25 (s, 1H), 7.72 (s, 1H), 7.35 (dd, *J* = 5.1, 1.4 Hz, 1H), 6.88 (s, 1H), 4.13 (t, *J* = 6.3 Hz, 2H), 3.71 (s, 3H), 2.91 (t, *J* = 6.3 Hz, 2H), 1.55 (s, 9H). **^{13}C NMR** (101 MHz, $CDCl_3$) δ 162.19, 159.51 (d, *J* = 16.7 Hz), 155.24, 154.86 (d, *J* = 3.7 Hz), 153.65, 151.33 (d, *J* = 258.9 Hz), 150.93, 144.01 (d, *J* = 22.7 Hz), 141.66,

141.08, 132.42, 128.25, 122.91, 115.94, 110.60, 82.81, 44.74, 32.95, 28.27, 22.32. **TLC-MS:** ESI(+) calcd. for $[M+Na]^+$: *m/z* = 512,1; found: 512.2. **HPLC:** t_{ret} = 16.06 min (99.7% at 254 nm, 98.7% at 230 nm, method B).

tert-Butyl 2-(2-((2-chloro-5-cyanopyrimidin-4-yl)thio)pyridin-4-yl)-1-methyl-4-oxo-1,4,6,7-tetrahydro-5H-pyrrolo[3,2-c]pyridine-5-carboxylate (201)

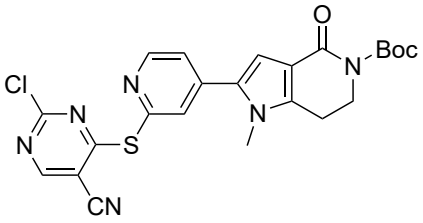

201

Chemical Formula: $C_{23}H_{21}ClN_6O_3S$
Exact Mass: 496.10844
Molecular Weight: 496.97000

tert-Butyl 2-(2-mercaptopyridin-4-yl)-1-methyl-4-oxo-1,4,6,7-tetrahydro-5*H*-pyrrolo[3,2-*c*]pyridine-5-carboxylate **185** (0.100 g, 0.278 mmol, 1.00 eq.) and 2,4-dichloropyrimidin-5-carbonitril (53.2 mg, 0.306 mmol, 1.10 eq.) were subjected to GSP 9 with a reaction time of 1 h. The residue was purified by flash column chromatography (Silica gel, 1 – 4% DCM/MeOH) which afforded the product **201** (35.0 mg, 48.4 µmol, 21%) as pale-yellow solid.

^{1}H NMR (400 MHz, $CDCl_3$) δ 8.67 (d, *J* = 5.1 Hz, 1H), 8.62 (s, 1H), 7.71 (d, *J* = 0.9 Hz, 1H), 7.41 (dd, *J* = 5.1, 1.6 Hz, 1H), 6.92 (s, 1H), 4.15 (t, *J* = 6.3 Hz, 2H), 3.70 (s, 3H), 2.92 (t, *J* = 6.3 Hz, 2H), 1.57 (s, 9H). **^{13}C NMR** (101 MHz, $CDCl_3$) δ 174.71, 162.79, 162.16, 161.35, 153.71, 151.33, 149.23, 141.80, 141.58, 132.24, 129.04, 123.47, 116.13, 112.45, 110.92, 105.67, 82.94, 44.75, 32.90, 28.32, 22.38. **TLC-MS:** ESI(+) calcd. for $[M+H]^+$: *m/z* = 519.1; found: 519.2. **HPLC:** t_{ret} = 15.13 min (95.1% at 254 nm, 94.4% at 230 nm, method B).

tert-Butyl 2-(2-((2-chloro-5-methoxypyrimidin-4-yl)thio)pyridin-4-yl)-1-methyl-4-oxo-1,4,6,7-tetrahydro-5H-pyrrolo[3,2-c]pyridine-5-carboxylate (202)

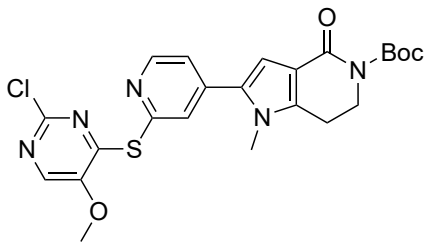

202

Chemical Formula: $C_{23}H_{24}ClN_5O_4S$
Exact Mass: 501.12375
Molecular Weight: 501.98600

tert-Butyl 2-(2-mercaptopyridin-4-yl)-1-methyl-4-oxo-1,4,6,7-tetrahydro-5*H*-pyrrolo[3,2-*c*]pyridine-5-carboxylate (**185**, 50.0 mg, 0.139 mmol, 1.00 eq.) and 2,4-dichloro-5-methoxypyrimidine (27.4 mg, 0.153 mmol, 1.10 eq.) were subjected to GSP 9 and stirred for 2 h. The residue was purified by flash column chromatography (Silica gel, 1 – 4% DCM/MeOH) which afforded the product **202** (59.0 mg, 0.118 mmol, 84%) as white powder.

^{1}H NMR (400 MHz, $CDCl_3$) δ 8.63 (d, *J* = 4.3 Hz, 1H), 8.36 (s, 1H), 7.71 (s, 1H), 7.32 (d, *J* = 4.4 Hz, 1H), 6.86 (s, 1H), 4.12 (t, *J* = 6.3 Hz, 2H), 4.00 (s, 3H), 3.65 (s, 3H), 2.89 (t, *J* = 6.3 Hz, 2H), 1.54 (s, 9H). **^{13}C NMR** (101 MHz, $CDCl_3$) δ 164.20, 162.19, 153.59, 152.57, 151.73, 151.62, 150.79, 146.74, 141.61, 140.91, 132.57, 128.90, 122.37, 115.87, 110.51, 82.78, 60.72, 44.70, 32.68, 28.24, 22.31. **TLC-MS:** ESI(+) calcd. for $[M+H]^+$: *m/z* = 524.1; found: 524.2. **HPLC:** t_{ret} = 16.32 min (99.3% at 254 nm, 98.6% at 230 nm, method B).

tert-Butyl 2-(2-((2-chloro-5-(trifluoromethyl)pyrimidin-4-yl)thio)pyridin-4-yl)-1-methyl-4-oxo-1,4,6,7-tetrahydro-5H-pyrrolo[3,2-c]pyridine-5-carboxylate (203)

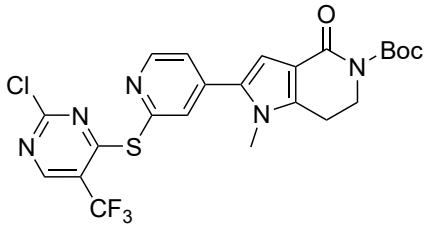

203
Chemical Formula: $C_{23}H_{21}ClF_3N_5O_3S$
Exact Mass: 539.10057
Molecular Weight: 539.95821

tert-Butyl 2-(2-mercaptopyridin-4-yl)-1-methyl-4-oxo-1,4,6,7-tetrahydro-5*H*-pyrrolo[3,2-*c*]pyridine-5-carboxylate (**185**, 0.100 g, 0.278 mmol, 1.00 eq.) and 2,4-dichloro-5-(trifluoromethyl)pyrimidine (**175**, 66.4 mg, 0.306 mmol, 1.10 eq.) were subjected to GSP 9 and stirred for 2 h. The residue was purified by two subsequent flash column chromatography methods (Silica gel, 1) 0.5 – 2% DCM/MeOH; 2) 10 – 70% hexane/EtOAc)) which afforded the product **203** (67.0 mg, 0.114 mmol, 41%) as white powder.

^{1}H NMR (400 MHz, $CDCl_3$) δ 8.67 (d, *J* = 5.1 Hz, 1H), 8.60 (d, *J* = 0.4 Hz, 1H), 7.69 (d, *J* = 0.9 Hz, 1H), 7.39 (dd, *J* = 5.1, 1.6 Hz, 1H), 6.89 (s, 1H), 4.13 (t, *J* = 6.3 Hz, 2H), 3.69 (s, 3H), 2.91 (t, *J* = 6.3 Hz, 2H), 1.55 (s, 9H). **^{13}C NMR** (101 MHz, $CDCl_3$) δ 171.21, 163.01 (d, *J* = 0.9 Hz), 162.17, 155.99 (q, *J* = 5.3 Hz), 153.66, 151.18, 149.53 (q, *J* = 1.7 Hz), 141.66, 141.29, 132.34, 129.84, 123.34, 122.48 (q, *J* = 273.4 Hz), 120.20 (q, *J* = 34.1 Hz), 115.99, 110.66, 82.85, 44.74, 32.86, 28.28, 22.33. **TLC-MS:** ESI(+) calcd. for $[M+H]^+$: *m/z* = 562.1; found: 562.3. **HPLC:** t_{ret} = 17.392 min (99.0% at 254 nm, 98.2% at 230 nm, method B).

2-(2-((2-Chloropyrimidin-4-yl)thio)pyridin-4-yl)-1-methyl-1,5,6,7-tetrahydro-4H-pyrrolo[3,2-c]pyridin-4-one (204)

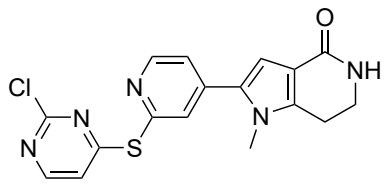

204
Chemical Formula: $C_{17}H_{14}ClN_5OS$
Exact Mass: 371.06076
Molecular Weight: 371.84300

tert-Butyl 2-(2-((2-chloropyrimidin-4-yl)thio)pyridin-4-yl)-1-methyl-4-oxo-1,4,6,7-tetrahydro-5*H*-pyrrolo[3,2-*c*]pyridine-5-carboxylate (**197**) (28.0 mg, 59.5 µmol, 1.00 eq.) was dissolved in DCM (dry, 1 mL) and subjected to GSP 7 and stirred for 30 min. The residue was dissolved in a DCM/5% MeOH mixture (10 mL) and washed with sat. Na_2CO_3 solution. The organic layer was dried over Na_2SO_4 and the solvent removed under reduced pressure. The raw product was purified by flash column chromatography (Silica gel, 2 – 10% DCM/MeOH) which afforded the product **204** (6.3 mg, 17.3 µmol, 29%) as light-yellow powder.

^{1}H NMR (400 MHz, DMSO) δ 8.63 (d, *J* = 5.2 Hz, 1H), 8.53 (d, *J* = 5.4 Hz, 1H), 7.92 (d, *J* = 1.2 Hz, 1H), 7.61 (dd, *J* = 5.2, 1.6 Hz, 1H), 7.50 (d, *J* = 5.4 Hz, 1H), 7.11 (s, 1H), 6.78 (s, 1H), 3.68 (s, 3H), 3.42 (dd, *J* = 8.2, 5.7 Hz, 3H), 2.86 (t, *J* = 6.8 Hz, 2H). **^{13}C NMR** (101 MHz, DMSO) δ 172.23, 164.49, 159.42, 159.14, 151.05, 150.93, 141.23, 140.98, 130.49, 126.46, 122.03, 118.27, 114.57, 108.98, 39.83, 32.69, 21.18. **HRMS:** ESI(+) calcd. for $[M+H]^+$: *m/z* = 372.06804; found: 372.06841; rel. deviation: 0.99 ppm. **HPLC:** t_{ret} = 9.80 min (94.9% at 254 nm, 96.1% at 230 nm, method B). **IR** (ATR) [cm^{-1}]:

3201, 3020, 1641, 1590, 1552, 1503, 1466, 1451, 1412, 1325, 1205, 1163, 1085, 977, 852, 815, 759, 735, 720, 689.

2-(2-((2-Bromopyrimidin-4-yl)thio)pyridin-4-yl)-1-methyl-1,5,6,7-tetrahydro-4H-pyrrolo[3,2-c]pyridin-4-one (205)

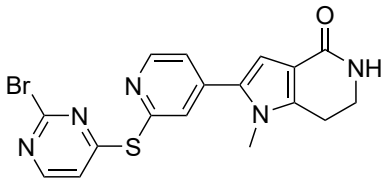

205
Chemical Formula: $C_{17}H_{14}BrN_5OS$
Exact Mass: 415.01024
Molecular Weight: 416.29700

tert-Butyl 2-(2-((2-bromopyrimidin-4-yl)thio)pyridin-4-yl)-1-methyl-4-oxo-1,4,6,7-tetrahydro-5*H*-pyrrolo[3,2-*c*]pyridine-5-carboxylate (**198**, 56.0 mg, 0.108 mmol) was dissolved in DCM (dry, 5 mL) and subjected to GSP 7 and stirred for 30 min. The residue was dissolved in DCM (10 mL) and washed with sat. Na_2CO_3 solution (10 mL). The aqueous phase was extracted with DCM (2x 10 mL). The organic layer was dried over Na_2SO_4 and the solvent evaporated. The residue was purified by flash column chromatography (Silica gel, 2 – 8% DCM/MeOH). The raw product was washed with pentane and dried in vacuum which afforded the product **205**, (15.0 mg, 35.8 µmol, 33%) as off-white solid.

^{1}H NMR (400 MHz, DMSO) δ 8.62 (d, *J* = 5.2 Hz, 2H), 8.44 (d, *J* = 5.4 Hz, 2H), 7.90 (d, *J* = 1.0 Hz, 2H), 7.60 (dd, *J* = 5.2, 1.7 Hz, 2H), 7.51 (d, *J* = 5.4 Hz, 2H), 7.11 (s, 2H), 6.78 (s, 2H), 3.68 (s, 6H), 3.46 – 3.40 (m, 7H, partially water residual peak), 2.86 (t, *J* = 6.9 Hz, 4H). **^{13}C NMR** (101 MHz, DMSO) δ 172.01, 164.56, 158.97, 151.41, 151.08, 150.98, 141.29, 141.04, 130.52, 126.46, 122.05, 118.60, 114.58, 109.03, 39.86, 32.78, 21.20. **HRMS:** ESI(+) calcd. for $[M+H]^+$: *m/z* = 416.01783; found: 416.01752; rel. deviation: 0.74 ppm. **HPLC:** t_{ret} = 10.03 min (96.2% at 254 nm, 95.2% at 230 nm, method B). **IR** (ATR) [cm^{-1}]: 3168, 3121, 3035, 3012, 2932, 2880, 1641, 1580, 1545, 1497, 1457, 1432, 1398, 1351, 1306, 1237, 1196, 1167, 1149, 1124, 1086, 1019, 974, 878, 858, 828, 785, 720, 679, 651.

2-(2-((2-Fluoropyrimidin-4-yl)thio)pyridin-4-yl)-1-methyl-1,5,6,7-tetrahydro-4H-pyrrolo[3,2-c]pyridin-4-one (206)

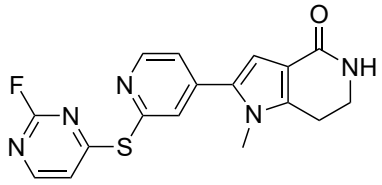

206
Chemical Formula: $C_{17}H_{14}FN_5OS$
Exact Mass: 355.09031
Molecular Weight: 355.39140

tert-Butyl 2-(2-((2-fluoropyrimidin-4-yl)thio)pyridin-4-yl)-1-methyl-4-oxo-1,4,6,7-tetrahydro-5*H*-pyrrolo[3,2-*c*]pyridine-5-carboxylate (**199**, 36.8 mg, 61.9 µmol) was dissolved in DCM (dry, 1 mL) and subjected to GSP 7 and stirred for 15 min. The residue was dissolved in a DCM (10 mL) and washed with sat. Na_2CO_3 solution. The aqueous phase was extracted with DCM (2x 10 mL). The combined organic layers were dried over Na_2SO_4 and the solvent removed under reduced pressure. The raw product was purified by flash column chromatography (Silica gel, 3 – 10% DCM/MeOH) which afforded the product **206** (20.0 mg, 56. 3µmol, 91%) as light-yellow powder.

^{1}H NMR (400 MHz, DMSO) δ 8.63 (d, *J* = 5.2 Hz, 1H), 8.55 (dd, *J* = 5.3, 2.0 Hz, 1H), 7.93 (d, *J* = 0.9 Hz, 1H), 7.61 (dd, *J* = 5.2, 1.6 Hz, 1H), 7.48 (dd, *J* = 5.2, 4.2 Hz, 1H), 7.10 (s, 1H), 6.78 (s, 1H), 3.68 (s, 3H), 3.47 – 3.40 (m, 2H), 2.87 (t, *J* = 6.8 Hz, 2H). **^{13}C NMR** (101 MHz, DMSO) δ 173.54 (d, *J* = 12.7 Hz), 164.45, 161.36 (d, *J* = 215.8 Hz), 160.27 (d, *J* = 12.5 Hz), 150.92, 150.86, 141.21, 140.96, 130.47, 126.67, 122.04, 117.56 (d, *J* = 4.4 Hz), 114.57, 108.95, 39.81, 32.58, 21.17. **HRMS:** ESI(+) calcd. for $[M+H]^+$: *m/z* = 356.09759; found: 356.09800; rel. deviation: 1.15 ppm. **HPLC:** t_{ret} = 8.54 min (96.2% at 254 nm, 95.2% at 230 nm, method B). **IR** (ATR) [cm^{-1}]: 3204, 3046, 1645, 1578, 1530, 1504, 1466, 1433, 1379, 1307, 1172, 931, 850, 805, 772, 708.

2-(2-((2-Chloro-5-fluoropyrimidin-4-yl)thio)pyridin-4-yl)-1-methyl-1,5,6,7-tetrahydro-4H-pyrrolo[3,2-c]pyridin-4-one (207)

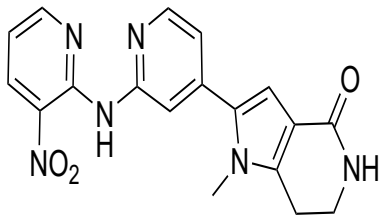

207
Chemical Formula: $C_{17}H_{13}ClFN_5OS$
Exact Mass: 389.05134
Molecular Weight: 389.83340

tert-Butyl 2-(2-((2-chloro-5-fluoropyrimidin-4-yl)thio)pyridin-4-yl)-1-methyl-4-oxo-1,4,6,7-tetrahydro-5*H*-pyrrolo[3,2-*c*]pyridine-5-carboxylate (**200**, 64.0 mg, 0.131 mmol) was dissolved in DCM (dry, 5 mL) and was subjected to GSP 7 and stirred for 30 min. The residue was dissolved in DCM (10 mL) and washed with sat. Na_2CO_3 solution (10 mL). The organic layer was dried over Na_2SO_4 and the solvent removed under reduced pressure. The raw product was washed with pentane and dried in vacuum which afforded the product **207** (34.4 mg, 89.1 µmol, 68%) as off-white powder.

^{1}H NMR (400 MHz, DMSO) δ 8.76 (d, *J* = 1.6 Hz, 1H), 8.56 (d, *J* = 5.2 Hz, 1H), 7.92 (d, *J* = 0.9 Hz, 1H), 7.58 (dd, *J* = 5.2, 1.6 Hz, 1H), 7.11 (s, 1H), 6.76 (s, 1H), 3.68 (s, 3H), 2.86 (t, *J* = 6.9 Hz, 2H) (2 H underneath water residual peak). **^{13}C NMR** (101 MHz, DMSO) δ 164.49, 158.01 (d, *J* = 17.1 Hz), 154.34 (d, *J* = 260.8 Hz), 153.66 (d, *J* = 3.6 Hz), 150.59, 150.31 (d, *J* = 2.0 Hz), 145.84, 145.61, 140.91, 130.52, 126.28, 121.96, 114.52, 108.83, 39.81, 32.62, 21.14. **HRMS:** ESI(+) calcd. for $[M+H]^+$: *m/z* = 390.05861; found: 390.058779; rel. deviation: 0.46 ppm. **HPLC:** t_{ret} = 11.00 min (96.1% at 254 nm, 95.3% at 230 nm, method B). **IR** (ATR) [cm^{-1}]: 3189, 3174, 3064, 2938, 2912, 1681, 1591, 1558, 1500, 1456, 1437, 1388, 1369, 1332, 1309, 1280, 1246, 1213, 1172, 1129, 1087, 988, 863, 827, 808, 768, 750, 720, 677.

2-(2-((2-chloro-5-methoxypyrimidin-4-yl)thio)pyridin-4-yl)-1-methyl-1,5,6,7-tetrahydro-4H-pyrrolo[3,2-c]pyridin-4-one (209)

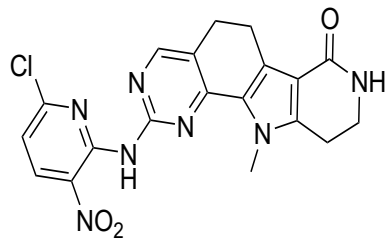

209

Chemical Formula: $C_{18}H_{16}ClN_5O_2S$
Exact Mass: 401,07132
Molecular Weight: 401,86900

tert-Butyl 2-(2-((2-chloro-5-methoxypyrimidin-4-yl)thio)pyridin-4-yl)-1-methyl-4-oxo-1,4,6,7-tetrahydro-5*H*-pyrrolo[3,2-*c*]pyridine-5-carboxylate (**202**, 59.0 mg, 0.118 mmol) was dissolved in DCM (dry, 5 mL) and subjected to GSP 7 and stirred for 30 min. The residue was dissolved in DCM (10 mL) and washed with sat. Na_2CO_3 solution. The aqueous phase was extracted twice with DCM (10 mL) and the organic layers dried over Na_2SO_4. The solvent was evaporated and purified by flash column chromatography (Silica gel, 0 - 10 % DCM/MeOH) which afforded the product **209** (27.9 mg, 69.9 µmol, 59%) as white powder.

^{1}H NMR (400 MHz, DMSO) δ 8.57 (d, *J* = 5.1 Hz, 1H), 8.54 (s, 1H), 7.89 (s, 1H), 7.55 (d, *J* = 4.2 Hz, 1H), 7.10 (s, 1H), 6.73 (s, 1H), 3.96 (s, 3H), 3.65 (s, 3H), 3.40 (d, *J* = 17.9 Hz, 29H), 2.85 (t, *J* = 6.7 Hz, 2H) (2 H underneath water residual peak). **^{13}C NMR** (101 MHz, DMSO) δ 164.60, 163.46, 152.85, 151.43, 150.97, 150.53, 146.27, 140.88, 140.63, 130.72, 127.54, 121.82, 114.52, 108.70, 60.68, 39.87, 32.63, 21.20. **HRMS:** ESI(+) calcd. for $[M+H]^+$: *m/z* = 402.07860; found: 402.07901; rel. deviation: 1.03 ppm. **HPLC:** t_{ret} = 11.62 min (97.0% at 254 nm, 96.5% at 230 nm, method B).

IR (ATR) [cm^{-1}]: 3364, 3185, 3054, 2938, 2879, 1718, 1653, 1589, 1532, 1497, 1457, 1438, 1415, 1348, 1309, 1279, 1227, 1196, 1167, 1126, 1087, 1046, 1018, 973, 800, 766, 727, 687.

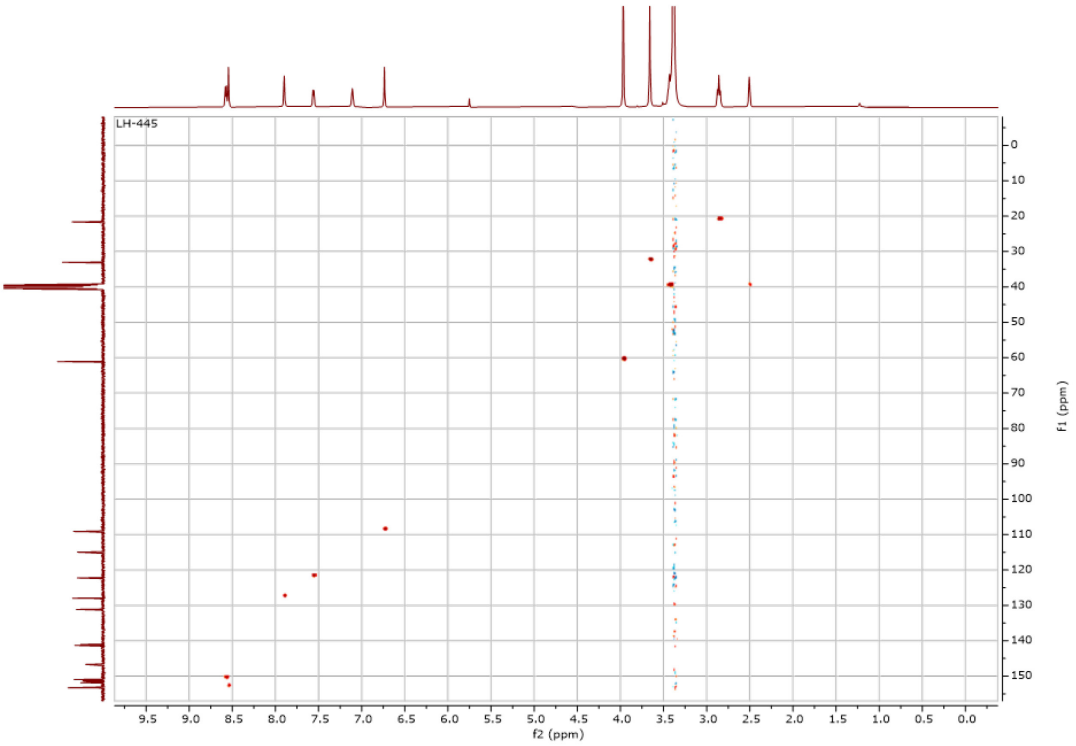

Figure 52: 2D-NMR spectra (HSQC) of **209**.

tert-Butyl 2-(2-((2-chloro-6,7-dimethoxyquinazolin-4-yl)thio)pyridin-4-yl)-1-methyl-4-oxo-1,4,6,7-tetrahydro-5H-pyrrolo[3,2-c]pyridine-5-carboxylate (211)

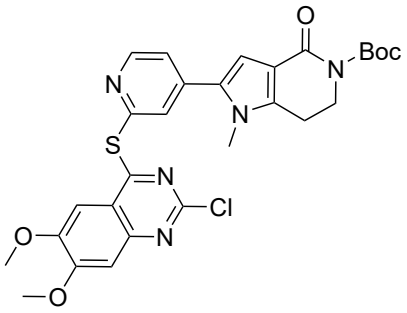

211
Chemical Formula: $C_{28}H_{28}ClN_5O_5S$
Exact Mass: 581.14997
Molecular Weight: 582.07200

2,4-Dichloro-6,7-dimethoxyquinazoline (39.7 mg, 0.153 mmol, 1.10 eq.), $Pd(OAc)_2$ (0.31 mg, 1.39 µmol, 10 mol%) and XantPhos (1.61 mg, 2.78 µmol, 20 mol%) were dissolved in DMF (degassed, dry, 1 mL) and stirred for 5 min. After adding *tert*-butyl 2-(2-mercaptopyridin-4-yl)-1-methyl-4-oxo-1,4,6,7-tetrahydro-5*H*-pyrrolo[3,2-*c*]pyridine-5-carboxylate (**185**, 50.0 mg, 0.139 mmol, 1.00 eq.) and K_3PO_4 (73.8 mg, 0.348 mmol, 2.50 eq.) the reaction was stirred at 50 °C for 1 hour. Then the solvent was evaporated and the residue purified by flash column chromatography (Silica gel, 2 – 6%) which afforded the product **211** (38.0 mg, 64.0 µmol, 46%) as white solid.

^{1}H NMR (400 MHz, $CDCl_3$) δ 8.55 (dd, *J* = 5.2, 0.5 Hz, 1H), 7.87 (d, *J* = 0.9 Hz, 1H), 7.29 (dd, *J* = 5.2, 1.6 Hz, 1H), 7.20 (s, 1H), 7.16 (s, 1H), 6.83 (s, 1H), 4.08 (t, *J* = 6.3 Hz, 2H), 3.98 (d, *J* = 5.3 Hz, 6H), 3.72 (s, 3H), 2.85 (t, *J* = 6.3 Hz, 2H), 1.49 (s, 9H). **^{13}C NMR** (101 MHz, $CDCl_3$) δ 167.91, 162.33, 157.22, 154.33, 153.70, 151.94, 150.80, 150.50, 148.58, 141.62, 140.88, 132.73, 128.35, 122.71, 117.43, 115.88, 110.44, 106.63, 101.57, 82.81, 56.73, 56.59, 44.79, 33.20, 28.29, 22.35. **TLC-MS:** ESI(+) calcd. for $[M+H]^+$: *m/z* = 604.1; found: 603.9. **HPLC:** t_{ret} = 18.11 min (99.2% at 254 nm, 98.0% at 230 nm, method B).

2-(2-((2-chloro-6,7-dimethoxyquinazolin-4-yl)thio)pyridin-4-yl)-1-methyl-1,5,6,7-tetrahydro-4H-pyrrolo[3,2-c]pyridin-4-one (212)

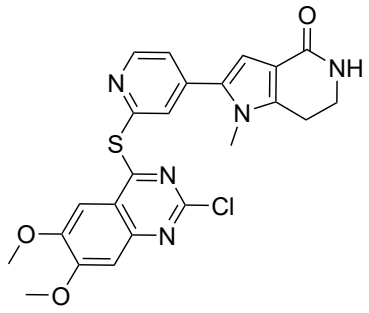

212
Chemical Formula: $C_{23}H_{20}ClN_5O_3S$
Exact Mass: 481.09754
Molecular Weight: 481.95500

tert-Butyl 2-(2-((2-chloro-6,7-dimethoxyquinazolin-4-yl)thio)pyridin-4-yl)-1-methyl-4-oxo-1,4,6,7-tetrahydro-5*H*-pyrrolo[3,2-*c*]pyridine-5-carboxylate (**211**, 38.0 mg, 64.0 µmol) was dissolved in DCM (dry, 2 mL) and subjected to GSP 7 and stirred for 15 min. The residue was dissolved in DCM (10 mL) and washed with sat. Na_2CO_3 solution (10 mL). The organic phase was dried over Na_2SO_4 and the solvent removed in vacuum. The raw product was purified by flash column chromatography (Silica gel, 2 – 10% DCM/MeOH) which afforded the product **212** (22.0 mg, 45.7 µmol, 71%) as white powder.

^{1}H NMR (400 MHz, $CdCl_3$/MeOD) δ 8.56 (d, *J* = 4.2 Hz, 1H), 7.87 (s, 1H), 7.79 (dd, *J* = 31.4, 8.7 Hz, 1H), 7.41 (d, *J* = 4.3 Hz, 1H), 7.28 (s, 1H), 7.16 (s, 1H), 6.81 (s, 1H), 4.00 (d, *J* = 4.3 Hz, 6H), 3.74 (s, 3H), 2.88 (t, *J* = 6.8 Hz, 2H); (2 proton signals underneath H_2O residual peak). **^{13}C NMR** (101 MHz,

$CdCl_3$/MeOD) δ 167.88, 157.29, 154.08, 151.10, 150.80, 150.01, 148.32, 141.47, 140.81, 133.14, 131.88, 129.79, 128.62, 122.73, 117.28, 109.40, 106.15, 101.41, 56.59, 56.46, 40.42, 33.15, 21.56. **HRMS:** ESI(+) calcd. for $[M+H]^+$: *m/z* = 482.10481; found: 482.10485; rel. deviation: 0.07 ppm. **HPLC:** t_{ret} = 13.85 min (96.2% at 254 nm, 96.6% at 230 nm, method B). **IR** (ATR) [cm^{-1}]: 3218, 2948, 2925, 1685, 1591, 1499, 1457, 1437, 1409, 1341, 1253, 1234, 1205, 1169, 1135, 1084, 1011, 983, 871, 842, 826, 809, 763, 743, 718, 674, 654.

6.2.12 Synthesis of the Compounds described in Section 3.3.2.4

tert-Butyl 2-bromo-1-(methoxymethyl)-4-oxo-1,4,6,7-tetrahydro-5H-pyrrolo[3,2-c]pyridine-5-carboxylate (213)

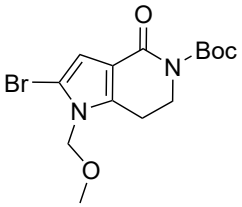

213
Chemical Formula: $C_{14}H_{19}BrN_2O_4$
Exact Mass: 358.05282
Molecular Weight: 359.22000

To *tert*-butyl 2-bromo-4-oxo-1,4,6,7-tetrahydro-5*H*-pyrrolo[3,2-*c*]pyridine-5-carboxylate (**151**, 0.200 g, 0.635 mmol, 1.00 eq.) and NaH (38.1 mg, 60% dispersion in mineral oil, 0.952 mmol, 1.50 eq.) under an argon atmosphere THF (dry, 12 mL) was added and stirred for 10 min in an ice bath. After bromomethyl methylether (**219**, 57.0 µL, 87.2 mg, 0.698 mmol, 1.10 eq.) was added, the reaction was stirred fur 1 h at 0°C. The reaction was quenched by adding NH_4Cl solution (20 mL) and DCM (30 mL). The layers were separated and the organic phase dried over Na_2SO_4. The solvent was removed under reduced pressure and the residue purified by flash column chromatography (Silica gel, 10 – 70% hexane/EA) which afforded the product **213** (0.186 g, 0.520 mmol, 82%) as white solid. **^{1}H NMR** (400 MHz, $CDCl_3$) δ 6.54 (s, 1H), 5.15 (s, 2H), 4.00 (t, *J* = 6.4 Hz, 2H), 3.22 (s, 3H), 2.83 (t, *J* = 6.4 Hz, 2H), 1.47 (s, 9H). **^{13}C NMR** (101 MHz, $CDCl_3$) δ 161.35, 153.25, 139.29, 116.72, 110.27, 104.56, 82.50, 75.47, 56.01, 44.62, 28.05, 22.05. **TLC-MS:** ESI(+) calcd. for $[M+Na]^+$: *m/z* = 381.1; found: 381.1. **HPLC:** t_{ret} = 13.96 min (97.5% at 254 nm, 96.3% at 230 nm, method B).

tert-Butyl 2-bromo-1-(4-methoxybenzyl)-4-oxo-1,4,6,7-tetrahydro-5H-pyrrolo[3,2-c]pyridine-5-carboxylate (214)

tert-Butyl 2-bromo-4-oxo-1,4,6,7-tetrahydro-5*H*-pyrrolo[3,2-*c*]pyridine-5-carboxylate (**151**, 0.200 g, 0.635 mmol, 1.00 eq.) and Cs_2CO_3 (0.310 g, 0.952 mmol, 1.50 eq.) were suspended in DMF (dry, 5 mL) and *p*-methoxybenzyl chloride (0.111 mL, 0.119 g, 0.761 mmol, 1.20 eq.) was added. After stirring at rt for 18 h NH_4Cl solution (20 mL) was added and the mixture extracted with DCM (3x 20 mL). The

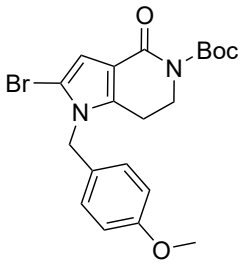

214
Chemical Formula: $C_{20}H_{23}BrN_2O_4$
Exact Mass: 434.08412
Molecular Weight: 435.31800

combined organic layers were dried over Na_2SO_4 and the solvent evaporated. The residue was purified by flash column chromatography (Silica gel, 30 – 60% hexane/EtOAc) which afforded the product **214** (91.0 mg, 0.209 mmol, 33%) as white solid.

^{1}H NMR (400 MHz, $CDCl_3$) δ 6.94 (d, *J* = 8.8 Hz, 2H), 6.87 – 6.82 (m, 2H), 6.68 (s, 1H), 5.05 (d, *J* = 7.6 Hz, 2H), 4.01 (t, *J* = 6.3 Hz, 2H), 3.78 (s, 3H), 2.68 (dd, *J* = 8.3, 4.4 Hz, 2H), 1.52 (d, *J* = 4.1 Hz, 9H). **^{13}C NMR** (101 MHz, $CDCl_3$) δ 161.65, 159.42, 153.66, 138.80, 127.86, 127.69, 116.40, 114.51, 110.35, 104.84, 82.72, 55.41, 48.56, 44.79, 28.26, 22.72. **TLC-MS:** ESI(+) calcd. for $[M+Na]^+$: *m/z* = 457.1; found: 457.2. **HPLC:** t_{ret} = 17.57 min (95.5% at 254 nm, 95.2% at 230 nm, method B).

tert-Butyl 2-bromo-4-oxo-1-pivaloyl-1,4,6,7-tetrahydro-5H-pyrrolo[3,2-c]pyridine-5-carboxylate (215)

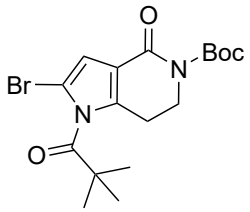

215
Chemical Formula: $C_{17}H_{23}BrN_2O_4$
Exact Mass: 398.08412
Molecular Weight: 399.28500

tert-Butyl 2-bromo-4-oxo-1,4,6,7-tetrahydro-5*H*-pyrrolo[3,2-*c*]pyridine-5-carboxylate (**151**, 0.200 g, 0.635 mmol, 1.00 eq.) and DMAP (7.75 mg, 63.5 µmol, 10 mol%) were dissolved in DCM (dry, 2 mL) under an argon atmosphere and cooled to 0 °C in an ice bath. TEA (0.123 mL, 96.3 mg, 0.952 mmol, 1.50 eq.) and pivaloyl chloride (93.8 µL, 91.8 mg, 0.761 mmol, 1.20 eq.) were added and the reaction was stirred at rt for 18 h. The volatiles were evaporated and the residue diluted with EtOAc (20 mL). The mixture was washed with a sat. NH_4Cl solution (20 mL) and the aqueous phase extracted twice with EtOAc (20 mL). The combined organic layers were dried over Na_2SO_4 and the solvent removed under reduced pressure. The raw product was purified by flash column chromatography (Silica gel, 0 – 20% hexane/EtOAc) which afforded the product **215** (0-183 g, 0.387 mmol, 61%) as white solid. **^{1}H NMR** (400 MHz, $CDCl_3$) δ 6.63 (s, 1H), 4.05 – 4.01 (m, 2H), 2.77 (t, *J* = 6.3 Hz, 2H), 1.52 (s, 9H), 1.31 (s, 9H). **^{13}C NMR** (101 MHz, $CDCl_3$) δ 183.95, 161.17, 153.28, 137.25, 117.30, 111.60, 99.85, 82.98, 44.89, 44.51, 28.18, 27.76, 23.24. **TLC-MS:** ESI(+) calcd. for $[M+Na]^+$: *m/z* =421.1; found: 420.6; ESI(-) calcd. for $[M-H]^-$: *m/z* = 397.1; found: 396.6. **HPLC:** t_{ret} = 17.32 min (98.2% at 254 nm, 96.7% at 230 nm, method B).

tert-Butyl 2-bromo-4-oxo-1-tosyl-1,4,6,7-tetrahydro-5H-pyrrolo[3,2-c]pyridine-5-carboxylate (216)

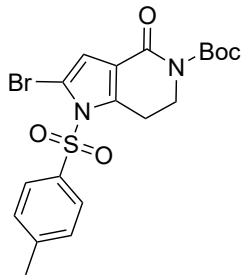

216
Chemical Formula: $C_{19}H_{21}BrN_2O_5S$
Exact Mass: 468.03546
Molecular Weight: 469.35000

tert-Butyl 2-bromo-4-oxo-1,4,6,7-tetrahydro-5*H*-pyrrolo[3,2-*c*]pyridine-5-carboxylate (**151**, 0.900 g, 2.86 mmol, 1.00 eq.), tosylchloride (0.817 g, 4.28 mmol, 1.50 eq.) and DMAP (35.0 mg, 0.286 mmol, 0.10 eq.) were dissolved in ACN (dry, 45 mL) and treated with TEA (0.796 mL, 0.578 g, 5.71 mmol, 2.00 eq.). The reaction was stirred at rt for 18 h. After complete conversion the solvent was evaporated. The residue was dissolved in EtOAc (50 mL) and washed with sat. NH_4Cl solution (50 mL). The aqueous phase was extracted again with EtOAc (50 mL) and the organic extracts dried over Na_2SO_4. The solvent was removed under reduced pressure and the raw product purified by flash column chromatography (Silica gel, 10 – 70% hexane/EtOAc) which afforded the product **216** (1.04 g, 2.23 mmol, 78%) as white solid. **^{1}H NMR** (400 MHz, $CDCl_3$) δ 7.80 (d, *J* = 8.4 Hz, 2H), 7.39 – 7.33 (m, 2H), 6.71 (s, 1H), 4.06 (t, *J* = 6.4 Hz, 2H), 3.32 (t, *J* = 6.4 Hz, 2H), 2.45 (s, 3H), 1.55 (s, 9H). **^{13}C NMR** (101 MHz, $CDCl_3$) δ 160.69, 152.95, 146.57, 141.24, 135.17, 130.41, 127.81, 120.04, 115.69, 102.97, 83.40, 44.66, 28.25, 25.33, 21.92. **TLC-MS:** ESI(+) calcd. for $[M+Na]^+$: *m/z* = 491.0; found: 491.2.; ESI(-) calcd. for $[M-H]^-$: *m/z* =467.0; found: 467.1. **HPLC:** t_{ret} = 18.31 min (96.0% at 254 nm, 95.4% at 230 nm, method B).

tert-Butyl (R)-2-bromo-1-((2,2-dimethyl-1,3-dioxolan-4-yl)methyl)-4-oxo-1,4,6,7-tetrahydro-5H-pyrrolo[3,2-c]pyridine-5-carboxylate (217)

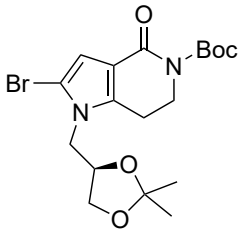

217
Chemical Formula: $C_{18}H_{25}BrN_2O_5$
Exact Mass: 428.09468
Molecular Weight: 429.31100

tert-Butyl 2-bromo-4-oxo-1,4,6,7-tetrahydro-5*H*-pyrrolo[3,2-*c*]pyridine-5-carboxylate (**151**, 1.10 g, 3.50 mmol, 1.00 eq.) and Cs_2CO_3 (2.85 g, 8.76 mmol, 2.50 eq.) were weighed into a flask and dried in vacuum before the addition of DMF (dry, 10 mL) under argon atmosphere and heated to 100 °C for 1 h (solution A).

Solution B was prepared by first drying Sodium iodide (1.84 g, 12.3 mmol, 3.50 eq.) at 150 °C for 18 h and dissolve it in acetone (dry, 4 mL). After addition of (*S*)-4-(chloromethyl)-2,2-dimethyl-1,3-dioxolane (***S*-223**, 1.43 mL, 1.58 g, 10.5 mmol, 3.00 eq.) the mixture was stirred at 40 °C for 1 h. The suspension was filtered and added to the flask containing solution A. The reaction was stirred at 110 °C for 48 h. After cooling down to rt, the solvent was evaporated and the residue dissolved in DCM (50 mL). The solution was washed with sat. NH_4Cl solution (50 mL) and the aqueous layer extracted with DCM (2x 50 mL). The combined organic layers were dried over Na_2SO_4 and the solvent removed under reduced pressure. The residue was purified by flash column chromatography

(Silica gel, 0.5 – 2.5% DCM/MeOH) which afforded the product **217** (0.902 g, 2.10 mmol, 60%) as colorless oil.

^{1}H NMR (400 MHz, $CDCl_3$) δ 6.65 (s, 1H), 4.32 (qd, *J* = 6.6, 3.7 Hz, 1H), 4.15 – 3.88 (m, 5H), 3.66 (dd, *J* = 8.7, 6.6 Hz, 1H), 3.03 – 2.77 (m, 2H), 1.54 (s, 9H), 1.36 (s, 3H), 1.31 (s, 3H). **^{13}C NMR** (101 MHz, $CDCl_3$) δ 161.63, 153.71, 139.80, 116.21, 110.62, 110.14, 104.01, 82.72, 74.88, 66.53, 48.02, 44.88, 28.28, 26.74, 25.35, 23.15. **TLC-MS:** ESI(+) calcd. for $[M+Na]^+$: *m/z* = 451.1; found: 451.9. **HPLC:** t_{ret} = 15.71 min (96.1% at 254 nm, 93.6% at 230 nm, method B).

tert-Butyl (S)-2-bromo-1-((2,2-dimethyl-1,3-dioxolan-4-yl)methyl)-4-oxo-1,4,6,7-tetrahydro-5H-pyrrolo[3,2-c]pyridine-5-carboxylate (218)

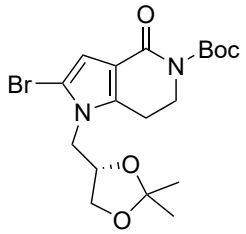

218

Chemical Formula: $C_{18}H_{25}BrN_2O_5$
Exact Mass: 428.09468
Molecular Weight: 429.31100

tert-Butyl 2-bromo-4-oxo-1,4,6,7-tetrahydro-5*H*-pyrrolo[3,2-*c*]pyridine-5-carboxylate (**151**, 0.400 g, 1.27 mmol, 1.00 eq.) and Cs_2CO_3 (1.04 g, 3.19 mmol, 2.50 eq.) were weighed into a flask and dried in vacuum before the addition of DMF (dry, 3 mL) under argon atmosphere and heated to 110 °C for 1 h (solution A).

Solution B was prepared by first drying Sodium iodide (1.84 g, 12.3 mmol, 3.50 eq.) at 150 °C for 1 h and dissolve it in acetone (dry, 4 mL). After addition of (*R*)-4-(chloromethyl)-2,2-dimethyl-1,3-dioxolane (***R*-223**, 1.43 mL, 1.58 g, 10.5 mmol, 3.00 eq.) the mixture was stirred at 40 °C for 1 h. The suspension was filtered and added to the flask containing solution A. The reaction was stirred at 110 °C for 48 h. After cooling down to rt the solvent was evaporated and the residue dissolved in DCM (20 mL). The solution was washed with sat. NH_4Cl solution (20 mL) and the aqueous layer extracted with DCM (2x 20 mL). The combined organic layers were dried over Na_2SO_4 and the solvent removed under reduced pressure. The residue was purified by flash column chromatography (Silica gel, 0.5 – 2.5% DCM/MeOH) which afforded the product **218** (0.315 g, 0.739 mmol, 58%) as colorless oil.

^{1}H NMR (400 MHz, $CDCl_3$) δ 6.57 (s, 2H), 4.27 (dd, *J* = 6.6, 3.5 Hz, 2H), 4.04 (ddd, *J* = 9.1, 6.8, 3.5 Hz, 6H), 3.96 – 3.82 (m, 4H), 3.61 (dd, *J* = 8.7, 6.6 Hz, 2H), 2.94 – 2.78 (m, 4H), 1.48 (s, 17H), 1.31 (s, 6H), 1.26 (s, 6H). **^{13}C NMR** (101 MHz, $CDCl_3$) δ 161.14, 153.10, 139.40, 115.64, 110.03, 109.59, 103.54, 82.12, 74.40, 66.03, 47.53, 44.44, 27.79, 26.24, 24.89, 22.64. **TLC-MS:** ESI(+) calcd. for $[M+Na]^+$: *m/z* = 451.1; found: 450.7; ESI(-) calcd. for $[M-H]^-$: *m/z* = 427.1; found: 426.9. **HPLC:** t_{ret} = 18.81 min (98.0% at 254 nm, 100% at 230 nm, method B).

tert-Butyl 2-(2-((tert-butoxycarbonyl)amino)pyridin-4-yl)-1-(methoxymethyl)-4-oxo-1,4,6,7-tetrahydro-5H-pyrrolo[3,2-c]pyridine-5-carboxylate (225)

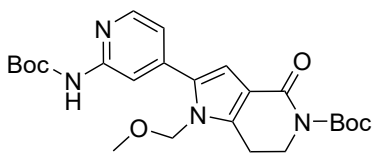

225

Chemical Formula: $C_{24}H_{32}N_4O_6$
Exact Mass: 472.23218
Molecular Weight: 472.54200

tert-Butyl 2-bromo-1-(methoxymethyl)-4-oxo-1,4,6,7-tetrahydro-5*H*-pyrrolo[3,2-*c*]pyridine-5-carboxylate (**213**, 50.0 mg, 0.139 mmol, 1.00 eq.) and *tert*-butyl (4-(4,4,5,5-tetramethyl-1,3,2-dioxaborolan-2-yl)pyridin-2-yl)carbamate (**123**, 53.5 mg, 0.167 mmol, 1.20 eq.) were combined with $Pd_2(dba)_3$ (6.37 mg, 6.96 µmol, 5 mol%) and XPhos (6.64 mg, 13.9 µmol, 10 mol%) and the flask purged with argon. 1,4-dioxane (degassed, 1.0 mL) and 2M Na_2CO_3 solution (degassed, 0.209 mL, 0.428 mmol, 3.00 eq.) were added and the reaction stirred at 80 °C for 2 h. After cooling down to rt the reaction was diluted with EtOAc (20 mL) and filtered through a pad of celite. The solution was washed with NH_4Cl solution, water and brine (20 mL). The organic layer was dried over Na_2SO_4 and the solvent evaporated. The residue was purified by flash column chromatography (Silica gel, 10 – 100% hexane/EtOAc) which afforded the product **225** (24.0 mg, 50.1 µmol, 36%) as white solid.

^{1}H NMR (400 MHz, $CDCl_3$) δ 8.67 (s, 1H), 8.31 (dd, *J* = 5.3, 0.5 Hz, 1H), 8.06 (s, 1H), 7.04 (dd, *J* = 5.3, 1.6 Hz, 1H), 6.85 (s, 1H), 5.22 (s, 2H), 4.14 (t, *J* = 6.3 Hz, 2H), 3.27 (s, 3H), 2.97 (t, *J* = 6.3 Hz, 2H), 1.56 (s, 9H), 1.53 (s, 9H). **^{13}C NMR** (101 MHz, $CDCl_3$) δ 162.37, 153.72, 152.99, 152.60, 148.37, 141.45, 141.35, 134.60, 117.63, 116.54, 111.26, 110.04, 82.80, 81.14, 75.31, 55.92, 44.93, 28.45, 28.31, 22.33. **TLC-MS:** ESI(+) calcd. for $[M+Na]^+$: *m/z* = 495.2; found: 495.3. **HPLC:** t_{ret} = 16.24 min (96.5% at 254 nm, 96.2% at 230 nm, method B).

tert-Butyl 2-(2-((tert-butoxycarbonyl)amino)pyridin-4-yl)-1-(4-methoxybenzyl)-4-oxo-1,4,6,7-tetrahydro-5H-pyrrolo[3,2-c]pyridine-5-carboxylate (226)

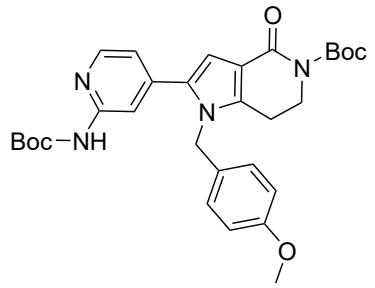

226

Chemical Formula: $C_{30}H_{36}N_4O_6$
Exact Mass: 548.26348
Molecular Weight: 548.64000

A flask containing *tert*-butyl 2-bromo-1-(4-methoxybenzyl)-4-oxo-1,4,6,7-tetrahydro-5*H*-pyrrolo[3,2-*c*]pyridine-5-carboxylate (**214**, 0.113 g, 0.260 mmol, 1.00 eq.), *tert*-butyl (4-(4,4,5,5-tetramethyl-1,3,2-dioxaborolan-2-yl)pyridin-2-yl)carbamate (**123**, 0.150 g, 0.467 mmol, 1.80 eq.), $Pd_2(dba)_3 \cdot CHCl_3$ (13.4 mg, 13.0 µmol, 5 mol%) and XPhos (12.4 mg, 26.0 µmol, 10 mol%) was purged with argon and 1,4.dioxane (degassed, 4.5 mL) added. After addition of a 2M Na_2CO_3 solution (degassed, 0.389 mL, 0.779 mmol, 3.00 eq.) the reaction mixture was stirred at 90 °C for 16 h. The reaction was cooled down to rt and the solvent evaporated. The residue was diluted with DCM (30 mL) and washed with sat. NH_4Cl solution (20 mL). The layers were separated and the aqueous layer extracted with DCM (2x 20 mL). The combined organic phases were dried over Na_2SO_4 and evaporated to dryness. The residue was purified by flash column

chromatography (Silica gel, 10 – 80% hexane/EtOAc) which afforded the product **226** (79.0 mg, 0.146 mmol, 56%) as light-yellow powder.

^{1}H NMR (400 MHz, $CDCl_3$) δ 8.18 – 8.15 (m, 1H), 7.96 (s, 1H), 7.65 (s, 1H), 6.89 (s, 1H), 6.87 (dd, *J* = 5.2, 1.6 Hz, 1H), 6.81 (s, 4H), 5.18 (s, 2H), 4.05 (t, *J* = 6.3 Hz, 2H), 3.76 (s, 3H), 2.70 (t, *J* = 6.3 Hz, 2H), 1.55 (s, 9H), 1.50 (s, 9H). **^{13}C NMR** (101 MHz, $CDCl_3$) δ 162.47, 159.30, 153.80, 152.49, 152.30, 148.19, 144.83, 141.79, 141.15, 134.26, 127.19, 117.76, 116.15, 114.55, 111.33, 110.10, 82.73, 81.27, 55.41, 48.09, 44.96, 28.39, 28.33, 22.55. **TLC-MS:** ESI(+) calcd. for $[M+Na]^+$: *m/z* = 571.3; found: 571.5. **HPLC:** t_{ret} = 9.50 min (100% at 254 nm, 99.6% at 230 nm, method A).

tert-Butyl 2-(2-((tert-butoxycarbonyl)amino)pyridin-4-yl)-4-oxo-1-tosyl-1,4,6,7-tetrahydro-5H-pyrrolo[3,2-c]pyridine-5-carboxylate (227)

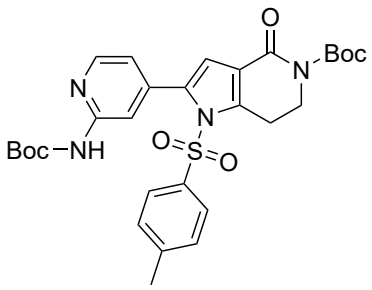

227
Chemical Formula: $C_{29}H_{34}N_4O_7S$
Exact Mass: 582.21482
Molecular Weight: 582.67200

tert-Butyl 2-bromo-4-oxo-1-tosyl-1,4,6,7-tetrahydro-5*H*-pyrrolo[3,2-*c*]pyridine-5-carboxylate (**216**, 0.360 g, 0.767 mmol, 1.00 eq.) and *tert*-Butyl (4-(4,4,5,5-tetramethyl-1,3,2-dioxaborolan-2-yl)pyridin-2-yl)carbamate (**123**, 0.368 g, 1.150 mmol, 1.50 eq.) were put into a flask and purged with argon. The solids were dissolved in 1,4-dioxane (degassed, 36 mL) and XPhos Pd g4 (33.0 mg, 38.3 µmol, 5 mol%) was added. After addition of a degassed 2M Na_2CO_3 solution (1.15 mL, 2.30 mmol, 3.00 eq.) the reaction was stirred at 80 °C for 18 h. After cooling to rt the solvent was removed under reduced pressure and the residue diluted with EtOAc (50 mL) and filtered through a pad of celite. After removal of the solvent the crude product was purified by flash column chromatography (Silica gel, 10 – 100% hexane/EtOAc) which afforded the product **227** (0.260 g, 0.445 mmol, 58%) as light-yellow powder.

^{1}H NMR (400 MHz, $CDCl_3$) δ 8.23 (d, *J* = 5.1 Hz, 1H), 8.16 (s, 1H), 7.83 (s, 1H), 7.37 (d, *J* = 8.3 Hz, 2H), 7.22 (d, *J* = 8.2 Hz, 2H), 6.97 (d, *J* = 5.3 Hz, 1H), 6.65 (s, 1H), 4.08 (t, *J* = 6.2 Hz, 2H), 3.31 (t, *J* = 6.3 Hz, 2H), 2.40 (s, 3H), 1.55 (s, 9H), 1.53 (s, 9H). **^{13}C NMR** (101 MHz, $CDCl_3$) δ 161.32, 152.98, 152.21, 151.80, 146.50, 146.23, 142.15, 141.88, 135.40, 135.17, 130.25, 127.14, 120.48, 119.96, 114.57, 113.75, 83.35, 81.34, 44.96, 28.44, 28.25, 24.94, 21.83. **TLC-MS:** ESI(+) calcd. for $[M+Na]^+$: *m/z* = 605.2; found: 605.7.; ESI(-) calcd. for $[M-H]^-$: *m/z* =581.2; found: 581.6. **HPLC:** t_{ret} = 19.20 min (97.9% at 254 nm, 96.4% at 230 nm, method B).

tert-Butyl 2-(2-((tert-butoxycarbonyl)(6-chloro-3-nitropyridin-2-yl)amino)pyridin-4-yl)-1-(methoxymethyl)-4-oxo-1,4,6,7-tetrahydro-5H-pyrrolo[3,2-c]pyridine-5-carboxylate (228)

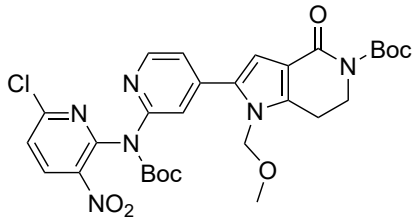

228

Chemical Formula: $C_{29}H_{33}ClN_6O_8$
Exact Mass: 628.20484
Molecular Weight: 629.06700

tert-Butyl 2-(2-((*tert*-butoxycarbonyl)amino)pyridin-4-yl)-1-(methoxymethyl)-4-oxo-1,4,6,7-tetrahydro-5*H*-pyrrolo[3,2-*c*]pyridine-5-carboxylate (**225**, 90.0 mg, 0.191 mmol, 1.00 eq.), 2-bromo-3-nitro-5-chloropyridine (67.9 mg, 0.286 mmol, 1.50 eq.) and Cs_2CO_3 (0.248 g, 0.762 mmol, 4.00 eq.) were weighed into a flask. The flask was purged with argon and toluene (degassed, 15 mL) added. XantPhos (5.51 mg, 9.53 µmol, 5 mol%) and $Pd(OAc)_2$ (2.14 mg, 9.53 µmol, 5 mol%) in toluene (0.5 mL, degassed) were stirred at 70 °C under an argon atmosphere for 15 min and then added to the reaction mixture. The reaction was stirred at 70 °C for 48 h. After cooling to rt the reaction was diluted with DCM (30 mL) and washed with water (50 mL). The aqueous phase was extracted with DCM and the combined organic layers dried over Na_2SO_4. The solvent was evaporated and the residue purified by flash column chromatography (Silica gel, 1.5 – 5% DCM/MeOH) which afforded the product **228** (91.0 mg, 0.145 mmol, 76%) as yellow solid.

^{1}H NMR (400 MHz, $CDCl_3$) δ 8.43 (d, *J* = 8.5 Hz, 1H), 8.19 (d, *J* = 5.2 Hz, 1H), 7.90 (s, 1H), 7.45 (d, *J* = 8.5 Hz, 1H), 7.16 (dd, *J* = 5.2, 1.5 Hz, 1H), 6.89 (s, 1H), 5.21 (s, 2H), 4.14 (t, *J* = 6.3 Hz, 2H), 3.34 (s, 3H), 2.99 (t, *J* = 6.3 Hz, 2H), 1.56 (s, 9H), 1.40 (s, 9H). **^{13}C NMR** (101 MHz, $CDCl_3$) δ 162.31, 153.77, 153.76, 153.68, 151.17, 148.36, 147.86, 141.90, 141.60, 140.84, 136.53, 134.04, 123.92, 119.71, 117.63, 116.59, 110.19, 84.23, 82.83, 75.17, 55.95, 44.86, 28.28, 27.91, 22.32. **TLC-MS:** ESI(+) calcd. for $[M+Na]^+$: *m/z* = 651.2; found: 651.4. **HPLC:** t_{ret} = 17.78 min (95.5% at 254 nm, 95.6% at 230 nm, method B).

tert-Butyl 2-(2-((tert-butoxycarbonyl)(6-chloro-3-nitropyridin-2-yl)amino)pyridin-4-yl)-1-(4-methoxybenzyl)-4-oxo-1,4,6,7-tetrahydro-5H-pyrrolo[3,2-c]pyridine-5-carboxylate (229)

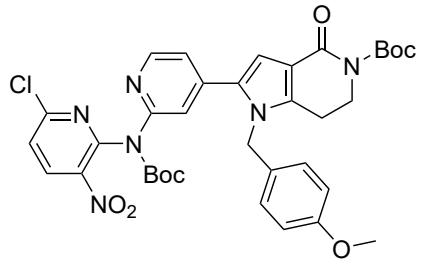

229

Chemical Formula: $C_{35}H_{37}ClN_6O_8$
Exact Mass: 704.23614
Molecular Weight: 705.16500

tert-Butyl 2-(2-((*tert*-butoxycarbonyl)amino)pyridin-4-yl)-1-(4-methoxybenzyl)-4-oxo-1,4,6,7-tetrahydro-5*H*-pyrrolo[3,2-*c*]pyridine-5-carboxylate (**226**, 25.0 mg, 45.6 µmol, 1.00 eq.), 2-bromo-3-nitro-5-chloropyridine (16.2 mg, 68.4 µmol, 1.50 eq.) and Cs_2CO_3 (59.4 mg, 0.182 mmol, 4.00 eq.) were weighed into a flask. The flask was purged with argon and toluene (degassed, 4 mL) added. XantPhos (1.58 mg, 2.73 µmol, 6 mol%) and $Pd(OAc)_2$ (0.61 mg, 2.73 µmol, 6 mol%) in toluene (0.1 mL, degassed) were stirred at 70 °C under an argon atmosphere for 15 min and then added to the reaction mixture. The reaction was stirred at 70 °C for 48 h. After cooling to rt the

reaction was diluted with DCM (10 mL) and washed with sat. NH_4Cl solution (10 mL). The aqueous phase was extracted with DCM and the combined organic layers dried over Na_2SO_4. The solvent was evaporated, and the residue purified by flash column chromatography (Silica gel, 10 – 80% hexane/EtOAc) which afforded the product **229** (15.0 mg, 21.3 µmol, 47%, containing ~5% of starting material) as yellow solid.

TLC-MS: ESI(+) calcd. for $[M+Na]^+$: *m/z* = 727.2; found: 727.4. **HPLC:** t_{ret} = 9.79 min (94.5% at 254 nm, 93.0% at 230 nm, method A).

tert-Butyl 2-(2-((tert-butoxycarbonyl)(6-chloro-3-nitropyridin-2-yl)amino)pyridin-4-yl)-4-oxo-1-tosyl-1,4,6,7-tetrahydro-5H-pyrrolo[3,2-c]pyridine-5-carboxylate (230)

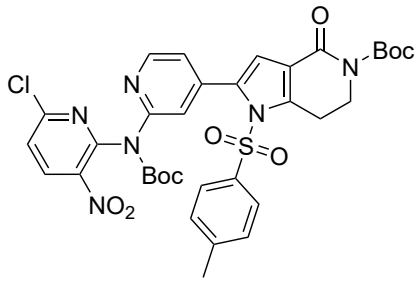

230

Chemical Formula: $C_{34}H_{35}ClN_6O_9S$
Exact Mass: 738.18748
Molecular Weight: 739.19700

tert-Butyl 2-(2-((tert-butoxycarbonyl)amino)pyridin-4-yl)-4-oxo-1-tosyl-1,4,6,7-tetrahydro-5*H*-pyrrolo[3,2-*c*]pyridine-5-carboxylate (**227**, 35.0 mg, 60.1 µmol, 1.00 eq.) was subjected to GSP 8, dissolved in toluene (10 mL) and stirred at 70 °C for 16 h. After cooling to rt the reaction was diluted with DCM (20 mL) and washed with sat. NH_4Cl solution (20 mL). The aqueous phase was extracted with DCM (2x 20 mL) and the combined organic layers dried over Na_2SO_4. After removal of the solvent the residue was purified by flash column chromatography (Silica gel, 10 - 90% hexane/EtOAc) which afforded the product **230** (38.5 mg, 51.4 µmol, 86%) as yellow solid.

^{1}H NMR (400 MHz, $CDCl_3$) δ 8.43 (d, *J* = 8.5 Hz, 1H), 8.16 (d, *J* = 5.1 Hz, 1H), 7.56 (s, 1H), 7.46 (d, *J* = 8.5 Hz, 1H), 7.33 (d, *J* = 8.4 Hz, 2H), 7.23 (d, *J* = 8.2 Hz, 2H), 7.02 (dd, *J* = 5.1, 1.4 Hz, 1H), 6.66 (s, 1H), 4.09 (d, *J* = 3.1 Hz, 2H), 3.38 (t, *J* = 6.3 Hz, 2H), 2.40 (s, 3H), 1.56 (s, 9H), 1.40 (s, 9H). **^{13}C NMR** (101 MHz, $CDCl_3$) δ 161.39, 153.77, 153.01, 153.00, 150.96, 147.81, 147.01, 146.39, 142.47, 141.77, 140.95, 136.53, 134.82, 134.70, 130.33, 127.36, 123.80, 122.79, 120.25, 119.73, 114.50, 84.27, 83.34, 44.96, 28.24, 27.96, 25.09, 21.86. **TLC-MS:** ESI(+) calcd. for $[M+Na]^+$: *m/z* = 761.2; found: 761.4; ESI(-) calcd. for $[M-H]^-$: *m/z* =737.2; found: 737.2. **HPLC:** t_{ret} = 19.75 min (95.7% at 254 nm, 95.1% at 230 nm, method B).

2-(2-((6-Chloro-3-nitropyridin-2-yl)amino)pyridin-4-yl)-1-(methoxymethyl)-1,5,6,7-tetrahydro-4H-pyrrolo[3,2-c]pyridin-4-one (232)

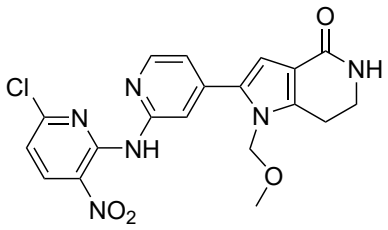

232
Chemical Formula: $C_{19}H_{17}ClN_6O_4$
Exact Mass: 428.09998
Molecular Weight: 428.83300

tert-Butyl 2-(2-((*tert*-butoxycarbonyl)(6-chloro-3-nitropyridin-2-yl)amino)pyridin-4-yl)-1-(methoxymethyl)-4-oxo-1,4,6,7-tetrahydro-5*H*-pyrrolo[3,2-*c*]pyridine-5-carboxylate (**228**, 49.0 mg, 77.9 µmol) was dissolved in DCM (4 mL) and subjected to GSP 7 and stirred for 1 h. The residue was dissolved in DCM (10 mL) and washed with sat. Na_2CO_3 solution. The organic layer was dried over Na_2SO_4 and the solvent evaporated. The raw product was purified by flash column chromatography (Silica gel, 3 – 10% DCM/MeOH) which afforded the product **232** (17.0 mg, 39.6 µmol, 51%) as yellow solid.

^{1}H NMR (400 MHz, DMSO) δ 10.47 (s, 1H), 8.61 (d, *J* = 8.6 Hz, 1H), 8.35 (d, *J* = 5.2 Hz, 1H), 8.22 (s, 1H), 7.34 (dd, *J* = 5.2, 1.2 Hz, 1H), 7.24 (s, 1H), 7.21 (d, *J* = 8.6 Hz, 1H), 6.74 (s, 1H), 5.36 (s, 2H), 3.49 – 3.42 (m, 2H), 3.24 (s, 3H), 2.96 (t, *J* = 6.8 Hz, 2H). **^{13}C NMR** (101 MHz, DMSO) δ 164.34, 153.50, 151.40, 148.52, 147.33, 141.04, 140.97, 138.82, 132.26, 129.70, 118.12, 115.74, 115.21, 112.06, 108.70, 74.69, 55.38, 21.42. **HRMS:** ESI(+) calcd. for $[M+H]^+$: *m/z* =429.10726; found: 429.10755; rel. deviation: 0.67 ppm. **HPLC:** t_{ret} = 13.60 min (98.3% at 254 nm, 97.2% at 230 nm, method B). **IR** (ATR) [cm^{-1}]: 3352, 3321, 1653, 1578, 1486, 1412, 1392, 1344, 1320, 1265, 1217, 1154, 1133, 1094, 1061, 1039, 992, 967, 898, 853, 814, 759, 675.

tert-Butyl 2-(2-((tert-butoxycarbonyl)amino)pyridin-4-yl)-4-oxo-1,4,6,7-tetrahydro-5H-pyrrolo[3,2-c]pyridine-5-carboxylate (139)

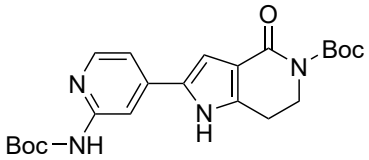

139
Chemical Formula: $C_{22}H_{28}N_4O_5$
Exact Mass: 428.20597
Molecular Weight: 428.48900

A) alternative method **A** described in section 6.2.7.

B) *tert*-Butyl 2-bromo-4-oxo-1-pivaloyl-1,4,6,7-tetrahydro-5*H*-pyrrolo[3,2-*c*]pyridine-5-carboxylate (**215**, 0.155 g, 0.388 mmol, 1.00 eq.), *tert*-butyl (4-(4,4,5,5-tetramethyl-1,3,2-dioxaborolan-2-yl)pyridin-2-yl)carbamate (**123**, 0.124 g, 0.388 mmol, 1.00 eq.) and XPhos Pd g4 (16.7 mg, 19.4 µmol, 5 mol%) were weighed into a flask and purged with argon. 1,4-dioxane (degassed, 4.0 mL) and a 2 M Na_2CO_3 solution (0.582 mL, 1.165 mmol, 3.00 eq.) were added and the reaction stirred at 80 °C for 18 h. Stirring was continued for 3 h at 90 °C before the reaction was cooled to rt and diluted with EtOAc (20 mL). The mixture was washed with sat. NH_4Cl solution, water and brine (20 mL) and the organic layer dried over Na_2SO_4. The solvent was removed under reduced pressure and the residue purified by flash column chromatography (Silica gel, 10 – 100% hexane/EtOAc) which afforded the product **139** (31.0 mg, 73.7µmol, 19%) as white solid.

^{1}H NMR (400 MHz, MeOD) δ 8.02 (d, *J* = 5.5 Hz, 1H), 7.82 (d, *J* = 0.9 Hz, 1H), 7.04 (dd, *J* = 5.5, 1.6 Hz, 1H), 6.95 (s, 1H), 3.99 (t, *J* = 6.4 Hz, 2H), 2.85 (t, *J* = 6.4 Hz, 2H), 1.43 (s, 18H). **TLC-MS:** ESI(+) calcd. for $[M+Na]^+$: *m/z* = 451.2; found: 451.4; ESI(-) calcd. for $[M-H]^-$: *m/z* = 427.2; found: 427.5. **HPLC:** t_{ret} = 14.69 min (96.9% at 254 nm, 97.5% at 230 nm, method B).

C) *tert*-Butyl 2-(2-((tert-butoxycarbonyl)amino)pyridin-4-yl)-4-oxo-1-tosyl-1,4,6,7-tetrahydro-5*H*-pyrrolo[3,2-*c*]pyridine-5-carboxylate (**227**, 0.160 g, 0.275 mmol, 1.00 eq.) and Cs_2CO_3 (0.179 g, 0.550 mmol, 2.00 eq.) were dissolved in an mixture of THF (1.5 mL) and MeOH (0.75 mL). After stirring the reaction for 30 min at rt, brine (15 mL) was added and the reaction extracted with EtOAc (15 mL) twice. The organic layer was dried over Na_2SO_4 and the solvent removed under reduced pressure. The crude product was purified by flash column chromatography (Silica gel, 30 – 100% hexane/EtOAc) which afforded the product **139** (54.6 mg, 0.127 mmol, 46%) as white solid.

^{1}H NMR (400 MHz, $CDCl_3$) δ 8.08 (d, *J* = 5.4 Hz, 1H), 7.86 (s, 1H), 7.09 (d, *J* = 5.3 Hz, 1H), 7.00 (s, 1H), 4.04 (t, *J* = 6.1 Hz, 2H), 2.89 (t, *J* = 6.2 Hz, 2H), 1.48 (s, 18H). **^{13}C NMR** (101 MHz, $CDCl_3$) δ 163.42, 153.46, 153.20, 152.38, 147.86, 141.36, 140.69, 130.76, 116.11, 116.04, 113.95, 107.87, 105.88, 82.88, 81.55, 45.27, 28.18, 27.99, 22.51. **TLC-MS:** ESI(+) calcd. for $[M+Na]^+$: *m/z* = 451.2; found: 451.2; ESI(-) calcd. for $[M-H]^-$: *m/z* = 427.2; found: 427.3. **HPLC:** t_{ret} = 7.66 min (96.7% at 254 nm, 96.7% at 230 nm, method A).

Di-tert-butyl 2-(2-((tert-butoxycarbonyl)amino)pyridin-4-yl)-4-oxo-6,7-dihydro-1H-pyrrolo[3,2-c]pyridine-1,5(4H)-dicarboxylate (145)

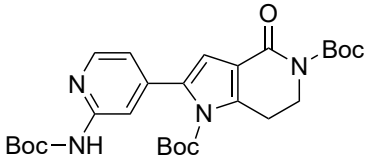

145

Chemical Formula: $C_{27}H_{36}N_4O_7$
Exact Mass: 528.25840
Molecular Weight: 528.60600

B) *tert*-Butyl 2-(2-((*tert*-butoxycarbonyl)amino)pyridin-4-yl)-4-oxo-1,4,6,7-tetrahydro-5*H*-pyrrolo[3,2-*c*]pyridine-5-carboxylate (**139**, 45.0 mg, 0.105 mmol, 1.00 eq.) was dissolved in DMF (0.5 mL) and cooled to 0 °C. NaH (60% dispersion in mineral oil, 4.20 mg, 0.105 mmol, 1.00 eq.) was added and the reaction stirred at rt for 30 min. Di-*tert*-butyldicarbonat (24.0 µL, 22.9 mg, 0.105 mmol, 1.00 eq.) and DMAP (1.28 mg, 10.5 µmol, 10 mol%) was added and the reaction stirred for 18 h at rt. An additional portion of di-*tert*-butyldicarbonat (24.0 µL, 22.9 mg, 0.105 mmol, 1.00 eq.) was added and the reaction stirred for 24 h. The reaction was diluted with DCM (10 mL) and washed with H_2O (10 mL). The organic layer was dried over Na_2SO_4 and the solvent evaporated. The residue was purified by flash column chromatography (Silica gel, 20 – 100% hexane/EtOAc) which afforded the product **145** (20.4 mg, 38.6 µmol, 37%) as white powder.

^{1}H NMR (400 MHz, $CDCl_3$) δ 8.56 (s, 1H), 8.26 (d, *J* = 5.0 Hz, 1H), 7.97 (s, 1H), 6.90 (dd, *J* = 5.2, 1.5 Hz, 1H), 6.72 (s, 1H), 4.09 (t, *J* = 6.4 Hz, 2H), 3.22 (t, *J* = 6.4 Hz, 2H), 1.56 (s, 9H), 1.51 (s, 9H), 1.35 (s, 9H). **^{13}C NMR** (101 MHz, $CDCl_3$) δ 161.98, 153.29, 152.51, 152.17, 148.55, 147.50, 143.67, 142.25, 134.08, 118.38, 117.92, 112.86, 112.02, 86.16, 82.98, 81.13, 44.76, 28.39, 28.28, 27.53, 24.71. **TLC-**

MS: ESI(+) calcd. for $[M+Na]^+$: *m/z* = 551.3; found: 551.0; ESI(-) calcd. for $[M-H]^-$: *m/z* =527.3; found: 527.3. **HPLC:** t_{ret} = 9.98 min (97.2% at 254 nm, 97.9% at 230 nm, method A).

An alternative (unsuccessful) attempt to for the synthesis of **145** is described in section 6.2.7.

Di-tert-butyl 2-(2-((tert-butoxycarbonyl)(6-chloro-3-nitropyridin-2-yl)amino)pyridin-4-yl)-4-oxo-6,7-dihydro-1H-pyrrolo[3,2-c]pyridine-1,5(4H)-dicarboxylate (233)

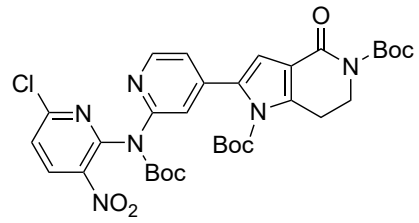

233

Chemical Formula: $C_{32}H_{37}ClN_6O_9$
Exact Mass: 684.23105
Molecular Weight: 685.13100

Di-*tert*-butyl 2-(2-((*tert*-butoxycarbonyl)amino)pyridin-4-yl)-4-oxo-6,7-dihydro-1*H*-pyrrolo[3,2-*c*]pyridine-1,5(4*H*)-dicarboxylate (**145**, 20.4 mg, 38.6 µmol, 1.00 eq.) was dissolved in DMF (1.0 mL, dry) under argon atmosphere and cooled to 0°C. After the addition of NaH (60 % dispersion in mineral oil, 2.32 mg, 57.9 µmol, 1.50 eq.) the mixture was stirred for 30 min at rt. Then 5-chloro-2-flouro-3-nitropyridine (20.6 mg, 0.116 mmol, 3.00 eq.) was added at 0 °C and then stirred for 18 h at room temperature. The reaction was quenched by the addition of sat. $NaHCO_3$ solution (10 mL) and extracted with DCM (4x 10 mL). the organic layer dried over Na_2SO_4. The solvent was removed under reduced pressure and the crude product purified by flash column chromatography (Silica gel, 0.5 – 8% DCM/MeOH) which afforded the product **233** (16.0 mg, 27.4 µmol, 71%) as yellow solid.**^{1}H NMR** (400 MHz, $CDCl_3$) δ 8.43 (d, *J* = 8.4 Hz, 1H), 8.17 (d, *J* = 5.1 Hz, 1H), 7.80 (s, 1H), 7.45 (d, *J* = 8.4 Hz, 1H), 6.99 (dd, *J* = 5.1, 1.2 Hz, 1H), 6.73 (s, 1H), 4.11 (t, *J* = 6.4 Hz, 2H), 3.26 (t, *J* = 6.4 Hz, 2H), 1.57 (s, 9H), 1.40 (s, 9H), 1.36 (s, 9H). **^{13}C NMR** (101 MHz, $CDCl_3$) δ 161.97, 153.78, 153.38, 153.33, 151.00, 148.57, 147.93, 147.31, 143.68, 142.44, 142.03, 136.46, 133.41, 123.88, 120.46, 118.48, 118.35, 112.94, 86.66, 84.28, 83.05, 44.77, 28.31, 27.96, 27.50, 24.70. **TLC-MS:** ESI(+) calcd. for $[M+Na]^+$: *m/z* = 707.2; found: 706.8; ESI(-) calcd. for $[M-Boc-H]^-$: *m/z* = 583.2; found: 583.1. **HPLC:** t_{ret} = 10.47 min (97.4% at 254 nm, 97.4% at 230 nm, method B).

2-(2-((6-Chloro-3-nitropyridin-2-yl)amino)pyridin-4-yl)-1,5,6,7-tetrahydro-4H-pyrrolo[3,2-c]pyridin-4-one (231)

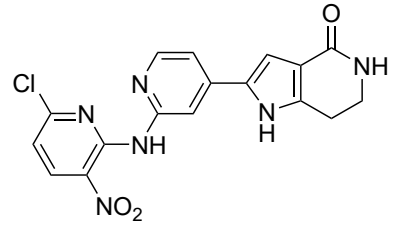

231

Chemical Formula: $C_{17}H_{13}ClN_6O_3$
Exact Mass: 384.07377
Molecular Weight: 384.78000

Di-*tert*-butyl 2-(2-((*tert*-butoxycarbonyl)(6-chloro-3-nitropyridin-2-yl)amino)pyridin-4-yl)-4-oxo-6,7-dihydro-1*H*-pyrrolo[3,2-*c*]pyridine-1,5(4*H*)-dicarboxylate (**233**, 16.0 mg, 27.4 µmol) was dissolved in DCM (2 mL, dry) and subjected to GSP 7 and stirred for 30 min. . The residue was dissolved in DCM (10 mL) and washed with sat. Na_2CO_3 solution (7 mL). The aqueous phase was extracted with DCM until the yellow color was removed. The combined organic layers were dried over Na_2SO_4 and the solvent evaporated. The raw product was

purified by flash column chromatography (Silica gel, 3 – 10% DCM/MeOH) which afforded the product (**231**, 3.0 mg, 7.8 µmol, 28%) as yellow powder.

^{1}H NMR (400 MHz, DMSO) δ 12.00 (s, 1H), 10.43 (s, 1H), 8.60 (d, *J* = 8.6 Hz, 1H), 8.31 – 8.19 (m, 2H), 7.38 (d, *J* = 5.4 Hz, 1H), 7.21 (d, *J* = 8.7 Hz, 1H), 7.11 (s, 1H), 6.88 (s, 1H), 3.41 (dt, *J* = 7.0, 3.6 Hz, 2H), 2.86 (t, *J* = 6.8 Hz, 2H). **HRMS:** ESI(+) calcd. for $[M+H]^+$: *m/z* = 385.08104; found: 385.08133; rel. deviation: 0.74 ppm. **HPLC:** t_{ret} = 5.78 min (100% at 254 nm, 100% at 230 nm, method A).

tert-Butyl (R)-2-(2-((tert-butoxycarbonyl)amino)pyridin-4-yl)-1-((2,2-dimethyl-1,3-dioxolan-4-yl)methyl)-4-oxo-1,4,6,7-tetrahydro-5H-pyrrolo[3,2-c]pyridine-5-carboxylate (234)

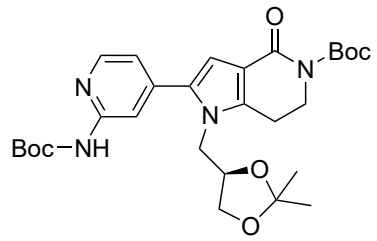

234
Chemical Formula: $C_{28}H_{38}N_4O_7$
Exact Mass: 542.27405
Molecular Weight: 542.63300

To a mixture of *tert*-butyl (*R*)-2-bromo-1-((2,2-dimethyl-1,3-dioxolan-4-yl)methyl)-4-oxo-1,4,6,7-tetrahydro-5*H*-pyrrolo[3,2-*c*]pyridine-5-carboxylate (**217**, 0.500 g, 1.52 mmol, 1.00 eq.) and *tert*-Butyl (4-(4,4,5,5-tetramethyl-1,3,2-dioxaborolan-2-yl)pyridin-2-yl)carbamate (**123**, 0.584 g, 1.82 mmol, 1.20 eq.) was added 1,4-dioxane (degassed, 20 mL) and 2.28 mL of a degassed 2 M Na_2CO_3 solution (2.25 mmol, 3.00 eq) was added dropwise. After adding XPhos Pd g4 (65.3 mg, 75.9 µmol, 5 mol%) the reaction was heated at 90 °C and stirred for 6h. After cooling down to room temperature the solvent was evaporated. The residue was suspended in EtOAc (50 mL), filtered through a pad of celite and the filtrated washed with sat. NH_4Cl solution (40 mL). The organic phase was dried over Na_2SO_4 and the solvent evaporated. The residue was purified by two consecutive flash column chromatography methods (Silica gel, 1: 1 – 6% DCM/MeOH; 2: 30 – 100% hexane/EtOAc) which afforded the product **234** (0.280 g, 0.516 mmol, 34%) as white powder.

^{1}H NMR (400 MHz, $CDCl_3$) δ 10.15 (s, 1H), 8.32 (d, *J* = 5.3 Hz, 1H), 7.98 (s, 1H), 7.01 – 6.90 (m, 1H), 6.79 (s, 1H), 4.28 – 4.19 (m, 2H), 4.17 – 4.08 (m, 1H), 4.08 – 3.91 (m, 3H), 3.46 (dd, *J* = 8.5, 6.2 Hz, 1H), 3.05 (ddd, *J* = 13.5, 8.4, 4.9 Hz, 1H), 2.88 (dt, *J* = 11.5, 5.1 Hz, 1H), 1.50 (d, *J* = 1.4 Hz, 18H), 1.28 (s, 3H), 1.22 (s, 3H). **^{13}C NMR** (101 MHz, $CDCl_3$) δ 162.26, 153.51, 153.24, 152.94, 148.13, 142.04, 141.82, 133.35, 117.50, 115.68, 110.94, 110.34, 109.99, 82.35, 80.90, 75.47, 66.52, 47.86, 44.88, 28.34, 28.12, 26.48, 25.03, 23.09. **TLC-MS:** ESI(+) calcd. for $[M+Na]^+$: *m/z* = 565.3; found: 565.4; ESI(-) calcd. for $[M-H]^-$: *m/z* = 541.3; found: 541.6. **HPLC:** t_{ret} = 17.77 min (97.6% at 254 nm, 98.6% at 230 nm, method B).

tert-Butyl (S)-2-(2-((tert-butoxycarbonyl)amino)pyridin-4-yl)-1-((2,2-dimethyl-1,3-dioxolan-4-yl)methyl)-4-oxo-1,4,6,7-tetrahydro-5H-pyrrolo[3,2-c]pyridine-5-carboxylate (235)

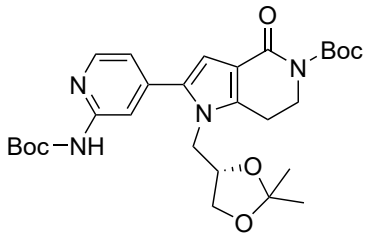

235

Chemical Formula: $C_{28}H_{38}N_4O_7$
Exact Mass: 542.27405
Molecular Weight: 542.63300

To a mixture of *tert*-butyl (*S*)-2-bromo-1-((2,2-dimethyl-1,3-dioxolan-4-yl)methyl)-4-oxo-1,4,6,7-tetrahydro-5*H*-pyrrolo[3,2-*c*]pyridine-5-carboxylate (**218**, 0.210 g, 0.638 mmol, 1.00 eq.) and *tert*-Butyl (4-(4,4,5,5-tetramethyl-1,3,2-dioxaborolan-2-yl)pyridin-2-yl)carbamate (**123**, 0.245 g, 0.765 mmol, 1.20 eq.) was added 1,4-dioxane (degassed, 9 mL) and a degassed 2 M Na_2CO_3 - solution (0,957 mL, 1.91 mmol, 3.00 eq) was added dropwise. After adding XPhos Pd g4 (27.4 mg, 31.9 µmol, 5 mol%) the reaction was heated to 90 °C and stirred for 6h. After cooling down to rt the solvent was evaporated. The residue suspended in EtOAc (20 mL), filtered through a pad of Celite and the filtrated washed with sat. NH_4Cl solution (20 mL). The organic phase was dried over Na_2SO_4 and the solvent evaporated. The residue was purified by two consecutive flash column chromatography methods (Silica gel, 1: 1 – 6% DCM/MeOH; 2: 30 – 100% hexane/EtOAc) which afforded the product **235** (86.0 mg, 0.160 mmol, 25%) as white powder.

^{1}H NMR (400 MHz, $CDCl_3$) δ 9.82 (s, 1H), 8.33 (d, *J* = 5.3 Hz, 1H), 7.99 (s, 1H), 6.97 (dd, *J* = 5.2, 1.3 Hz, 1H), 6.81 (s, 1H), 4.26 (dd, *J* = 11.4, 4.1 Hz, 2H), 4.15 (dd, *J* = 12.5, 5.7 Hz, 1H), 4.09 – 4.03 (m, 1H), 4.02 – 3.95 (m, 2H), 3.47 (dd, *J* = 8.6, 6.2 Hz, 1H), 3.13 – 3.01 (m, 1H), 2.98 – 2.81 (m, 1H), 1.53 (s, 9H), 1.52 (s, 9H), 1.31 (s, 3H), 1.25 (s, 3H). **^{13}C NMR** (101 MHz, $CDCl_3$) δ 162.34, 153.64, 153.20, 152.95, 148.27, 142.09, 141.89, 133.42, 117.68, 115.80, 110.98, 110.45, 110.10, 82.49, 81.04, 75.55, 66.62, 53.48, 47.95, 44.95, 28.41, 28.21, 26.56, 25.11, 23.18. **TLC-MS:** ESI(+) calcd. for $[M+Na]^+$: *m/z* = 565.3; found: 564.8; ESI(-) calcd. for $[M-H]^-$: *m/z* = 541.3; found: 541.6. **HPLC:** t_{ret} = 17.78 min (99.2% at 254 nm, 98.7% at 230 nm, method B).

tert-Butyl (R)-2-(2-((tert-butoxycarbonyl)(6-chloro-3-nitropyridin-2-yl)amino)pyridin-4-yl)-1-((2,2-dimethyl-1,3-dioxolan-4-yl)methyl)-4-oxo-1,4,6,7-tetrahydro-5H-pyrrolo[3,2-c]pyridine-5-carboxylate (236)

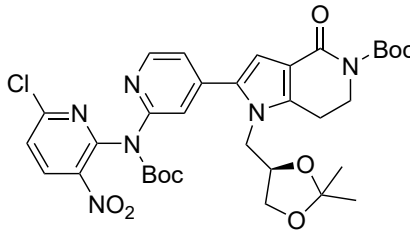

236

Chemical Formula: $C_{33}H_{39}ClN_6O_9$
Exact Mass: 698.24670
Molecular Weight: 699.15800

tert-Butyl (*R*)-2-(2-((*tert*-butoxycarbonyl)amino)pyridin-4-yl)-1-((2,2-dimethyl-1,3-dioxolan-4-yl)methyl)-4-oxo-1,4,6,7-tetrahydro-5*H*-pyrrolo[3,2-*c*]pyridine-5-carboxylate (**234**, 0.200 g, 0.369 mmol, 1.00 eq.) was subjected to GSP 8 (4 mL toluene) and stirred at 55 °C for 18 h. After cooling to rt the reaction was diluted with EtOAc (20 mL) and filtered through a pad of celite. The filtrate was washed with sat. NH_4Cl solution, brine and H_2O (20 mL) and organic layer dried over Na_2SO_4 and the solvent evaporated. The raw product was

purified in a two-step procedure by flash column chromatography (Silica gel, 1: 0 – 5% DCM/MeOH; 2: 10 – 80% hexane /EtOAc) which afforded the product **236** (0.177 g, 0.253 mmol, 69%) as yellow oil. **^{1}H NMR** (400 MHz, $CDCl_3$) δ 8.47 (d, *J* = 5.2 Hz, 1H), 8.25 (d, *J* = 8.8 Hz, 1H), 7.96 (d, *J* = 8.8 Hz, 1H), 7.36 (d, *J* = 0.8 Hz, 1H), 7.26 (s, 1H), 6.87 (s, 1H), 4.14 (t, *J* = 6.3 Hz, 2H), 3.65 (s, 3H), 2.91 (t, *J* = 6.3 Hz, 2H), 1.56 (s, 9H), 1.44 (s, 9H). **^{13}C NMR** (101 MHz, $CDCl_3$) δ 162.49, 153.85, 153.52, 151.23, 148.40, 147.72, 142.26, 142.01, 141.45, 136.55, 133.07, 124.16, 120.23, 117.20, 116.01, 110.65, 110.33, 84.32, 82.67, 75.65, 66.66, 48.12, 45.01, 28.33, 27.93, 26.65, 25.19, 23.31. **TLC-MS:** ESI(+) calcd. for $[M+H]^+$: *m/z* = 721.2. **HPLC:** t_{ret} = 18.62 min (95.7% at 254 nm, 93.8% at 230 nm, method B).

tert-Butyl (S)-2-(2-((tert-butoxycarbonyl)(6-chloro-3-nitropyridin-2-yl)amino)pyridin-4-yl)-1-((2,2-dimethyl-1,3-dioxolan-4-yl)methyl)-4-oxo-1,4,6,7-tetrahydro-5H-pyrrolo[3,2-c]pyridine-5-carboxylate (237)

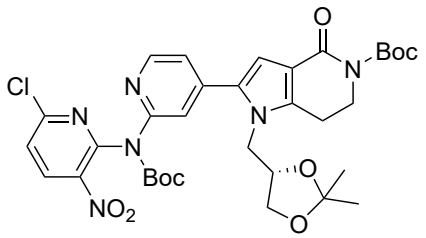

237
Chemical Formula: $C_{33}H_{39}ClN_6O_9$
Exact Mass: 698.24670
Molecular Weight: 699.15800

tert-Butyl (*S*)-2-(2-((*tert*-butoxycarbonyl)amino)pyridin-4-yl)-1-((2,2-dimethyl-1,3-dioxolan-4-yl)methyl)-4-oxo-1,4,6,7-tetrahydro-5*H*-pyrrolo[3,2-*c*]pyridine-5-carboxylate (**235**, 86.0 mg, 0.158 mmol, 1.00 eq.) was subjected to GSP 8 (2 mL toluene) and stirred at 60 °C for 18 h. After cooling to rt, the reaction was quenched by addition of sat. $NaHCO_3$ solution and extracted with DCM (3x 20 mL). The organic layer was dried over Na_2SO_4 and the solvent evaporated. The raw product was purified in a two-step procedure by flash column chromatography (Silica gel, 1: 0 – 5% DCM/MeOH; 2: 10 – 80% hexane /EtOAc) which afforded the product **237** (68.0 mg, 97.3 µmol, 61%) as yellow oil.

^{1}H NMR (400 MHz, $CDCl_3$) δ 8.43 (d, *J* = 8.5 Hz, 1H), 8.15 (d, *J* = 5.2 Hz, 1H), 7.81 (s, 1H), 7.47 (d, *J* = 8.5 Hz, 1H), 7.06 (dd, *J* = 5.2, 1.4 Hz, 1H), 6.84 (s, 1H), 4.31 – 4.15 (m, 3H), 4.11 – 3.98 (m, 3H), 3.54 (dd, *J* = 8.7, 6.3 Hz, 1H), 3.16 – 3.04 (m, 1H), 2.92 (ddd, *J* = 16.4, 6.7, 4.8 Hz, 1H), 1.56 (s, 9H), 1.39 (s, 9H), 1.34 (s, 3H), 1.26 (s, 3H). **^{13}C NMR** (101 MHz, $CDCl_3$) δ 162.41, 153.82, 153.78, 153.50, 151.20, 148.35, 147.67, 142.21, 141.97, 141.50, 136.52, 133.04, 124.14, 120.17, 117.17, 115.97, 110.59, 110.27, 84.26, 82.63, 75.61, 66.76, 48.08, 44.98, 28.28, 27.89, 26.60, 25.16, 23.27. **TLC-MS:** ESI(+) calcd. for $[M+Na]^+$: *m/z* = 721.3; found: 720.8. **HPLC:** t_{ret} = 18.69 min (98.7% at 254 nm, 97.9% at 230 nm, method B).

(R)-2-(2-((6-Chloro-3-nitropyridin-2-yl)amino)pyridin-4-yl)-1-(2,3-dihydroxypropyl)-1,5,6,7-tetrahydro-4H-pyrrolo[3,2-c]pyridin-4-one (238)

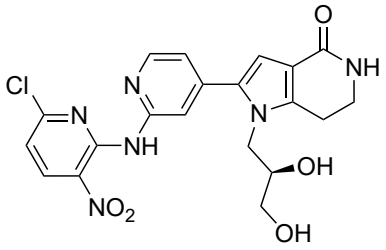

238

Chemical Formula: $C_{20}H_{19}ClN_6O_5$
Exact Mass: 458.11055
Molecular Weight: 458.85900

tert-Butyl (*R*)-2-(2-((tert-butoxycarbonyl)(6-chloro-3-nitropyridin-2-yl)amino)pyridin-4-yl)-1-((2,2-dimethyl-1,3-dioxolan-4-yl)methyl)-4-oxo-1,4,6,7-tetrahydro-5*H*-pyrrolo[3,2-*c*]pyridine-5-carboxylate (**236**, 42.0 mg, 74.4 µmol, 1.00 eq.) was dissolved in DCM (2 mL) and water (18 µL) in TFA (87 µL) added. The reaction was stirred at rt for 18 h. $NaHCO_3$ solution (2 mL) was added and the mixture extracted with DCM (3x 5 mL). The combined organic layers were dried over Na_2SO_4 and the solvent removed under reduced pressure. The aqueous phase was lyophilized and combined with the extracted fraction. The crude product was purified by reversed phase column chromatography (43 g, CHROMABOND® Flash RS 40 C_{18} ec, 10 - 60% water/MeCN + 0.2% TFA, 60 min). The product containing fractions were lyophilised and purified by flash column chromatography (Silica gel, 5 – 10% DCM/MeOH) which afforded the product **238** (2.0 mg, 5.8%) as yellow powder.

^{1}H NMR (400 MHz, DMSO) δ 10.47 (s, 1H), 8.62 (d, *J* = 8.6 Hz, 1H), 8.32 (d, *J* = 5.2 Hz, 1H), 8.20 (s, 1H), 7.35 (dd, *J* = 5.2, 1.2 Hz, 1H), 7.24 – 7.17 (m, 1H), 7.08 (s, 1H), 6.61 (s, 1H), 4.97 (d, *J* = 4.4 Hz, 1H), 4.63 (d, *J* = 4.9 Hz, 1H), 4.31 (dd, *J* = 14.8, 3.3 Hz, 1H), 4.01 (dd, *J* = 14.7, 8.7 Hz, 1H), 3.54 (dd, *J* = 9.0, 4.3 Hz, 1H), 3.42 (dd, *J* = 6.7, 4.6 Hz, 2H), 3.22 (d, *J* = 4.1 Hz, 2H), 3.01 – 2.83 (m, 2H). **^{13}C NMR** (101 MHz, DMSO) δ 164.69, 153.47, 151.31, 148.33, 147.26, 142.09, 141.14, 138.78, 131.78, 129.68, 118.41, 115.62, 114.44, 112.16, 108.39, 71.08, 63.51, 47.91, 21.99. **HPLC:** t_{ret} = 9.95 min (95.7% at 254 nm, 95.5% at 230 nm, method B). **IR** (ATR) [cm^{-1}]: 3313, 3270, 3230, 3124, 3085, 2946, 2927, 2871, 1632, 1575, 1483, 1416, 1380, 1320, 1249, 1214, 1153, 1100, 1045, 992, 968, 938, 891, 872, 850, 817, 759, 726, 699, 658.

(S)-2-(2-((6-Chloro-3-nitropyridin-2-yl)amino)pyridin-4-yl)-1-(2,3-dihydroxypropyl)-1,5,6,7-tetrahydro-4H-pyrrolo[3,2-c]pyridin-4-one (239)

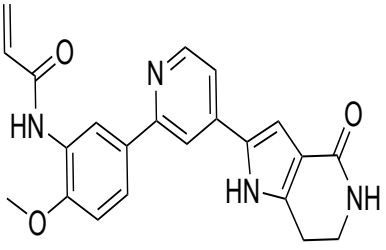

239

Chemical Formula: $C_{20}H_{19}ClN_6O_5$
Exact Mass: 458.11055
Molecular Weight: 458.85900

tert-Butyl (*S*)-2-(2-((tert-butoxycarbonyl)(6-chloro-3-nitropyridin-2-yl)amino)pyridin-4-yl)-1-((2,2-dimethyl-1,3-dioxolan-4-yl)methyl)-4-oxo-1,4,6,7-tetrahydro-5*H*-pyrrolo[3,2-*c*]pyridine-5-carboxylate (**237**, 68.0 mg, 97.3 µmol, 1.00 eq.) was dissolved in DCM (3 mL) and water (27 µL) in TFA (130 µL) added. The reaction was stirred at rt for 18 h. $NaHCO_3$ solution (6 mL) was added and the mixture extracted with DCM (5x 25 mL). The combined organic layers were dried over Na_2SO_4 and the solvent removed under reduced

pressure. The crude product was purified by flash column chromatography (Silica gel, 5 – 10% DCM/MeOH) which afforded the product **239** (3.5 mg, 7.63 µmol, 7.8%) as yellow solid.

^{1}H NMR (400 MHz, DMSO) δ 10.48 (s, 1H), 8.62 (d, *J* = 8.6 Hz, 1H), 8.32 (d, *J* = 5.2 Hz, 1H), 8.20 (s, 1H), 7.35 (dd, *J* = 5.2, 1.4 Hz, 1H), 7.22 (d, *J* = 8.6 Hz, 1H), 7.10 (s, 1H), 6.61 (s, 1H), 4.98 (d, *J* = 5.2 Hz, 1H), 4.65 (t, *J* = 5.5 Hz, 1H), 4.31 (dd, *J* = 14.7, 3.3 Hz, 1H), 4.01 (dd, *J* = 14.9, 8.5 Hz, 1H), 3.58 – 3.48 (m, 2H), 3.44 – 3.39 (m, 2H), 3.22 (td, *J* = 5.5, 2.1 Hz, 2H), 2.99 – 2.85 (m, 2H). **^{13}C NMR** (101 MHz, DMSO) δ 164.69, 153.46, 151.32, 148.34, 147.27, 142.09, 141.14, 138.79, 131.78, 129.70, 118.42, 115.64, 114.45, 112.15, 108.40, 71.08, 63.52, 47.92, 22.00. **HRMS:** ESI(+) calcd. for $[M+Na]^{+}$: *m/z* = 481.09977; found: 481.10008; rel. deviation: 0.65 ppm. **HPLC:** t_{ret} = 9.92 min (95.8% at 254 nm, 95.8% at 230 nm, method B).

7 Literature

[1] L. Revesz, A. Schlapbach, R. Aichholz, J. Dawson, R. Feifel, S. Hawtin, A. Littlewood-Evans, G. Koch, M. Kroemer, H. Möbitz, C. Scheufler, J. Velcicky, C. Huppertz, *Bioorg Med Chem Lett* **2010**, *20*, 4719-4723.

[2] M. Hagel, C. Miduturu, M. Sheets, N. Rubin, W. Weng, N. Stransky, N. Bifulco, J. L. Kim, B. Hodous, N. Brooijmans, A. Shutes, C. Winter, C. Lengauer, N. E. Kohl, T. Guzi, *Cancer Discov* **2015**, *5*, 424-437.

[3] L. Revesz, A. Schlapbach, R. Aichholz, R. Feifel, S. Hawtin, R. Heng, P. Hiestand, W. Jahnke, G. Koch, M. Kroemer, H. Möbitz, C. Scheufler, J. Velcicky, C. Huppertz, *Bioorg Med Chem Lett* **2010**, *20*, 4715-4718.

[4] Yosaatmadja, Y., Squire, C.J., *Protein Data Bank*, 4WKQ, https://doi.org/10.2210/pdb4wkq/pdb (accessed 13.05.2024)

[5] D. S. Weinstein, B. V. Yang, S.-H. Kim, W. Vaccaro, J. Sheppeck, J. Gilmore, (Ed.: B.-M. S. company), **2005**, p. 148.

[6] X. Zhang, J. Gureasko, K. Shen, P. A. Cole, J. Kuriyan, *Cell* **2006**, *125*, 1137-1149.

[7] A. Y. Kovalevsky, H. Johnson, B. L. Hanson, M. J. Waltman, S. Z. Fisher, S. Taylor, P. Langan, *Acta Crystallographica Section D* **2012**, *68*, 854-860.

[8] V. Sharma, M. Gupta, *Chemical Biology & Drug Design* **2022**, *100*, 968-980.

[9] D. R. Anderson, M. J. Meyers, R. G. Kurumbail, N. Caspers, G. I. Poda, S. A. Long, B. S. Pierce, M. W. Mahoney, R. J. Mourey, *Bioorganic & Medicinal Chemistry Letters* **2009**, *19*, 4878-4881.

[10] R. C. Hillig, U. Eberspaecher, F. Monteclaro, M. Huber, D. Nguyen, A. Mengel, B. Muller-Tiemann, U. Egner, *Journal of Molecular Biology* **2007**, *369*, 735-745.

[11] K. W. Underwood, K. D. Parris, E. Federico, L. Mosyak, R. M. Czerwinski, T. Shane, M. Taylor, K. Svenson, Y. Liu, C.-L. Hsiao, S. Wolfrom, M. Maguire, K. Malakian, J.-B. Telliez, L.-L. Lin, R. W. Kriz, J. Seehra, W. S. Somers, M. L. Stahl, *Structure* **2003**, *11*, 627-636.

[12] R. A. Fairhurst, T. Knoepfel, C. Leblanc, N. Buschmann, C. Gaul, J. Blank, I. Galuba, J. Trappe, C. Zou, J. Voshol, C. Genick, P. Brunet-Lefeuvre, F. Bitsch, D. Graus-Porta, P. Furet, *MedChemComm* **2017**, *8*, 1604-1613.

[13] F. Solca, G. Dahl, A. Zoephel, G. Bader, M. Sanderson, C. Klein, O. Kraemer, F. Himmelsbach, E. Haaksma, G. R. Adolf, *Journal of Pharmacology and Experimental Therapeutics* **2012**, *343*, 342-350.

[14] X. Pan, C. Yang, J. L. Cleveland, T. D. Bannister, *The Journal of Organic Chemistry* **2016**, *81*, 2194-2200.

[15] M. D. Alexander*, Vol. WO/2014/149164* (Ed.: I. Celgene Avilomics Rresearch), **2014**.

[16] A. Schlapbach, L. Révész, G. Koch, (Ed.: N. AG), **2008**.

[17] aM. G. Netea, F. Balkwill, M. Chonchol, F. Cominelli, M. Y. Donath, E. J. Giamarellos-Bourboulis, D. Golenbock, M. S. Gresnigt, M. T. Heneka, H. M. Hoffman, R. Hotchkiss, L. A. B. Joosten, D. L. Kastner, M. Korte, E. Latz, P. Libby, T. Mandrup-Poulsen, A. Mantovani, K. H. G. Mills, K. L. Nowak, L. A. O'Neill, P. Pickkers, T. van der Poll, P. M. Ridker, J. Schalkwijk, D. A. Schwartz, B. Siegmund, C. J. Steer, H. Tilg, J. W. M. van der Meer, F. L. van de Veerdonk, C. A. Dinarello, *Nature Immunology* **2017**, *18*, 826-831; bJ. M. Bennett, G. Reeves, G. E. Billman, J. P. Sturmberg, *Frontiers in Medicine* **2018**, *5*.

[18] aR. Medzhitov, *Nature* **2008**, *454*, 428-435; bR. Chovatiya, R. Medzhitov, *Molecular Cell* **2014**, *54*, 281-288.

[19] S. Kany, J. T. Vollrath, B. Relja, *International Journal of Molecular Sciences* **2019**, *20*, 6008.

[20] D. Furman, J. Campisi, E. Verdin, P. Carrera-Bastos, S. Targ, C. Franceschi, L. Ferrucci, D. W. Gilroy, A. Fasano, G. W. Miller, A. H. Miller, A. Mantovani, C. M. Weyand, N. Barzilai, J. J. Goronzy, T. A. Rando, R. B. Effros, A. Lucia, N. Kleinstreuer, G. M. Slavich, *Nature Medicine* **2019**, *25*, 1822-1832.

[21] D. Wu, Y. Jin, Y. Xing, M. D. Abate, M. Abbasian, M. Abbasi-Kangevari, Z. Abbasi-Kangevari, F. Abd-Allah, M. Abdelmasseh, M.-A. Abdollahifar, D. M. Abdulah, A. Abedi, V. Abedi, H. Abidi, R. G. Aboagye, H. Abolhassani, K. Abuabara, M. Abyadeh, I. Y. Addo, K. N. Adeniji, A. V. Adepoju, M. A. Adesina, Q. E. Sakilah Adnani, M. Afarideh, S. Aghamiri, A. Agodi, A. Agrawal, C. E. Aguilera Arriagada, A. Ahmad, D. Ahmad, S. Ahmad, S. Ahmad, A. Ahmadi, A. Ahmed, A. Ahmed, J. P. Aithala, A. A. Ajadi, M. Ajami, M. Akbarzadeh-Khiavi, F. Alahdab, M. T. AlBataineh, S. Alemi, A. A. Saeed Al-Gheethi, L. Ali, S. M. Alif, J. U. Almazan, S. Almustanyir, J. S. Alqahtani, I. Alqasmi, I. U. Khan Altaf, N. Alvis-Guzman, N. J. Alvis-Zakzuk, Y. M. Al-Worafi, H. Aly, R. Amani, H. Amu, G. A. Amusa, C. L. Andrei, A. Ansar, H. Ansariniya, A. E. Anyasodor, J. Arabloo, R. Arefnezhad, J. Arulappan, M. Asghari-Jafarabadi, T. Ashraf, J. A. Atata, S. S. Athari, D. Atlaw, M. M. d. Wahbi Atout, A. Aujayeb, A. T. Awan, H. Ayatollahi, S. Azadnajafabad, A. Y. Azzam, A. Badawi, A. D. Badiye, S. Bagherieh, A. A. Baig, B. B. Bantie, M. Barchitta, M. Bardhan, S. L. Barker-Collo, F. Barone-Adesi, K. Batra, N. S. Bayileyegn, A. H. Behnoush, U. I. Belgaumi, M. Bemanalizadeh, I. M. Bensenor, K. A. Beyene, A. S. Bhagavathula, P. Bhardwaj, S. Bhaskar, A. N. Bhat, S. Bitaraf, V. R. Bitra, A. Boloor, K. Bora, J. S. Botelho, et al., *eClinicalMedicine* **2023**, *64*.

[22] World Health Organisation, **2023**. *Rheumatoide arthritis*. https://www.who.int/news-room/fact-sheets/detail/rheumatoid-arthritis (accessed 15.05.2024)

[23] R. J. Black, M. Cross, L. M. Haile, G. T. Culbreth, J. D. Steinmetz, H. Hagins, J. A. Kopec, P. M. Brooks, A. D. Woolf, K. L. Ong, D. R. Kopansky-Giles, K. E. Dreinhoefer, N. Betteridge, A. Aali, M. Abbasifard, M. Abbasi-Kangevari, A. M. Abdurehman, A. Abedi, H. Abidi, R. G. Aboagye, H. Abolhassani, E. Abu-Gharbieh, A. Abu-Zaid, K. Adamu, I. Y. Addo, M. A. Adesina, Q. E. S. Adnani, M. S. Afzal, A. Ahmed, J. P. Aithala, M. Akhlaghdoust, A. Alemayehu, S. Alvand, N. J. Alvis-Zakzuk, H. Amu, B. Antony, J. Arabloo, A. Y. Aravkin, J. Arulappan, T. Ashraf, S. S. Athari, S. Azadnajafabad, A. Badawi, N. Baghcheghi, A. A. Baig, A. B. Balta, M. Banach, P. C. Banik, A. Barrow, A. Bashiri, L. M. Bearne, A. Bekele, I. M. Bensenor, A. Y. Berhie, A. S. Bhagavathula, P. Bhardwaj, A. N. Bhat, V. S. Bhojaraja, S. Bitaraf, B. B. A. Bodicha, J. S. Botelho, A. M. Briggs, R. Buchbinder, C. A. Castañeda-Orjuela, P. Charalampous, V. K. Chattu, K. Coberly, N. Cruz-Martins, O. Dadras, X. Dai, K. de Luca, F. N. Dessalegn, G. Dessie, M. Dhimal, L. E. Digesa, M. Diress, P. N. Doku, H. A. Edinur, M. Ekholuenetale, M. Elhadi, Y. M. El-Sherbiny, F. Etaee, R. Ezzeddini, S. Faghani, I. Filip, F. Fischer, T. Fukumoto, B. Ganesan, M. A. Gebremichael, U. Gerema, M. E. Getachew, A. Ghashghaee, T. K. Gill, B. Gupta, S. Gupta, V. B. Gupta, V. K. Gupta, R. Halwani, M. A. Hannan, S. Haque, et al., *The Lancet Rheumatology* **2023**, *5*, e594-e610.

[24] aM. A. Muzammil, F. N. U. Fariha, T. Patel, R. Sohail, M. Kumar, E. Khan, B. Khanam, S. Kumar, M. Khatri, G. Varrassi, P. Vanga, *Cureus* **2023**, *15*, e41120; bY.-J. Lin, M. Anzaghe, S. Schülke, *Cells* **2020**, *9*, 880.

[25] G. Frazzei, A. Musters, N. de Vries, S. W. Tas, R. F. van Vollenhoven, *Autoimmunity Reviews* **2023**, *22*, 103217.

[26] G. Geisslinger, S. Menzel, T. Gudermann, B. Hinz, P. Ruth, E. Mutschler, BiblioScout, **2019**.

[27] J. C. Lee, J. T. Laydon, P. C. McDonnell, T. F. Gallagher, S. Kumar, D. Green, D. McNulty, M. J. Blumenthal, J. R. Keys, S. W. Land vatter, J. E. Strickler, M. M. McLaughlin, I. R. Siemens, S. M. Fisher, G. P. Livi, J. R. White, J. L. Adams, P. R. Young, *Nature* **1994**, *372*, 739-746.

[28] D. Li, *Cell Research* **2012**, *22*, 1-2.

[29] H. Kia-Ki, A. Martinage, *International Journal of Biochemistry* **1992**, *24*, 19-28.

[30] F. Ardito, M. Giuliani, D. Perrone, G. Troiano, L. Lo Muzio, *Int J Mol Med* **2017**, *40*, 271-280.
[31] S. Cheek, H. Zhang, N. V. Grishin, *Journal of Molecular Biology* **2002**, *320*, 855-881.
[32] G. Manning, D. B. Whyte, R. Martinez, T. Hunter, S. Sudarsanam, *Science* **2002**, *298*, 1912-1934.
[33] aD. Fabbro, S. W. Cowan-Jacob, H. Moebitz, *British Journal of Pharmacology* **2015**, *172*, 2675-2700; b; cN. Moret, C. Liu, B. M. Gyori, J. A. Bachman, A. Steppi, C. Hug, R. Taujale, L.-C. Huang, M. E. Berginski, S. M. Gomez, *BioRxiv* **2020**, 2020.2004. 2002.022277.
[34] B. Nolen, S. Taylor, G. Ghosh, *Molecular Cell* **2004**, *15*, 661-675.
[35] R. Roskoski, *Pharmacological Research* **2015**, *100*, 1-23.
[36] Daniel K. Treiber, Neil P. Shah, *Chemistry & Biology* **2013**, *20*, 745-746.
[37] aD. K. Morrison, *Cold Spring Harbor Perspectives in Biology* **2012**, *4*; bH. Enslen, J. Raingeaud, R. J. Davis, *Journal of Biological Chemistry* **1998**, *273*, 1741-1748.
[38] aR. Paudel, L. Fusi, M. Schmidt, *International Journal of Molecular Sciences* **2021**, *22*, 7594; bY. J. Guo, W. W. Pan, S. B. Liu, Z. F. Shen, Y. Xu, L. L. Hu, *Exp Ther Med* **2020**, *19*, 1997-2007.
[39] Y. T. Ip, R. J. Davis, *Current Opinion in Cell Biology* **1998**, *10*, 205-219.
[40] D. Morgan, K. L. Berggren, C. D. Spiess, H. M. Smith, A. Tejwani, S. J. Weir, C. E. Lominska, S. M. Thomas, G. N. Gan, *Molecular Carcinogenesis* **2022**, *61*, 173-199.
[41] J. M. Kyriakis, J. Avruch, *Physiological Reviews* **2001**, *81*, 807-869.
[42] aK. Deacon, J. L. Blank, *Journal of Biological Chemistry* **1999**, *274*, 16604-16610; bK. Shirakabe, K. Yamaguchi, H. Shibuya, K. Irie, S. Matsuda, T. Moriguchi, Y. Gotoh, K. Matsumoto, E. Nishida, *Journal of Biological Chemistry* **1997**, *272*, 8141-8144; cJ. Ninomiya-Tsuji, K. Kishimoto, A. Hiyama, J.-i. Inoue, Z. Cao, K. Matsumoto, *Nature* **1999**, *398*, 252-256; dB. D. Cuevas, A. N. Abell, G. L. Johnson, *Oncogene* **2007**, *26*, 3159-3171.
[43] aS.-i. Hirai, M. Katoh, M. Terada, J. M. Kyriakis, L. I. Zon, A. Rana, J. Avruch, S. Ohno, *Journal of Biological Chemistry* **1997**, *272*, 15167-15173; bS.-i. Hirai, K. Noda, T. Moriguchi, E. Nishida, A. Yamashita, T. Deyama, K. Fukuyama, S. Ohno, *Journal of Biological Chemistry* **1998**, *273*, 7406-7412; cL. A. Tibbles, Y. L. Ing, F. Kiefer, J. Chan, N. Iscove, J. R. Woodgett, N. J. Lassam, *The EMBO Journal* **1996**, *15*, 7026-7035.
[44] C.-Y. Fang, T.-C. Lai, M. Hsiao, Y.-C. Chang, *International Journal of Molecular Sciences* **2020**, *21*, 7463.
[45] H. J. Schaeffer, M. J. Weber, *Molecular and Cellular Biology* **1999**, *19*, 2435-2444.
[46] J. Han, J.-D. Lee, L. Bibbs, R. J. Ulevitch, *Science* **1994**, *265*, 808-811.
[47] J. Rouse, P. Cohen, S. Trigon, M. Morange, A. Alonso-Llamazares, D. Zamanillo, T. Hunt, A. R. Nebreda, *Cell* **1994**, *78*, 1027-1037.
[48] aZ. Li, Y. Jiang, R. J. Ulevitch, J. Han, *Biochemical and Biophysical Research Communications* **1996**, *228*, 334-340; bY. Jiang, H. Gram, M. Zhao, L. New, J. Gu, L. Feng, F. Di Padova, R. J. Ulevitch, J. Han, *Journal of Biological Chemistry* **1997**, *272*, 30122-30128.
[49] P. Ganguly, T. Macleod, C. Wong, M. Harland, D. McGonagle, *Pharmaceuticals* **2023**, *16*, 1286.
[50] T. Y. Yeung, F. Aziz, A. Guerrero-Castilla, S. Arguelles, *Current Pharmaceutical Design* **2018**, *24*, 1449-1484.
[51] aK. Ono, J. Han, *Cellular Signalling* **2000**, *12*, 1-13; bB. Canovas, A. R. Nebreda, *Nature Reviews Molecular Cell Biology* **2021**, *22*, 346-366; cJ. M. Kyriakis, J. Avruch, *Physiological Reviews* **2012**, *92*, 689-737; dA. Martínez-Limón, M. Joaquin, M. Caballero, F. Posas, E. de Nadal, *International Journal of Molecular Sciences* **2020**, *21*.
[52] aF. Y. Liew, D. Xu, E. K. Brint, L. A. J. O'Neill, *Nature Reviews Immunology* **2005**, *5*, 446-458; bE. Beamer, S. A. L. Corrêa, *Frontiers in Cell and Developmental Biology* **2021**, *9*.
[53] aD. Faust, C. Schmitt, F. Oesch, B. Oesch-Bartlomowicz, I. Schreck, C. Weiss, C. Dietrich, *Cell Communication and Signaling* **2012**, *10*, 6; bM. Raman, S. Earnest, K. Zhang, Y. Zhao, M. H.

Cobb, *The EMBO Journal* **2007**, *26*, 2005-2014; cG. Sabio, R. J. Davis, *Seminars in Immunology* **2014**, *26*, 237-245.

[54] aT. Moriguchi, N. Kuroyanagi, K. Yamaguchi, Y. Gotoh, K. Irie, T. Kano, K. Shirakabe, Y. Muro, H. Shibuya, K. Matsumoto, E. Nishida, M. Hagiwara, *Journal of Biological Chemistry* **1996**, *271*, 13675-13679; bJ. Raingeaud, A. J. Whitmarsh, T. Barrett, B. Dérijard, R. J. Davis, *Molecular and Cellular Biology* **1996**, *16*, 1247-1255.

[55] M. Gaestel, *Frontiers in Cell and Developmental Biology* **2016**, *3*.

[56] aP. Juyoux, I. Galdadas, D. Gobbo, J. von Velsen, M. Pelosse, M. Tully, O. Vadas, F. L. Gervasio, E. Pellegrini, M. W. Bowler, *Science* **2023**, *381*, 1217-1225; bT. Tanoue, M. Adachi, T. Moriguchi, E. Nishida, *Nature Cell Biology* **2000**, *2*, 110-116.

[57] J. Raingeaud, S. Gupta, J. S. Rogers, M. Dickens, J. Han, R. J. Ulevitch, R. J. Davis, *Journal of Biological Chemistry* **1995**, *270*, 7420-7426.

[58] D. Brancho, N. Tanaka, A. Jaeschke, J.-J. Ventura, N. Kelkar, Y. Tanaka, M. Kyuuma, T. Takeshita, R. A. Flavell, R. J. Davis, *Genes & Development* **2003**, *17*, 1969-1978.

[59] aG. F. De Nicola, E. D. Martin, A. Chaikuad, R. Bassi, J. Clark, L. Martino, S. Verma, P. Sicard, R. Tata, R. A. Atkinson, S. Knapp, M. R. Conte, M. S. Marber, *Nature Structural & Molecular Biology* **2013**, *20*, 1182-1190; bM. Tanno, R. Bassi, D. A. Gorog, A. T. Saurin, J. Jiang, R. J. Heads, J. L. Martin, R. J. Davis, R. A. Flavell, M. S. Marber, *Circulation Research* **2003**, *93*, 254-261; cJ. Li, E. J. Miller, J. Ninomiya-Tsuji, R. R. Russell, L. H. Young, *Circulation Research* **2005**, *97*, 872-879; dA. Wolf, K. Beuerlein, C. Eckart, H. Weiser, B. Dickkopf, H. Müller, H. Sakurai, M. Kracht, *PLOS ONE* **2011**, *6*, e29256.

[60] J. M. Salvador, P. R. Mittelstadt, T. Guszczynski, T. D. Copeland, H. Yamaguchi, E. Appella, A. J. Fornace, J. D. Ashwell, *Nature Immunology* **2005**, *6*, 390-395.

[61] G. Maik-Rachline, L. Lifshits, R. Seger, *International Journal of Molecular Sciences* **2020**, *21*, 6102.

[62] X. Gong, X. Ming, P. Deng, Y. Jiang, *Journal of Cellular Biochemistry* **2010**, *110*, 1420-1429.

[63] B. Cánovas, A. Igea, A. A. Sartori, R. R. Gomis, T. T. Paull, M. Isoda, H. Pérez-Montoyo, V. Serra, E. González-Suárez, T. H. Stracker, A. R. Nebreda, *Cancer Cell* **2018**, *33*, 1094-1110.e1098.

[64] R. Seger, E. G. Krebs, *The FASEB Journal* **1995**, *9*, 726-735.

[65] aJ. S. Mudgett, J. Ding, L. Guh-Siesel, N. A. Chartrain, L. Yang, S. Gopal, M. M. Shen, *Proceedings of the National Academy of Sciences* **2000**, *97*, 10454-10459; bR. H. Adams, A. Porras, G. Alonso, M. Jones, K. Vintersten, S. Panelli, A. Valladares, L. Perez, R. Klein, A. R. Nebreda, *Molecular Cell* **2000**, *6*, 109-116.

[66] J. F. Schindler, A. Godbey, W. F. Hood, S. L. Bolten, R. M. Broadus, T. P. Kasten, A. J. Cassely, J. L. Hirsch, M. A. Merwood, M. A. Nagy, K. F. Fok, M. J. Saabye, H. M. Morgan, R. P. Compton, R. J. Mourey, A. J. Wittwer, J. B. Monahan, *Biochimica et Biophysica Acta (BBA) - Proteins and Proteomics* **2002**, *1598*, 88-97.

[67] aT. Wu, J.-X. Shi, S. Geng, W. Zhou, Y. Shi, X. Su, *BMC Pulmonary Medicine* **2016**, *16*, 84; bV. Lafarga, A. Cuadrado, I. Lopez de Silanes, R. Bengoechea, O. Fernandez-Capetillo, A. R. Nebreda, *Molecular and Cellular Biology* **2009**, *29*, 4341-4351.

[68] C. Tiedje, N. Ronkina, M. Tehrani, S. Dhamija, K. Laass, H. Holtmann, A. Kotlyarov, M. Gaestel, *PLOS Genetics* **2012**, *8*, e1002977.

[69] K. M. S. E. Reyskens, J. S. C. Arthur, *Frontiers in Cell and Developmental Biology* **2016**, *4*.

[70] aB. Ritschka, M. Storer, A. Mas, F. Heinzmann, M. C. Ortells, J. P. Morton, O. J. Sansom, L. Zender, W. M. Keyes, *Genes & Development* **2017**, *31*, 172-183; bN. Frey, S. Venturelli, L. Zender, M. Bitzer, *Nature Reviews Gastroenterology & Hepatology* **2018**, *15*, 81-95.

[71] M. S. Phong, R. D. Van Horn, S. Li, G. Tucker-Kellogg, U. Surana, X. S. Ye, *Molecular and Cellular Biology* **2010**, *30*, 3816-3826.

[72] aK. Tamura, T. Sudo, U. Senftleben, A. M. Dadak, R. Johnson, M. Karin, *Cell* **2000**, *102*, 221-231; bF. B. Engel, M. Schebesta, M. T. Duong, G. Lu, S. Ren, J. B. Madwed, H. Jiang, Y. Wang, M. T. Keating, *Genes & Development* **2005**, *19*, 1175-1187.

[73] P. L. Puri, Z. Wu, P. Zhang, L. D. Wood, K. S. Bhakta, J. Han, J. R. Feramisco, M. Karin, J. Y. J. Wang, *Genes & Development* **2000**, *14*, 574-584.

[74] Z. S. Tan, A. S. Beiser, R. S. Vasan, R. Roubenoff, C. A. Dinarello, T. B. Harris, E. J. Benjamin, R. Au, D. P. Kiel, P. A. Wolf, S. Seshadri, *The Framingham Study* **2007**, *68*, 1902-1908.

[75] aA. Lloret, T. Fuchsberger, E. Giraldo, J. Viña, *Free Radical Biology and Medicine* **2015**, *83*, 186-191; bP. R. Asih, E. Prikas, K. Stefanoska, A. R. P. Tan, H. I. Ahel, A. Ittner, *Frontiers in Molecular Neuroscience* **2020**, *13*; cN. Maphis, S. Jiang, G. Xu, O. N. Kokiko-Cochran, S. M. Roy, L. J. Van Eldik, D. M. Watterson, B. T. Lamb, K. Bhaskar, *Alzheimer's Research & Therapy* **2016**, *8*, 54; dL. R. Coulthard, D. E. White, D. L. Jones, M. F. McDermott, S. A. Burchill, *Trends in Molecular Medicine* **2009**, *15*, 369-379.

[76] aE. Manieri, G. Sabio, *Journal of Molecular Endocrinology* **2015**, *55*, R11-R22; bS. Wang, L. Ding, H. Ji, Z. Xu, Q. Liu, Y. Zheng, *International Journal of Molecular Sciences* **2016**, *17*, 1037.

[77] aG. Chen, M. Hitomi, J. Han, D. W. Stacey, *Journal of Biological Chemistry* **2000**, *275*, 38973-38980; bJ. J. Ventura, S. Tenbaum, E. Perdiguero, M. Huth, C. Guerra, M. Barbacid, M. Pasparakis, A. R. Nebreda, *Nature Genetics* **2007**, *39*, 750-758.

[78] L. Hui, L. Bakiri, A. Mairhorfer, N. Schweifer, C. Haslinger, L. Kenner, V. Komnenovic, H. Scheuch, H. Beug, E. F. Wagner, *Nature Genetics* **2007**, *39*, 741-749.

[79] J. Urosevic, X. Garcia-Albéniz, E. Planet, S. Real, M. V. Céspedes, M. Guiu, E. Fernandez, A. Bellmunt, S. Gawrzak, M. Pavlovic, R. Mangues, I. Dolado, F. M. Barriga, C. Nadal, N. Kemeny, E. Batlle, A. R. Nebreda, R. R. Gomis, *Nature Cell Biology* **2014**, *16*, 685-694.

[80] aA. K. Greenberg, S. Basu, J. Hu, T.-a. Yie, K. M. Tchou-Wong, W. N. Rom, T. C. Lee, *American Journal of Respiratory Cell and Molecular Biology* **2002**, *26*, 558-564; bK. Leelahavanichkul, P. Amornphimoltham, A. A. Molinolo, J. R. Basile, S. Koontongkaew, J. S. Gutkind, *Molecular Oncology* **2014**, *8*, 105-118.

[81] aJ. Tang, X. Qi, D. Mercola, J. Han, G. Chen, *Journal of Biological Chemistry* **2005**, *280*, 23910-23917; bA. Tomás-Loba, E. Manieri, B. González-Terán, A. Mora, L. Leiva-Vega, A. M. Santamans, R. Romero-Becerra, E. Rodríguez, A. Pintor-Chocano, F. Feixas, J. A. López, B. Caballero, M. Trakala, Ó. Blanco, J. L. Torres, L. Hernández-Cosido, V. Montalvo-Romeral, N. Matesanz, M. Roche-Molina, J. A. Bernal, H. Mischo, M. León, A. Caballero, D. Miranda-Saavedra, J. Ruiz-Cabello, Y. A. Nevzorova, F. J. Cubero, J. Bravo, J. Vázquez, M. Malumbres, M. Marcos, S. Osuna, G. Sabio, *Nature* **2019**, *568*, 557-560.

[82] X. Guo, N. Ma, J. Wang, J. Song, X. Bu, Y. Cheng, K. Sun, H. Xiong, G. Jiang, B. Zhang, M. Wu, L. Wei, *BMC Cancer* **2008**, *8*, 375.

[83] aS. Y. Yang, A. Miah, K. M. Sales, B. Fuller, A. M. Seifalian, M. Winslet, *Int J Oncol* **2011**, *38*, 1695-1702; bL. Pereira, A. Igea, B. Canovas, I. Dolado, A. R. Nebreda, *EMBO Molecular Medicine* **2013**, *5*, 1759-1774.

[84] R. Rudalska, D. Dauch, T. Longerich, K. McJunkin, T. Wuestefeld, T.-W. Kang, A. Hohmeyer, M. Pesic, J. Leibold, A. von Thun, P. Schirmacher, J. Zuber, K.-H. Weiss, S. Powers, N. P. Malek, M. Eilers, B. Sipos, S. W. Lowe, R. Geffers, S. Laufer, L. Zender, *Nature Medicine* **2014**, *20*, 1138-1146.

[85] aF. R. Greten, S. I. Grivennikov, *Immunity* **2019**, *51*, 27-41; bE. I. Deryugina, J. P. Quigley, *Cancer and Metastasis Reviews* **2006**, *25*, 9-34.

[86] aX. Song, E. Voronov, T. Dvorkin, E. Fima, E. Cagnano, D. Benharroch, Y. Shendler, O. Bjorkdahl, S. Segal, C. A. Dinarello, R. N. Apte, *The Journal of Immunology* **2003**, *171*, 6448-6456; bB. S. Paugh, L. Bryan, S. W. Paugh, K. M. Wilczynska, S. M. Alvarez, S. K. Singh, D.

Kapitonov, H. Rokita, S. Wright, I. Griswold-Prenner, S. Milstien, S. Spiegel, T. Kordula, *Journal of Biological Chemistry* **2009**, *284*, 3408-3417; cB. M. Emerling, L. C. Platanias, E. Black, A. R. Nebreda, R. J. Davis, N. S. Chandel, *Molecular and Cellular Biology* **2005**, *25*, 4853-4862; dM. Limoge, A. Safina, A. M. Truskinovsky, I. Aljahdali, J. Zonneville, A. Gruevski, C. L. Arteaga, A. V. Bakin, *Oncotarget* **2017**, *8*; eM. Curtis, H. A. Kenny, B. Ashcroft, A. Mukherjee, A. Johnson, Y. Zhang, Y. Helou, R. Batlle, X. Liu, N. Gutierrez, X. Gao, S. D. Yamada, R. Lastra, A. Montag, N. Ahsan, J. W. Locasale, A. R. Salomon, A. R. Nebreda, E. Lengyel, *Cell Metabolism* **2019**, *29*, 141-155.e149; fF. M. S. Gurgis, Y. T. Yeung, M. X. M. Tang, B. Heng, M. Buckland, A. J. Ammit, J. Haapasalo, H. Haapasalo, G. J. Guillemin, T. Grewal, L. Munoz, *Oncogene* **2015**, *34*, 2934-2942; gS. I. Grivennikov, M. Karin, *Annals of the Rheumatic Diseases* **2011**, *70*, i104-i108; hC. Suarez-Cuervo, M. A. Merrell, L. Watson, K. W. Harris, E. L. Rosenthal, H. K. Väänänen, K. S. Selander, *Clinical & Experimental Metastasis* **2004**, *21*, 525-533.

[87] aT. Shasha, M. Gruijs, M. van Egmond, *Cellular and Molecular Life Sciences* **2022**, *79*, 607; bY. Niu, W. Yang, H. Qian, Y. Sun, *Cancer Cell International* **2022**, *22*, 341.

[88] A. Igea, A. R. Nebreda, *Cancer Research* **2015**, *75*, 3997-4002.

[89] D. Stokoe, D. G. Campbell, S. Nakielny, H. Hidaka, S. J. Leevers, C. Marshall, P. Cohen, *The EMBO Journal* **1992**, *11*, 3985-3994.

[90] D. Stokoe, K. Engel, D. G. Campbell, P. Cohen, M. Gaestel, *FEBS Letters* **1992**, *313*, 307-313.

[91] I. A. Manke, A. Nguyen, D. Lim, M. Q. Stewart, A. E. H. Elia, M. B. Yaffe, *Molecular Cell* **2005**, *17*, 37-48.

[92] A. Kotlyarov, A. Neininger, C. Schubert, R. Eckert, C. Birchmeier, H.-D. Volk, M. Gaestel, *Nature Cell Biology* **1999**, *1*, 94-97.

[93] aD. Stokoe, B. Caudwell, P. T. W. Cohen, P. Cohen, *Biochemical Journal* **1993**, *296*, 843-849; bM. Gaestel, *Biological Chemistry* **2013**, *394*, 1301-1315.

[94] N. Ronkina, A. Kotlyarov, O. Dittrich-Breiholz, M. Kracht, E. Hitti, K. Milarski, R. Askew, S. Marusic, L. L. Lin, M. Gaestel, J. B. Telliez, *Molecular and Cellular Biology* **2007**, *27*, 170-181.

[95] P. Trulley, G. Snieckute, D. Bekker-Jensen, M. B. Menon, R. Freund, A. Kotlyarov, J. V. Olsen, M. D. Diaz-Muñoz, M. Turner, S. Bekker-Jensen, M. Gaestel, C. Tiedje, *Cell Reports* **2019**, *27*, 2859-2870.e2856.

[96] aY.-L. Zu, Y. Ai, C.-K. Huang, *Journal of Biological Chemistry* **1995**, *270*, 202-206; bM. Gaestel, in *Encyclopedia of Signaling Molecules* (Ed.: S. Choi), Springer International Publishing, Cham, **2018**, pp. 2958-2963; cM. Gaestel, *Nature Reviews Molecular Cell Biology* **2006**, *7*, 120-130.

[97] W. Meng, L. L. Swenson, M. J. Fitzgibbon, K. Hayakawa, E. ter Haar, A. E. Behrens, J. R. Fulghum, J. A. Lippke, *Journal of Biological Chemistry* **2002**, *277*, 37401-37405.

[98] S. Soni, P. Anand, Y. S. Padwad, *Journal of Experimental & Clinical Cancer Research* **2019**, *38*, 121.

[99] M. Fiore, S. Forli, F. Manetti, *Journal of Medicinal Chemistry* **2016**, *59*, 3609-3634.

[100] aL. N. Johnson, M. E. M. Noble, D. J. Owen, *Cell* **1996**, *85*, 149-158; bS. S. Taylor, A. P. Kornev, *Trends in Biochemical Sciences* **2011**, *36*, 65-77.

[101] R. Ben-Levy, I. A. Leighton, Y. N. Doza, P. Attwood, N. Morrice, C. J. Marshall, P. Cohen, *The EMBO Journal* **1995**, *14*, 5920-5930-5930.

[102] W. A. Linke, N. Hamdani, *Circulation Research* **2014**, *114*, 1052-1068.

[103] Y. L. Zu, F. Y. Wu, A. Gilchrist, Y. X. Ai, M. E. Labadia, C. K. Huang, *Biochemical and Biophysical Research Communications* **1994**, *200*, 1118-1124.

[104] N. Ronkina, M. B. Menon, J. Schwermann, C. Tiedje, E. Hitti, A. Kotlyarov, M. Gaestel, *Biochemical Pharmacology* **2010**, *80*, 1915-1920.

[105] aR. Ben-Levy, S. Hooper, R. Wilson, H. F. Paterson, C. J. Marshall, *Current Biology* **1998**, *8*, 1049-1057; bA. White, C. A. Pargellis, J. M. Studts, B. G. Werneburg, B. T. Farmer, *Proceedings of the National Academy of Sciences* **2007**, *104*, 6353-6358.

[106] K. Engel, A. Kotlyarov, M. Gaestel, *The EMBO Journal* **1998**, *17*, 3363-3371.

[107] E. t. Haar, P. Prabakhar, X. Liu, C. Lepre, *Journal of Biological Chemistry* **2007**, *282*, 9733-9739.

[108] N. Gutierrez-Prat, M. Cubillos-Rojas, B. Cánovas, A. Kuzmanic, J. Gupta, A. Igea, E. Llonch, M. Gaestel, A. R. Nebreda, *Proceedings of the National Academy of Sciences* **2021**, *118*, e2024562118.

[109] aP. R. Dunkley, L. Bobrovskaya, M. E. Graham, E. I. Von Nagy-Felsobuki, P. W. Dickson, *Journal of Neurochemistry* **2004**, *91*, 1025-1043; bG. Thomas, J. Haavik, P. Cohen, *European Journal of Biochemistry* **1997**, *247*, 1180-1189.

[110] L. Suarez-Lopez, G. Sriram, Y. W. Kong, S. Morandell, K. A. Merrick, Y. Hernandez, K. M. Haigis, M. B. Yaffe, *Proceedings of the National Academy of Sciences* **2018**, *115*, E4236-E4244.

[111] M. B. Menon, N. Ronkina, J. Schwermann, A. Kotlyarov, M. Gaestel, *Cell Motility* **2009**, *66*, 1041-1047.

[112] aM. M. Gorska , Q. Liang , S. J. Stafford , N. Goplen , N. Dharajiya , L. Guo , S. Sur , M. Gaestel , R. Alam *Journal of Experimental Medicine* **2007**, *204*, 1637-1652; bA. T. Funding, C. Johansen, M. Gaestel, B. M. Bibby, L. L. Lilleholt, K. Kragballe, L. Iversen, *Journal of Investigative Dermatology* **2009**, *129*, 891-898; cY. Y. Li, B. Yuece, C. Mh, L. Xh, S. Lv, C. Cj, S. Ochs, A. Sibaev, E. Deindl, C. Schaefer, M. Storr, *Laboratory Investigation* **2013**, *93*, 322-333.

[113] T. Bakheet, M. Frevel, B. R. G. Williams, W. Greer, K. S. A. Khabar, *Nucleic Acids Research* **2001**, *29*, 246-254.

[114] S. A. Brooks, P. J. Blackshear, *Biochimica et Biophysica Acta (BBA) - Gene Regulatory Mechanisms* **2013**, *1829*, 666-679.

[115] G. A. Taylor, E. Carballo, D. M. Lee, W. S. Lai, M. J. Thompson, D. D. Patel, D. I. Schenkman, G. S. Gilkeson, H. E. Broxmeyer, B. F. Haynes, P. J. Blackshear, *Immunity* **1996**, *4*, 445-454.

[116] E. Carballo, W. S. Lai, P. J. Blackshear, *Blood* **2000**, *95*, 1891-1899.

[117] C. Tiedje, M. D. Diaz-Muñoz, P. Trulley, H. Ahlfors, K. Laaß, P. J. Blackshear, M. Turner, M. Gaestel, *Nucleic Acids Research* **2016**, *44*, 7418-7440.

[118] aE. A. Van Tubergen, R. Banerjee, M. Liu, R. V. Broek, E. Light, S. Kuo, S. E. Feinberg, A. L. Willis, G. Wolf, T. Carey, C. Bradford, M. Prince, F. P. Worden, K. L. Kirkwood, N. J. D'Silva, *Clinical Cancer Research* **2013**, *19*, 1169-1179; bW. S. Lai, D. J. Stumpo, L. Qiu, R. Faccio, P. J. Blackshear, *Molecular and Cellular Biology* **2018**, *38*, e00488-00417.

[119] aF. Bollig, R. Winzen, M. Gaestel, S. Kostka, K. Resch, H. Holtmann, *Biochemical and Biophysical Research Communications* **2003**, *301*, 665-670; bH. C. Reinhardt, P. Hasskamp, I. Schmedding, S. Morandell, M. A. T. M. van Vugt, X. Wang, R. Linding, S.-E. Ong, D. Weaver, S. A. Carr, M. B. Yaffe, *Molecular Cell* **2010**, *40*, 34-49; cS. Rousseau, N. Morrice, M. Peggie, D. G. Campbell, M. Gaestel, P. Cohen, *The EMBO Journal* **2002**, *21*, 6505-6514.

[120] C. Tiedje, M. Lubas, M. Tehrani, M. B. Menon, N. Ronkina, S. Rousseau, P. Cohen, A. Kotlyarov, M. Gaestel, *RNA* **2015**, *21*, 262-278.

[121] Y. Li, K. Inoki, P. Vacratsis, K.-L. Guan, *Journal of Biological Chemistry* **2003**, *278*, 13663-13671.

[122] N. Herranz, S. Gallage, M. Mellone, T. Wuestefeld, S. Klotz, C. J. Hanley, S. Raguz, J. C. Acosta, Andrew J. Innes, A. Banito, A. Georgilis, A. Montoya, K. Wolter, G. Dharmalingam, P. Faull, T. Carroll, J. P. Martínez-Barbera, P. Cutillas, F. Reisinger, M. Heikenwalder, Richard A. Miller, D. Withers, L. Zender, G. J. Thomas, J. Gil, *Nature Cell Biology* **2015**, *17*, 1205-1217.

[123] X. Wang, M. A. Khaleque, M. J. Zhao, R. Zhong, M. Gaestel, S. K. Calderwood, *Journal of Biological Chemistry* **2006**, *281*, 782-791.
[124] A. Shrestha, H. Bruckmueller, H. Kildalsen, G. Kaur, M. Gaestel, H. L. Wetting, I. Mikkola, O.-M. Seternes, *Scientific Reports* **2020**, *10*, 11388.
[125] M. E. Borisova, A. Voigt, M. A. X. Tollenaere, S. K. Sahu, T. Juretschke, N. Kreim, N. Mailand, C. Choudhary, S. Bekker-Jensen, M. Akutsu, S. A. Wagner, P. Beli, *Nature Communications* **2018**, *9*, 1017.
[126] A. Steven, M. Friedrich, P. Jank, N. Heimer, J. Budczies, C. Denkert, B. Seliger, *Cellular and Molecular Life Sciences* **2020**, *77*, 4049-4067.
[127] aM. Rolli, A. Kotlyarov, K. M. Sakamoto, M. Gaestel, A. Neininger, *Journal of Biological Chemistry* **1999**, *274*, 19559-19564; bO. Heidenreich, A. Neininger, G. Schratt, R. Zinck, M. A. Cahill, K. Engel, A. Kotlyarov, R. Kraft, S. Kostka, M. Gaestel, A. Nordheim, *Journal of Biological Chemistry* **1999**, *274*, 14434-14443; cY. Tan, J. Rouse, A. Zhang, S. Cariati, P. Cohen, M. J. Comb, *The EMBO Journal* **1996**, *15*, 4629-4642.
[128] N. Ronkina, J. Lafera, A. Kotlyarov, M. Gaestel, *Scientific Reports* **2016**, *6*, 31219.
[129] H. C. Reinhardt, A. S. Aslanian, J. A. Lees, M. B. Yaffe, *Cancer Cell* **2007**, *11*, 175-189.
[130] Ian G. Cannell, Karl A. Merrick, S. Morandell, C.-Q. Zhu, Christian J. Braun, Robert A. Grant, Eleanor R. Cameron, M.-S. Tsao, Michael T. Hemann, Michael B. Yaffe, *Cancer Cell* **2015**, *28*, 623-637.
[131] H. O. Weber, R. L. Ludwig, D. Morrison, A. Kotlyarov, M. Gaestel, K. H. Vousden, *Oncogene* **2005**, *24*, 1965-1972.
[132] G. Fadi Maged Shokry, Z. William, M. Lenka, *Molecular Pharmacology* **2014**, *85*, 345.
[133] J. Tang, X. Yang, X. Liu, *Oncogene* **2008**, *27*, 6635-6645.
[134] L. Wang, H. Yang, P. L. Palmbos, G. Ney, T. A. Detzler, D. Coleman, J. Leflein, M. Davis, M. Zhang, W. Tang, J. K. Hicks, C. M. Helchowski, J. Prasad, T. S. Lawrence, L. Xu, X. Yu, C. E. Canman, M. Ljungman, D. M. Simeone, *Cancer Research* **2014**, *74*, 1778-1788.
[135] I. Jaco, A. Annibaldi, N. Lalaoui, R. Wilson, T. Tenev, L. Laurien, C. Kim, K. Jamal, S. Wicky John, G. Liccardi, D. Chau, J. M. Murphy, G. Brumatti, R. Feltham, M. Pasparakis, J. Silke, P. Meier, *Molecular Cell* **2017**, *66*, 698-710.e695.
[136] Y. Wei, Z. An, Z. Zou, R. Sumpter, Jr., M. Su, X. Zang, S. Sinha, M. Gaestel, B. Levine, *eLife* **2015**, *4*, e05289.
[137] Z. Xiao, J. Xue, T. J. Sowin, H. Zhang, *Molecular Cancer Therapeutics* **2006**, *5*, 1935-1943.
[138] D. Luo, E. Mladenov, A. Soni, M. Stuschke, G. Iliakis, *Cells* **2023**, *12*, 1387.
[139] M. Vicente-Manzanares, A. R. Horwitz, in *Cell Migration: Developmental Methods and Protocols* (Eds.: C. M. Wells, M. Parsons), Humana Press, Totowa, NJ, **2011**, pp. 1-24.
[140] J. C. Hedges, M. A. Dechert, I. A. Yamboliev, J. L. Martin, E. Hickey, L. A. Weber, W. T. Gerthoffer, *Journal of Biological Chemistry* **1999**, *274*, 24211-24219.
[141] aA. Vidyasagar, N. A. Wilson, A. Djamali, *Fibrogenesis & Tissue Repair* **2012**, *5*, 7; bM. K. Singh, B. Sharma, Pramod K. Tiwari, *Journal of Thermal Biology* **2017**, *69*, 149-154.
[142] L. M. Hoffman, C. C. Jensen, M. C. Beckerle, *Molecular Biology of the Cell* **2022**, *33*, ar100.
[143] L. Xu, S. Chen, R. C. Bergan, *Oncogene* **2006**, *25*, 2987-2998.
[144] M. Kobayashi, M. Nishita, T. Mishima, K. Ohashi, K. Mizuno, *The EMBO Journal* **2006**, *25*, 713-726-726.
[145] Y. Wu, L. Zhan, Y. Ai, M. Hannigan, M. Gaestel, C.-K. Huang, J. A. Madri, *Biochemical and Biophysical Research Communications* **2007**, *358*, 170-175.
[146] A. Kotlyarov, Y. Yannoni, S. Fritz, K. Laaß, J.-B. Telliez, D. Pitman, L.-L. Lin, M. Gaestel, *Molecular and Cellular Biology* **2002**, *22*, 4827.
[147] Manoj B. Menon, C. Tiedje, J. Lafera, N. Ronkina, T. Konen, A. Kotlyarov, M. Gaestel, *Biochemical Journal* **2013**, *456*, 163-172.

[148] M. A. X. Tollenaere, B. H. Villumsen, M. Blasius, J. C. Nielsen, S. A. Wagner, J. Bartek, P. Beli, N. Mailand, S. Bekker-Jensen, *Nature Communications* **2015**, *6*, 10075.
[149] Kirsty F. MacKenzie, Derek A. Wallace, Elaine V. Hill, Diana F. Anthony, David J. P. Henderson, Daniel M. Houslay, J. Simon C. Arthur, George S. Baillie, Miles D. Houslay, *Biochemical Journal* **2011**, *435*, 755-769.
[150] N. Flamand, M. Luo, M. Peters-Golden, T. G. Brock, *Journal of Biological Chemistry* **2009**, *284*, 306-313.
[151] H. Li, Y. Liu, Z. Gu, L. Li, Y. Liu, L. Wang, L. Su, *Oncol Lett* **2018**, *15*, 775-782.
[152] aA. L. Ray, E. F. Castillo, K. T. Morris, R. A. Nofchissey, L. L. Weston, V. G. Samedi, J. A. Hanson, M. Gaestel, I. V. Pinchuk, E. J. Beswick, *International Journal of Cancer* **2016**, *138*, 770-775; bA. L. Ray, K. L. Berggren, S. Restrepo Cruz, G. N. Gan, E. J. Beswick, *International Journal of Cancer* **2018**, *142*, 1702-1711.
[153] L. Yang, B. Liu, F. Qiu, B. Huang, Y. Li, D. Huang, R. Yang, X. Yang, J. Deng, Q. Jiang, Y. Zhou, J. Lu, *Carcinogenesis* **2013**, *35*, 46-52.
[154] K. L. Berggren, S. Restrepo Cruz, M. D. Hixon, A. T. Cowan, S. B. Keysar, S. Craig, J. James, M. Barry, M. A. Ozbun, A. Jimeno, D. J. McCance, E. J. Beswick, G. N. Gan, *Oncogene* **2019**, *38*, 7329-7341.
[155] B. Liu, L. Yang, B. Huang, M. Cheng, H. Wang, Y. Li, D. Huang, J. Zheng, Q. Li, X. Zhang, W. Ji, Y. Zhou, J. Lu, *The American Journal of Human Genetics* **2012**, *91*, 384-390.
[156] F. Qeadan, P. Bansal, J. A. Hanson, E. J. Beswick, *Journal of Translational Medicine* **2020**, *18*, 137.
[157] C. McCormick, D. Ganem, *Science* **2005**, *307*, 739-741.
[158] M. Matsumoto, T. Sudo, T. Saito, H. Osada, M. Tsujimoto, *Journal of Biological Chemistry* **2000**, *275*, 31155-31161.
[159] B. Murali, Q. Ren, X. Luo, D. V. Faget, C. Wang, R. M. Johnson, T. Gruosso, K. C. Flanagan, Y. Fu, K. Leahy, E. Alspach, X. Su, M. H. Ross, B. Burnette, K. N. Weilbaecher, M. Park, G. Mbalaviele, J. B. Monahan, S. A. Stewart, *Cancer Research* **2018**, *78*, 5618-5630.
[160] J. Samulin Erdem, V. Skaug, A. Haugen, S. Zienolddiny, *Journal of Cancer* **2016**, *7*, 512-515.
[161] S. Morandell, H. C. Reinhardt, Ian G. Cannell, Jacob S. Kim, Daniela M. Ruf, T. Mitra, Anthony D. Couvillon, T. Jacks, Michael B. Yaffe, *Cell Reports* **2013**, *5*, 868-877.
[162] M. Guo, D. Sun, Z. Fan, Y. Yuan, M. Shao, J. Hou, Y. Zhu, R. Wei, Y. Zhu, J. Qian, F. Li, Y. Yang, C. Gu, *Frontiers in Oncology* **2019**, *9*.
[163] D. Alimbetov, B. Umbayev, A. Tsoy, D. Begimbetova, T. Davis, D. Kipling, S. Askarova, *BMC Cancer* **2023**, *23*, 895.
[164] F. Köpper, A. M. Binkowski, C. Bierwirth, M. Dobbelstein, *Cell Cycle* **2014**, *13*, 884-889.
[165] N. M. Anderson, M. C. Simon, *Current Biology* **2020**, *30*, R921-R925.
[166] L.-Y. Yu-Lee, G. Yu, Y.-C. Lee, S.-C. Lin, J. Pan, T. Pan, K.-J. Yu, B. Liu, C. J. Creighton, J. Rodriguez-Canales, P. A. Villalobos, I. I. Wistuba, E. de Nadal, F. Posas, G. E. Gallick, S.-H. Lin, *Cancer Research* **2018**, *78*, 2911-2924.
[167] B. Kumar, S. Koul, J. Petersen, L. Khandrika, J. S. Hwa, R. B. Meacham, S. Wilson, H. K. Koul, *Cancer Research* **2010**, *70*, 832-841.
[168] W. Zhou, X. Yu, S. Sun, X. Zhang, W. Yang, J. Zhang, X. Zhang, Z. Jiang, *Biomedicine & Pharmacotherapy* **2019**, *118*, 109369.
[169] G. Landskron, M. De la Fuente, P. Thuwajit, C. Thuwajit, M. A. Hermoso, *Journal of Immunology Research* **2014**, *2014*, 149185.
[170] aS. Soni, M. K. Saroch, B. Chander, N. V. Tirpude, Y. S. Padwad, *Journal of Experimental & Clinical Cancer Research* **2019**, *38*, 175; bX. León, C. Bothe, J. García, M. Parreño, S. Alcolea, M. Quer, L. Vila, M. Camacho, *Oncotarget* **2015**, *6*.

[171] aS. A. Duffy, J. M. G. Taylor, J. E. Terrell, M. Islam, Y. Li, K. E. Fowler, G. T. Wolf, T. N. Teknos, *Cancer* **2008**, *113*, 750-757; bJ. Zhang, S. Sarkar, R. Cua, Y. Zhou, W. Hader, V. W. Yong, *Carcinogenesis* **2011**, *33*, 312-319.

[172] M. A. Coelho, S. de Carné Trécesson, S. Rana, D. Zecchin, C. Moore, M. Molina-Arcas, P. East, B. Spencer-Dene, E. Nye, K. Barnouin, A. P. Snijders, W. S. Lai, P. J. Blackshear, J. Downward, *Immunity* **2017**, *47*, 1083-1099.e1086.

[173] M. M. McLaughlin, S. Kumar, P. C. McDonnell, S. Van Horn, J. C. Lee, G. P. Livi, P. R. Young, *Journal of Biological Chemistry* **1996**, *271*, 8488-8492.

[174] C. Ehlting, N. Ronkina, O. Böhmer, U. Albrecht, K. A. Bode, K. S. Lang, A. Kotlyarov, D. Radzioch, M. Gaestel, D. Häussinger, J. G. Bode, *Journal of Biological Chemistry* **2011**, *286*, 24113-24124.

[175] C. Ehlting, J. Rex, U. Albrecht, R. Deenen, C. Tiedje, K. Köhrer, O. Sawodny, M. Gaestel, D. Häussinger, J. G. Bode, *Scientific Reports* **2019**, *9*, 11021.

[176] aR. Roskoski, *Pharmacological Research* **2024**, *199*, 107036; bR. Roskoski Jr., **2024**. *Protein Kinase Inhbibitors*. https://brimr.org/protein-kinase-inhibitors/ (accessed 15.05.2024)

[177] aC. Bournez, F. Carles, G. Peyrat, S. Aci-Sèche, S. Bourg, C. Meyer, P. Bonnet, *Molecules* **2020**, *25*, 3226; b. *PKIDB: A Curated, Annotated and Updated Database of Protein Kinase Inhibitors in Clinical Trials.* **2024.** https://www.icoa.fr/pkidb/ (accessed 15.05.2024)

[178] P. Cohen, D. Cross, P. A. Jänne, *Nature Reviews Drug Discovery* **2021**.

[179] A. Talevi, *Frontiers in Pharmacology* **2015**, *6*.

[180] Z. A. Knight, K. M. Shokat, *Chemistry & Biology* **2005**, *12*, 621-637.

[181] J. Zhang, P. L. Yang, N. S. Gray, *Nature Reviews Cancer* **2009**, *9*, 28-39.

[182] J. M. Grimes, K. V. Grimes, *Journal of Molecular and Cellular Cardiology* **2020**, *144*, 63-65.

[183] aM. Adams, T. Kobayashi, J. D. Lawson, M. Saitoh, K. Shimokawa, S. V. Bigi, M. S. Hixon, C. R. Smith, T. Tatamiya, M. Goto, J. Russo, C. E. Grimshaw, S. Swann, *Bioorganic & Medicinal Chemistry Letters* **2016**, *26*, 1086-1089; bX. Yang, D. Fan, A. H. Troha, H. M. Ahn, K. Qian, B. Liang, Y. Du, H. Fu, A. A. Ivanov, *Bioorganic & Medicinal Chemistry* **2021**, *45*, 116324; cM.-L. Tang, H. Li, J.-F. Ning, X. Shen, X. Sun, *Journal of Medicinal Chemistry* **2022**, *65*, 6690-6709; dS. Scarneo, P. Hughes, R. Freeze, K. Yang, J. Totzke, T. Haystead, *ACS Chemical Biology* **2022**, *17*, 536-544.

[184] aS. Iwano, Y. Asaoka, H. Akiyama, S. Takizawa, H. Nobumasa, H. Hashimoto, Y. Miyamoto, *Journal of Applied Toxicology* **2011**, *31*, 671-677; bN. Damjanov, R. S. Kauffman, G. T. Spencer-Green, *Arthritis & Rheumatism* **2009**, *60*, 1232-1241.

[185] M. C. GENOVESE, S. B. COHEN, D. WOFSY, M. E. WEINBLATT, G. S. FIRESTEIN, E. BRAHN, V. STRAND, D. G. BAKER, S. E. TONG, *The Journal of Rheumatology* **2011**, *38*, 846-854.

[186] aS. B. Cohen, T.-T. Cheng, V. Chindalore, N. Damjanov, R. Burgos-Vargas, P. DeLora, K. Zimany, H. Travers, J. P. Caulfield, *Arthritis & Rheumatism* **2009**, *60*, 335-344; bS. Schreiber, B. Feagan, G. D'Haens, J. F. Colombel, K. Geboes, M. Yurcov, V. Isakov, O. Golovenko, C. N. Bernstein, D. Ludwig, T. Winter, U. Meier, C. Yong, J. Steffgen, *Clinical Gastroenterology and Hepatology* **2006**, *4*, 325-334.

[187] J. H. Ronald, D. Karim, P. Deborah, L. Ching, T. S. Rebecca, W. Mary, P. Eva, W. S. Kyung, C. Kung-ching, L. David, K. Yong-Nam, T. R. Richard, S. Z. Tanja, A. Dee, P. Joseph Dal, M. M. Anthony, L. P. Stanford, M. G. David, R. W. Brian, *Journal of Pharmacology and Experimental Therapeutics* **2008**, *327*, 610.

[188] A. Cuenda, J. Rouse, Y. N. Doza, R. Meier, P. Cohen, T. F. Gallagher, P. R. Young, J. C. Lee, *FEBS Letters* **1995**, *364*, 229-233.

[189] S. C. Koeberle, J. Romir, S. Fischer, A. Koeberle, V. Schattel, W. Albrecht, C. Grütter, O. Werz, D. Rauh, T. Stehle, S. A. Laufer, *Nature Chemical Biology* **2012**, *8*, 141-143.

[190] aQ. Zheng, S. Li, A. Wang, M. Zhe, P. Yang, Y. Wu, M. Zhao, Y. Zhu, Y. Luo, G. Wang, L. Ouyang, *MedComm – Oncology* **2023**, *2*, e53; bJ. Regan, A. Capolino, P. F. Cirillo, T. Gilmore, A. G. Graham, E. Hickey, R. R. Kroe, J. Madwed, M. Moriak, R. Nelson, C. A. Pargellis, A. Swinamer, C. Torcellini, M. Tsang, N. Moss, *Journal of Medicinal Chemistry* **2003**, *46*, 4676-4686; cC. Pargellis, L. Tong, L. Churchill, P. F. Cirillo, T. Gilmore, A. G. Graham, P. M. Grob, E. R. Hickey, N. Moss, S. Pav, J. Regan, *Nature Structural Biology* **2002**, *9*, 268-272.

[191] J. W. Goldman, L. S. Rosen, A. W. Tolcher, K. Papadopoulos, M. Beeram, P. Shi, C. Pitou, R. Bell, P. Kulanthaivel, X. Zhang, A. Fink, E. M. Chan, A. Shahir, D. Farrington, A. Patnaik, *Investigational New Drugs* **2018**, *36*, 629-637.

[192] aJ. S. C. Arthur, S. C. Ley, *Nature Reviews Immunology* **2013**, *13*, 679-692; bS. Rakesh Kumar, S. Reena, S. Sameer, D. Sunanda Ghosh, T. Ruchi, *bioRxiv* **2022**, 2022.2007.2017.500377.

[193] W. Davidson, L. Frego, G. W. Peet, R. R. Kroe, M. E. Labadia, S. M. Lukas, R. J. Snow, S. Jakes, C. A. Grygon, C. Pargellis, B. G. Werneburg, *Biochemistry* **2004**, *43*, 11658-11671.

[194] aD. Gordon, A. Kivitz, A. Singhal, D. Burt, M. C. Bangs, E. E. Huff, H. R. Hope, J. B. Monahan, *ACR Open Rheumatology* **2023**, *5*, 63-70; bC. Wang, S. Hockerman, E. J. Jacobsen, Y. Alippe, S. R. Selness, H. R. Hope, J. L. Hirsch, S. J. Mnich, M. J. Saabye, W. F. Hood, S. L. Bonar, Y. Abu-Amer, A. Haimovich, H. M. Hoffman, J. B. Monahan, G. Mbalaviele, *Journal of Experimental Medicine* **2018**, *215*, 1315-1325.

[195] Ress release; Aclaris Therapeutics, Inc., **2023**. *Aclaris Therapeutics Announces Top-line Results from 12-Week Phase 2b Trial of Oral Zunsemetinib (ATI-450) for Moderate to Severe Rheumatoid Arthritis and Provides Corporate Update.* https://investor.aclaristx.com/news-releases/news-release-details/aclaris-therapeutics-announces-top-line-results-12-week-phase-2b (accessed 19.01.2024)

[196] aJ. G. Cumming, J. É. Debreczeni, F. Edfeldt, E. Evertsson, M. Harrison, G. A. Holdgate, M. J. James, S. G. Lamont, K. Oldham, J. E. Sullivan, S. L. Wells, *Journal of Medicinal Chemistry* **2015**, *58*, 278-293; bU. Hedström, M. Norberg, E. Evertsson, S. R. Lever, M. Munck af Rosenschöld, H. Lönn, P. Bold, H. Käck, P. Berntsson, J. Vinblad, J. Liu, A. Welinder, J. Karlsson, A. Snijder, K. Pardali, U. Andersson, A. M. Davis, M. Mogemark, *ChemMedChem* **2019**, *14*, 1701-1709.

[197] D. C. Swinney, *Nature Reviews Drug Discovery* **2004**, *3*, 801-808.

[198] A. Schlapbach, C. Huppertz, *Future Medicinal Chemistry* **2009**, *1*, 1243-1257.

[199] B. C. Evans, K. M. Hocking, M. J. Osgood, I. Voskresensky, J. Dmowska, K. V. Kilchrist, C. M. Brophy, C. L. Duvall, *Science Translational Medicine* **2015**, *7*, 291ra295-291ra295.

[200] Q. T. N. Tran, P. X. L. Gan, W. Liao, Y. K. Mok, C. L. L. Chai, W. S. F. Wong, *Pharmacological Research* **2023**, *194*, 106861.

[201] B. Yang, M. M. Weiss, X. Zhu, H. Dong, I. Marx, (Ed.: I. Kymera Therapeutics), **2023**.

[202] R. J. Mourey, B. L. Burnette, S. J. Brustkern, J. S. Daniels, J. L. Hirsch, W. F. Hood, M. J. Meyers, S. J. Mnich, B. S. Pierce, M. J. Saabye, J. F. Schindler, S. A. South, E. G. Webb, J. Zhang, D. R. Anderson, *Journal of Pharmacology and Experimental Therapeutics* **2010**, *333*, 797-807.

[203] A. A. Antolin, D. Sanfelice, A. Crisp, E. Villasclaras Fernandez, I. L. Mica, Y. Chen, I. Collins, A. Edwards, S. Müller, B. Al-Lazikani, P. Workman, *Nucleic Acids Research* **2022**, *51*, D1492-D1502.

[204] S. J. Daniels, Y. Lai, S. South, P.-C. Chiang, D. Walker, B. Feng, R. Mireles, O. L. Whiteley, W. J. McKenzie, J. Stevens, R. Mourey, D. Anderson, W. D. J. Ii, *Drug Metabolism Letters* **2013**, *7*, 15-22.

[205] aM. D. Alexander, C. Chuaqui, J. Malona, J. J. McDonald, Y. Ni, D. Niu, R. C. Petter, J. Singh, C. Pabba, (Ed.: C. C. LLC), **2016**; bJ. Malona, A. L. Ruchelman, (Ed.: C. C. LLC), **2018**.

[206] D. R. Anderson, M. J. Meyers, W. F. Vernier, M. W. Mahoney, R. G. Kurumbail, N. Caspers, G. I. Poda, J. F. Schindler, D. B. Reitz, R. J. Mourey, *Journal of Medicinal Chemistry* **2007**, *50*, 2647-2654.

[207] R. Pengal, A. J. Guess, S. Agrawal, J. Manley, R. F. Ransom, R. J. Mourey, R. Benndorf, W. E. Smoyer, *American Journal of Physiology-Renal Physiology* **2011**, *301*, F509-F519.

[208] C. Hanau, S. M. Mershon, M. J. Graneto, M. J. Meyers, S. G. Hegde, I. P. Buchler, K. K. Wu, S. Liu, K. Nacro, (Ed.: P. corporation), **2004**, p. 265.

[209] T. Barf, A. Kaptein, S. d. Wilde, R. v. d. Heijden, R. v. Someren, D. Demont, C. Schultz-Fademrecht, J. Versteegh, M. v. Zeeland, N. Seegers, B. Kazemier, B. v. d. Kar, M. v. Hoek, J. d. Roos, H. Klop, R. Smeets, C. Hofstra, J. Hornberg, A. Oubrie, *Bioorganic & Medicinal Chemistry Letters* **2011**, *21*, 3818-3822.

[210] A. Oubrie, A. Kaptein, E. de Zwart, N. Hoogenboom, R. Goorden, B. van de Kar, M. van Hoek, V. de Kimpe, R. van der Heijden, J. Borsboom, B. Kazemier, J. de Roos, M. Scheffers, J. Lommerse, C. Schultz-Fademrecht, T. Barf, *Bioorganic & Medicinal Chemistry Letters* **2012**, *22*, 613-618.

[211] J. Velcicky, A. Schlapbach, R. Heng, L. Revesz, D. Pflieger, E. Blum, S. Hawtin, C. Huppertz, R. Feifel, R. Hersperger, *ACS Medicinal Chemistry Letters* **2018**, *9*, 392-396.

[212] J. A. H. Schwöbel, Y. K. Koleva, S. J. Enoch, F. Bajot, M. Hewitt, J. C. Madden, D. W. Roberts, T. W. Schultz, M. T. D. Cronin, *Chemical Reviews* **2011**, *111*, 2562-2596.

[213] M. Gehringer, S. A. Laufer, *Journal of Medicinal Chemistry* **2019**, *62*, 5673-5724.

[214] L. Boike, N. J. Henning, D. K. Nomura, *Nature Reviews Drug Discovery* **2022**, *21*, 881-898.

[215] L. Hillebrand, X. J. Liang, R. A. M. Serafim, M. Gehringer, *Journal of Medicinal Chemistry* **2024**.

[216] R. Roskoski Jr, *Pharmacological Research* **2023**, *194*, 106847.

[217] A. Chaikuad, P. Koch, S. A. Laufer, S. Knapp, *Angewandte Chemie International Edition* **2018**, *57*, 4372-4385.

[218] Z. Zhao, P. E. Bourne, *Pharmaceuticals* **2022**, *15*, 1322.

[219] R. Banerjee, N. J. Pace, D. R. Brown, E. Weerapana, *Journal of the American Chemical Society* **2013**, *135*, 2497-2500.

[220] F. Terrier, *Chemical Reviews* **1982**, *82*, 77-152.

[221] E. E. Kwan, Y. Zeng, H. A. Besser, E. N. Jacobsen, *Nature Chemistry* **2018**, *10*, 917-923.

[222] aA. Elbrecht, Y. Chen, A. Adams, J. Berger, P. Griffin, T. Klatt, B. Zhang, J. Menke, G. Zhou, R. G. Smith, D. E. Moller, *Journal of Biological Chemistry* **1999**, *274*, 7913-7922; bL. M. Leesnitzer, D. J. Parks, R. K. Bledsoe, J. E. Cobb, J. L. Collins, T. G. Consler, R. G. Davis, E. A. Hull-Ryde, J. M. Lenhard, L. Patel, K. D. Plunket, J. L. Shenk, J. B. Stimmel, C. Therapontos, T. M. Willson, S. G. Blanchard, *Biochemistry* **2002**, *41*, 6640-6650.

[223] K. X. Chen, C. A. Lesburg, B. Vibulbhan, W. Yang, T.-Y. Chan, S. Venkatraman, F. Velazquez, Q. Zeng, F. Bennett, G. N. Anilkumar, J. Duca, Y. Jiang, P. Pinto, L. Wang, Y. Huang, O. Selyutin, S. Gavalas, H. Pu, S. Agrawal, B. Feld, H.-C. Huang, C. Li, K.-C. Cheng, N.-Y. Shih, J. A. Kozlowski, S. B. Rosenblum, F. G. Njoroge, *Journal of Medicinal Chemistry* **2012**, *55*, 2089-2101.

[224] W. Hou, Y. Ren, Z. Zhang, H. Sun, Y. Ma, B. Yan, *Bioorganic & Medicinal Chemistry* **2018**, *26*, 1740-1750.

[225] S. Gerstenecker, L. Haarer, M. Schröder, M. Kudolo, M. P. Schwalm, V. Wydra, R. A. M. Serafim, A. Chaikuad, S. Knapp, S. Laufer, M. Gehringer, *Cancers (Basel)* **2021**, *13*.

[226] R. A. M. Serafim, A. da Silva Santiago, M. P. Schwalm, Z. Hu, C. V. dos Reis, J. E. Takarada, P. Mezzomo, K. B. Massirer, M. Kudolo, S. Gerstenecker, A. Chaikuad, L. Zender, S. Knapp, S. Laufer, R. M. Couñago, M. Gehringer, *Journal of Medicinal Chemistry* **2022**, *65*, 3173-3192.

[227] M. Schwarz, M. Kurkunov, F. Wittlinger, R. Rudalska, G. Wang, M. P. Schwalm, A. Rasch, B. Wagner, S. A. Laufer, S. Knapp, D. Dauch, M. Gehringer, *Journal of Medicinal Chemistry* **2024**.

[228] J. Malona, C. Chuaqui, B. M. Seletsky, L. Beebe, S. Cantin, D. V. Kalken, K. Fahnoe, Z. Wang, B. Browning, H. Szabo, L. A. Koopman, T. Oravecz, J. J. McDonald, F. Ramirez-Valle, R. Gaur, K. A. Mensah, M. Thomas, J. N. Connarn, H. Hu, M. D. Alexander, A. F. Corin, *Translational Research* **2022**.

[229] I. Miyahisa, T. Sameshima, M. S. Hixon, *Angewandte Chemie International Edition* **2015**, *54*, 14099-14102.

[230] J. M. Strelow, *SLAS Discovery* **2017**, *22*, 3-20.

[231] D. P. Williams, *Toxicology* **2006**, *226*, 1-11.

[232] L. Petri, P. Ábrányi-Balogh, P. R. Varga, T. Imre, G. M. Keserű, *Bioorganic & Medicinal Chemistry* **2020**, *28*, 115357.

[233] R. A. M. Serafim, L. Haarer, J. G. B. Pedreira, M. Gehringer, *Current Research in Chemical Biology* **2023**, *3*, 100040.

[234] aR. A. Ward, P. Bethel, C. Cook, E. Davies, J. E. Debreczeni, G. Fairley, L. Feron, V. Flemington, M. A. Graham, R. Greenwood, N. Griffin, L. Hanson, P. Hopcroft, T. D. Howard, J. Hudson, M. James, C. D. Jones, C. R. Jones, S. Lamont, R. Lewis, N. Lindsay, K. Roberts, I. Simpson, S. St-Gallay, S. Swallow, J. Tang, M. Tonge, Z. Wang, B. Zhai, *Journal of Medicinal Chemistry* **2017**, *60*, 3438-3450; bP. A. Schwartz, P. Kuzmic, J. Solowiej, S. Bergqvist, B. Bolanos, C. Almaden, A. Nagata, K. Ryan, J. Feng, D. Dalvie, J. C. Kath, M. Xu, R. Wani, B. W. Murray, *Proceedings of the National Academy of Sciences* **2014**, *111*, 173-178.

[235] R. Gaur, K. A. Mensah, J. Stricker, M. Adams, A. Parton, D. Cedzik, J. Connarn, M. Thomas, G. Horan, P. Schafer, S. Mair, M. Palmisano, F. Ramírez-Valle, *Arthritis Research & Therapy* **2022**, *24*, 199.

[236] National Library of Mediicne, **2023.** NCT04947579. *A Study of CC-99677 in Participants With Active Ankylosing Spondylitis (AS SpA axSpA)*. https://clinicaltrials.gov/study/NCT04947579?term=%20Study%20of%20CC-99677%20in%20Participants%20with%20Active%20Ankylosing%20Spondylitis%20&rank=1 (accessed 30.01.2024)

[237] S. Duraisamy, M. Bajpai, U. Bughani, S. G. Dastidar, A. Ray, P. Chopra, *Expert Opinion on Therapeutic Targets* **2008**, *12*, 921-936.

[238] aA. Hantzsch, *Berichte der deutschen chemischen Gesellschaft* **1890**, *23*, 1474-1476; bM. Leonardi, V. Estévez, M. Villacampa, J. C. Menéndez, *Synthesis* **2019**, *51*, 816-828.

[239] M. Armitage, G. Bret, B. M. Choudary, M. Kingswood, M. Loft, S. Moore, S. Smith, M. W. J. Urquhart, *Organic Process Research & Development* **2012**, *16*, 1626-1634.

[240] in *Chemistry of Heterocyclic Compounds*, **1962**, pp. 1-30.

[241] J. A. Ortega, J. M. Arencibia, E. Minniti, J. A. W. Byl, S. Franco-Ulloa, M. Borgogno, V. Genna, M. Summa, S. M. Bertozzi, R. Bertorelli, A. Armirotti, A. Minarini, C. Sissi, N. Osheroff, M. De Vivo, *Journal of Medicinal Chemistry* **2020**, *63*, 12873-12886.

[242] aP. Ruiz-Castillo, S. L. Buchwald, *Chemical Reviews* **2016**, *116*, 12564-12649; bX. Yang, Y. Zhang, D. Ma, *Advanced Synthesis & Catalysis* **2012**, *354*, 2443-2446.

[243] aL. Qin, H. Cui, D. Zou, J. Li, Y. Wu, Z. Zhu, Y. Wu, *Tetrahedron Letters* **2010**, *51*, 4445-4448; bS. Bhagwanth, A. G. Waterson, G. M. Adjabeng, K. R. Hornberger, *The Journal of Organic Chemistry* **2009**, *74*, 4634-4637.

[244] S. M. Hickey, S. O. Nitschke, M. J. Sweetman, C. J. Sumby, D. A. Brooks, S. E. Plush, T. D. Ashton, *The Journal of Organic Chemistry* **2020**, *85*, 7986-7999.

[245] E. V. Vinogradova, N. H. Park, B. P. Fors, S. L. Buchwald, *Organic Letters* **2013**, *15*, 1394-1397.

[246] aB. Jolicoeur, E. E. Chapman, A. Thompson, W. D. Lubell, *Tetrahedron* **2006**, *62*, 11531-11563; bin *Greene's Protective Groups in Organic Synthesis*, **2006**, pp. 696-926.

[247] aE. Vanotti, R. Amici, A. Bargiotti, J. Berthelsen, R. Bosotti, A. Ciavolella, A. Cirla, C. Cristiani, R. D'Alessio, B. Forte, A. Isacchi, K. Martina, M. Menichincheri, A. Molinari, A. Montagnoli, P. Orsini, A. Pillan, F. Roletto, A. Scolaro, M. Tibolla, B. Valsasina, M. Varasi, D. Volpi, C. Santocanale, *Journal of Medicinal Chemistry* **2008**, *51*, 487-501; bM. Menichincheri, A. Bargiotti, J. Berthelsen, J. A. Bertrand, R. Bossi, A. Ciavolella, A. Cirla, C. Cristiani, V. Croci, R. D'Alessio, M. Fasolini, F. Fiorentini, B. Forte, A. Isacchi, K. Martina, A. Molinari, A. Montagnoli, P. Orsini, F. Orzi, E. Pesenti, D. Pezzetta, A. Pillan, I. Poggesi, F. Roletto, A. Scolaro, M. Tatò, M. Tibolla, B. Valsasina, M. Varasi, D. Volpi, C. Santocanale, E. Vanotti, *Journal of Medicinal Chemistry* **2009**, *52*, 293-307.

[248] H. Huang, L. Acquaviva, V. Berry, H. Bregman, N. Chakka, A. O'Connor, E. F. DiMauro, J. Dovey, O. Epstein, B. Grubinska, J. Goldstein, H. Gunaydin, Z. Hua, X. Huang, L. Huang, J. Human, A. Long, J. Newcomb, V. F. Patel, D. Saffran, R. Serafino, S. Schneider, C. Strathdee, J. Tang, S. Turci, R. White, V. Yu, H. Zhao, C. Wilson, M. W. Martin, *ACS Medicinal Chemistry Letters* **2012**, *3*, 1059-1064.

[249] F. Scott, A. M. Fala, J. E. Takarada, M. P. Ficu, L. E. Pennicott, T. D. Reuillon, R. M. Couñago, K. B. Massirer, J. M. Elkins, S. E. Ward, *Bioorganic & Medicinal Chemistry Letters* **2022**, *60*, 128588.

[250] aF. Voss, S. Ritter, S. Nordhoff, S. Wachten, S. Oberbörsch, A. Kless, (Ed.: G. GmbH), **2015**, p. 135; bA. Hart, W. J. Pitts, H. Mastalerz, J. Guo, G. Brown, (Ed.: B.-M. S. Company), **2016**, p. 148; cV. Schulze, A. Mengel, A. C. Faria Alvares de Lemos, U. Rauh, U. Bömer, R. Hillig, C. Lechner, J. X. Mortier, D. Sülzle, (Ed.: B. Aktiengesellschaft), **2022**, p. 219; dS. Siegel, F. Siegel, V. Schulze, M. Berger, K. Graham, D. Sülzle, U. Bömer, D. Korr, J. Schröder, U. Mönning, M. Niehues, M. Meyerson, H. Greulich, B. Kaplan, (Ed.: B. Aktiengesellschaft), **2020**, p. 273; eB. Milgram, B. F. Rahemtulla, J. M. Bateman, E. Talbot, T. A. Mulhern, (Ed.: S. T. Inc.), **2023**, p. 220.

[251] W. K. Anderson, D. C. Dean, T. Endo, *Journal of Medicinal Chemistry* **1990**, *33*, 1667-1675.

[252] S. Nahm, S. M. Weinreb, *Tetrahedron Letters* **1981**, *22*, 3815-3818.

[253] F. Ansideri, S. Andreev, A. Kuhn, W. Albrecht, S. A. Laufer, P. Koch, *Molecules* **2018**, *23*, 221.

[254] M. A. Düfert, K. L. Billingsley, S. L. Buchwald, *Journal of the American Chemical Society* **2013**, *135*, 12877-12885.

[255] aY. Garcia, F. Schoenebeck, C. Y. Legault, C. A. Merlic, K. N. Houk, *Journal of the American Chemical Society* **2009**, *131*, 6632-6639; bJ. P. Knowles, A. Whiting, *Organic & Biomolecular Chemistry* **2007**, *5*, 31-44.

[256] P. Skolnick, (Ed.: I. Dov Pharmaceutical), **2005**, p. 63.

[257] M. P. Hay, S. Turcotte, J. U. Flanagan, M. Bonnet, D. A. Chan, P. D. Sutphin, P. Nguyen, A. J. Giaccia, W. A. Denny, *Journal of Medicinal Chemistry* **2010**, *53*, 787-797.

[258] aM. D. Walkinshaw, S. N. Pettit, A. Highton, I. W. McNae, (Ed.: T. U. c. o. t. U. o. Edinborugh), **2019**, p. 117; bV. Cee, F. Chavez Jr., J. J. Chen, E. H. Harrington, B. Herberich, C. L. M. Jackson, B. A. Lanman, T. T. Nguyen, M. H. Norman, L. H. Pettus, A. B. Reed, A. L. Smith, N. A. Tamayo, A. Tasker, H.-L. Wang, B. Wu, R. Wurz, (Ed.: A. Inc.), **2013**, p. 708.

[259] S. Routier, L. Saugé, N. Ayerbe, G. Coudert, J.-Y. Mérour, *Tetrahedron Letters* **2002**, *43*, 589-591.

[260] M. Menichincheri, M. Angiolini, J. Bertrand, M. Caruso, P. Polucci, F. Quartieri, B. Salom, M. Salsa, F. Zuccotto, **2014**, p. 156.

[261] L. I. Belen'kii, T. G. Kim, I. A. Suslov, N. D. Chuvylkin, *Russian Chemical Bulletin* **2005**, *54*, 853-863.

[262] G. A. Cordell, *The Journal of Organic Chemistry* **1975**, *40*, 3161-3169.

[263] L. I. Belen'Kii, in *Advances in Heterocyclic Chemistry, Vol. 99* (Ed.: A. R. Katritzky), Academic Press, **2010**, pp. 143-183.
[264] H. M. Gilow, D. E. Burton, *The Journal of Organic Chemistry* **1981**, *46*, 2221-2225.
[265] A. H. Jackson, A. H. Jackson, M. Artico, H. J. Anderson, C. E. Loader, A. Gossauer, P. Nesvadba, N. Dennis, in *Chemistry of Heterocyclic Compounds*, **1990**, pp. 295-548.
[266] aC. Zambaldo, E. V. Vinogradova, X. Qi, J. Iaconelli, R. M. Suciu, M. Koh, K. Senkane, S. R. Chadwick, B. B. Sanchez, J. S. Chen, A. K. Chatterjee, P. Liu, P. G. Schultz, B. F. Cravatt, M. J. Bollong, *Journal of the American Chemical Society* **2020**, *142*, 8972-8979; bM. M. Pichon, D. Drelinkiewicz, D. Lozano, R. Moraru, L. J. Hayward, M. Jones, M. A. McCoy, S. Allstrum-Graves, D.-I. Balourdas, A. C. Joerger, R. J. Whitby, S. M. Goldup, N. Wells, G. J. Langley, J. M. Herniman, M. G. J. Baud, *Bioconjugate Chemistry* **2023**, *34*, 1679-1687.
[267] J. L. Maurel, J.-M. Autin, P. Funes, A. Newman-Tancredi, F. Colpaert, B. Vacher, *Journal of Medicinal Chemistry* **2007**, *50*, 5024-5033.
[268] O. Rabal, E. San José-Enériz, X. Agirre, J. A. Sánchez-Arias, A. Vilas-Zornoza, A. Ugarte, I. de Miguel, E. Miranda, L. Garate, M. Fraga, P. Santamarina, R. Fernandez Perez, R. Ordoñez, E. Sáez, S. Roa, M. J. García-Barchino, J. A. Martínez-Climent, Y. Liu, W. Wu, M. Xu, F. Prosper, J. Oyarzabal, *Journal of Medicinal Chemistry* **2018**, *61*, 6518-6545.
[269] M. M. K. Amer, M. A. Aziz, W. S. Shehab, M. H. Abdellattif, S. M. Mouneir, *Journal of Saudi Chemical Society* **2021**, *25*, 101259.
[270] L. D. Hatherley, R. D. Brown, P. D. Godfrey, A. P. Pierlot, W. Caminati, D. Damiani, S. Melandri, L. B. Favero, *The Journal of Physical Chemistry* **1993**, *97*, 46-51.
[271] aP. Beak, J. B. Covington, S. G. Smith, *Journal of the American Chemical Society* **1976**, *98*, 8284-8286; bP. Beak, *Accounts of Chemical Research* **1977**, *10*, 186-192; cM. R. Nimlos, D. F. Kelley, E. R. Bernstein, *The Journal of Physical Chemistry* **1989**, *93*, 643-651; dM. J. Nowak, L. Lapinski, J. Fulara, A. Les, L. Adamowicz, *The Journal of Physical Chemistry* **1992**, *96*, 1562-1569; eM. K. Hazra, T. Chakraborty, *The Journal of Physical Chemistry A* **2006**, *110*, 9130-9136; fS. Mata, V. Cortijo, W. Caminati, J. L. Alonso, M. E. Sanz, J. C. López, S. Blanco, *The Journal of Physical Chemistry A* **2010**, *114*, 11393-11398.
[272] aN. M. Chung, H. Tieckelmann, *The Journal of Organic Chemistry* **1970**, *35*, 2517-2520; bG. Vavilina, A. Zicmanis, P. Mekss, M. Klavins, *Chemistry of Heterocyclic Compounds* **2008**, *44*, 549-558; cH. Meislich, in *Chemistry of Heterocyclic Compounds*, **1962**, pp. 509-890.
[273] M. Breugst, H. Mayr, *Journal of the American Chemical Society* **2010**, *132*, 15380-15389.
[274] aX.-H. Li, A.-H. Ye, C. Liang, D.-L. Mo, *Synthesis* **2018**, *50*, 1699-1710; bR. A. Altman, S. L. Buchwald, *Organic Letters* **2007**, *9*, 643-646.
[275] T. Chen, Q. Huang, Y. Luo, Y. Hu, W. Lu, *Tetrahedron Letters* **2013**, *54*, 1401-1404.
[276] M. Kuriyama, N. Hanazawa, Y. Abe, K. Katagiri, S. Ono, K. Yamamoto, O. Onomura, *Chemical Science* **2020**, *11*, 8295-8300.
[277] D. Huang, G. Xu, S. Peng, J. Sun, *Chemical Communications* **2017**, *53*, 3197-3200.
[278] Q. Zhou, F. Du, X. Liang, W. Liu, T. Fang, G. Chen, *Molecules* **2018**, *23*, 1784.
[279] B. K. Singh, C. Cavalluzzo, M. De Maeyer, Z. Debyser, V. S. Parmar, E. Van der Eycken, *Synthesis* **2009**, *2009*, 2725-2728.
[280] N. Kornblum, R. A. Smiley, H. E. Ungnade, A. M. White, B. Taub, S. A. Herbert, Jr., *Journal of the American Chemical Society* **1955**, *77*, 5528-5533.
[281] J. Holenz, S. Karlström, J. Kihlström, K. Kolmodin, J. Lindström, L. Rakos, D. Rotticci, B.-M. Swahn, S. von Berg, (Ed.: A. AB), **2011**, p. 72.
[282] aJ. Chen, Y. Zhang, L. Yang, X. Zhang, J. Liu, L. Li, H. Zhang, *Tetrahedron* **2007**, *63*, 4266-4270; bC.-Y. Chen, Y.-Y. Huang, W.-N. Su, K. Kaneko, M. Kimura, H. Takayama, F. F. Wong, *Journal of Heterocyclic Chemistry* **2012**, *49*, 183-189; cM. W. Hooper, J. F. Hartwig,

Organometallics **2003**, *22*, 3394-3403; dL. Jedinák, R. Zátopková, H. Zemánková, A. Šustková, P. Cankař, *The Journal of Organic Chemistry* **2017**, *82*, 157-169.

[283] G. Zhang, Y. Xie, Z. Wang, Y. Liu, H. Huang, *Chemical Communications* **2015**, *51*, 1850-1853.

[284] T. Amelia, J. P. D. van Veldhoven, M. Falsini, R. Liu, L. H. Heitman, G. J. P. van Westen, E. Segala, G. Verdon, R. K. Y. Cheng, R. M. Cooke, D. van der Es, A. P. Ijzerman, *Journal of Medicinal Chemistry* **2021**, *64*, 3827-3842.

[285] aJ. Becher, J. Lundsgaard, *Phosphorus and Sulfur and the Related Elements* **1983**, *14*, 131-138; bN. Stuhr-Hansen, *Synthetic Communications* **2003**, *33*, 641-646.

[286] aB. Wang, T. Xu, L. Zhu, Y. Lan, J. Wang, N. Lu, Z. Wei, Y. Lin, H. Duan, *Organic Chemistry Frontiers* **2017**, *4*, 1266-1271; bL. Testaferri, M. Tiecco, M. Tingoli, D. Chianelli, M. Montanucci, *Synthesis* **1983**, *1983*, 751-755.

[287] R. N. Adamek, C. V. Credille, B. L. Dick, S. M. Cohen, *JBIC Journal of Biological Inorganic Chemistry* **2018**, *23*, 1129-1138.

[288] M. Kreis, S. Bräse, *Advanced Synthesis & Catalysis* **2005**, *347*, 313-319.

[289] aS. N. Mthembu, A. Sharma, F. Albericio, B. G. de la Torre, *ChemBioChem* **2020**, *21*, 1947-1954; bR. E. Humphrey, J. M. Hawkins, *Analytical Chemistry* **1964**, *36*, 1812-1814; cR. E. Humphrey, J. L. Potter, *Analytical Chemistry* **1965**, *37*, 164-165.

[290] S.-i. Fukuzawa, D. Tanihara, S. Kikuchi, *Synlett* **2006**, *2006*, 2145-2147.

[291] aR. Jones, A. Katritzky, *Journal of the Chemical Society (Resumed)* **1958**, 3610-3613; bM. Breugst, H. Zipse, J. P. Guthrie, H. Mayr, *Angewandte Chemie International Edition* **2010**, *49*, 5165-5169; cÁ. Horváth, B. D. Lőrincz, Z. Benkő, *Chemistry – A European Journal* **2023**, *29*, e202300611.

[292] S. S. M. Bandaru, S. Bhilare, J. Cardozo, N. Chrysochos, C. Schulzke, Y. S. Sanghvi, K. C. Gunturu, A. R. Kapdi, *The Journal of Organic Chemistry* **2019**, *84*, 8921-8940.

[293] D. M. Goldstein, T. Alfredson, J. Bertrand, M. F. Browner, K. Clifford, S. A. Dalrymple, J. Dunn, J. Freire-Moar, S. Harris, S. S. Labadie, J. La Fargue, J. M. Lapierre, S. Larrabee, F. Li, E. Papp, D. McWeeney, C. Ramesha, R. Roberts, D. Rotstein, B. San Pablo, E. B. Sjogren, O.-Y. So, F. X. Talamas, W. Tao, A. Trejo, A. Villasenor, M. Welch, T. Welch, P. Weller, P. E. Whiteley, K. Young, S. Zipfel, *Journal of Medicinal Chemistry* **2006**, *49*, 1562-1575.

[294] P. M. Grima Povedal, N. Aguilar Izquierdo, M. Mir Cepeda, M. Carrascal Riera, E. Terricabras Bellart, (Ed.: S. A. Almirall), **2011**, p. 90.

[295] H. Ma, S. Deacon, K. Horiuchi, *Expert Opinion on Drug Discovery* **2008**, *3*, 607-621.

[296] T. Anastassiadis, S. W. Deacon, K. Devarajan, H. Ma, J. R. Peterson, *Nature Biotechnology* **2011**, *29*, 1039-1045.

[297] https://www.assayquant.com/our-technology/ (accessed 08.05.2024)

[298] X. Lin, Y. Yosaatmadja, M. Kalyukina, M. J. Middleditch, Z. Zhang, X. Lu, K. Ding, A. V. Patterson, J. B. Smaill, C. J. Squire, *ACS Medicinal Chemistry Letters* **2019**, *10*, 1180-1186.

[299] N. A. Senger, B. Bo, Q. Cheng, J. R. Keeffe, S. Gronert, W. Wu, *The Journal of Organic Chemistry* **2012**, *77*, 9535-9540.

[300] B. Cordero, V. Gómez, A. E. Platero-Prats, M. Revés, J. Echeverría, E. Cremades, F. Barragán, S. Alvarez, *Dalton Transactions* **2008**, 2832-2838.

[301] E. Mons, S. Roet, R. Q. Kim, M. P. C. Mulder, *Current Protocols* **2022**, *2*, e419.

[302] X. Zhai, R. A. Ward, P. Doig, A. Argyrou, *Biochemistry* **2020**, *59*, 1428-1441.

[303] M. D. Shults, B. Imperiali, *Journal of the American Chemical Society* **2003**, *125*, 14248-14249.

[304] C. Yung-Chi, W. H. Prusoff, *Biochemical Pharmacology* **1973**, *22*, 3099-3108.

[305] W. C. Chan, S. Sharifzadeh, S. J. Buhrlage, J. A. Marto, *Chemical Society Reviews* **2021**, *50*, 8361-8381.

[306] aA. Keeley, P. Ábrányi-Balogh, G. M. Keserű, *MedChemComm* **2019**, *10*, 263-267; bV. J. Cee, L. P. Volak, Y. Chen, M. D. Bartberger, C. Tegley, T. Arvedson, J. McCarter, A. S. Tasker, C.

Fotsch, *Journal of Medicinal Chemistry* **2015**, *58*, 9171-9178; cA. Birkholz, D. J. Kopecky, L. P. Volak, M. D. Bartberger, Y. Chen, C. M. Tegley, T. Arvedson, J. D. McCarter, C. Fotsch, V. J. Cee, *Journal of Medicinal Chemistry* **2020**, *63*, 11602-11614; dR. Lonsdale, J. Burgess, N. Colclough, N. L. Davies, E. M. Lenz, A. L. Orton, R. A. Ward, *Journal of Chemical Information and Modeling* **2017**, *57*, 3124-3137.

[307] R. A. Ward, M. J. Anderton, S. Ashton, P. A. Bethel, M. Box, S. Butterworth, N. Colclough, C. G. Chorley, C. Chuaqui, D. A. E. Cross, L. A. Dakin, J. É. Debreczeni, C. Eberlein, M. R. V. Finlay, G. B. Hill, M. Grist, T. C. M. Klinowska, C. Lane, S. Martin, J. P. Orme, P. Smith, F. Wang, M. J. Waring, *Journal of Medicinal Chemistry* **2013**, *56*, 7025-7048.

[308] aK. Słoczyńska, A. Gunia-Krzyżak, P. Koczurkiewicz, K. Wójcik-Pszczoła, D. Żelaszczyk, J. Popiół, E. Pękala, *Acta Pharmaceutica* **2019**, *69*, 345-361; bK. M. Knights, D. M. Stresser, J. O. Miners, C. L. Crespi, *Current Protocols in Pharmacology* **2016**, *74*, 7.8.1-7.8.24.

[309] U. Boelsterli, H. Ho, S. Zhou, K. Leow, *Current drug metabolism* **2006**, *7*, 715-727.

[310] D. Steinhilber, M. Schubert-Zsilavecz, H. Roth, BiblioScout, **2017**, p. 704.

[311] T. J. Wilke, W. R. Jondorf, G. Powis, *Xenobiotica* **1989**, *19*, 1013-1022.

[312] L. Di, P. V. Fish, T. Mano, *Drug Discovery Today* **2012**, *17*, 486-495.

[313] N. A. Meanwell, *Chemical Research in Toxicology* **2011**, *24*, 1420-1456.

[314] G. R. Fulmer, A. J. M. Miller, N. H. Sherden, H. E. Gottlieb, A. Nudelman, B. M. Stoltz, J. E. Bercaw, K. I. Goldberg, *Organometallics* **2010**, *29*, 2176-2179.

[315] aK. Gao, R. Oerlemans, M. R. Groves, *Biophysical Reviews* **2020**, *12*, 85-104; bO. Fedorov, F. H. Niesen, S. Knapp, in *Kinase Inhibitors: Methods and Protocols* (Ed.: B. Kuster), Humana Press, Totowa, NJ, **2012**, pp. 109-118.

[316] K. Huynh, C. L. Partch, *Current Protocols in Protein Science* **2015**, *79*, 28.29.21-28.29.14.

[317] aT. G. Erbay, D. P. Dempe, B. Godugu, P. Liu, K. M. Brummond, *The Journal of Organic Chemistry* **2021**, *86*, 11926-11936; bM. E. Flanagan, J. A. Abramite, D. P. Anderson, A. Aulabaugh, U. P. Dahal, A. M. Gilbert, C. Li, J. Montgomery, S. R. Oppenheimer, T. Ryder, B. P. Schuff, D. P. Uccello, G. S. Walker, Y. Wu, M. F. Brown, J. M. Chen, M. M. Hayward, M. C. Noe, R. S. Obach, L. Philippe, V. Shanmugasundaram, M. J. Shapiro, J. Starr, J. Stroh, Y. Che, *Journal of Medicinal Chemistry* **2014**, *57*, 10072-10079; cR. N. Reddi, E. Resnick, A. Rogel, B. V. Rao, R. Gabizon, K. Goldenberg, N. Gurwicz, D. Zaidman, A. Plotnikov, H. Barr, Z. Shulman, N. London, *Journal of the American Chemical Society* **2021**, *143*, 4979-4992.